Summer 2021

Development of tripodal and bipodal ligand frameworks and first-row transition metal reagents for selective C-N bond construction methodologies

Anshika Kalra

Department: Chemistry

DEVELOPMENT OF TRIPODAL AND BIPODAL LIGAND FRAMEWORKS AND FIRST-ROW TRANSITION METAL REAGENTS FOR SELECTIVE C–N BOND CONSTRUCTION METHODOLOGIES

by

ANSHIKA KALRA

A DISSERTATION

Presented to the Graduate Faculty of the

MISSOURI UNIVERSITY OF SCIENCE AND TECHNOLOGY

In Partial Fulfillment of the Requirements for the Degree

DOCTOR OF PHILOSOPHY

in

CHEMISTRY

2021

Approved by:

Dr. Pericles Stavropoulos, Advisor
Dr. Chariklia Sotiriou Leventis
Dr. Amitava Choudhury
Dr. V. Prakash Reddy
Dr. Melanie R. Mormile

PUBLICATION DISSERTATION OPTION

This dissertation consists of the following three articles, formatted in the style used by the Missouri University of Science and Technology:

Paper I, found on pages 23–94, has been published in *ACS Catal.*, **2018**, *8*, 9183-9206.

Paper II, found on pages 95–164, has been published in *Organometallics.*

Paper III, found on pages 165–212, is intended for submission to *ACS Catal.*

ABSTRACT

We present a family of anionic Mn(II) reagents supported by trisphenylamido-amine frameworks that offer guidance with regards to ligand selection for developing C─N bond construction methodologies (extensively used in the synthesis of petrochemicals, household chemicals) through nitrene- transfer chemistry. We subsequently extend the study to include the corresponding Fe(II), Co(II), and Ni(II) reagents, to gain insights in their comparative reactivity/selectivity patterns. Attenuated levels of electrophilicity of anionic complexes proved to be more suitable for discriminating aromatic from aliphatic olefins for aziridination purposes, especially for Mn(II) complexes. However, in the case of Co(II) reagents, we observe that additional stereoelectronic parameters can occasionally override the electron-affinity of the metal nitrene as the sole guiding force, which is established as the dominant factor for Mn(II) complexes. We conclude from experimental and computational investigations that carboradical intermediates are generated by initial rate-determining nitrene-addition to one of the olefinic carbons followed by fast ring closure to form the aziridine, with rates that largely depend on the ligand and metal choice.

This study was extended to start exploring intermolecular aziridinations of alkenes catalyzed by metal reagents (Cu, Ag) supported by the rigid cyclic guanidinyl arms possessing chiral elements. In this study, we synthesized a series of cyclic chiral guanidinyl precursors and corresponding metal regents which proved to have good reactivity, but still modest enantioselectivities, in the aziridination of styrenes.

ACKNOWLEDGMENTS

I am sincerely grateful to my advisor, Dr.Pericles Stavropoulos, for his constant advice and motivation, immense support, his kind, reassuringly soft and muted presence, his gentleman aura, ever hovering in the wings to row me out of troubled waters, whenever i needed direction and help. Such unbounded and beautiful has been his constant presence that, finally speaking aloud of it is such relief to the grateful and indebted heart and silence would be a lie to my shying nature to express in words what I strongly feel about him. I am extremely thankful to him for giving me the opportunity to work with him and being a great advisor throughout my journey.

I am thankful to Dr. Chariklia Sotiriou Leventis, Dr. Amitava Choudhury, Dr. V. Prakash Reddy and Dr. Melanie Mormile for their support, guidance and accepting to be a part of my committee.

I am grateful to the National Institute of General Medical Sciences (NIGMS) for supporting my research. I would like to thank the Department of Chemistry at Missouri University of Science & Technology for their help and support.

I am immensely thankful to my parents, Madan Kalra, and Kalpana Kalra, my brother, Akansh Kalra, and my sister, Gauri Kalra, for their never-ending love and continuous support. No words can express my deep gratitude to them for bearing me, believing in me and always having my back. A special thank you to all my family members and friends for their love and emotional support. Thank you for always being there for me and making my life here in Rolla fun!

TABLE OF CONTENTS

LIST OF ILLUSTRATIONS

SECTION Page

PAPER II

PAPER III

SECTION

LIST OF SCHEMES

SECTION Page

LIST OF TABLES

1. INTRODUCTION

1.1. IMPORTANCE OF AND STRATEGIES FOR CONSTRUCTING C–N BOND FUNCTIONALITIES

Essential saturated and unsaturated hydrocarbons (especially light alkanes, alkenes, and aromatics) derived via natural gas processing and crude petroleum refining are extensively used for their energy content as fuels and space heating materials, but to a much lesser extent as feedstock for producing commodity[1] chemicals. They commonly require initial functionalization (for instance, halogenation, nitrogenation, carbonylation, oxidation/reduction) prior to becoming available for the synthesis of targeted commodity chemicals. For instance, the synthesis of methanol from methane requires initial deep oxidation, followed by reduction of synthesis gas ($CO+H_2$) over heterogeneous catalysts at high pressures and temperatures. The synthetic methodologies employed in this process are energetically wasteful and environmentally hazardous.

The direct activation of C–H bonds of light alkanes and unadorned benzenes to selectively generate C–X bonds of high value is a most sought-after enterprise with numerous applications for X = C, N O, S, B, and halogen atoms[2-12]. Among them, the C–N bond provides an astonishing array of functionality to a diverse body of chemicals (polymers, pharmaceuticals, agrochemicals, semiconductors, ligands, diverse natural products, catalytic materials, solvents, and household chemicals), although its selective generation from unfunctionalized sp^3-C–H (prim, sec), C–H (aromatic) and C=C bonds is not trivial[13].

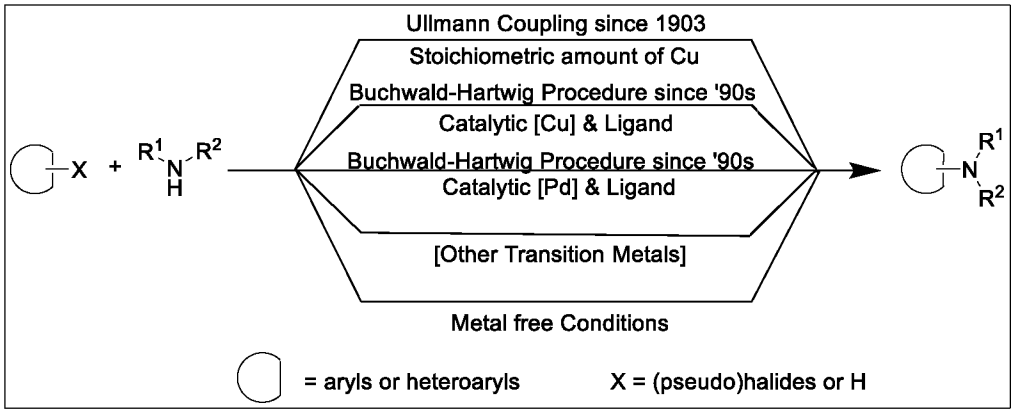

Scheme 1.1. C—N Bond Construction Strategies

The most common way of building a C–N bond (Scheme 1) is by cross-coupling methodologies (Ullmann-Goldberg, Buchwald-Hartwig, Chan-Lam)[14], which, however, require prior derivatization of the C–H bond to an energetic C–X surrogate (X = halide, pseudohalide, boronic acids, stannanes, siloxanes) and frequently extensive heating. An effective strategy for introducing a new C−N bond into a molecule is through transition metal- catalyzed nitrene transfer chemistry.

For olefinic substrates, a metal-supported nitrene group/entity can add across a C=C bond to form an aziridine or insert into an allylic C−H bond to yield the corresponding amine. These organic transformations are promoted by diverse metals, including first-row transition elements such as Cu, Fe, Co, and Mn. Aziridines are highly strained three membered rings, the smallest members in the family of nitrogen-containing rings, and potential carriers of optical activity. They are useful building blocks and end products in synthesis by means of stereo- and regiospecific transformations, including ring opening, ring expansion, and rearrangement[15]. A handful of natural products that exert antineoplastic or antibiotic activity via DNA alkylation[16], cleavage, or cross-linking have been found to contain aziridine moieties. Many synthetic aziridine-containing

agents have been intended as pharmaceuticals[17] and fine chemicals[18], and a significant number of materials containing aziridine frameworks are currently emerging as intermediates or end products[19]. Aziridines are also useful intermediates in natural product synthesis, as in the case of the kainoids, (-)-mesembrine, (-)-platynesine, sphingosines, actinomycin D, L-epicapreomycidine, and feldamycin. Scheme 2 highlights various ring opening pathways of aziridines to provide a range of useful products.

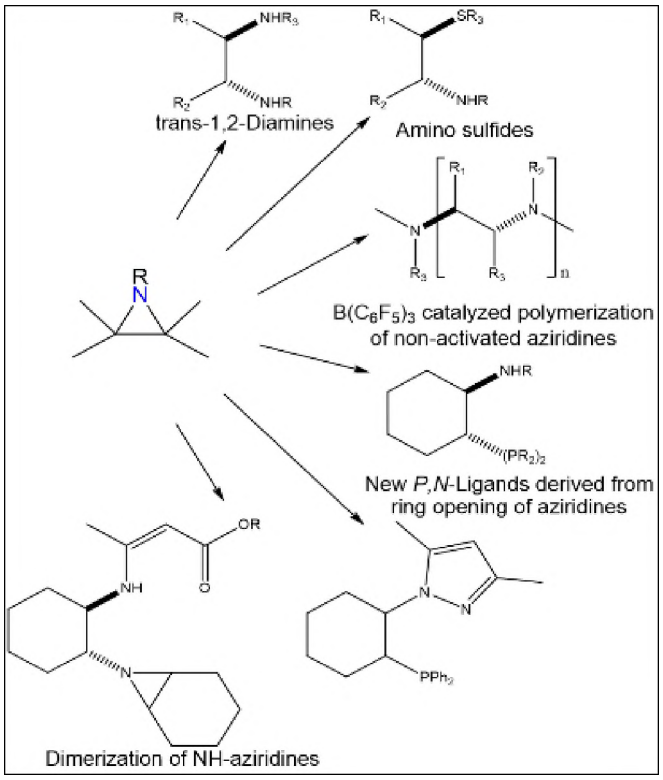

Scheme 1.2. Various Ring Opening Pathways of Aziridines

Three approaches are more frequently employed among the different known methodologies for effecting the synthesis of aziridines, namely, cyclization of 1,2-amino derivatives, addition of C_1 sources to imines, and nitrene transfer to alkenes[20] (Scheme 3). Catalytic nitrene transfer to alkenes ("C_2+N_1" addition) involves reaction of a metal-

supported singlet or triplet nitrene intermediate with an olefinic substrate. The "C_2+N_1" addition approach is more extensively practiced due to its operational simplicity and availability of a wide range of suitable substrates and catalysts and the potential for stereo/regio-specific and atom-economical nitrene addition to olefins. The N_1 donors include a variety of nitrene/nitrenoids precursor oxidants such as iminoiodanes (ArI=NR), haloamines (RNNaX, X = Cl, Br), O/N-substituted hydroxylamines and *N*-tosyloxycarbamates (RN(X)–OR′, X = H, leaving group) or atom-economical organic azides (RN_3). These N-donor groups react with reduced metals to generate high-valent metal-nitrene or nitrenoid species.

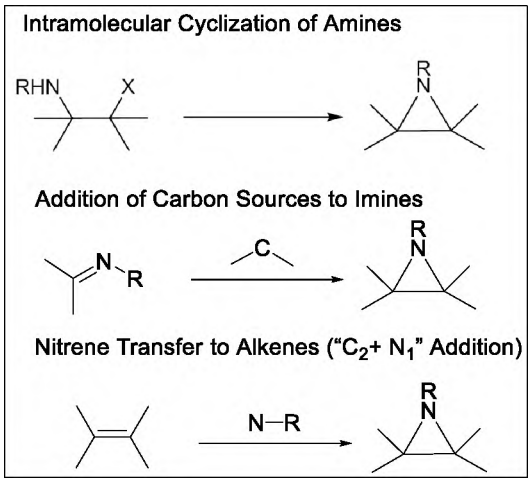

Scheme 1.3. Synthesis of Aziridines by Various Methodologies

The desirable direct aziridination of C=C or amination of C–H bonds by means of metal-nitrene, metal-nitrenoid or metal-imido/amido entities, has become a field of intense exploration, involving largely platinum-group elements, but also earth's abundant and nonprecious metals[20-25] (Scheme 4).

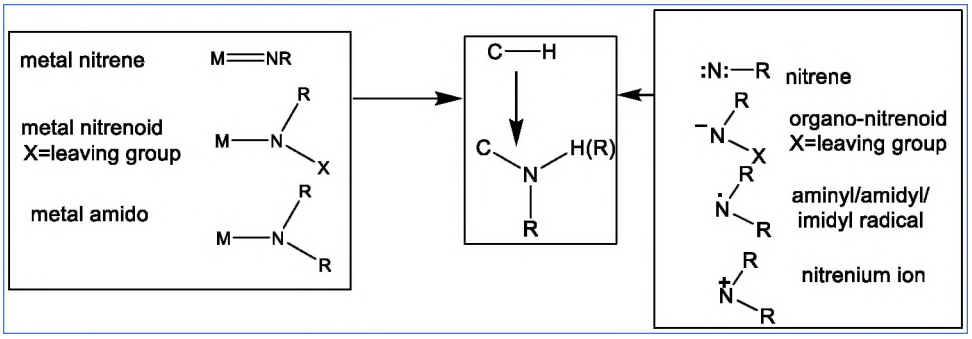

Scheme 1.4. Metal-Bound and Metal Free Nitrogen-Group Donors for C─H Amination

Metal-free nitrenes, nitrenoids and aminyl/amidyl/imidyl radicals or even nitrenium ions can also be effective, albeit not always selective agents. To employ raw starting materials from primary energy sources (natural gas, petroleum), the C–N bond construction technology requires further development to extend the substrates scope beyond the current feedstock of rather weak or energetic C–H bonds (usually benzylic, tertiary, or heteroatom-activated C–H bonds). The methodology that recently has garnered much attention relies on substrate-appended directing groups to guide site-selective functionalization of inert C–H bonds. For the selective synthesis of pharmaceutical agents[26-30], this methodology is certainly beneficial but generally not applicable to synthetic targets derived directly from nonfunctionalized energy-related feedstock (for instance, C_1-C_8 alkanes and aromatics).

The direct amination of two iconic substrates (methane, benzene) by ammonia to afford methylamine and aniline respectively is quite challenging[31-33] (Scheme 5), as both are endergonic processes and require a hydrogen scavenger to render them thermodynamically feasible. In heterogeneous catalysis, a suitable metal oxide (for instance, "cataloreactant" NiO) is required that can eliminate hydrogen as water and render these reactions exergonic.

In homogeneous catalysis, an analogous "oxidant" is needed to provide a similar thermodynamic driving force. Common oxidants employed are hypervalent iodine(III) reagents (ArI=NR), organic azides (RN_3), haloamines (RNNaX, X = halogen), and F^+ reagents (R_2N–F), or the less explored O/N-substituted hydroxylamines (RO-NR′R″)[34-42].

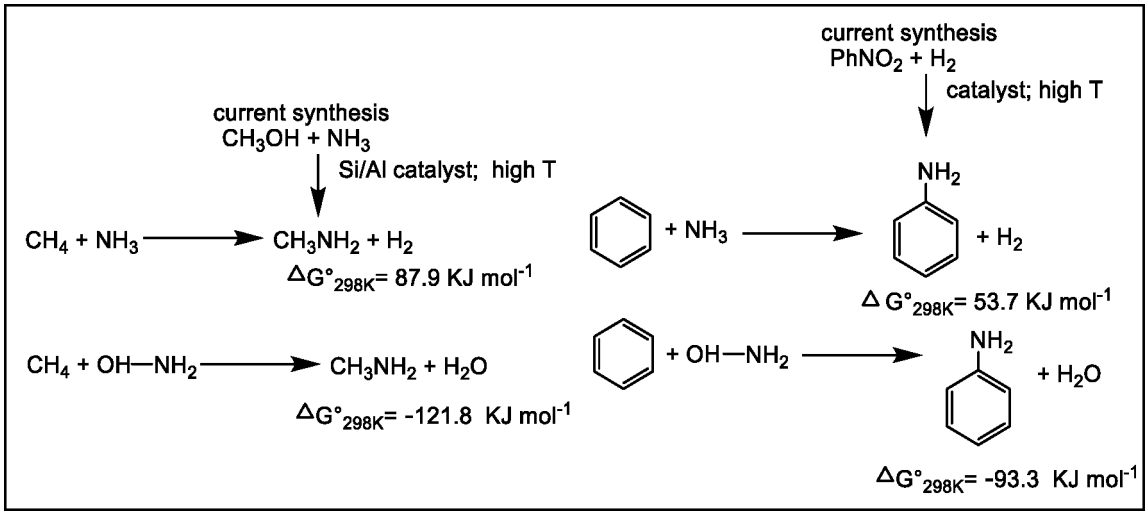

Scheme 1.5. Thermodynamic Requirements for the Amination of Methane or Benzene by Ammonia

These oxidants transfer the nitrogen moiety (NR, NR_2) to be inserted in the C–H bond or added to C=C bonds, via metal-nitrene/nitrenoid chemistry. For example, if ammonia is replaced by the parent hydroxylamine ($HO–NH_2$), the reactions (Scheme 5) become highly exergonic (eqs. 1, 2), because of the strong O–H bond generated. Kinetic barriers for H-atom abstraction from inert C–H bonds by metal-bound N-group moieties can also be formidable, and these require the employment of highly electrophilic M–NR/NR(X)/NR_2 moieties. For this purpose, the nitrogen-group sources frequently carry electron deficient groups (SO_2R, COOR), which provide stability and compatibility with oxidants.

1.2. DIFFERENT NITROGEN DONORS SUITABLE FOR CATALYTIC AZIRIDINATION REACTIONS AND FACTORS AFFECTING THE REACTIVITY/SELECTIVITY OF METAL NITRENES

An important class of nitrogen-group donors are nitrene sources (NR) that carry not only electron-withdrawing R groups (Ts, Ns), but also alkyl (1-Adamantyl, tert-Bu) and aryl moieties (Mesityl, 2,6- $^{i}Pr_2C_6H_3$, 4-$MeOC_6H_4$, C_6F_5). Similarly, aryl nitrenes have been instrumental in rhodium[43] and iridium-catalyzed[44] aminations, despite their known instability via rearrangement, yet their engagement with first row middle/late transition elements (with the exception of Ni) has not been fully evaluated. A caveat with respect to these alkyl and aryl nitrenes is the need for delivering them as azides (RN_3).

Metal-nitrenoids (M–NR(X)), formally combining an electrofuge and a nucleofuge nitrogen substituent[45], have been less explored for olefin aziridination and alkane amination, especially from hydroxylamine sources (RO–NHR). The nitrene sources such as *O*/*N*-substituted hydoxylamines (Scheme 6)[46] and organic azides (RN_3) may be required for difficult substrates, because of the superior thermodynamic driving force provided by N−O bond cleavage in the case of hydroxylamines or N_2 extrusion from organic azides, but these nitrene sources do not always undergo facile activation at metal sites. The nitrenoid units can further enhance the electrophilicity of the N atom by means of electron-withdrawing X leaving groups, and are expected to accelerate H-atom abstraction from light alkanes by placing the reaction under thermodynamic control due to formation of a strong X–H bond (Bell-Evans-Polanyi principle). Geometric and electronic structures of metal-nitrenoids are scarcely available, and their mode of operation is not well understood.

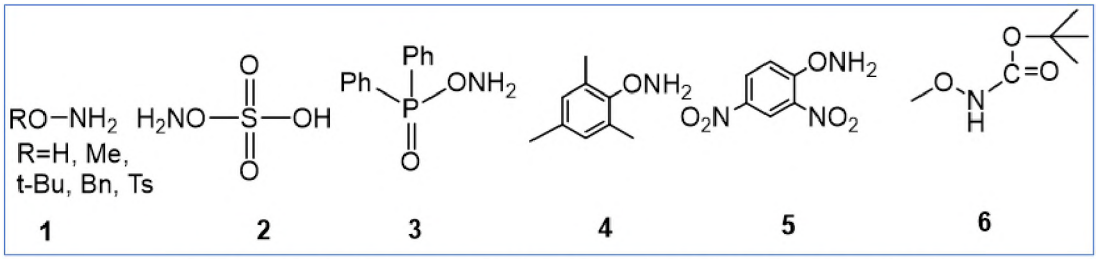

Scheme 1.6. Common O-Substituted Hydroxylamines (1-6)

As opposed to oxo-transfer chemistry, the corresponding nitrene/nitrenoid-transfer reactions rely significantly on the choice of the attendant R group, to control the electrophilicity of the active moiety and provide activated (R = SO_2R, CO_2R, COR, carbamoyl, sulfamoyl) or nonactivated aziridines (R = H, alkyl, aryl, silyl) with differential reactivity. Shaik[47] has advanced arguments that support, counterintuitively, lower barriers for H-atom abstraction by Fe=NH vs. $Fe=NSO_2Me$ units (P-450 related). Moreover, whereas copper-nitrenes with sulfonamides invariably support triplet spin states, alkyl nitrenes such as Cu=N(1-Adamantyl) tend to stabilize the open-shell singlet state.

The latter should exhibit very low barriers for recombination with substrate-centered radicals. The chemo-, site- and stereoselectivity of these reactions can be impacted by whether addition or insertion of this species occurs into a C=C or C–H bond in a concerted or stepwise fashion (Scheme 7).

Activated aziridines feature an electron-withdrawing protective R group (SO_2R, CO_2R, COR, carbamoyl, sulfamoyl)[48] that enhances electrophilicity to enable aziridine synthesis and facilitate further aziridine transformation, but suffers in terms of reduced atom economy and often requires a harsh deprotection protocol. On the other hand,

nonactivated aziridines[49] (R = H, alkyl, aryl, silyl), although more challenging to synthesize, are naturally desirable as terminal products.

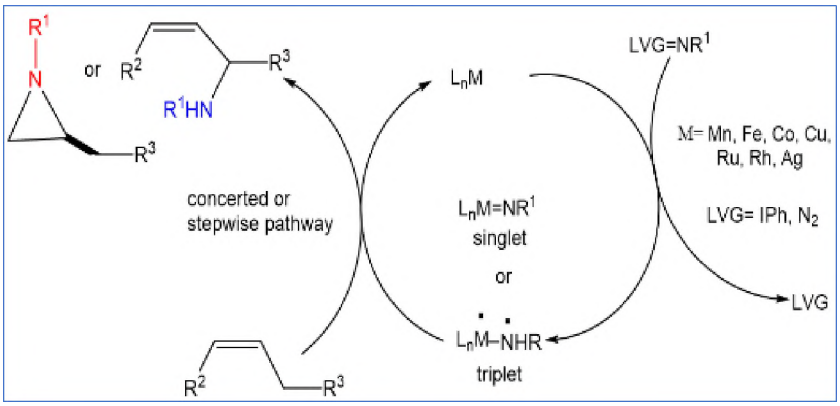

Scheme 1.7. Plausible Mechanism for Nitrene Transfer Chemistry to Olefins

Terminal metal carbenes or nitrenes are notoriously difficult to isolate, especially with moieties frequently used in catalysis, possessing electron-withdrawing substituents. Recent studies by Davies/Berry[50] and Fürstner[51] highlighted the importance of carbenes with "donor-acceptor" and "donor-donor" substituents, giving rise to isolable dirhodium carbenes. With respect to nitrenes, recent work has documented an isolable Cu=NAr moiety trapped within a macrocyclic framework[52]. Other studies resort to assistance by Sc^{3+} ions[53] to stabilize electron-deficient NTs/NMes entities or require employment of phosphino-nitrenes. Betley's group[54] also reported the isolation of copper nitrene intermediates They employed electron deficient aryl azides as a nitrogen source with a copper(I) dinitrogen complex bearing a sterically encumbered dipyrrin ligand to produce isolable terminal copper nitrene complexes.

1.3. TRANSITION METAL REAGENTS EXPLORED FOR CATALYTIC AZIRIDINATION REACTIONS

A wide range of transition metal catalysts has been explored to influence reactivity and selectivity outcomes in nitrene transfer to alkenes, frequently supported by chiral ligands for enantioselective aziridinations, starting from historic Mn or Fe porphyrinoids[55] and more recent biomimetic and artificial hemoprotein versions. Mansuy and his group were the first to report that that Fe(III) tetraarylporphyrins in the presence of PhI=NTs as a nitrogen donor, catalyzed aziridination of alkenes, although the NTs nitrene moiety can also bridge between the iron and a porphyrin nitrogen atom.

Although porphyrin and salen-based systems were effective for alkene epoxidation, they had initially found limited utility as aziridination catalysts, and no enantioselective systems had been reported employing these classes of metal complexes.

In the early 90's, Jacobsen's[56] group successfully reported the first asymmetric aziridination of alkenes using Cu(I) based benzylidene derivatives of 1,2-diaminocyclohexane ligands (Scheme 8).

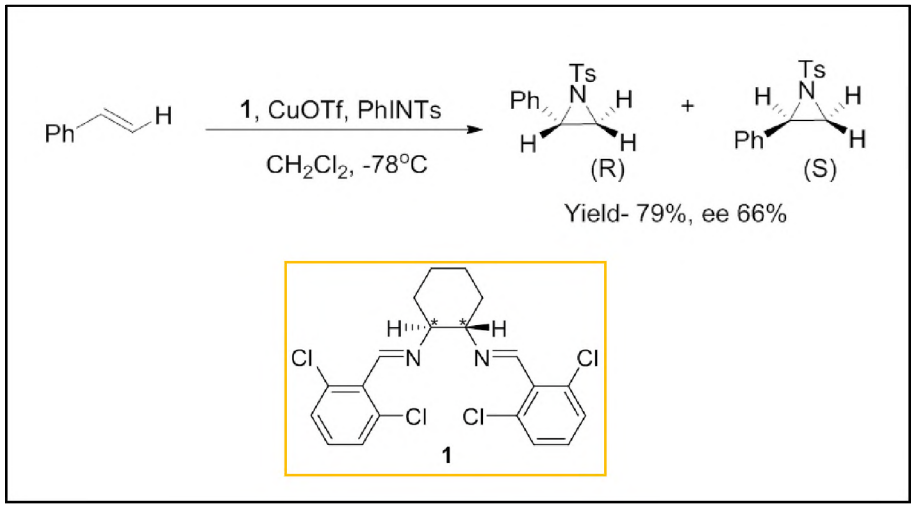

Scheme 1.8. Asymmetric Aziridination Catalyzed by Jacobsen Ligand

Around the same time, Evans' group[57] also demonstrated that copper complexes of bis-oxazolines are efficient catalysts for the asymmetric aziridination of olefins (Scheme 9).

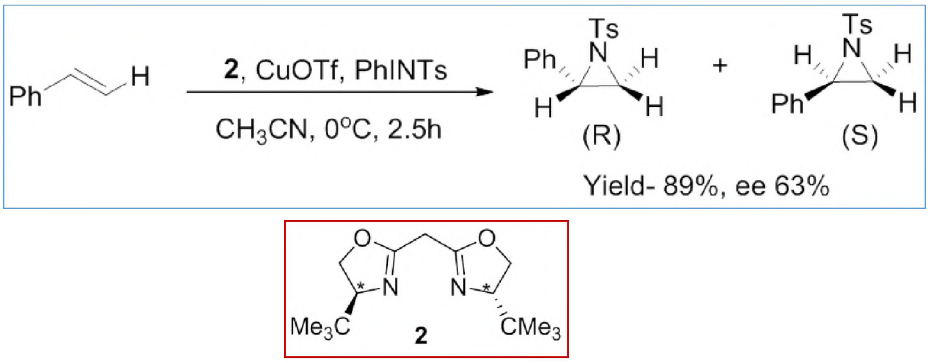

Scheme 1.9. Asymmetric Aziridination Catalyzed by Evans' Ligand

Lebel et al reported the use of a stable, readily available chiral *N*-tosyloxycarbamate[58] as a nitrene precursor to perform stereoselective intermolecular amination of alkenes in the presence of a chiral rhodium catalyst (Scheme 10).

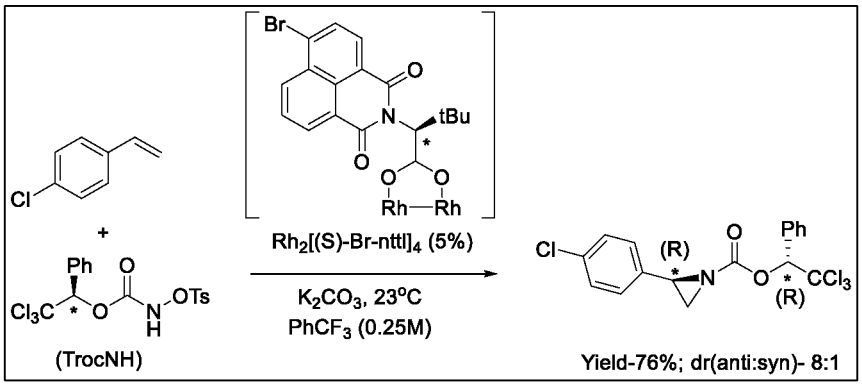

Scheme 1.10. Intermolecular Aziridination in the Presence of a Chiral Rhodium Catalyst

Zhang's group[59] showed that commercially available cobalt(II) complex of *meso*-tetraphenylporphyrin ([Co(TPP)]) can effectively activate aryloxysulfonyl azides at room temperature for selective radical aziridination of alkenes via metalloradical catalysis. In addition to generating the environmentally benign N_2 as the only byproduct, this Co(II)-based metalloradical aziridination process features neutral, nonoxidative conditions and operational simplicity. More recently, Zhang also reported that cobalt(II) complexes of D_2-symmetric chiral porphyrins[60], can catalyze asymmetric olefin aziridination with diphenylphosphoryl azide (DPPA) as a nitrene source, forming the desired N-phosphorus-substituted aziridines in moderate to high yields and good enantioselectivities (Scheme 11).

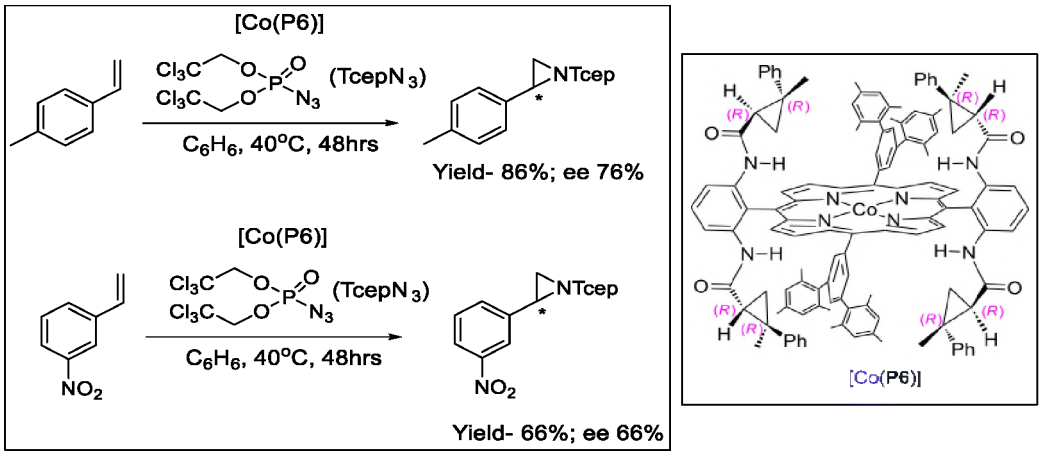

Scheme 1.11. Enantioselective Aziridination Catalyzed by a Chiral Co-Porphyrin System

The importance of stereoselectivity in the synthesis of biologically active aziridines and its derivatives is well established, but chemo- and regioselectivity are also crucial in nitrene insertions, especially in the presence of other unsaturated organic moieties and/or a multitude of C−H bonds[61]. While an inverse reactivity/selectivity correlation may hold true in many instances, as demonstrated in Mn-catalyzed

epoxidations[62], there are many exceptions to this relationship as well[63]. Our group[64] used Cu(I) based trisphenyl-amido amine tripodal ligand having (Scheme 12) tetramethylguanidinyl as pendent arms and showed that a range of olefinic substrates can undergo aziridination with good yields and selectivity. Betley's group[65] reported the use of dipyrrinato iron catalyst with organic azides to generate a reactive, high-spin iron imido species that directs the chemoselectivity for intermolecular nitrene transfer with olefinic substrates towards allylic C–H bonds to give rise to predominantly allylic aminated products rather than aziridinated products.

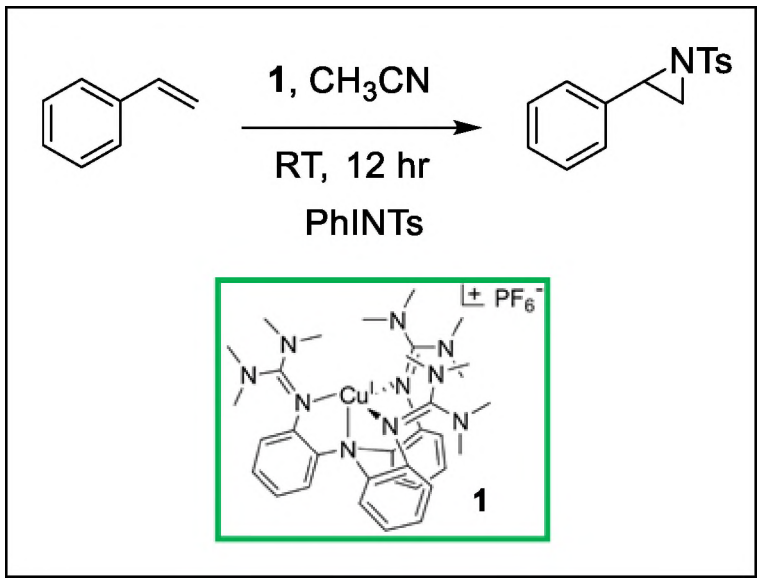

Scheme 1.12. Aziridination Catalyzed by Cu(I) based Trisphenyl-amido amine Tripodal Ligand

N-Heterocyclic carbene (NHC) ligands are increasingly used in transition-metal catalysis because of the strong σ-donor character of the ligand that helps in increasing the reactivity of the trans metal-carbene or nitrene moeity unit. Che's group[66] showed that the high reactivity of bis(NHC)ruthenium(II)–porphyrin complexes towards alkene aziridination by aryl azides (RN_3) could be attributed to the stabilization of the reactive

[Ru(Por)(NHC)(NR)] intermediate owing to a strong NHC–Ru–NHC interaction (Scheme 13).

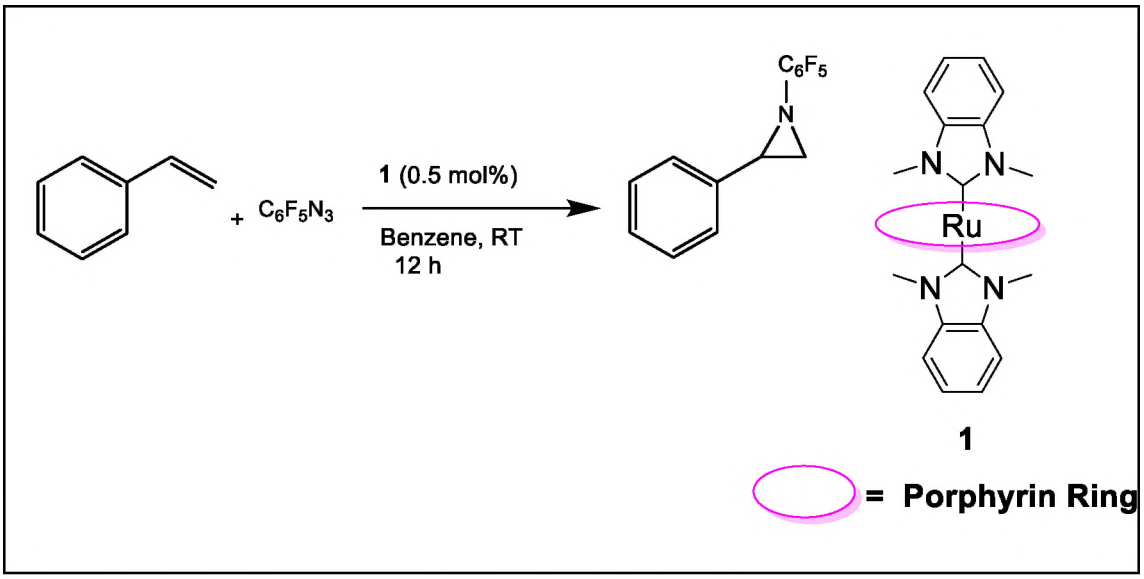

Scheme 1.13. Aziridination Catalyzed by NHC Supported Ru Porphyrin Complexes

1.4. FACTORS AFFECTING THE REACTIVITY OF COMPETING OLEFINS IN AZIRIDINATIONS

In the literature, several instances of terminal vs internal (multiple substitution), electron-poor vs electron-rich, or aromatic vs aliphatic alkenes have been reported that may be competing for aziridination. Using commercially available $Rh_2(esp)_2$ and hydroxylamine-O-sulfonic acid (HOSA) as the aminating agent, Kurti and co-workers[67] achieved, the chemoselective aziridination of the more substituted alkene (Scheme 14). Evans's group[68] demonstrated the Cu-catalyzed aziridination of aromatic olefins and observed better yields with electron-rich substituents as compared to the electron-withdrawing substrates. Halfen and co-workers[69] used non-heme Fe(II) complexes for the

catalytic aziridination of styrene and 1-hexene by PhINTs. They observed lower yields in the case of 1-hexene (30%) as compared to styrene (68%).

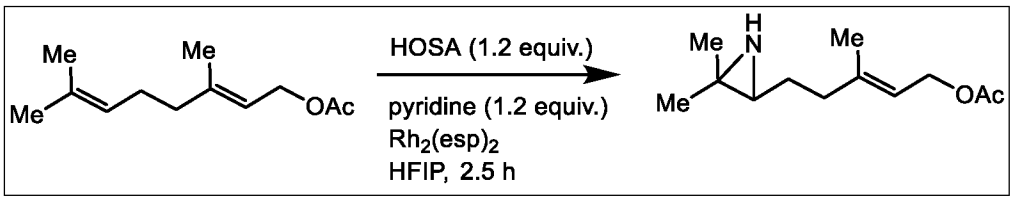

Scheme 1.14. Chemoselective Aziridination of Alkenes using $Rh_2(esp)_2$ and HOSA

Generally, electron rich alkenes tend to be more productive with an electrophilic nitrene, but this predilection may be undercut by steric requirements. Accordingly, it has been observed that aromatic olefins are favored over nonconjugated olefinic substrates in the competition for aziridination between styrenes and acyclic aliphatic olefins. Indeed, aromatic or conjugated olefins enjoy better reactivity than their nonconjugated congeners in several metal-catalyzed aziridinations (Rh, Cu, Fe, Co, Ru, Ag). Alkyl-substituted olefins, on the other hand undergo aziridination in a significantly more stereospecific manner than styrenes. Aziridination for aliphatic alkenes have been found to be more productive with Cu, Fe and Ru reagents supported by salen and/or NHC ligands. For instance, the aziridination of a variety of aliphatic alkenes, using copper compounds supported by N-heterocyclic carbene ligands, has been demonstrated by Appella and co-workers[70] (Scheme 15).

Apparently, N-Heterocyclic carbenes (NHC) stabilizes the reactive intermediates (Cu^{III}-nitrene) in the catalytic cycle and could potentially serve as a better ligand in case of aliphatic olefins as the substrate. The product balance also depends on the ligand framework employed, or the number of ligands coordinated at the metal site. Du Bois and

co-workers showed that the mixed-valent paddlewheel complex tetrakis-(2-oxypyridinato)diruthenium(II,III)chloride, $[Ru_2(hp)_4Cl]$, displayed a preference for amination of allylic and benzylic centers, in contract to its dirhodium tetracarboxylate counterpart, which tends to favor aziridination (Scheme 16)[71].

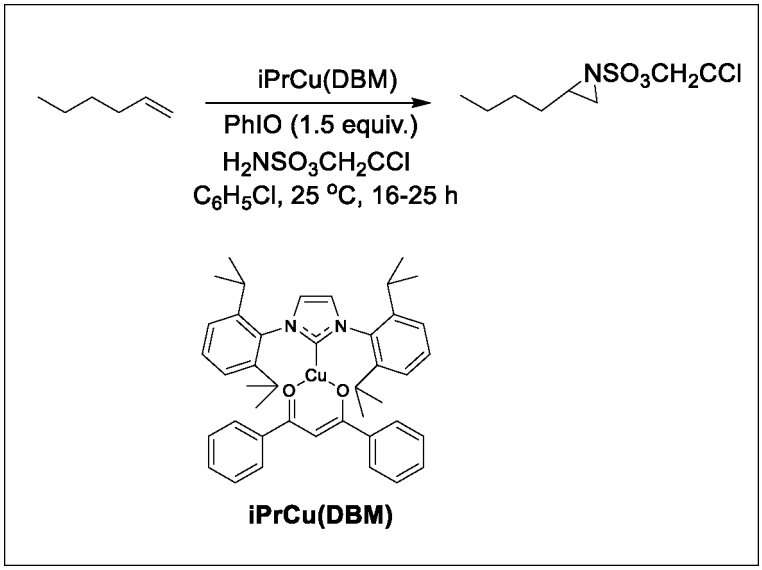

Scheme 1.15. Aziridination of Aliphatic Alkenes using Copper-NHC Catalysts

Both computational and experimental data revealed a two-step nitrene addition/insertion to olefinic/C−H substrates mechanism for the Ru based catalyst through the intermediacy of a short-lived diradical species, while the counterpart Rh analog proceeds via a concerted mechanism.

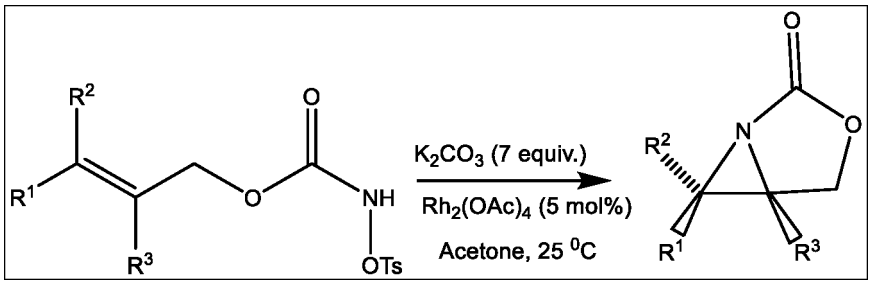

Scheme 1.16. Intramolecular Aziridine Formation Catalyzed by $Rh_2(OAc)_4$

Schomaker and her co-workers[72] developed a catalyst system based on silver triflate and phenanthroline but with different stoichiometries (Ag(OTf)phen vs. Ag(OTf)$(phen)_2$) to achieve either aziridination or allylic C−H aminatin in good yields. This was achieved because of the ability for Ag to readily adopt multiple coordination numbers and geometries, thereby manipulating the ligand environment of the active Ag catalyst (Scheme 17).

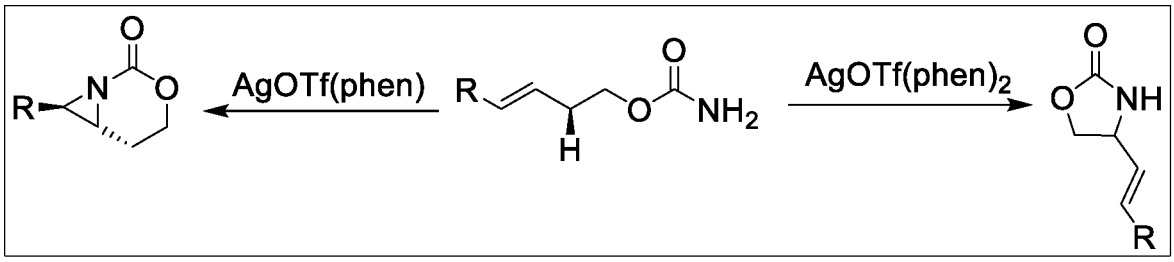

Scheme 1.17. Silver Catalyzed Intramolecular Aziridination and Allylic Amination Reaction

1.5. MECHANISM OF NITRENE TRANSFER IN AROMATIC AND ALIPHATIC OLEFINS FOR AZIRIDINATION REACTIONS

With the exception of Rh, the metal-catalyzed nitrene-transfer to aromatic alkenes is more consistent with a stepwise mechanism (successive formation of two C−N bonds), whereas the corresponding addition to aliphatic olefins has been occasionally associated with a concerted (asynchronous) mechanism (Scheme 18). One possible explanation is that electron rich aliphatic olefins undergo facile, essentially barrierless oxidation of the incipient α-carbon centered radical upon ring closure. The time elapsed between the first and second C−N bond constructions, in case of the aliphatic olefins is usually in the femtosecond regime, as opposed to picoseconds for the aromatic olefins. Therefore, although aliphatic alkenes are less reactive than the aromatic, they show better stereo-control than the aromatics upon ring formation.

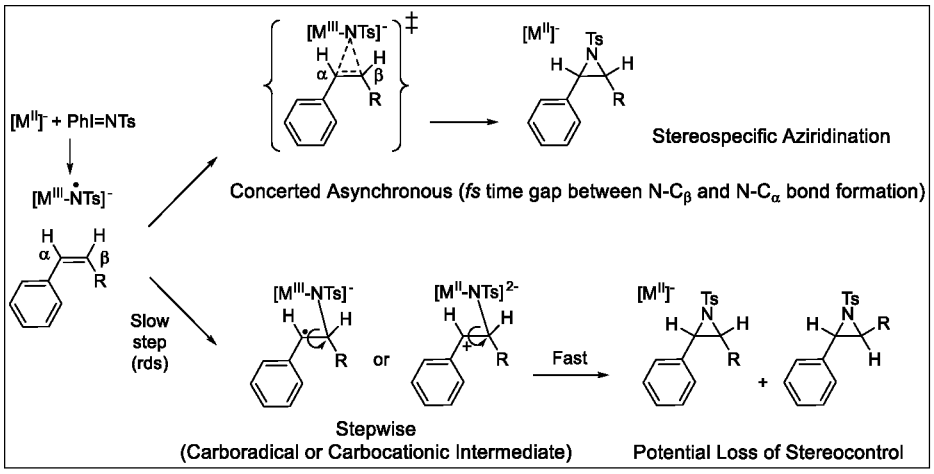

Scheme 1.18. Mechanistic Considerations for Transfer of Metal Nitrenes

As shown in our studies, the redox potential M^{II}/M^{III} tends to be the dominant factor (but not always the sole) in determining the rate of aziridine reaction and in deciding the stereo-selectivity for aziridine-ring formation by aromatic olefins. For aliphatic olefins, the relative energy of the metal-centered orbital that is ultimately receiving the single electron upon ring closure (rather than the redox potential) might be the dominant factor in deciding the stereo-selectivity for aziridine-ring formation.

1.6. MOTIVATION FOR THE WORK

In recent years, we have tested the hypothesis that if the classic $N(CH_2CH_2NH_2)_3$ (TREN) framework[73] (Scheme 19) were to be modified to include phenylene bridges, then the resulting trisphenylamido-amine (TRPHEN, Fig. 1.1) would be more supportive of metal-centered atom/group-transfer catalysis due to scaffold rigidity, resistance to β-hydride cleavage and, most importantly, weaker equatorial coordination field. We thus embarked in the synthesis of a series of trisphenyl-amido amine tripodal and bipodal ligands.

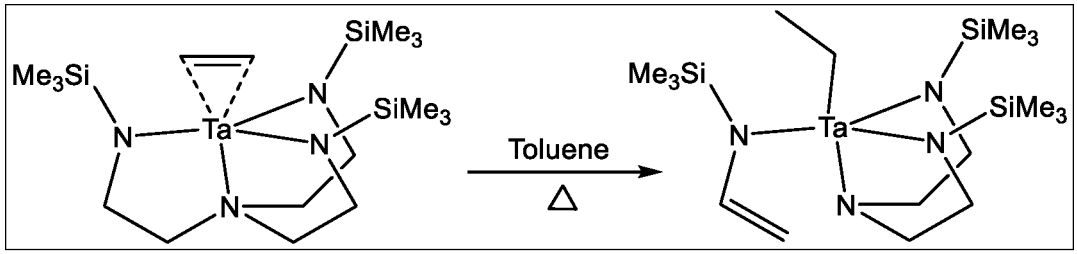

Scheme 1.19. TREN Decomposition by C−N Bond Cleavage

This family of reagents has been developed gradually, in an iterative, rather than a blindly heuristic or combinatorial manner. First, we employed the three major categories of carbonaceous arms (aryl, acyl, alkyl) to investigate the salient stereo-electronic properties exerted by each type of group with regards to atom/group-transfer chemistry.

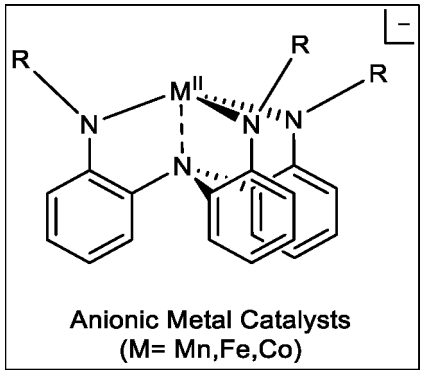

Figure 1.1. Anionic Metal Complexes

Secondly, within each category we varied the substituents in a manner that extended the redox range of the resulting ligands and compounds (closely followed by electrochemistry) as well as the steric profile (including rotational restrictions) of the reaction cavity. We thus developed a library of seventeen TRPHEN based ligands and metalated most of them with three different base metals i.e., Mn, Fe and Co as well as with Ni in a handful of cases. In total, we synthesized approximately fifty new anionic metal complexes.

The first part of the dissertation concentrates on a synthetic, catalytic (nitrene transfer chemistry), and mechanistic study with the assistance of fifteen new anionic Mn(II) catalysts, and a few Fe(II) and Co(II) congeners, supported by the TRPHEN framework to address the selective aziridination of aromatic over aliphatic alkenes in a competitive manner. Anionic metal complexes possess attenuated levels of electrophilicity as compared to cationic or neutral metal reagents but proved to be more suitable for discriminating aromatic from aliphatic olefins for aziridination purposes, and, are therefore, advantageous for chemo- and regio-selective applications. The motivation for this segment of the work was the need to identify combinations of ligands and metals that are most suitable for effecting high reactivity but also practicable selectivity to differentiate between aromatic and aliphatic alkenes in aziridination reactions.

The second part of this dissertation focuses on seventeen new anionic high-spin Co(II) catalysts as nitrene-transfer reagents, supported by the same trisphenylamido-amine ligand framework, to provide insights in their operational characteristics, not only in comparison with the previously examined libraries of Mn(II) (and to a lesser extent Fe(II) reagents), but also with respect to reported low-spin (Por)Co(II) paradigms and related congeners. In this work, we observed that even an otherwise small change in ligand substitution can have a significant effect on the rate of nitrene-transfer reactivity in aziridination reactions. This work unravels stereoelectronic parameters that can occasionally override the electron-affinity of the metal nitrene as the sole guiding force in nitrene transfer chemistry (a dominant factor in the first part of this study).

The motivation for this segment of the work was to study how the Co (II) reagents which in the first part were shown to be more reactive than Mn (II) analogs, may be

affected in their catalytic activity by additional electronic and steric factors (beyond the metal-nitrene electrophilicity), likely to arise from the tighter disposition of the Co(II) reaction cavity.

The third section of this dissertation consists of our initial attempts to address intermolecular aziridination of alkenes, mediated by metal complexes (Cu^{I}, Ag^{I}) that are supported with rigid chiral ligands. In 2014, our group reported a C−N bond construction methodology using a versatile trisphenyl-amido amine tripodal based copper(I) complex having tetramethylguanidinyl (TMG) as pendent arms[64] (Figure. 1.2). Such a moiety changes the nature of the catalyst by generating cationic metal complexes, which are expected to be more reactive than the anionic complexes discussed in the previous section, due to the electrophilic nature of the reaction. Three different kinds of C−N construction methodologies were explored in this earlier study, namely, amination of C−H bonds, amidination of C−H bonds in the presence of nitriles, and aziridination of olefins, with good yields and selectivity.

However, new challenges were noted in that study that required closer attention. First, there is significant rotational freedom for the guanidyl residue, which can be problematic for selectivity purposes during C−N bond construction, and, secondly, the N–Me substituents of the guanidyl arms may be susceptible to amination. To address these shortcomings, in addition to further efforts to enhance the electrophilicity of the key metal-nitrene moieties, we intended to initially employ cyclic guanidyl arms (Fig. 1.3), which enjoy superior rigidity and provide opportunities for examining various N-atom appended moieties, as well as exploring various chiral auxiliaries for enantioselective C−N bond construction.

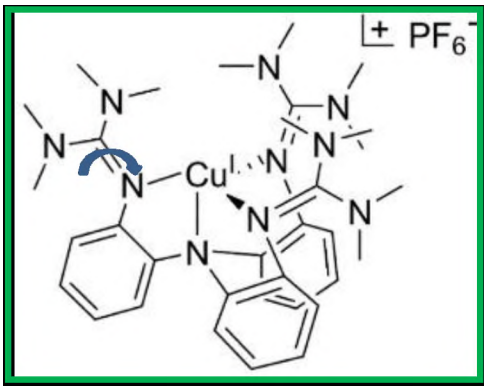

Figure 1.2. [(TMG$_3$trphen)Cu^{I})][PF$_6$]

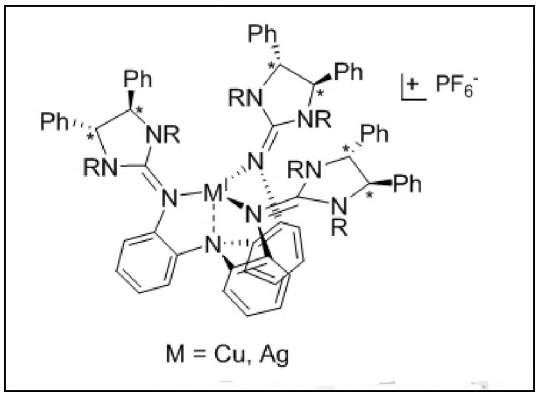

Figure 1.3. Chiral Cyclic Guanidinyl-Arms Catalyst

Enantioselective intermolecular C−N bond construction has been reported in the literature mostly relying on platinum-group transition metals such as rhodium, ruthenium and iridium. The major problem with these metals is that they are quite expensive and toxic. We opted to concentrate more on earth abundant transition metal such as copper, which has been used in asymmetric nitrene transfer chemistry, but the range of substrates has remained limited.

PAPER

I. COMPARATIVE NITRENE-TRANSFER CHEMISTRY TO OLEFINIC SUBSTRATES MEDIATED BY A LIBRARY OF ANIONIC Mn(II) TRIPHENYLAMIDO-AMINE REAGENTS AND M(II) CONGENERS (M = Fe, Co, Ni) FAVORING AROMATIC OVER ALIPHATIC ALKENES

Vivek Bagchi,[†] Anshika Kalra,[†] Purak Das,[†] Patrina Paraskevopoulou,[†§] Saidulu Gorla,[†] Lin Ai,[†¶] Qiuwen Wang,[†] Sudip Mohapatra,[†] Amitava Choudhury,[†] Zhicheng Sun,[#] Thomas R. Cundari*[#] and Pericles Stavropoulos*[†]

[†] Department of Chemistry, Missouri University of Science and Technology, Rolla, Missouri 65409.

[§] Laboratory of Inorganic Chemistry, Department of Chemistry, National and Kapodistrian University of Athens, Panepistimiopolis Zografou 15771, Athens, Greece.

[¶] College of Chemistry, Beijing Normal University, Beijing 100875, PRC.

[#] Department of Chemistry, Center for Advanced Scientific Computing and Modeling (CASCaM), University of North Texas, Denton, Texas 76203

ABSTRACT

Selective amination of σ and π–entities such as C–H and C=C bonds of substrates remains a challenging endeavor for current catalytic methodologies devoted to the synthesis of abundant nitrogen-containing chemicals. The present work addresses an approach towards discriminating aromatic over aliphatic alkenes in aziridination reactions, relying on the use of anionic metal reagents (M = Mn, Fe, Co, Ni) to attenuate reactivity in a metal-dependent manner. A family of Mn^{II} reagents bearing a triphenylamido-amine scaffold and various pendant arms has been synthesized and characterized by various techniques, including cyclic voltammetry. Aziridination of styrene by PhI=NTs in the presence of each Mn^{II} catalyst establishes a trend of increasing

yield with increasing $Mn^{II/III}$ anodic potential. The Fe^{II}, Co^{II}, and Ni^{II} congeners of the highest yielding Mn^{II} catalyst have been synthesized and explored in the aziridination of aromatic and aliphatic alkenes, exhibiting good to high yields with *para*-substituted styrenes, low to modest yields with sterically congested styrenes, and invariably low yields with aliphatic olefins. Co^{II} mediates faster styrene aziridination by comparison to Mn^{II}, but is less selective than Mn^{II} in competitive aziridinations of conjugated versus non-conjugated olefins. Indeed, Mn^{II} proved to be highly selective even versus well-established copper and rhodium aziridination reagents. Mechanistic investigations and computational studies indicate that all metals follow a two-step styrene aziridination pathway (successive formation of two N–C bonds), featuring a turnover-limiting metal-nitrene addition to an olefinic carbon, followed by product-determining ring closure. Both steps exhibit activation barriers in the order Fe > Mn > Co, most likely stemming from relevant metal-nitrene electrophilicities and $M^{II/III}$ redox potentials. The aziridination of aliphatic olefins follows the same stepwise path, albeit with a considerably higher activation barrier and a weaker driving force for the formation of the initial N–C bond, succeeded by ring closure with a miniscule barrier.

Keywords: Manganese, Iron, Cobalt, Trisamidoamine ligands, Nitrene-transfer Catalysis, Electrochemistry, Mechanistic Studies, Computational Studies

1. INTRODUCTION

As highly strained three-atom membered rings and potential carriers of optical activity, aziridines are valuable intermediates as building blocks for a plethora of chemicals by means of stereo- and regiospecific transformations, including ring opening, ring expansion or rearrangement.[1] The aziridine framework is further evidenced in a handful of natural products that exert antineoplastic or antibiotic activity via DNA alkylation, cleavage or crosslinking.[2] Naturally, many synthetic aziridine-containing agents have been targeted as pharmaceuticals[3] and fine chemicals.[4] A significant number of aziridine-functionalized tailored-made materials are currently emerging as end-products or intermediates.[5]

Among different methodologies for effecting the synthesis of aziridines, three approaches are more frequently employed, namely, cyclization of 1,2-amino derivatives, addition of C_1 sources to imines, or nitrene transfer to alkenes.[6] Catalytic nitrene transfer to alkenes ("C_2+N_1" addition) is extensively practiced due to the wide availability of substrates, and the potential for stereo/regio-specific and atom-economical nitrene addition to olefins.[7] Organocatalytic[8] and metal-mediated[7,9] approaches have been advanced, with the latter being more suitable for unactivated alkenes. A wide variety of transition metal compounds have been employed, frequently supported by chiral ligands for enantioselective aziridinations, starting from historic Mn or Fe porphyrinoids,[10] and more recent biomimetic[11] and artificial hemoprotein[12] versions. Many other catalytic systems have been subsequently developed, including iconic copper reagents bearing C_2-symmetric chiral salen[13] or bis(oxazoline)[14] ligands and other more recently established copper-containing frameworks,[15] highly practical Rh tetracarboxylate and related

paddlewheel structures,[16] versatile Mn,[17] Fe,[18] Co,[19] Ni,[20] Ru,[21] and Pd[22] reagents, frequently supported by porphyrinoid- or salen-type ligands, as well as intriguing silver-[23] and gold-centered[24] reagents featuring nitrogen-rich coordination spheres such as polypyridines and tris-pyralozyl-borates.

All these metal sites are purported to transfer a nitrene moiety (NR) to olefinic substrates or C–H bonds[25] from sources such as pre-formed or *in situ* assembled iminoiodanes (ArI=NR),[7] haloamines (RNNaX, X = Cl, Br),[26] organic azides (RN_3),[27] and cleavable N–O bond-containing precursors (RN(X)–OR′, X = H or leaving group).[16a,b,h] Activated aziridines feature NR moieties with an electron-withdrawing protective R group (SO_2R, CO_2R, COR, carbamoyl, sulfamoyl) that enhances electrophilicity to enable aziridine synthesis and facilitates further aziridine transformations, but often requires harsh deprotection protocols[28] and may suffer in terms of reduced atom economy. On the other hand, non-activated aziridines (R = H, alkyl, aryl, silyl)[16a,b,18e,l,m,27,29] are naturally desirable as terminal products, albeit more challenging to synthesize. The superior thermodynamic driving force provided by N–O bond cleavage of O/N-substituted hydroxylamines or N_2 extrusion from organic azides may be required for difficult substrates,[30] but these nitrene sources do not always undergo facile activation at metal sites.

Despite the explosive development of synthetic methodologies to access various aziridine scaffolds, many challenges remain surrounding the range of addressable olefin/N-donor substrates and attendant reaction selectivity. Naturally, matters of stereoselectivity are central in the synthesis of biologically active aziridines and derivatives thereof,[6] but important questions regarding chemo- and regioselectivity are

also crucial in nitrene insertions, especially in the presence of other unsaturated organic moieties and/or a multitude of C–H bonds.[31] While an inverse reactivity/selectivity relationship, as exemplified in Mn-catalyzed epoxidations,[32] may hold, there are many exceptions to this correlation in hydrocarbon aminations,[33] especially for a reaction that may successively form two N–C bonds (olefin aziridination) or an N–H/N–C bond combination (alkane amination). A common conundrum arises when competitive aziridination and allylic amination occurs with many metal-mediated nitrene-transfer catalysts.[31a] Metal choice may influence the product ratio of aziridination vs. allylic amination (for instance, certain Rh[16c,h,34] or Cu[15a,g,p] catalysts may have a higher predilection for aziridination, whereas Mn,[33] Fe,[18e,35] Co[19i,36] or Ru[21d,e,37] reagents tend to favor allylic aminations). The balance can also vary significantly as a function of the type of nitrene used (for instance dirhodium sulfamates favor aziridination, whereas carbamates enhance competing C–H amination) and of the ligand framework employed[21d,e] or the number of ligands coordinated at the metal site, as Schomaker and coworkers have established for Ag(I) catalysts,[23f,h] even if the underlying mechanism remains largely the same (for instance, concerted (asynchronous) or two-step nitrene addition/insertion to olefinic/C–H substrates for Rh[16c,d] and Ru,[21d] respectively). However, intramolecular and intermolecular versions can be mechanistically distinct.[38] Parallel advances in achieving selectivity in the amination of C–H bonds (usually allylic > α-heteroatom-substituted-C–H $\approx$ 3° > benzylic > 2° >>1°) via nitrene insertion are notable.[16c,31,33,39]

Another less frequently discussed but equally important issue of site selectivity arises when multiple π acceptors are present on the substrate. If we limit the discussion to

various olefins, several instances of terminal vs. internal (multiple substitution),[16a,b] electron-poor vs. electron-rich,[15g,p,19b] or aromatic vs. aliphatic alkenes[16e,f] may compete for aziridination. Naturally, electron-rich alkenes are more susceptible to accept an electrophilic nitrene, but this predilection may be undercut by steric requirements.[15p] Of particular interest is the competition for aziridination between styrenes and acyclic aliphatic olefins, which generally tends to favor the aromatic rather than the non-conjugated olefinic substrates.[19e,21a,b,23b,c,j] However, most effective and practical aziridination catalysts usually provide appreciable product yields (≥25%) for the aziridination of terminal alkyl olefins, while simultaneously perform aziridination of styrenes at high yields (≥75%).[15p,16e,f] More specifically for intermolecular reactions, conjugated olefins enjoy better reactivity than their non-conjugated congeners in several metal-catalyzed aziridinations (Rh,[16b] Cu,[15l] Fe,[18h-j] Co,[19e] Ru,[21a,b,e] Ag[15d,23b,c,j]); inversely, alkyl-substituted olefins undergo aziridination in a significantly more stereospecific manner than styrenes.[15p,16f] In a competition experiment between styrene and 1-hexene, Evans and co-workers report that the copper-mediated aziridination of styrene is favored by a "modest" ratio of 5:1.[15p] Notably, the aziridination of aliphatic alkenes and/or β-substituted styrenes has been in passing deemed unproductive with a handful of Mn,[17a] Fe,[18n] and Co[19g] reagents. Conversely, outstanding aziridination catalysts for aliphatic akenes have been developed with Cu,[40] Fe[18l,m] and Ru[21a,b,e] reagents supported by salen and/or NHC ligands.

Among the many mechanistic dilemmas confronting metal-catalyzed aziridination reactions,[15d,17a,18g,19d,21d,23e,38a] a potential mechanism switch has been contemplated in conjunction with copper-mediated aziridinations,[15p] inasmuch as nitrene transfer to

styrenes is more consistent with a stepwise mechanism (successive formation of two C–N bonds), whereas the corresponding addition to aliphatic olefins has been deemed more in line with a concerted (asynchronous) mechanism by virtue of its stereospecificity and lack of discernible radical intermediates. Among other considerations, this mechanistic differentiation hinges on a delicate, but crucial for selectivity purposes, evaluation of the time elapsed between the first and second C–N bond construction.

In the present publication, we examine a family of catalytic systems that rely on anionic metal reagents (M = Mn, Fe, Co, Ni) to selectively mediate aziridination of styrenes, while many alkyl olefins remain largely intact (≤10% yield). The electrophilicity and potential radical character[41] of the putative metal nitrene (M=NR) are heavily influenced by the stereoelectronic attributes of the R substituent and the metal center, but can also be modulated by the overall anionic charge of the complexes. The overwhelming majority of metal-nitrene units noted above, feature positive or zero overall charge in order to retain enhanced electrophilic character of the active site. In the current work, we explore mono-anionic metal sites and demonstrate that attenuated levels of electrophilicity are more suitable for discriminating aromatic from aliphatic olefins for aziridination purposes, while reactivity can still remain high by means of fine-tuning the electrophilicity levels via electron-withdrawing, ligand-centered residues. In addition, we make use of divalent, first-row transition-metal sites that have historically found extensive application within porphyrinoid frameworks,[11] but have more recently been explored in non-heme environments.[18b] These elements are more likely to operate via odd-electron governed, successive steps, posing significant reactivity/selectivity related questions with regards to each step that are better addressable with systems of more

moderate reactivity and in a metal-comparative manner. In fact, very few studies provide a parallel examination of a series of first-row M^{II} catalyst precursors with the same ligand framework in aziridination reactions,[42] potentially guiding future catalyst design. Moreover, the high-spin nature of the compounds encountered in the present work gives rise to putative metal-nitrene intermediates possessing more complex electronic structures than the common singlet/triplet manifolds explored with Cu,[15g] Ag[15f] or Ru[21k,l] nitrenes. In this combined experimental and computational research, a family of anionic Mn^{II} reagents is presented that offers guidance with regards to ligand selection for effecting olefin aziridination. These studies are subsequently extended to the corresponding Fe^{II}, Co^{II}, and Ni^{II} reagents to gain insights in their comparative reactivity/selectivity patterns that enable aromatic over aliphatic alkene aziridinations. For additional insights, the reader is also referred to a complementary report by Mat Lani and Schomaker on Rh and Ag-catalyzed competitive alkene aziridinations that was published while the present work was under review.[43]

2. RESULTS

2.1. SYNTHESIS OF LIGANDS

The synthesis of ligands L^1H_3 - $L^{10}H_3$ and $L^{13}H_3$ have already been reported.[44-47] The remaining ligands ($L^{11}H_3$, $L^{12}H_3$, $L^{14}H_3$, $L^{15}H_3$) are prepared by similar methodologies, namely (i) application of Pd-based Buchwald-Hartwig protocols ($Pd_2(dba)_3$/BINAP/NaO^{t}Bu in refluxing toluene)[48] for the arylation (ArBr) of trphen ($L^{11}H_3$, $L^{12}H_3$) or (ii) condensation of trphen with the corresponding acyl chloride in the

presence of Et_3N in dichloromethane ($L^{14}H_3$, $L^{15}H_3$). Ligands $L^{11}H_3$ (Figure S1) and $L^{15}H_3$ (Figure S2) have been characterized by X-ray diffraction analysis.

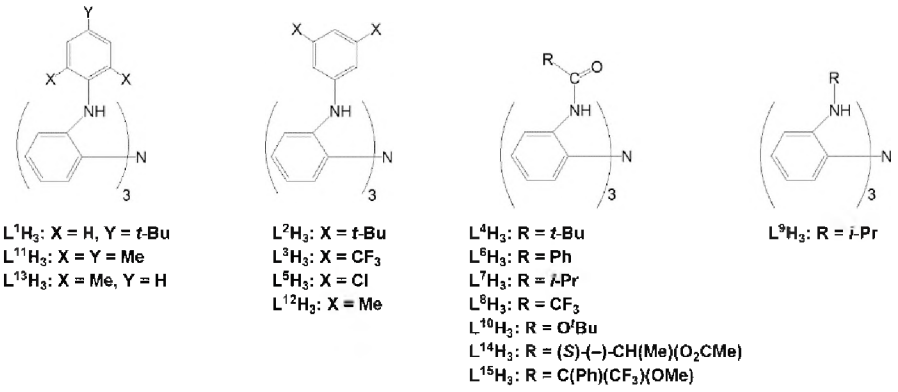

Figure 1. Ligands Used in this Study

2.2. SYNTHESIS AND CHARACTERIZATION OF Mn^{II} COMPLEXES

All Mn^{II} compounds were prepared by deprotonation of the ligands with three equivalents of KH in THF (aryl or alkyl-armed ligands) or in *N*,*N*-dimethylacetamide (DMA) (acyl-armed ligands), followed by metallation with anhydrous $MnCl_2$. Minimal representations of the first coordination sphere, as derived by single-crystal X-ray data, are shown in Figure 2. The vast majority of compounds demonstrate distorted trigonal bipyramidal geometries featuring ligand-derived [$N_{3(amido)}N_{amine}$] coordination and a solvent moiety (THF, DMA, MeCN) occupying a site trans to the axial N_{amine} atom. In a single-instance ([L^8Mn–DMA]$^-$), one N_{amido} moiety coordinates as an N_{imino} group instead (Mn–N(Ar)=C(CF_3)–O^-). A few compounds with acyl-armed ligands (see below) employ ligand-derived rather than solvent moieties in their first coordination sphere. These structures exhibit weak O-atom coordination of carbonyl or ether residues, and/or strong coordination of an iminato moiety via the O-terminus (Mn–O–C(R)=N–Ar).

Finally, the alkyl-armed [L^9MnK] reveals a four-coordinate [N_3N] geometry, devoid of any coordinated or solvated solvent molecule. Specific structural features for each category of Mn^{II} compounds are summarized below. Detailed crystallographic data are collected in Tables S1 - S3, and additional interatomic distances and angles are reported in Tables S4 - S8.

(a) Aryl-armed Mn^{II} Compounds**.** All seven Mn^{II} compounds featuring metal cavities surrounded by aryl arms possess the minimal [$(L^x)Mn^{II}$–THF]$^-$ structure (x = 1-3, 5, 11-13)

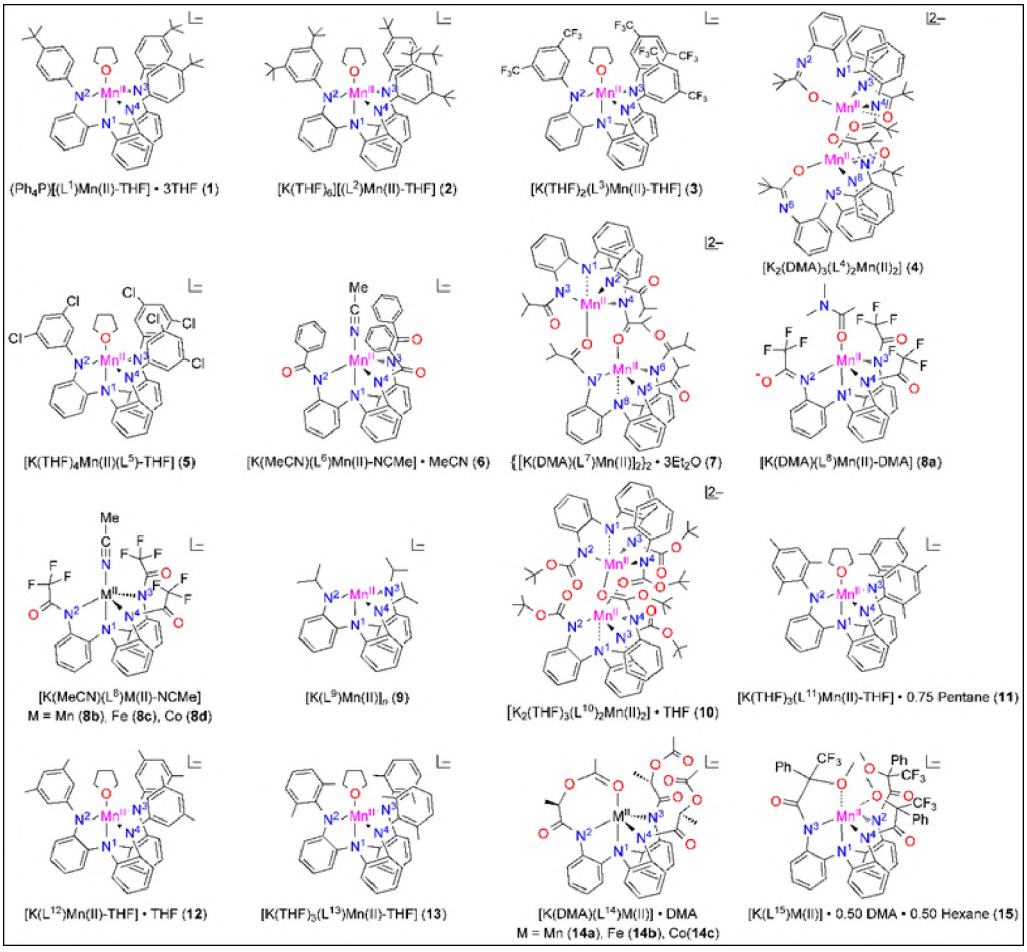

Figure 2. Minimal Coordination of Mn^{II} and Other Metal Complexes with Ligands

The five-coordinate Mn^{II} site adopts a distorted trigonal bipyramidal geometry, defined by the presence of three equatorial N_{amido} residues, and two axial moieties (N_{amine}, O (THF)). The level of distortion varies significantly, as evidenced by the evaluation of the trigonality index τ (0.97 (L^1), 0.96 (L^2), 0.50 (L^3), 0.47 (L^5), 0.96 (L^{11}), 0.45 (L^{12}), 0.99 (L^{13})).[50] Indeed, for those structures with $\tau \leq 0.50$, a square pyramidal geometrical description might be more appropriate.

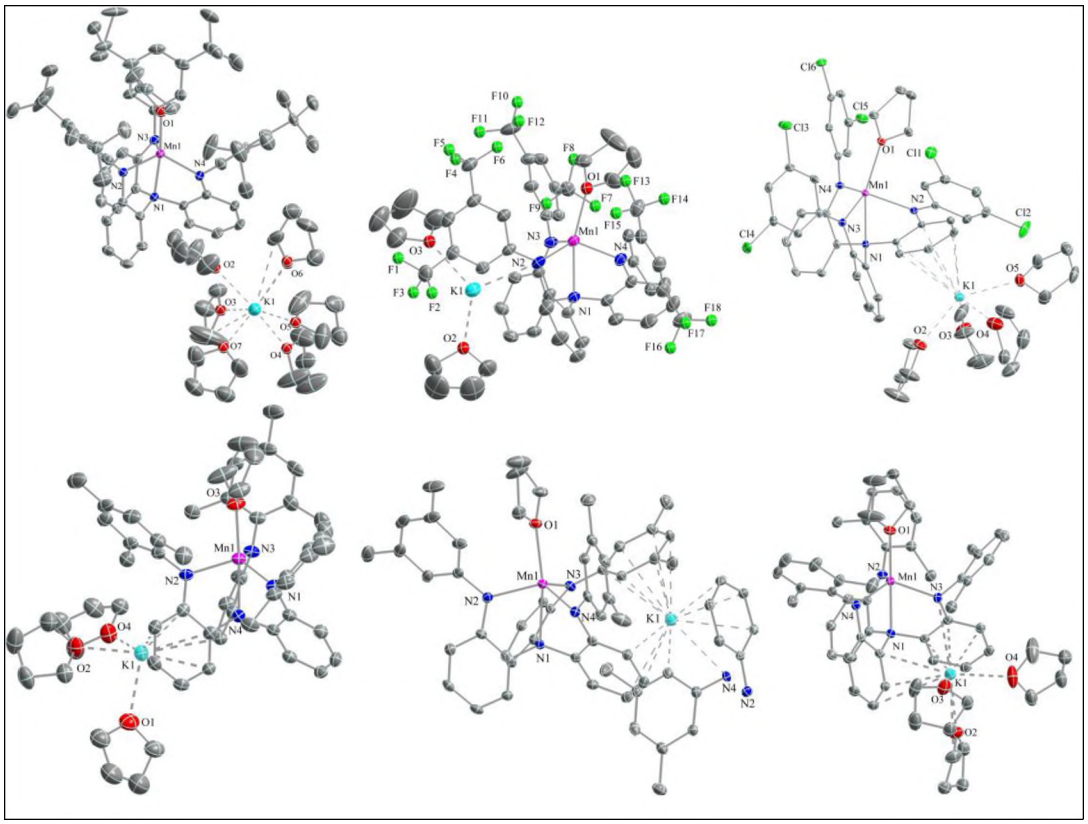

Figure 3. ORTEP Diagrams of Mn^{II} Compounds 2, 3, 5, 11, 12, and13, Bearing Aryl Arms. Drawn with 40% thermal ellipsoids. Selective interatomic distances [Å] and angles [°]

With the exception of the previously disclosed structure of the L^1-containing Mn^{II} compound that features a PPh_4^+ cation, all other structures possess a K^+ ion that further

impacts metrical variances. Compound $[K(THF)_6][(L^2)Mn^{II}–THF]$ (**2**) is the only case in which K^+ is solely coordinated by THF molecules. In all other cases, the potassium ion generates additional K^+–arene contacts[51] with one or more aromatic rings of the triphenylamine core, and even with an aryl arm (L^{12}). In all cases, the most prominent effect of K^+ contacts with ligand-centered arene and occasionally N_{amido} residues is the elongation of the Mn–N bonds associated with these moieties. Otherwise, the range of Mn–N_{amide} bond distances (2.103 (L^5) – 2.138 (L^{11}) Å), Mn–N_{amine} (2.296 (L^2) – 2.357 (L^{11}) Å), and Mn–O_{THF} (2.198 (L^3) - 2.272 (L^{11}) Å) is fairly narrow and consistent with metrical parameters for Mn^{II} sites.

2: Mn(1)–N(1) = 2.2959(19), Mn(1)–N(2) = 2.105(2), Mn(1)–N(3) = 2.113(2), Mn(1)–N(4) = 2.105(2), Mn(1)–O(1) = 2.2175(18), N(1)–Mn(1)–N(2) = 76.35(7), N(1)–Mn(1)–N(3) = 76.81(8), N(1)–Mn(1)–N(4) = 77.18(7), N(2)–Mn(1)–N(3) = 114.53(8), N(2)–Mn(1)–N(4) = 116.19(8), N(3)–Mn(1)–N(4) = 114.07(8); **3:** Mn(1)–N(1) = 2.350(3), Mn(1)–N(2) = 2.102(4), Mn(1)–N(3) = 2.126(3), Mn(1)–N(4) = 2.120(3), Mn(1)–O(1) = 2.198(3), N(1)–Mn(1)–N(2) = 76.64(12), N(1)–Mn(1)–N(3) = 75.01(11), N(1)–Mn(1)–N(4) = 74.19(12), N(2)–Mn(1)–N(3) = 105.05(14), N(2)–Mn(1)–N(4) = 106.81(14), N(3)–Mn(1)–N(4) = 128.36(13); **5:** Mn(1)–N(1) = 2.3385(16), Mn(1)–N(2) = 2.1284(17), Mn(1)–N(3) = 2.0839(17), Mn(1)–N(4) = 2.0972(17), Mn(1)–O(1) = 2.2266(14), N(1)–Mn(1)–N(2) = 73.46(6), N(1)–Mn(1)–N(3) = 77.60(6), N(1)–Mn(1)–N(4) = 75.77(6), N(2)–Mn(1)–N(3) = 101.40(6), N(2)–Mn(1)–N(4) = 123.70(7), N(3)–Mn(1)–N(4) = 116.40(7); **11:** Mn(1)–N(1) = 2.359(3), Mn(1)–N(2) = 2.139(3), Mn(1)–N(3) = 2.144(3), Mn(1)–N(4) = 2.125(3), Mn(1)–O(3) = 2.272(3), N(1)–Mn(1)–N(2) = 77.07(10), N(1)–Mn(1)–N(3) = 75.80(10), N(1)–Mn(1)–N(4) = 77.28(11), N(2)–Mn(1)–

N(3) = 112.59(12), N(2)–Mn(1)–N(4) = 112.60(12), N(3)–Mn(1)–N(4) = 119.40(11); **12:** Mn(1)–N(1) = 2.345(2), Mn(1)–N(2) = 2.098(2), Mn(1)–N(3) = 2.122(2), Mn(1)–N(4) = 2.114(2), Mn(1)–O(1) = 2.273(3), N(1)–Mn(1)–N(2) = 75.81(9), N(1)–Mn(1)–N(3) = 73.50(8), N(1)–Mn(1)–N(4) = 75.90(9), N(2)–Mn(1)–N(3) = 122.55(9), N(2)–Mn(1)–N(4) = 111.20(9), N(3)–Mn(1)–N(4) = 106.72(9); **13:** Mn(1)–N(1) = 2.3356(14), Mn(1)–N(2) = 2.1102(14), Mn(1)–N(3) = 2.1367(14), Mn(1)–N(4) = 2.1024(14), Mn(1)–O(1) = 2.2481(13), N(1)–Mn(1)–N(2) = 75.81(5), N(1)–Mn(1)–N(3) = 76.22(5), N(1)–Mn(1)–N(4) = 76.54(5), N(2)–Mn(1)–N(3) = 112.44(6), N(2)–Mn(1)–N(4) = 119.65(6), N(3)–Mn(1)–N(4) = 111.30(6).

(b) Acyl-Armed Mn^{II} Compounds. Seven Mn^{II} compounds with ligands providing acyl-fortified cavities (L^4, L^6, L^7, L^8, L^{10}, L^{14}, L^{15}) have been isolated and crystallographically characterized (Figure 4), with the exception of the L^{14}-supported compound that has not provided X-ray quality crystals. The structures of $[(L^4)_2Mn^{II}_2K_2(DMA)_3]$ (**4**), $[(L^7)_2Mn^{II}_2K_2(DMA)_2]_n$ (**7**), and $[(L^{10})_2Mn^{II}_2K_2(THF)_3]$ (**10**) possess a similar dimeric unit either as a molecular entity (**4**, **10**) or as part of a polymeric assembly (**7**), featuring a building block consisted of a symmetry-related dimer of dimers (–Mn(1)-Mn(2)---Mn(2)-Mn(1)–). The L^4 and L^{10} containing structures are very similar, although the former features a slightly asymmetric dinuclear unit, whereas the latter is symmetric with respect to an axis passing through the two nonequivalent potassium ions. Furthermore, although the two molecules exhibit essentially four-coordinate Mn^{II} sites, they differ in the residue composition (N_2O_2 (L^4), N_3O (L^{10})). For both structures, the bridging between the two metal sites is further strengthened by the two K^+ ions, which, in addition to solvent coordination, generate contacts with corresponding O/N residues of

both ligands. Finally, the structure of $[(L^7)_2Mn^{II}_2K_2(DMA)_2]_n$ (**7**) reveals a Mn^{II} coordination sphere (N_3O) that is very similar to that observed for the L^{10}-containing molecule, and an asymmetric dimeric unit similar to that demonstrated by the L^4-containing molecule.

The acyl-armed $[K(MeCN)(L^6)Mn^{II}–NCMe]_n$ (**6**) and $[K(DMA)(L^8)Mn^{II}–DMA]_n$ (**8a**), as well as the related $[K(MeCN)(L^8)Mn^{II}–NCMe]_n$ (**8b**) and $[K(THF)(L^8)Mn^{II}–NCMe]_n$ versions (see below), are all very similar polymeric structures that feature distorted trigonal-bipyramidal Mn^{II} sites coordinated by the typical $[(N_{amido})_3N_{amine}]$ ligand-derived moieties and an axial residue due to the corresponding solvent. As anticipated, the ligand field of the L^8-derived compounds is the weakest among all compounds surveyed in this study ($Mn–N_{amido}$ (av. 2.163 – 2.184 Å), $Mn–N_{amine}$ (2.440 – 2.475 Å)). The polymeric nature of the L^6 and L^8 containing compounds arises from the almost identical function of the K^+ solvated ion, which generates contacts with all O atoms (O(1), O(2), O(3)) of the three CF_3CO arms, albeit each belonging to a different molecule.

As noted above, the $[L^{14}Mn^{II}]^-$ compound (**14a**) has not been amenable to crystallographic crystallization, but clues to its structure may be glimpsed by the isostructural congeners $\{[K(DMA)(L^{14})^{II})]•DMA\}_n$ (M = Fe (**14b**), Co(**14c**)) (Figures S3 and S4), which exhibit a seven-membered atom metallacycle loop that positions an ester C=O moiety of the side arm in the coordination sphere of the metal in lieu of solvent (M–O = 2.153 (Fe), 2.163 (Co) Å).

Finally, compound $[K(DMA)_{0.5}(L^{15})Mn^{II}]_n$ (**15**) exhibits a polymeric structure, owing to an identical network of K^+ contacts as noted in the case of L^6- and L^8-containing

molecules, although the solvent molecule (DMA) associated with K^+ exhibits half-occupancy as a result of the racemic nature of this compound.

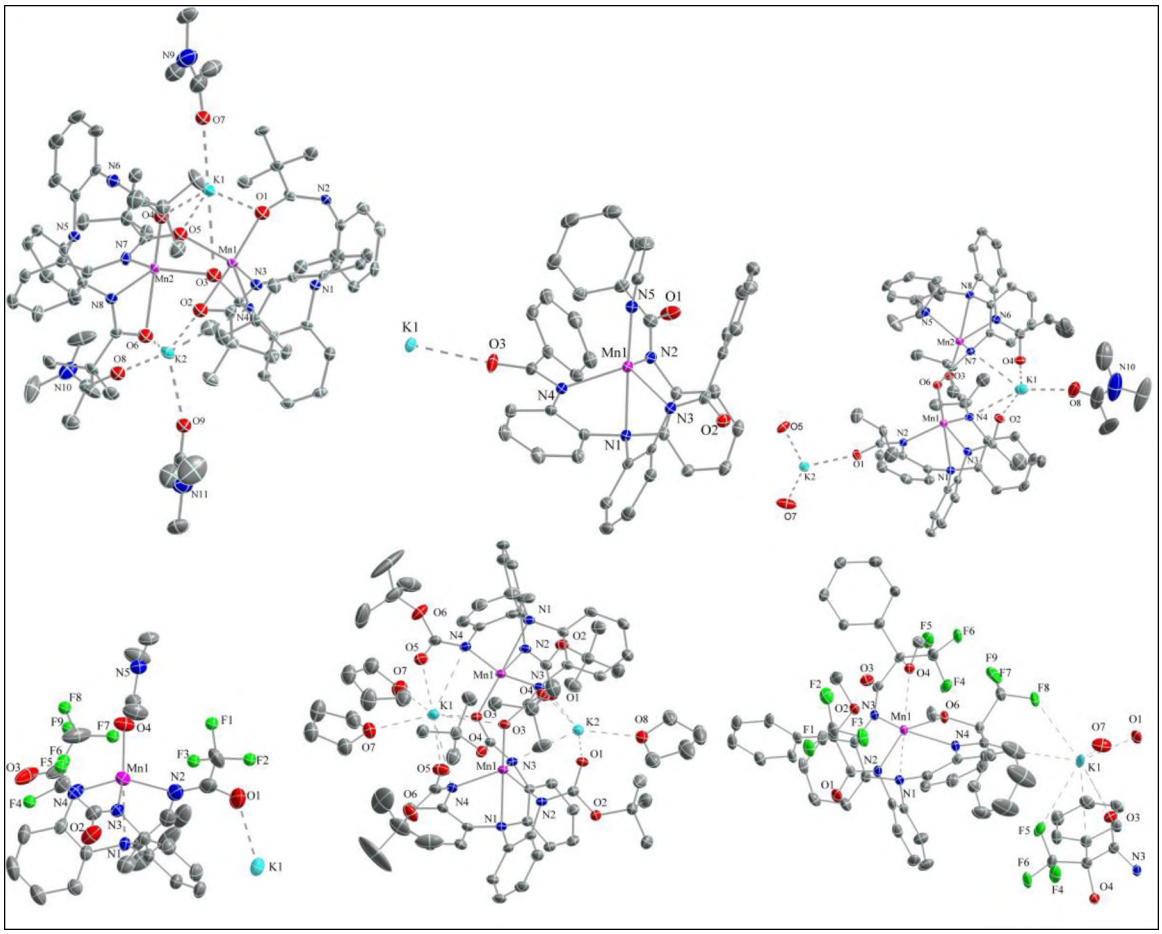

Figure 4. ORTEP Diagrams of Mn^{II} Compounds 4, 6, 7, 8a, 10, and 15, Bearing Acyl Arms. Drawn with 40% thermal ellipsoids. Selective interatomic distances [Å] and angles [°]

The Mn^{II} coordination sphere features a regular [N_3N] ligand field, further stabilized by two novel Mn–O long contacts (av. 2.407 Å) provided by MeO residues, at the expense of any solvent coordination.

4: Mn(1)–N(3) = 2.148(5), Mn(1)–N(4) = 2.163(5), Mn(1)–O(1) = 2.083(4), Mn(1)–O(2) = 2.395(5), Mn(1)–O(5) = 2.094(4), N(3)–Mn(1)–N(4) = 100.99(19); **6:**

Mn(1)–N(1) = 2.386(2), Mn(1)–N(2) = 2.141(2), Mn(1)–N(3) = 2.1541(19), Mn(1)–N(4) = 2.155(2), Mn(1)–N(5) = 2.171(2), N(1)–Mn(1)–N(2) = 73.08(7), N(1)–Mn(1)–N(3) = 73.22(7), N(1)–Mn(1)–N(4) = 72.89(7), N(2)–Mn(1)–N(3) = 110.74(8), N(2)–Mn(1)–N(4) = 112.15(7), N(3)–Mn(1)–N(4) = 112.75(7); **7:** Mn(1)–N(1) = 2.543(2), Mn(1)–N(2) = 2.152(2), Mn(1)–N(3) = 2.140(3), Mn(1)–N(4) = 2.189(3), Mn(1)–O(6) = 2.039(2), N(1)–Mn(1)–N(2) = 70.22(9), N(1)–Mn(1)–N(3) = 69.61(9), N(1)–Mn(1)–N(4) = 70.51(8), N(2)–Mn(1)–N(3) = 108.36(10), N(2)–Mn(1)–N(4) = 113.57(10), N(3)–Mn(1)–N(4) = 105.15(10); **8a:** Mn(1)–N(1) = 2.475(3), Mn(1)–N(2) = 2.224(4), Mn(1)–N(3) = 2.171(3), Mn(1)–N(4) = 2.158(3), Mn(1)–O(2) = 2.042(3), Mn(1)–O(4) = 2.044(3), N(1)–Mn(1)–N(2) = 69.48(13), N(1)–Mn(1)–N(3) = 70.47(11), N(1)–Mn(1)–N(4) = 70.81(11), N(2)–Mn(1)–N(3) = 109.75(13), N(2)–Mn(1)–N(4) = 112.36(14), N(3)–Mn(1)–N(4) = 105.35(13); **10:** Mn(1)–N(1) = 2.540(2), Mn(1)–N(2) = 2.101(2), Mn(1)–N(3) = 2.158(2), Mn(1)–N(4) = 2.137(2), Mn(1)–O(3) = 2.0902(19), N(1)–Mn(1)–N(2) = 69.76(8), N(1)–Mn(1)–N(3) = 70.71(8), N(1)–Mn(1)–N(4) = 71.39(8), N(2)–Mn(1)–N(3) = 107.22(9), N(2)–Mn(1)–N(4) = 119.45(9), N(3)–Mn(1)–N(4) = 101.39(9); **15:** Mn(1)–N(1) = 2.429(4), Mn(1)–N(2) = 2.179(4), Mn(1)–N(3) = 2.158(4), Mn(1)–N(4) = 2.178(4), Mn(1)–O(4) = 2.446(4), Mn(1)–O(6) = 2.366(4), N(1)–Mn(1)–N(2) = 71.84(15), N(1)–Mn(1)–N(3) = 72.10(15), N(1)–Mn(1)–N(4) = 71.16(15), N(2)–Mn(1)–N(3) = 110.34(16), N(2)–Mn(1)–N(4) = 111.05(16), N(3)–Mn(1)–N(4) = 110.45(16).

(c) Alkyl-armed Mn^{II} Compound. The structure of the isopropyl-armed $[K(L^{9})Mn^{II}]_n$ (**9**) (Figure 5) is a simpler version of that reported for the ferrous congener ($[K_2(L^{9})_2Fe^{II}_2]_n$).[44a] The local Mn^{II} site exhibits a distorted trigonal-pyramidal [N_3N]

coordination, featuring short Mn–N_{amido} (av. 2.072 Å) and Mn–N_{amine} (2.212 Å) bond distances. The polymeric structure arises from a repeating –[Mn(1)–K(1)]– unit, characterized by K^+–(η^6-arene) contacts (phenylene rings between N(1)/N(4) and N(1)/N(2)) and long-range K^+ interactions with N_{amido} residues (N(3), N(4)), involving adjacent ligands.

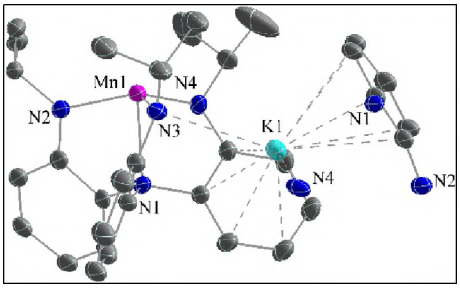

Figure 5. ORTEP Diagram of Mn^{II} Compound 9, Bearing Alkyl Arms. Drawn with 40% thermal ellipsoids. Selective interatomic distances [Å] and angles [°]

9: Mn(1)–N(1) = 2.212(4), Mn(1)–N(2) = 2.036(5), Mn(1)–N(3) = 2.085(6), Mn(1)–N(4) = 2.094(5), N(1)–Mn(1)–N(2) = 81.07(18), N(1)–Mn(1)–N(3) = 79.6(2), N(1)–Mn(1)–N(4) = 78.68(16), N(2)–Mn(1)–N(3) = 121.47(19), N(2)–Mn(1)–N(4) = 111.0(2), N(3)–Mn(1)–N(4) = 118.19(19).

(d) Other [(L^8)M^{II}]-containing Structures (M = Mn, Fe, Co, Ni). The structures for the catalytically important [K(MeCN)(L^8)Mn^{II}–NCMe]$_n$ (Figure 6; M = Mn (**8b**), Fe (**8c**; previously reported,[45a] not shown), Co (**8d**)) are all similarly polymeric, featuring a distorted trigonal-bipyramidal geometry around the metal site, assembled by the typical [N_3N] coordination of the ligand and an acetonitrile moiety located trans with respect to the N_{amine} atom. All three side-arm carbonyl units are oriented *exo* with respect to the metal cavity, and each provides essential coordination to a unique potassium ion, further supported by two more carbonyl moieties belonging to different molecules. Moreover,

the K^+ ion is coordinated by an acetonitrile molecule and forms a long contact with an adjacent F atom (K–F = 3.189 (Mn), 3.253 (Fe), 3.315 (Co) Å). Metrical parameters are consistent with decreasing ionic radii from Mn to Co, whereas the corresponding bond angles associated with the $[N_3N]$–M coordination increase as a result of bond distance decreases from Mn to Co.

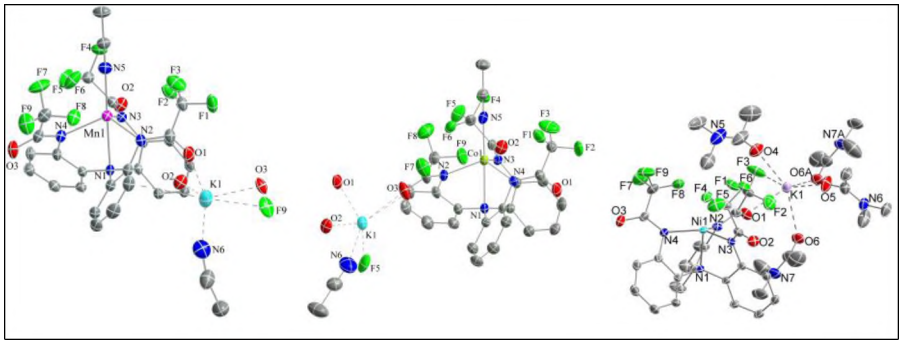

Figure 6. ORTEP Diagrams of Divalent Compounds 8b (Mn), 8d (Co) and 8e (Ni). Possessing the L^8 Ligand (drawn with 40% thermal ellipsoids). Selective interatomic distances [Å] and angles [°]:

The structure of the Ni^{II} compound $[K(DMA)_3(L^8)Ni^{II}]_2$ (**8e**; Figure 6), obtained from crystals formed in DMA solutions, reveals a molecular dimer related by inversion symmetry. The coordination of Ni^{II} displays a distorted trigonal pyramidal $[N_3N]$ geometry ($Ni–N_{amido}$ = av. 1.980 Å; $Ni–N_{amine}$ (2.038 Å)) and is devoid of any solvent coordination, although a potential Ni–F (2.564 Å) long contact may be present. The dimer is bridged by a $K_2(O_{DMA})_2$ parallelogram that features additional K–O contacts of each K^+ ion with two terminal DMA molecules and, most importantly, a carbonyl residue of a specific CF_3CO moiety.

8b: Mn(1)–N(1) = 2.440(4), Mn(1)–N(2) = 2.161(3), Mn(1)–N(3) = 2.165(3), Mn(1)–N(4) = 2.174(3), Mn(1)–N(5) = 2.176(4), N(1)–Mn(1)–N(2) = 71.32(11), N(1)–

Mn(1)–N(3) = 70.50(11), N(1)–Mn(1)–N(4) = 71.42(11), N(2)–Mn(1)–N(3) = 109.13(12), N(2)–Mn(1)–N(4) = 113.60(12), N(3)–Mn(1)–N(4) = 107.29(11); **8d:** Co(1)–N(1) = 2.345(4), Co(1)–N(2) = 2.060(3), Co(1)–N(3) = 2.076(3), Co(1)–N(4) = 2.069(3), Co(1)–N(5) = 2.055(5), N(1)–Co(1)–N(2) = 73.53(13), N(1)–Co(1)–N(3) = 73.98(13), N(1)–Co(1)–N(4) = 73.18(13), N(2)–Co(1)–N(3) = 115.40(14), N(2)–Co(1)–N(4) = 111.52(14), N(3)–Co(1)–N(4) = 110.05(13). **8e:** Ni(1)–N(1) = 2.038(3), Ni(1)–N(2) = 1.987(3), Ni(1)–N(3) = 1.972(2), Ni(1)–N(4) = 1.982(3), N(1)–Ni(1)–N(2) = 82.90(8), N(1)–Ni(1)–N(3) = 84.77(8), N(1)–Ni(1)–N(4) = 83.31(9), N(2)–Ni(1)–N(3) = 109.91(11), N(2)–Ni(1)–N(4) = 114.63(10), N(3)–Ni(1)–N(4) = 131.79(9).

2.3. CYCLIC VOLTAMMETRY

Electrochemical data for representative Mn^{II} compounds are listed in Table S9, and selective waves tentatively assigned to the Mn^{II}/Mn^{III} couple are shown in Figure 7. The aryl-armed compound $[K(THF)_3(L^{13})Mn^{II}–THF]$ (**13**), which bears the electron-donating aryl substituent 2,6-$(CH_3)_2$, is oxidized at the most negative potential (-1.255 V vs. Fc^+/Fc in DMA), and is only among a handful of Mn^{II} compounds noted in Table S9 that show semi-reversible waves. Compound $[K(THF)_6][(L^2)Mn^{II}–THF]$ (**2**), which also possesses aryl arms, substituted by electron-donating 3,5-^{t}Bu$_2$ moieties, is the next more easily oxidized Mn^{II} reagent, albeit in an irreversible manner. As anticipated, the presence of the electron-withdrawing aryl substituents 3,5-$(CF_3)_2$ and 3,5-Cl_2 in $[K(THF)_2(L^3)Mn^{II}–THF]$ (**3**) and $[K(THF)_4(L^5)Mn^{II}–THF]$ (**5**) respectively, shifts the oxidation potential to more positive values by approximately 300 mV (in THF) versus that observed for **2**. The unique alkyl-substituted $[K(L^9)Mn^{II}]_n$ (**9**) shows one redox wave at 0.245 V, which is higher than expected for a Mn^{II}/Mn^{III} couple. The acyl-substituted

compounds examined (**4**, **6-8**, **10**, **14**, **15**) are all anodically shifted versus the aryl-substituted congeners, as expected for the electron-withdrawing character of the acyl moiety. Specifically for [K(MeCN)(L^8)Mn^{II}–NCMe] (**8b**), which carries the trifluoromethylacyl arm, an additional anodic shift is observed by approximately 500 mV versus that of the other acyl-armed compounds (**4**, **6**, **7**). Compound {[K(DMA)(L^7)Mn^{II}]$_2$}$_2$•3Et_2O (**7**), as well as [K(DMA)(L^{14})Mn^{II}]•DMA (**14a**) and [(L^{15})Mn^{II}]•0.5DMA•0.5hexane (**15**), demonstrate two oxidation waves (Figure S5), which in the case of **7** may reflect the two distinct Mn^{II} ions observed in the solid-state structure. These results are consistent with the electronic character of the ligands and prior electrochemical data obtained for analogous Fe^{II} and Co^{II} complexes,[45a,47] with anodic shifts observed in the order Fe < Mn < Co. Indeed, for the catalytically important series of [K(MeNC)(L^8)M^{II}–NCMe] (M = Mn (**8b**), Fe (**8c**), Co (**8d**)) complexes (see below), their cyclic voltammograms in MeCN/(^{n}Bu$_4$)NPF_6 provide $E_{p,a}$ values at 0.228 (Fe), 0.518 (Mn), and 0.837 (Co) V, presumably due to the M^{II}/M^{III} couple (Figure 8). CV of compounds, [K(MeCN)(L^8)Fe^{II}–NCMe] (**8c**)[44a], [K(MeCN)(L^8)Mn^{II}–NCMe] (**8b**) and [K(MeCN)(L^8)Co^{II}–NCMe] (**8d**) in MeCN/(^{n}Bu$_4$N)PF_6, as indicated, with a Au disk electrode (1.6 mm in diameter); scan rate 0.1 V/s is shown in Figure 8. The metal complexes with more electron-withdrawing substituents are found towards the anodic side as it stabilizes the metal in its lower oxidation state, while the metals with the more electron-releasing substitutents are present towards the cathodic side. L^{13}Mn, was found out to have the most negative reduction potential, on the other hand L^8Mn was found to be the most stable of all, as the electron-withdrawing subsitituent (CF_3) stablizes it.

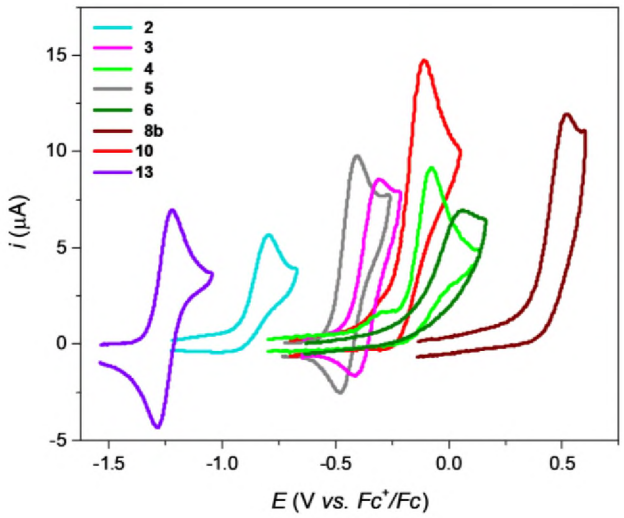

Figure 7. Cyclic voltammograms (first oxidation wave) of selected Mn^{II} compounds:

$[K(NCMe)][(L^{6})Mn^{II}–NCMe]•MeCN$ (6) and $[K(MeCN)(L^{8})Mn^{II}–NCMe]$ (8b) in $MeCN/(^{n}Bu_4N)PF_6$, $[K(THF)_6][(L^{2})Mn^{II}\text{-}THF]$ (2), $[K(THF)_2(L^{3})Mn^{II}\text{-}THF]$ (3), $[K(THF)_4(L^{5})Mn^{II}–THF]$ (5) and $[K_2(THF)_3(L^{10})_2Mn^{II}_2]•2THF$ (10) in $DMF/(^{n}Bu_4N)PF_6$, and $[K_2(DMA)_3(L^{4})_2Mn^{II}_2]$ (4) and $[K(THF)_3(L^{13})Mn^{II}–THF]$ (13) in $DMA/(^{n}Bu_4N)PF_6$, as indicated, with a Au disk electrode (1.6 mm in diameter); scan rate 0.1 V/s.

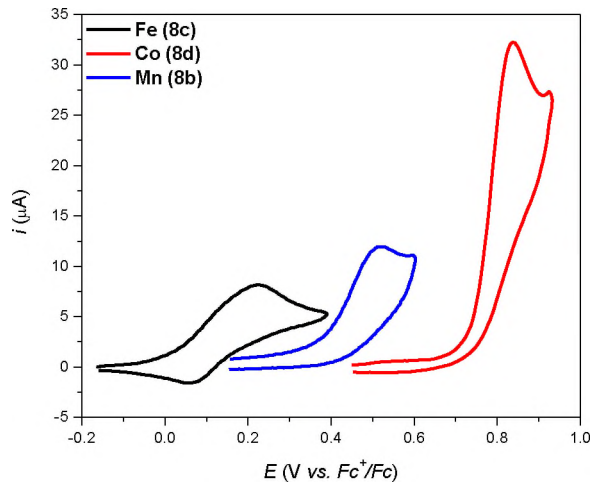

Figure 8. Cyclic Voltammograms (M^{II}/M^{III} Redox Couple)

2.4. CATALYTIC STUDIES

Table 1 reveals a wide range of yields (11 – 75%) for the aziridination of styrene as a function of the ligand system employed for the corresponding Mn^{II} compounds. The aryl-armed ligands exhibit a particularly low yield for the electron-rich members of the group (L^1, L^2, L^{11}–L^{13}). Better, but still modest yields, are achieved with the electron-deficient congeners (L^3, L^5). The alkyl-armed ligand (L^9), is similarly a poor supporter of styrene aziridination. As detailed previously for metal complexes (M = Cr, Mn, Fe) with ligands L^1 and L^2,[44b,49,52] the electron-rich aryl-substituted ligands are particularly vulnerable to one-electron oxidation, leading to a specific ligand rearrangement, which may in turn be responsible for poor catalytic performance. The seven acyl-armed ligands examined (L^4, L^6–L^8, L^{10}, L^{14}, L^{15}) are instead redox robust, and support aziridination of styrene with widely variable yields. The lower and higher limits of the yield range are provided by the structurally related –$COCMe_3$ (L^4, 12%) and –$COCF_3$ (L^8, 75%) moieties, respectively. Indeed, the L^8Mn compound 8b is the highest yielding and most electron-deficient metal site of the entire series of reagents examined in this work, followed by the L^{14}Mn compound 14a. The latter possesses chirality, and will be addressed in a separate study exploring enantioselective aziridinations. In general, the yield levels ascend with increasing electrophilicity of the metal site in accordance with the electrochemical data noted above. However, the exceptionally low-yielding L^4Mn and L^7Mn reagents may be further limited due to the *t*-Bu/*i*-Pr group's encumbrance of the metal site and/or susceptibility to H-atom abstraction by the putative, electrophilic metal-nitrene moiety.

Table 1. Yields of Styrene Aziridination Mediated by Mn^{II} Reagents **1-15**

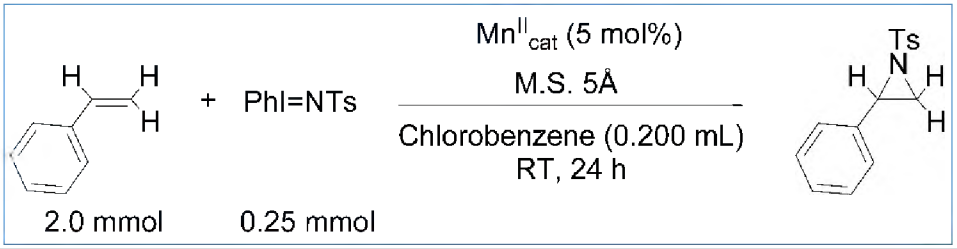

Compound	**Yield (%)**
$[K(THF)_x][(L^1)Mn^{II}–THF]$ (**1a**)[49]	11
$[K(THF)_6][(L^2)Mn^{II}–THF]$ (**2**)	23
$[K(THF)_2(L^3)Mn^{II}–THF]$ (**3**)	43
$[K_2(DMA)_3(L^4)_2Mn^{II}_2]$ (**4**)	12
$[K(THF)_4(L^5)Mn^{II}–THF]$ (**5**)	31
$[K(NCMe)][(L^6)Mn^{II}–NCMe]$•MeCN (**6**)	57
$\{[K(DMA)(L^7)Mn^{II}]_2\}_2$•3$Et_2O$ (**7**)	26
$[K(NCMe)(L^8)Mn^{II}–NCMe]$ (**8b**)	**75**
$[K(L^9)Mn^{II}]_n$ (**9**)	25
$[K_2(THF)_3(L^{10})_2Mn^{II}_2]$•2THF (**10**)	50
$[K(THF)_3(L^{11})Mn^{II}–THF]$•0.75 Pentane (**11**)	18
$[K(L^{12})Mn^{II}–THF]$•THF (**12**)	17
$[K(THF)_3][(L^{13})Mn^{II}–THF]$ (**13**)	25
$[K(DMA)(L^{14})Mn^{II}]$•DMA (**14a**)	67
$[K(L^{15})Mn^{II}]$•0.5DMA•0.5hexane (**15**)	39

(b) Aziridination of a Series of Olefins Mediated by $[L^8Mn^{II}$-NCMe][K(NCMe)]. The most productive L^8Mn reagent **8b** was further selected to explore the catalytic aziridination of a wide range of alkenes under the conditions noted for styrene aziridination. A subset of catalytic reactions (entries 1-11) was also conducted in methylene chloride. Table 2 summarizes pertinent product profiles. A panel of styrenes with electron-donating or electron-withdrawing *para*-substituents (entries 1- 9) undergoes

facile aziridination with yields ranging from 56% (p-NO_2) to 81% (p-^{t}Bu) in chlorobenzene. For indeterminate reasons, more modest and narrowly distributed yields (42-55%) are obtained in dichloromethane, with the exception of p-NO_2-styrene, which affords low amounts of product (25%). *Ortho*-positioned methyl substituents introduce significant steric and electronic effects, as evidenced in the low yields obtained for the aziridination of 2,4,6-trimethylstyrene (entry 10). The β-carbon of this substrate is off the plane of the aromatic ring and the α-carbon, thus causing disruption of electron delocalization between the aromatic and the olefinic carbons.[53] On the other hand, the electron-rich α-substituted methylstyrene provides the corresponding aziridine in respectable yields (entry 11), along with minor amounts of the allylic amination product, most likely derived via ring opening of the sensitive aziridine.[54] In accordance with previous observations,[15g,55] the ring-opened product is significantly more pronounced in the aziridination profile of the α-Ph substituted styrene (in this case, an olefinic amine; entry 12), although the combined yield of aziridine and olefinic amine (38%) is significantly lower than that observed with α-methylstyrene (62%), probably due to the steric encumbrance of the α-Ph group. Subsequent aziridinations were performed only in chlorobenzene, since yields were invariably lower in dichloromethane. Styrenes with β-substitution (Me, Ph) show dramatic drop in overall yields (entries 13-16), accompanied by stereochemical scrambling that is naturally more pronounced for the *cis* isomers, along with low yields of allylic amination products (entries 13, 14). Notably, allylic or benzylic aminations are also favorably competing with aziridinations of *trans*- or *cis*-disubstituted aromatic olefins, albeit at low yields (entries 17, 18). Overall, the L^8Mn

reagent **8b** favors aziridination of unhindered terminal styrenes and exhibits sharp decline in reactivity with disubstituted reagents, especially when the β position is involved.

In sharp contrast to the sterically unhindered styrenes, all aliphatic olefins examined provide products of aziridination in very low yields, with the exception of Co^{II} mediated reactions. For instance, a series of cycloalkenes (entries 19 - 21) furnishes the corresponding aziridines in essentially trace amounts (cyclopentene, cyclohexene) for Mn^{II} or Fe^{II} catalyzed reactions, in favor of low yields for the competing product of allylic amination, whereas low yields of aziridine are obtained as the sole product only for the more electron rich cyclooctene. Similarly, the *exo*-ene methylenecyclohexane affords a mixture of aziridination and allylic amination products in low yields (entry 22). Other terminal and internal aliphatic alkenes consistently provide very low yields of aziridination products (Table S10).

(c) Comparative Aziridination of Olefins with other L^8 Supported Fe, Co and Ni Compounds. The L^8-containing Fe^{II} and Co^{II} congeners have been further evaluated as catalysts for the aziridination of the olefin series noted in Table 2, under the same conditions detailed for Mn^{II} catalysis for comparative purposes. Moreover, a narrow selection of styrenes has been tested in aziridinations mediated by the corresponding Ni^{II} reagent, albeit with low yields (styrene: 19%, 4-methylstyrene: 16%, 4-fluorostyrene: 20%). The readily available $[L^8M^{II}\text{-NCMe}][K(NCMe)]$ (M = Fe (8c), Co (8d)) and $[K(DMA)_3(L^8)Ni^{II}]_2$ (8e) compounds have been employed for the comparative aziridinations of the olefinic substrates. Not unlike Mn^{II} catalysis, the aziridination of the electron-diverse styrenes (entries 1-9) affords products with a wide range of yields (Fe: 38-80%; Co: 46-83%).

Table 2. Yields of Aziridination/Amination (PhINTs) of Olefins by [L^8M^{II}–NCMe][K(NCMe)][a]

Entry No.	Substrate	Products		Yield (%) CH_2Cl_2/PhCl L^8Mn	Yield (%) PhCl L^8Fe	Yield (%) PhCl L^8Co
1.	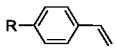	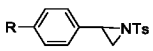	R = H	44/ 75	73	69
2.			R = Me	42/ 71	58	77
3.			R = ^{t}Bu	46/ 81	69	83
4.			R = OMe	55/ 72	80	11
5.			R = O^{t}Bu	44/ 85	78	76
6.			R = F	50/ 71	79	82
7.			R = Cl	48/ 79	67	79
8.			R = CF_3	46/ 67	57	65
9.			R = NO_2	25/ 56	38	46
10.	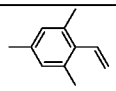	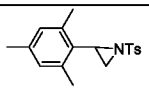		18/ 25	9	54
11.	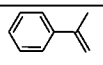	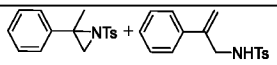		22, 8/ 59, 3	49, 8	33, 7
12.	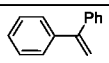	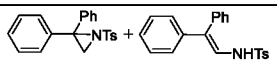		19, 19	7, 11	8, 16
13.	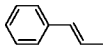	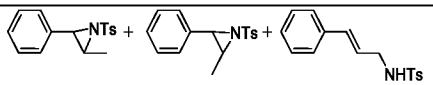		10, 2, 5	12, 2, 1	72, trace, 4
14.		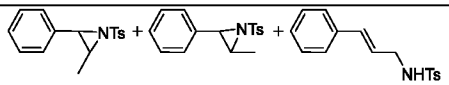		8, 7, 5	8, 12, trace	38, 30, trace
15.		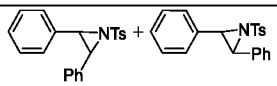		2, 7	3, 8	10, 28
16.	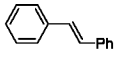	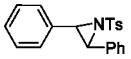		6	11	23
17.	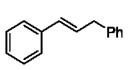	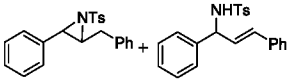		6, 28	5, 12	32, 26
18.		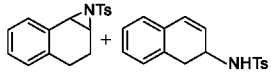		10, 10	10, 10	36, nd
19.		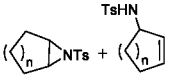	n = 1	1, 13	3, 7	16, 23
20.			n = 2	1, 17	5, 11	17, 16
21.			n = 4	14, nd	24, nd	59, nd
22.		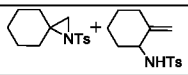		13, 10	22, 15	33, 19

[a]Olefin, 2.0 mmol; PhINTs, 0.25 mmol; M^{II}_{cat}, 0.0125 mmol (5 mol%); M.S. 5Å, 20 mg; Solvent (chlorobenzene or dichloromethane), 0.200 mL; RT, 24 h.

An exceptionally low yield (11%), not included in the given range, is observed for the aziridination of *p*-MeO-styrene by Co^{II}. However, this product is known to be

susceptible to transformation,[15p,16f,55] apparently accelerated under Co^{II} catalysis.With a few exceptions, the Mn^{II}-mediated aziridinations of *para*-substituted styrenes tend to be more productive than those catalyzed by Fe^{II}, and fairly competitive to those facilitated by Co^{II} reagents.

The bulky 2,4,6-trimethylstyrene (entry 10) is even more sluggish in aziridinations mediated by the Fe^{II} vs. the Mn^{II} reagent, but significantly more productive with the Co^{II} congener (54% yield). The α-substituted styrenes (entries 11, 12), especially the more reactive α-Me styrene, are better handled by the Mn^{II} reagent, presumably due to a more spacious reaction cavity. In sharp contrast, β-substituted styrenes are significantly more reactive towards aziridination under Co^{II} catalysis, with less extensive stereochemical scrambling and higher propensity for aziridination vs. allylic/benzylic amination (entries 13 - 18).The superior reactivity (but not selectivity; see below) of Co^{II} vs. Mn^{II} or Fe^{II} is also evident in entries 19 - 22 (Table 2) and 1-6 (Table S10) with aliphatic olefins, albeit with low to modest yields.

(d) Comparative Reaction Profile and Selectivity for Different Olefins. Aziridination of styrene mediated by [K(NCMe)(L^8)M^{II}–NCMe] (M = Mn, Fe, Co) under the general heterogeneous conditions noted above, albeit in 0.50 mL of d_5-chlorobenzene at 30 °C, highlight differences in the rate of aziridine formation by the three metals, as monitored by ^{1}H-NMR with the assistance of an internal standard (Figure 9). Whereas the yield for all three metals is approximately 60% under the dilute conditions of the experiment, this maximum value is essentially reached in 6.0 hours in the Co^{II}-catalyzed reaction, at which time the kinetically more comparable Fe- and Mn-catalyzed aziridinations have only achieved 28% yield.

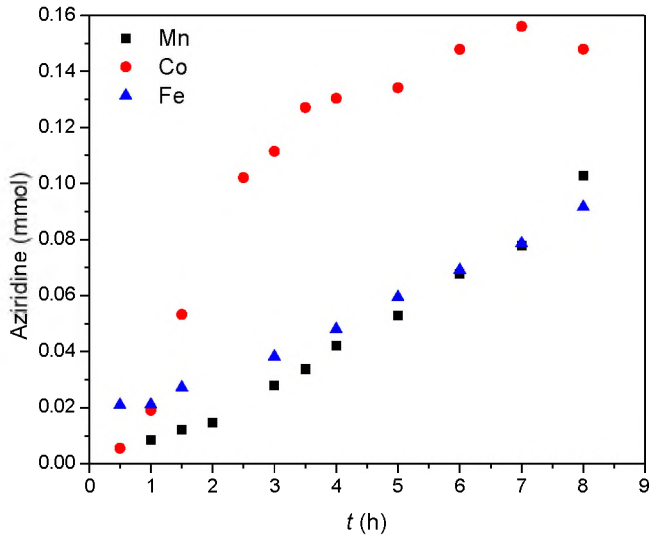

Figure 9. Production of Aziridine as a Function of Time. Reaction of Styrene (2.0 mmol) by PhI=NTs (0.25 mmol) Catalyzed by [K(NCMe)(L^8)M^{II}–NCMe] (M = Mn, Fe, Co; 0.0125 mmol) in d_5-chlorobenzene (0.50 mL) at 30 °C.

Competitive aziridination of styrene (1.0 mmol) versus allylbenzene (1.0 mmol), styrene (1.0 mmol) versus 4-phenyl-1-butene (1.0 mmol), and styrene versus 1-hexene by PhI=NTs (0.25 mmol), catalyzed by [K(NCMe)(L^8)M^{II}–NCMe] (M = Mn, Fe, Co; 0.0125 mmol) in chlorobenzene (0.20 mL), demonstrates considerable predilection for the aziridination of aromatic olefins (Table 3), significantly more enhanced for Mn-catalyzed reactions, and consistently in the order Mn > Co > Fe. In contrast, lower selectivities are largely obtained for the same competitive reactions mediated by [$Cu(CH_3CN)_4$](PF_6) (5 mol%) in MeCN. For the styrene versus 1-hexene aziridination, Evans and co-workers have reported[15p] a relative olefin reactivity of 5:1 with $CuClO_4$, CuOTf and $Cu(OTf)_2$ (5-10 mol%) in MeCN at –20 °C. A wide range of ratios (from >19:1 to 1:5.6) for the competitive aziridination of styrenes vs. aliphatic alkenes by sulfamate nitrene donors has been recently noted with Rh and Ag catalysts.[43]

We also witnessed poor selectivity with $[Rh_2(OAc)_4]$ (2 mol%) in dichloromethane, further complicated by the observation of more than one product in the aziridination (NTs) of styrene. Overall these results are consistent with an inverse reactivity/selectivity correlation, with the exception of Fe^{II} mediated reactions.

Table 3. Ratio and Yield of Aziridines obtained by Competitive Aziridination. Styrene vs. Allylbenzene, Styrene vs. 4-Phenyl-1-Butene, and Styrene vs. 1-Hexene[a]

Compound	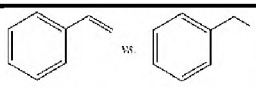	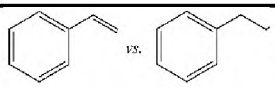	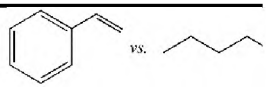
[K(MeCN)(L^8)Mn^{II}–NCMe] (**8b**)	25:1 (78%)	17:1 (72%)	62:1 (75%)
[K(MeCN)(L^8)Fe^{II}–NCMe] (**8c**)	11:1 (72%)	9:1 (70%)	16:1 (68%)
[K(MeCN)(L^8)Co^{II}–NCMe] (**8d**)	16:1 (68%)	11:1 (72%)	28:1 (73%)
$[Cu(NCMe)_4](PF_6)$	8:1 (90%)	6:1 (89%)	17:1 (91%)

[a]Olefin, 1.0 mmol each; PhINTs, 0.25 mmol; Catalyst, 0.0125 mmol (5 mol%); M.S. 5Å, 20 mg; Solvent, chlorobenzene (**8b-8d**) or MeCN (Cu^I), 0.200 mL; RT, 24 h.

2.5. MECHANISTIC STUDIES

Scheme 1 presents the general features of two major mechanistic scenarios that are explored in experimental and computational studies detailed below. Both are predicated on the formation of an initial metal-nitrene entity, whose electronic and structural characteristics are investigated computationally for three metals (Mn, Fe, Co; see below). An effectively concerted pathway of nitrene transfer to a styrene is expected to provide aziridine in a stereospecific manner, relying on concerted (albeit potentially asynchronous) formation of two C–N bonds (in succession N–C_β and N–C_α), with an intervening time gap that is essentially within the vibrational timescale. In contrast, a

two-step process is characterized by a well-defined carboradical and/or carbocationic intermediate, featuring a lifetime that permits competitive C_α–C_β bond rotation and N–C_α bond formation (aziridine-ring closure).

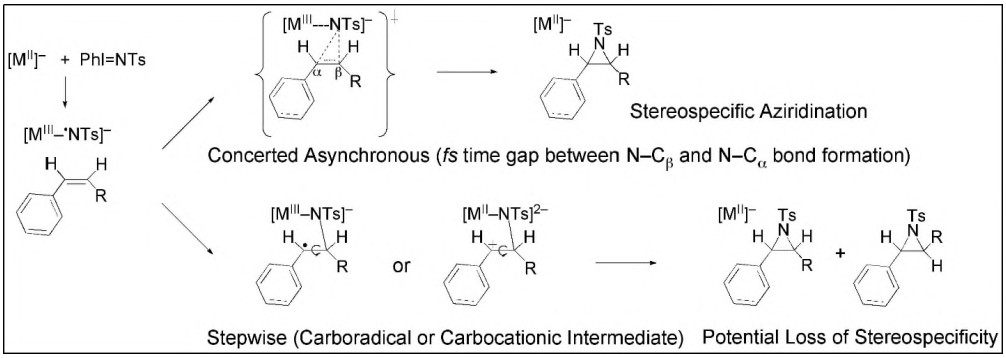

Scheme 1. Mechanistic Study of Nitrene Transfer to Olefins

(a) Hammett plots. Competitive aziridination of a series of *para*-substituted styrenes (1.0 mmol) versus styrene (1.0 mmol) by PhI=NTs (0.25 mmol) in the presence of [K(MeCN)(L^8)M^{II}–NCMe] (M = Mn, Fe, Co) generates log(k_X/k_H) values (Tables S11 - S13) that cannot provide linear free energy correlations with typical polar parameters such as σ_P and σ_{mb}, and only marginal ones with the resonance responsive σ^+ parameter (for Mn: $\rho^+ = -0.36$, $R^2 = 0.86$; for Co: $\rho^+ = -0.52$, $R^2 = 0.90$; poor correlation for Fe; Figure S6). As has been previously noted,[15g] electron-withdrawing substituents such as F and Cl exhibit a significant accelerating effect in the aziridination of the corresponding *para*-substituted styrene versus styrene, whereas others (NO_2, CF_3) demonstrate a surprisingly modest decelerating effect. These effects are better accommodated by Jiang's dual-parameter correlation (log (k_X/k_H) = $\rho_{mb}\sigma_{mb} + \rho_{JJ}{}^{\bullet}\sigma_{JJ}{}^{\bullet} + C$) that include both polar (σ_P, σ_{mb}) and spin-delocalizing ($\sigma_{JJ}{}^{\bullet}$) elements.[56] Indeed, aziridinations by [L^8M^{II}–

solv]$^{-}$ can be reasonably fit with the dual-parameter approach for Mn (ρ_{mb} = -0.38, $\rho_{JJ}^{\bullet}$ = 0.51, R^2 = 0.95) and Co (ρ_{mb} = -0.56, $\rho_{JJ}^{\bullet}$ = 0.56, R^2 = 0.97), and rather poorly for Fe (ρ_{mb} = -0.28, $\rho_{JJ}^{\bullet}$ = 0.24, R^2 = 0.84) (Figure 10). As expected, all ρ_{mb} values are moderately negative, consistent with a small incipient positive charge developing at the benzylic carbon as a result of the electrophilic attack of the putative metal-nitrene moiety.

In accordance with the electrochemical data noted above, the metal-nitrene site is anticipated to exhibit increased electron deficiency in the order Fe < Mn < Co, reflecting the trend in the negative ρ_{mb} values observed (*i.e.*, higher polar contribution for Co). The spin-responsive (radical) component ($\rho_{JJ}^{\bullet}$) is instead positive, since all *para*-substituents are effectively spin delocalizing. Its contribution to polar-over-spin effects ($|\rho_{mb}/\rho_{JJ}^{\bullet}|$; Mn = 0.75, Fe = 1.17, Co = 1.0) seems to be more enhanced for the Mn site, potentially due to a comparatively later transition state versus Co, although the poor correlation provided by Fe makes comparisons with Mn more difficult to assess. These results are consistent with the more modest rate for aziridine production noted above for Mn versus Co, and inconclusive with respect to Fe. A similar requirement for dual-parameter Hammett analysis has been previously applied in the competitive aziridination (NR) of styrene vs. *para*-substituted styrenes by Tp^{x}M (M = Cu, Ag) catalysts [$|\rho^{+}/\rho^{\bullet}|$ = 0.925–1.625 (R = Ts);[15d] $\rho^{\bullet}$ refers to Jackson's spin-delocalization scale[57]], [Cu^{I}(TMG$_3$trphen)](PF$_6$) [($|\rho_{mb}/\rho_{JJ}^{\bullet}|$ = 0.50 (R = Ts)],[15g] and several [Ru(Por)(NR)$_2$] compounds [($|\rho_{mb}/\rho_{JJ}^{\bullet}|$ = 0.55, 2.02 (R = Ts), 1.46 (R = Ns)],[21f,g] all exhibiting competitive contributions by polar and spin-delocalization effects.

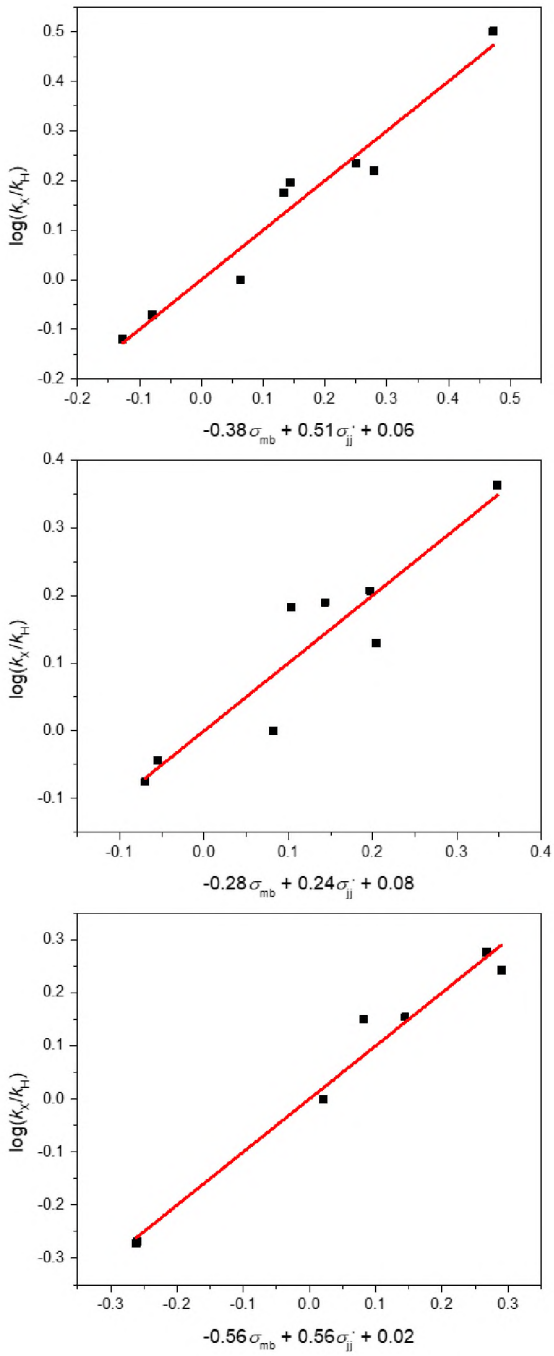

Figure 10. Linear free energy correlation of $\log(k_X/k_H)$ *vs.* (σ_{mb}, $\sigma_{JJ}^{\bullet}$). Aziridination of *para*-substituted styrenes catalyzed by $[L^{8}M^{II}\text{–solv}]^{-}$ (M = Mn (top), Fe (middle), Co (bottom)).

In contrast, Fe^{II}-dipyrrinato complexes demonstrate an overwhelming preponderance of spin effects [($|\rho_{mb}/\rho_{JJ}^{\bullet}|$ = 0.04 (R = Ad)].[18e] Conversely, dominant polar

effects are observed in many instances in which kinetic data for competitive aziridinations can be fitted by polar substituent parameters alone (σ_P, σ^+, σ_{mb}), as for instance with $[Rh_2(OAc)_4]$ [$\rho^+ = -0.61$ (R = Ns)],[16f] $[Cu(acac)_2]$ [$\rho^+ = -0.49$ (R = Ns)],[16f] and $[Cu(tfac)_2]$ [$\rho^+ = -0.60$ (R = (5-Me)-2-$PySO_2$)],[58] as well as with several non-heme Fe catalysts by Latour [$\rho^+ = -0.71$ (R = Ts)],[18g] Che [$\rho^+ = -0.72$ (R = Ts)][59] and Jensen [$\rho^+ = -0.58$ (R = Ts)].[42a]

Table 4. Secondary Deuterium Kinetic Isotope Effect Values vs. Styrene

Compound	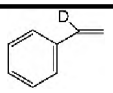	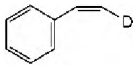	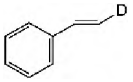	**Calculated cis × trans**	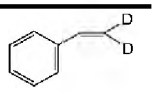
[K(MeCN)(L^8)Mn^{II}–NCMe] (**8b**)	1.01(±0.01)	0.89(±0.02)	1.03(±0.01)	0.92(±0.03)	0.89(±0.01)
[K(MeCN)(L^8)Fe^{II}–NCMe] (**8c**)	1.02(±0.01)	0.86(±0.02)	1.04(±0.01)	0.89(±0.03)	0.93(±0.01)
[K(MeCN)(L^8)Co^{II}–NCMe] (**8d**)	1.00(±0.01)	0.96(±0.02)	0.98(±0.02)	0.94(±0.04)	0.98(±0.01)

(b) Deuterium Kinetic Isotope Effects and Stereocontrol Studies. The comparative effect of the metal was further investigated by secondary kinetic isotope effect experiments (k_H/k_D) for the aziridination of suitably deuterated styrenes (0.5 mmol) versus styrene (0.5 mmol) by PhI=NTs (0.125 mmol) mediated by [K(NCMe)(L^8)M^{II}–NCMe] (6.25 μmol; M = Mn^{II}, Fe^{II}, Co^{II}) in chlorobenzene. The α-styrene position was first examined (Table 4), and proved to give rise to normal KIE values very close to 1, signifying that the α-styrene site is unlikely to be involved in the electrophilic attack by the nitrene (NTs). The β-styrene site was evaluated with the assistance of *cis*- and *trans*-β-d^1 styrene (Table 4) and exhibited inverse KIE values for all metals for the *cis* isomer,

although the *trans* isomer provided KIE values in the vicinity of 1 for all metals. The secondary KIE value trend for the *cis*-β-d^1 styrene (Mn: 0.89(±0.02); Fe: 0.86(±0.02); Co: 0.96(±0.02) indicates a more pronounced inverse effect for Mn and Fe rather than for Co, whereas the corresponding values for *trans*-β-d^1 styrene suggest that the trans position has little contribution to the KIE value. The overall product k_H/k_D(cis) × k_H/k_D(trans) further narrows the range of KIE values with respect to the metal (Table 4). This combined effect was further explored with the assistance of β-d^2 styrene (Table 4) and found to provide rather small inverse KIE values for Mn and Fe, and a value approaching 1 for Co. Che and co-workers report a k_H/k_D value of 0.85 for the aziridination of β-d^2 styrene and 0.97 for the aziridination of α-d^1 styrene by $[Ru^{VI}(TPP)(NTs)_2]$.[21g] Overall, these values point towards an engagement of the β-styrene site in the electrophilic phase of the nitrene attack, with a transition state that is comparatively early for Co (resulting in small deviation from sp^2 hybridization at the β-carbon of styrene) and more advanced for Mn and Fe. The deuterium KIE values associated with *cis*-β-d^1 styrene most likely provide the best guidance (as also exemplified in Mn epoxidations),[32] and further underscore the correlation between the anticipated electrophilicity of the putative M^{III}–$^{\bullet}$NTs unit (Fe < Mn < Co) and the position of the transition state associated with the addition of the metal-nitrene to the β-carbon of styrene. However, the accuracy of the KIE experimental data, and the occasionally small deviation of KIE values from 1, make the metal-dependent comparisons tentative, especially between Mn and Fe.

The *cis*- and *trans*-β-d^1 styrenes are also useful in the evaluation of the stereochemical integrity upon styrene aziridination (Table 5). The degree of cis/trans

partitioning, due to competitive aziridine-ring closer vs. C_α–C_β bond rotation, was determined by ^{2}H NMR (and ^{1}H NMR) and indicated a clear trend for increasing stereochemical scrambling in the order Co < Mn < Fe, thus suggesting that the Co^{II} reagent effects a shorter time gap between N–C_β and N–C_α bond formation. The same trend was observed in the aziridination of both *cis*- and *trans*-*β*-methylstyrene as noted above (Table 2). In sharp contrast to the L^8Fe reagent **8c**, Betley's Fe-dippyrinato catalyst shows no loss of stereochemistry in the aziridination (NAd) of *cis*-*β*-d^1 styrene,[18e] although the nature of the nitrene group (NTs vs. NAd) is known to impart significant kinetic differentiation, affecting reactivity and selectivity in aziridinations.[60]

Table 5. Investigation of Stereochemistry in the Aziridination of *cis*- and *trans*-*β*-d^1-styrene

Compound	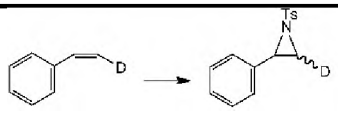 **cis/trans aziridine**	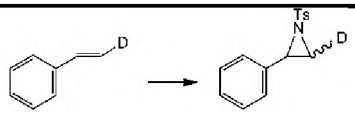 **trans/cis aziridine**
[K(MeCN)(L^8)Mn^{II}–NCMe] (**8b**)	78/22	79/21
[K(MeCN)(L^8)Fe^{II}–NCMe] (**8c**)	67/33	67/33
[K(MeCN)(L^8)Co^{II}–NCMe] (**8d**)	89/11	92/8

Again, the effect of the metal (Mn, Fe, Co) in the present study correlates well with established M^{II}/M^{III} reduction potentials (Figure 8), since the rate of formation of the N–C_α bond from a carbon-centered radical and a nitrogen-centered, metal-bound nucleophile (three-electron oxidative process) has been previously shown[15g,61] to be thermodynamically controlled either by the ease of oxidation of the benzyl (styrenyl) radical and/or by the ease of reduction of the metal (from M^{III} to M^{II} in the present case). Hence, the more electron-deficient catalyst (Co) affects not only the formation of the first

N–Cα bond (relatively early transition state) but also the closure of the second N–Cβ bond (reduced stereochemical scrambling). Similar electronic effects have been noted by Jacobsen with respect to Mn^{III}(salen)-mediated epoxidations[32] and by Che for aziridinations enabled by [Ru^{VI}(Por)($NSO_2R)_2$].[21f,g]

(c) Radical Probe. The radical clock *trans*-2-phenyl-1-vinylcyclopropane[62] (16, Scheme 2) was further employed to evaluate the comparative lifetime of the anticipated radical intermediate, following nitrene addition to olefins at the terminal carbon atom, albeit for an aliphatic olefin. Although this radical probe has found good use,[15p,16i,63] not much is known about the product profile and/or the spectroscopic signature of key products in aziridinations. The rate constant for ring opening of the *trans*-2-phenylcyclopropyl-1-methyl radical has been experimentally determined to be 3×10^{11} s^{-1} at 25 °C.[64]

The catalytic amination of **16** (4 equiv.) by PhI=NTs (1.0 equiv.) in the presence of catalysts [K(NCMe)(L^8)M^{II}–NCMe] (M = Mn, Fe, Co) (0.0125 equiv.) and molecular sieves in chlorobenzene affords both ring-closed (aziridine) and ring-opened (olefinic amines) products in modest yields (Scheme 2). Care is required in the evaluation of ring-closed vs. ring-opened products, because the aziridine (**17**) is prone to ring opening on silica affording alcohol **18** (one diastereomer is particularly vulnerable), hence the product distribution was determined by ^{1}H NMR on samples obtained in situ and/or after solvent extraction (hexane/ethyl acetate 3:1). The genuine ring-opened amination products are the olefinic diamine **19** and the conjugate diene **20**, presumably arising due to the generation of an intermediary ring-opened radical or carbocation that can be captured by NHTs and/or be subjected to *E*1-type proton elimination, respectively. The

competitive distribution of the two ring-opened products is evidenced by the enhancement of the olefinic diamine at the expense of the diene product in separate experiments in the presence of $TsNH_2$ (1 equiv. versus the radical clock).

The calculated ratio of ring-closed (aziridine) over ring-opened (olefinic amines) products (Mn: 6.2(±1.0), Fe: 1.9(±0.2), Co: 0.40(±0.10)) establishes a trend that indicates a shorter radical or carbocation lifetime (relatively faster aziridine ring closure) for Mn versus the other metals. Because trace amounts of one or two additional olefinic products can also be detected, the aforementioned values should be considered approximate, although the trend is secure. Specifically for the Co^{II} catalyst, trace amounts of the cyclopropane ring-opened $PhCH{=}CHCH_2$-aziridine(NTs)[65] are observed, although the provenance of this product is unclear.

For comparison, amination of the same radical clock by typical cationic copper(I) reagents such as $[Cu(NCMe)_4](PF_6)$ or $[Cu(TMG_3\text{-trphen})](PF_6)$, under the same conditions, save for MeCN used as solvent, favors the aziridine over the olefinic amines by a large margin (24(±1.0) and 19.0(±1.0), respectively) and at higher overall yields (48% and 37%, respectively). Interestingly, $CuClO_4$ in MeCN has been reported by Evans and co-workers[15p] to afford only the aziridine. These results indicate that the aziridination of aliphatic olefins by Cu(I) reagents may still obey a two-step mechanism, but with a much shorter time gap between the first and second C–N bond construction.

Most importantly, the trend observed in these radical clock experiments, especially for the well-behaved Mn- and Co-catalyzed reactions, differs from that previously noted in conjunction with the stereocontrol studies in styrene aziridinations (Table 5). On the other hand, the trend is consistent with stereocontrol results for the

aziridination of *cis*-2-hexene (stereochemical integrity decreases in the order Mn > Fe > Co; Table S10), albeit in low yields for the Mn and Fe-catalyzed reactions.

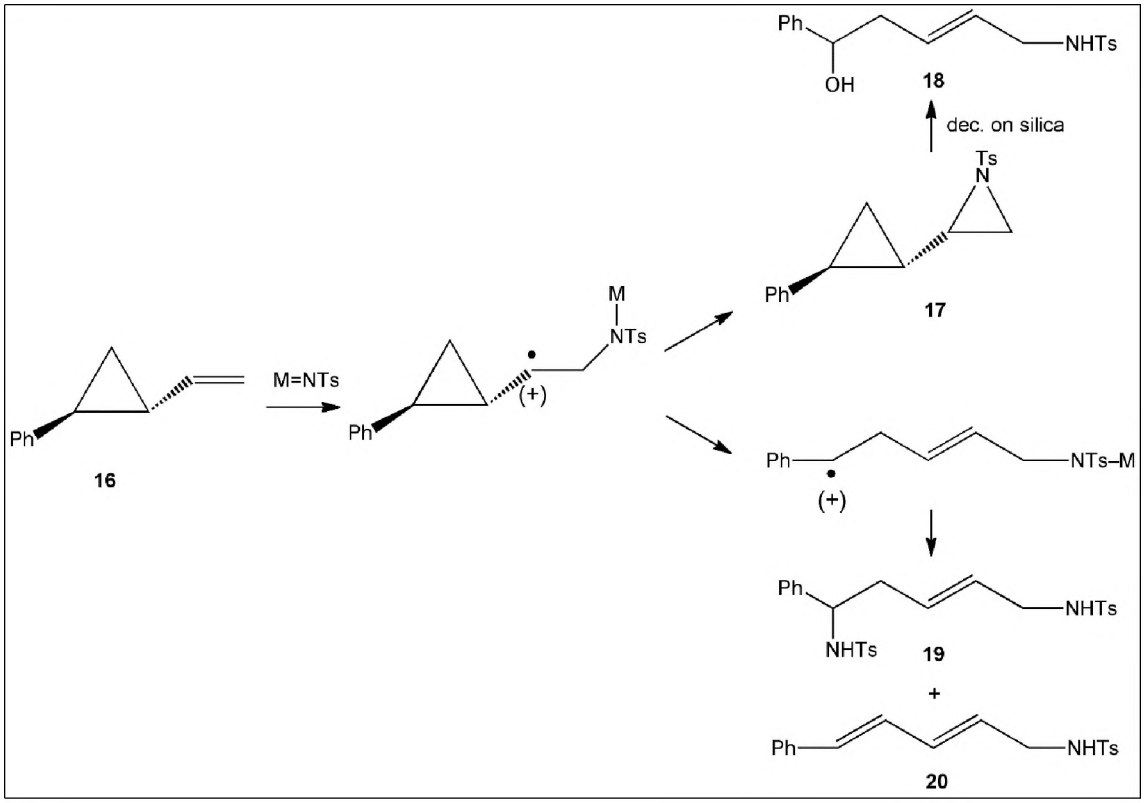

Scheme 2. Radical Clock Experiment

One possible explanation is that whereas the barrier for ring closure (radical rebound) in styrene aziridinations is largely determined by the ease of M^{III} to M^{II} reduction, electron-rich aliphatic olefins (which invariably show higher levels of retaining stereochemistry versus styrenes) undergo facile, essentially barrierless oxidation of the incipient α-carbon-centered radical upon ring closure (see also computational studies below). Hence, any residual barrier for aziridine-ring formation by aliphatic olefins will be influenced by parameters other than the relative M^{II}/M^{III} redox potentials.

One such parameter, identified in conjunction with P450-related alkane oxidations and olefin epoxidations,[61] is the relative energy of the metal-centered orbital that ultimately receives the single electron upon ring closure. More extensive experimentation with aliphatic olefins will further shed light on these intriguing variations.

2.6. COMPUTATIONAL STUDIES

(a) Geometry and Structure of Nitrene Intermediates. The presumptive metal-nitrene intermediates (M = Co, Fe, Mn) are calculated at the same B3LYP/6-31+G(d) level of theory used in a previous study of copper azirdination catalysts.[15g] Free energy calculations indicate that nitrenes favor intermediate or high spin ground states: $S_{Co} = {}^5/_2$, $S_{Fe} = 2$, $S_{Mn} = {}^3/_2$. For [Co]NTs ($S = {}^5/_2$), the computed spin density is ~1.1 unpaired e^- on nitrene nitrogen and ~3.3 unpaired e^- on Co; the remaining spin density is spread over other atoms. The ΔG differences among doublet, quartet and sextet states of [Co]NTs are small, with the sextet being 1.5 kcal/mol lower than quartet and 0.4 kcal/mol lower than the doublet in free energy. The geometry of sextet cobalt nitrene intermediate is distorted with a fluorine (F1) of the trifluoromethyl substituent on the supporting ligand interacting with Co (Co–F1 = 2.37 Å) while one equatorial Co–N and the axial Co–N are elongated (> 3 Å; Figure 11).

For [Fe]NTs (S = 2) and [Mn]NTs ($S = {}^3/_2$), the Mulliken spin density shows ~5 e^- on Fe and 3.2 e^- on Mn and -0.67 e^- on nitrene nitrogen for both complexes with the rest of the spin density spread among other atoms. Unrestricted Kohn-Sham calculations were used to model singlet [Fe]NTs; its free energy is 25.4 kcal/mol higher than the quintet; a triplet minimum could not be located. As expected, the M–NTs is calculated to be the shortest M–N for all three metals [1.79 Å (Co), 1.86 Å (Fe), 1.81 Å (Mn)]. Optimized

bond angles for [M]–N–S are 147° (Co), 170° (Fe), 160° (Mn) (Figure 11), and thus intermediate between bent and linear nitrene coordination modes.

Among many well-characterized terminal metal imido compounds L_nM–NR (M = Mn,[66] Fe,[67] Co,[68] Ni[69]) at various oxidation and spin states, only a handful are available featuring one oxidizing equivalent above the M^{III} state, either metal centered or residue localized.[41,70,71] Most relevant to the present investigation from an electronic standpoint are Betley's four-coordinate ($^{t\text{Bu}}$L)FeCl(NC$_6$H$_3$-2,6-^{i}Pr$_2$)[18d] (Fe–NR = 1.768(4) Å, Fe–N–C_{Ar} = 178.7(4)°) and (^{Ar}L)FeCl(N(*p*-^{t}BuC$_6$H$_4$))[18f] (Fe–NR = 1.768(2) Å, Fe–N–C_{Ar} = 156.43(17)°) ($^{t\text{Bu}}$L and ^{Ar}L are *t*-butyl- and aryl-substituted dipyrromethene ligands, respectively), whose high-spin (S = 2) is accounted by a high-spin Fe^{III} site (S = 5/2) coupled antiferromagnetically to an imidyl based radical.

(b) Aziridination Reaction Coordinate. The aziridination of styrene using [M^{III}]NTs as the catalytic active species is also calculated (Figures 12–15). Spin states of aziridination transition states (TSs) for Co, Fe and Mn are calculated to be quartet, triplet and quartet, respectively. Upon C_β in styrene binding to N_{Ts}, there is an elongation of the C_α–C_β bond in the organic substrate, 1.34 Å → 1.38 Å, for the cobalt system (Figure 13). Calculations show asymmetry of the two C–N_{Ts} bonds to the styrene substrate during aziridination; C_β–N_{Ts} = 2.24 Å (Co), 2.23 Å (Fe), 2.20 Å (Mn), C_α–N_{Ts} = 3.06 Å (Co), 3.04 Å (Fe), 3.02 Å (Mn) (Table 6). The asymmetry in this TS suggests aziridination of styrene is a two-step process: initial C–N formation leading to an open "diradical" intermediate, which is then followed by radical rebound (RR) to close the three-membered aziridine ring, instead of one-step formation of both C–N bonds. Interestingly, a similar, two-step mechanism was proposed for related Cu-nitrene intermediates in a

joint experiment-theory study by our groups.[15g] Notably, dirhodium carboxylate catalysts have also been conceived to undergo two-step aziridination processes, albeit with high stereospecifity due to triplet-singlet interconversion via a minimum energy crossing point.[16b] Calculations also show a decrease of spin density (e^-) on N_{Ts} upon $C_\beta \cdots N_{Ts}$ bond formation: 1.08 → 0.53 (Co), -0.62 → -0.41 (Fe), -0.64 → -0.5 (Mn), which might be due to electron transfer from N_{Ts} to C_α after activation. Spin densities change at the metal center as well: 3.34 → 2.38 (Co), 5.08 → 3.56 (Fe), 3.24 → 4.23 (Mn).

Activation free energy barriers for the initial $C_\beta \cdots N_{Ts}$ bond forming step of aziridination are calculated: $\Delta G_{az}^{\ddagger}$ = 23.4 kcal/mol (Co), 27.9 kcal/mol (Fe) and 25.1 kcal/mol (Mn) (Figure 12). For the 1st TS of Co aziridination, the quartet is 5.0 kcal/mol lower than doublet in free energy. The iron complexes unrestricted singlet TS is 31.1 kcal/mol higher than the triplet. For the Mn system, the doublet TS is 27.3 kcal/mol higher in free energy than quartet. Although calculations show a distorted cobalt nitrene complex with fluorine-cobalt interaction, in the first TS structure the Co complex possesses a disphenoidal structure with no Co–F interaction As expected, it is exergonic upon going from the $C_\beta \cdots N_{Ts}$ bond forming TS to the diradical intermediate for all three metals (by 8.7 kcal/mol for Co, 28.6 kcal/mol for Fe and 20.5 kcal/mol for Mn; Figure 12). The cobalt diradical intermediate favors a low spin doublet spin state with 0.51 unpaired e^- on the benzylic carbon and 0.11 e^- on Co. The Fe diradical intermediate, however, favors a high spin quintet intermediate with spin density of 0.79 e^- on benzylic carbon (C_α) and 5.13 e^- on Fe. The Mn diradical intermediate is calculated to be a high spin sextet with 0.79 e^- on C_α and 3.50 e^- on Mn. Compared to the initial aziridination TSs, these three intermediates have an increase in spin density (in e^-) on C_α upon

formation of the first C–N bond: 0.42 → 0.51 (Co), -0.41 → 0.79 (Mn), -0.40 → 0.79 (Fe). The accumulating spin density on benzylic carbon C_α further supports the proposal that the overall aziridination reaction coordinate is non-concerted.

Table 6. Key bond lengths (Å) among active site atoms by [M]NTs. For the initial $C_\beta \cdots N_{Ts}$ bond formation transition states, radical intermediate, and radical rebound transition states (RR TSs) for the three metals studied. See Figures 13 - 15 for optimized geometries.

	C_β–N_{Ts}	C_α–N_{Ts}	C_α–C_β	M–N_{Ts}
$C_\beta \cdots N_{Ts}$ TS Co (4)	2.24	3.06	1.38	1.84
Intermediate Co (4)	1.48	2.48	1.42	2.00
RR TS Co (4)	1.50	2.39	1.49	2.01
$C_\beta \cdots N_{Ts}$ TS Fe (3)	2.23	3.04	1.38	1.87
Intermediate Fe (5)	1.48	2.48	1.50	1.93
RR TS Fe (5)	1.49	2.17	1.48	2.06
$C_\beta \cdots N_{Ts}$ TS Mn (4)	2.20	3.02	1.38	1.91
Intermediate Mn (6)	1.48	2.48	1.50	1.97
RR TS Mn (6)	1.49	2.25	1.48	2.07

The C_α of the open intermediate bonds to the nitrogen of the NTs moiety after the initial TS, to give aziridine product via a 2nd TS that we have termed the radical rebound transition state. For the RR step, the TSs for all three metals maintain the same spin state as the rebound intermediates. The barriers for radical rebound are small to non-existent: $\Delta G_{RR}^{\ddagger}$ = 1.4 kcal/mol (Co), 14.8 kcal/mol (Fe), 4.7 kcal/mol (Mn) relative to the diradical intermediates. Different from Fe and Mn, C_α–C_β keeps elongating along the reaction coordinate for Co [1.38 Å (HAA TS) → 1.42 (intermediate) → 1.49 (RR TS)] (Figure 13). For Fe and Mn complexes, the value of this bond remains closer to a carbon-carbon single bond after the initial C_β–N_{Ts} bond forming step. The C_α–C_β bond length of the

cobalt intermediate (1.42 Å) is in between the C=C double bond in styrene (1.34 Å) and a C–C single bond (1.54 Å), which suggests that the π-bond between C_α and C_β is weakened but not yet fully broken upon activation step (*i.e.*, bond order of C_α–C_β between 1 and 2). As such, the presence of a two-step aziridination mechanism with an intermediate that has a finite lifetime is consistent with the observed C_α–C_β rotation that is experimentally observed.

(c) Thermodynamics of Aziridination. The ligand-supported [M^{II}] catalysts are calculated separately with isolated aziridine. Calculations suggest that on the free energy surface, separated products are more stable than an aziridine complex given the bulky ligand substituents. The overall reaction, [M]NTs + styrene → [M^{II}] + aziridine is highly exergonic for all the metals: ΔG of the reactions = -20.4 kcal/mol (Co), -41.1 kcal/mol (Fe), -48.6 kcal/mol (Mn) (Figure 12). The spin density on the metal center of the three catalyst complexes [M] did not change significantly compared to reactant complexes with nitrene: spin density of metal center [M]NTs vs. [M^{II}]: 3.3 vs. 3.1 e^- (Co), 5.1 vs. 4.6 e^- (Fe), 3.2 vs. 3.4 e^- (Mn). For the product complex, calculations show that there is an interaction between fluorine and metal center for both Co and Mn product complexes, [M–F = 2.39 Å (Mn), 2.33 Å (Co)], which may serve to stabilize the low-coordinate complex for another round of catalysis. Figure 11 depicts the three representative metal nitrene active species (M = Mn, Fe, Co) optimized at the B3LYP/6-31+G(d) level of theory. All hydrogen atoms are omitted for clarity Figure 12. Two-step aziridination (initial N-C⌟ bond formation + radical rebound) of styrene with metal nitrene active species are calculated B3LYP/6-31+G(d) for Mn (red), Fe (blue) and Co (black). Calculated free energies in kcal/mol.

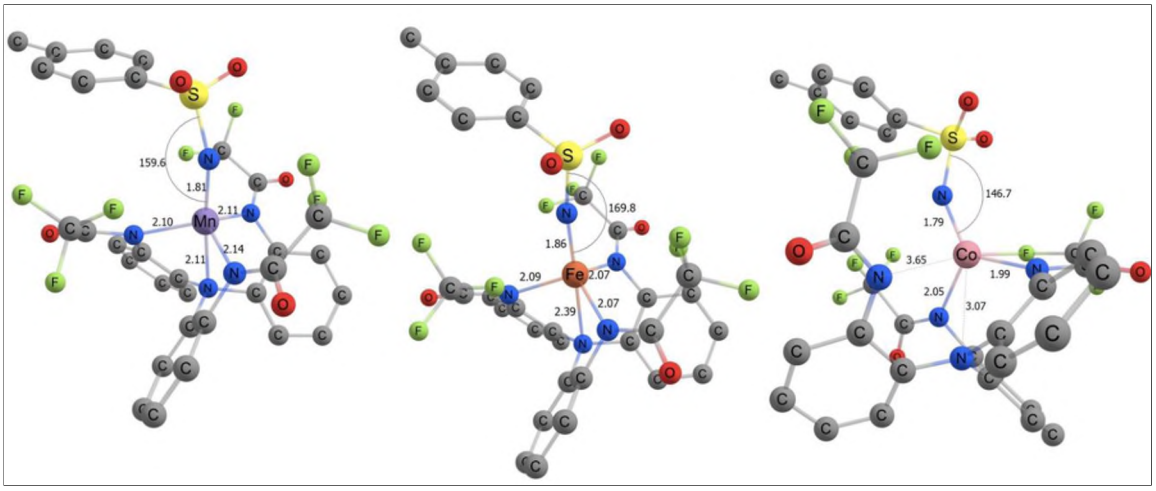

Figure 11. Three representative metal nitrene active species (M = Mn, Fe, Co). Optimized at the B3LYP/6-31+G(d) level of theory. All hydrogen atoms are omitted for clarity.

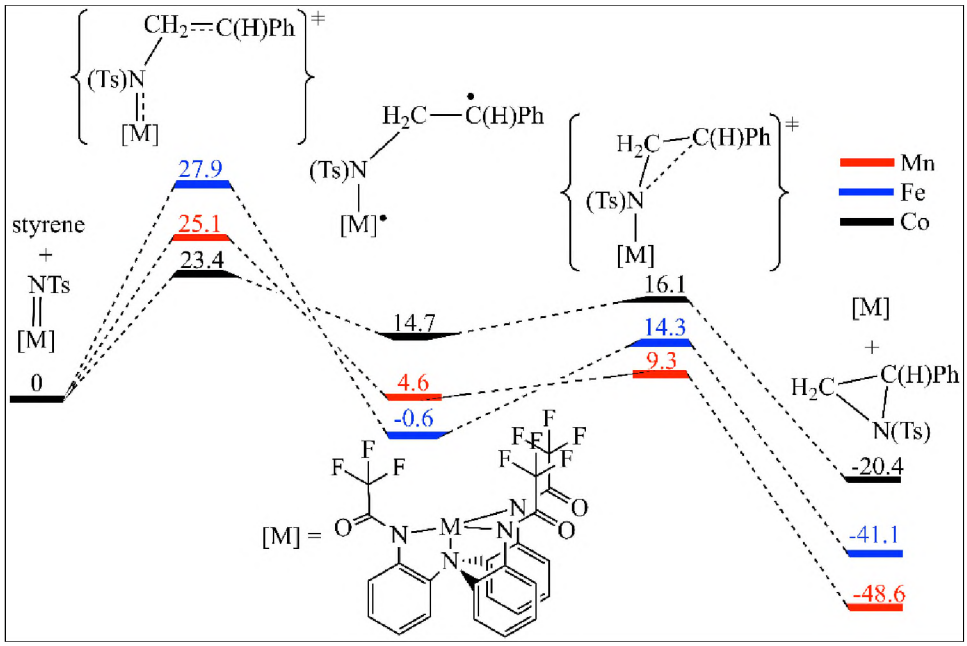

Figure 12. Two-step aziridination of styrene with metal nitrene active species. Calculated B3LYP/6-31+G(d) for Mn (red), Fe (blue) and Co (black). Calculated free energies in kcal/mol. (initial N-Cβ bond formation + radical rebound)

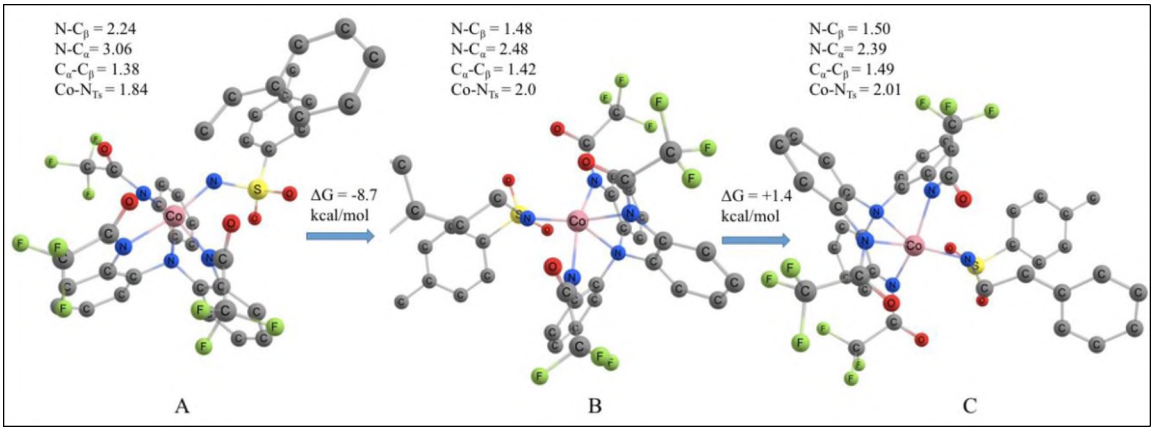

Figure 13. B3LYP/6-31+G(d) calculated (bond lengths in Å) for (A) Co. Quartet initial $C_{\beta}\cdots N_{Ts}$ bond forming TS; (B) Quartet intermediate; and (C) Quartet radical rebound TS.

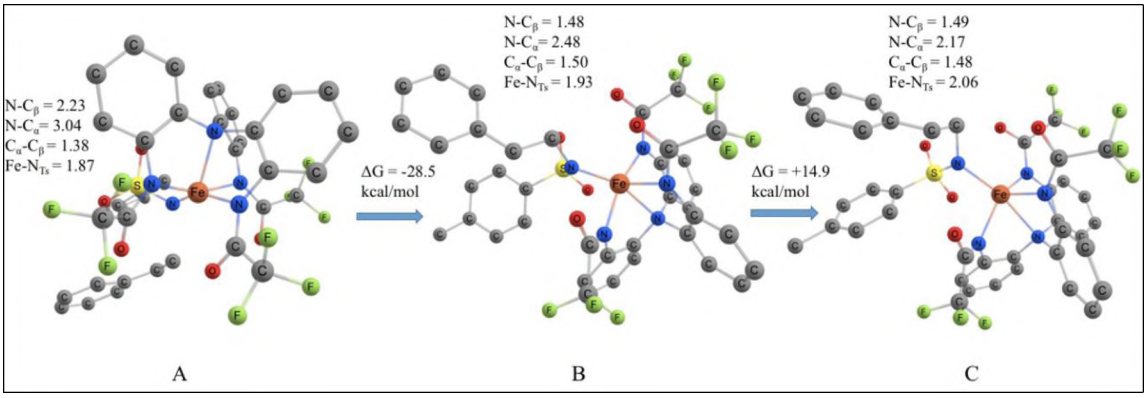

Figure 14. B3LYP/6-31+G(d) calculated (bond lengths in Å) for (A) Fe. Triplet initial $C_{\beta}\cdots N_{Ts}$ bond forming TS; (B) Quintet intermediate; and (C) Quintet radical rebound TS.

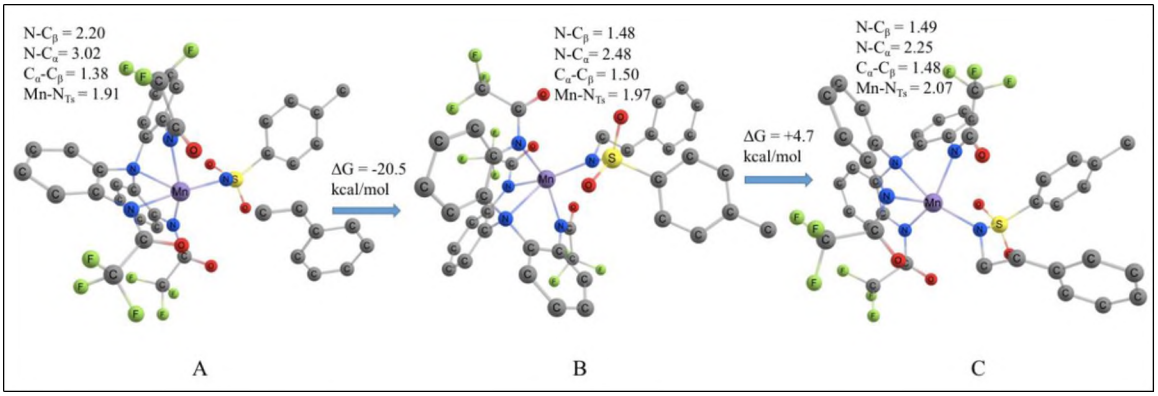

Figure 15. B3LYP/6-31+G(d) calculated (bond lengths in Å) for (A) Mn. Quartet initial $C_{\beta}\cdots N_{Ts}$ bond forming TS; (B) Sextet intermediate; and (C) Sextet radical rebound TS.

(d) DFT Calculations of Manganese Nitrene Intermediate Reacting with Isopentene. Isopentene is modeled as an alternative substrate to study the competition of aziridination between styrene and acyclic aliphatic olefins. Mn-meditated nitrene addition to isopentene is calculated at the same reaction conditions and same level of theory as styrene. Spin states are the same for initial nitrene addition TSs (quartet) and rebound intermediates (sextet) for both styrene and isopentene reactions. The difference in key bond lengths (C_β–N_{Ts}, C_α–N_{Ts}, C_α–C_β) at the reaction center is ~ 0.2 Å. Upon C_β–N_{Ts} bond forming, elongation of C_α–C_β (1.34 Å → 1.38 Å) is also observed at the initial nitrene addition TS (Figure S7). The same type of asymmetry of two C–NTs bonds in styrene is also observed in TS with isopentene: C_β–N_{Ts} = 2.13 Å and C_α–N_{Ts} = 2.92 Å. Spin density at the Mn center increases from 3.24 e^- to 4.68 e^-, while it decreases at the N_{Ts} -0.64 e^- to -0.52 e^-. However, the activation energy barrier ($\Delta G_{aZ}^{\ddagger}$) of C_β–N_{Ts} bond forming step for isopentene is 32.8 kcal/mol, which is higher than that of styrene (25.1 kcal/mol). Calculations show that HOMO energy of styrene is 0.7 eV higher than that of isopentene, which makes styrene a better nucleophile for attack by the electrophilic nitrene catalyst, yielding a lower activation barrier.

From nitrene addition TS to rebound intermediate for isopentene, it is also exergonic by 18.6 kcal/mol. The Mn radical intermediate is a high-spin sextet, which is the same as the intermediate from reaction with styrene as substrate. Spin density on the Mn center increases from 4.69 e^- to 5.18 e^-, and increases from -0.52 e^- to -0.67 e^- on the C_α, which supports the non-concerted aziridination of isopentene. RR TS for isopentene is calculated to be sextet. The majority of the spin density resides on Mn (5.35 e^-) and C_α (0.79 e^-). Going from radical intermediate to RR TS, spin density decreases on C_α from

1.09 e^- to 0.79 e^- and C_α-N_{Ts} bond shortens from 2.5 Å to 2.3 Å, which is also a trend observed for the styrene pathway. The $\Delta G_{RR}^{\ddagger}$ is +3.4 kcal/mol, which is lower than that for styrene (+4.7 kcal/mol). This is expected due to the higher reactivity of alkyl radical than that of benzyl radical.

The overall reaction, [M]NTs + isopentene → $[M^{II}]$ + aziridine, is exergonic: ΔG of the reactions = -3.6 kcal/mol, which is much closer to thermoneutral than with styrene (-48.6 kcal/mol) using the same Mn catalyst. The much smaller thermodynamic driving force along with the less stable alkyl radical intermediate than benzyl radical intermediate, makes the aziridination of isopentene more difficult.

3. CONCLUSIONS

The following are the major findings observed and insights gained in the present study:

(a) A family of fifteen anionic Mn^{II} compounds, supported by an N_3N^{3-} triphenylamido-amine framework and various carbonaceous arms, has been synthesized and characterized. Electrochemical data support a wide range of Mn^{II}/Mn^{III} redox potentials that span 1.8 V, and correlate with observed yields of Mn^{II}-mediated styrene aziridination by PhI=NTs, inasmuch as higher yields are largely obtained with less easily oxidized Mn^{II} catalyst precursors.

(b) The most productive catalyst, [K(NCMe)(L^8)Mn^{II}–NCMe], and the synthesized Fe^{II}, Co^{II} and Ni^{II} congeners, have been further evaluated with a panel of *para*-substituted styrenes, to afford good to high yields of aziridines at comparable ranges, with the exception of Ni^{II} that mediates low aziridine production (≤20%). In sharp

contrast, *ortho*-, α-, and β-substituted styrenes undergo aziridination in lower yields, especially for those reactions mediated by Mn^{II} or Fe^{II} precursors, whereas Co^{II} catalyzed reactions remain more productive and selective with respect to cis/trans isomerizations. Further curtailing of aziridine production is observed with aliphatic olefins for all catalysts employed.

(c) A comparative study of the reaction profile for the aziridination of styrene establishes a superior rate of aziridine formation for the L^8Co-catalyzed reaction versus that mediated by the L^8Mn and L^8Fe analogs. On the other hand, L^8Mn proved to be significantly more discriminating than L^8Co, as well as common Cu and Rh catalysts, in competitive aziridinations involving aromatic and non-conjugated alkenes. Indeed, the attenuated aziridination reactivity of the anionic L^8Mn reagent enables differentiation of styrene and 1-hexene by a practicable margin (62:1) versus a modest edge (5:1) previously reported for leading Cu reagents.[15p]

(d) Mechanistic investigations (Hammett plots, secondary KIE, cis/trans isomerization) and computational studies (DFT) strongly support a two-step pathway associated with the successive construction of two C–N bonds as a result of a close interaction between a plausible high-spin M–NTs unit and an aromatic alkene. The initial C_β–N_{Ts} bond formation that also generates a radical C_α site, is perceived as turnover-limiting, with barriers in the order Fe > Mn > Co, consistent with the anticipated electrophilicity of the metal nitrene moiety. The ring-closing and product-determining C_α–N_{Ts} bond formation consists of an intramolecular radical rebound within a M^{III}–$N(Ts)$–$C_\beta H_2$–$^\bullet C_\alpha(H)Ph$ fragment involving a C_α-centered radical and an open-shell M^{III}–NR site. This three-electron step proceeds with an experimentally and computationally

confirmed barrier in the order Fe > Mn > Co, presumably governed by the ease of metal reduction ($M^{III} \rightarrow M^{II}$).

(e) The observed preponderance for the aziridination of aromatic over aliphatic alkenes by the L^8Mn reagent is further reflected in the computed lower activation barrier for styrene versus isopentene aziridination as a result of the higher styrene HOMO energy, as well as due to the thermodynamic stability of the incipient, resonance-stabilized α-styrenyl radical. On the other hand, the more easily oxidized aliphatic-substituted C_α radical lowers the barrier for the radical rebound step, hence it exerts better control on stereoselectivity. Interestingly, the radical clock experiment reveals that the aliphatic radical exhibits longer lifetime in the Co- rather than the Mn-mediated reaction, in sharp contrast to the behavior of the α-styrenyl radical. It is conceivable that the $M^{III} \rightarrow M^{II}$ reduction potential no longer controls the miniscule activation barrier, and other still unidentified parameters are responsible for the metal selectivity observed.

Future studies will address the trends observed for the aziridination of aliphatic alkenes, and further explore the structural and functional characteristics of the metal nitrenes assumed to participate in the present study.

ACKNOWLEDGMENTS

This work was generously supported by the National Institute of General Medical Sciences of the National Institutes of Health under Award Number R15GM117508 (to P.S.), and in part by the National Science Foundation through grant CHE-0412959 (to P.S.). The authors also thank the U.S. Department of Energy, Office of Basic Energy Sciences, Division of Chemical Sciences, Geosciences, and Biosciences for support of

this research via grant DE-FG02-03ER15387 (to T.R.C.). The authors further acknowledge the National Science Foundation for their support of the UNT Chemistry CASCaM high performance computing facility through grant CHE-1531468. The authors also thank the Special Account of Research Grants of the National and Kapodistrian University of Athens for partial support.

REFERENCES

(1) (a) *Aziridines and Epoxides in Organic Synthesis*; Yudin, A. K., Ed.; Wiley-VCH: Weinheim, 2006. (b) Padwa, A. "Aziridines and Azirines: Monocyclic" in *Comprehensive Heterocyclic Chemistry III*, Katritzky, A. R.; Ramsden, C. A.; Scriven, E. F. V.; Taylor, R. J. K., Eds.; Elsevier Science: Amsterdam, 2008, Vol. 1, pp 1-104 (c) Sweeney, J. B. Aziridines: epoxides' ugly cousins? *Chem. Soc. Rev.* **2002**, *31*, 247-258. (d) Lapinsky, D. J. Three-Membered Ring Systems. *Prog. Heterocycl. Chem.* **2015**, *27*, 61-85. (e) Botuha, C.; Chemla, F.; Ferreira, F.; Pérez-Luna, A. Aziridines in Natural Product Synthesis, in *Heterocycles in Natural Product Synthesis*, Majumdar, K. C.; Chattopadhyay, S. K., Eds.; Wiley-VCH: Weinheim, 2011, pp 1-39. (f) Padwa, A.; Murphree, S. S. Epoxides and aziridines – A mini review. *Arkivoc* **2006**, 6-33.

(2) (a) Tomasz, M.; Mitomycin C. Small, fast and deadly (but very selective). *Chem. Biol.* **1995**, *2*, 575-579. (b) Coleman, R. S.; Li, J.; Navarro, A. Total Synthesis of Azinomycin A. *Angew. Chem. Int. Ed.* **2001**, *40*, 1736-1739. (c) Zhao, Q.; He, Q.; Ding, W.; Tang, M.; Kang, Q.; Yu, Y.; Deng, W.; Zhang, Q.; Fang, J.; Tang, G.; Liu, W. Characterization of the Azinomycin B Biosynthetic Gene Cluster Revealing a Different Iterative Type I Polyketide Synthase for Naphthoate Biosynthesis. *Chem. Biol.* **2008**, *15*, 693-705. (d) Ogasawara, Y.; Liu, H.-W. Biosynthetic Studies of Aziridine Formation in Azicemicins. *J. Am. Chem. Soc.* **2009**, *131*, 18066-18068. (e) Nakao, Y.; Fujita, M.; Warabi, K.; Matsunaga, S.; Fusetani, N. Miraziridine A, a Novel Cysteine Protease Inhibitor from the Marine Sponge *Theonella* aff. *Mirabilis*. *J. Am. Chem. Soc.* **2000**, *122*, 10462-10463. (f) Liu, Y.; Li, M.; Mu, H.; Song, S.; Zhang, Y.; Chen, K.; He, X.; Wang, H.; Dai, Y.; Lu, F.; Yan, Z.; Zhang, H. Identification and characterization of the ficellomycin biosynthesis gene cluster from *Streptomyces ficellus*. *Appl. Microbiol. Biotechnol.* **2017**, *101*, 7589-7602. (g) Foulke-Abel, J.; Agbo, H.; Zhang, H.; Mori, S.; Watanabe, C. M. H. Mode of action and biosynthesis of the azabicycle-containing natural products azinomycin and ficellomycin. *Nat. Prod. Rep.* **2011**, *28*, 693-704.

(3) (a) Ismail, F. M. D.; Levitsky, D. O.; Dembitsky, V. M. Aziridine alkaloids as potential therapeutic agents. *Eur. J. Med. Chem.* **2009**, *44*, 3373-3387. (b) Ballereau, S.; Andrieu-Abadie, N.; Saffon, N.; Génisson, Y. Synthesis and biological evaluation of aziridine-containing analogs of phytosphingosine. *Tetrahedron* **2011**, *67*, 2570-2578. (c) Dorr, R. T.; Wisner, L.; Samulitis, B. K.; Landowski, T. H.; Remers, W. A. Anti-tumor activity and mechanism of action for a cyanoaziridine-derivative, AMP423. *Cancer Chemother. Pharmacol.* **2012**, *69*, 1039-1049. (d) Pillai, B.; Cherney, M. M.; Diaper, C. M.; Sutherland, A.; Blanchard, J. S.; Vederas, J. C.; James, M. N. G. Structural insights into stereochemical inversion by diaminopimelate epimerase: An antibacterial drug target. *Proc. Natl. Acad. Sci. U.S.A.* **2006**, *103*, 8668-8673.

(4) (a) Rotstein, B. H.; Zaretsky, S.; Rai, V.; Yudin, A. K. Small Heterocycles in Multicomponent Reactions. *Chem. Rev.* **2014**, *114*, 8323-8359. (b) Huang, C.-Y. Doyle, A. G. The Chemistry of Transition Metals with Three-Membered Ring Heterocycles. *Chem. Rev.* **2014**, *114*, 8153-8198. (c) Stankovic, S.; D'hooghe, M.; Catak, S.; Eum, H.; Waroquier, M.; Van Speybroeck, V.; De Kimpe, N.; Ha, H.-J. Regioselectivity in the ring opening of non-activated aziridines. *Chem. Soc. Rev.* **2012**, *41*, 643-665. (d) Lu, P. Recent developments in regioselective ring opening of aziridines. *Tetrahedron* **2010**, *66*, 2549-2560. (e) Schneider, C. Catalytic, Enantioselective Ring Opening of Aziridines. *Angew. Chem. Int. Ed.* **2009**, *48*, 2082-2084. (f) Hu, X. E. Nucleophilic ring opening of aziridines. *Tetrahedron* **2004**, *60*, 2701-2743. (g) McCoull, W.; Davis, F. A. Recent Synthetic Applications of Chiral Aziridines. *Synthesis* **2000**, 1347-1365.

(5) (a) Moon, H. K.; Kang, S.; Yoon, H. J. Aziridine-functionalized polydimethylsiloxanes for tailorable polymeric scaffolds: aziridine as a clickable moiety for structural modification of materials. *Polym. Chem.* **2017**, *8*, 2287-2291. (b) Chen, R.; Chen, J. S.; Zhang, C.; Kessler, M. R. Rapid room-+temperature polymerization of bio-based multiaziridine-containing compounds. *RSC Adv.* **2015**, *5*, 1557-1563.

(6) (a) Degennaro, L.; Trinchera, P.; Luisi, R. Recent Advances in the Stereoselective Synthesis of Aziridines. *Chem. Rev.* **2014**, *114*, 7881-7929. (b) Pellissier, H. Recent Developments in Asymmetric Aziridination. *Adv. Synth. Catal.* **2014**, *356*, 1899-1935. (c) Pellissier, H. Recent developments in asymmetric aziridination. *Tetrahedron* **2010**, *66*, 1509-1555. (d) Singh, G. S.; D'hooghe, M.; De Kimpe, N. Synthesis and Reactivity of *C*-Heteroatom-Substituted Aziridines. *Chem. Rev.* **2007**, *107*, 2080-2135. (e) Watson, I. D. G.; Yu, L.; Yudin, A. K. Advances in Nitrogen Transfer Reactions Involving Aziridines. *Acc. Chem. Res.* **2006**, *39*, 194-206. (f) Osborn, H. M. I.; Sweeney, J. The asymmetric synthesis of aziridines. *Tetrahedron: Asymmetry* **1997**, *8*, 1693-1715. (g) Tanner, D. Chiral Aziridines–Their Synthesis and Use in Stereoselective Transformations. *Angew. Chem. Int. Ed.* **1994**, *33*, 599-619.

(7) (a) Darses, B.; Rodrigues, R.; Neuville, L. Mazurais, M.; Dauban, P. Transition metal-catalyzed iodine(III)-mediated nitrene transfer reactions: efficient tools for challenging syntheses. *Chem. Commun.* **2017**, *53*, 493-508. (b) Chang, J. W. W.; Ton, T. M. U.; Chan, P. W. H. Transition-metal-catalyzed aminations and aziridinations of C–H and C=C bonds with iminoiodinanes. *Chem. Rec.* **2011**, *11*, 331-357. (c) Karila, D.; Dodd, R. H. Recent Progress in Iminoiodane-Mediated Aziridination of Olefins. *Curr. Org. Chem.* **2011**, *15*, 1507-1538.

(8) (a) Zhu, Y.; Wang, Q.; Cornwall, R. G.; Shi, Y. Organocatalytic Asymmetric Epoxidation and Aziridination of Olefins and Their Synthetic Applications. *Chem. Rev.* **2014**, *114*, 8199-8256. (b) Zhang, Y.; Lu, Z.; Wulff, W. D. Catalytic Asymmetric Aziridination with Catalysts Derived from VAPOL and VANOL. *Synlett* **2009**, 2715-2739. (c) Yoshimura, A.; Middleton, K. R.; Zhu, C.; Nemykin, V. N.; Zhdankin, V. V. Hypoiodite-Mediated Metal-Free catalytic Aziridination of Alkenes. *Angew. Chem. Int. Ed.* **2012**, *51*, 8059-8062. (d) Siu, T.; Yudin, A. K. Practical Olefin Aziridination with a Broad Substrate Scope. *J. Am. Chem. Soc.* **2002**, *124*, 530-531.

(9) (a) Chandrachud, P. P.; Jenkins, D. M. Transition Metal Aziridination Catalysts, in *Encyclopedia of Inorganic and Bioinorganic Chemistry*; Wiley Online Library, 2017; pp. 1-11. (b) Che, C.-M.; Lo, V. K.-Y.; Zhou, C.-Y. Oxidation by Metals (Nitrene), in *Comprehensive Organic Synthesis II*, 2nd ed.; Knochel, P.; Molander, G. A., Eds.; Elsevier: Amsterdam, 2014, Vol. 7; pp. 26-85. (c) Jung, N.; Bräse, S. New Catalysts for the Transition-Metal-Catalyzed Synthesis of Aziridines. *Angew. Chem. Int. Ed.* **2012**, *51*, 5538-5540. (d) Jiang, H.; Zhang, X. P. Oxidation: C–N Bond Formation by Oxidation (Aziridines), in *Comprehensive Chirality*; Carreira, E. M.; Yamamoto, H., Eds.; Elsevier: Amsterdam, 2012, Vol. 5; pp. 168-182. (e) Mößner, C.; Bolm, C. Catalyzed Asymmetric Aziridinations, in *Transition Metals for Organic Synthesis*, 2nd ed.; Beller, M.; Bolm, C., Eds.; Wiley-VCH: Weinheim, Germany, 2004; pp. 389-402. (f) Halfen, J. A. Recent Advances in Metal-Mediated Carbon-Nitrogen Bond Formation Reactions: Aziridination and Amidation. *Curr. Org. Chem.* **2005**, *9*, 657-669. (g) Müller, P.; Fruit, C. Enantioselective Catalytic Aziridinations and Asymmetric Nitrene Insertions into CH Bonds. *Chem. Rev.* **2003**, *103*, 2905-2919.

(10) (a) Mansuy, D.; Mahy, J.-P.; Dureault, A.; Bedi, G.; Battioni, P. Iron- and manganese-porphyrin catalysed aziridination of alkenes by tosyl- and acyl-iminoiodobenzene. *J. Chem. Soc., Chem. Commun.* **1984**, 1161-1163. (b) Mahy, J.-P.; Battioni, P.; Mansuy, D. Formation of an Iron(III) Porphyrin Complex with a Nitrene Moiety Inserted into a Fe–N Bond during Alkene Aziridination by [(Tosylimido)iodo]benzene Catalyzed by Iron(III) Porphyrins. *J. Am. Chem. Soc.* **1986**, *108*, 1079-1080. (c) Mahy, J.-P.; Bedi, G.; Battioni, P.; Mansuy, D. Aziridination of alkenes catalysed by porphyrinirons: Selection of catalysts for optimal efficiency and stereospecificity. *J. Chem. Soc., Perkin Trans 2* **1988**, 1517-1524. (d) Groves, J. T.; Takahashi, T. Activation and Transfer of Nitrogen from Nitridomanganese(V) Porphyrin Complex. The Aza Analogue of Epoxidation. *J. Am. Chem. Soc.* **1983,** *105*, 2073-2074.

(11) (a) Intrieri, D.; Carminati, D. M.; Gallo, E. Recent Advances in Metal Porphyrinoid-Catalyzed Nitrene and Carbene Transfer Reactions, in *Handbook of Porphyrin Science*; Kadish, K. M.; Smith, K. M.; Guilard, R., Eds.; World Scientific, 2016, Vol. 38, pp. 1-99. (b) Anding, B. J.; Woo, L. K. An Overview of Metalloporphyrin-Catalyzed Carbon and Nitrogen Group Transfer Reactions, in *Handbook of Porphyrin Science*; Kadish, K. M.; Smith, K. M.; Guilard, R., Eds.; World Scientific, 2012, Vol. 21, pp. 145-319. (c) Ruppel, J. V.; Fields, K. B.; Snyder, N. L.; Zhang, X. P. Metalloporphyrin-Catalyzed Asymmetric Atom/Group Transfer Reactions, in *Handbook of Porphyrin Science*; Kadish, K. M.; Smith, K. M.; Guilard, R., Eds.; World Scientific, 2010, Vol. 10, pp. 1-84. (d) Fantauzzi, S.; Caselli, A.; Gallo, E. Nitrene transfer reactions mediated by metallo-porphyrin complexes. *Dalton Trans.* **2009**, 5434-5443.

(12) (a) Brandenberg, O. F.; Fasan, R.; Arnold, F. H. Exploiting and engineering hemoproteins for abiological carbene and nitrene transfer reactions. *Curr. Opin. Biotechnol.* **2017**, *47*, 102-111. (b) Farwell, C. C.; Zhang, R. K.; McIntosh, J. A.; Hyster, T. K.; Arnold, F. H. Enantioselective Enzyme-Catalyzed Aziridination Enabled by Active-Site Evolution of a Cytochrome P450. *ACS Cent. Sci.* **2015**, *1*, 89-93. (c) Gober, J. G.; Brustad, E. M. Non-natural carbenoid and nitrenoid insertion reactions catalyzed by heme proteins. *Curr. Opin. Chem. Biol.* **2016**, *35*, 124-132.

(13) (a) Li, Z.; Quan, R. W.; Jacobsen, E. N. Mechanism of the (Diimine)copper-Catalyzed Asymmetric Aziridination of Alkenes. Nitrene Transfer via Ligand-Accelerated Catalysis. *J. Am. Chem. Soc.* **1995**, *117*, 5889-5890. (b) Li, Z.; Conser, K. R.; Jacobsen, E. N. Asymmetric Alkene Aziridination with Readily Available Chiral Diimine-Based Catalysts. *J. Am. Chem. Soc.* **1993**, *115*, 5326-5327.

(14) Evans, D. A.; Faul, M. M.; Bilodeau, M. T.; Anderson, B. A.; Barnes, D. M. Bis(oxazoline)-copper complexes as chiral catalysts for the enantioselective aziridination of olefins. *J. Am. Chem. Soc.* **1993**, *115*, 5328-5329.

(15) (a) Gephart, R. T., III; Warren, T. H. Copper-Catalyzed sp^3 C–H Amination. *Organometallics* **2012**, *31*, 7728-7752. (b) Lebel, H.; Parmentier, M. Copper-catalyzed enantioselective aziridination of styrenes. *Pure App. Chem.* **2010**, *82*, 1827-1833. (c) Lebel, H.; Parmentier, M.; Leogane, O.; Ross, K.; Spitz, C. Copper bis(oxazolines) as catalysts for stereoselective aziridination of styrenes with *N*-tosyloxycarbamates. *Tetrahedron* **2012**, *68*, 3396-3409. (d) Maestre, L.; Sameera, W. M. C.; Díaz-Requejo, M. M.; Maseras, F.; Pérez, P. J. A General Mechanism for the Copper- and Silver-Catalyzed Olefin Aziridination Reactions: Concomitant Involvement of the Singlet and Triplet Pathways. *J. Am. Chem. Soc.* **2013**, *135*, 1338-1348. (e) Mairena, M. A.; Díaz-Requejo, M. M.; Belderraín, T. R.; Nicasio, M. C.; Trofimenko, S.; Pérez, P. J. Copper-Homoscorpionate Complexes as Very Active Catalysts for the Olefin Aziridination Reaction. *Organometallics* **2004**, *23*, 253-256. (f) Díaz-Requejo, M. M.; Pérez, P. J.; Brookhart, M.; Templeton, J. L. Substituent Effects on the Reaction Rates of Copper-Catalyzed Cyclopropanation and Aziridination of para-Substituted Styrenes. *Organometallics* **1997**, *16*, 4399-4402. (g) Bagchi, V.; Paraskevopoulou, P.; Das, P.; Chi, L.; Wang, Q.; Choudhury, A.; Mathieson, J. S.; Cronin, L.; Pardue, D. B.; Cundari, T. R.; Mitrikas, G.; Sanakis, Y.; Stavropoulos, P. A Versatile Tripodal Cu(I) Reagent for C–N Bond Construction via Nitrene-Transfer Chemistry: Catalytic Perspectives and Mechanistic Insights on C–H Aminations/Amidinations and Olefin Aziridinations. *J. Am. Chem. Soc.* **2014**, *136*, 11362-11381. (h) Lam, T. L.; Tso, K. C.-H.; Cao, B.; Yang, C.; Chen, D.; Chang, X.-Y.; Huang, J.-S.; Che, C.-M. Tripodal S.

(16) Ligand Complexes of Copper(I) as Catalysts for Alkene Aziridination, Sulfide Sulfimidation, and C–H Amination. *Inorg. Chem.* **2017**, *56*, 4253-4257. (i) Li, Y.; He, J.; Khankhoje, V.; Herdtweck, E.; Köhler, K.; Storcheva, O.; Cokoja, M.; Kühn, F. E. Copper(II) complexes incorporating poly/perfluorinated alkoxyaluminate-type weakly coordinating anions: Syntheses, characterization and catalytic application in stereoselective olefin aziridination. *Dalton Trans.* **2011**, *40*, 5746-5754. (j) Comba, P.; Haaf, C.; Lienke, A.; Muruganantham, A.; Wadepohl, H. Synthesis, Structure, and Highly Efficient Copper-Catalyzed Aziridination with a Tetraaza-Bispidine Ligand. *Chem. Eur. J.* **2009**, *15*, 10880-10887. (k) Wang, X.; Ding, K. One-Pot Enantioselective Aziridination of Olefins Catalyzed by a Copper(I) Complex of a Novel Diimine Ligand by Using $PhI(OAc)_2$ and Sulfonamide as Nitrene Precursors. *Chem. Eur. J.* **2006**, *12*, 4568-4575. (l) Robert-Peillard, F.; Di Chenna, P. H.; Liang, C.; Lescot, C.; Collet, F.; Dodd, R. H.; Dauban, P. Catalytic stereoselective alkene aziridination with sulfonimidamides. *Tetrahedron: Asymmetry* **2010**, *21*, 1447-1457. (m) Kundu, S.; Miceli, E.; Farquhar, E.; Pfaff, F. F.; Kuhlmann, U.; Hildebrandt, P.; Braun, B.; Greco, C.; Ray, K. Lewis Acid Trapping of an Elusive Copper–Tosylnitrene Intermediate Using Scandium Triflate. *J. Am. Chem. Soc.* **2012**, *134*, 14710-14713. (n) Ma, L.; Jiao, P.; Zhang, Q.; Du, D.-M.; Xu, J. Ligand and substrate π-stacking interaction controlled enantioselectivity in the asymmetric aziridination. *Tetrahedron: Asymmetry* **2007**, *18*, 878-884. (o) Vedernikov, A. N.; Caulton, K. G. Angular Ligand Constraint Yields an Improved Olefin Aziridination Catalyst. *Org. Lett.* **2003**, *5*, 2591-2594. (p) Evans, D. A.; Faul, M. M.; Bilodeau, M. T. Development of the Copper-Catalyzed Olefin Aziridination Reaction. *J. Am. Chem. Soc.* **1994**, *116*, 2742-2753. (q) Kwart, H.; Khan, A. A. Copper-Catalyzed Decomposition of Benzenesulfonyl Azide in Cyclohexene Solution. *J. Am. Chem. Soc.* **1967**, *89*, 1951-1953.

(17) (a) Ma, Z.; Zhou, Z.; Kürti, L. Direct and Stereospecific Synthesis of N-H and N-Alkyl Aziridines from Unactivated Olefins Using Hydroxylamine-O-Sulfonic Acids. *Angew. Chem. Int. Ed.* **2017**, *56*, 9886-9890. (b) Jat, J. L.; Paudyal, M. P.; Gao, H.; Xu, Q.-L.; Yousufuddin, M.; Devarajan, D.; Ess, D. H.; Kürti, L.; Falck, J. R. Direct Stereospecific Synthesis of Unprotected N-H and N-Me Aziridines from Olefins. *Science* **2014**, *343*, 61-65. (c) Roizen, J. L.; Harvey, M. E.; Du Bois, J. Metal-Catalyzed Nitrogen-Atom Transfer Methods for the Oxidation of Aliphatic C–H Bonds. *Acc. Chem. Res.* **2012**, *45*, 911-922. (d) Fiori, K. W.; Espino, C. G.; Brodsky, B. H.; Du Bois, J. A mechanistic analysis of the Rh-catalyzed intramolecular C–H amination reaction. *Tetrahedron* **2009**, *65*, 3042-3051. (e) Fruit, C.; Robert-Peillard, F.; Bernardinelli, G.; Müller, P.; Dodd, R. H.; Dauban, P. Diastereoselective rhodium-catalyzed nitrene transfer starting from chiral sulfonimidamide-derived iminoiodanes. *Tetrahedron: Asymmetry* **2005,** *16*, 3484-3487. (f) Müller, P.; Baud, C.; Jacquier, Y. The rhodium(III)-catalyzed aziridination of olefins with {[(4-Nitrophenyl)-sulfonyl]imino}phenyl-λ^3-iodane. *Can. J. Chem.* **1998**, *76*, 738-750. (g) Nägeli, I.; Baud, C.; Bernardinelli, G.; Jacquier, Y.; Moran, M.; Müller, P. Rhodium(II)-Catalyzed CH Insertions with {[(4-Nitrophenyl)-sulfonyl]imino}phenyl-λ^3-iodane. *Helv. Chim Acta* **1997**, *80*, 1087-1105. (h) Lebel, H.; Huard, K.; Lectard, S. *N*-Tosyloxycarbamates as a Source of Metal Nitrenes: Rhodium-Catalyzed C−H Insertion and Aziridination Reactions. *J. Am. Chem. Soc.* **2005**, *127*, 14198-14199. (i) Catino, A. J.; Nichols, J. M.; Forslund, R. E.; Doyle, M. P. Efficient Aziridination of Olefins Catalyzed by Mixed-Valent Dirhodium(II, III) Caprolactamate. *Org. Lett.* **2005**, *7*, 2787-2790. (j) Liang, J.-L.; Yuan, S.-X.; Chan, P. W. H.; Che, C.-M. Rhodium(II,II) Dimer as an Efficient Catalyst for Aziridination of Sulfonamides and Amidation of Steroids. *Org. Lett.* **2002**, *4*, 4507-4510.

(18) (a) Zdilla, M. J.; Abu-Omar, M. M. Mechanism of Catalytic Aziridination with Manganese Corrole: The Often Postulated High-Valent Mn(V) Imido Is Not the Group Transfer Reagent. *J. Am. Chem. Soc.* **2006**, *128*, 16971-16979. (b) Nishikori, H.; Katsuki, T. Catalytic and highly enantioselective aziridination of styrene derivatives. *Tetrahedron Lett.* **1996**, *37*, 9245-9248. (c) Minakata, S.; Ando, T.; Nishimura, M.; Ryu, I.; Komatsu, M. Novel Asymmetric and Stereospecific Aziridination of Alkenes with a Chiral Nitridomanganese Complex. *Angew. Chem. Int. Ed.* **1998**, *37*, 3392-3394. (d) Du Bois, J;.Hong, J.; Carreira, E. M. Nitridomanganese(V) Complexes: Design, Preparation, and Use as Nitrogen Atom-Transfer Reagents. *Acc. Chem. Res.* **1997**, *30*, 364-372. (e) Lai, T.-S,Che, C.-M.; Peng, S.-M. Catalytic and asymmetric aziridination of alkenes catalyzed by a chiral manganese porphyrin complex. *Chem. Commun.* **1997**, 2373-2374. (f) Liang, J.-L.; X.-Q.; Zhu, N.; Che, C.-M. Metalloporphyrin-Mediated Asymmetric Nitrogen-Atom Transfer to Hydrocarbons: Aziridination of Alkenes and Amidation of Saturated C−H Bonds Catalyzed by Chiral Ruthenium and Manganese Porphyrins. *Chem. Eur. J.* **2002**, *8*, 1563-1572. (g) O'Connor, K. J.; Wey, S.-J.; Burrows, C. J. Alkene aziridination and epoxidation catalyzed by chiral metal salen complexes. *Tetrahedron Lett.* **1992**, *33*, 1001-1004.

(19) (a) Damiano, C.; Intrieri, D.; Gallo, E. Aziridination of alkenes promoted by iron or ruthenium complexes. *Inorg. Chim. Acta* **2018**, *470*, 51-67. (b) Fingerhut, A.; Serdyuk, O. V.; Tsogoeva, S. B. *Non-heme iron* catalysts for epoxidation and aziridination reactions of challenging terminal alkenes: towards sustainability. *Green Chem.* **2015**, *17*, 2042-2058. (c) Correa, A.; Mancheño, O. G.; Bolm, C. Iron-catalysed carbon-heteroatom and heteroatom-heteroatom bond forming processes. *Chem. Soc. Rev.* **2008**, *37*, 1108-1117. (d) Iovan, D. A.; Betley, T. A. Characterization of Iron-Imido Species Relevant for *N*-Group Transfer Chemistry. *J. Am. Chem. Soc.* **2016**, *138*, 1983-1993. (e) Hennessy, E. T.; Liu, R. Y.; Iovan, D. A.; Duncan, R. A.; Betley, T. A. Iron-mediated intermolecular N-group transfer chemistry with olefinic substrates. *Chem. Sci.* **2014**, *5*, 1526-1532. (f) King, E. R.; Hennessy, E. T.; Betley, T. A. Catalytic C−H Bond Amination from High-Spin Iron Imido Complexes. *J. Am. Chem. Soc.* **2011**, *133*, 4917-4923. (g) Patra, R.; Coin, G.; Castro, L.; Dubourdeaux, P.; Clémancey, M.; Pécaut, J.; Lebrun, C.; Maldivi, P.; Latour, J.-M. Rational design of Fe catalysts for olefin aziridination through DFT-based mechanistic analysis. *Catal. Sci. Technol.* **2017**, *7*, 4388-4400. (h) Avenier, F.; Latour, J.-M. Catalytic aziridination of olefins and amidation of thioanisole by a non-heme iron complex. *Chem. Commun.* **2004**, 1544-1545. (i) Liu, Y.; Che, C. M. [$Fe^{III}(F_{20}$-tpp)Cl] Is an Effective Catalyst for Nitrene Transfer Reactions and Amination of Saturated Hydrocarbons with Sulfonyl and Aryl Azides as Nitrogen Source under Thermal and Microwave-Assisted Conditions. *Chem. Eur. J.* **2010**, *16*, 10494-10501. (j) Klotz, K. L.; Slominski, L. M.; Hull, A. V.; Gottsacker, V. M.; Mas-Ballesté, R.; Que, L., Jr.; Halfen, J. A. Non-heme iron(II) complexes are efficient olefin aziridination catalysts. *Chem. Commun.* **2007**, 2063-2065. (k) Klotz, K. L.; Slominski, L. M.; Riemer, M. E.; Phillips, J. A.; Halfen, J. A. Mechanism of the Iron-Mediated Alkene Aziridination reaction: Experimental and Computational Investigations. *Inorg. Chem.* **2009**, *48*, 801-803. (l) Chandrachud, P. P.; Bass, H. M.; Jenkins, D. M. Synthesis of Fully Aliphatic Aziridines with a Macrocycle Tetracarbene Iron Catalyst. *Organometallics* **2016**, *35*, 1652-1657. (m) Cramer, S. A.; Jenkins, D. M. Synthesis of Aziridines from Alkenes and Aryl Azides with a Reusable Macrocyclic Tetracarbene Iron Catalyst. *J. Am. Chem. Soc.* **2011**, *133*, 19342-19345. (n) Muñoz, S. B., Jr.: Lee, W.-T.; Dickie, D. A.; Scepaniak, J. J.; Subedi, D.; Pink, M.; Johnson, M. D.; Smith, J. M. Styrene Aziridination by Iron(IV) Nitrides. *Angew. Chem. Int. Ed.* **2015**, *54*, 10600-10603. (o) Nakanishi, M.; Salit, A.-F.; Bolm, C. Iron-Catalyzed Aziridination Reactions. *Adv. Synth. Catal.* **2008**, *350*, 1835-1840. (p) Mayer, A. C.; Salit, A.-F.; Bolm, C. Iron-catalysed aziridination reactions promoted by an ionic liquid. *Chem. Commun.* **2008**, 5975-5977. (q) Heuss, B. D.; Mayer, M. F.; Dennis, S.; Hossain, M. M. Iron mediated nitrenoid transfer: $[(\eta^5\text{-}C_5H_5)Fe(CO)_2(THF)]^+[BF_4]^-$ catalyzed aziridination of olefins. *Inorg. Chim. Acta* **2003**, *342*, 301-304.

(20) (a) Subbarayan, V.; Jin, L.-M.; Cui, X.; Zhang, X. P. Room temperature activation of aryloxysulfonyl azides by [Co(II)(TPP)] for selective radical aziridination of alkenes via metalloradical catalysis. *Tetrahedron Lett.* **2015**, *56*, 3431-3434. (b) Tao, J.; Jin, L.-M.; Zhang, X. P. Synthesis of chiral N-phosphoryl aziridines through enantioselective aziridination of alkenes with phosphoryl azide via Co(II)-based metalloradical catalysis. *Beilstein J. Org. Chem.* **2014**, *10*, 1282-1289. (c) Jin, L.-M.; Xu, X.; Lu, H.; Cui, X.; Wojtas, L.; Zhang, X. P. Effective Synthesis of Chiral *N*-Fluoroaryl Aziridines through Enantioselective Aziridination of Alkenes with Fluoroaryl Azides. *Angew. Chem. Int. Ed.* **2013**, *52*, 5309-5313. (d) Suarez, A. I. O.; Jiang, H.; Zhang, X. P.; de Bruin, B. The radical mechanism of cobalt(II) porphyrin-catalyzed olefin aziridination and the importance of cooperative H-bonding. *Dalton Trans.* **2011**, *40*, 5697-5705. (e) Subbarayan, V.; Ruppel, J. V.; Zhu, S.; Perman, J. A.; Zhang, X. P. Highly asymmetric cobalt-catalyzed aziridination of alkenes with trichloroethoxysulfonyl azide ($TcesN_3$). *Chem. Commun.* **2009**, 4266-4268. (f) Jones, J. E.; Ruppel, J. V.; Gao, G.-Y.; Moore, T. M.; Zhang, X. P. Cobalt-Catalyzed Asymmetric Olefin Aziridination with Diphenylphosphoryl Azide. *J. Org. Chem.* **2008**, *73*, 7260-7265. (g) Ruppel, J. V.; Jones, J. E.; Huff, C. A.; Kamble, R. M.; Chen, Y.; Zhang, X. P. A Highly Effective Cobalt Catalyst for Olefin Aziridination with Azides: Hydrogen Bonding Guided Catalyst Design. *Org. Lett.* **2008**, *10*, 1995-1998. (h) Gao, G.-Y.; Jones, J. E.; Vyas, R.; Harden, J. D.; Zhang, X. P. Cobalt-Catalyzed Aziridination with Diphenylphosphoryl Azide (DPPA): Direct Synthesis of *N*-Phosphorus-Substituted Aziridines from Alkenes. *J. Org. Chem.* **2006**, *71*, 6655-6658. (i) Gao, G.-Y.; Harden, J. D.; Zhang, X. P. Cobalt-Catalyzed Efficient Aziridination of Alkenes. *Org. Lett.* **2005**, *7*, 3191-3193. (j) Caselli, A.; Gallo, E.; Fantauzzi, S.; Morlacchi, S.; Ragaini, F.; Cenini, S. Allylic Amination and Aziridination of Olefins by Aryl Azides Catalyzed by Co^{II}(tpp): A Synthetic and Mechanistic Study. *Eur. J. Inorg. Chem.* **2008**, 3009-3019. (k) Caselli, A.; Gallo, E.; Ragaini, F.; Ricatto, F.; Abbiati, G.; Cenini, S. Chiral porphyrin complexes of cobalt(II) and ruthenium(II) in catalytic cyclopropanation and amination reactions. *Inorg. Chim. Acta* **2006**, *359*, 2924-2932. (l) Cenini, S.; Tollari, S.; Penoni, A.; Cereda, C. Catalytic amination of unsaturated hydrocarbons: reactions of p-nitrophenylazide with alkenes catalyzed by metallo-porphyrins. *J. Mol. Catal. A: Chem.* **1999**, *137*, 135-146.

(21) (a) Waterman, R.; Hillhouse, G. L. Group Transfer from Nickel Imido, Phosphinidine, and Carbene Complexes to Ethylene with Formation of Aziridine, Phosphirane, and Cyclopropane Products. *J. Am. Chem. Soc.* **2003**, *125*, 13350-13351. (b) Lin, B. L.; Clough, C. R.; Hillhouse, G. L. Interactions of Aziridines with Nickel Complexes: Oxidative-Addition and Reductive-Elimination Reactions that Break and Make C–N Bonds. *J. Am. Chem. Soc.* **2002**, *124*, 2890-2891.

(22) (a) Uchida, T.; Katsuki, T. Asymmetric Nitrene Transfer Reactions: Sulfimidation, Aziridination and C–H Amination Using Azide Compounds as Nitrene Precursors. *Chem. Rec.* **2014**, *14*, 117. (b) Kim, C.; Uchida, T.; Katsuki, T. Asymmetric olefin aziridination using a newly designed Ru(CO)(salen) complex as the catalyst. *Chem. Commun.* **2012**, *48*, 7188. (c) Kawabata, H.; Omura, K.; Uchida, T.; Katsuki, T. Construction of Robust Ru(salen)(CO) Complexes and Asymmetric Aziridination with Nitrene Precursors in the Form of Azide Compounds That Bear Easily Removable *N*-Sulfonyl Groups. *Chem. Asian J.* **2007**, *2*, 248-256. (d) Harvey, M. E.; Musaev, D.; Du Bois, J. A Diruthenium Catalyst for Selective, Intramolecular Allylic C–H Amination: Reaction Development and Mechanistic Insight Gained through Experiment and Theory. *J. Am. Chem. Soc.* **2011**, *133*, 17207. (e) Chan, K.-H.; Guan, X.; Lo, V. K.-Y.; Che, C.-M. Elevated Catalytic Activity of Ru(II)–Porphyrin-Catalyzed Carbene/Nitrene Transfer and Insertion Reactions with N-Heterocyclic Carbene Ligands. *Angew. Chem. Int. Ed.* **2014**, *53*, 2982-2987. (f) Leung, S. K.-Y.; Tsui, W.-M.; Huang, J.-S.; Che, C.-M.; Liang, J.-L.; Zhu, N. Imido Transfer from Bis(imido)Ru(VI) Porphyrins to Hydrocarbons: Effect of Imido Substituents, C−H Bond Dissociation Energies, and $Ru^{VI/V}$ Reduction Potentials. *J. Am. Chem. Soc.* **2005**, *127*, 16629-16640. (g) Au, S.-M.; Huang, J.-S.; Yu, W.-Y.; Fung, W.-H.; Che, C.-M. Aziridination of Alkenes and Amidation of Alkanes by Bis(tosylimido)Ru(VI) Porphyrins. A Mechanistic Study. *J. Am. Chem. Soc.* **1999**, *121*, 9120-9132. (h) Fantauzzi, S.; Ragaini, F.; Re, N.; Cenini, S. Rearrangement of *N*-Aryl-2-Vinylaziridines to Benzoazepines and Dihydropyrroles: A Synthetic and Theoretical Study. *Chem. Eur. J.* **2009**, *15*, 1241-1251. (i) Fantauzzi, S.; Gallo, E.; Caselli, A.; Piangiolino, C.; Ragaini, F.; Cenini, S. The (Porphyrin)ruthenium-Catalyzed Aziridination of Olefins Using Aryl Azides as Nitrogen Sources. *Eur. J. Org. Chem.* **2007**, 6053-6059. (j) Fantauzzi, S.; Cenini, S. Origin of the Deactivation in Styrene Aziridination by Aryl Azides, Catalyzed by Ruthenium Porphyrin Complexes. Structural Characterization of a Δ^2-1,2,3-triazoline Ru^{II}(TPP)CO Complex. *Organometallics* **2005**, *24*, 4710-4713. (k) Zardi, P.; Pozzoli, A.; Ferretti, F.; Manca, G.; Mealli, C.; Gallo, E. A mechanistic investigation of the ruthenium porphyrin catalyzed aziridination of olefins by aryl azides. *Dalton Trans.* **2015**, *44*, 10479-10489. (l) Manca, G.; Gallo, E.; Intrieri, D.; Mealli, C. DFT Mechanistic Proposal of the Ruthenium Porphyrin-Catalyzed Allylic Amination by Organic Azides. *ACS Catal.* **2014**, *4*, 823-832.

(23) (a) Okamoto, K.; Oda, T.; Kohigashi, S.; Ohe, K. Palladium-catalyzed Decarboxylative Intramolecular Aziridination from 4*H*-Isoxazol-5-ones Leading to 1-Azabicyclo[3.1.0]hex-2-enes. *Angew. Chem. Int. Ed.* **2011**, *50*, 11470-11473. (b) Han, J.; Li, Y.; Zhi, S.; Pan, Y.; Timmons, C.; Li, G. Palladium-catalyzed aziridination of alkenes using *N*,*N*-dichloro-p-toluenesulfonamide as nitrogen source. *Tetrahedron Lett.* **2006**, *47*, 7225-7228. (c) Timsina, Y. N.; Gupton, B. F.; Ellis, K. C. Palladium-Catalyzed C–H Amination of $C(sp^2)$ and $C(sp^3)$–H Bonds: Mechanism and Scope for N-Based Molecule Synthesis. *ACS Catal.* **2018**, *8*, 5732-5776.

(24) (a) Li, Z.; He, C. Recent Advances in Silver-Catalyzed Nitrene, Carbene, and Silylene-Transfer Reactions. *Eur. J. Org. Chem.* **2006**, 4313-4322. (b) Cui, Y.; He, C. Efficient Aziridination of Olefins Catalyzed by a Unique Disilver(I) Compound. *J. Am. Chem. Soc.* **2003**, *125*, 16202-16203. (c) Llaveria, J.; Beltrán, Á.; Díaz-Requejo, M. M.; Matheu, M. I.; Castillón, S.; Pérez, P. J. Efficient Silver-Catalyzed Regio-and Stereospecific Aziridination of Dienes. *Angew. Chem. Int. Ed.* **2010**, *49*, 7092-7095. (d) Ju, M.; Weatherly, C. D.; Guzei, I. A.; Schomaker, J. M. Chemo- and Enantioselective Intramolecular Silver-Catalyzed Aziridinations. *Angew. Chem. Int. Ed.* **2017**, *56*, 9944-9948. (e) Dolan, N. S.; Scamp, R. J.; Yang, T.; Berry, J. F.; Schomaker, J. M. Catalyst-Controlled and Tunable, Chemoselective Silver-catalyzed Intermolecular Nitrene Transfer: Experimental and Computational Studies. *J. Am. Chem. Soc.* **2016**, *138*, 14658-14667. (f) Rigoli, J. W.; Weatherly, C. D.; Alderson, J. M.; Vo, B. T.; Schomaker, J. M. Tunable, Chemoselective Amination via Silver Catalysis. *J. Am. Chem. Soc.* **2013**, *135*, 17238-17241. (g) Huang, M.; Corbin, J. R.; Dolan, N. S.; Fry, C. G.; Vinokur, A. I.; Guzei, I. A.; Schomaker, J. M. Synthesis, Characterization, and Variable-Temperature NMR Studies of Silver(I) Complexes for Selective Nitrene Transfer. *Inorg. Chem.* **2017**, *56*, 6725-6733. (h) Weatherly, C.; Alderson, J. M.; Berry, J. F.; Hein, J. E.; Schomaker, J. M. Catalyst-Controlled Nitrene Transfer by Tuning Metal:Ligand Ratios: Inshight into the Mechanisms of Chemoselectivity. *Organometallics* **2017**, *36*, 1649-1661. (i) Rigoli, J. W.; Weatherly, C. D.; Vo, B. T.; Neale, S.; Meis, A. R.; Schomaker, J. M. Chemoselective Allene Aziridination via Ag(I) Catalysis. *Org. Lett.* **2013**, *15*, 290-293. (j) Scamp, R. J.; Rigoli, J. W.; Schomaker, J. M. Chemoselective silver-catalyzed nitrene insertion reactions. *Pure Appl. Chem.* **2014**, *86*, 381-393.

(25) (a) Li, Z.; Ding, X.; He, C. Nitrene Transfer Reactions Catalyzed by Gold Complexes. *J. Org. Chem.* **2006**, *71*, 5876-5880. (b) Deng, X.; Baker, T. A.; Friend, C. M. A Pathway for NH Addition to Styrene Promoted by Gold. *Angew. Chem. Int. Ed.* **2006**, *45*, 7075-7078.

(26) Park, Y.; Kim, Y.; Chang, S. Transition Metal-Catalyzed C–H Amination: Scope, Mechanism, and Applications. *Chem. Rev.* **2017**, *117*, 9247-9301.

(27) (a) Chanda, B. M.; Vyas, R.; Landge, S. S. Synthesis of aziridines using new catalytic systems with bromamine-T as the nitrene source. *J. Mol. Catal. A: Chem.* **2004**, *223*, 57-60. (b) Chanda, B. M.; Vyas, R.; Bedekar, A. V. Investigations in the Transition Metal catalyzed Aziridination of Olefins, Amination, and Other Insertion Reactions with Bromamine-T as the Source of Nitrene. *J. Org. Chem.* **2001**, *66*, 30-34.

(28) Driver, T. G. Recent advances in transition metal-catalyzed *N*-atom transfer reactions of azides. *Org. Biomol. Chem.* **2010**, *8*, 3831-3846.

(29) (a) Li, L.; Zhang, J. Lewis Acid-catalyzed [3+2]Cyclo-addition of Alkynes with N-Tosyl-aziridines via Carbon–Carbon Bond Cleavage: Synthesis of Highly Substituted 3-Pyrrolines. *Org. Lett.* **2011**, *13*, 5940-5943. (b) Dauban, P.; Dodd, R. H. PhI=NSes: A New Iminoiodinane Reagent for the Copper-Catalyzed Aziridination of Olefins. *J. Org. Chem.* **1999**, *64*, 5304-5307. (c) Alonso, D. A.; Andersson, P. G. Deprotection of Sulfonyl Aziridines. *J. Org. Chem.* **1998**, *63*, 9455-9461. (d) Bergmeier, S. C.; Seth, P. P. A general method for deprotection of *N*-toluenesulfonyl aziridines using sodium naphthalenide. *Tetrahedron Lett.* **1999**, *40*, 6181-6184.

(30) Warner, D. L.; Hibberd, A. M.; Kalman, M.; Klapars, A.; Vedejs, E. *N*-Silyl Protecting Groups for Labile Aziridines: Application toward the Synthesis of *N*-H Aziridinomitosenes. *J. Org. Chem.* **2007**, *72*, 8519-8522.

(31) Stavropoulos, P. Metal-Catalyzed and Metal-Free Intermolecular Amination of Light Alkanes and Benzenes. *Comm. Inorg. Chem.* **2017**, *37*, 1-57.

(32) (a) Hazelard, D.; Nocquet, P.-A.; Compain, P. Catalytic C–H amination at its limits: challenges and solutions. *Org. Chem. Front.* **2017**, *4*, 2500-2521. (b) Collet, F.; Lescot, C.; Dauban, P. Catalytic C–H amination: the stereoselectivity issue. *Chem. Soc. Rev.* **2011**, *40*, 1926-1936. (c) Zalatan, D.N.; Du Bois, J. Metal-Catalyzed Oxidations of C–H to C–N Bonds. *Top. Curr. Chem.* **2010**, *292*, 347-378. (d) Díaz-Requejo, M. M.; Pérez, P. J. Coinage Metal Catalyzed C−H Bond Functionalization of Hydrocarbons. *Chem Rev.* **2008**, *108*, 3379-3394.

(33) Palucki, M.; Finney, N. S.; Pospisil, P. J.; Güler, M. L.; Ishida, T.; Jacobsen, E. N. The Mechanistic Basis for Electronic Effects on Enantioselectivity in the (salen)Mn(III)-Catalyzed Epoxidation Reaction. *J. Am. Chem. Soc.* **1998**, *120*, 948-954.

(34) (a) Paradine, S. M.; Griffin, J. R.; Zhao, J.; Petronico, A. L.; Miller, S. M.; White, M. C. A manganese catalyst for highly reactive yet chemoselective intramolecular C(sp^3)–H amination. *Nat. Chem.* **2015**, *7*, 987-994. (b) Clark, J. R.; Feng, K.; Sookezian, A.; White, M. C. Manganese-catalysed benzylic C(sp^3)–H amination for late-stage functionalization. *Nat. Chem.* **2018**, *10*, 583-591.

(35) (a) Zalatan, D. N.; Du Bois, J. A Chiral Rhodium Carboxamidate Catalyst for Enantioselective C–H Amination. *J. Am. Chem. Soc.* **2008**, *130*, 9220-9221. (b) Zhang, X.; Xu, H.; Zhao, C. Mechanistic Investigation of Dirhodium-Catalyzed Intramolecular Allylic C–H Amination versus Alkene Aziridination. *J. Org. Chem.* **2014**, *79*, 9799-9811.

(36) (a) Liu, Y.; Guan, X.; Wong, E. L.-M.; Liu, P.; Huang, J.-S.; Che, C.-M. Nonheme Iron-Mediated Amination of C(sp^3)–H Bonds. Quinquepyridine-Supported Iron-Imide/Nitrene Intermediates by Experimental Studies and DFT Calculations. *J. Am. Chem. Soc.* **2013**, *135*, 7194-7204. (b) Paradine, S. M.; White, M. C. Iron-Catalyzed Intramolecular Allylic C–H Amination. *J. Am. Chem. Soc.* **2012**, *134*, 2036-2039.

(37) (a) Lu, H.; Lang, K.; Jiang, H.; Wojtas, L.; Zhang, X. P. Intramolecular 1,5-C(sp^3)–H radical amination *via* Co(II)-based metalloradical catalysis for five-membered cyclic sulfamides. *Chem. Sci.* **2016**, *7*, 6934-6939. (b) Lu, H.; Jiang, H.; Hu, Y.; Wojtas, L.; Zhang, X. P. Chemoselective intramolecular allylic C–H amination *versus* C=C aziridination through Co(II)-based metalloradical catalysis. Chem. *Sci.* **2011**, *2*, 2361-2366. (c) Lyaskovskyy, V.; Suarez, A. I. O.; Lu, H.; Jiang, H.; Zhang, X. P.; de Bruin, B. Mechanism of Cobalt(II) Porphyrin-Catalyzed C–H Amination with Organic Azides: Radical Nature and H-Atom Abstraction Ability of the Key Cobalt(III)–Nitrene Intermediates. *J. Am. Chem. Soc.* **2011**, *133*, 12264-12273.

(38) (a) Xiao, W.; Wei, J.; Zhou, C.-Y.; Che, C.-M. [Ru^{IV}(F_{20}-TPP)Cl_2] efficiently catalysed inter- and intra-molecular nitrene insertion into sp^3 C–H bonds of hydrocarbons using phosphoryl azides as nitrene sources. *Chem. Commun.* **2013**, *49*, 4619-462. (b) Milczek, E.; Boudet, N.; Blakey, S. Enantioselective C–H Amination Using Cationic Ruthenium(II)–pybox Catalysts. *Angew. Chem. Int. Ed.* **2008**, *47*, 6825-6828.

(39) (a) Varela-Álvarez, A.; Musaev, D. G. Rh_2(II,III) Catalysts with Chelating Carboxylate and Carboxamidate Supports: Electronic Structure and Nitrene Transfer Reactivity. *J. Am. Chem. Soc.* **2016**, *138*, 2327-2341. (b) Kornecki, K. P.; Berry, J. F. Evidence for a One-Electron Mechanistic Regime in Dirhodium-Catalyzed Intermolecular C–H Amination. *Chem. Eur. J.* **2011**, *17*, 5827-5832. (c) Kornecki, K. P.; Introducing a mixed-valent dirhodium((II,III) catalyst with increased stability in C–H amination. *Chem. Commun.* **2012**, *48*, 12097-12099.

(40) (a) Alderson, J. M.; Corbin, J. R.; Schomaker, J. M. Tunable, Chemo-and Site-Selective Nitrene Transfer Reactions through the Rational Design of Silver(I) Catalysts. *Acc. Chem. Res.* **2017**, *50*, 2147-2158. (b) Du Bois, J. Rhodium-Catalyzed C–H Amination. An Enabling Method for Chemical Synthesis. *Org. Process Res. Dev.* **2011**, *15*, 758-762. (c) Collet, F.; Lescot, C.; Liang, C.; Dauban, P. Studies in catalytic C–H amination involving nitrene C–H insertion. *Dalton Trans.* **2010**, *39*, 10401-10413.

(41) Xu, Q.; Appella, D. H. Aziridination of Aliphatic Alkenes Catalyzed by *N*-Heterocyclic Carbene Copper Complexes. *Org. Lett.* **2008**, *10*, 1497-1500.

(42) (a) Kuijpers, P. F.; van der Vlugt, J. I.; Schneider, S.; de Bruin, B. Nitrene Radical Intermediates in Catalytic Synthesis. *Chem. Eur. J.* **2017**, *23*, 13819-13829. (b) Xiong, T.; Zhang, Q. New amination strategies based on nitrogen-centered radical chemistry. *Chem. Soc. Rev.* **2016**, *45*, 3069-3087.

(43) (a) Liang, S.; Jensen, M. P. Half-Sandwich Scorpionates as Nitrene Transfer Catalysts. *Organometallics* **2012**, *31*, 8055-8058. (b) Yan, S.-Y.; Wang, Y.; Shu, Y.-J.; Liu, H.-H.; Zhou, X.-G. Nitrene transfer reaction catalyzed by substituted metallophthalocyanines. *J. Mol. Catal. A: Chem.* **2006**, *248*, 148-151.

(44) Mat Lani, A. S.; Schomaker, J. M. Site-Selective, Catalyst-Controlled Alkene Aziridination. *Synthesis* **2018**, DOI: 10.1055/s-0037-1609858.

(45) (a) Jones, M. B.; MacBeth, C. E. Tripodal Phenylamine-Based Ligands and Their Co^{II} Complexes. *Inorg. Chem.* **2007**, *46*, 8117-8119. (b) Çelenligil-Çetin, R.; Paraskevopoulou, P.; Dinda, R.; Staples, R. J.; Sinn, E.; Rath, N. P.; Stavropoulos, P. Synthesis, Characterization, and Reactivity of Iron Trisamidoamine Complexes that Undergo both Metal- and Ligand-Centered Oxidative Transformations. *Inorg. Chem.* **2008**, *47*, 1165-1172. (c) Çelenligil-Çetin, R. *Synthesis, Characterization, and Reactivity of Iron Complexes with N-Donor Ligands in Relation to Oxygenation of Hydrocarbons*, Ph.D. Thesis, Boston University, Boston, MA, **2004**.

(46) (a) Paraskevopoulou, P.; Lin, A.; Wang, Q.; Pinnapareddy, D.; Acharrya, R.; Dinda, R.; Çelenligil-Çetin, R.; Floros, G.; Sanakis, Y.; Choudhury, A.; Rath, N. P.; Stavropoulos, P. Synthesis and Characterization of a Series of Structurally and Electronically Diverse Fe(II) Complexes Featuring a Family of Triphenylamido-amine Ligands. *Inorg. Chem.* **2010**, *49*, 108-122. (b) Pinnapareddy, D. *Synthesis and Characterization of Metal Reagents Mediating C–X Activation (X = Cl, H) of Hydrocarbons*, Ph.D. Thesis, University of Missouri-Rolla, Rolla, MO, **2007**.

(47) (a) Jones, M. B.; Hardcastle, K. I.; MacBeth, C. E. Synthetic, spectral and structural studies of mononuclear tris(κ^2-amidate) aluminium complexes supported by tripodal ligands. *Polyhedron* **2010**, *29*, 116-119. (b) Jones, M. B.; Hardcastle, K. I.; Hagen, K. S.; MacBeth, C. E. Oxygen Activation and Intramolecular C–H Bond Activation by an Amidate-Bridged Diiron(II) Complex. *Inorg. Chem.* **2011**, *50*, 6402-6404. (c) Villanueva, O.; Weldy, N. M.; Blakey, S. B.; MacBeth, C. E. Cobalt catalyzed sp^3 C–H amination utilizing aryl azides. *Chem. Sci.* **2015**, *6*, 6672-6675.

(48) Bagchi, V.; Raptopoulos, G.; Das, P.; Christodoulou, S.; Wang, Q.; Ai, L.; Choudhury, A.; Pitsikalis, M.; Paraskevopoulou, P.; Stavropoulos, P. Synthesis and characterization of a family of Co(II) triphenylamido-amine complexes and catalytic activity in controlled radical polymerization of olefins. *Polyhedron* **2013**, *52*, 78-90.

(49) (a) Hartwig, J. F.; Kawatsura, M.; Hauck, S. I.; Shaughnessy, K. H.; Alcazar-Roman, L. M. Room-Temperature Palladium-Catalyzed Amination of Aryl Bromides and Chlorides and Extended Scope of Aromatic C–N Bond Formation with a Commercial Ligand. *J. Org. Chem.* **1999**, *64*, 5575-5580. (b) Wolfe, J. P.; Buchwald, S. L. Scope and Limitations of the Pd/BINAP-Catalyzed Amination of Aryl Bromides. *J. Org. Chem.* **2000**, *65*, 1144-1157.

(50) Çelenligil-Çetin, R.; Paraskevopoulou, P.; Lalioti, N.; Sanakis, Y.; Staples, R. J.; Rath, N. P.; Stavropoulos, P. Metalloradical Complexes of Manganese and Chromium Featuring an Oxidatively Rearranged Ligand. *Inorg. Chem.* **2008**, *47*, 10998-11009.

(51) Addison, A. W.; Rao, T. N.; Reedijk, J.; van Rijn, J.; Verschoor, G. C. Synthesis, structure, and spectroscopic properties of copper(II) compounds containing nitrogen-sulfur donor ligands; the crystal and molecular structure of aqua[1,7-bis(*N*-methylbenzimidazol-2′-yl)-2,6-dithiaheptane]copper(II) perchlorate. *J. Chem. Soc., Dalton Trans.* **1984**, 1349-1356.

(52) Fukin, G. K.; Lindeman, S. V.; Kochi, J. K. Molecular Structures of Cations•••π-(Arene) Interactions for Alkali Metals with π- and σ-Modalities. *J. Am. Chem. Soc.* **2002**, *124*, 8329-8336.

(53) Çelenligil-Çetin, R.; Paraskevopoulou, P.; Dinda, R.; Lalioti, N.; Sanakis, Y.; Rawashdeh, A. M.; Staples, R. J.; Sinn, E.; Stavropoulos, P. Oxidative Ligand Rearrangement due to Incipient Aminyl Radicals in the Oxidation of Iron(II) Species with Dioxygen. *Eur. J. Inorg. Chem.* **2008**, 673-677.

(54) Al-Ajlouni, A.; Espenson, J. H. Epoxidation of Styrenes by Hydrogen Peroxide As Catalyzed by Methylrhenium Trioxide. *J. Am. Chem. Soc.* **1995**, *117*, 9243-9250.

(55) Souto, J. A.; Zian, D.; Muñiz, K. Iodine(III)-Mediated Intermolecular Allylic Amination under Metal-Free Conditions. *J. Am. Chem. Soc.* **2012**, *134*, 7242-7245.

(56) Müller, P.; Baud, C.; Jacquier, Y. A Method for Rhodium(II)-Catalyzed Aziridination of Olefins. *Tetrahedron* **1996**, *52*, 1543-1548.

(57) Jiang, X.-K. Establishment and Successful Application of the σ_{JJ}• Scale of Spin-Delocalization Substituent Constants. *Acc. Chem. Res.* **1997**, *30*, 283-289.

(58) Dinçtürk, S.; Jackson, R. A. Free radical reactions in solution. Part 7. Substituent effects on free radical reactions: comparison of the σ• scale with other measures of radical stabilization. *J. Chem. Soc., Perkin Trans. 2* **1981**, 1127-1131.

(59) Han, H.; Park, S. B.; Kim, S. K.; Chang, S. Copper–Nitrenoid Formation and Transfer in Catalytic Olefin Aziridination Utilizing Chelating 2-Pyridylsulfonyl Moieties. *J. Org. Chem.* **2008**, *73*, 2862-2870.

(60) Liu, P.; Wong, E. L.-M.; Yuen, A. W.-H.; Che, C.-M. Highly Efficient Alkene Epoxidation and Aziridination catalyzed by Iron(II) Salt + 4,4′,4″-Trichloro-2,2′:6′,2″-terpyridine/4,4″-Dichloro-4′-*O*-PEG-OCH_3-2,2′:6′,2″-terpyridine. *Org. Lett.* **2008**, *10*, 3275-3278.

(61) Moreau, Y.; Chen, H.; Derat, E.; Hirao, H.; Bolm, C.; Shaik, S. NR Transfer Reactivity of Azo-Compound I of P450. How Does the Nitrogen Substituent Tune the Reactivity of the Species toward C–H and C=C Activation? *J. Phys. Chem. B* **2007**, *111*, 10288-10299.

(62) (a) Ogliaro, F.; Harris, N.; Cohen, S.; Filatov, M.; de Visser, S. P.; Shaik, S. A Model "Rebound" Mechanism of Hydroxylation by Cytochrome P450: Stepwise and Effectively Concerted Pathways, and Their Reactivity Patterns. *J. Am. Chem. Soc.* **2000**, *122*, 8977-8989. (b) Shaik, S.; de Visser, S. P.; Ogliaro, F.; Schwarz, H.; Schröder, D. Two-state reactivity mechanisms of hydroxylation and epoxidation by cytochrome P-450 revealed by theory. *Curr. Opin. Chem. Biol.* **2002**, *6*, 556-567.

(63) (a) Marvell, E. N.; Lin, C. The Aromatic Cope Rearrangement. Thermal Reactions of *cis*-1-Aryl-2-vinylcyclopropanes. *J. Am. Chem. Soc.* **1978**, *100*, 877-883. (b) Goh, S. H.; Closs, L. E.; Closs, G. L. Carbenoid Decomposition of Aryldiazomethanes with Lithium and Zinc Halides. A Convenient Method for the Synthesis of Arylcyclopropanes. *J. Org. Chem.* **1969**, *34*, 25-31. (c) Feldman, K. S.; Simpson, R. E. Oxygenation of Substituted Vinylcyclopropanes: Preparative and Mechanistic Studies. *J. Am. Chem. Soc.* **1989**, *111*, 4878-4886. (d) Ganesh, V.; Kundu, T.; Chandrasekaran, S. Electrophile-Induced C–C Bond Activation of Vinylcyclopropanes for the Synthesis of Z-Alkylidenetetrahydrofurans. *J. Org. Chem.* **2013**, *78*, 380-399.

(64) (a) Fu, H.; Look, G. C.; Zhang, W.; Jacobsen, E. N.; Wong, C.-H. Mechanistic Study of a Synthetically Useful Monooxygenase Model Using the Hypersensitive Probe *trans*-2-Phenyl-1-vinylcyclopropane. *J. Org. Chem.* **1991**, *56*, 6497-6500. (b) Baik, J. S.; Lee, N. H. Mechanistic Studies on the O_2-mediated Oxidation of Olefins in the Presence of (Schiff-base)Mn(III) Catalyst and $NaBH_4$. *Bull. Korean Chem. Soc.* **2006**, *27*, 765-768. (c) Lu, D.-F.; Zhu, C.-L.; Sears, J. D.; Xu, H. Iron(II)-Catalyzed Intermolecular Aminofluorination of Unfunctionalized Olefins Using Fluoride Ion. *J. Am. Chem. Soc.* **2016**, *138*, 11360-11367. (d) Yuan, Y.-A.; Lu, D.-F.; Chen, Y.-R.; Xu, H. Iron-Catalyzed Direct Diazidation for a Broad Range of Olefins. *Angew. Chem. Int. Ed.* **2016**, *55*, 534-538. (e) Hiraoka, T.; Yano, S.; Hara, S. Iodoazidation of Alkenes by Using Iodine Pentafluoride–Pyridine–Hydrogen Fluoride and Trimethylsilyl Azide. *Synthesis* **2016**, *48*, 1353-1358. (f) Taniguchi, T.; Zaimoku, H.; Ishibashi, H. A Mild Oxidative Aryl Radical Addition into Alkenes by Aerobic Oxidation of Arylhydrazines. *Chem. Eur. J.* **2011**, *17*, 4307-4312. (g) Tokuyasu, T.; Kunikawa, S.; Masuyama, A.; Nojima, M. Co(III)–Alkyl Complex- and Co(III)–Alkylperoxo Complex-Catalyzed Triethylsilylperoxidation of Alkenes with Molecular Oxygen and Triethylsilane. *Org. Lett.* **2002**, *4*, 3595-3598.

(65) (a) Newcomb, M.; Johnson, C. C.; Manek, M. B.; Varick, T. R. Picosecond Radical Kinetics. Ring Openings of Phenyl Substituted Cyclopropylcarbinyl Radicals. *J. Am. Chem. Soc.* **1992**, *114*, 10915-10921. (b) Nonhebel, D. C. The chemistry of cyclopropylmethyl and related radicals. *Chem. Soc. Rev.* **1993**, *22*, 347-359.

(66) P. S.; Raje, V. P.; Dourado, J.; Gordo, J. Catalyst-free aziridination and unexpected homologation of aziridines from imines. *Org. Biomol. Chem.* **2010**, *8*, 2968-2974.

(67) (a) Lansky, D. E.; Kosack, J. R.; Sarjeant, A. A. N.; Goldberg, D. P. An Isolable, Nonreducible High-Valent Manganese(V) Imido Corrolazine Complex. *Inorg. Chem.* **2006**, *45*, 8477-8479. (b) Eikey, R. A.; Khan, S. I.; Abu-Omar, M. M. The Elusive Terminal Imido of Manganese(V). *Angew. Chem. Int. Ed.* **2002**, *41*, 3592-3595.

(68) (a) Bucinsky, L.; Breza, M.; Lee, W.-T.; Hickey, A. K.; Dickie, D. A.; Nieto, I.; DeGayner, J. A.; Harris, T. D.; Meyer, K.; Krzystek, J.; Ozarowski, A.; Nehrkorn, J.; Schnegg, A.; Holldack, K.; Herber, R. H.; Telser, J.; Smith, J. M. Spectroscopic and Computational Studies of Spin States of Iron(IV) Nitrido and Imido Complexes. *Inorg. Chem.* **2017**, *56*, 4751-4768. (b) Hong, S.; Lu, X.; Lee, Y.-M.; Seo, M. S.; Ohta, T.; Ogura, T.; Clémancey, M.; Maldivi, P.; Latour, J.-M.; Sarangi, R.; Nam, W. Achieving One-Electron Oxidation of a Mononuclear Nonheme Iron(V)-Imido Complex. *J. Am. Chem. Soc.* **2017**, *139*, 14372-14375. (c) Hong, S.; Sutherlin, K. D.; Vardhaman, A. K.; Yan, J. J.; Park, S.; Lee, Y.-M.; Jang, S.; Lu, X.; Ohta, T.; Ogura, T.; Solomon, E. I.; Nam, W. A Mononuclear Nonheme Iron(V)-Imido Complex. *J. Am. Chem. Soc.* **2017**, *139*, 8800-8803. (d) Gouré, E.; Senthilnathan, D.; Coin, G.; Albrieux, F.; Avenier, F.; Dubourdeaux, P.; Lebrun, C.; Maldivi, P.; Latour, J.-M. Redox Self-Adaptation of a Nitrene Transfer Catalyst to the Substrate Needs. *Angew. Chem. Int. Ed.* **2017**, *56*, 4305-4309. (e) Leeladee, P.; Jameson, G. N. L.; Siegler, M. A.; Kumar, D.; de Visser, S. P.; Goldberg, D. P. Generation of a High-Valent Iron Imido Corrolazine Complex and NR Group Transfer Reactivity. *Inorg. Chem.* **2013**, *52*, 4668-4682. (f) Moret, M.-E.; Peters, J. C. Terminal Iron Dinitrogen and Iron Imide Complexes Supported by a Tris(phosphino)borane Ligand. *Angew. Chem. Int. Ed.* **2011**, *50*, 2063-2067. (g) Cowley, R. E.; DeYonker, N. J.; Eckert, N. A.; Cundari, T. R.; DeBeer, S.; Bill, E.; Ottenwaelder, X.; Flaschenriem, C.; Holland, P. L. Three-Coordinate Terminal Imidoiron(III) Complexes: Structure, Spectroscopy, and Mechanism of Formation. *Inorg. Chem.* **2010**, *49*, 6172-6187. (h) Eckert, N. A.; Vaddadi, S.; Stoian, S.; Lachicotte, R. J.; Cundari, T. R.; Holland, P. L. Coordination-Number Dependence of Reactivity in an Imidoiron(III) Complex. *Angew. Chem. Int. Ed.* **2006**, *45*, 6868-6871. (i) Scepaniak, J. J.; Young, J. A.; Bontchev, R. P.; Smith, J. M. Formation of Ammonia from an Iron Nitrido Complex. *Angew. Chem. Int. Ed.* **2009**, *48*, 3158-3160. (j) Ni, C.; Fettinger, J. C.; Long, G. J.; Brynda, M.; Power, P. P. Reaction of a sterically encumbered iron(I) aryl/arene with organoazides: formation of an iron(V) bis(imide). *Chem. Commun.* **2008**, 6045-6047. (k) Lu, C. C.; Saouma, C. T.; Day, M. W.; Peters, J. C. Fe(I)-Mediated Reductive Cleavage and Coupling of CO_2: An $Fe^{II}(\mu\text{-}O,\mu\text{-}CO)Fe^{II}$ Core. *J. Am. Chem. Soc.* **2007**, *129*, 4-5. (l) Mehn, M. P.; Brown, S. D.; Jenkins, D. M.; Peters, J. C.; Que, L., Jr. Vibrational Spectroscopy and Analysis of Pseudo-tetrahedral Complexes with Metal Imido Bonds. *Inorg. Chem.* **2006**, *45*, 7417-7427. (m) Brown, S. D.; Peters, J. C. Ground-State Singlet $L_3Fe\text{-}(\mu\text{-}N)\text{-}FeL_3$ and $L_3Fe(NR)$ Complexes Featuring Pseudotetrahedral Fe(II) Centers. *J. Am. Chem. Soc.* **2005**, *127*, 1913-1923.

(69) (a) Liu, Y.; Du, J.; Deng, L. Synthesis, Structure, and Reactivity of Low-Spin Cobalt(II) Imido Complexes $[(Me_3P)_3Co(NAr)]$. *Inorg. Chem.* **2017**, *56*, 8278-8286. (b) Yao, X.-N.; Du, J.-Z.; Zhang, Y.-Q.; Leng, X.-B.; Yang, M.-W.; Jiang, S.-D.; Wang, Z.-X.; Ouyang, Z.-W.; Deng, L.; Wang, B.-W.; Gao, S. Two-Coordinate Co(II) Imido Complexes as Outstanding Single-Molecule Magnets. *J. Am. Chem. Soc.* **2017**, *139*, 373-380. (c) Du, J.; Wang, L.; Xie, M.; Deng, L. A Two-Coordinate Cobalt(II) Imido Complex with NHC Ligation: Synthesis, Structure, and Reactivity. *Angew. Chem. Int. Ed.* **2015**, *54*, 12640-12644. (d) Wu, B.; Sánchez, R. H.; Bezpalko, M. W.; Foxman, B. M.; Thomas, C. M. Formation of Heterobimetallic Zirconium/Cobalt Diimido Complexes via a Four-Electron Transformation. *Inorg. Chem.* **2014**, *53*, 10021-10023. (e) King, E. R.; Sazama, G. T.; Betley, T. A. Co(III) Imidos Exhibiting Spin Crossover and C–H Bond Activation. *J. Am. Chem. Soc.* **2012**, *134*, 17858-17861. (f) Jones, C.; Schulten, C.; Rose, R. P.; Stasch, A.; Aldridge, S.; Woodul, W. D.; Murray, K. S.; Moubaraki, B.; Brynda, M.; La Macchia, G.; Gagliardi, L. Amidinato– and Guanidinato–Cobalt(I) Complexes: Characterization of Exceptionally Short Co–Co Interactions. *Angew. Chem. Int. Ed.* **2009**, *48*, 7406-7410. (g) Cowley, R. E.; Bontchev, R. P.; Sorrell, J.; Sarracino, O.; Feng, Y.; Wang, H.; Smith, J. M. Formation of a Cobalt(III) Imido from a Cobalt(II) Amido Complex. Evidence for Proton-Coupled Electron Transfer. *J. Am. Chem. Soc.* **2007**, *129*, 2424-2425. (h) Shay, D. T.; Yap, G. P. A.; Zakharov, L. N.; Rheingold, A. L.; Theopold, K. H. Intramolecular C–H Activation by an Open-Shell Cobalt(III) Imido Complex. *Angew. Chem. Int. Ed.* **2005**, *44*, 1508-1510. (i) Dai, X.; Kapoor, P.; Warren, T. H. $[Me_2NN]Co(\eta^6$-toluene): O=O, N=N, and O=N Bond Cleavage Provides β-Diketiminato Cobalt μ-Oxo and Imido Complexes. *J. Am. Chem. Soc.* **2004**, *126*, 4798-4799. (j) Hu, X.; Meyer, K. Terminal Cobalt(III) Imido Complexes Supported by Tris(Carbene) Ligands: Imido Insertion into the Cobalt–Carbene Bond. *J. Am. Chem. Soc.* **2004**, *126*, 16322-16323.

(70) 2300-2308. (b) Kogut, E.; Wiencko, H. L.; Zhang, L.; Cordeau, D. E.; Warren, T. H. A Terminal Ni(III)–Imide with Diverse Reactivity Pathways. *J. Am. Chem. Soc.* **2005**, *127*, 11248-11249. (c) Iluc, V. M.; Miller, A. J. M.; Anderson, J. S.; Monreal, M. J.; Mehn, M. P.; Hillhouse, G. L. Synthesis and Characterization of Three-Coordinate Ni(III)-Imide Complexes. *J. Am. Chem. Soc.* **2011**, *133*, 13055-13063. (d) Laskowski, C. A.; Hillhouse, G. L. Group-Transfer Reactions of Ni(II)–Ni(II) Bridging Imido Complexes. Catalytic Formation of Carbodiimides and Isocyanates via Nitrene Transfer from Organoazides. *Organometallics* **2009**, *28*, 6114-6120. (e) Waterman, R.; Hillhouse, G. L. η^2-Organoazide Complexes of Nickel and Their Conversion to Terminal Imido Complexes *via* Dinitrogen Extrusion. *J. Am. Chem. Soc.* **2008**, *130*, 12628-12629. (f) Mindiola, D. J.; Hillhouse, G. L. Terminal Amido and Imido Complexes of Three-Coordinate Nickel. *J. Am. Chem. Soc.* **2001**, *123*, 4623-4624.

(71) (a) Wang, L.; Hu, L.; Zhang, H.; Chen, H.; Deng, L. Three-Coordinate Iron(IV) Bisimido Complexes with Aminocarbene Ligation: Synthesis, Structure, and Reactivity. *J. Am. Chem. Soc.* **2015**, *137*, 14196-14207. (b) Searles, K.; Fortier, S.; Khusniyarov, M. M.; Carroll, P. J.; Sutter, J.; Meyer, K.; Mindiola, D. J.; Caulton, K. G. A *cis*-Divacant Octahedral and Mononuclear Iron(IV) Imide. *Angew. Chem. Int. Ed.* **2014**, *53*, 14139-14143. (c) Bowman, A. C.; Milsmann, C.; Bill, E.; Turner, Z. R.; Lobkovsky, E.; DeBeer, S.; Wieghardt, K.; Chirik, P. J. Synthesis and Electronic Structure Determination of N-Alkyl-Substituted Bis(Imino)pyridine Iron Imides Exhibiting Spin Crossover Behavior. *J. Am. Chem. Soc.* **2011**, *133*, 17353-17369. (d) Bart, S. C.; Lobkovsky, E.; Bill, E.; Chirik, P. J. Synthesis and Hydrogenation of Bis(imino)pyridine Iron Imides. *J. Am. Chem. Soc.* **2006**, *128*, 5302-5303. (e) Klinker, E. J.; Jackson, T. A.; Jensen, M. P.; Stubna, A.; Juhász, G.; Bominaar, E. L.; Münck, E.; Que, L., Jr. A Tosylimido Analogue of a Nonheme Oxoiron(IV) Complex. *Angew. Chem. Int. Ed.* **2006**, *45*, 7394-7397. (f) Kumar, S.; Faponle, A. S.; Barman, P.; Vardhaman, A. K.; Sastri, C. V.; Kumar, D.; de Visser, S. P. Long-Range Electron Transfer Triggers Mechanistic Differences between Iron(IV)-Oxo and Iron(IV)-Imido Oxidants. *J. Am. Chem. Soc.* **2014**, *136*, 17102-17115. (g) Thomas, C. M.; Mankad, N. P.; Peters, J. C. Characterization of the Terminal Iron(IV) Imides $\{[PhBP^{tBu}_2(pz')]Fe^{IV}{\equiv}NAd\}^+$. *J. Am. Chem. Soc.* **2006**, *128*, 4956-4957. (h) Nieto, I.; Ding, F.; Bontchev, R. P.; Wang, H.; Smith, J. M. Thermodynamics of Hydrogen Atom Transfer to a High-Valent Iron Imido Complex. *J. Am. Chem. Soc.* **2008**, *130*, 2716-2717. (i) Lucas, R. L.; Powell, D. R.; Borovik, A. S. Preparation of Iron Amido Complexes via Putative Fe(IV) Imido Intermediates. *J. Am. Chem. Soc.* **2005**, *127*, 11596-11597.

(72) (a) Goswami, M.; Rebreyend, C.; de Bruin, B. Porphyrin Cobalt(III) "Nitrene Radical" Reactivity; Hydrogen Atom Transfer from *Ortho*-YH Substituents to the Nitrene Moiety of Cobalt-Bound Aryl Nitrene Intermediates (Y = O, NH). *Molecules* **2016**, *21*, 242. (b) Goswami, M.; Lyaskovskyy, V.; Domingos, S. R.; Buma, W. J.; Woutersen, S.; Troeppner, O.; Ivanović-Burmazović, I.; Lu, H.; Cui, X.; Zhang, X. P.; Reijerse, E. J.; DeBeer, S.; van Schooneveld, M. M.; Pfaff, F. F.; Ray, K.; de Bruin, B. Characterization of Porphyrin-Co(III)-'Nitrene Radical' Species Relevant in Catalytic Nitrene Transfer Reactions. *J. Am. Chem. Soc.* **2015**, *137*, 5468-5479. (c) Zhang, L.; Liu, Y.; Deng, L. Three-Coordinate Cobalt(IV) and Cobalt(V) Imido Complexes with N-Heterocyclic Carbene Ligation: Synthesis, Structure, and Their Distinct Reactivity in C–H Bond Amination. *J. Am. Chem. Soc.* **2014**, *136*, 15525-15528. (d) Hopmann, K. H.; Ghosh, A. Mechanism of Cobalt-Porphyrin–Catalyzed Aziridination. *ACS Catal.* **2011**, *1*, 597-600.

II. IS THE ELECTROPHILICITY OF THE METAL NITRENE THE SOLE PREDICTOR OF METAL-MEDIATED NITRENE TRANSFER TO OLEFINS? SECONDARY CONTRIBUTING FACTORSAS REVEALED BY A LIBRARY OF HIGH-SPIN Co(II) REAGENTS

Anshika Kalra,[†] Vivek Bagchi,[†,⊥] Patrina Paraskevopoulou,[‡] Purak Das,[†] Lin Ai,[†,§] Yiannis Sanakis,[^] Grigorios Raptopoulos,[‡] Sudip Mohapatra,[†] Amitava Choudhury,[†] Zhicheng Sun,[‖] Thomas R. Cundari,[*,‖] and Pericles Stavropoulos[*,†]

[†]Department of Chemistry, Missouri University of Science and Technology, Rolla, Missouri 65409, United States

[‡]Inorganic Chemistry Laboratory, Department of Chemistry, National and Kapodistrian University of Athens, Panepistimiopolis Zografou 15771, Athens, Greece

[§]College of Chemistry, Beijing Normal University, Beijing 100875, People's Republic of China

[^]Institute of Advanced Materials, Physicochemical Processes, Nanotechnology and Microsystems, NCSR "Demokritos", Ag. Paraskevi 15310, Athens, Greece

[‖]Department of Chemistry, Center for Advanced Scientific Computing and Modeling (CASCaM), University of North Texas, Denton, Texas 76203, United States

ABSTRACT

Recent research has highlighted the key role played by the electron affinity of the active metal-nitrene/imido oxidant as the driving force in nitrene additions to olefins to afford valuable aziridines. The present work showcases a library of Co(II) reagents that, unlike the previously examined Mn(II) and Fe(II) analogs, demonstrate reactivity trends in olefin aziridinations that cannot be solely explained by the electron affinity criterion. A family of Co(II) catalysts (seventeen members) has been synthesized with the assistance of a trisphenylamido-amine scaffold decorated by various alkyl, aryl and acyl groups attached to the equatorial amidos. Single-crystal X-ray diffraction analysis, cyclic voltammetry and EPR data reveal that the high-spin Co(II) sites ($S = 3/2$) feature a

minimal [N_3N] coordination and span a range of 1.4 V in redox potentials. Surprisingly, the Co(II)-mediated aziridination of styrene demonstrates reactivity patterns that deviate from those anticipated by the relevant electrophilicities of the putative metal nitrenes. The representative L^4Co catalyst (-$COCMe_3$ arm) is operating faster than the L^8Co analog (-$COCF_3$ arm), in spite of diminished metal-nitrene electrophilicity. Mechanistic data (Hammett plots, KIE, stereocontrol studies) reveal that although both reagents follow a two-step reactivity path (turnover-limiting metal-nitrene addition to the C_b atom of styrene, followed by product-determining ring-closure), the L^4Co catalyst is associated with lower energy barriers in both steps. DFT calculations indicate that the putative [L^4Co]NTs and [L^8Co]NTs species are electronically distinct, inasmuch as the former exhibits a single-electron oxidized ligand arm. In addition, DFT calculations suggest that including London dispersion corrections for L^4Co (due to the polarizability of the *tert*-Bu substituent) can provide significant stabilization of the turnover-limiting transition state.

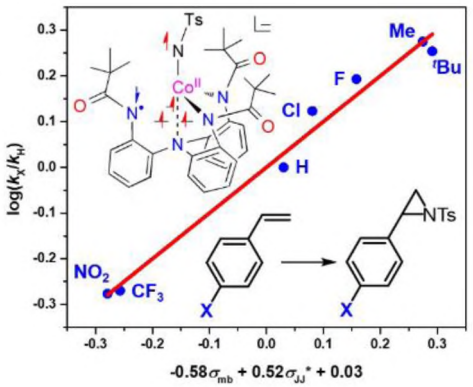

This study highlights how small ligand modifications can generate stereoelectronic variants that in certain cases are even capable of overriding the preponderance of the metal-nitrene electrophilicity as a driving force.

Keywords: Cobalt, Trisamidoamine ligands, Nitrene-transfer Catalysis, Electrochemistry

1. INTRODUCTION

1.1. BACKGROUND

The role of aziridines[1] as intermediates and end products of synthetic and biological chemistry is hard to overstate. Not only do aziridines afford avenues for further structural development by taking advantage of the energetic content and stereochemical disposition of their strained three-atom ring (ring opening, expansion or rearrangement),[2] but also constitute valuable functionalities in the framework of several natural products possessing antibiotic or antineoplastic activities.[3] In addition to the central role exercised by aziridines as fine chemicals and pharmaceutical agents,[4] their contribution to the chemistry of maretials has been increasingly recognized,[5] especially as key entities for the development and post-modification of polymeric scaffolds.

Synthetic protocols for the generation of aziridines abound, but largely rely on three major methodologies. The cyclization of 1,2-amino precursors constitutes a traditional approach that has been more recently complemented by addition of either C_1 sources to imines or electrophilic N_1 donors to alkenes.[6] The latter "C_2+N_1" addition is extensively implemented due to its operational simplicity and availability of a wide range of suitable substrates and catalysts. The N_1 donors encompass a variety of nitrene/nitrenoid precursor oxidants such as iminoiodanes (ArI=NR),[7] haloamines (RNNaX, X = Cl, Br),[8] *O*/*N*-substituted hydroxylamines and *N*-tosyloxycarbamates (RN(X)–OR′, X = H, leaving group)[9] or atom-economical organic azides (RN_3).[10] As

opposed to oxo-transfer chemistry, the corresponding nitrene/nitrenoid transfer relies significantly on the choice of the attendant R group to control the electrophilicity of the active moiety and provide activated (R = SO_2R, CO_2R, COR, carbamoyl, sulfamoyl) or nonactivated aziridines (R = H, alkyl, aryl, silyl) with differential reactivity.[11]

A wide range of catalysts has been explored to influence reactivity and selectivity outcomes in nitrene transfer to alkenes, including several organocatalytic[12] and metal-mediated processes.[13] In the latter case, the presumptive and rather elusive metal-nitrene (M=NR) active species are entities with rich and variable stereoelectronic attributes, inherent and/or ligand induced, whose operation vis-à-vis olefinic substrates is a matter of intense investigation. The variety of transition metals employed, both from the first-row (Mn, Fe, Co, Ni, Cu)[14-22] and from the heavier platinum-group[23-25] and coinage elements,[26,27] coupled with a range of ancillary ligand frameworks (e.g., porphyrinoids, salens, bis-oxazolines, tetracarboxylate paddlewheels, trispyrazolyl-borates/methanes, polypyridines) is a testament to the vigorous activity in this field and that of the closely related C–H bond amination reactions.[28]

Among the late 3*d* transition elements, the case of cobalt is most intriguing, inasmuch as isolable or even putative Co=NR units have been invoked with a variety of oxidation states (from II to V), electronic ground-state spins (S = 0, ½, 1, 3/2, 2) and coordination numbers (from 2 to 5).[29] The most common configuration is that of diamagnetic Co(III) imidos (S = 0),[30] mostly supported by C_3 or C_2 symmetric ligands. In a handful of cases, open-shell spin-states were observed for Co(III) imidos, as for instance with (trispyrazolylborato)Co^{III}(NAd) (S = 1, at T > 280K),[31] (dipyrrin)Co^{III}(NR) (S = 1 for R = Mes; S = 0 or 0 $\rightarrow$ 2 transition, for R = ^{t}Bu, 1-Ad, other alkyls),[32]

$[(hmds)_2Co^{III}(N^tBu)]^-$ ($S = 1$; hmds = $N(SiMe_3)_2$),[33] and possibly bimetallic Zr(μ-NMes)Co^{III}(NMes) ($S = 0 \rightarrow 2$ transition, near room temperature).[34] None of these compounds has been reported to mediate nitrene-transfer to alkenes. Observable reactivity includes (i) nitrene-transfer to carbon monoxide;[30g,31a,35] (ii) insertion of nitrene into ligand-derived carbene residues;[30e] (iii) formal hydrogen-atom abstraction from a ^{t}Bu or Mes ligand moiety by open-shell Co=NR, presumably generating an amido Co–NHR unit and a carbon centered radical; the latter can then recombine with the amido,[31a] dimerize,[31b] or generate a Co–C bond;[31b,32a] (iv) intramolecular C–H bond insertion into alkyl azides (source of imido), mediated by (dipyrrin)Co^{III}(NR), to generate substituted N-heterocycles;[32b,c] and (v) a rare instance of intermolecular hydrogen-atom abstraction from C–H bonds of various substrates with $BDE_{C-H} \leq 92$ kcal mol^{-1} by $[(hmds)_2Co^{III}(N^tBu)]^-$,[33] leading to the corresponding Co(II) amido; the amido can then react with another equivalent of substrate (C–H) to perform either proton transfer (frequently with the concomitant formation of Co^{II}–C organometallics) or formal hydrogen-atom abstraction via stepwise proton/electron transfer or direct HAT, giving rise to Co(I) and substrate dehydrogenation product. In several instance noted above, the carbophilic character of cobalt is notable as a product-determining factor.

Cobalt(II) imidos are more recent additions to the repertoire of cobalt reagents, and encompass both high-spin ($S = 3/2$)[36] and low-spin ($S = ½$)[37] cases as two- and four-coordinate compounds, respectively. The high-spin examples have been reported to perform nitrene-transfer to ethylene to afford RN=CH–CH_3, presumably due to a [2π+2π] activation mode. Similarly, certain C(*sp*)–H and Si–H bonds are activated not via H-atom abstraction, but by means of [2π+2σ] interactions.[36b] On the other hand, the low-spin

Co(II) imidos are unreactive versus alkenes, although they engage in nitrene-transfer and/or nitrene-exchange with O/S with respect to substrates such as CO, PMe_3, PhCHO, and CS_2.[37] Finally, two examples of high-valent Co(IV) and Co(V) bis-imido complexes ($[IMes]Co(NDipp)_2]^{0/+}$), possessing low-spin ground states of $S = ½$ and 0, respectively, proved to be rather unreactive.[38] The open-shell Co(IV) congener is the only one that exhibits intramolecular nitrene C–H insertion into the o-Me group of the Mes residue, possibly via an ortho-cobaltation intermediate (Co–C).[29]

Whereas the catalytic formation of new C–N bonds by means of the isolable cobalt imidos noted above is only rarely observed, the advent of a library of Co^{II}(Por) complexes that give rise to Co^{III}–nitrenoid radicals [(Por)Co^{III}–$^{\bullet}$NR] or [(Por$^{\bullet}$)Co^{III}–($^{\bullet}$NR)$_2$], has provided numerous instances of highly effective catalytic systems for the stereo-, chemo- and site-selective aziridination of alkenes and amination of C–H bonds.[19] Starting with Co(TPP), and electron-deficient analogs, several generations of Co^{II}(Por) reagents with richly decorated porphyrins have been introduced in the past two decades to facilitate the activation of various organic azides, leading to the generation of well characterized low-spin ($S = ½$) Co^{III}–$^{\bullet}$NR moieties, with spin density largely localized on the N atom.[19f,39] These relatively long-lived Co^{III}–nitrene-radical intermediates owe their stability to hydrogen-bonding interactions of the nitrene moieties with porphyrin-appended amido residues (–NHCOR*), which can further introduce and metal-orient chiral auxiliaries via their R* functionality in D_2-symmetric overall geometries. Detailed theoretical and experimental studies[19f,39] have established that the mode of operation of [(Por)Co^{III}–$^{\bullet}$NR] metalloradicals vis-à-vis C=C or C–H bonds consists of a two-step process: initial formation of a new N–C bond with alkenes and relocation of the spin

density on the distal carbon atom (Co^{III}–N(R)–C–$^{\bullet}$C–) (or formation of a Co^{III}–NHR amido and a substrate-bound radical via hydrogen-atom abstraction from a C–H bond), followed by an essentially barrierless collapse of the carbon-centered radical with the N atom to generate the product of aziridination (or amination) along with Co^{II}(Por).

More recently, the structurally related $[Co^{III}(TAML^{red})]^{-}$ and $[Co^{III}(TAML^{sq})]$ compounds, featuring the tetraamido macrocyclic ligand TAML in its intact reduced form $TAML^{red}$ and one-electron oxidized variant $TAML^{sq}$ (sometimes denoted as $TAML^{+\bullet}$), have been shown to give rise to $[Co^{III}(TAML^{q})(^{\bullet}NR)_2]^{-}$ ($S = 1$) and $[Co^{III}(TAML^{q})(^{\bullet}NR)]$ ($S = 1/2$), respectively ($TAML^{q}$ = doubly oxidized, diamagnetic ligand; Co^{III} site is low-spin, $S = 0$).[40] These cobalt nitrenes have emerged as capable catalysts for the aziridination of largely styrene substrates by imidoiodinanes (PhINNs, PhINTs, PhINTces).[41] Their mode of operation is considered to be unique, inasmuch as the turnover-limiting, initial N–C bond formation with styrenes features an asynchronous transition state, encompassing a partial electron-transfer to form a styrenyl radical cation, in turn undergoing a *nucleophilic* attack by the nitrene lone pair (see below for more details). This initial charge-transfer has also emerged as a central component of the operation of iron(IV) imido species developed by Latour and co-workers for alkene aziridinations, further underscoring the importance of the electron affinity of the metal nitrene as a commonly encountered driving force.[42]

Finally, of great interest are recently reported Co(II) organoazides,[43] which either thermally or photolytically can extrude N_2 to give rise to nitrenoids best described as iminyl [Co^{III}–$^{\bullet}$NR] units (R = aryl, alkyl). Although the electronics of these fleeting intermediates are not yet known, crystal structures of such species (R = alkyl) have been

determined following N_2 expulsion from single crystals of metal azides in the solid state. For R = aryl, the cobalt(II) organozide can promote nitrene-transfer by means of unisolable [Co^{III}–$^{\bullet}$NR], both intramolecularly ([3+2] annulation) and intermolecularly (C–H allylic amination or styrene aziridination in modest yields). The reactivity of the Co(II) aliphatic azides is more complex and includes (i) α-H atom abstraction via the incipient [Co^{III}–$^{\bullet}$$NCH_2R$] to generate the imine (RCH=NH), if strong δ-C–H bonds (sec, prim) are present; (ii) δ-H atom abstraction and amination of relatively weaker δ-C–H bonds (benzylic, tertiary) by the cobalt alkylazide itself (initial N_2 extrusion is not needed), leading to substituted pyrrolidines; and (iii) intramolecular 1,3-dipolar cycloaddition of cobalt-bound CH_2=$CH(CH_2)_4N_3$ to afford 1,2,3-dihydrotriazole.

In the present work, we examine a library of high-spin Co(II) reagents (S = 3/2), supported by a modular trisphenylamido-amine ligand framework, giving rise to a weak equatorial field. Previous DFT calculations[44] on one member of this library of reagents indicated that exposure to a nitrene source (PhI=NTs) generates a Co(III)–nitrene radical (Co^{III}–$^{\bullet}$NTs) with a high-spin ground state (S = 5/2). The corresponding doublet and quartet [Co]NTs states lie slightly higher than the sextet by ΔG values of 0.4 and 1.5 kcal mol^{-1}, respectively. The computed spin density for the S = 5/2 state places ~1.1 unpaired electron on the nitrene N atom, and ~3.3 unpaired electrons on Co, with the remaining spin density being distributed to other atoms. Similarly to the low-spin porphyrin-supported Co^{III}–nitrene-radical (S = ½) noted above, the high-spin congener is capable of performing alkene aziridinations in a two-step process (successive formation of two N–C bonds). Remarkably, the computed transition-state barrier ($\Delta G^{\ddagger}$ = 23.4 kcal mol^{-1} vs. Co^{III}–$^{\bullet}$NTs/styrene) for the rate-determining, initial Cβ···NTs bond-forming step of the

high-spin system is very similar to that reported for the corresponding low-spin Co(Por) ($\Delta G^{\ddagger}$ = 24.1 kcal mol^{-1}) or Co(AmidoPor) ($\Delta G^{\ddagger}$ = 22.8 kcal mol^{-1}) with respect to Co^{III}–$^{\bullet}$NSO$_2$Ph/styrene.[19f] The present work significantly enlarges the scope of high-spin Co(II) compounds as nitrene-transfer reagents, and provides insights in their operational characteristics, not only vis-à-vis the reported low-spin (Por)Co(II) paradigms, but also in comparison with the previously examined libraries of Mn(II) and Fe(II) reagents, supported by the same trisphenylamido-amine ligand framework.[44] Whereas the nitrene-transfer reactivity of the Mn(II) reagents in alkene aziridinations largely depends on the electrophilicity of the presumptive Mn^{III}–$^{\bullet}$NR (S = 3/2) moiety, underscoring the role of the electron affinity of the metal nitrene as a dominant factor, the reactivity of the corresponding, more reactive, Co(II) reagents is affected by additional subtle electronic and steric factors. These most likely arise from the tighter disposition of the reaction cavity, resulting in ligand-coordination flexibility, electronic rearrangement, and secondary stabilizing interactions. In this publication we show that even an otherwise small change in ligand substitution can have a significant effect on nitrene-transfer reactivity in aziridination reactions, occasionally overriding the preponderance of the metal-nitrene electrophilicity as a driving force.

2. RESULTS AND DISCUSSION

2.1. SYNTHESIS AND CHARACTERIZATION OF NEW LIGANDS AND Co(II) COMPLEXES

The family of trisphenylamido-amine ligands (L^1H_3 - $L^{17}H_3$) employed in this study is shown in Figure 1. The majority of these ligands (L^1H_3 - $L^{15}H_3$) have been used and reported in previous studies.[44-48] They are all derivatives of the common 2,2′,2″-

triaminotriphenylamine framework,[45] featuring carbonaceous arm substituents (alkyl, aryl acyl).

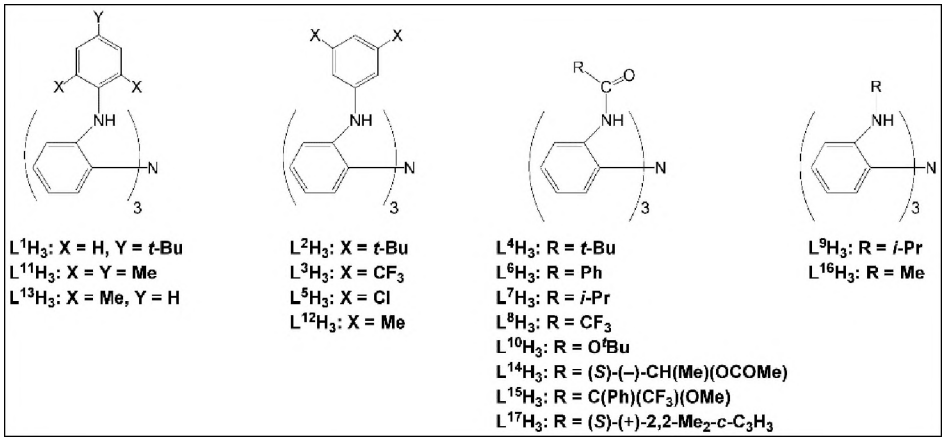

Figure 1. Ligands Employed in the Present Study

Ligand $L^{16}H_3$ is prepared by methylation of deprotonated (KH) 2,2′,2″-triaminotriphenylamine by MeI in THF, and ligand $L^{17}H_3$ is derived via condensation of the same triamine with the corresponding chiral acyl chloride in the presence of Et_3N in dichloromethaneThe solid-state structures of these two new ligands (Figure S1) are indicative of their favorable preorganization for metalation, in a cavity that is buttressed by alkyl and acyl arms, respectively.Co^{II} complexes were synthesized with all ligands, by reacting the deprotonated (KH) ligand with anhydrous beads of $CoCl_2$ in THF (alkyl and aryl armed ligands) or *N*,*N*-dimethylacetamide (DMA) (acyl armed ligands). A subset of Co^{II} compounds, namely L^3Co (**3**), L^5Co (**5**), L^8Co (**8a**), L^9Co (**9**), $L^{10}Co$ (**10**), and $L^{13}Co$ (**13**), has been previously reported in a study that examined the use of these catalysts in controlled radical polymerization of olefins.[48] In addition, L^8Co (**8b**) has been explored in conjunction with the L^8Mn and L^8Fe congeners, towards establishing metal-dependent trends in catalytic nitrene transfer to olefins[44].

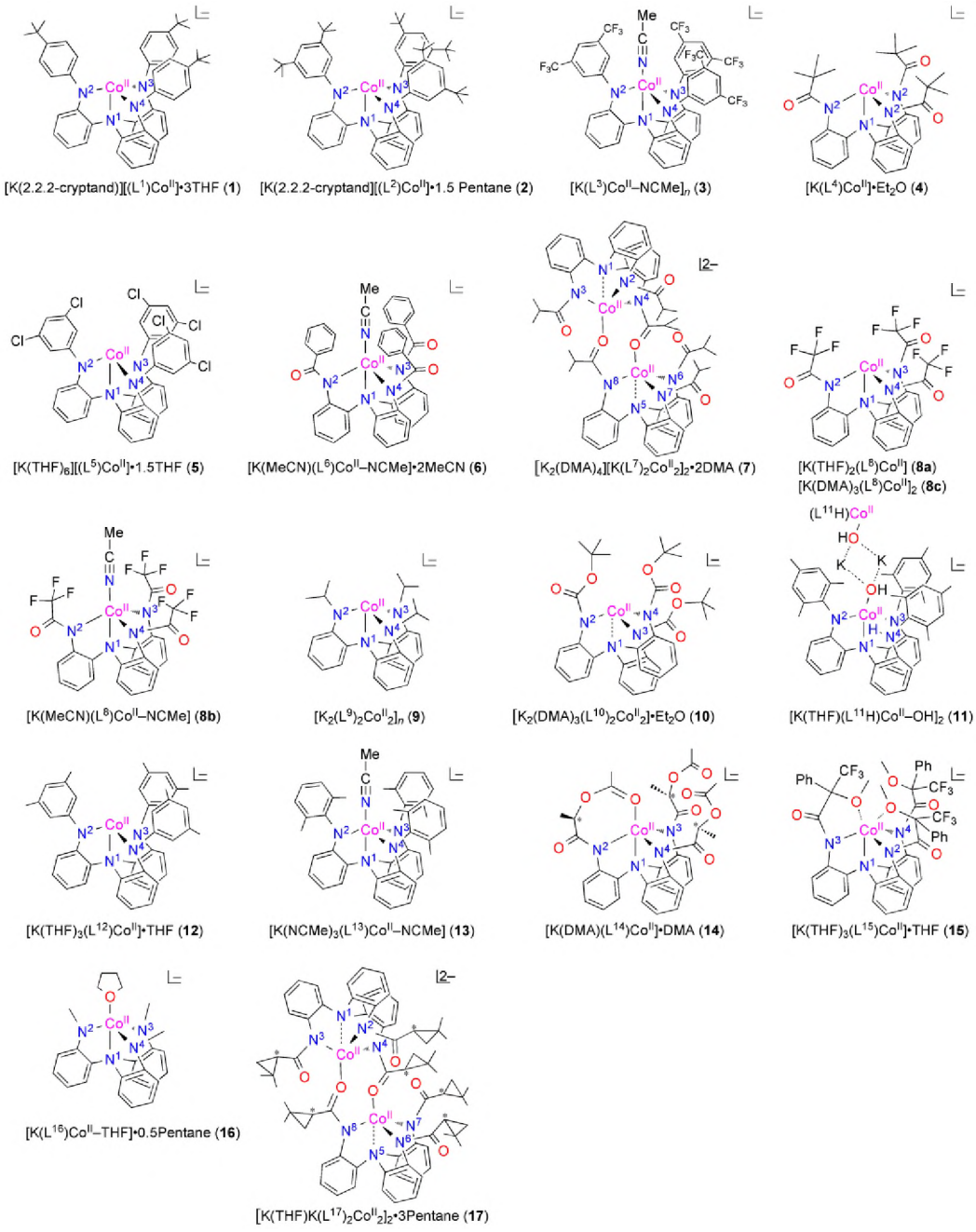

Figure 2. Minimal Coordination of Co^{II} Compounds with Ligands L^1–L^{17}. The Ligands Explored in this Study

Figure 2 depicts representations of the minimal coordination site of each Co^{II} site, derived from single-crystal X-ray diffraction data. In all cases the ligand coordinates in a trigonal pyramidal [$N_{3(amido)}N_{amine}$] mode, exhibiting various degrees of distortion, although in two instances (**7**, **17**) the coordination to the axial N_{amine} residue can be best described as a long contact. Moreover, compound **11** features a non-coordinating amido residue that has been protonated. The dominant four-coordinate [N_3N] pattern is retained as the sole ligand field of seven Co^{II} compounds (**4**, **5**, **8a**, **8c**, **9**, **10**, **12**).

Additional elements of metal coordination, essentially located trans to the axial N_{amine} residue, are observed with all other compounds, and include solvent moieties, especially for compounds crystallized from MeCN (**3**, **6**, **13**) and THF (**16**), as well as carbonyl units (–C(R)=O–Co^{II}) deriving from acyl residues belonging to the ligand (**7**, **14**, **17**). In a single case (**15**), a six-coordinate Co^{II} site arises from the presence of two ligand-derived ether residues in the metal coordination sphere, in addition to the usual [N_3N] framework. Importantly, most structures are polymeric, largely due to an intricate network of intermolecular interactions generated by K^+ ions. Mononuclear (**1**, **2**, **5**, **12**, **13**) or oligonuclear (**8c**, **11**, **17**) compounds (molecular or ionic) are only encountered in a handful of cases. A more detailed description of the structural features of the new Co^{II} compounds is provided below.

2.2. Co^{II} COMPOUNDS WITH ACYL-ARMED LIGANDS

The seven new compounds (**4**, **6**, **7**, **8c**, **14**, **15**, **17**; Figure 3) that belong in this category are polymeric, with the exception of [$K(DMA)_3(L^8)Co^{II}]_2$ (**8c**) and [$K_2(THF)_2K_2(L^{17})_4Co^{II}_4$] (**17**) that feature a dimeric and tetrameric molecular unit, respectively. The catalytically important {[$K(L^4)Co^{II}$]•Diethyl Ether}$_n$ (**4**) exhibits higher

symmetry than all other compounds, consisting of a rigorous three-fold axis along the Co–N_{amine} direction as well as through K^+ ions relating three different molecules in the crystal lattice. This compound is characterized by an exclusive four-coordinate [N_3N] ligand field and an open metalated cavity fortified by the three –CO^{t}Bu arms. The carbonyl residues are positioned *exo* with respect to the cavity and are further engaged in contacts with K^+ ions, inasmuch as each potassium is coordinated by three oxygen (carbonyl) atoms belonging to different molecules, and is also involved in K^+–arene π contacts. These structural features are largely retained in the structure of [K(NCMe)(L^6)Co^{II}–NCMe]•2MeCN (**6**), but important deviations also apply, mostly because of the presence of a coordinated MeCN molecule in a trans position versus the N_{amine} (N_{amine}–Co–N_{MeCN} = 178.75(14)°) and the lack of a strict three-fold crystallographic symmetry. Otherwise, each K^+ ion is still coordinated by three carbonyl residues belonging to different molecules in addition to a single MeCN, in lieu of any K^+–arene contacts.

The structure of [K_2(DMA)$_4$][K(L^7)$_2Co^{II}_2$]$_2$•2DMA (**7**) is organized in a much more complex manner, featuring an "one-dimensional" array of a repeating unit, [Co(1)/Co(2)--K(1)--Co(3)/Co(4)--K(2)]$_n$, connected to identical arrays via lateral links provided by a DMA solvated K(3)/K(4) dimer (K_2(DMA)$_4$). Within the repeating unit, the Co(II) sites are arranged in two similar dimers linked via K^+ contacts. The dimeric unit is composed of two slightly different Co(II) centers, each featuring the usual [N_3N] ligand coordination, but with a long axial Co–N_{amine} interaction (av. 2.49 Å). In addition, each Co(II) is coordinated by an oxygen atom (carbonyl) positioned *trans* with respect to the axial Co–N_{amine} direction (av. N_{amine}–Co–$O_{C=O}$ = 173.2 °, Co–$O_{C=O}$ = 1.98 Å).

Importantly, the oxygen atom (carbonyl) coordinated to each Co^{II} center belongs to the ligand surrounding the partner Co^{II} site, hence giving rise to a dimer.

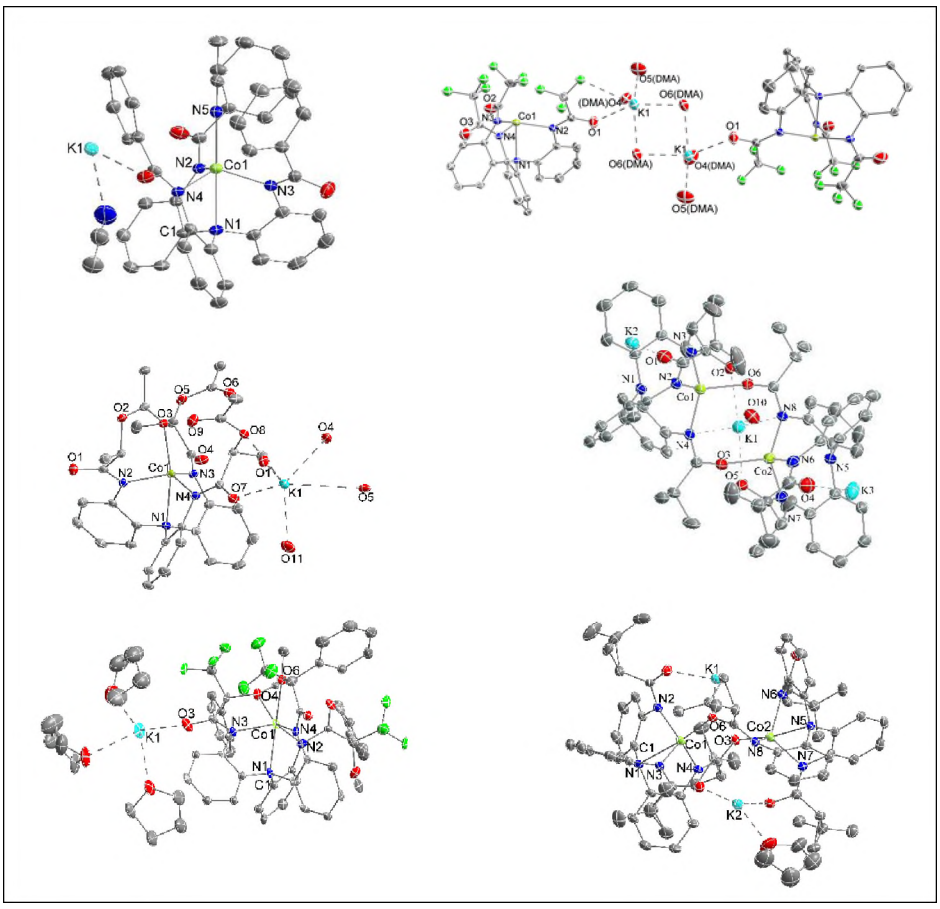

Figure 3. ORTEP diagrams. From left to right of $\{[K(L^4)Co^{II}]\bullet$Diethyl Ether$\}_n$ (4), $[K(MeCN)(L^6)Co^{II}$–NCMe]•2MeCN (6), $[K_2(DMA)_4][[K(L^7)_2Co^{II}_2]_2$•2DMA (7), $[K_2(DMA)_3(L^8)Co^{II}]_2$ (8c), $[K(DMA)(L^{14})Co^{II}]$•DMA (14), $[K(THF)_3(L^{15})Co^{II}]$•THF (15), and $[K(THF)K(L^{17})_2Co^{II}_2]_2$•3Pentane (17), drawn with 40% thermal ellipsoids. Hydrogen atoms are omitted for clarity. Selective interatomic distances (Å) and angles (°)

The K^+ ions interconnecting the dimers in a pseudo 1-D array are coordinated by two carbonyl and, more weakly, two N_{amido} residues all belonging to one dimer, and by only a single carbonyl moiety (O(10)) belonging to the adjacent dimer. A much more simplified version of this structure is adopted by $[K(DMA)_3(L^8)Co^{II}]_2$ (**8c**), exhibiting a

dimeric structure comprised of two inversion symmetry related $[N_3N]Co^{II}$ units connected via carbonyl O atoms of acyl residues to a central $K_2(\mu\text{-DMA})_2(DMA)_4$ core.

Compound $[K(DMA)(L^{14})Co^{II}]\bullet DMA$ (**14**) retains the usual $[N_3N]$ trigonal-pyramidal coordination but exhibits an additional unique feature, inasmuch as one of the chiral arms generates a seven-member loop by positioning the ester carbonyl in the coordination sphere of Co^{II}, trans to the axial N_{amine} residue (N_{amine}–Co–$O_{C=O}$ = 167.33(12)°, Co–$O_{C=O}$ = 2.162(3) Å). The polymeric nature of the compound arises again due to identical K^+ ions, coordinated by one DMA, forming contacts with oxygen residues (amidato carbonyls, MeC(=O)O–) belonging to three different Co^{II} sites in the crystal lattice.

Compound $[K(THF)_3(L^{15})Co^{II}]\bullet THF$ (**15**) is the only six-coordinate species observed, in as much as two acyl arms generate five-membered loops that place two ether residues (ROMe) in the coordination sphere of the $[N_3N]Co^{II}$ site (Co–O = 2.302(14), 2.405(13) Å; N_{amine}–Co–O = 146.4(6), 129.3(6)°). Identical K^+ ions are coordinated by three THF molecules and two acyl residues, each located in neighboring molecules, thus giving rise to pseudo 1-D polymeric structures.

Finally, the structure of $[K_2(THF)_2][K(L^{17})_2Co^{II}_2]_2$ (**17**) is very similar to that observed for **7** with respect to the formation of two interconnecting dimers, but the K^+ ions are organized differently, to afford a molecular (tetranuclear) rather than a polymeric complex. First, two K^+ ions link the two dimers in **17**, by employing the same contact pattern noted for the single K^+ ion connecting the two dimers in **7**. Secondly, the remaining two K^+ ions in **17** are terminated by THF molecules, and thus do not provide connections that could generate an 1-D array of repeating tetranuclear units as in **7**.

Otherwise, the coordination and arrangement of the Co^{II} sites in **17** and **7** is very similar, with somewhat more pronounced contact for the N_{amine} residue (av. Co–N_{amine} = 2.40 Å), and concomitant weaker attachment of the oxygen (carbonyl) moiety (av. Co–$O_{C=O}$ = 2.00 Å), along the axial coordination of Co^{II} sites in **17** versus that of **7**.

4, Co(1)–N(1) = 2.151(11), Co(1)–N(2) = 1.986(6), Co(1)–[N(2), N(2), N(2)] = 0.32(2) (distance of Co from mean plane) Å, N(2)–Co(1)–N(2) = 117.48(11), N(2)–Co(1)–N(1) = 80.8(2); **6**, Co(1)–N(1) = 2.235(3), Co(1)–N(2) = 2.046(4), Co(1)–N(3) = 2.049(4), Co(1)–N(4) = 2.053(4), Co(1)–N(5) = 2.063(4), Co(1)–[N(2), N(3), N(4)] = 0.48(2) (distance of Co from mean plane), N(2)–Co(1)–N(4) = 115.18(15), N(2)–Co(1)–N(3) = 117.17(15), N(3)–Co(1)–N(4) = 111.69(15), N(2)–Co(1)–N(1) = 76.70(14), N(4)–Co(1)–N(1) = 76.49(14), N(3)–Co(1)–N(1) = 76.15(14), N(3)–Co(1)–N(5) = 103.24(15), N(2)–Co(1)–N(5) = 104.55(14), N(4)–Co(1)–N(5) = 102.81(15), N(1)–Co(1)–N(5) = 178.75(14); **7**, Co(1)–N(1) = 2.463(4), Co(1)–N(2) = 2.053(4), Co(1)–N(3) = 2.054(5), Co(1)–N(4) = 2.054(4), Co(1)–O(6) = 1.975(4), Co(1)–[N(2), N(3), N(4)] = 0.61(2) (distance of Co from mean plane), Co(2)–N(5) = 2.517(5), Co(2)–N(6) = 2.081(5), Co(2)–N(7) = 2.033(5), Co(2)–N(8) = 2.069(5), Co(2)–O(3) = 1.984(4), Co(2)–[N(6), N(7), N(8)] = 0.67(2) (distance of Co from mean plane), N(2)–Co(1)–N(4) = 109.51(18), N(2)–Co(1)–N(3) = 113.66(17), N(3)–Co(1)–N(4) = 111.52(18), N(2)–Co(1)–N(1) = 73.14(16), N(4)–Co(1)–N(1) = 73.24(16), N(3)–Co(1)–N(1) = 71.83(16), N(3)–Co(1)–O(6) = 103.19(17), N(2)–Co(1)–O(6) = 106.85(17), N(4)–Co(1)–O(6) = 111.92(16), N(1)–Co(1)–O(6) = 174.16(15), N(6)–Co(2)–N(7) = 111.14(19), N(6)–Co(2)–N(8) = 112.01(19), N(7)–Co(2)–N(8) = 106.34(19), N(6)–Co(2)–N(5) = 70.48(19), N(7)–Co(2)–N(5) = 70.69(16), N(8)–Co(2)–N(5) = 71.42(17), N(6)–Co(2)–O(3) = 105.77(19), N(7)–

Co(2)–O(3) = 105.15(18), N(8)–Co(2)–O(3) = 116.27(17), N(5)–Co(2)–O(3) = 172.25(16); **8c**, Co(1)–N(1) = 2.1422(13), Co(1)–N(2) = 1.9941(14), Co(1)–N(3) = 1.9899(14), Co(1)–N(4) = 1.9872(13), Co(1)–[N(2), N(3), N(4)] = 0.306(4) (distance of Co from mean plane), K(1)–O(1) = 2.7298(14), N(2)–Co(1)–N(4) = 114.79(6), N(2)–Co(1)–N(3) = 118.04(6), N(3)–Co(1)–N(4) = 120.18(6), N(2)–Co(1)–N(1) = 80.83(5), N(4)–Co(1)–N(1) = 81.54(5), N(3)–Co(1)–N(1) = 81.06(5); **14**, Co(1)–N(1) = 2.224(3), Co(1)–N(2) = 2.018(4), Co(1)–N(3) = 2.031(4), Co(1)–N(4) = 2.021(4), Co(1)–O(3) = 2.162(3), Co(1)–[N(2), N(3), N(4)] = 0.42(1) (distance of Co from mean plane), N(2)–Co(1)–N(4) = 110.16(14), N(2)–Co(1)–N(3) = 121.11(15), N(3)–Co(1)–N(4) = 115.82(15), N(2)–Co(1)–N(1) = 76.31(14), N(4)–Co(1)–N(1) = 78.82(13), N(3)–Co(1)–N(1) = 78.58(14), N(3)–Co(1)–O(3) = 106.07(14), N(2)–Co(1)–O(3) = 91.35(13), N(4)–Co(1)–O(3) = 108.68(13), N(1)–Co(1)–O(3) = 167.33(12); **15**, Co(1)–N(1) = 2.337(17), Co(1)–N(2) = 2.041(17), Co(1)–N(3) = 2.048(18), Co(1)–N(4) = 2.033(17), Co(1)–O(4) = 2.405(13), Co(1)–O(6) = 2.302(14), Co(1)–[N(2), N(3), N(4)] = 0.53(2) (distance of Co from mean plane), N(2)–Co(1)–N(4) = 103.6(7), N(2)–Co(1)–N(3) = 118.1(7), N(3)–Co(1)–N(4) = 117.9(7), N(2)–Co(1)–N(1) = 74.3(6), N(4)–Co(1)–N(1) = 76.4(7), N(3)–Co(1)–N(1) = 73.5(6), N(3)–Co(1)–O(6) = 107.6(6), N(2)–Co(1)–O(6) = 127.7(6), N(4)–Co(1)–O(6) = 73.7(6), N(1)–Co(1)–O(6) = 146.4(6), N(3)–Co(1)–O(4) = 72.9(6), N(2)–Co(1)–O(4) = 89.5(6), N(4)–Co(1)–O(4) = 154.0(6), N(1)–Co(1)–O(4) = 129.3(6), O(4)–Co(1)–O(6) = 80.5(5); **17**, Co(1)–N(1) = 2.428(5), Co(1)–N(2) = 2.055(5), Co(1)–N(3) = 2.038(5), Co(1)–N(4) = 2.047(5), Co(1)–O(6) = 1.990(4), Co(1)–[N(2), N(3), N(4)] = 0.58(1) (distance of Co from mean plane), Co(2)–N(5) = 2.375(5), Co(2)–N(6) = 2.049(5), Co(2)–N(7) = 2.026(5), Co(2)–N(8) = 2.100(5), Co(2)–O(3) = 2.027(4), Co(2)–

[N(6), N(7), N(8)] = 0.56(1) (distance of Co from mean plane), N(2)–Co(1)–N(4) = 110.2(2), N(2)–Co(1)–N(3) = 118.9(2), N(3)–Co(1)–N(4) = 107.2(2), N(2)–Co(1)–N(1) = 73.94(18), N(4)–Co(1)–N(1) = 74.25(18), N(3)–Co(1)–N(1) = 72.09(18), N(3)–Co(1)–O(6) = 109.47(18), N(2)–Co(1)–O(6) = 99.64(18), N(4)–Co(1)–O(6) = 110.20(18), N(1)–Co(1)–O(6) = 172.96(17), N(6)–Co(2)–N(7) = 112.3(2), N(6)–Co(2)–N(8) = 113.4(2), N(7)–Co(2)–N(8) = 112.71(19), N(6)–Co(2)–N(5) = 74.71(18), N(7)–Co(2)–N(5) = 74.52(19), N(8)–Co(2)–N(5) = 73.18(17), N(6)–Co(2)–O(3) = 97.07(18), N(7)–Co(2)–O(3) = 112.18(19), N(8)–Co(2)–O(3) = 108.06(17), N(5)–Co(2)–O(3) = 171.18(17).

2.3. Co^{II} COMPOUNDS WITH ALKYL-ARMED LIGANDS

The new methyl-substituted compound **16** and the previously reported isopropyl congener (**9**),[48] are the only members of the alkyl-armed category of Co(II) compounds explored in this study. Compound **16** (Figure 4) demonstrates the familiar [N_3N] coordination, but unlike the more bulky isopropyl analog, exhibits a five-coordinate Co^{II} site due to the presence of a coordinated THF molecule trans to the N_{amine} residue (N_{amine}–Co–O_{THF} = 175.75(13)°). The electron-rich alkyl substitution dictates a stronger +equatorial ligand field (av. Co–N_{amido} = 2.000 Å) by comparison to all other five-coordinate Co^{II} sites investigated in this study. The polymeric nature of the compound arises by means of a repeating –[Co(1)–K(1)]– sequence, which features K(1) ions engaging in K–N_{amido} and K^+–arene contacts with both ligands of adjacent Co(1) sites. Co(1)–N(1) = 2.226(3), Co(1)–N(2) = 2.007(4), Co(1)–N(3) = 1.990(4), Co(1)–N(4) = 2.004(4), Co(1)–O(1) = 2.207(3), Co(1)–[N(2), N(3), N(4)] = 0.37(2) (distance of Co from mean plane), N(2)–Co(1)–N(4) = 112.70(15), N(2)–Co(1)–N(3) = 114.04(15),

N(3)–Co(1)–N(4) = 122.94(15), N(2)–Co(1)–N(1) = 79.40(13), N(4)–Co(1)–N(1) = 78.61(14), N(3)–Co(1)–N(1) = 79.64(14), N(3)–Co(1)–O(1) = 100.45(14), N(2)–Co(1)–O(1) = 104.32(13), N(4)–Co(1)–O(1) = 97.91(14), N(1)–Co(1)–O(1) = 175.75(13).

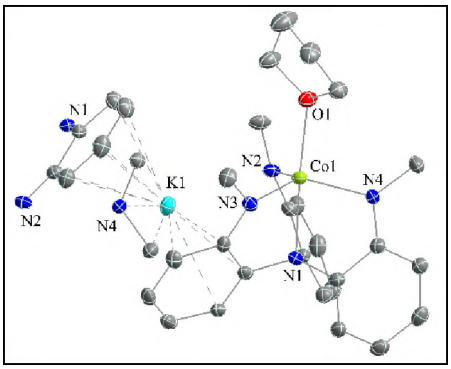

Figure 4. ORTEP diagram of [K(L^{16})Co^{II}–THF]•0.5Pentane (16). Drawn with 40% thermal ellipsoids. Hydrogen atoms are omitted for clarity. Selective interatomic distances (Å) and angles (°)

2.4. Co^{II} COMPOUNDS WITH ARYL-ARMED LIGANDS

Among the seven aryl-supported Co(II) reagents shown in Figure 2 (**1**, **2**, **11**, **12** are new; **3**, **5**, **13** have been previously reported[48]), only those crystallized from MeCN solutions (**3**, **13**) feature a solvent molecule coordinated to the Co(II) center. All others, crystallized from THF solutions, exhibit four-coordinate [N_3N]Co(II) sites devoid of any axial THF residues, in sharp contrast to analogous five-coordinate Mn and Fe reagents previously reported.

Among the four new Co(II) complexes (Figure 5), (L^1)Co (**1**) provides nice green crystals from concentrated THF solutions, but single-crystal specimens (albeit of low quality) were only obtained in the presence of the exceptional K^+ binder 2.2.2-cryptand. The resulting ionic complex [K(2.2.2-cryptand)][(L^1)Co^{II}]•3THF (**1**) exhibits a distorted [N_3N] coordination with an equatorial ligand field (av. Co–N = 1.927 Å) that is equal or

stronger than that demonstrated by similar four-coordinate Co(II) sites supported by aryl substituents (**2**, **5**, **12**), presumably due to the electron-rich character of the 4-^{t}Bu-substituted phenyl arm. Similarly, the 3,5-^{t}Bu$_2$ disubstituted compound (L^2)Co (**2**) proved to be isolable only in the presence of 2.2.2-cryptand, in the form of green crystals of [K(2.2.2-cryptand)][(L^2)Co^{II}]•1.5 Pentane (**2**) of marginal quality. Its structure is almost identical to that of **1**, with a similarly strong equatorial field (av. Co–N = 1.927 Å). The corresponding 3,5-Me$_2$ disubstituted compound [K(THF)$_3$(L^{12})Co^{II}]•THF (**12**) is monomeric and geometrically analogous to **2**, with a weaker equatorial field (av. Co–N = 1.956 Å), but, as opposed to **1** and **2**, can be isolated without the assistance of 2.2.2-cryptand. The K^+ ion in **12** is supported by three THF molecules and a host of contacts with aromatic moieties and N-atom residues. Although both the 3,5-Me$_2$ and 2,6-Me$_2$ disubstituted compounds **12** and **13**, respectively, can be isolated and characterized, the corresponding 2,4,6-Me$_3$ trisubstituted species (L^{11})Co^{II} has proven to be difficult to synthesize, apparently due to extreme sensitivity to even traces of water. In contrast, the analogous [K(THF)$_3$(L^{11})Mn^{II}–THF] can be readily prepared.[44] Indeed, after initial formation of a deep green species in the reaction of deprotonated $L^{11}H_3$ and $CoCl_2$ in THF, the color soon fades and ligand can be recovered intact along with separation of blue $Co(OH)_2$. In one instance, under scrupulous water exclusion, a few green crystals of [K(THF)(L^{11}H)Co^{II}–OH)]$_2$ (**11**) have been isolated, amounting to a species that can be viewed as the formal product of water addition to (L^{11})Co^{II}. Indeed, **11** features protonation and dissociation of one nitrogen residue from the equatorial field, with concomitant formation of a Co^{II}–OH moiety. The hydroxide is further coordinated by two

$K(THF)^{+}$ ions in an overall dimeric structure that connects two inversion-related $(L^{11}H)Co^{II}$–OH monomers by means of a $K_2(OH)_2$ rhomb.

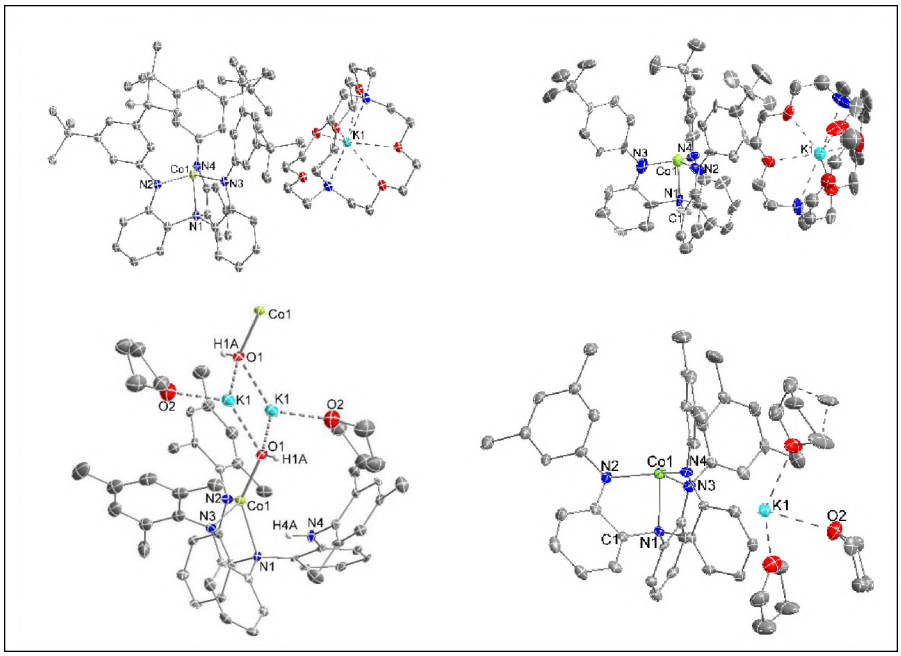

Figure 5. ORTEP diagrams. From left to right) of $[K(2.2.2\text{-cryptand})][(L^{1})Co^{II}]\bullet 3THF$ (1), $[K(2.2.2\text{-cryptand})][(L^{2})Co^{II}]\bullet 1.5Pentane$ (2), $[K(THF)(L^{11}H)Co^{II}\text{–}OH]_2$ (11), and $[K(THF)_3(L^{12})Co^{II}]\bullet THF$ (12) drawn with 40% thermal ellipsoids. Hydrogen atoms are omitted for clarity. Selective interatomic distances (Å) and angles (°)

1, Co(1)–N(1) = 2.102(18), Co(1)–N(2) = 1.946(18), Co(1)–N(3) = 1.92(2), Co(1)–N(4) = 1.915(19), Co(1)–[N(2), N(3), N(4)] = 0.17(2) (distance of Co from mean plane), N(2)–Co(1)–N(4) = 122.7(8), N(2)–Co(1)–N(3) = 118.0(8), N(3)–Co(1)–N(4) = 117.0(8), N(2)–Co(1)–N(1) = 84.0(8), N(4)–Co(1)–N(1) = 85.1(8), N(3)–Co(1)–N(1) = 85.6(8); **2**, Co(1)–N(1) = 2.085(8), Co(1)–N(2) = 1.921(7), Co(1)–N(3) = 1.933(8), Co(1)–N(4) = 1.926(7), Co(1)–[N(2), N(3), N(4)] = 0.14(1) (distance of Co from mean plane), N(2)–Co(1)–N(4) = 120.4(3), N(2)–Co(1)–N(3) = 118.2(3), N(3)–Co(1)–N(4) = 119.8(3), N(2)–Co(1)–N(1) = 85.9(3), N(4)–Co(1)–N(1) = 86.0(3), N(3)–Co(1)–N(1) = 85.5(3); **11**, Co(1)–N(1) = 2.260(5), Co(1)–N(2) = 1.956(5), Co(1)–N(3) = 1.939(5),

Co(1)–O(1) = 1.947(4), K(1)–O(1) = 2.675(5), K(1)–O(2) = 2.677(5), Co(1)–[N(2), N(3), N(4)] = 0.62(2) (distance of Co from mean plane), N(2)–Co(1)–N(3) = 118.7(2), N(2)–Co(1)–N(1) = 81.6(2), N(3)–Co(1)–N(1) = 80.1(2), N(1)–Co(1)–O(1) = 139.41(18), N(2)–Co(1)–O(1) = 108.5(2), N(3)–Co(1)–O(1) = 122.9(2), Co(1)–O(1)–K(1) = 113.83(18), O(1)–K(1)–O(2) = 116.95(15); **12**, Co(1)–N(1) = 2.121(7), Co(1)–N(2) = 1.950(8), Co(1)–N(3) = 1.964(8), Co(1)–N(4) = 1.955(7), Co(1)–[N(2), N(3), N(4)] = 0.20(1) (distance of Co from mean plane), N(2)–Co(1)–N(4) = 119.2(3), N(2)–Co(1)–N(3) = 121.5(3), N(3)–Co(1)–N(4) = 116.2(3), N(2)–Co(1)–N(1) = 84.3(3), N(4)–Co(1)–N(1) = 84.0(2), N(3)–Co(1)–N(1) = 84.0(3).

Structures Featuring Ligand Rearrangement**.** In two instances, we have isolated a few compounds that exhibit a characteristic oxidative ligand rearrangement in the presence of traces of dioxygen or one-electron oxidants. Similarly reorganized compounds, featuring electron-donor substituents, have been previously studied in our lab and attributed, to the formation of an incipient aminyl radical.[45b,49] Indeed, the electron-rich $(L^2)Co^{II}$ (**2**) is highly sensitive to oxidative rearrangement, and provided two crystallographically characterized species, $[K(THF)_3(L^2_{re})Co^{II}–THF]$ (**2b**) and $[(L^2_{re,ox})Co^{II}–THF]$•0.5 Pentane (**2c**) (Scheme 1 and Figure S2; bonds broken in **2** and formed in **2b** and **2c** are shown in red), formed in comparable amounts. Compound **2c** is not only ligand-rearranged, but also one-electron oxidized, as noted by relevant metrical parameters associated with the phenylene ring between atoms N_1 and N_2 (Figure S2). A possible overall stoichiometry for this reaction can be written as: $2\ [(L^2)Co^{II}]^- \rightarrow [(L^2_{re})Co^{II}]^- + [(L^2_{re,ox})Co^{II}] + e^-$

Compound (L^{16})Co^{II} (**16**) is also highly sensitive to the same type of ligand rearrangement in the presence of traces of dioxygen, affording the isolable dimer $[K(THF)_2(L^{16}{}_{re})Co^{II}]_2$ (**16b**, Figure S3), which is equivalent to **2b** in terms of ligand reorganization. In this case, we were not able to isolate any other compound that might provide evidence for the location of the oxidizing equivalent(s).

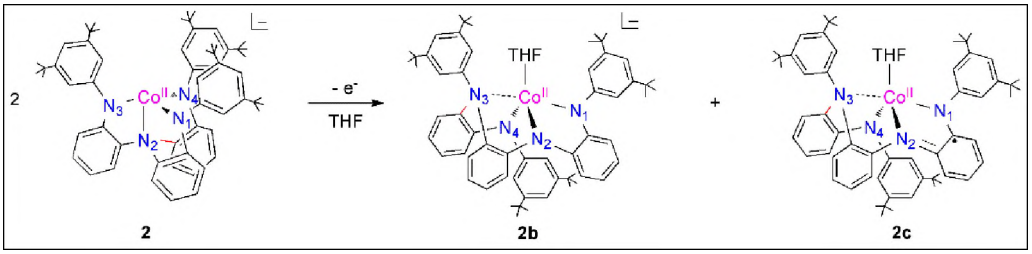

Scheme 1. Structural Rearrangement of L^{16}Co Complex

2.5. ELECTROCHEMISTRY

Ten Co(II) compounds possessing aryl (L^3Co, L^5Co, L^{13}Co), alkyl (L^9Co) and acyl arms (L^4Co, L^6Co, L^7Co, L^8Co, L^{10}Co, L^{17}Co) were selected as representative examples for examination by cyclic voltammetry. Electrochemical data for a handful of these examples have been previously reported.[48] Figure 6 provides a collective presentation of the corresponding waves (first oxidation event), and Table S2 summarizes relevant electrochemical data (potentials are reported versus the ferrocenium/ferrocene (Fc^+/Fc) couple). All aryl- and alkyl-armed Co(II) compounds examined by cyclic voltammetry feature semi-reversible waves at negative potentials, ranging from -0.665 (L^{13}Co) to -0.090 V (L^3Co), in accordance with the electron-rich nature of the corresponding substituents. Specifically for the alkyl-armed L^9Co, the two closely spaced, semi-reversible waves observed (-0.654, -0.500 V), may represent the two

slightly different Co(II) sites in the crystal structure. Given the almost identical wave currents for all these aryl- and alkyl-armed Co(II) compounds (3.0 M), and their anodic shifts with respect to the analogous Mn(II)/Mn(III) and Fe(II)/Fe(III) couples[44,46a] by approximately 0.65 and 0.25 V, respectively, we assign the corresponding semi-reversible waves to essentially metal-centered Co(II)/Co(III) cycles. In sharp contrast, the acyl-armed Co(II) compounds examined, demonstrate irreversible anodic ways with variable $i_{p,a}$ values (mostly large versus the aryl/alkyl-substituted congeners), suggesting significant ligand-centered contributions. In addition, the first anodic wave shown in Figure 6 overlaps with a subsequent oxidation wave (not shown), rendering any attempts to garner further information from exhaustive electrolysis futile. Nevertheless, all initial anodic waves for the acyl-armed Co(II) sites are shifted to positive potentials (0.032 ($L^{17}Co$) – 0.719 V ($L^{8}Co$)), reflecting the effect of the electron-withdrawing acyl arm on the Co(II) center, albeit in an order not always consistent with the electronic nature of each individual acyl group. The most significant deviation is observed for $L^{10}Co$ ($E_{p,a}$ = 0.559 V), whose anodic shift versus that of $L^{10}Mn$ ($E_{p,a}$ = -0.108 V; tentatively assigned to Mn(II)/Mn(III))[44] betrays very little, if any, metal-centered contributions to the anodic wave. The intervention of ligand-centered oxidation events does not permit any secure identification of the solution structure of species such as $L^{7}Co$ and $L^{10}Co$, which exhibit single anodic waves even in the presence of dinuclear units in their polymeric solid-state structures. On the other hand, the dual anodic-wave feature for $L^{17}Co$ (solid-state tetramer) may signify a dinuclear structure in solution.

Finally, the catalytically important L^8Co (-$COCF_3$ arm), possesses the indisputably most electrochemically stable Co(II) site encountered in this series of Co(II) compounds, in agreement with previous findings for the L^8Mn and L^8Fe analogs.[44,46a]

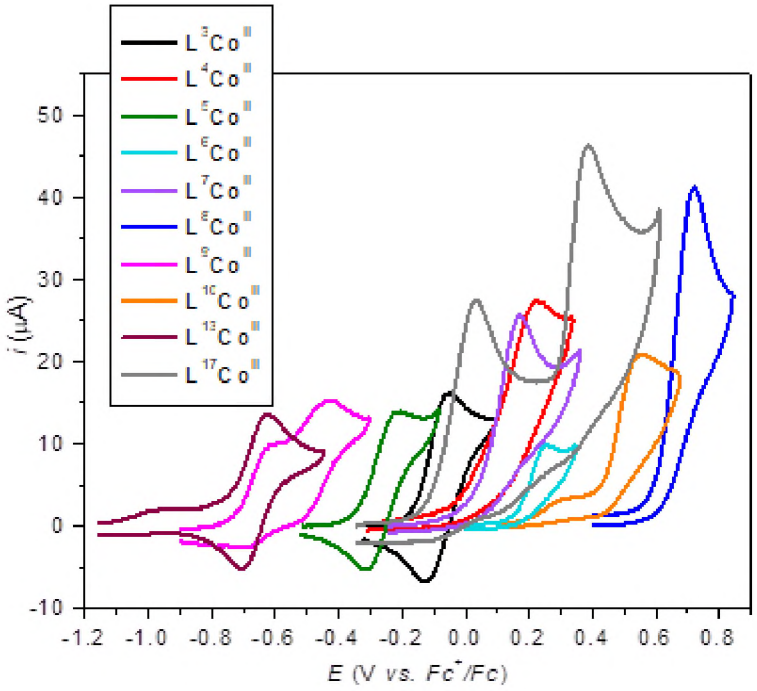

Figure 6. Cyclic voltammograms of compounds. [K(L^3)Co^{II}–NCMe] (3) and [K(NCMe)$_3$(L^{13})Co^{II}–NCMe] (13) in MeCN/(^{n}Bu$_4$N)PF_6, [K(L^4)Co^{II}]•Et_2O (4), [K(THF)$_6$][(L^5)Co^{II}]•1.5THF (5), [K(MeCN)(L^6)Co^{II}–NCMe]•2MeCN (6), [K$_2$(DMA)$_4$][K(L^7)$_2Co^{II}_2$]$_2$•2DMA (7), [K(THF)$_2$(L^8)Co^{II}] (8a), [K$_2$(L^9)$_2Co^{II}_2$] (9) and [K(THF)K(L^{17})$_2Co^{II}_2$]$_2$•3Pentane (17) in DMF/(^{n}Bu$_4$N)PF_6, and [K$_2$(DMA)$_3$(L^{10})$_2Co^{II}_2$]•0.5Et_2O (10) in DMA/(^{n}Bu$_4$N)PF_6, with a Au disk electrode (1.6 mm in diameter); scan rate 0.1 V/s.

2.6. EPR SPECTROSCOPY

EPR spectra of selected Co(II) compounds were recorded from frozen DMF solutions of **3**, **4**, **5**, **6**, 7, **8a**, **9**, **10**, **13**, **14**, **15** and **17**. In all cases, the samples give rise to signals that are consistent with isolated Co^{II} (S=3/2) species.[50] Spectra recorded at 10 K

are shown in Figure 7. The spectra can be interpreted within the framework of the spin Hamiltonian[51]:

$$\hat{H}_{zfs} = D\left[\hat{S}_z^2 - \frac{S(S+1)}{3} + \frac{E}{D}\left(\hat{S}_x^2 - \hat{S}_y^2\right)\right] + \hat{\mathbf{S}} \cdot \boldsymbol{A} \cdot \hat{\mathbf{I}} + \beta \mathbf{B} \cdot \boldsymbol{g_0} \cdot \hat{\boldsymbol{S}} \qquad (1)$$

In eq. 1, D and E are the zero field splitting (zfs) parameters. $\boldsymbol{A}$ is the hyperfine tensor relevant to the hyperfine interactions of the electronic (S = 3/2) and nuclear (I =7/2 for ^{59}Co) spins, and $\boldsymbol{g_0}$ is the intrinsic $\boldsymbol{g}$-tensor of the Co(II) ion. For simplicity we assume that the principle axes of the tensors are parallel to each other. Often, due to large spin orbit coupling effects for Co^{II} (S=3/2), the zfs parameter $|D|$ is quite large, whereas $\boldsymbol{A}$ and $\boldsymbol{g_0}$ are characterized by significant anisotropy. Under the influence of zfs, the four-fold degeneracy is partially lifted in zero magnetic field, yielding two Kramers' doublets, $|\pm 1/2\rangle$ and $|\pm 3/2\rangle$ separated by $2|D|$. The $|\pm 1/2\rangle$ (or $|\pm 3/2\rangle$) doublet is the ground state for positive (or negative) D. For $|D| \gg h\nu$ (≈ 0.31 cm^{-1} at X-band), each Kramers' doublet can be described by an effective S_{eff} = ½, giving rise to an EPR spectrum characterized by an anisotropic $\boldsymbol{g_{eff}}$ tensor.

The EPR signals shown in Figure 7 are consistent with the $|\pm 1/2\rangle$ doublet. No detailed temperature dependence of the spectra was pursued in the present work. However, spectra recorded at 4.2 and/or 20 K (not shown) indicate that the intensity of the signals (scaled as Intensity × Temperature) decreases as temperature increases. This suggests that the $|\pm 1/2\rangle$ doublet is the ground state, implying a positive value for D. For $|D| \gg h\nu$, the spectra observed do not depend on D but rather on the rhombic zfs parameter E/D, the values of the intrinsic $\boldsymbol{g_0}$-tensor[52] and the hyperfine term. With the exception of the spectrum for complex **15**, the $\boldsymbol{g_0}$-tensor was assumed axial ($g_{0x} = g_{0y} =$

$g_{0\perp} \neq g_{0z} = g_{\|}$). In several cases (**3**, **4**, **6**, 7, **8a**, **10**, **17**), the spectra indicated the presence of two Co(II) species, characterized by a different value for the parameter *E/D*. Assuming a common value for |*D*|, the simulations determine the relative abundance of each Co(II) site. The specific line shape of the spectra results from a combination of factors, including distributions on the parameter *E/D* (*E/D* strain), unresolved hyperfine interactions, and residual line-broadening mechanisms.[53] The EPR parameters for all samples, as well as the relative ratios of the two species when applicable, are presented in Table S3. Because an unequivocal deconvolution of the line broadening mechanisms is not feasible, the quoted values for the relevant parameters are indicative.

With the exception of the six-coordinate **15**, all other complexes (four- or five-coordinate) exhibit rhombic parameters (*E/D*) that lie in the interval [0, 0.19], indicating different degrees of rhombicity. All complexes (except **15**) demonstrate a valley-shaped signal at g~2.0 which corresponds to the $g_{\|}$ component of the $\boldsymbol{g}_{\boldsymbol{eff}}$-tensor. This signal is broadened due to hyperfine interactions and in some cases (**7**, **9**, **17**) the hyperfine lines are well resolved. The simulations indicate that $A_{\|}$ values in all cases are in the range of 200 - 300 MHz and that the hyperfine term has to be taken into account in order to reproduce the low field region of the spectra, corresponding to the perpendicular components of the tensors in eq. 1. Due to restrictions in the determination of the line-broadening mechanisms, it is not possible to unambiguously evaluate the magnitudes of the A_x and A_y. Therefore an average value, $A_{\perp} = (A_x + A_y)/2$, is quoted in Table S3. This value ranges in the 30-90 MHz range. Complex **15** exhibits a relatively sharp peak at g = 6.24 and an extremely broad derivative feature with an apparent zero crossing at ca. g = 2.07. This behavior indicates a rhombic system with E/D = 0.33. From this point of view,

complex **15** exhibits unique EPR properties in this series, most likely due to its special, six-coordinate ligand field, featuring two O residues in addition to the familiar [N_3N] coordination. The origin of dual EPR-active species in DMF solutions of some compounds cannot be ascertained at the present time, especially since structural data from crystals derived from DMF solutions are not available. Possible sources are small deviations in the coordination of Co(II) sites in polymeric species (as noted for **7**, crystallized from DMA solutions), and also potential differentiation arising from partial DMF coordination to Co(II) and even K^+ sites.

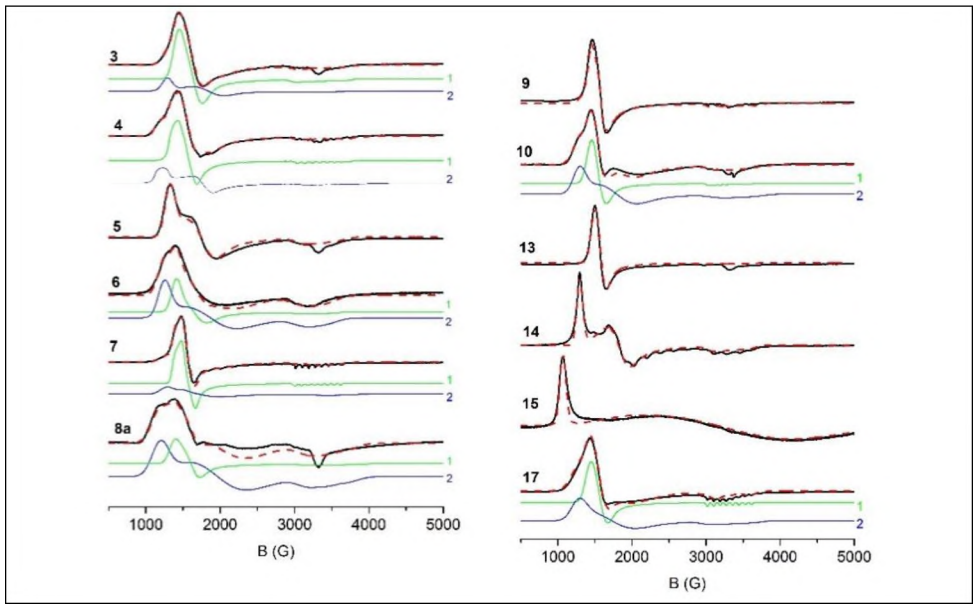

Figure 7. Experimental and theoretical EPR spectra.

In summary, the EPR studies from frozen DMF solutions of the complexes indicate that all complexes feature a Co(II) (S=3/2) ion with a large and positive zfs term, D, and variable degree of rhombicity. The existence of more than one species in some cases suggest that the coordination environment of the Co ion can be quite flexible in solution.

2.7. CATALYTIC AZIRIDINATIONS OF OLEFINS

(a) Styrene The seventeen Co^{II} compounds shown in Figure 2 were first explored as catalysts (5 mol%) for the aziridination of styrene (8.0 equiv.) by PhINTs (1.0 equiv.) in chlorobenzene at room temperature (Table 1). The high-yielding L^4Co^{II} was first investigated as catalyst in several solvents (MeCN, 50%; 2,2,2-Trifluoroethanol, 62%; $PhCF_3$, 61%; CH_2Cl_2, 61%; Benzene, 53%; PhCl, 70%) and found to afford superior levels of aziridine in chlorobenzene (similar solvent-screening results were previously obtained with Mn^{II} reagents[44]). The yield drops significantly (25%) if equimolar amounts of styrene and PhINTs are employed in PhCl, whereas a two-fold excess of styrene over PhINTs improves the yield to 46%. Increasing the amount of the L^4Co catalyst to 10 mol% suppresses the yield to 53%. The styrene aziridination yields obtained with various Co^{II} catalysts (Table 1) vary significantly (18 – 70%) as a function of the ligand employed. As opposed to the corresponding L^xMn^{II} reagents (x = 1-15)[44] that reveal a dominant relationship between increasing styrene aziridination yields with anodically shifting Mn^{II}/Mn^{III} redox potentials (and, by extension, with increasing electrophilicity of the putative Mn^{III}–$^{\bullet}$NR), the Co^{II} catalysts provide yields that indicate a more complex pattern of electronic and steric contributions. For example, although the comparatively electron-deficient, acyl-armed reagents remain, on average, more productive than aryl- or alkyl-armed congeners, a comparison between the $-COCMe_3$ (L^4) and $-COCF_3$ (L^8) supported Co^{II} reagents furnishes essentially the same aziridination yields, in spite of the fact that the Co(II)/Co(III) couple for L^8Co is anodically shifted by ~500 mV versus L^4Co. In addition, L^8Co is potentially less congested than L^4Co.

Table 1. Yields of Styrene Aziridination Mediated by Co^{II} Reagents **1-17**

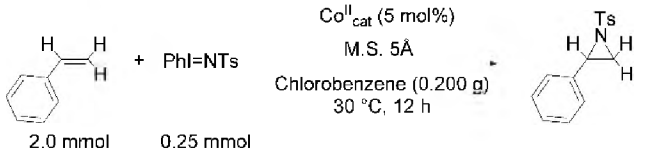

Compound	Yield (%)
[K(2.2.2-cryptand)][(L^1)Co^{II}]•3THF (**1**)	18
[K(2.2.2-cryptand)][(L^2)Co^{II}]•1.5Pentane (**2**)	18
[K(L^3)Co^{II}–NCMe] (**3**)	36
[K(L^4)Co^{II}]•Diethyl Ether (**4**)	**70**
[K(THF)$_6$](L^5)Co^{II}] • 1.5THF (**5**)	32
[K(NCMe)(L^6)Co^{II}–NCMe]•MeCN•0.5H_2O (**6**)	50
[K_2(DMA)$_4$][K(L^7)$_2Co^{II}_2$]$_2$•2DMA (**7**)	59
[K(NCMe)(L^8)Co^{II}–NCMe] (**8b**)	69
[K(DMA)$_3$(L^8)Co^{II}]$_2$ **(8c)**	68
[K_2(L^9)$_2Co^{II}_2$]$_n$ (**9**)	38
[K_2(DMA)$_3$(L^{10})$_2Co^{II}_2$]•0.5Et_2O (**10**)	49
[K(THF)(L^{11}H)Co^{II}–OH)]$_2$ (**11**)	–
[K(THF)$_3$(L^{12})Co^{II}]•THF (**12**)	25
[K(NCMe)$_3$(L^{13})Co^{II}–NCMe] (**13**)	38
[K(DMA)(L^{14})Co^{II}]•DMA (**14**)	36
[K(THF)$_3$(L^{15})Co^{II}]•THF (**15**)	45
[K(L^{16})Co^{II}–THF] (**16**)	25
[K(THF)K(L^{17})$_2Co^{II}_2$]$_2$ (**17**)	35

[a]Conditions: Catalyst, 0.0125 mmol (5 mol %); PhINTs, 0.25 mmol; styrene, 2.0 mmol; MS 5 Å, 20 mg; PhCl, 0.200 g; 30 °C; 12 h.

In contrast, the Mn^{II} and Fe^{II} congeners are associated with significantly diverging yields in favor of the more electron-deficient L^8M reagents (L^4Mn, 12%; L^8Mn, 75%; L^4Fe, 45%; L^8Fe, 73%), correlating with an anodic potential shift of approximately 600 mV for both the L^8Mn and L^8Fe catalysts with respect to their L^4M analogs. More

importantly, as indicated below, L^4Co (**4**) is faster than L^8Co (**8b**, **8c**) in mediating styrene aziridination.

The closely related L^7Co (–CO^{i}Pr arm) is in principle slightly less electron rich and sterically congested than the L^4Co congener, but affords lower yields than L^4Co in a slower reaction (the opposite is true for the corresponding Mn(II) catalysts).[44]. Two other acyl-substituted Co^{II} catalysts ($L^{14}Co$, $L^{17}Co$), exhibiting significantly lower yields, are indicative of how the metal-nitrene electron-affinity bias may be overridden by other electronic or steric factors in the fairly restricted reaction cavity of Co reagents. The corresponding $L^{14}Mn$ catalyst, by contrast, is among the most productive Mn^{II} aziridination reagents examined (yield: 67%).[44] As expected, the aryl-substituted ligands generate Co^{II} reagents that are poor mediators of styrene aziridination. These sites are oxidatively and even hydrolytically sensitive and tend to generate thermodynamic sinks. Nevertheless, the muted role of the electron-affinity criterion can still be discerned in the series of the electron-rich, aryl-armed reagents (**1**, **2**, **3**, **5**, **12**, **13**), inasmuch as the highest-yielding $L^{13}Co$ (**13**) is the most electron rich member of the group. Finally, the alkyl-substituted L^9Co and $L^{16}Co$ reagents are only modestly productive, as anticipated for electron-rich Co^{II} sites, but again the more electron rich, isopropyl-substituted L^9Co provides higher yields than the methyl-substituted congener $L^{16}Co$. However, the latter undergoes facile oxidative ligand rearrangement that may compromise its structural integrity.

(b) Alkene Aziridinations by $[K(L^4)Co^{II}]$•Diethyl Ether (4)**.** The highest yielding L^4Co (**4**) catalyst was subsequently investigated as a nitrene-transfer (NTs) mediator with a panel of aromatic, cyclo (Table 2) and aliphatic alkenes (Table S4). Styrenes substituted

at the *para* position with both electron-donor and electron-acceptor groups were examined first (entries 1-9) under the conditions noted in the previous section. Both methylene chloride and chlorobenzene were employed (as well as acetonitrile in a few instances), invariably resulting in better aziridination yields in chlorobenzene. In the majority of cases, yields above 70% were recorded irrespective of the electron-rich or poor character of the substituent, with the exception of two moderately yielding cases involving strong electron-withdrawing groups (*p*-CF_3, *p*-NO_2). Moreover, the product of 4-MeO-styrene aziridination is known to be unstable,[54] and is thus associated with modest yields. Overall, the aziridination yields for these para-substituted styrenes, save for the parent styrene, are comparable to those previously reported for L^8Co. Ortho substitution (entry 10) affects aziridination yields, presumably interfering with nitrene-transfer both sterically and electronically (due to the orthogonal orientation of the aromatic versus the olefinic plane of the substrate[55]).

Similar steric inhibition is also observed for α-substituted styrenes (methyl, phenyl; entries 11 and 12), especially for the bulkier α-phenyl-styrene. An allylic amination product is also obtained in both cases, ascribed to aziridine-ring opening,[56] which is more pronounced for the α-phenyl-substituted product.[54]

Steric hindrance is also evident in the aziridination of β-substituted styrenes (entries 13-16), especially for the bulky *cis*- and *trans*-stilbene (entries 15, 16). In agreement with previous observations in the application of L^8Co,[44] the cis congeners are more productive (entries 14, 15), with significant loss of stereochemical integrity. For all these encumbered substrates, L^8Co is on average more productive than L^4Co, presumably reflecting the somewhat more voluminous reaction cavity of L^8Co. Allylic or benzylic

aminations compete successfully with aziridinations (entries 17-22), unless cis (entry 18) and/or electron-rich (entry 21) olefins are involved.

Table 2. Yields of Aziridination/Amination of Olefins by [K(L^4)Co^{II}]•Et_2O (**4**)[a]

Entry No.	Substrate	Products		Yield (%) CH_2Cl_2/PhCl L^4Co
1.	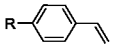	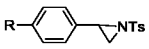	R = H	61/70
2.			R = Me	52/70
3.			R = ^{t}Bu	55/72
4.			R = OMe	30/40
5.			R = O^{t}Bu	33/72
6.			R = F	31[b]/56/71
7.			R = Cl	45[b]/52/71
8.			R = CF_3	36/49
9.			R = NO_2	36/39
10.	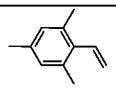	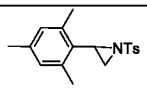		39
11.		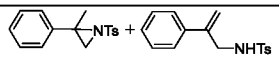		59, 3
12.	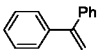	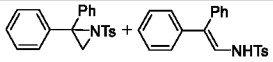		5, 15
13.	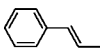	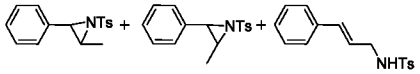		41, nd, 1
14.		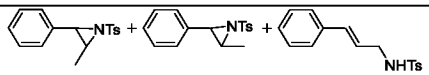		21, 31, tr
15.		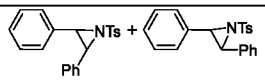		6, 8
16.	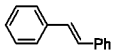	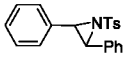		7
17.	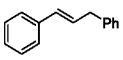	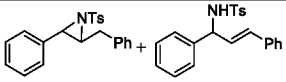		24, 21
18.		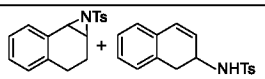		27, nd
19.		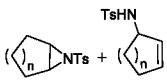	n = 1	9, 12
20.			n = 2	7, 10
21.			n = 4	41, nd
22.		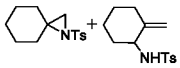		19, 20

[a]Conditions: **4**, 0.0125 mmol (5 mol %); PhINTs, 0.25 mmol; olefin, 2.0 mmol; MS 5 Å, 20 mg; solvent (MeCN/CH_2Cl_2/PhCl) 0.200 g; 30 °C; 12 h. [b]In MeCN.

Beyond cycloalkenes, other terminal or internal aliphatic olefins exhibit low aziridination yields (Table S4), in accordance with previous results pertaining to the application of L^8Co in aziridinations of aromatic and aliphatic olefins.[44] A competitive styrene versus 1-hexene (1.0 mmol each) aziridination by PhINTs (0.25 mmol) catalyzed by L^4Co (5 mol%) in chlorobenzene provided a ratio of 25:1 in favor of the styrene aziridination product (combined aziridine yield: 72%), not unlike the L^8Co catalyst (28:1, yield 73%).[44]

2.8. MECHANISTIC STUDIES

(a) Comparative Reaction Profile**.** The formation of the product of styrene aziridination was monitored as a function of time (Figure 8) for catalysts L^4Co (**4**), L^7Co (**7**) and L^8Co (**8c**) (all crystallized from DMA/ether), under the conditions noted above (Table 1), with the exception of the amount of PhCl used (500 mg). Yields were determined after quenching the reaction at various time intervals. Surprisingly, the more electron rich and sterically congested L^4Co (**4**) exhibits faster product generation than L^8Co (**8c**) during the first hour, whereas L^7Co (**7**) is kinetically comparable to **8c**. At the 1.0 hour mark, the reaction is complete by 88% for L^4Co (**4**), 65% for L^8Co (**8c**) and 76% for L^7Co (**7**). Interestingly, the MeCN-crystallized version of L^8Co, $[K(NCMe)(L^8)Co^{II}–NCMe]$ (**8b**), has been previously shown[44] to be significantly slower; only 14% of the reaction is complete after 1.0 hour in d^5-PhCl, indicating potential interference by the strongly coordinating acetonitrile. However, **8b** is still much faster than the corresponding $[K(NCMe)(L^8)M^{II}–NCMe]$ (M = Mn, Fe) reagents, presumably reflecting the superior electrophilicity of $Co^{III}–^{\bullet}NR$ as discerned from $E_{p,a}$ values associated with the M^{II}/M^{III} couple of the divalent catalysts (Fe: 0.228 V, Mn: 0.518 V, Co: 0.837 V).[44]

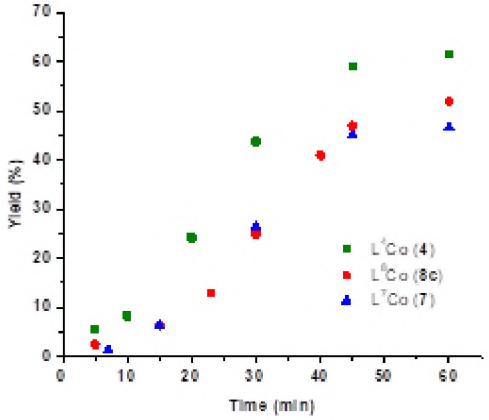

Figure 8. Yield of aziridine (%) as a function of time (min). Reaction of styrene (2.0 mmol) by PhI=NTs (0.25 mmol) mediated by L^4Co (4), L^8Co (8c), and L^7Co (7) (0.0125 mmol with respect to Co) in chlorobenzene (0.500 g) at 30 °C.

(b) Hammett Analysis**.** Several para-substituted styrenes (para substituent: Me, ^{t}Bu, F, Cl, CF_3, NO_2; 1.0 mmol each) were subjected to competitive aziridination (PhINTs, 0.25 mmol) versus styrene (1.0 mmol), mediated by L^4Co (5 mol %) in chlorobenzene (0.200 g), in the presence of 5 Å molecular sieves (25 mg). Hammett plots of $\log(k_X/k_H)$ (determined by ^{1}H NMR from the ratio of the corresponding aziridines) as a function of the substituent polar parameter σ_P or even the resonance-responsive parameter σ^+, did not provide any reliable linear free-energy correlations (Figure S4, Table S5). In contrast, Jiang's dual-parameter correlation that incorporates both polar (σ_{mb}) and spin-responsive (σ_{JJ}^*) parameters ($\log(k_X/k_H) = \rho_{mb}\sigma_{mb} + \rho_{JJ}^*\sigma_{JJ}^* + C$),[57] provides a reasonable linear correlation ($R^2 = 0.98$; Figure 9). The negative ρ_{mb} value is consistent with a small positive charge developing at the benzylic carbon, whereas the always positive ρ_{JJ}^* value denotes an incipient radical character for the same site. The ratio $|\rho_{mb}/\rho_{JJ}^*| = 1.12$ is similar to the one previously observed for L^8Co catalyzed

aziridinations ($|\rho_{mb}/\rho_{JJ}^{*}| = 1.0$),[44] and indicates competitive contributions of polar and spin-delocalization effects. Polar effects are dominant in many Rh,[24d] Cu[24d,58] and Fe[18g,59,60] catalyzed aziridinations, for which Hammett plots can be fit with the assistance of polar parameters alone (σ_p, σ^+), but the need for incorporating spin-delocalization parameters (σ^*, σ_{JJ}^*)[57,61] with a wide range of $|\rho_{mb}/\rho_{JJ}^{*}|$ values (0.04 – 2.02), is also evident in many other metal-catalyzed aziridinations.[18e,22d,g,23f,g] More recently, larger $|\rho^+/\rho_{JJ}^{*}|$ values have been reported for the aziridination of styrene by PhINNs mediated by $[Co^{III}(TAML^{red})]^-$ (5.71) and $[Co^{III}(TAML^{sq})]$ (8.64), in accordance with a novel mechanism that involves a partial single-electron transfer from the styrene to the metal-nitrene as a component of the turnover-determining step.[41]

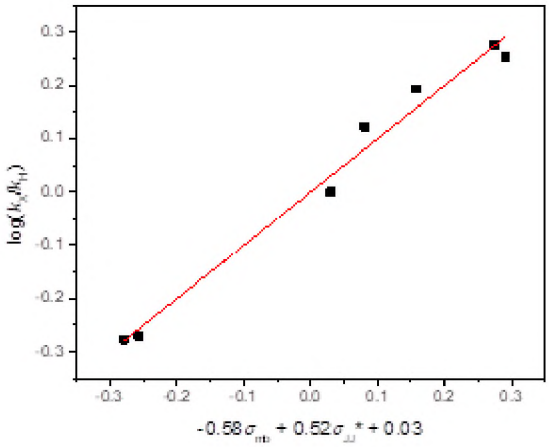

Figure 9. Linear free energy correlation of $\log(k_X/k_H)$ vs σ_{mb}, σ_{JJ}^*. Aziridination of para-substituted styrenes (X = Me, ^{t}Bu, F, Cl, CF_3, NO_2) mediated by L^4Co (4).

A similar mechanistic scenario has also been advanced for Fe-mediated aziridinations, but in this case Hammett correlations can be successfully accommodated with polar parameters alone (σ^+).[42]

(c) Kinetic Isotope Effect and Stereochemical Integrity. Evaluation of the secondary kinetic isotope effect was accomplished by ^{1}H and ^{2}H-NMR with the assistance of deuterated styrenes (α-*d*-styrene, cis- and trans-β-*d*-styrene; 1.0 mmol each) in competitive aziridinations (PhINTs, 0.25 mmol) with styrene (1.0 mmol) catalyzed by L^4Co (**4**) or L^8Co (**8c**) (5 mol %) in chlorobenzene (Table 3). KIE values close to 1.0 were obtained with α-*d*-styrene for both catalysts, indicating that the α-styrenyl is unlikely to be involved in the initial nitrene attack to styrene. In contrast, the β-styrenes are associated with inverse KIE values for L^4Co (cis: 0.90 (±0.02), trans: 0.92 (±0.02)) that can be attributed to a limited $sp^2 \rightarrow sp^3$ rehybridization of styrene's Cβ site upon development of the initial N–Cβ bond (Scheme 2). More modest inverse KIE values are also noted in cis- and trans-β-*d*-styrene aziridinations mediated by L^8Co (**8b**[44] or **8c**) (cis: 0.96 (±0.02), trans: 0.98 (±0.02)), suggesting only minimal N–Cβ bond formation in the transition state.

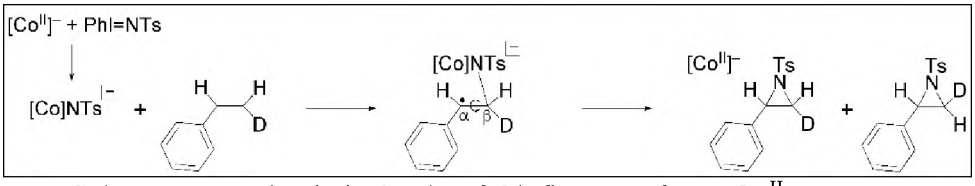

Scheme 2. Mechanistic Study of Olefin Transfer to Co^{II} Reagents

The kinetics of the aziridine ring closure (formation of the second N–Cα bond) was further evaluated by ^{2}H-NMR in the aziridinations of cis- and trans-β-*d*-styrene (Table 4), by examining the degree of stereochemical scrambling in the resulting aziridines (cis/trans partitioning due to Cα–Cβ bond rotation; Scheme 2) in competition with N–Cα bond formation. The ratio of cis/trans aziridine (94:6) and trans/cis aziridine

(92:8) resulting from the L^4Co-mediated aziridination of cis-*β-d*-styrene and trans-*β-d*-styrene, respectively, signifies the interference of very small energy barriers in aziridine-ring closure.

Table 3. Secondary KIE Values in Aziridination of Deuterated Styrenes vs Styrene

Catalyst	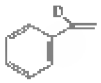		
$[K(L^4)Co^{II}]_n$ (**4**)	1.01(±0.01)	0.90(±0.02)	0.92(±0.02)
$[K(DMA)_3(L^8)Co^{II}]_2$ (**8c**)	1.00(±0.01)	0.96(±0.02)	0.98(±0.02)

Table 4. Exploration of Stereochemical Integrity in the Aziridination of cis- and trans-β-d-Styrene

Catalyst	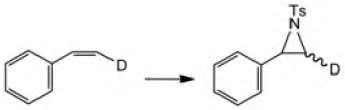	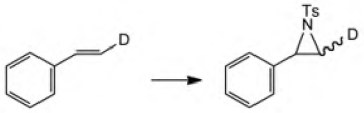
$[K(L^4)Co^{II}]_n$ (**4**)	94:6 (cis:trans aziridine)	92:8 (trans:cis aziridine)
$[K(DMA)_3(L^8)Co^{II}]_2$(**8c**)	89:11 (cis:trans aziridine)	92:8 (trans:cis aziridine)

A slightly larger barrier is indicated for the aziridination of the more sensitive cis-*β-d*-styrene by L^8Co (cis/trans aziridine: 89/11).

On the other hand, the sterochemical scrambling observed in the aziridination of cis-β-methyl-styrene is more pronounced with L^4Co than L^8Co.

2.9. COMPUTATIONAL STUDIES

The structure and electronic description of the presumptive [L^4Co]NTs intermediate were explored by DFT calculations at the B3LYP/6-31+G(d) level of theory. Free energy calculations suggest that the intermediate-spin quartet ground state (S = 3/2) lies only 0.1 kcal mol^{-1} lower than the high-spin sextet state (S = 5/2), and 2.8 kcal mol^{-1} below the doublet state (S = ½). As mentioned above, the calculated free energies for [L^8Co]NTs indicate that the high-spin sextet is the ground state, in agreement with the weaker ligand field provided by the L^8 versus L^4 ligand.

Calculated structures for the three spin-states of [L^4Co]NTs along with key metrical parameters are presented in Figure 10. The most conspicuous feature of these structures is the dissociation of one arm from the equatorial coordination sphere of the metal (Co–N = 3.93 (quartet), 3.67 (sextet), 4.08 (doublet) Å). The axial Co–N_{amine} bond is also elongated (Co–N = 2.43 (quartet), 2.63 (sextet), 2.99 (doublet) Å), if not dissociated, by comparison to that of L^4Co (2.151(11) Å). These features have been previously noted in the DFT structure of [L^8Co]NTs, although the latter exhibits an additional Co–F equatorial contact (Co–F = 2.37 Å).[44]

Most importantly, the calculated spin densities for all three spin states of [L^4Co]NTs place a full oxidizing equivalent over the dissociated arm, hence generating a widely delocalized *N*-aryl amidyl radical (Figure 11). For the ground-state quartet, the computed spin density consists of ~3.2 unpaired e^- on Co, 0.79 e^- on the nitrene N atom and –1.0 unpaired e^- on the non-coordinating arm. Similar spin densities are calculated

for the sextet (Co: 2.9 e^-, N: 0.9 e^-, ligand arm: 1.0 e^-) and the doublet state (Co: 2.8 e^-, N: –0.66 e^-, ligand arm: –1.0 e^-). This spin density distribution is accommodated by an electronic structure such as $[(^{\bullet}L^4)Co(II)–^{\bullet}NTs]^-$, featuring a high-spin Co(II) center (S = 3/2) and two oxidizing equivalents on the non-coordinating ligand arm and the N atom of the nitrene residue, respectively. In sharp contrast, the spin density of the ground-state sextet of $[L^8Co]NTs$ (Figure 11) is largely distributed on Co (3.3 e^-) and the N atom of the nitrene (1.1 e^-).

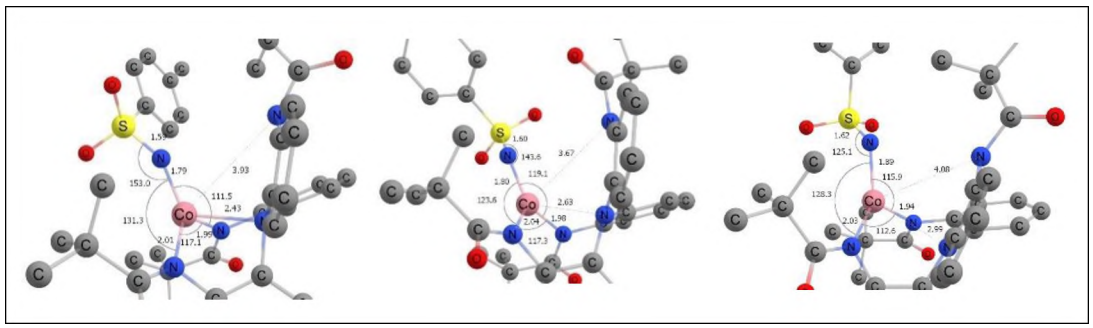

Figure 10. DFT structures for $[L^4Co]NTs$ active species in different spin states.From left to right: quartet, sextet, doublet, optimized at the B3LYP/6-31+G(d) level of theory. Hydrogen atoms omitted from the figure for clarity.

In this case, the non-coordinating arm is redox innocent, and the residual spin density is centered over ligating N atoms in a typical spin polarization fashion. Hence, the sextet state of $[L^8Co]NTs$ is better accommodated with an $[(L^8)Co(III)–^{\bullet}NTs]^-$ electronic description (S_{Co} = 2).

A global electrophilicity index (GEI) was also computed for $[L^4Co]NTs$ and $[L^8Co]NTs$ by employing Stephan's improved methodology.[62] For the quartet spin state, GEI is calculated to be 5.0 eV for $[L^4Co]NTs$ and 5.7 eV for $[L^8Co]NTs$. The corresponding values for the sextet spin state are 4.7 and 6.1 eV for $[L^4Co]NTs$ and

[L^8Co]NTs, respectively. Thus, [L^8Co]NTs is more electrophilic than [L^4Co]NTs on the basis of the GEI criterion.

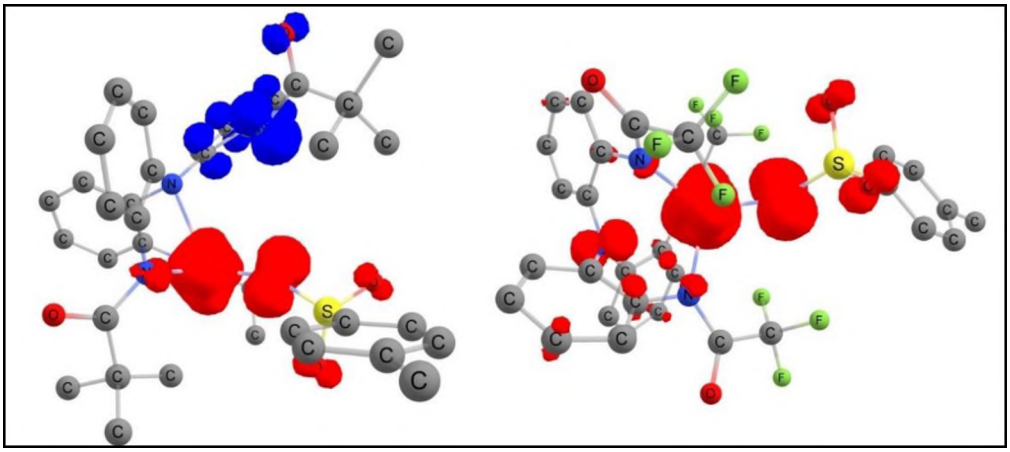

Figure 11. Spin density of the putative cobalt nitrenoid intermediates. Quartet [L^4Co]NTs (left) and sextet [L^8Co]NTs (right).

Unfortunately, all efforts to map the aziridination reaction coordinate starting from [L^4Co]NTs and styrene have not been successful in locating an acceptable transition state for the initial N–C_b bond formation. All three spin states (quartet, sextet, doublet) of [L^4Co]NTs generated large activation barriers for this initial step (~50 kcal/mol). However, when dispersion-corrected DFT was applied,[63] as appropriate for polarizable bulky groups such as the *tert*-Bu, the corresponding barriers were reduced by approximately 20 kcal/mol. These barriers are still significant by comparison to those we have previously identified for the reaction of [L^8Co]NTs (sextet) and styrene (23.4 kcal/mol for the turnover-limiting N–C_b bond formation).[44] Further experimentation and attendant DFT calculations will be required to unravel reliable trends and contributing factors with the assistance of catalysts that feature substituents spanning the CF_3 to CMe_3 range.

3. FURTHER DISCUSSION AND CONCLUSIONS

In a rigorous account, Latour and co-workers[42] highlight the importance of the electron affinity (EA) of iron-nitrene/imido species as a guiding principle for predicting their reactivity in a wide range of iron-mediated aziridinations. In these catalytic reactions, the iconic substrate styrene undergoes aziridinations by various iron-nitrene compounds (Fe=NR), under a general mechanistic scheme that designates the formation of the initial N–C_b bond as the rate-determining step, usually encountered in aziridinations with a two-step mechanism ([M]NR radical addition to styrene, ring-closure radical rebound). More importantly, this first step is front-loaded by significant charge transfer from styrene to the iron-nitrene and, thus, is crucially influenced by the EA of the active oxidant. The applicability of the EA as a general predictor of reactivity seems to be wide, but at the present time is largely confined within the realm of catalysts that provide Hammett correlations for the aziridination of para-substituted styrenes that can be accommodated with polar parameters alone (σ_P, σ^+), or by a combination of polar and spin-delocalization parameters (σ^*, σ_{JJ}^*) with dominant polar contribution.

In an almost concurrent publication, de Bruin and co-workers[41] advance a similar argument with the assistance of electrophilic Co(III)-nitrene radical aziridination reagants, generated from the reaction of anionic $[Co^{III}(TAML^{red})]^-$ or the one-electron oxidized and neutral $[Co^{III}(TAML^{sq})]$ with PhINNs. Hammett plots for para-substituted styrene aziridinations are fitted with both polar (σ^+) and spin-delocalization parameters (σ_{JJ}^*) with large $|\rho^+/\rho_{JJ}^*|$ values (5.71 for $[Co^{III}(TAML^{red})]^-$ and 8.64 for $[Co^{III}(TAML^{sq})]$), hence these systems can also be considered as good candidates for testing the EA criterion. Indeed, the larger $|\rho^+/\rho_{JJ}^*|$ value for $[Co^{III}(TAML^{sq})]$ and DFT

calculations indicate that the energy barrier for the initial, rate-limiting reaction of the incipient [Co^{III}]NNs and styrene to generate the N–C_b bond is lower for [$Co^{III}(TAML^{sq})$] versus [$Co^{III}(TAML^{red})]^-$, in agreement with an anticipated higher EA value for the nitrene species generated from [$Co^{III}(TAML^{sq})$]. Surprisingly, the experimental rate for the aziridination of styrene by these two catalysts favors [$Co^{III}(TAML^{red})]^-$ versus [$Co^{III}(TAML^{sq})$], but this has been attributed largely to the instability of the latter reagent. A distinctive feature of the Co(III) systems is associated with the redox noninnocent character of the tetraanionic ligand $(TAML^{red})^{4-}$, which can be successively oxidized in one-electron steps to $(TAML^{sq})^{3-}$ and $(TAML^{q})^{2-}$. The authors argue convincingly that the emerging radical nitrene species [$Co^{III}(TAML^{sq})(^{\bullet}NNs)]^-$/$Co^{III}(TAML^{q})(^{\bullet}NNs)_2]^-$ and [$Co^{III}(TAML^{q})(^{\bullet}NNs)$], resulting from [$Co^{III}(TAML^{red})]^-$ and [$Co^{III}(TAML^{sq})$], respectively, interact with styrene in the rate-limiting step by means of an asynchronous transition state, encompassing significant single-electron transfer from styrene to the oxidized TAML ligand and a nucleophilic attack by the nitrene lone pair (in lieu of the $^{\bullet}$NNs *p* radical) at the incipient styrenyl radical cation. The attendant single-electron relocation (TAML $\rightarrow$ Co(III) $\rightarrow$ $^{\bullet}$NNs) reestablishes the N lone pair and retains the Co(III) oxidation state. Similar participation of charge transfer in the rate-limiting transition state between high-valent metal nitrenes/imidos and sulfides has been recently showcased for many other nitrene-transfer catalysts[64] and is now established as a common mechanistic feature.

In a previous comprehensive study from our lab,[44] we have shown that a library of Mn(II) catalysts, supported by the vast majority of the ligands used in the present work ($L^{1\text{-}15}H_3$), mediates alkene aziridinations with reactivity that increases in parallel with

increasing electrophilicity of the putative $[Mn^{III}]$–$^{\bullet}$NTs active oxidant. Moreover, the electrophilicity criterion holds across the base metals, inasmuch as the reactivity of the best performing Mn(II) reagent L^8Mn is inferior to that of the more acidic L^8Co. Although the electron affinity of the metal-nitrene reigns supreme for all these reagents, the molecular interaction between $[M^{III}]$–$^{\bullet}$NR and styrene in the rate-limiting formation of the initial N–C_b bond, is quite distinct with respect to the reagents explored by Latour and deBruin. Indeed, Hammett correlations for the aziridination of styrenes mediated by our L^8M reagents (M = Mn, Fe, Co) reveal rather modest positive charge buildup on the α-styrenyl carbon (increasing with metal acidity in the expected order: Fe < Mn < Co), and require the inclusion of competitive spin-delocalization contributions ($|\rho_{mb}/\rho_{JJ}^{*}|$ = 0.75 (Mn), 1.17 (Fe), 1.00 (Co); the correlation for Fe was rather weak). The fact that these reagents demonstrate more modest charge-transfer characteristics is consistent with the operation of presumptive metal nitrenes ($[M^{III}]$–$^{\bullet}$NR) resting at a lower oxidizing level than the high-valent iron and cobalt nitrenes of Latour and de Bruin, respectively. Overall, these Mn(II) reagents and congeners can also be accommodated under the general EA criterion advanced by Latour (after all, they are catalysts engaged in typical electrophilic radical reactions), although they are not characterized by a dominant charge-transfer component. Incidentally, a strongly enhanced radical contribution, as in the case of Betley's iron dipyrrinato complexes ($|\rho_{mb}/\rho_{JJ}^{*}|$ = 0.04 for NAd),[18e] has been interpreted[42] as the result of a competitive energy barrier for the second, ring-closing step (radical rebound).

The library of the Co(II) reagents (S = 3/2) reported in this work showcases some surprising deviations from the EA criterion. Although the importance of the

electrophilicity of the metal-nitrene can still be detected in the relative enhanced yields provided by the Co(II) compounds possessing acyl- versus aryl- or alkyl-substituted ligands, the trend is certainly not as smooth and predictable as that previously encountered with the Mn(II) reagents.[44] Indeed, a closer inspection of the acyl-substituted subset of the Co(II) library of reagents reveals a wide range of yields in the aziridination of styrene that cannot be correlated with the anticipated electrophilicities of the corresponding cobalt-nitrene moieties. To further pinpoint the provenance of these disparities, we selected the high-yielding L^8Co (-$COCF_3$ arm) and L^4Co (-$COCMe_3$ arm) for further investigation. The L^8Co was previously studied[44] in tandem with the L^8Mn and L^8Fe congeners and found to be more reactive and selective than the other two base metal analogs. Mechanistic and computational studied showed that all three L^8M reagents follow a two-step styrene aziridination path (turnover-limiting addition of $[L^8M^{III}]$–$^{\bullet}$NTs to the β-styrenyl carbon followed by product-determing ring-closure via radical rebound), with activation barriers in the order Fe > Mn > Co for both steps. The trend is consistent with the anticipated metal-nitrene electrophilicities (first step) and ease of reduction from M(III) to M(II) (second step), hence highlighting the dominant role of EA *in both steps* of styrene aziridination (aliphatic olefins do not follow the same trend for the second step).

The representative case of L^4Co, however, presents a conundrum, inasmuch as its reactivity in terms of styrene aziridination yields is comparable to that provided by L^8Co. More importantly, the rate of product buildup in the first hour of the reaction mediated by L^4Co is superior to that of L^8Co (Figure 8). These results are difficult to reconcile for a reagent such as L^4Co, whose Co(II/III) couple is cathodically shifted by 500 mV versus that of L^8Co, and its nitrene derivative $[L^4Co]NTs$ is computed to have a lower global

electrophilicity index (GEI) than that of [L^8Co]NTs, in agreement with the electronic nature of the CMe_3 and CF_3 substituents. In addition, the enhanced reactivity of L^4Co deviates from that of the corresponding L^4Mn and L^4Fe reagents, which exhibit significantly lower yields (and rates) in styrene aziridinations by comparison to the L^8Mn and L^8Fe analogs, in line with their electrophilic characteristics.

Mechanistic analysis of the operation of L^4Co in styrene aziridination indicate that both polar (σ_{mb}) and spin-delocalization (σ_{JJ}^*) parameters are needed to fit Hammett plots, suggesting that both modest positive charge buildup and radical stabilization participate in the turnover-limiting step. The unexpected preponderance of the polar effect for L^4Co by comparison to L^8Co can be traced both in the slightly higher values of absolute ρ_{mb} (-0.58) and relative $|\rho_{mb}/\rho_{JJ}^*|$ (1.17) than those observed for L^8Co (ρ_{mb} = -0.56, $|\rho_{mb}/\rho_{JJ}^*|$ = 1.0). The secondary KIE values obtained from the competition between styrene and selectively deuterated styrene in aziridinations, confirm that both catalysts operate via an initial, turnover-limiting N–C_b bond formation step, but also indicate that the L^4Co mediated pathway incorporates more significant rehybridization of the β-styrenyl carbon in the transition state, hence placing this TS energetically closer to the resulting radical intermediate [L^4Co]N(Ts)–CH_2–$^{\bullet}CH_2$Ph. Moreover, the ring-closing step (radical rebound) seems to operate via a miniscule energy barrier for both L^4Co and L^8Co styrene aziridinations, but the one for L^4Co is even more suppressed than that for L^8Co, as judged by the superior retention of stereochemistry in the aziridination of the sensitive substrate cis-β-styrene. This runs counter to what is usually the main driving force for the aziridine-ring closure of styrene, namely the ease of reduction from Co(III) to

Co(II).[22g,44,65] All these mechanistic observations would have been perfectly in line, had the supporting L^4 ligand been more electron-withdrawing than L^8.

DFT calculations on the electronic and geometric disposition of the presumptive [L^4Co]NTs vis-à-vis the previously explored [L^8Co]NTs, highlight how a small ligand modification can result in a major electronic rearrangement. First, the ground state of [L^4Co]NTs is computed to be the quartet (S = 3/2), positioned slightly underneath the sextet (S = 5/2). The sextet is the clear ground state of [L^8Co]NTs, presumably due to the weaker ligand field provided by the L^8 ligand. Geometrically, both cobalt nitrenes are quite similar, their most outstanding feature being the elongation of one of the equatorial N residues to a non-coordinating position. However, spin-density calculations reveal that the non-coordinating arm of [L^4Co]NTs is one-electron oxidized, whereas the corresponding arm of [L^8Co]NTs is redox innocent. The single-electron distribution of the resulting *N*-aryl amidyl radical in [L^4Co]NTs is spread throughout the non-coordinating arm, with almost half of the spin density being localized on the N atom. Apparently, the electron withdrawing CF_3 residue protects the non-coordinating arm of [L^8Co]NTs from a similar one-electron oxidation. The overall electronic picture for the ground state of the two cobalt nitrenes is schematically summarized in Figure 12. As noted above, the [L^4Co]NTs sextet (α-spin on the N-aryl amidyl radical) is calculated to be only 0.1 kcal/mol higher in free energy relative to the quartet. Whereas a definitive justification for the higher reactivity of L^4Co, in spite of lower electrophilicity, versus L^8Co cannot be provided at the present time, the following observations should be taken into account:

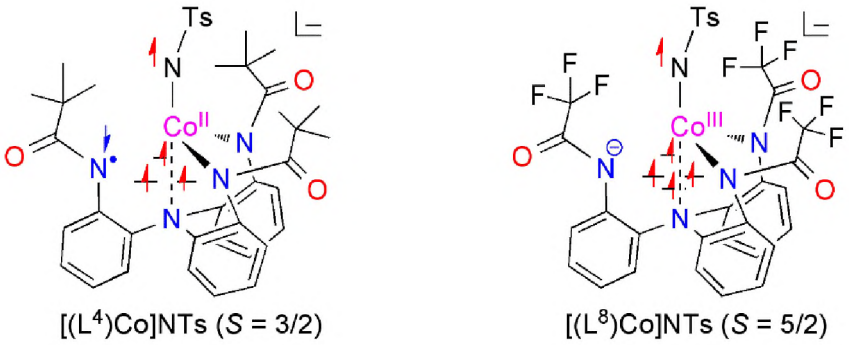

Figure 12. Schematic distribution of spins in the ground state of [L^4Co]NTs and [L^8Co]NTs

(i) Although it cannot be excluded, it is deemed rather unlikely that the ease of formation of the cobalt-nitrene itself (presumably favoring [L^4Co]NTs) will be a contributing factor, since our previous calculations for the reaction of [L^8M^{II}] (M = Mn, Fe, Co) and PhINTs indicate almost instantaneous generation of [L^8M]NTs. Rate-limiting metal-nitrene formation is more common with organic azides (RN_3).[66]

(ii) The fact that L^4M (M = Mn, Fe), as well as a wide range of other Mn(II) reagents, exhibit reactivities consistent with the EA criterion, whereas L^4Co and other Co(II) reagents demonstrate deviations, suggest that ligand-centered contributions to the overall oxidizing ability of the reagent may enable more favorable reactivity channels. Indeed, [LCo^{III}]NTs is more likely to store oxidizing equivalents on ligand residues, as inferred by the cyclic voltammograms of the LCo^{II} reagents, and anticipated due to the superior oxidizing power of Co(III) versus Mn(III) or Fe(III). Among other possibilities, *N*-aryl amidyl radicals are known to add to alkenes, at least intramolecularly,[67] and more electrophilic *N*-aryl sulfonamidyl radicals can even add intermolecularly.[68] Although they are not expected to outcompete the metal-bound nitrene radical, they might offer stabilizing interactions not yet realized. On the other hand, the similarity of the Hammett

parameters for L^4Co and L^8Co suggests that the electronic differences in the ground states of [L^4Co]NTs and [L^8Co]NTs may have only a small effect on their reactivities, but this point requires further elaboration once more information is available for the corresponding transition states.

(iii) Multiple spin-state reactivity channels,[65c,69] such as those offered by the almost isoenergetic quartet and sextet states of [L^4Co]NTs, may afford enhanced reactivity profiles in aziridinations[70] by comparison to a potentially single spin-state operation by the [L^8Co]NTs sextet.

(iv) London dispersion (LD) interactions applying intramolecularly between highly polarizable alkyl substituents (also known as σ–σ interactions), are now well established stabilizing forces of sterically congested molecules in solution, by means of favorable enthalpic contributions.[71] The *tert*-Bu group and other conformationally rigid alkyl groups (flexible alkyl groups have an unfavorable entropic impact)[72] have been credited as "dispersion energy donors",[73] and deemed responsible for stabilizing many highly congested organic and inorganic compounds.[71-74] More importantly, LD forces have started receiving recognition as contributors to observed chemical reactivity and catalytic outcomes.[75] In the more tight reaction cavity of cobalt reagents, the stabilization offered by *tert*-Bu groups via LD interactions can play a significant role, as already noted in our initial dispersion-corrected DFT calculations. Interestingly, the L^7Co reagent, which carries the less polarizable *i*-Pr substituent, demonstrates lower aziridination rates, not unlike those of L^8Co.

Future experimental and computational work will seek to disentangle and quantify the factors contributing to the enhancement of catalytic reactivity above and beyond the

underlying electrophilic character of the active oxidant, and further explore whether reagents with other rigid alkyl substituents can be superior mediators of nitrene-transfer chemistry.

ACKNOWLEDGEMENTS

This work was generously supported by the National Institute of General Medical Sciences of the National Institutes of Health under Award Numbers R15GM117508 and R15GM139071 (to P.S.), and in part by the National Science Foundation through grant CHE-0412959 (to P.S.). Authors Z. S. and T. R. C. further acknowledge the U.S. National Science Foundation for partial support of this research through grants CHE-1464943 and CHE-1953547. Authors G. R. and P. P. also thank the Special Account of Research Grants of the National and Kapodistrian University of Athens for partial support. We thank the reviewers for many insightful comments.

REFERENCES

(1) (a) *Aziridines and Epoxides in Organic Synthesis*; Yudin, A. K., Ed.; Wiley-VCH: Weinheim, 2006. (b) Padwa, A. "Aziridines and Azirines: Monocyclic" in *Comprehensive Heterocyclic Chemistry III*, Katritzky, A. R.; Ramsden, C. A.; Scriven, E. F. V.; Taylor, R. J. K., Eds.; Elsevier Science: Amsterdam, 2008, Vol. 1, pp 1-104 (c) Sweeney, J. B. Aziridines: epoxides' ugly cousins? *Chem. Soc. Rev.* **2002**, *31*, 247-258. (d) Lapinsky, D. J. Three-Membered Ring Systems. *Prog. Heterocycl. Chem.* **2015**, *27*, 61-85. (e) Botuha, C.; Chemla, F.; Ferreira, F.; Pérez-Luna, A. Aziridines in Natural Product Synthesis, in *Heterocycles in Natural Product Synthesis*, Majumdar, K. C.; Chattopadhyay, S. K., Eds.; Wiley-VCH: Weinheim, 2011, pp 1-39. (f) Padwa, A.; Murphree, S. S. Epoxides and aziridines – A mini review. *Arkivoc* **2006**, 6-33.

(2) (a) Ouyang, K.; Hao, W.; Zhang, W.-X.; Xi, Z. Transition-Metal-Catalyzed Cleavage of C–N Single Bonds. *Chem. Rev.* **2015**, *115*, 12045-12090. (b) Rotstein, B. H.; Zaretsky, S.; Rai, V.; Yudin, A. K. Small Heterocycles in Multicomponent Reactions. *Chem. Rev.* **2014**, *114*, 8323-8359. (c) Huang, C.-Y. Doyle, A. G. The Chemistry of Transition Metals with Three-Membered Ring Heterocycles. *Chem. Rev.* **2014**, *114*, 8153-8198. (d) Stankovic, S.; D'hooghe, M.; Catak, S.; Eum, H.; Waroquier, M.; Van Speybroeck, V.; De Kimpe, N.; Ha, H.-J. Regioselectivity in the ring opening of non-activated aziridines. *Chem. Soc. Rev.* **2012**, *41*, 643-665. (e) Cardoso, A. L.; Pinho e Melo, T. M. V. D. Aziridines in Formal [3+2] Cycloadditions: Synthesis of Five-Membered Heterocycles. *Eur. J. Org. Chem.* **2012**, 6479-6501. (f) Lu, P. Recent developments in regioselective ring opening of aziridines. *Tetrahedron* **2010**, *66*, 2549-2560. (g) Schneider, C. Catalytic, Enantioselective Ring Opening of Aziridines. *Angew. Chem. Int. Ed.* **2009**, *48*, 2082-2084. (h) Hu, X. E. Nucleophilic ring opening of aziridines. *Tetrahedron* **2004**, *60*, 2701-2743. (i) McCoull, W.; Davis, F. A. Recent Synthetic Applications of Chiral Aziridines. *Synthesis* **2000**, 1347-1365.

(3) a) Tomasz, M.; Mitomycin C. Small, fast and deadly (but very selective). *Chem. Biol.* **1995**, *2*, 575-579. (b) Coleman, R. S.; Li, J.; Navarro, A. Total Synthesis of Azinomycin A. *Angew. Chem. Int. Ed.* **2001**, *40*, 1736-1739. (c) Zhao, Q.; He, Q.; Ding, W.; Tang, M.; Kang, Q.; Yu, Y.; Deng, W.; Zhang, Q.; Fang, J.; Tang, G.; Liu, W. Characterization of the Azinomycin B Biosynthetic Gene Cluster Revealing a Different Iterative Type I Polyketide Synthase for Naphthoate Biosynthesis. *Chem. Biol.* **2008**, *15*, 693-705. (d) Ogasawara, Y.; Liu, H.-W. Biosynthetic Studies of Aziridine Formation in Azicemicins. *J. Am. Chem. Soc.* **2009**, *131*, 18066-18068. (e) Nakao, Y.; Fujita, M.; Warabi, K.; Matsunaga, S.; Fusetani, N. Miraziridine A, a Novel Cysteine Protease Inhibitor from the Marine Sponge *Theonella* aff. *Mirabilis*. *J. Am. Chem. Soc.* **2000**, *122*, 10462-10463

(4) (a) Ismail, F. M. D.; Levitsky, D. O.; Dembitsky, V. M. Aziridine alkaloids as potential therapeutic agents. *Eur. J. Med. Chem.* **2009**, *44*, 3373-3387. (b) Ballereau, S.; Andrieu-Abadie, N.; Saffon, N.; Génisson, Y. Synthesis and biological evaluation of aziridine-containing analogs of phytosphingosine. *Tetrahedron* **2011**, *67*, 2570-2578. (c) Dorr, R. T.; Wisner, L.; Samulitis, B. K.; Landowski, T. H.; Remers, W. A. Anti-tumor activity and mechanism of action for a cyanoaziridine-derivative, AMP423. *Cancer Chemother. Pharmacol.* **2012**, *69*, 1039-1049. (d) Pillai, B.; Cherney, M. M.; Diaper, C. M.; Sutherland, A.; Blanchard, J. S.; Vederas, J. C.; James, M. N. G. Structural insights into stereochemical inversion by diaminopimelate epimerase: An antibacterial drug target. *Proc. Natl. Acad. Sci. U.S.A.* **2006**, *103*, 8668-8673.

(5) (a) Ujjain, S. K.; Bhatia, R.; Ahuja, P. Aziridine-functionalized graphene: Effect of aromaticity for aryl functional groups on enhanced power conversion efficiency of organic photovoltaic cells. *J. Saudi Chem. Soc.* **2019**, *23*, 655-665. (b) Tuci, G.; Filippi, J.; Ba, H.; Rossin, A.; Luconi, L.; Pham-Huu, C.; Vizza, F.; Giambastiani, G. How to teach an old dog new (electrochemical) tricks: aziridine-functionalized CNTs as efficient electrocatalysts for the selective CO_2 reduction to CO. *J. Mater. Chem. A* **2018**, *6*, 16382-16389. (c) Moon, H. K.; Kang, S.; Yoon, H. J. Aziridine-functionalized polydimethylsiloxanes for tailorable polymeric scaffolds: aziridine as a clickable moiety for structural modification of materials. *Polym. Chem.* **2017**, *8*, 2287-2291. (d) Tuci, G.; Luconi, L.; Rossin, A.; Berretti, E.; Ba, H.; Innocenti, M.; Yakhvarov, D.; Caporali, S.; Pham-Huu, C.; Giambastiani, G. Aziridine-Functionalized Multiwalled Carbon Nanotubes: Robust and Versatile Catalysts for the Oxygen Reduction Reaction and Knoevenagel Condensation. *ACS Appl. Mater. Interfaces* **2016**, *8*, 30099-30106. (e) Chen, R.; Chen, J. S.; Zhang, C.; Kessler, M. R. Rapid room-temperature polymerization of bio-based multiaziridine-containing compounds. *RSC Adv.* **2015**, *5*, 1557-1563. (f) Kim, H.-J.; Chaikittisilp, W.; Jang, K.-S.; Didas, S. A.; Johnson, J. R.; Koros, W. J.; Nair, S.; Jones, C. W. Aziridine-Functionalized Mesoporous Silica Membranes on Polymeric Hollow Fibers: Synthesis and Single-Component CO_2 and N_2 Permeation Properties. *Ind. Eng. Chem. Res.* **2015**, *54*, 4407-4413.

(6) (a) Degennaro, L.; Trinchera, P.; Luisi, R. Recent Advances in the Stereoselective Synthesis of Aziridines. *Chem. Rev.* **2014**, *114*, 7881-7929. (b) Pellissier, H. Recent Developments in Asymmetric Aziridination. *Adv. Synth. Catal.* **2014**, *356*, 1899-1935. (c) Pellissier, H. Recent developments in asymmetric aziridination. *Tetrahedron* **2010**, *66*, 1509-1555. (d) Singh, G. S.; D'hooghe, M.; De Kimpe, N. Synthesis and Reactivity of *C*-Heteroatom-Substituted Aziridines. *Chem. Rev.* **2007**, *107*, 2080-2135. (e) Watson, I. D. G.; Yu, L.; Yudin, A. K. Advances in Nitrogen Transfer Reactions Involving Aziridines. *Acc. Chem. Res.* **2006**, *39*, 194-206. (f) Osborn, H. M. I.; Sweeney, J. The asymmetric synthesis of aziridines. *Tetrahedron: Asymmetry* **1997**, *8*, 1693-1715.

(7) (a) Darses, B.; Rodrigues, R.; Neuville, L. Mazurais, M.; Dauban, P. Transition metal-catalyzed iodine(III)-mediated nitrene transfer reactions: efficient tools for challenging syntheses. *Chem. Commun.* **2017**, *53*, 493-508. (b) Chang, J. W. W.; Ton, T. M. U.; Chan, P. W. H. Transition-metal-catalyzed aminations and aziridinations of C–H and C=C bonds with iminoiodinanes. *Chem. Rec.* **2011**, *11*, 331-357. (c) Karila, D.; Dodd, R. H. Recent Progress in Iminoiodane-Mediated Aziridination of Olefins. *Curr. Org. Chem.* **2011**, *15*, 1507-1538.

(8) (a) Chanda, B. M.; Vyas, R.; Landge, S. S. Synthesis of aziridines using new catalytic systems with bromamine-T as the nitrene source. *J. Mol. Catal. A: Chem.* **2004**, *223*, 57-60. (b) Chanda, B. M.; Vyas, R.; Bedekar, A. V. Investigations in the Transition Metal catalyzed Aziridination of Olefins, Amination, and Other Insertion Reactions with Bromamine-T as the Source of Nitrene. *J. Org. Chem.* **2001**, *66*, 30-34.

(9) (a) Ma, Z.; Zhou, Z.; Kürti, L. Direct and Stereospecific Synthesis of N-H and N-Alkyl Aziridines from Unactivated Olefins Using Hydroxylamine-O-Sulfonic Acids. Angew. Chem. Int. Ed. 2017, 56, 9886-9890. (b) Jat, J. L.; Paudyal, M. P.; Gao, H.; Xu, Q.-L.; Yousufuddin, M.; Devarajan, D.; Ess, D. H.; Kürti, L.; Falck, J. R. Direct Stereospecific Synthesis of Unprotected N-H and N-Me Aziridines from Olefins. *Science* **2014**, *343*, 61-65. (c) Lebel, H.; Huard, K.; Lectard, S. *N*-Tosyloxycarbamates as a Source of Metal Nitrenes: Rhodium-Catalyzed C–H Insertion and Aziridination Reactions. *J. Am. Chem. Soc.* **2005**, *127*, 14198-14199.

(10) (a) Driver, T. G. Recent advances in transition metal-catalyzed *N*-atom transfer reactions of azides. *Org. Biomol. Chem.* **2010**, *8*, 3831-3846. (b) Intrieri, D.; Zardi, P.; Caselli, A.; Gallo, E. Organic azides: *"energetic reagents"* for the *inter*molecular amination of C–H bonds. *Chem. Commun.* **2014**, *50*, 11440-11453.

(11) (a) Hao, W.; Wu, X.; Sun, J. Z.; Siu, J. C.; MacMillan, S. N.; Lin, S. Radical Redox-Relay Catalysis: Formal [3+2] Cycloaddition of *N*-Acylaziridines and Alkenes. *J. Am. Chem. Soc.* **2017**, *139*, 12141-12144. (b) Goossens, H.; Vervisch, K.; Catak, S.; Stanković, S.; D'hooghe, M.; De Proft, F.; Geerlings, P.; De Kimpe, N.; Waroquier, M.; Van Speybroeck, V. Reactivity of Activated versus Nonactivated 2-(Bromomethyl)aziridines with respect to Sodium Methoxide: A Combined Computational and Experimental Study. *J. Org. Chem.* **2011**, *76*, 8698-8709. (c) Li, L.; Zhang, J. Lewis Acid-catalyzed [3+2] Cycloaddition of Alkynes with N-Tosyl-aziridines via Carbon–Carbon Bond Cleavage: Synthesis of Highly Substituted 3-Pyrrolines. *Org. Lett.* **2011**, *13*, 5940-5943. (d) Dauban, P.; Dodd, R. H. PhI=NSes: A New Iminoiodinane Reagent for the Copper-Catalyzed Aziridination of Olefins. *J. Org. Chem.* **1999**, *64*, 5304-5307. (e) Alonso, D. A.; Andersson, P. G. Deprotection of Sulfonyl Aziridines. *J. Org. Chem.* **1998**, *63*, 9455-9461. (f) Bergmeier, S. C.; Seth, P. P. A general method for deprotection of *N*-toluenesulfonyl aziridines using sodium naphthalenide. *Tetrahedron Lett.* **1999**, *40*, 6181-6184.

(12) (a) Zhu, Y.; Wang, Q.; Cornwall, R. G.; Shi, Y. Organocatalytic Asymmetric Epoxidation and Aziridination of Olefins and Their Synthetic Applications. *Chem. Rev.* **2014**, *114*, 8199-8256. (b) Zhang, Y.; Lu, Z.; Wulff, W. D. Catalytic Asymmetric Aziridination with Catalysts Derived from VAPOL and VANOL. *Synlett* **2009**, 2715-2739. (c) Yoshimura, A.; Middleton, K. R.; Zhu, C.; Nemykin, V. N.; Zhdankin, V. V. Hypoiodite-Mediated Metal-Free catalytic Aziridination of Alkenes. *Angew. Chem. Int. Ed.* **2012**, *51*, 8059-8062. (d) Siu, T.; Yudin, A. K. Practical Olefin Aziridination with a Broad Substrate Scope. *J. Am. Chem. Soc.* **2002**, *124*, 530-531.

(13) (a) Chandrachud, P. P.; Jenkins, D. M. Transition Metal Aziridination Catalysts, in *Encyclopedia of Inorganic and Bioinorganic Chemistry*; Wiley Online Library, 2017; pp. 1-11. (b) Che, C.-M.; Lo, V. K.-Y.; Zhou, C.-Y. Oxidation by Metals (Nitrene), in *Comprehensive Organic Synthesis II*, 2nd ed.; Knochel, P.; Molander, G. A., Eds.; Elsevier: Amsterdam, 2014, Vol. 7; pp. 26-85. (c) Jung, N.; Bräse, S. New Catalysts for the Transition-Metal-Catalyzed Synthesis of Aziridines. *Angew. Chem. Int. Ed.* **2012**, *51*, 5538-5540. (d) Jiang, H.; Zhang, X. P. Oxidation: C–N Bond Formation by Oxidation (Aziridines), in *Comprehensive Chirality*; Carreira, E. M.; Yamamoto, H., Eds.; Elsevier: Amsterdam, 2012, Vol. 5; pp. 168-182. (e) Mößner, C.; Bolm, C. Catalyzed Asymmetric Aziridinations, in *Transition Metals for Organic Synthesis*, 2nd ed.; Beller, M.; Bolm, C., Eds.; Wiley-VCH: Weinheim, Germany, 2004; pp. 389-402. (f) Halfen, J. A. Recent Advances in Metal-Mediated Carbon-Nitrogen Bond Formation Reactions: Aziridination and Amidation. *Curr. Org. Chem.* **2005**, *9*, 657-669.

(14) Historic Mn/Fe Porphyrinoid Systems: (a) Mansuy, D.; Mahy, J.-P.; Dureault, A.; Bedi, G.; Battioni, P. Iron- and manganese-porphyrin catalysed aziridination of alkenes by tosyl- and acyl-iminoiodobenzene. *J. Chem. Soc., Chem. Commun.* **1984**, 1161-1163. (b) Mahy, J.-P.; Battioni, P.; Mansuy, D. Formation of an Iron(III) Porphyrin Complex with a Nitrene Moiety Inserted into a Fe–N Bond during Alkene Aziridination by [(Tosylimido)iodo]benzene Catalyzed by Iron(III) Porphyrins. *J. Am. Chem. Soc.* **1986**, *108*, 1079-1080. (c) Mahy, J.-P.; Bedi, G.; Battioni, P.; Mansuy, D. Aziridination of alkenes catalysed by porphyrinirons: Selection of catalysts for optimal efficiency and stereospecificity. *J. Chem. Soc., Perkin Trans 2* **1988**, 1517-1524. (d) Groves, J. T.; Takahashi, T. Activation and Transfer of Nitrogen from Nitridomanganese(V) Porphyrin Complex. The Aza Analogue of Epoxidation. *J. Am. Chem. Soc.* **1983,** *105*, 2073-2074.

(15) For select reviews of metal porphyrinoid nitrene-transfer systems, see: (a) Intrieri, D.; Carminati, D. M.; Gallo, E. Recent Advances in Metal Porphyrinoid-Catalyzed Nitrene and Carbene Transfer Reactions, in *Handbook of Porphyrin Science*; Kadish, K. M.; Smith, K. M.; Guilard, R., Eds.; World Scientific, 2016, Vol. 38, pp. 1-99. (b) Anding, B. J.; Woo, L. K. An Overview of Metalloporphyrin-Catalyzed Carbon and Nitrogen Group Transfer Reactions, in *Handbook of Porphyrin Science*; Kadish, K. M.; Smith, K. M.; Guilard, R., Eds.; World Scientific, 2012, Vol. 21, pp. 145-319. (c) Ruppel, J. V.; Fields, K. B.; Snyder, N. L.; Zhang, X. P. Metalloporphyrin-Catalyzed Asymmetric Atom/Group Transfer Reactions, in *Handbook of Porphyrin Science*; Kadish, K. M.; Smith, K. M.; Guilard, R., Eds.; World Scientific, 2010, Vol. 10, pp. 1-84. (d) Fantauzzi, S.; Caselli, A.; Gallo, E. Nitrene transfer reactions mediated by metallo-porphyrin complexes. *Dalton Trans.* **2009**, 5434-5443.

(16) For select reviews of engineered hemoproteins for nitrene transfer to alkenes, see: (a) Brandenberg, O. F.; Fasan, R.; Arnold, F. H. Exploiting and engineering hemoproteins for abiological carbene and nitrene transfer reactions. *Curr. Opin. Biotechnol.* **2017**, *47*, 102-111. (b) Farwell, C. C.; Zhang, R. K.; McIntosh, J. A.; Hyster, T. K.; Arnold, F. H. Enantioselective Enzyme-Catalyzed Aziridination Enabled by Active-Site Evolution of a Cytochrome P450. *ACS Cent. Sci.* **2015**, *1*, 89-93. (c) Gober, J. G.; Brustad, E. M. Non-natural carbenoid and nitrenoid insertion reactions catalyzed by heme proteins. *Curr. Opin. Chem. Biol.* **2016**, *35*, 124-132.

(17) For select examples of Mn-based nitrene-transfer to alkenes, see: (a) Zdilla, M. J.; Abu-Omar, M. M. Mechanism of Catalytic Aziridination with Manganese Corrole: The Often Postulated High-Valent Mn(V) Imido Is Not the Group Transfer Reagent. *J. Am. Chem. Soc.* **2006**, *128*, 16971-16979. (b) Nishikori, H.; Katsuki, T. Catalytic and highly enantioselective aziridination of styrene derivatives. *Tetrahedron Lett.* **1996**, *37*, 9245-9248. (c) Minakata, S.; Ando, T.; Nishimura, M.; Ryu, I.; Komatsu, M. Novel Asymmetric and Stereospecific Aziridination of Alkenes with a Chiral Nitridomanganese Complex. *Angew. Chem. Int. Ed.* **1998**, *37*, 3392-3394. (d) Du Bois, J.; Tomooka, C. S.; Hong, J.; Carreira, E. M. Nitridomanganese(V) Complexes: Design, Preparation, and Use as Nitrogen Atom-Transfer Reagents. *Acc. Chem. Res.* **1997**, *30*, 364-372. (e) Lai, T.-S.; Kwong, H.-L.; Che, C.-M.; Peng, S.-M. Catalytic and asymmetric aziridination of alkenes catalyzed by a chiral manganese porphyrin complex. *Chem. Commun.* **1997**, 2373-2374. (f) Liang, J.-L.; Huang, J.-S.; Yu, X.-Q.; Zhu, N.; Che, C.-M. Metalloporphyrin-Mediated Asymmetric Nitrogen-Atom Transfer to Hydrocarbons: Aziridination of Alkenes and Amidation of Saturated C−H Bonds Catalyzed by Chiral Ruthenium and Manganese Porphyrins. *Chem. Eur. J.* **2002**, *8*, 1563-1572. (g) O'Connor, K. J.; Wey, S.-J.; Burrows, C. J. Alkene aziridination and epoxidation catalyzed by chiral metal salen complexes. *Tetrahedron Lett.* **1992**, *33*, 1001-1004.

(18) For select examples of Fe-based nitrene-transfer to alkenes, see: (a) Damiano, C.; Intrieri, D.; Gallo, E. Aziridination of alkenes promoted by iron or ruthenium complexes. *Inorg. Chim. Acta* **2018**, *470*, 51-67. (b) Fingerhut, A.; Serdyuk, O. V.; Tsogoeva, S. B. *Non-heme iron* catalysts for epoxidation and aziridination reactions of challenging terminal alkenes: towards sustainability. *Green Chem.* **2015**, *17*, 2042-2058. (c) Correa, A.; Mancheño, O. G.; Bolm, C. Iron-catalysed carbon-heteroatom and heteroatom-heteroatom bond forming processes. *Chem. Soc. Rev.* **2008**, *37*, 1108-1117. (d) Iovan, D. A.; Betley, T. A. Characterization of Iron-Imido Species Relevant for *N*-Group Transfer Chemistry. *J. Am. Chem. Soc.* **2016**, *138*, 1983-1993. (e) Hennessy, E. T.; Liu, R. Y.; Iovan, D. A.; Duncan, R. A.; Betley, T. A. Iron-mediated intermolecular N-group transfer chemistry with olefinic substrates. *Chem. Sci.* **2014**, *5*, 1526-1532. (f) King, E. R.; Hennessy, E. T.; Betley, T. A. Catalytic C−H Bond Amination from High-Spin Iron Imido Complexes. *J. Am. Chem. Soc.* **2011**, *133*, 4917-4923. (g) Patra, R.; Coin, G.; Castro, L.; Dubourdeaux, P.; Clémancey, M.; Pécaut, J.; Lebrun, C.; Maldivi, P.; Latour, J.-M. Rational design of Fe catalysts for olefin aziridination through DFT-based mechanistic analysis. *Catal. Sci. Technol.* **2017**, *7*, 4388-4400. (h) Avenier, F.; Latour, J.-M. Catalytic aziridination of olefins and amidation of thioanisole by a non-heme iron complex. *Chem. Commun.* **2004**, 1544-1545. (i) Liu, Y.; Che, C. M. [$Fe^{III}(F_{20}$-tpp)Cl] Is an Effective Catalyst for Nitrene Transfer Reactions and Amination of Saturated Hydrocarbons with Sulfonyl and Aryl Azides as Nitrogen Source under Thermal and Microwave-Assisted Conditions. *Chem. Eur. J.* **2010**, *16*, 10494-10501. (j) Klotz, K. L.; Slominski, L. M.; Hull, A. V.; Gottsacker, V. M.; Mas-Ballesté, R.; Que, L., Jr.; Halfen, J. A. Non-heme iron(II) complexes are efficient olefin aziridination catalysts. *Chem. Commun.* **2007**, 2063-2065. (k) Klotz, K. L.; Slominski, L. M.; Riemer, M. E.; Phillips, J. A.; Halfen, J. A. Mechanism of the Iron-Mediated Alkene Aziridination reaction: Experimental and Computational Investigations. *Inorg. Chem.* **2009**, *48*, 801-803. (l) Chandrachud, P. P.; Bass, H. M.; Jenkins, D. M. Synthesis of Fully Aliphatic Aziridines with a Macrocycle Tetracarbene Iron Catalyst. *Organometallics* **2016**, *35*, 1652-1657. (m) Cramer, S. A.; Jenkins, D. M. Synthesis of Aziridines from Alkenes and Aryl Azides with a Reusable Macrocyclic Tetracarbene Iron Catalyst. *J. Am. Chem. Soc.* **2011**, *133*, 19342-19345. (n) Muñoz, S. B., Jr.: Lee, W.-T.; Dickie, D. A.; Scepaniak, J. J.; Subedi, D.; Pink, M.; Johnson, M. D.; Smith, J. M. Styrene Aziridination by Iron(IV) Nitrides. *Angew. Chem. Int. Ed.* **2015**, *54*, 10600-10603. (o) Nakanishi, M.; Salit, A.-F.; Bolm, C. Iron-Catalyzed Aziridination Reactions. *Adv. Synth. Catal.* **2008**, *350*, 1835-1840. (p) Mayer, A. C.; Salit, A.-F.; Bolm, C. Iron-catalysed aziridination reactions promoted by an ionic liquid. *Chem. Commun.* **2008**, 5975-5977.

(19) For select examples of Co-based nitrene-transfer to alkenes, see: (a) Jiang, H.; Lang, K.; Lu, H.; Wojtas, L.; Zhang, X. P. Asymmetric Radical Bicyclization of Allyl Azidoformates via Cobalt(II)-Based Metalloradical Catalysis. *J. Am. Chem. Soc.* **2017**, *139*, 9164-9167. (b) Jiang, H.; Lang, K.; Lu, H.; Wojtas, L.; Zhang, X. P. Intramolecular Radical Aziridination of Allylic Sulfamoyl Azides by Cobalt(II)-Based Metalloradical Catalysis: Effective Construction of Strained Heterobicyclic Structures. *Angew. Chem. Int. Ed.* **2016**, *55*, 11604-11608. (c) Subbarayan, V.; Jin, L.-M.; Cui, X.; Zhang, X. P. Room temperature activation of aryloxysulfonyl azides by [Co(II)(TPP)] for selective radical aziridination of alkenes via metalloradical catalysis. *Tetrahedron Lett.* **2015**, *56*, 3431-3434. (d) Tao, J.; Jin, L.-M.; Zhang, X. P. Synthesis of chiral N-phosphoryl aziridines through enantioselective aziridination of alkenes with phosphoryl azide via Co(II)-based metalloradical catalysis. *Beilstein J. Org. Chem.* **2014**, *10*, 1282-1289. (e) Jin, L.-M.; Xu, X.; Lu, H.; Cui, X.; Wojtas, L.; Zhang, X. P. Effective Synthesis of Chiral *N*-Fluoroaryl Aziridines through Enantioselective Aziridination of Alkenes with Fluoroaryl Azides. *Angew. Chem. Int. Ed.* **2013**, *52*, 5309-5313. (f) Suarez, A. I. O.; Jiang, H.; Zhang, X. P.; de Bruin, B. The radical mechanism of cobalt(II) porphyrin-catalyzed olefin aziridination and the importance of cooperative H-bonding. *Dalton Trans.* **2011**, *40*, 5697-5705. (g) Lu, H.; Jiang, H.; Hu, Y.; Wojtas, L.; Zhang, X. P. Chemoselective intramolecular allylic C–H amination *versus* C=C aziridination through Co(II)-based metalloradical catalysis. *Chem. Sci.* **2011**, *2*, 2361-2366. (h) Subbarayan, V.; Ruppel, J. V.; Zhu, S.; Perman, J. A.; Zhang, X. P. Highly asymmetric cobalt-catalyzed aziridination of alkenes with trichloroethoxysulfonyl azide ($TcesN_3$). *Chem. Commun.* **2009**, 4266-4268. (i) Jones, J. E.; Ruppel, J. V.; Gao, G.-Y.; Moore, T. M.; Zhang, X. P. Cobalt-Catalyzed Asymmetric Olefin Aziridination with Diphenylphosphoryl Azide. *J. Org. Chem.* **2008**, *73*, 7260-7265. (j) Ruppel, J. V.; Jones, J. E.; Huff, C. A.; Kamble, R. M.; Chen, Y.; Zhang, X. P. A Highly Effective Cobalt Catalyst for Olefin Aziridination with Azides: Hydrogen Bonding Guided Catalyst Design. *Org. Lett.* **2008**, *10*, 1995-1998. (k) Gao, G.-Y.; Jones, J. E.; Vyas, R.; Harden, J. D.; Zhang, X. P. Cobalt-Catalyzed Aziridination with Diphenylphosphoryl Azide (DPPA): Direct Synthesis of *N*-Phosphorus-Substituted Aziridines from Alkenes. *J. Org. Chem.* **2006**, *71*, 6655-6658. (l) Gao, G.-Y.; Harden, J. D.; Zhang, X. P. Cobalt-Catalyzed Efficient Aziridination of Alkenes. *Org. Lett.* **2005**, *7*, 3191-3193. (m) Caselli, A.; Gallo, E.; Fantauzzi, S.; Morlacchi, S.; Ragaini, F.; Cenini, S. Allylic Amination and Aziridination of Olefins by Aryl Azides Catalyzed by Co^{II}(tpp): A Synthetic and Mechanistic Study. *Eur. J. Inorg. Chem.* **2008**, 3009-3019. (n) Caselli, A.; Gallo, E.; Ragaini, F.; Ricatto, F.; Abbiati, G.; Cenini, S. Chiral porphyrin complexes of cobalt(II) and ruthenium(II) in catalytic cyclopropanation and amination reactions. *Inorg. Chim. Acta* **2006**, *359*, 2924-2932.

(20) For select examples of Ni-based nitrene-transfer to alkenes, see: (a) Waterman, R.; Hillhouse, G. L. Group Transfer from Nickel Imido, Phosphinidine, and Carbene Complexes to Ethylene with Formation of Aziridine, Phosphirane, and Cyclopropane Products. *J. Am. Chem. Soc.* **2003**, *125*, 13350-13351. (b) Lin, B. L.; Clough, C. R.; Hillhouse, G. L. Interactions of Aziridines with Nickel Complexes: Oxidative-Addition and Reductive-Elimination Reactions that Break and Make C–N Bonds. *J. Am. Chem. Soc.* **2002**, *124*, 2890-2891.

(21) For historic examples of Cu-based enantioselective aziridinations, see: (a) Li, Z.; Quan, R. W.; Jacobsen, E. N. Mechanism of the (Diimine)copper-Catalyzed Asymmetric Aziridination of Alkenes. Nitrene Transfer via Ligand-Accelerated Catalysis. *J. Am. Chem. Soc.* **1995**, *117*, 5889-5890. (b) Li, Z.; Conser, K. R.; Jacobsen, E. N. Asymmetric Alkene Aziridination with Readily Available Chiral Diimine-Based Catalysts. *J. Am. Chem. Soc.* **1993**, *115*, 5326-5327. (c) Evans, D. A.; Faul, M. M.; Bilodeau, M. T.; Anderson, B. A.; Barnes, D. M. Bis(oxazoline)-copper complexes as chiral catalysts for the enantioselective aziridination of olefins. *J. Am. Chem. Soc.* **1993**, *115*, 5328-5329.

(22) For select examples of Cu-based nitrene-transfer to alkenes, see: (a) Gephart, R. T., III; Warren, T. H. Copper-Catalyzed sp^3 C–H Amination. *Organometallics* **2012**, *31*, 7728-7752. (b) Lebel, H.; Parmentier, M. Copper-catalyzed enantioselective aziridination of styrenes. *Pure App. Chem.* **2010**, *82*, 1827-1833. (c) Lebel, H.; Parmentier, M.; Leogane, O.; Ross, K.; Spitz, C. Copper bis(oxazolines) as catalysts for stereoselective aziridination of styrenes with *N*-tosyloxycarbamates. *Tetrahedron* **2012**, *68*, 3396-3409. (d) Maestre, L.; Sameera, W. M. C.; Díaz-Requejo, M. M.; Maseras, F.; Pérez, P. J. A General Mechanism for the Copper- and Silver-Catalyzed Olefin Aziridination Reactions: Concomitant Involvement of the Singlet and Triplet Pathways. *J. Am. Chem. Soc.* **2013**, *135*, 1338-1348. (e) Mairena, M. A.; Díaz-Requejo, M. M.; Belderraín, T. R.; Nicasio, M. C.; Trofimenko, S.; Pérez, P. J. Copper-Homoscorpionate Complexes as Very Active Catalysts for the Olefin Aziridination Reaction. *Organometallics* **2004**, *23*, 253-256. (f) Díaz-Requejo, M. M.; Pérez, P. J.; Brookhart, M.; Templeton, J. L. Substituent Effects on the Reaction Rates of Copper-Catalyzed Cyclopropanation and Aziridination of para-Substituted Styrenes. *Organometallics* **1997**, *16*, 4399-4402. (g) Bagchi, V.; Paraskevopoulou, P.; Das, P.; Chi, L.; Wang, Q.; Choudhury, A.; Mathieson, J. S.; Cronin, L.; Pardue, D. B.; Cundari, T. R.; Mitrikas, G.; Sanakis, Y.; Stavropoulos, P. A Versatile Tripodal Cu(I) Reagent for C–N Bond Construction via Nitrene-Transfer Chemistry: Catalytic Perspectives and Mechanistic Insights on C–H Aminations/Amidinations and Olefin Aziridinations. *J. Am. Chem. Soc.* **2014**, *136*, 11362-11381. (h) Lam, T. L.; Tso, K. C.-H.; Cao, B.; Yang, C.; Chen, D.; Chang, X.-Y.; Huang, J.-S.; Che, C.-M. Tripodal S-Ligand Complexes of Copper(I) as Catalysts for Alkene Aziridination, Sulfide Sulfimidation, and C–H Amination. *Inorg. Chem.* **2017**, *56*, 4253-4257. (i) Li, Y.; He, J.; Khankhoje, V.; Herdtweck, E.; Köhler, K.; Storcheva, O.; Cokoja, M.; Kühn, F. E. Copper(II) complexes incorporating poly/perfluorinated alkoxyaluminate-type weakly coordinating anions: Syntheses, characterization and catalytic application in stereoselective olefin aziridination. *Dalton Trans.* **2011**, *40*, 5746-5754. (j) Comba, P.; Haaf, C.; Lienke, A.; Muruganantham, A.; Wadepohl, H. Synthesis, Structure, and Highly Efficient Copper-Catalyzed Aziridination with a Tetraaza-Bispidine Ligand. *Chem. Eur. J.* **2009**, *15*, 10880-10887. (k) Wang, X.; Ding, K. One-Pot Enantioselective Aziridination of Olefins Catalyzed by a Copper(I) Complex of a Novel Diimine Ligand by Using $PhI(OAc)_2$ and Sulfonamide as Nitrene Precursors. *Chem. Eur. J.* **2006**, *12*, 4568-4575. (l) Robert-Peillard, F.; Di Chenna, P. H.; Liang, C.; Lescot, C.; Collet, F.; Dodd, R. H.; Dauban, P. Catalytic stereoselective alkene aziridination with sulfonimidamides. *Tetrahedron: Asymmetry* **2010**, *21*, 1447-1457. (m) Kundu, S.; Miceli, E.; Farquhar, E.; Pfaff, F. F.; Kuhlmann, U.; Hildebrandt, P.; Braun, B.; Greco, C.; Ray, K. Lewis Acid Trapping of an Elusive Copper–Tosylnitrene Intermediate Using Scandium Triflate. *J. Am. Chem. Soc.* **2012**, *134*, 14710-14713.

(23) For select examples of Ru-based nitrene-transfer to alkenes, see: (a) Uchida, T.; Katsuki, T. Asymmetric Nitrene Transfer Reactions: Sulfimidation, Aziridination and C–H Amination Using Azide Compounds as Nitrene Precursors. *Chem. Rec.* **2014**, *14*, 117-129. (b) Kim, C.; Uchida, T.; Katsuki, T. Asymmetric olefin aziridination using a newly designed Ru(CO)(salen) complex as the catalyst. *Chem. Commun.* **2012**, *48*, 7188-7190. (c) Kawabata, H.; Omura, K.; Uchida, T.; Katsuki, T. Construction of Robust Ruthenium(salen)(CO) Complexes and Asymmetric Aziridination with Nitrene Precursors in the Form of Azide Compounds That Bear Easily Removable *N*-Sulfonyl Groups. *Chem. Asian J.* **2007**, *2*, 248-256. (d) Harvey, M. E.; Musaev, D.; Du Bois, J. A Diruthenium Catalyst for Selective, Intramolecular Allylic C–H Amination: Reaction Development and Mechanistic Insight Gained through Experiment and Theory. *J. Am. Chem. Soc.* **2011**, *133*, 17207-17216. (e) Chan, K.-H.; Guan, X.; Lo, V. K.-Y.; Che, C.-M. Elevated Catalytic Activity of Ruthenium(II)–Porphyrin-Catalyzed Carbene/Nitrene Transfer and Insertion Reactions with N-Heterocyclic Carbene Ligands. *Angew. Chem. Int. Ed.* **2014**, *53*, 2982-2987. (f) Leung, S. K.-Y.; Tsui, W.-M.; Huang, J.-S.; Che, C.-M.; Liang, J.-L.; Zhu, N. Imido Transfer from Bis(imido)ruthenium(VI) Porphyrins to Hydrocarbons: Effect of Imido Substituents, C−H Bond Dissociation Energies, and $Ru^{VI/V}$ Reduction Potentials. *J. Am. Chem. Soc.* **2005**, *127*, 16629-16640. (g) Au, S.-M.; Huang, J.-S.; Yu, W.-Y.; Fung, W.-H.; Che, C.-M. Aziridination of Alkenes and Amidation of Alkanes by Bis(tosylimido)ruthenium(VI) Porphyrins. A Mechanistic Study. *J. Am. Chem. Soc.* **1999**, *121*, 9120-9132. (h) Fantauzzi, S.; Gallo, E.; Caselli, A.; Piangiolino, C.; Ragaini, F.; Re, N.; Cenini, S. Rearrangement of *N*-Aryl-2-Vinylaziridines to Benzoazepines and Dihydropyrroles: A Synthetic and Theoretical Study. *Chem. Eur. J.* **2009**, *15*, 1241-1251. (i) Fantauzzi, S.; Gallo, E.; Caselli, A.; Piangiolino, C.; Ragaini, F.; Cenini, S. The (Porphyrin)ruthenium-Catalyzed Aziridination of Olefins Using Aryl Azides as Nitrogen Sources. *Eur. J. Org. Chem.* **2007**, 6053-6059. (j) Fantauzzi, S.; Gallo, E.; Caselli, A.; Ragaini, F.; Macchi, P.; Casati, N.; Cenini, S. Origin of the Deactivation in Styrene Aziridination by Aryl Azides, Catalyzed by Ruthenium Porphyrin Complexes. Structural Characterization of a Δ^2-1,2,3-triazoline Ru^{II}(TPP)CO Complex. *Organometallics* **2005**, *24*, 4710-4713. (k) Zardi, P.; Pozzoli, A.; Ferretti, F.; Manca, G.; Mealli, C.; Gallo, E. A mechanistic investigation of the ruthenium porphyrin catalyzed aziridination of olefins by aryl azides. *Dalton Trans.* **2015**, *44*, 10479-10489. (l) Manca, G.; Gallo, E.; Intrieri, D.; Mealli, C. DFT Mechanistic Proposal of the Ruthenium Porphyrin-Catalyzed Allylic Amination by Organic Azides. *ACS Catal.* **2014**, *4*, 823-832.

(24) For select examples of Rh-based nitrene-transfer to alkenes, see ref. 9 and the following: (a) Roizen, J. L.; Harvey, M. E.; Du Bois, J. Metal-Catalyzed Nitrogen-Atom Transfer Methods for the Oxidation of Aliphatic C–H Bonds. *Acc. Chem. Res.* **2012**, *45*, 911-922. (b) Fiori, K. W.; Espino, C. G.; Brodsky, B. H.; Du Bois, J. A mechanistic analysis of the Rh-catalyzed intramolecular C–H amination reaction. *Tetrahedron* **2009**, *65*, 3042-3051. (c) Fruit, C.; Robert-Peillard, F.; Bernardinelli, G.; Müller, P.; Dodd, R. H.; Dauban, P. Diastereoselective rhodium-catalyzed nitrene transfer starting from chiral sulfonimidamide-derived iminoiodanes. *Tetrahedron: Asymmetry* **2005,** *16*, 3484-3487. (d) Müller, P.; Baud, C.; Jacquier, Y. The rhodium(III)-catalyzed aziridination of olefins with {[(4-Nitrophenyl)-sulfonyl]imino}phenyl-λ^3-iodane. *Can. J. Chem.* **1998**, *76*, 738-750. (e) Nägeli, I.; Baud, C.; Bernardinelli, G.; Jacquier, Y.; Moran, M.; Müller, P. Rhodium(II)-Catalyzed CH Insertions with {[(4-Nitrophenyl)-sulfonyl]imino}phenyl-λ^3-iodane. *Helv. Chim Acta* **1997**, *80*, 1087-1105. (f) Catino, A. J.; Nichols, J. M.; Forslund, R. E.; Doyle, M. P. Efficient Aziridination of Olefins Catalyzed by Mixed-Valent Dirhodium(II, III) Caprolactamate. *Org. Lett.* **2005**, *7*, 2787-2790. (g) Liang, J.-L.; Yuan, S.-X.; Chan, P. W. H.; Che, C.-M. Rhodium(II,II) Dimer as an Efficient Catalyst for Aziridination of Sulfonamides and Amidation of Steroids. *Org. Lett.* **2002**, *4*, 4507-4510.

(25) For select examples of Pd-based nitrene-transfer to alkenes, see: (a) Okamoto, K.; Oda, T.; Kohigashi, S.; Ohe, K. Palladium-catalyzed Decarboxylative Intramolecular Aziridination from 4*H*-Isoxazol-5-ones Leading to 1-Azabicyclo[3.1.0]hex-2-enes. *Angew. Chem. Int. Ed.* **2011**, *50*, 11470-11473. (b) Han, J.; Li, Y.; Zhi, S.; Pan, Y.; Timmons, C.; Li, G. Palladium-catalyzed aziridination of alkenes using *N*,*N*-dichloro-p-toluenesulfonamide as nitrogen source. *Tetrahedron Lett.* **2006**, *47*, 7225-7228.

(26) For select examples of Ag-based nitrene-transfer to alkenes, see: (a) Mat Lani, A. S.; Schomaker, J. M. Site-Selective, Catalyst-Controlled Alkene Aziridination. *Synthesis* **2018**, *50*, 4462-4470. (b) Ju, M.; Weatherly, C. D.; Guzei, I. A.; Schomaker, J. M. Chemo- and Enantioselective Intramolecular Silver-Catalyzed Aziridinations. *Angew. Chem. Int. Ed.* **2017**, *56*, 9944-9948. (c) Dolan, N. S.; Scamp, R. J.; Yang, T.; Berry, J. F.; Schomaker, J. M. Catalyst-Controlled and Tunable, Chemoselective Silver-catalyzed Intermolecular Nitrene Transfer: Experimental and Computational Studies. *J. Am. Chem. Soc.* **2016**, *138*, 14658-14667. (d) Rigoli, J. W.; Weatherly, C. D.; Alderson, J. M.; Vo, B. T.; Schomaker, J. M. Tunable, Chemoselective Amination via Silver Catalysis. *J. Am. Chem. Soc.* **2013**, *135*, 17238-17241. (e) Huang, M.; Corbin, J. R.; Dolan, N. S.; Fry, C. G.; Vinokur, A. I.; Guzei, I. A.; Schomaker, J. M. Synthesis, Characterization, and Variable-Temperature NMR Studies of Silver(I) Complexes for Selective Nitrene Transfer. *Inorg. Chem.* **2017**, *56*, 6725-6733. (f) Weatherly, C.; Alderson, J. M.; Berry, J. F.; Hein, J. E.; Schomaker, J. M. Catalyst-Controlled Nitrene Transfer by Tuning Metal:Ligand Ratios: Inshight into the Mechanisms of Chemoselectivity. *Organometallics* **2017**, *36*, 1649-1661. (g) Scamp, R. J.; Rigoli, J. W.; Schomaker, J. M. Chemoselective silver-catalyzed nitrene insertion reactions. *Pure Appl. Chem.* **2014**, *86*, 381-393. (h) Rigoli, J. W.; Weatherly, C. D.; Vo, B. T.; Neale, S.; Meis, A. R.; Schomaker, J. M. Chemoselective Allene Aziridination via Ag(I) Catalysis. *Org. Lett.* **2013**, *15*, 290-293. (i) Llaveria, J.; Beltrán, Á.; Díaz-Requejo, M. M.; Matheu, M. I.; Castillón, S.; Pérez, P. J. Efficient Silver-Catalyzed Regio-and Stereospecific Aziridination of Dienes. *Angew. Chem. Int. Ed.* **2010**, *49*, 7092-7095. (j) Li, Z.; He, C. Recent Advances in Silver-Catalyzed Nitrene, Carbene, and Silylene-Transfer Reactions. *Eur. J. Org. Chem.* **2006**, 4313-4322. (k) Cui, Y.; He, C. Efficient Aziridination of Olefins Catalyzed by a Unique Disilver(I) Compound. *J. Am. Chem. Soc.* **2003**, *125*, 16202-16203.

(27) For select examples of Au-based nitrene-transfer to alkenes, see: (a) Li, Z.; Ding, X.; He, C. Nitrene Transfer Reactions Catalyzed by Gold Complexes. *J. Org. Chem.* **2006**, *71*, 5876-5880. (b) Deng, X.; Baker, T. A.; Friend, C. M. A Pathway for NH Addition to Styrene Promoted by Gold. *Angew. Chem. Int. Ed.* **2006**, *45*, 7075-7078.

(28) (a) Singh, R.; Mukherjee, A. Metalloporphyrin Catalyzed C–H Amination. *ACS Catal.* **2019**, *9*, 3604-3617. (b) Park, Y.; Kim, Y.; Chang, S. Transition Metal-Catalyzed C–H Amination: Scope, Mechanism, and Applications. *Chem. Rev.* **2017**, *117*, 9247-9301. (c) Stavropoulos, P. Metal-Catalyzed and Metal-Free Intermolecular Amination of Light Alkanes and Benzenes. *Comm. Inorg. Chem.* **2017**, *37*, 1-57. (d) Hazelard, D.; Nocquet, P.-A.; Compain, P. Catalytic C–H amination at its limits: challenges and solutions. *Org. Chem. Front.* **2017**, *4*, 2500-2521. (e) Collet, F.; Lescot, C.; Dauban, P. Catalytic C–H amination: the stereoselectivity issue. *Chem. Soc. Rev.* **2011**, *40*, 1926-1936. (f) Zalatan, D.N.; Du Bois, J. Metal-Catalyzed Oxidations of C–H to C–N Bonds. *Top. Curr. Chem.* **2010**, *292*, 347-378. (g) Díaz-Requejo, M. M.; Pérez, P. J. Coinage Metal Catalyzed C−H Bond Functionalization of Hydrocarbons. *Chem Rev.* **2008**, *108*, 3379-3394.

(29) Hu, L.; Chen, H. What Factors Control the Reactivity of Cobalt–Imido Complexes in C–H Bond Activation via Hydrogen Abstraction? *ACS Catal.* **2017**, *7*, 285-292.

(30) (a) Jones, C.; Schulten, C.; Rose, R. P.; Stasch, A.; Aldridge, S.; Woodul, W. D.; Murray, K. S.; Moubaraki, B.; Brynda, M.; La Macchia, G.; Gagliardi, L. Amidinato– and Guanidinato–Cobalt(I) Complexes: Characterization of Exceptionally Short Co–Co Interactions. *Angew. Chem. Int. Ed.* **2009**, *48*, 7406-7410. (b) Cowley, R. E.; Bontchev, R. P.; Sorrell, J.; Sarracino, O.; Feng, Y.; Wang, H.; Smith, J. M. Formation of a Cobalt(III) Imido from a Cobalt(II) Amido Complex. Evidence for Proton-Coupled Electron Transfer. *J. Am. Chem. Soc.* **2007**, *129*, 2424-2425. (c) Mehn, M. P.; Brown, S. D.; Jenkins, D. M.; Peters, J. C. Que, L., Jr. Vibrational Spectroscopy and Analysis of Pseudo-tetrahedral Complexes with Metal Imido Bonds. *Inorg. Chem.* **2006**, *45*, 7417-7427. (d) Dai, X.; Kapoor, P.; Warren, T. H. [Me_2NN]Co(η^6-toluene): O=O, N=N, and O=N Bond Cleavage Provides β-Diketiminato Cobalt μ-Oxo and Imido Complexes. *J. Am. Chem. Soc.* **2004**, *126*, 4798-4799. (e) Hu, X.; Meyer, K. Terminal Cobalt(III) Imido Complexes Supported by Tris(Carbene) Ligands: Imido Insertion into the Cobalt–Carbene Bond. *J. Am. Chem. Soc.* **2004**, *126*, 16322-16323. (f) Betley, T. A.; Peters, J. C. Dinitrogen Chemistry from Trigonally Coordinated Iron and Cobalt Platforms. *J. Am. Chem. Soc.* **2003**, *125*, 10782-10783. (g) Jenkins, D. M.; Betley, T. A.; Peters, J. C. Oxidative Group Transfer to Co(I) Affords a Terminal Co(III) Imido Complex. *J. Am. Chem. Soc.* **2002**, *124*, 11238-11239.

(31) (a) Shay, D. T.; Yap, G. P. A.; Zakharov, L. N.; Rheingold, A. L.; Theopold, K. H. Intramolecular C–H Activation by an Open-Shell Cobalt(III) Imido Complex. *Angew. Chem. Int. Ed.* **2005**, *44*, 1508-1510. (b) Thyagarajan, S.; Shay, D. T.; Incarvito, C. D.; Rheingold, A. L.; Theopold, K. H. Intramolecular C–H Activation by Inferred Terminal Cobalt Imido Intermediates. *J. Am. Chem. Soc.* **2003**, *125*, 4440-4441.

(32) (a) King, E. R.; Sazama, G. T.; Betley, T. A. Co(III) Imidos Exhibiting Spin Crossover and C–H Bond Activation. *J. Am. Chem. Soc.* **2012**, *134*, 17858-17861. (b) Baek, Y.; Betley, T. A. Catalytic C–H Amination Mediated by Dipyrrin Cobalt Imidos. *J. Am. Chem. Soc.* **2019**, *141*, 7797-7806. (c) Baek, Y.; Hennessy, E. T.; Betley, T. A. Direct Manipulation of Metal Imido Geometry: Key Principles to Enhance C–H Amination Efficacy. *J. Am. Chem. Soc.* **2019**, *141*, 16944-16953.

(33) Reckziegel, A.; Pietzonka, C.; Kraus, F.; Werncke, C. G. C–H Bond Activation by an Imido Cobalt(III) and the Resulting Amido Cobalt(II) Complex. *Angew. Chem. Int. Ed.* **2020**, *59*, 8527-8531.

(34) Wu, B.; Sánchez, R. H.; Bezpalko, M. W.; Foxman, B. M.; Thomas, C. M. Formation of Heterobimetallic Zirconium/Cobalt Diimido Complexes via a Four-Electron Transformation. *Inorg. Chem.* **2014**, *53*, 10021-10023.

(35) Chomitz, W. A.; Arnold, J. Reactivity of a Co(I) [N_2P_2] complex with azides: evidence for a transient Co(III) imido species. *Chem. Commun.* **2008**, 3648-3650.

(36) (a) Yao, X.-N.; Du, J.-Z.; Zhang, Y.-Q.; Leng, X.-B.; Yang, M.-W.; Jiang, S.-D.; Wang, Z.-X.; Ouyang, Z.-W.; Deng, L.; Wang, B.-W.; Gao, S. Two-Coordinate Co(II) Imido Complexes as Outstanding Single-Molecule Magnets. *J. Am. Chem. Soc.* **2017**, *139*, 373-380. (b) Du, J.; Wang, L.; Xie, M.; Deng, L. A Two-Coordinate Cobalt(II) Imido Complex with NHC Ligation: Synthesis, Structure, and Reactivity. *Angew. Chem. Int. Ed.* **2015**, *54*, 12640-12644.

(37) Liu, Y.; Du, J.; Deng, L. Synthesis, Structure, and Reactivity of Low-Spin Cobalt(II) Imido Complexes [$(Me_3P)_3Co(NAr)$]. *Inorg. Chem.* **2017**, *56*, 8278-8286.

(38) Zhang, L.; Liu, Y.; Deng, L. Three-Coordinate Cobalt(IV) and Cobalt(V) Imido Complexes with N-Heterocyclic Carbene Ligation: Synthesis, Structure, and Their Distinct Reactivity in C–H Bond Amination. *J. Am. Chem. Soc.* **2014**, *136*, 15525-15528.

(39) (a) Goswami, M.; Rebreyend, C.; de Bruin, B. Porphyrin Cobalt(III) "Nitrene Radical" Reactivity; Hydrogen Atom Transfer from *Ortho*-YH Substituents to the Nitrene Moiety of Cobalt-Bound Aryl Nitrene Intermediates (Y = O, NH). *Molecules* **2016**, *21*, 242. (b) Goswami, M.; Lyaskovskyy, V.; Domingos, S. R.; Buma, W. J.; Woutersen, S.; Troeppner, O.; Ivanović-Burmazović, I.; Lu, H.; Cui, X.; Zhang, X. P.; Reijerse, E. J.; DeBeer, S.; van Schooneveld, M. M.; Pfaff, F. F.; Ray, K.; de Bruin, B. Characterization of Porphyrin-Co(III)-'Nitrene Radical' Species Relevant in Catalytic Nitrene Transfer Reactions. *J. Am. Chem. Soc.* **2015**, *137*, 5468-5479. (c) Hopmann, K. H.; Ghosh, A. Mechanism of Cobalt-Porphyrin–Catalyzed Aziridination. *ACS Catal.* **2011**, *1*, 597-600.

(40) van Leest, N. P.; Tepaske, M. A.; Oudsen, J.-P. H.; Venderbosch, B.; Rietdijk, N. R.; Siegler, M. A.; Tromp, M.; van der Vlugt, J. I.; de Bruin, B. Ligand Redox Noninnocence in $[Co^{III}(TAML)]^{0/-}$ Complexes Affects Nitrene Formation. *J. Am. Chem. Soc.* **2020**, *142*, 552-563.

(41) van Leest, N. P.; Tepaske, M. A.; Venderbosch, B.; Oudsen, J.-P. H.; Tromp, M.; van der Vlugt, J. I.; de Bruin, B. Electronically Asynchronous Transition States for C–N Bond Formation by Electrophilic $[Co^{III}(TAML)]$-Nitrene Radical Complexes Involving Substrate-to-Ligand Single-Electron Transfer and a Cobalt-Centered Spin Shuttle. *ACS Catal.* **2020**, *10*, 7449-7463.

(42) Coin, G.; Patra, R.; Rana, S.; Biswas, J. P.; Dubourdeaux, P.; Clémancey, M.; de Visser, S. P.; Maiti, D.; Maldivi, P.; Latour, J.-M. Fe-Catalyzed Aziridination Is Governed by the Electron Affinity of the Active Imido-Iron Species. *ACS Catal.* **2020**, *10*, 10010-10020.

(43) Baek, Y.; Das, A.; Zheng, S.-L.; Reibenspies, J. H.; Powers, D. C.; Betley, T. A. C–H Amination Mediated by Cobalt Organoazide Adducts and the Corresponding Cobalt Nitrenoid Intermediates. *J. Am. Chem. Soc.* **2020**, *142*, 11232-11243.

(44) Bagchi, V.; Kalra, A.; Das, P.; Paraskevopoulou, P.; Gorla, S.; Ai, L.; Wang, Q.; Mohapatra, S.; Choudhury, A.; Sun, Z.; Cundari, T. R.; Stavropoulos, P. Comparative Nitrene-Transfer Chemistry to Olefinic Substrates Mediated by a Library of Anionic Mn(II) Triphenylamido-Amine Reagents and M(II) Congeners (M = Fe, Co, Ni) Favoring Aromatic over Aliphatic Alkenes. *ACS Catal.* **2018**, *8*, 9183-9206.

(45) (a) Jones, M. B.; MacBeth, C. E. Tripodal Phenylamine-Based Ligands and Their Co^{II} Complexes. *Inorg. Chem.* **2007**, *46*, 8117-8119. (b) Çelenligil-Çetin, R.; Paraskevopoulou, P.; Dinda, R.; Staples, R. J.; Sinn, E.; Rath, N. P.; Stavropoulos, P. Synthesis, Characterization, and Reactivity of Iron Trisamidoamine Complexes that Undergo both Metal- and Ligand-Centered Oxidative Transformations. *Inorg. Chem.* **2008**, *47*, 1165-1172. (c) Çelenligil-Çetin, R. *Synthesis, Characterization, and Reactivity of Iron Complexes with N-Donor Ligands in Relation to Oxygenation of Hydrocarbons*, Ph.D. Thesis, Boston University, Boston, MA, **2004**.

(46) (a) Paraskevopoulou, P.; Lin, A.; Wang, Q.; Pinnapareddy, D.; Acharrya, R.; Dinda, R.; Çelenligil-Çetin, R.; Floros, G.; Sanakis, Y.; Choudhury, A.; Rath, N. P.; Stavropoulos, P. Synthesis and Characterization of a Series of Structurally and Electronically Diverse Fe(II) Complexes Featuring a Family of Triphenylamido-amine Ligands. *Inorg. Chem.* **2010**, *49*, 108-122. (b) Pinnapareddy, D. *Synthesis and Characterization of Metal Reagents Mediating C–X Activation (X = Cl, H) of Hydrocarbons*, Ph.D. Thesis, University of Missouri-Rolla, Rolla, MO, **2007**.

(47) (a) Jones, M. B.; Hardcastle, K. I.; MacBeth, C. E. Synthetic, spectral and structural studies of mononuclear tris(κ^2-amidate) aluminium complexes supported by tripodal ligands. *Polyhedron* **2010**, *29*, 116-119. (b) Jones, M. B.; Hardcastle, K. I.; Hagen, K. S.; MacBeth, C. E. Oxygen Activation and Intramolecular C–H Bond Activation by an Amidate-Bridged Diiron(II) Complex. *Inorg. Chem.* **2011**, *50*, 6402-6404. (c) Villanueva, O.; Weldy, N. M.; Blakey, S. B.; MacBeth, C. E. Cobalt catalyzed sp^3 C–H amination utilizing aryl azides. *Chem. Sci.* **2015**, *6*, 6672-6675.

(48) Bagchi, V.; Raptopoulos, G.; Das, P.; Christodoulou, S.; Wang, Q.; Ai, L.; Choudhury, A.; Pitsikalis, M.; Paraskevopoulou, P.; Stavropoulos, P. Synthesis and characterization of a family of Co(II) triphenylamido-amine complexes and catalytic activity in controlled radical polymerization of olefins. *Polyhedron* **2013**, *52*, 78-90.

(49) Çelenligil-Çetin, R.; Paraskevopoulou, P.; Lalioti, N.; Sanakis, Y.; Staples, R. J.; Rath, N. P.; Stavropoulos, P. Metalloradical Complexes of Manganese and Chromium Featuring an Oxidatively Rearranged Ligand. *Inorg. Chem.* **2008**, *47*, 10998-11009.

(50) (a) Bencini, A.; Benelli, C.; Gatteschi, D.; Zanchini, C. ESR Spectra of Low-Symmetry High-Spin Cobalt(II) Complexes. 2. Pseudotetrahedral Dichlorobis(triphenylphospine oxide)cobalt(II). *Inorg. Chem.* **1979**, *18*, 2137-2140. (b) Benelli, C.; Gatteschi, D. ESR Spectra of Low-Symmetry High-Spin Cobalt(II) Complexes. 10. Five-Coordinated Trigonal-Bipyramidal Complexes. *Inorg. Chem.* **1982**, *21*, 1788-1790. (c) Drulis, H.; Dyrek, K.; Hoffmann, K. P.; Hoffmann, S. K.; Weselucha-Berczynska, A. ESR Spectra of Low-Symmetry Tetrahedral High-Spin Cobalt(II) in a Cinchoninium Tetrachlorocobaltate(II) Dihydrate Single Crystal. *Inorg. Chem.* **1985**, *24*, 4009-4012. (d) Makinen, M. W.; Kuo, L. C.; Yim, M. B.; Wells, G. B.; Fukuyama, J. M.; Kim, J. E. Ground Term Splitting of High-Spin Co^{2+} as a Probe of Coordination Structure. 1. Dependence of the Splitting on Coordination Geometry. *J. Am. Chem. Soc.* **1985**, *107*, 5245-5255. (e) Bennett, B. EPR of Cobalt-Substituted Zinc Enzymes, In *Metals in Biology: Applications of High-Resolution EPR to Metalloenzymes*, *Biological Magnetic Resonance*, Hanson, G.; Berliner, L.;, Eds.; Springer-Verlag: New York, 2010, Vol. 29, pp 345-366. (f) Zolnhhofer, E. M.; Käß, M.; Khusniyarov, M. M.; Heinemann, F. W.; Maron, L.; van Gastel, M.; Bill, E.; Meyer, K. An Intermediate Cobalt(IV) Nitrido Complex and its N-Migratory Insertion Product. *J. Am. Chem. Soc.* **2014**, *136*, 15072-15078. (g) Antholine, W. E. Resolved Hyperfine at L-band for High-Spin CoEDTA, A Model for Co Sites in Proteins. *Int. J. Mol. Sci.* **2019**, *20*, 2385.

(51) Abragam, A.; Bleaney, B. Electron Paramagnetic Resonance of Transition Ions. Clarendon Press: Oxford, 1970.

(52) Pilbrow, J. R. Effective g values for $S = 3/2$ and $S = 5/2$. *J. Magn. Reson.* **1978**, *31*, 479-490.

(53) Petasis, D. T.; Hendrich, M. P. Chapter Eight – Quantitative Interpretation of Multifrequency Multimode EPR Spectra of Metal Containing Proteins, Enzymes, and Biomimetic Complexes. In Electron Paramagnetic Resonance Investigations of Biological Systems by Using Spin Labels, Spin Probes, and Intrinsic Metal Ions, Part A., Qin, P. Z.; Warncke, K. Eds. Methods in Enzymology 2015, 563, 171-208.

(54) Müller, P.; Baud, C.; Jacquier, Y. A Method for Rhodium(II)-Catalyzed Aziridination of Olefins. *Tetrahedron* **1996**, *52*, 1543-1548.

(55) Al-Ajlouni, A.; Espenson, J. H. Epoxidation of Styrenes by Hydrogen Peroxide As Catalyzed by Methylrhenium Trioxide. *J. Am. Chem. Soc.* **1995**, *117*, 9243-9250.

(56) Souto, J. A.; Zian, D.; Muñiz, K. Iodine(III)-Mediated Intermolecular Allylic Amination under Metal-Free Conditions. *J. Am. Chem. Soc.* **2012**, *134*, 7242-7245.

(57) Jiang, X.-K. Establishment and Successful Application of the σ_{JJ}• Scale of Spin-Delocalization Substituent Constants. *Acc. Chem. Res.* **1997**, *30*, 283-289.

(58) Han, H.; Park, S. B.; Kim, S. K.; Chang, S. Copper–Nitrenoid Formation and Transfer in Catalytic Olefin Aziridination Utilizing Chelating 2-Pyridylsulfonyl Moieties. *J. Org. Chem.* **2008**, *73*, 2862-2870.

(59) Liang, S.; Jensen, M. P. Half-Sandwich Scorpionates as Nitrene Transfer Catalysts. *Organometallics* **2012**, *31*, 8055-8058.

(60) Liu, P.; Wong, E. L.-M.; Yuen, A. W.-H.; Che, C.-M. Highly Efficient Alkene Epoxidation and Aziridination catalyzed by Iron(II) Salt + 4,4′,4″-Trichloro-2,2′:6′,2″-terpyridine/4,4″-Dichloro-4′-*O*-PEG-OCH_3-2,2′:6′,2″-terpyridine. *Org. Lett.* **2008**, *10*, 3275-3278.

(61) Dinçtürk, S.; Jackson, R. A. Free radical reactions in solution. Part 7. Substituent effects on free radical reactions: comparison of the σ• scale with other measures of radical stabilization. *J. Chem. Soc., Perkin Trans. 2* **1981**, 1127-1131.

(62) Jupp, A. R.; Johnstone, T. C.; Stephan, D. W. Improving the Global Electrophilicity Index (GEI) as a Measure of Lewis Acidity. *Inorg. Chem.* **2018**, *57*, 14764-14771.

(63) (a) Johnson, E. R.; Becke, A. D. A post-Hartree–Fock model of intermolecular interactions. *J. Phys. Chem.* 2005, 123, 024101. (b) Grimme, S.; Ehrlich, S.; Goerigk, L. Effect of the Damping Function in Dispersion Corrected Density Functional Theory. *J. Comput. Chem.* **2011**, *32*, 1456-1465. (c) Grimme, S.; Antony, J.; Ehrlich, S.; Krieg, H. A consistent and accurate ab initio parametrization of density functional dispersion correction (DFT-D) for the 94 elements H-Pu. *J. Chem. Phys.* **2010**, *132*, 154104.

(64) (a) Lu, X.; Li, X.-X.; Lee, Y.-M.; Jang, Y.; Seo, M. S.; Hong, S.; Cho, K.-B.; Fukuzumi, S.; Nam, W. Electron-Transfer and Redox Reactivity of High-Valent Iron Imido and Oxo Complexes with the Formal Oxidation States of Five and Six. *J. Am. Chem. Soc.* **2020**, *142*, 3891-3904. (b) Sabenya, G.; Gamba, I.; Gómez, L.; Clémancey, M.; Frisch, J. R.; Klinker, E. J.; Blondin, G.; Torelli, S.; Que, L., Jr.; Martin-Diaconescu, V.; Latour, J.-M.; Lloret-Fillol, J.; Costas, M. Octahedral iron(iv)–tosylimido complexes exhibiting single electron-oxidation reactivity. *Chem. Sci.* **2019**, *10*, 9513-9529. (c) Hong, S.; Lu, X.; Lee, Y.-M.; Seo, M. S.; Ohta, T.; Ogura, T.; Clémancey, M.; Maldivi, P.; Latour, J.-M.; Sarangi, R.; Nam, W. Achieving One-Electron Oxidation of a Mononuclear Nonheme Iron(V)-Imido Complex. *J. Am. Chem. Soc.* **2017**, *139*, 14372-14375. (d) Kumar, S.; Faponle, A. S.; Barman, P.; Vardhaman, A. K.; Sastri, C. V.; Kumar, D.; de Visser, S. P. Long-range Electron Transfer Triggers Mechanistic Differences between Iron(IV)-Oxo and Iron(IV)-Imido Oxidants. *J. Am. Chem. Soc.* **2014**, *136*, 17102-17115.

(65) (a) Ogliaro, F.; Harris, N.; Cohen, S.; Filatov, M.; de Visser, S. P.; Shaik, S. A Model "Rebound" Mechanism of Hydroxylation by Cytochrome P450: Stepwise and Effectively Concerted Pathways, and Their Reactivity Patterns. *J. Am. Chem. Soc.* **2000**, *122*, 8977-8989. (b) Shaik, S.; de Visser, S. P.; Ogliaro, F.; Schwarz, H.; Schröder, D. Two-state reactivity mechanisms of hydroxylation and epoxidation by cytochrome P-450 revealed by theory. *Curr. Opin. Chem. Biol.* **2002**, *6*, 556-567. (c) Moreau, Y.; Chen, H.; Derat, E.; Hirao, H.; Bolm, C.; Shaik, S. NR Transfer Reactivity of Azo-Compound I of P450. How Does the Nitrogen Substituent Tune the Reactivity of the Species toward C–H and C=C Activation? *J. Phys. Chem. B* **2007**, *111*, 10288-10299.

(66) (a) Kuijpers, P. F.; van der Vlugt, J. I.; Schneider, S.; de Bruin, B. Nitrene Radical Intermediates in Catalytic Synthesis. *Chem. Eur. J.* **2017**, *23*, 13819-13829. (b) Xiong, T.; Zhang, Q. New amination strategies based on nitrogen-centered radical chemistry. *Chem. Soc. Rev.* **2016**, *45*, 3069-3087.

(67) (a) Xiong, P.; Xu, H.-C. Chemistry with Electrochemically Generated N-Centered Radicals. *Acc. Chem. Res.* **2019**, *52*, 3339-3350. (b) Wang, P.; Zhao, Q.; Xiao, W.; Chen, J. Recent advances in visible-light photoredox-catalyzed nitrogen radical cyclization. *Green Synth.Catal.* **2020**, *1*, 42-51. (c) Zheng, S.; Gutiérrez-Bonet, Á.; Molander, G. A. Merging Photoredox PCET with Ni-Catalyzed Cross-Coupling: Cascade Amidoarylation of Unactivated Olefins. *Chem* **2019**, *5*, 339-352. (d) Davies, J.; Svejstrup, T. D.; Reina, D. F.; Sheikh, N. S.; Leonori, D. Visible-Light-Mediated Synthesis of Amidyl Radicals: Transition-Metal-Free Hydroamination and *N*-Arylation Reactions. *J. Am. Chem. Soc.* **2016**, *138*, 8092-8095.

(68) Wang, Q.; Wang, P.; Gao, X.; Wang, D.; Wang, S.; Liang, X.; Wang, L.; Zhang, H.; Lei, A. Regioselective/electro-oxidative intermolecular [3 + 2] annulation for the preparation of indolines. *Chem. Sci.* **2020**, *11*, 2181-2186.

(69) (a) Usharani, D.; Janardanan, D.; Shaik, S. A Theory for Bioinorganic Chemical Reactivity of Oxometal Complexes and Analogous Oxidants: The Exchange and Orbital-Selection Rules. *Acc. Chem. Res.* **2013**, *46*, 471-482. (b) Swart, M.; Gruden, M. Spinning around in Transition-Metal Chemistry. *Acc. Chem. Res.* **2016**, *49*, 2690-2697.

(70) Ren, Y.; Cheaib, K.; Jacquet, J.; Vezin, H.; Fensterbank, L.; Orio, M.; Blanchard, S.; Desage-El Murr, M. Copper-Catalyzed Aziridination with Redox-Active Ligands: Molecular Spin Catalysis. *Chem. Eur. J.* **2018**, *24*, 5086-5090.

(71) Schümann, J. M.; Wagner, J. P.; Eckhardt, A. K.; Quanz, H.; Schreiner, P. R. Intramolecular London Dispersion Interactions Do Not Cancel in Solution. *J. Am. Chem. Soc.* **2021**, *143*, 41-45.

(72) (a) Rösel, S.; Becker, J.; Allen, W. D.; Schreiner, P. R. Probing the Delicate Balance between Pauli Repulsion and London Dispersion with Triphenylmethyl Derivatives. *J. Am. Chem. Soc.* **2018**, *140*, 14421-14432. (b) Rösel, S.; Balestrieri, C.; Schreiner, P. R. Sizing the role of London dispersion in the dissociation of all-*meta tert*-butyl hexaphenylethane. *Chem. Sci.* **2017**, *8*, 405-410. (c) Grimme, S.; Schreiner, P. R. Steric Crowding Can Stabilize a Labile Molecule: Solving the Hexaphenylethane Riddle. *Angew. Chem. Int. Ed.* **2011**, *50*, 12639-12642.

(73) (a) Bursch, M.; Caldeweyher, E.; Hansen, A.; Neugebauer, H.; Ehlert, S.; Grimme, S. Understanding and Quantifying London Dispersion Effects in Organometallic Complexes. *Acc. Chem. Res.* **2019**, *52*, 258-266. (b) Grimme, S.; Huenerbein, R.; Ehrlich, S. On the Importance of the Dispersion Energy for the Thermodynamic Stability of Molecules. *ChemPhysChem*. **2011**, *12*, 1258-1261.

(74) (a) Power, P. P. An Update on Multiple Bonding between Heavier Main Group Elements: The Importance of Pauli Repulsion, Charge-Shift Character, and London Dispersion Force Effects. *Organometallics* **2020**, *39*, 4127-4138. (b) Liptrot, D.; Power, P. P. London dispersion forces in sterically crowded inorganic and organometallic molecules. *Nat. Rev. Chem.* **2017**, *1*, 0004.

III. STUDIES DIRECTED TOWARDS THE INTERMOLECULAR AZIRIDINATION OF ALKENES CATALYZED BY METAL REAGENTS (Cu, Ag) SUPPORTED BY BULKY LIGANDS WITH A CHIRAL FRAMEWORK

Anshika Kalra, Amitava Choudhury and Pericles Stavropoulos

Department of Chemistry, Missouri University of Science and Technology, Rolla, Missouri 65409, United States

ABSTRACT

This study explores intermolecular aziridinations of alkenes catalyzed by metal reagents (Cu, Ag) supported by the same triphenylamine scaffold but with rigid cyclic guanidinyl arms possessing chiral elements. Guanidines are known as powerful organic bases and act as organocatalysts in a variety of asymmetric organic synthetic reactions. In this study, a series of cyclic chiral guanidinyl precursors and corresponding metal reagents were synthesized, and proved to have good reactivity, but modest enantioselectivity, in the aziridination of styrenes. These results are expected to provide insights for further catalyst development.

Keywords. Chiral cyclic guanidinyl catalyst, Earth's-abundant metal, Asymmetric aziridination.

1. INTRODUCTION

1.1. C—N BOND CONSTRUCTION VIA NITRENE-TRANSFER CHEMISTRY

Enantiomerically pure compounds are extremely important in fields such as medicine and pharmacy, nutrition or materials with optical properties. When the reaction between the nitrene source complexed to the chiral catalyst and the substrate takes place,

it traverses through two alternative diastereomeric transition states. A difference in energy of only 2 kcal/mol between these two transition states can lead to enantiomeric excess (ee) of ≥ 90%. Small changes in any of the participants in the catalytic process (it can either be temperature, catalyst/substrate ratio, modification of the chiral pocket, conformational variations of the chiral ligand) can alter significantly this difference in energy. The efficiency of the chirality transfer is measured as enantiomeric excess [% ee= (R-S)/(R+S) x 100].

Enantioselective intermolecular C─N bond construction has been reported in the literature mostly relying on platinum-group transition metals such as rhodium, ruthenium and iridium. The major problem with these metals is that they are quite expensive and toxic.

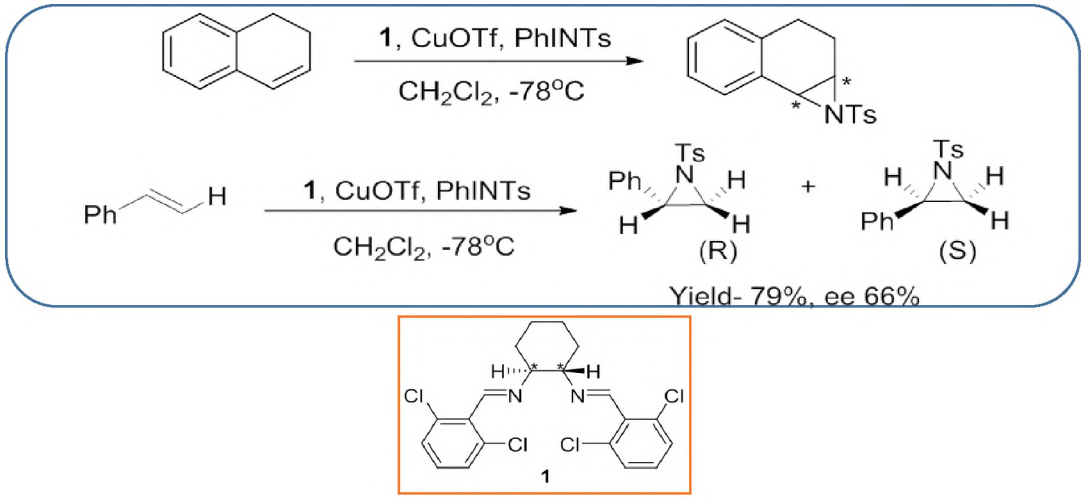

Jacobsen Ligand

Scheme 1. Asymmetric Bond Construction Using Jacobsen Ligand

In the early 90's, Jacobsen's and Evans' groups reported the asymmetric aziridination of alkenes. They are known to be the pioneers in this field Jacobsen's group reported that copper reagents bearing a C_2-symmetric chiral salen framework ligand[1] can

catalyze the asymmetric aziridination of olefins by PhI=NTs (Scheme 1) to achieve products with moderate yields and enantiomeric excess (around 60-67 ee%). However, one of the limitations was that the substrate scope was quite narrow. Around the same time, the Evans' group also reported the aziridination of olefins using Cu(I) based bis(oxazoline) ligands[2]. They obtained comparable yield and ee values as those reported by Jacobsen, especially in the case of styrene as a substrate.

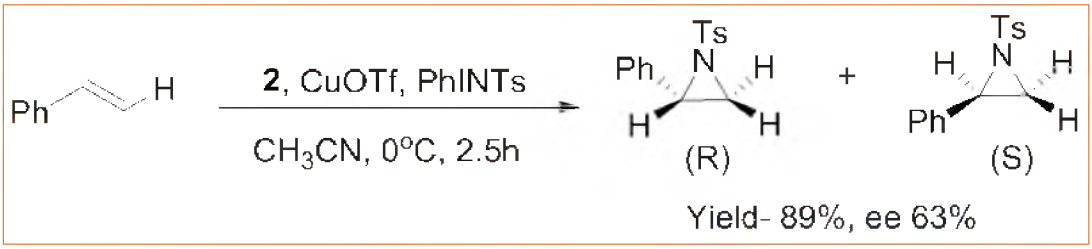

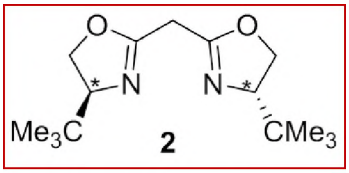

Evans Ligand

Scheme 2. Asymmetric Bond Construction Using Evans' Ligand

However, in this case too, the substrate scope was restricted to cinnamate esters, and the range of other olefinic substrates that can undergo asymmetric aziridination was limited (Scheme 2).

Later, the Evans' group also reported the enantioselective amination of *N*-acyloxazolidinones in high yields and ee values using chiral magnesium bis(sulfonamide)[3] complexes as catalysts. The conditions were specific to only one type of substrate (Scheme 3). The late 90's witnessed the diversification of catalytic

frameworks, with researchers exploring different types of metals such as rhodium, iridium, palladium and platinum.

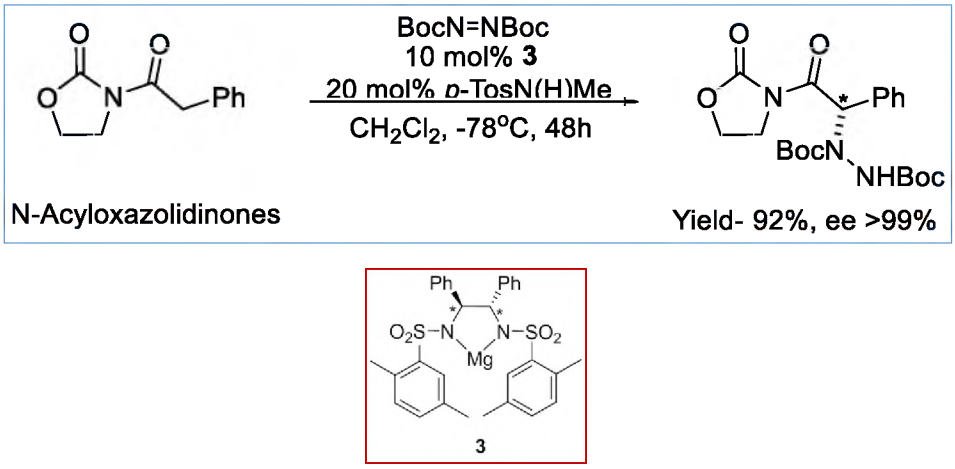

Scheme 3. Enantioselective Amination of *N*-acyloxazolidinones using Evans' Ligand

Lebel et al reported the use of a stable, readily available chiral *N*-tosyloxycarbamate[4] as a nitrene precursor to perform stereoselective intermolecular aziridination ofalkenes in the presence of a chiral rhodium catalyst. The use of a chiral *N*-tosyloxycarbamate would allow for double stereo differentiation in the product. A range of substituted styrenes with electron-releasing and electron-donating groups at ortho, meta and para position was tested; however, expensive Rh catalysts as well as chiral N-donors are needed (Scheme 4).

The Du Bois group documented a catalytic intermolecular C—H amination through the use of a dimeric Rh tetracarboxylate ($Rh_2(esp)_2$), which is a commercially available catalyst (0.5g, 237$). This catalyst has a paddlewheel structure. The electron-deficient trichloroethylsulfamate ($TcesNH_2$) was used as the N-source, along with an oxidant ($PhI(O_2C^tBu)_2$) (Scheme 5). A 5-fold enhanced rate for the C—H insertion reaction with $TcesNH_2$ was observed in comparison to other N-donor sources that are less electron

deficient in nature[5]. The intermediate Rh-nitrene shows discriminate reactivity, oxidizing preferentially benzylic C—H groups over all others. Reactions are typically conducted using limiting amounts of the starting alkane, a second distinguishing feature of this process.

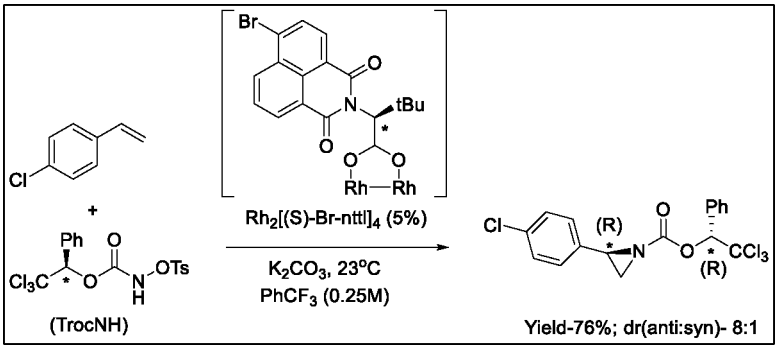

Scheme 4. Stereoselective Intermolecular Aziridination in the Presence of a Chiral Rhodium Catalyst

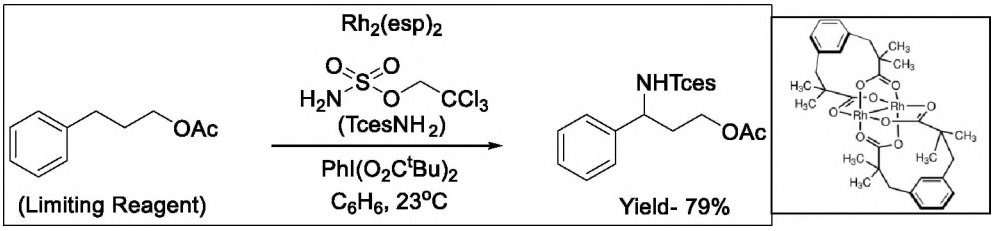

Scheme 5. C—H Amination Using $Rh_2(esp)_2$ and $TcesNH_2$

Katsuki et. al achieved a highly enantio- and regioselective intermolecular benzylic and allylic C—H bond amination using chiral Ru(CO)–salen and Ir(CO)–salen complexes, along with SES azide as the nitrene precursor[6] (Scheme 6). They were able to achieve moderate reactivity and good stereoselectivity. One of the limitations of this method is that the chiral Ru or Ir catalysts and $SeSNH_2$ are quite costly.

Zhang et. al reported enantioselective aziridination of alkenes with bis(2,2,2-trichloroethyl)phosphoryl azide ($TcepN_3$) as a nitrene source, mediated by Co(II)-based

catalysts that possess D_2 -symmetric chiral amidoporphyrins as the supporting ligand[7] (Scheme 7).

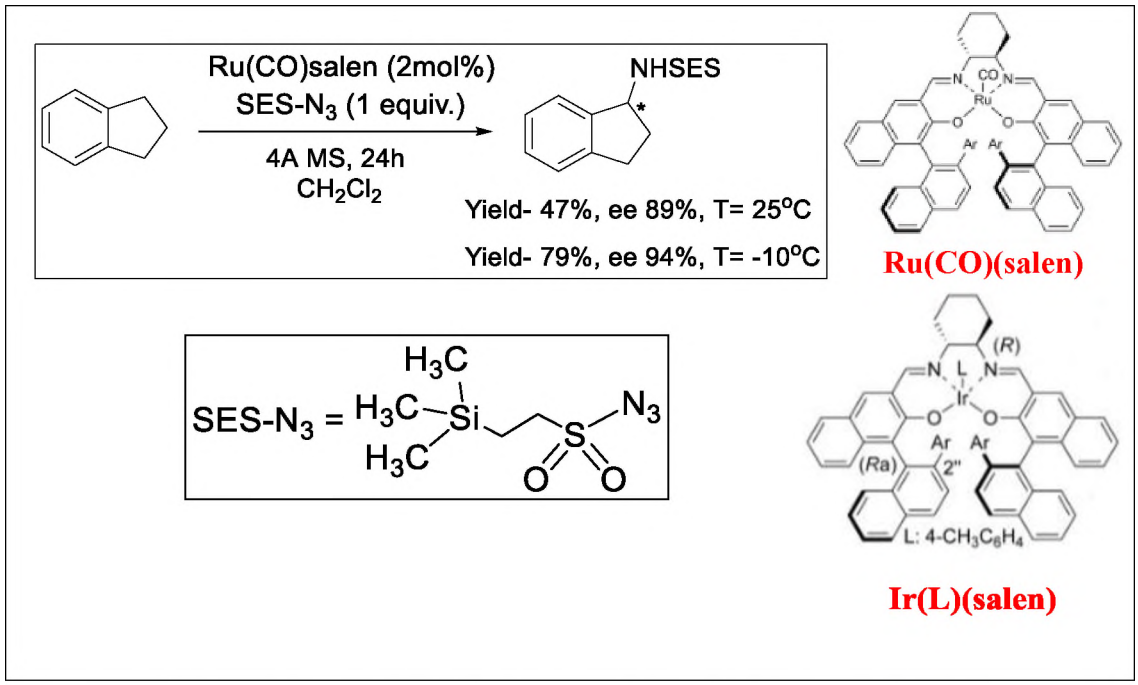

Scheme 6. Ru and Ir Catalyzed Enantioselective C—H Amination

These researchers noted the rigid amide spacers not only provide support and orient the chiral environments toward the cobalt metalloradical center but also the P=O group of phosphoryl azides engages in H-bonding with the chiral amide units of the ligand. These secondary hydrogen bonding interactions are expected to lower the energy barrier of the transition state and thus lead to acceleration of the reaction rate as well as improvement of the stereoselectivity. This method is mostly restricted to aromatic olefins, and though a comparatively cheap metal (Co) has been used, the overall cost of the chiral ligand is quite high, due to its elaborate structure. They also showed by both computational and experimental studies a stepwise radical mechanism for the Co(II)-

catalyzed metalloradical aziridination that involves an Co(III)–nitrene radical intermediate.

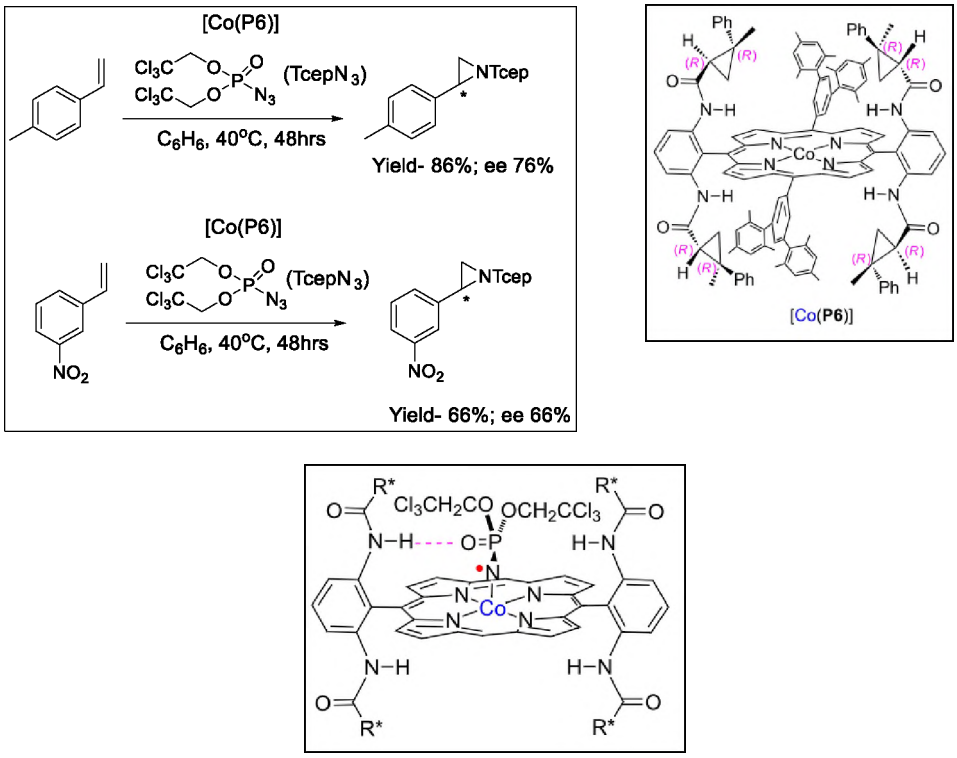

Scheme 7. Enantioselective Aziridination by Chiral Cobalt Porphyrin Catalysts

Dr. Frances H. Arnold, Nobel Prize winner in chemistry in 2018 for her work on genetically engineered enzymes, genetically modified the naturally existing enzyme P-450, and made a new variant (P411) that can catalyze a variety of reactions that nature cannot perform on its own. In one report[8], Dr. Arnold showed that enantioselective, intermolecular benzylic C─H amination can be catalyzed by the engineered iron-heme enzyme P411 (Scheme 8).

Tosyl azide was used as a N-source to afford high ee values, but with modest yields. Biocatalysts for non-natural reactions have alternatively been created by introducing precious metals (such as iridium and rhodium) into proteins.

However, this new iron based variant P411 is much more cost effective compared to the Rh/Ir functionalized proteins, due to the high abundance of Fe.

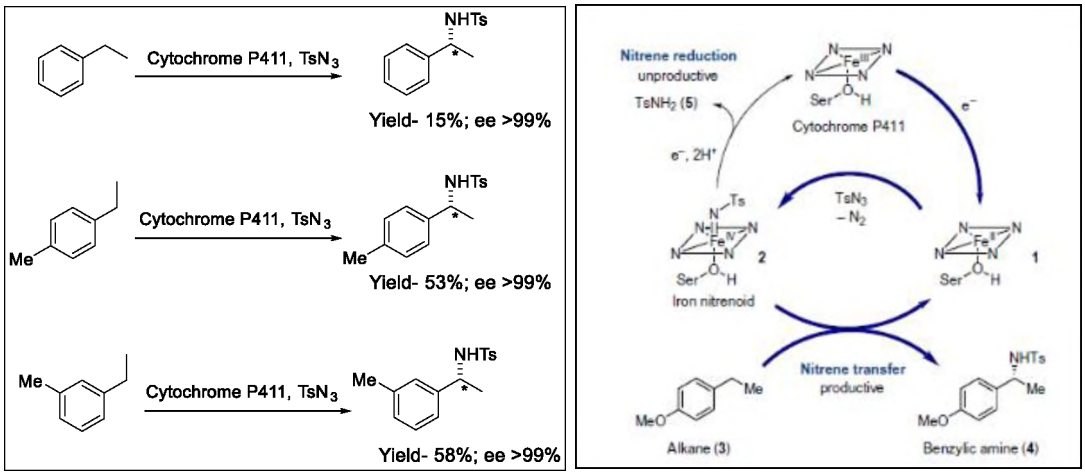

Scheme 8. P411 Catalyzed Enantioselective Amination and Proposed Mechanism of Nitrene Transfer

The Arnold group also attempted aziridination reactions of aromatic olefins using this new genetically modified variant enzyme P411. In this case also, they obtained high ee values, but the yields remain low[9] (Scheme 9).

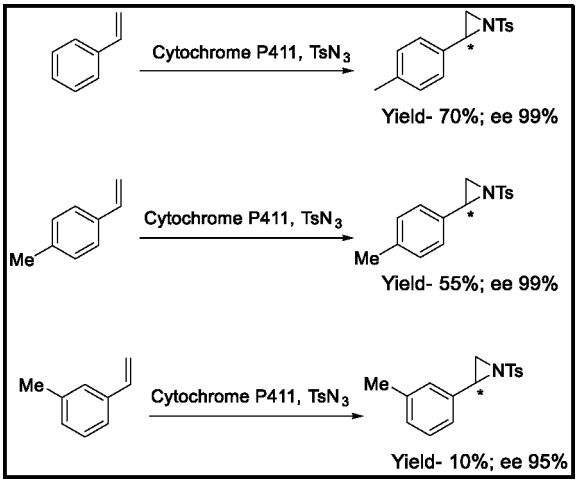

Scheme 9. P411 Catalyzed Enantioselective Aziridination

1.2. C−C BOND CONSTRUCTION VIA CARBENE-TRANSFER CHEMISTRY

In cyclopropanation reactions, a transition-metal complex acting as catalyst reacts with a diazo carbene compound to form an electrophilic metallocarbene intermediate with the evolution of nitrogen (Scheme 10). The transfer of the carbene unit to a nucleophile affords the desired product and releases the metal center to reinitiate the catalytic cycle. The main drawback of this methodology is the existence of an undesirable side reaction, the possible homocoupling of the diazo compound. This problem has been usually overcome by using slow addition of the carbene source and/or an excess of the nucleophilic substrate.

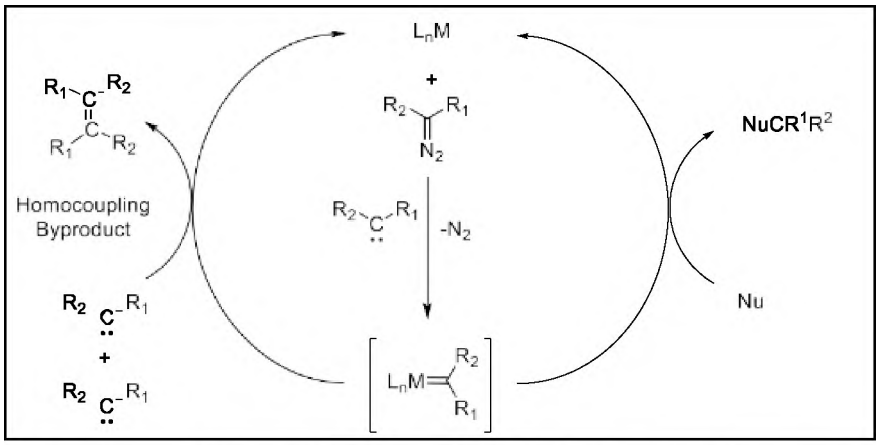

Scheme 10. Mechanism of Cyclopropanation

The mechanism of cyclopropanation reactions by metalcomplexes has been experimentally investigated by several groups, demonstrating by kinetic experiments and other means that the rate-determining step of the cyclopropanation mechanism is frequently the dinitrogen extrusion from the diazo compound, to form a metal-carbene intermediate, a veryreactive species and, therefore, elusive to experimental detection.

Subsequent addition of the carbenoid moiety of this intermediate to the olefin double bond results in the cyclopropane product.

One of the initial contributions to this field was by the Evans group. In the early 90's, Evans et. al demonstrated the asymmetric cyclopropanation of styrenes using a chiral copperbis(oxazoline)(BOX) reagent (Scheme 11)[10]. The catalyst was only tested on styrene as a substrate with a range of diazoacetate sources. Good yields and modest ee values were obtained, but again this methodology was restricted to just a single substrate.

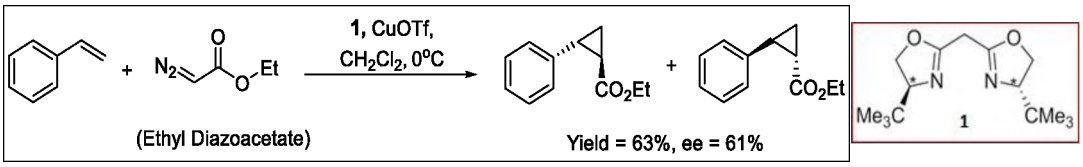

Scheme 11. Enantioselective C−C Bond Formation using Evans Ligand

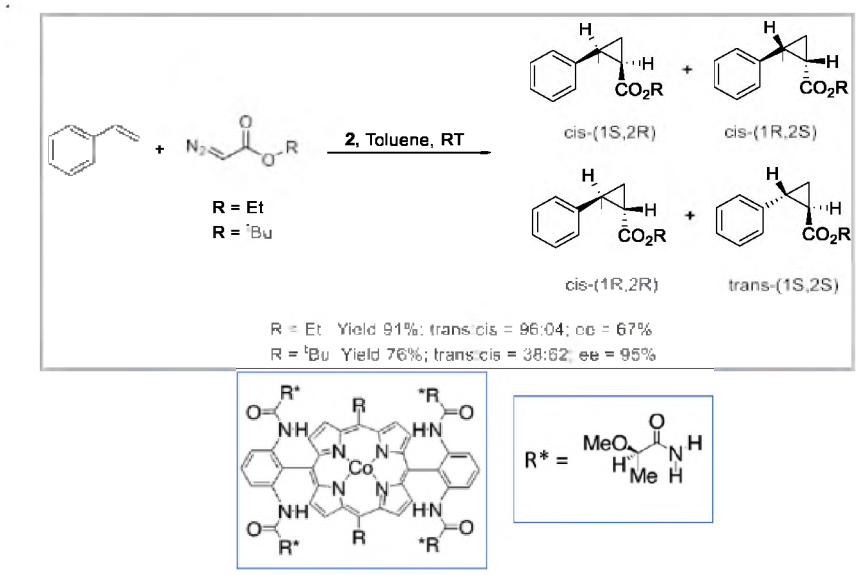

Scheme 12. Asymmetric Cyclopropanation of Styrene Catalyzed by Co Chiral Porphyrins Catalyst

Peter Zhang et. al used cobalt complexes of chiral porphyrins[11] for the enantioselective and diastereoselective cyclopropanation with styrene as a model

substrate. They used ethyl diazoacetate and tert-butyl diazoacetate as the carbene source (Scheme 12) and showed that withcertain Co chiral porphyrin catalysts, enantioselectivity can be improved by employing the tert-butyl group instead of the ethyl in the diazo compounds.

Ghanem et al. used chiral dirhodium (II) carboxylate complexes for asymmetric cyclopropanation reactions. They screened a number of different donor–acceptor diazo systems, for example 2,2,2-trifluromethyl-1-phenyldiazoethane and p-methyl methoxyphenyldiazoacetate[12] (Scheme 13).These donor-acceptor carbenes are less reactive, but more selective than acceptor-acceptor carbenes. This is because of the presence of a donor group that stabilizes the electron deficient metal carbene and decreases its reactivity but improves its selectivity.

The Huw M. L. Davies group has greatly contributed to the field of enantioselective and site selective C−H functionalization. The site selectivity is controlled by a delicate balance of steric and electronic effects. Highly substituted sites (tert C−H) are electronically favored because buildup of positive charge occurs at the carbon during the C−H insertion step, but this is counterbalanced by the steric demands of the carbene complex. Therefore, in general, bulkier catalysts will preferentially functionalize primary C−H bonds (i.e., the less hindered site). Davies et al. described a major change in the site selectivity of carbene-induced C−H functionalization through the use of bulky chiral dirhodium catalysts, which results in a strong preference for reactions to occur at primary C−H bonds (Scheme 14). This research group has used methyl (4-bromophenyl)diazoacetate as a donor/acceptor carbene source,[13] resulting in attenuated reactivity, but enabling high selectivity in C−H bond functionalizations.

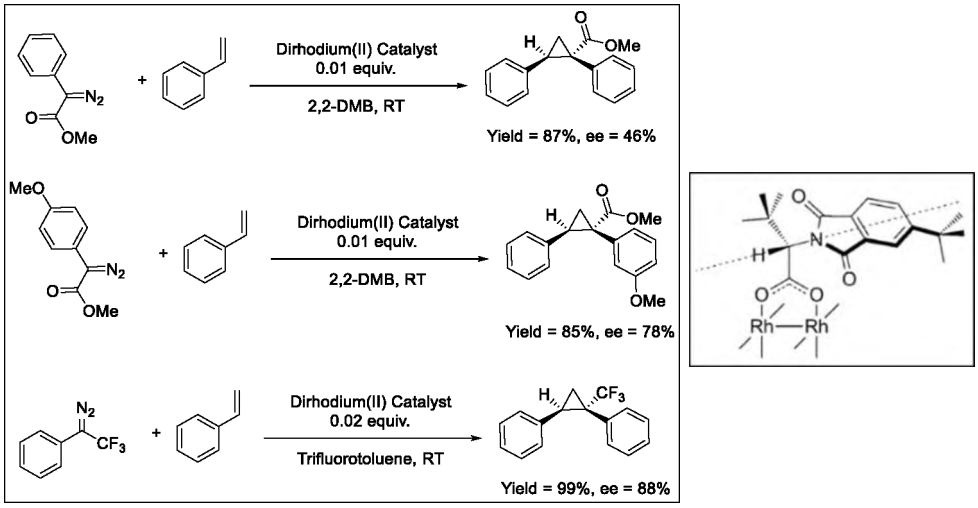

Scheme 13. Chiral Dirhodium(II) Carboxylate Catalyzed Asymmetric Cyclopropanation Reaction

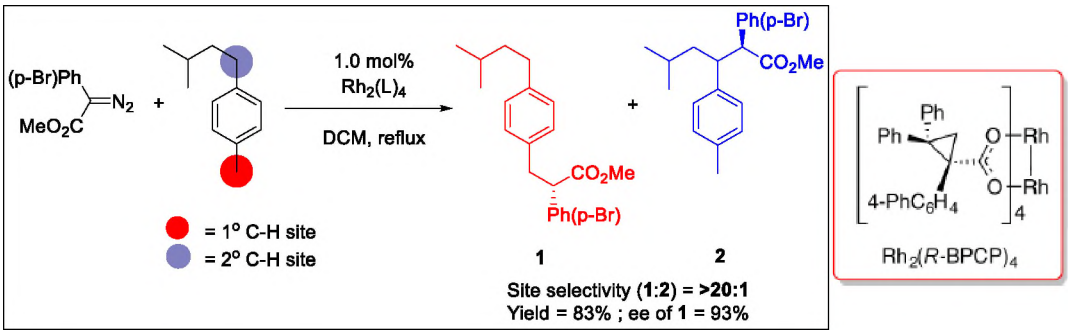

Scheme 14. Enantioselective and Site Selective C–H Functionalization

2. RESULTS AND DISCUSSIONS

2.1. DEVELOPMENT OF CATALYST WITH CYCLIC CHIRAL GUANIDINE RESIDUES

In 2014, our group reported a C–N bond construction methodology using a versatile tripodal copper(I) complex[14]. We synthesized a trisphenyl-amido amine tripodal ligand having tetramethylguanidinyl (TMG) as pendent arms. A TMG moiety changes the nature of the catalyst by generating cationic metal complexes that are more reactive

than the anionic complexes discussed in the previous sections, as expected for an electrophilic reaction.

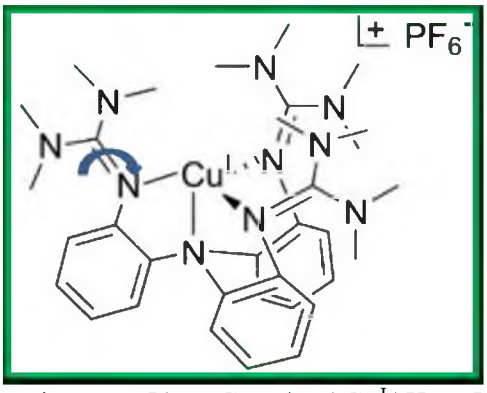

Figure 1. [(TMG_3trphen)Cu^I)][PF_6]

Three different kinds of C−N bond construction methodologies were explored, namely, amination of C−H, amidination of C−H bonds in the presence of nitriles and aziridination of olefins with good yields and selectivity.

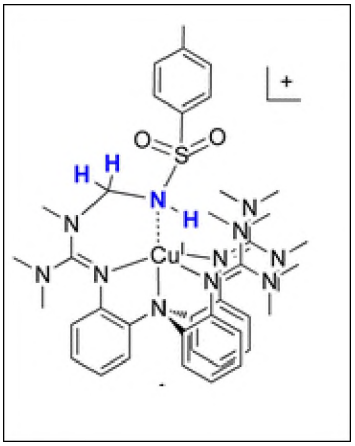

Figure 2. Nitrene insertion into Cu^I TMG

The major drawbacks of this catalyst were that first, the formally C=N double bond of TMG (Figure. 1) exhibits a significant degree of rotation which may suppress

selectivity; and secondly, the nitrogen of the NTsmoiety can insert into the C−H bond of the methyl group (Figure. 2), eventually leading to oxidative demethylation. In order to overcome these limitations, we thought of designing a catalyst with a more rigid framework and with the potential inclusion of chiral sites to start exploring asymmetric C−N bond construction.

2.2. SYNTHESIS OF LIGANDS

We first synthesized a chiral ligand featuring guanidinyl arms (Figure. 3) that possess superior rigidity and permit the incorporation of chiral centers in the backbone of the cyclic framework. We opted for using mostly earth abundant first-row transition metals such as Cu , and Ag as a representative second-row element for comparative purposes. Chiral guanidinyl-centered organo-catalysts have been widely explored, although not as components of metal complexes.

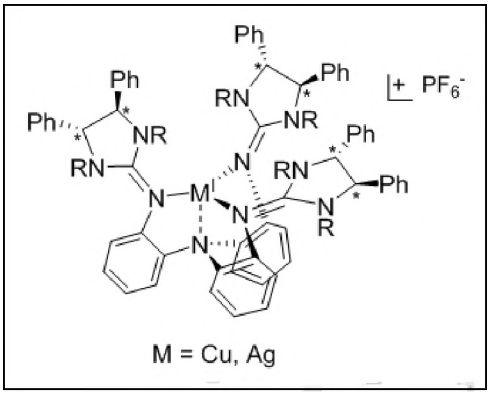

Figure 3. Cyclic Chiral Complex Featuring Guanidinyl-Arms

(i) Synthesis of a Tripodal Triphenyl amido-amine Scaffold [N_3N] with Chiral Cyclic Guanidinyl Arms. We first designed a cyclic guanidinyl chiral ligand featuring N−Me groups (**4**, Scheme 15). For the synthesis of the chiral ligand scaffold, we start

from the commercially available chiral 1R, 2R-(+)-1, 2- diphenylethylenediamine, which we convert to the corresponding urea **1** using di-tert-butyl dicarbonate (BOC_2O, 1.08equiv.) and 4-dimethyaminopyridine (DMAP, 1.08 equiv.) in acetonitrile at room temperature for 24 hours. We then alkylate the urea, by first deprotonating with 3 equiv. of sodium hydride, and then methylating with 3.3 equiv. of methyl iodide in THF at room temperature. The methylated urea **2** is then converted into the (4R,5R)-2-chloro-1,3-dimethyl-4,5-diphenyl-4,5-dihydro-1H-imidazol-3-ium chloride **(3)** using 5 equiv. of oxalyl chloride in refluxing toluene for 20 hours to afford a white solid. The solid was filtered and washed with diethyl ether under inert atmosphere to afford the compound **3** (85%).

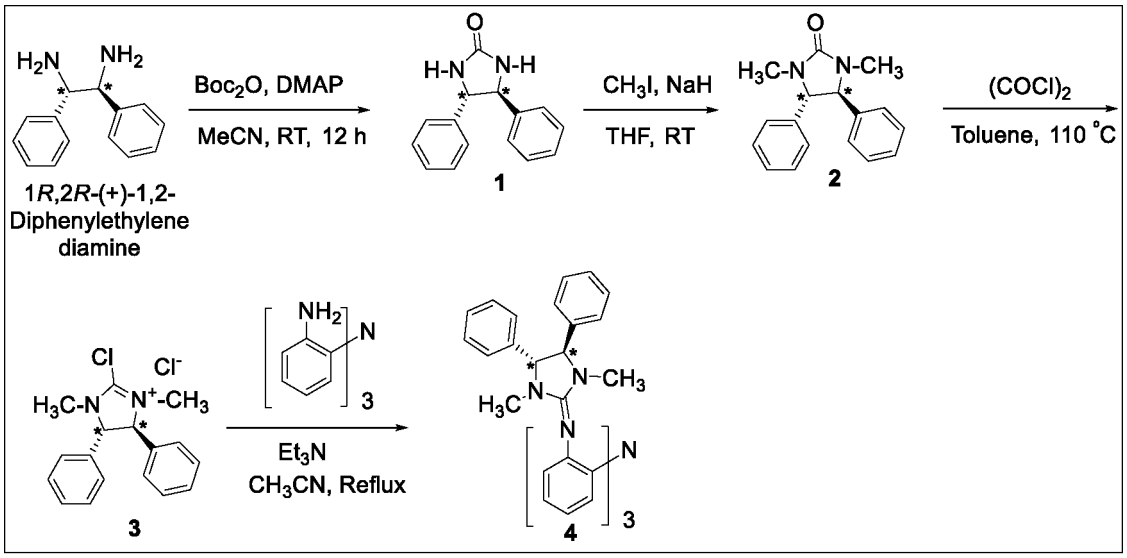

Scheme 15. Synthesis of $DMDPI_3-$ trphen- Ligand **4**

The chloro salt **3** (3 equiv.) is then coupled with our parent 2, 2′, 2-″ triaminotriphenylamine in the presence of 3 equiv. of triethylamine in acetonitrile and refluxed overnight to form (4R,5R)-1,3-dimethyl-4,5-diphenylimidazolidin-2-imine-

trphen (DMDPI$_3$−trphen, 70%) **(4),** featuring the chiral cyclic guanidinyl residue (Scheme 15). The ligand was characterized by ^{1}H-NMR (400 MHz) which showed the C−H of the cyclic ring at 3.81 ppm and the CH_3 group of the N−Me arm at 2.26 ppm in $CDCl_3$ (Figure. 4).

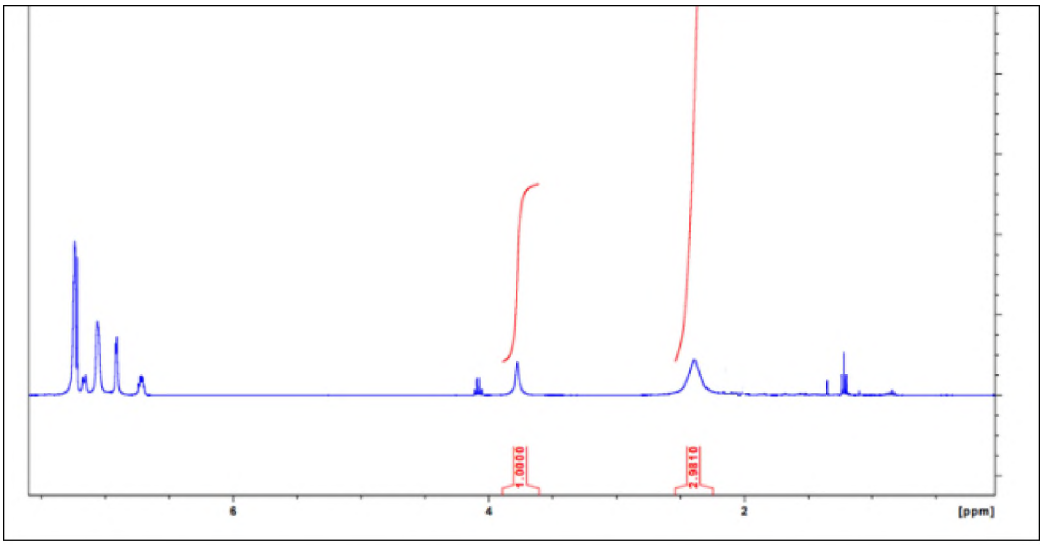

Figure 4. ^{1}H NMR of DMDPI$_3$− trphen Ligand **4** in $CDCl_3$

We also generated the same tripodal ligand with the deuterated N-CD_3 group (**7**, Scheme 16), in case it is less prone to oxidative damage as compared to the N-Me analog. The ligand (4R,5R)-1,3-bis(methyl-d_3)-4,5-diphenylimidazolidin-2-imine-trphen (d-DMDPI$_3$−trphen, 65%) **(7)** obtained as a white solid was synthesized exactly in the same manner as the procedure described above for the synthesis of ligand **4**, with the exception that the source of alkylating agent is deuterated iodomethane (CD_3I**).**). ^{1}H-NMR (400 MHz) of **7** shows the C−H of the cyclic ring at 3.85 ppm in $CDCl_3$.The deuterated urea was then converted into deuterated chloro imidazolium salt using oxalyl chloride in refluxing toluene for a period of 20 hrs.

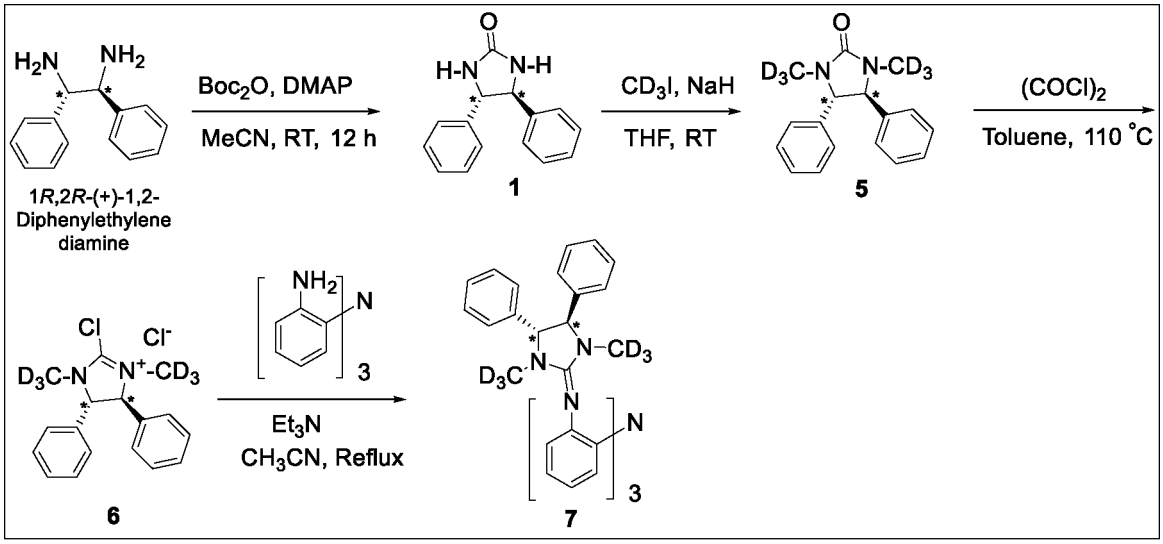

Scheme 16. Synthesis of d-DMDPI$_3$-trphen Ligand **7**

(ii) Synthesis of a Bipodal Bisphenyl amido-methyl amine Scaffold [N_2N-Me] with Chiral Cyclic Guanidinyl Arms. The tripodal ligand noted above was also modified to provide a bipodal framework, by replacing one of the phenyl legs with a terminal Me group (**11**, Scheme 18). It was designed while keeping in mind that the tripodal framework might be sterically too bulky to accommodate bulky substrates in catalytic reactions. For its synthesis, we first synthesized *N*-methyl-2-nitro-*N*-(2-nitrophenyl) benzenamine **9** (Scheme 17) by deprotonating bis(2-nitrophenyl)amine **8** (prepared according to the literature protocol) with sodium hydroxide in THF, and subsequently methylating with 4.0 equiv. of Me_2SO_4 under reflux to give **9** as yellow needles (97%).

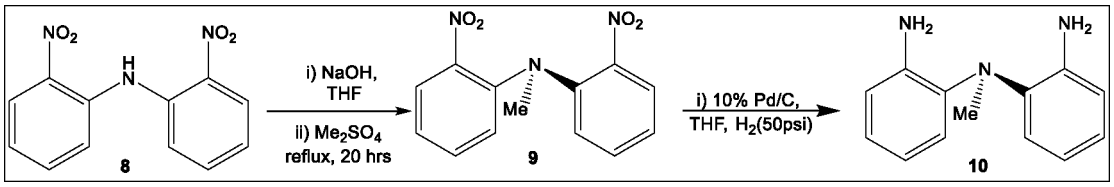

Scheme 17. Synthesis of N-methyl-2,2′-diamino-diphenylamine **10**

The nitro derivative **9** was reduced to the corresponding diamine by employing 50 psig hydrogen gas over Pd/C (10%) in THF to afford *N*-methyl-2,2′-diamino-diphenylamine **10** (Scheme 17) as a white solid (90 %).

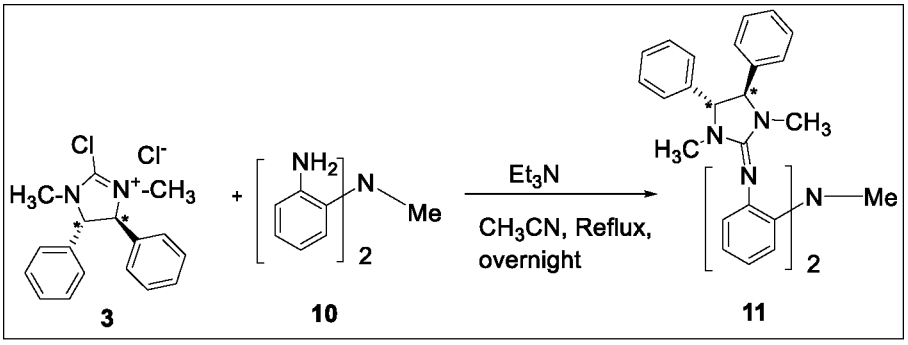

Scheme 18. Synthesis of DMDPI$_3$-biphen **11**

The chloro salt **3** (3 equiv.) noted above, is then coupled with our parent N-methyl-2,2′-diamino-diphenylamine **10** in the presence of 2 equiv. of triethylamine in acetonitrile under reflux to afford the bipodal chiral ligand, (4R,5R**)-**1,3-bis(methyl)-4,5-diphenylimidazolidin-2-imine- biphen (DMDPI$_3$-biphen, 75%) **(11)**, featuring the same chiral cyclic guanidinyl residue as the one used in the tripodal analog (Scheme 18).

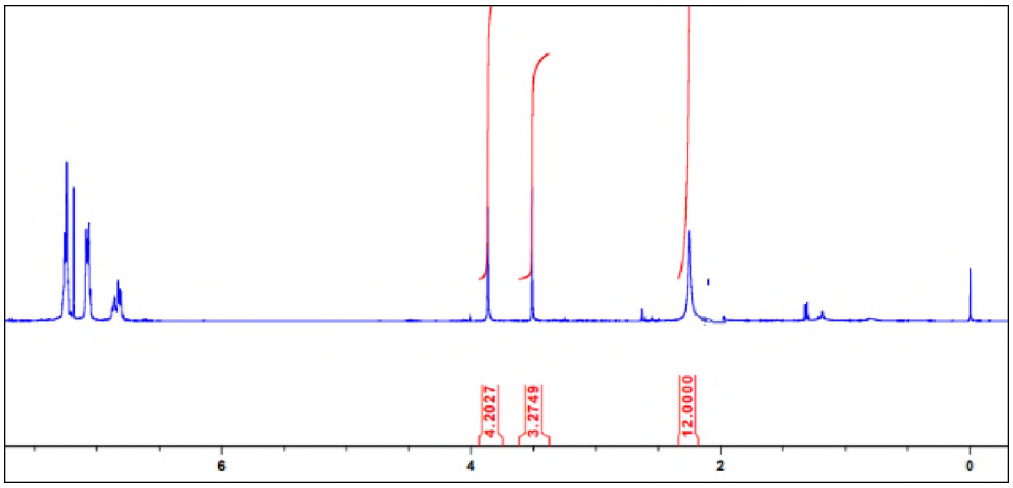

Figure 5. ^{1}H NMR of DMDPI$_3$– biphen Ligand **11** in $CDCl_3$

^{1}H-NMR (400MHz) of **11** shows the C—H protons of the cyclic guanidinyl ring at 3.91 ppm and the N−Me substituents at 2.31 ppm in $CDCl_3$ (Figure. 5).

2.3. SYNTHESIS OF TRIPODAL METAL COMPLEXES

Synthesis of Chiral [Cu^I(DMDPI$_3$-trphen)][PF_6] **(12).** For the synthesis of this chiral reagent, the ligand DMDPI$_3$-trphen **4** and 1 equiv. of [$Cu(CH_3CN)_4$][PF_6] was stirred in THF overnight at room temperature (Scheme 19). The light white crystalline material of chiral [Cu^I(DMDPI$_3$-trphen)][PF_6] **12** (80%), suitable for X-ray diffraction analysis, was obtained from acetonitrile over layered with diethyl ether and kept at – 30° C.

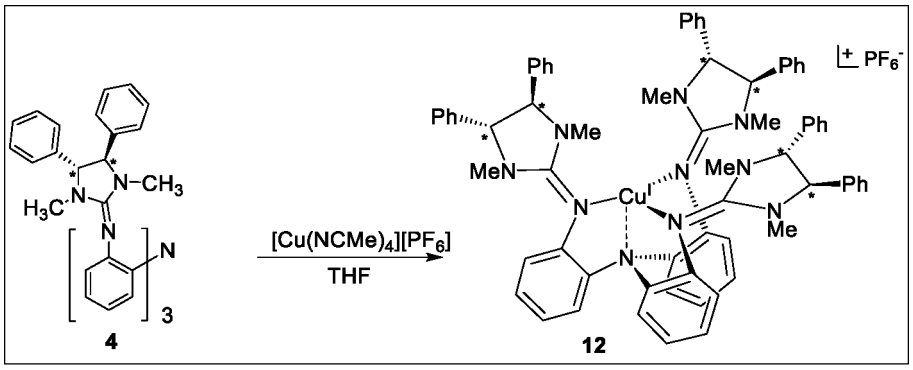

Scheme 19. Synthesis of Chiral [Cu^I(DMDPI$_3$-trphen)][PF_6] **(12)**

^{1}H-NMR (400MHz) of **12** in CD_3CN shows the C—H protons of the cyclic guanidinyl ring as doublets at 4.80-4.32 and 3.82-3.83 ppm. The N—Me arm also resolves to two distinct peaks at 2.82 and 2.05 ppm (Figure. 6). Figure. 7 shows the ORTEP diagram of chiral [Cu^I(DMDPI$_3$-trphen)][PF_6] (**12**) which essentially has a distorted trigonal pyramidal geometry. There does not seem to be a solvent molecule coordinating to the central metal atom.

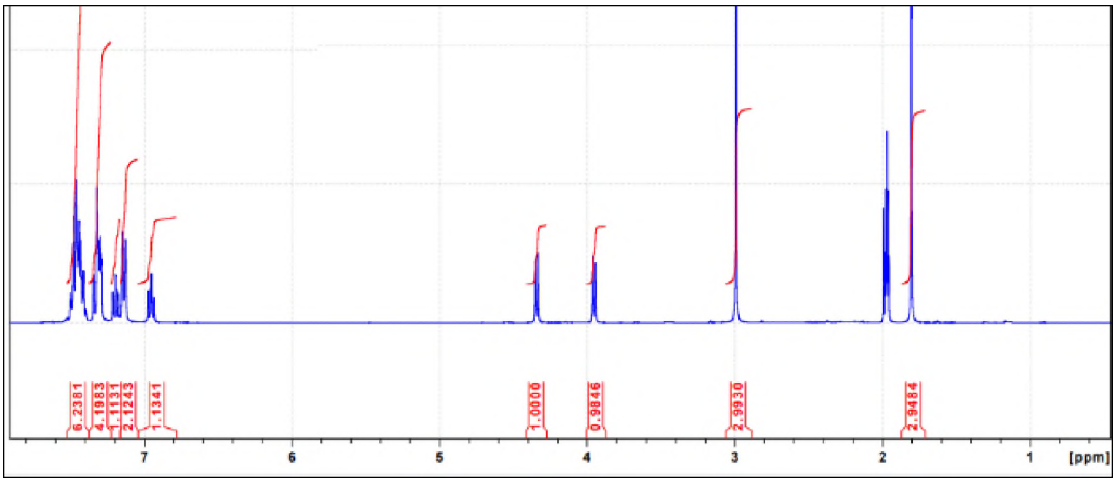

Figure 6. ^{1}H-NMR (400MHz) of **12** in CD_3CN

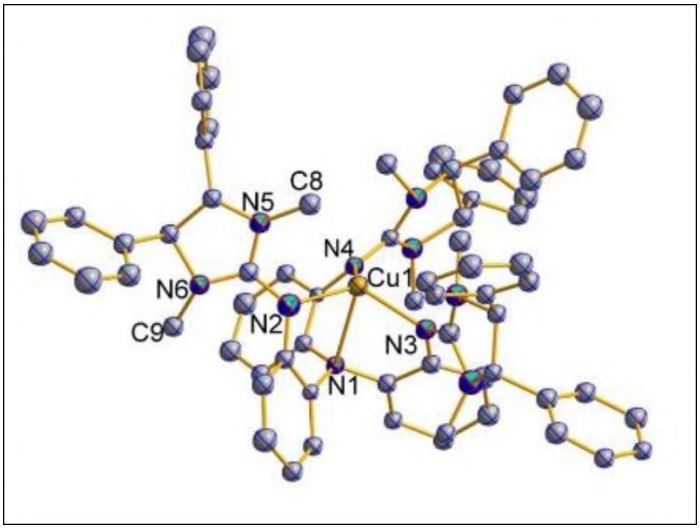

Figure 7. ORTEP Diagram of Chiral [CuI(DMDPI$_3$-trphen)][PF_6] (**12**)

Synthesis of Chiral [Cu^{I}(d-DMDPI$_3$-trphen)][PF_6] **(13)**. For the synthesis of the chiral reagent **13** (Scheme 20), the ligand d-DMDPI$_3$ trphen **7** and 1 equiv. of [$Cu(CH_3CN)_4$][PF_6] were heated in THF at 55°C. The compound [Cu^{I}(d-DMDPI$_3$-trphen)][PF_6] **(13)** was recrystallized from acetonitrile and diethyl ether at -30 ^{0}C, to afford off white crystalline material (78%). We initially monitored the synthesis of this

metal complex **13** at room temperature through ^{1}H-NMR analysis (an aliquot was taken from reaction mixture after 12 hours). We observed that most of the ligand **7** remained unreacted in the solution. For the synthesis of this catalyst, we had to heat the reaction at 55°C in order to fully convert the ligand **7** to the desired metal catalyst **13**.

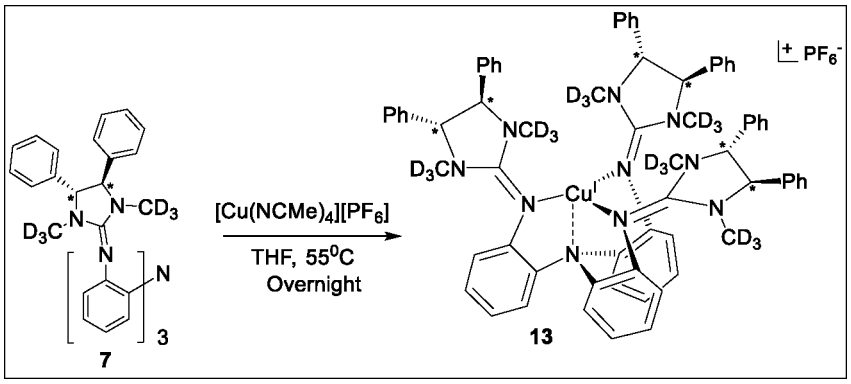

Scheme 20. Synthesis of Chiral [Cu^I(d-DMDPI$_3$-trphen)][PF$_6$] (**13**)

Synthesis of Chiral [Cu^I(DMDPI$_3$-trphen)][B(C$_6$F$_5$)$_4$] **(14).** We have also synthesized the Cu (I) cyclic chiral catalyst **14** by replacing the hexafluorophosphate (PF_6^-) as a counter anion with the more soluble tetrakis pentafluorophenylborate $B(C_6F_5)_4^-$ anion.

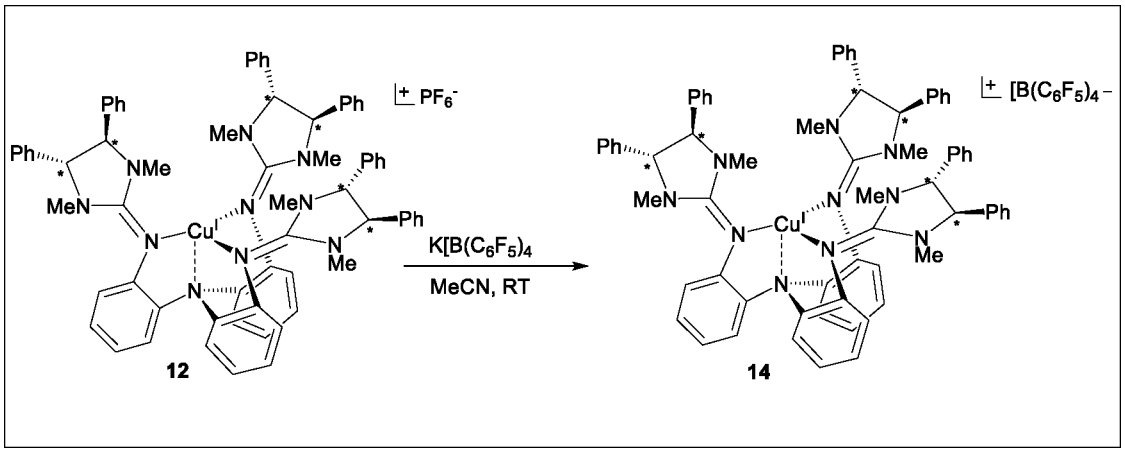

Scheme 21. Synthesis of Chiral [Cu^I(DMDPI$_3$-trphen)][(B(C$_6$F$_5$)$_4$] **(14)**

For catalytic reactions, and even more for mechanistic studies, keeping reagents and substrates in solution can be advantageous. In the case of the $B(C_6F_5)_4^-$ anion, fluorine increases the lipophilicity of the catalyst and thus its solubility. For its synthesis, the metal complex $[Cu^I(DMDPI_3\ trphen)][PF_6]$ **(12)** was dissolved in acetonitrile and 1.3 equiv. of potassium tetrakispentafluorophenylborate, $K[B(C_6F_4]$ was added to this solution (Scheme 21) to afford **14** as a white solid (75%).

Synthesis of Chiral $[Ag^I(DMDPI_3\text{-trphen})][PF_6]$ **(15).** For the synthesis of this chiral reagent, the ligand $DMDPI_3$ trph**e**n **4** and 1 equiv. of $AgPF_6$ was stirred in acetonitrile overnight at room temperature (Scheme 22). The white crystalline material of chiral $[Ag^I(DMDPI_3\text{-trphen})][PF_6]$ **15** (78%) suitable for X-ray diffraction analysis (Fig. 8), was obtained from acetonitrile over layered with diethyl ether and kept at – 30° C.

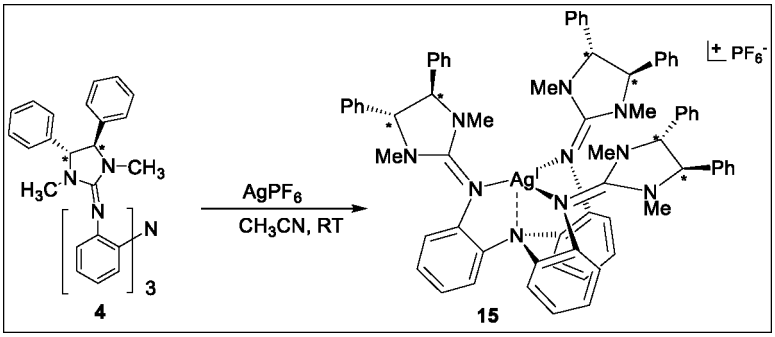

Scheme 22. Synthesis of Chiral $[Ag^I(DMDPI_3\text{-trphen})][PF_6]$ **(15)**

2.4. SYNTHESIS OF BIPODAL METAL COMPLEXES

Synthesis of Chiral $[Cu^I(DMDPI_3\text{-biphen})][PF_6].Et_2O$ **(16).** The ligand $DMDPI_3$-biphen **11** was dissolved in degassed THF and 1 equiv. of $[Cu(CH_3CN)_4][PF_6]$ was added to this solution (Scheme 23) and stirred overnight.

Compound **16** was obtained from acetonitrile and diethyl ether solutions at – 30 °C as off-white crystalline material (82%), suitable for X-ray diffraction analysis (Figure. 8).

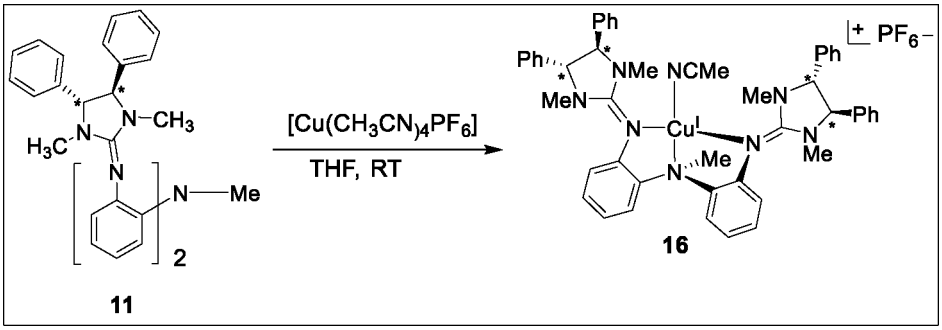

Scheme 23. Synthesis of Chiral [Cu^{I}(DMDPI$_3$-biphen)][PF_6].Et_2O (**16**)

Type of bond	Bond Angle
N(8)-Cu(1)-N(2)	125.74(10)
N(8)-Cu(1)-N(3)	124.14(10)
N(2)-Cu(1)-N(3)	107.01(9)
N(8)-Cu(1)-N(1)	125.45(9)
N(2)-Cu(1)-N(1)	79.31(9)
N(3)-Cu(1)-N(1)	77.26(8)

Type of Bond	Bond length
Cu(1)-N(8)	1.867(2)
Cu(1)-N(2)	2.044(2)
Cu(1)-N(3)	2.063(2)
Cu(1)-N(1)	2.268(2)

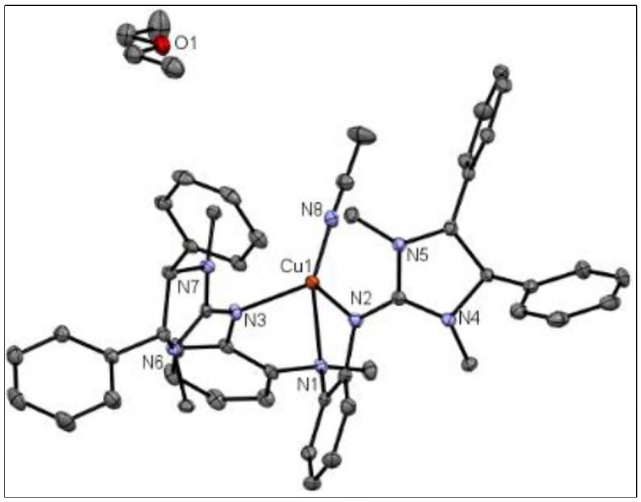

Figure 8. ORTEP Diagram of Chiral [Cu I(DMDPI$_3$-biphen)][PF_6].Et_2O (**16**)

Compound **16** possessed a distorted tetrahedral coordination environment in the solid state. In addition to the [N_2NMe] coordination, acetonitrile (used as a solvent for recrystallization) is also binding to Cu(I). The calculated bond lengths (Å) and bond angles (°) are given below. As expected, the Cu−N(1) bond length between N_{amine} atom and Cu(I) is longer as compared to the bonds of Cu with the N_{amido} atoms, N(2) and N(3).

2.5. CATALYTIC STUDIES

Catalytic Studies with [Cu^{I}(DMDPI$_3$-trphen)][PF_6] **(12).** We first tried asymmetric aziridination reactions (Scheme 24) with styrene (2.0 mmol) as the substrate and PhINTs as a nitrene source (0.25 mmol.; limiting reagent), in the presence of 5 mol% of [Cu^{I}(DMDPI$_3$-trphen)][PF_6] **(12)** and molecular sieves (MS). Initially, the aziridination of styrene (2.0 mmol) by PhINTs (0.25 mmol) was conducted in various (0.20 mL) solvents (MeCN, benzene, chlorobenzene, pentane, CH_2Cl_2, fluorobenzene, trifluoroethanol; 0.20 mL) in the presence of catalytic amounts of **12** (0.0125 mmol) at 30 ^{0}C (Table 1). The reaction was stirred for 12 hours, after which the crude mixture was purified by silica column chromatography to give pure aziridinated product**,** which was quantified by ^{1}H NMR in $CDCl_3$ versus an internal standard (4′-methoxyacetophenone). The % ee values were determined with the assistance of chiral HPLC on a commercial (R, R)-Whelk-O1 column.

The highest yield (99%) was obtained in acetonitrile, although all other solvents also afforded good yields. At the temperature of this experiment (30 ^{0}C), all % ee values are insignificant in all solvents.

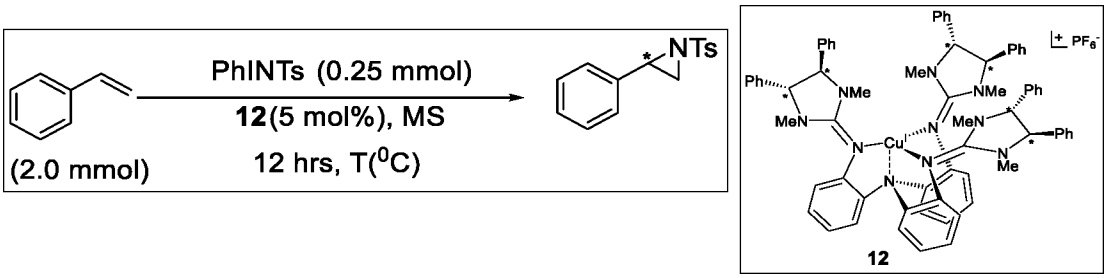

Scheme 24. Asymmetric Aziridination Reaction with [Cu^{I}(DMDPI$_3$-trphen)][PF_6] **(12)**

It is common for such types of asymmetric reactions to require low temperatures in order to suppress the reaction rate in favor of selectivity. We thus explored the reaction at 10 ^{0}C in all the solvents noted above (Table 1).

Table 1 . Asymmetric Aziridination of Styrene by PhINTs Catalytic Data Mediated by 12 at 30 0C, 10 0C and 0 0C in Various Solvents[a]

Solvent	Yield(%) **30 ^{0}C**	ee (%) **30 ^{0}C**	Yield(%) **10 ^{0}C**	ee (%) **10 ^{0}C**	Yield(%) **0 ^{0}C**	ee (%) **0 ^{0}C**
CH_3CN	99	0	85	0	35	12
CH_2Cl_2	92	0	78	5	30	10
C_6H_6	88	5	70	38	32	40
C_6H_5Cl	90	10	**72**	**60**	35	58
C_6H_5F	87	10	70	55	30	50
Pentane	85	5	70	50	25	45
CF_3CH_2OH	83	0	75	10	48	10

[a]Conditions: Styrene, 2.0 mmol; PhINTs, 0.25 mmol; cat 12, 0.0125 mmol (5 mol %); MS 5 Å, 20 mg; solvent , 0.200 mL; 12 h.

As expected, the yields dropped upon decreasing the temperature from 30 ^{0}C to 10 ^{0}C. The highest yield was obtained in acetonitrile (85%) at 10 ^{0}C, although the % ee value did not improve in this solvent. Other solvents also gave low to modest % ee

values. The best balance between yield and ee at 10 ^{0}C was found in chlorobenzene (yields, 70%; ee, 60%), followed closely by fluorobenzene and pentane. Selected solvents were then screened at 0 ^{0}C (Table 1). At 0 ^{0}C, the yields dropped significantly as expected with the highest yield recorded in acetonitrile (35%). In the case of chlorobenzene, the yield was low and the ee values were roughly the same as those obtained at 10 ^{0}C. Upon decreasing the temperature to -78 ^{0}C in dichloromethane, both the yield (6%) and ee (35%) values remained significantly low. Overall, in the case of **12** as a chiral catalyst for the asymmetric aziridination of styrene, the best balance between yield and ee is achieved in chlorobenzene at 10 ^{0}C.

Styrene, as well many other non-functionalized terminal olefins, has always been a challenging substrate for enantioselective aziridination. To our knowledge, the best % ee values with styrene as a substrate and PhINTs as a nitrene source has been reported by Jacobsen's[1] and Evans'[2] group (60-67 ee%). The Jacobsen group used copper reagents bearing C_2-symmetric chiral salen-framework, while the Evans' group used Cu(I) bis(oxazoline) ligands for asymmetric aziridination of styrenes at -78 ^{0}C and 0 ^{0}C, respectively. The % ee value with our Cu(I) catalyst **12** supported by cyclic chiral guanidinyl arms is moderate (60 ee%), at roughly the same level as that achieved in the iconic work of Jacobsen and Evans, although the temperature required for **12** (10 ^{0}C) is significantly higher. The Arnold group also attempted aziridination reactions of styrenes and other aromatic olefins using the new genetically modified variant enzyme P411 and tosyl azide (TsN_3) as a nitrene source. High ee values (>90%) were obtained, but at very low yields. Unfortunately, the feasibility of such reactions for a practicing synthetic chemist may be challenging in a common laboratory setting at the present time.

After establishing the optimum working conditions with styrene as a substrate in the case of the Cu(I) chiral catalyst **12** (5 mol %), we tried asymmetric aziridination reactions with other p-substituted styrenes (2.0 mmol), PhINTs (0.25 mmol, limiting agent) as a nitrene source, and stirred for 12 hours in PhCl (0.2 mL) at 10 ^{0}C (Table 2).

Table 2 . Asymmetric Aziridination of para-Substituted Styrene by PhINTs Catalytic Data Mediated by **12** at, 10 ^{0}C in Chlorobenzene.

Entry	Substrates	Products	Yield (%)	%ee
1.	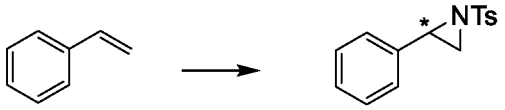		72	60
2.	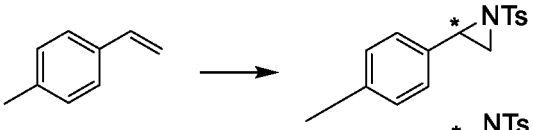		68	50
3.	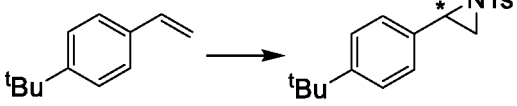		65	45
4.	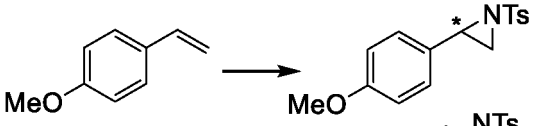		62	40
5.	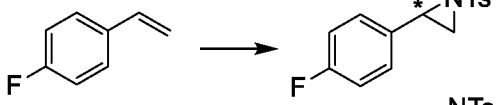		65	50
6.	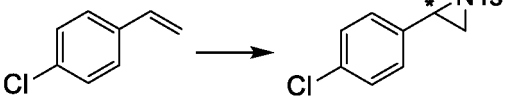		60	50
7.	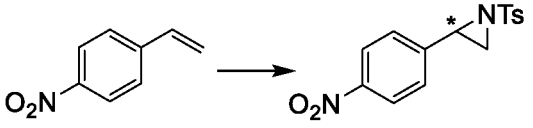		25	51
8.	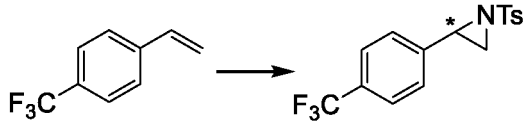		20	50

[a]Conditions: Olefin, 2.0 mmol; PhINTs, 0.25 mmol; cat **12** 0.0125 mmol MS (5mol%);5 Å, 20 mg; chlorobenzene,0.200 mL; room temperature; 12 h.

The crude product was purified by column chromatography to give pure substituted aziridinated product which was quantified by ^{1}H NMR in $CDCl_3$ versus an internal standard (4′-methoxyacetophenone) to obtain yields. The % ee values were determined with the assistance of chiral HPLC on a commercial (R, R)-Whelk-O1 column.

At 10 °C, the yields were modest with both electron-donating and electron-withdrawing para-substituents (Table 2, entries 2-4 and 5-8, respectively). The yield dropped drastically for the more electron-withdrawing substituents i.e., 4-nitro styrene and 4-trifluoromethyl styrene (Table 2, entries 7 and 8). This is an expected trend, as these reactions are all electrophilic in nature, therefore, generally tend to favor more electron-rich substrates as compared to electron-deficient substrates. The % ee values remain modest with p-substituted styrenes (Table 2, entries 2-8), with the parent styrene providing the best yield and ee values (Table 2, entry 1).

Catalytic Studies with [Cu^I(d-DMDPI-trphen)][PF_6] **(13).** Representative examples in the exploration of different solvents and temperatures in the case of the deuterated analog (N−CD_3) analog **13** are shown in Table 3. The highest yield was obtained at 30 °C in acetonitrile (92%). As expected, the yields drop significantly upon decreasing the temperature from 30 °C to -78 °C. Surprisingly, ee values were quite low even in chlorobenzene at 10 °C, by comparison to **12**. In this case, the highest ee values obtained (only 25% ee) were in dichloromethane at -78 °C. We designed [Cu^I(d-DMDPI-trphen)][PF_6] **(13)** to possess N-CD_3 substituents, to impede oxidative demethylation as compared to the N-Me arm. Although this catalyst shows good reactivity, ee values are surprising very low to non-existent., for reasons not well understood at the present time.

Table 3. Asymmetric Aziridination of Styrene by PhINTs Catalytic Data Mediated by **13** at 30 °C, 10 °C and 0 °C in Various Solvents[a]

Solvent	Temp (°C)	Yield(%)	% ee
CH_3CN	30	92	0
CH_3CN	0	30	20
CH_2Cl_2	0	25	12
CH_2Cl_2	-78	8	25
C_6H_5Cl	30	80	5
C_6H_5Cl	10	65	20

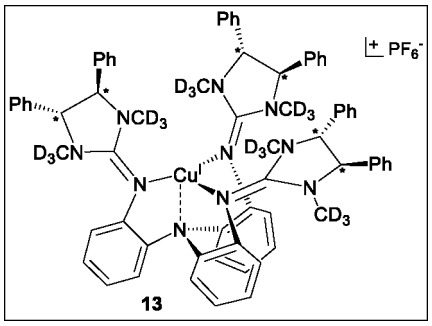

[a]Conditions: Styrene, 2.0 mmol; PhINTs, 0.25 mmol; cat **13**, 0.0125 mmol (5 mol %); MS (5 Å), 20 mg; solvent , 200 mg; 12 h.

Catalytic Studies with Chiral [Cu^I(DMDPI$_3$-biphen)]. Et_2O (**16**). Representative examples in the exploration of different solvents and temperatures in the case of the bipodal Cu(I) catalyst **16** are shown in Table 4. The highest yield was obtained at 30 °C in acetonitrile (90%), followed by chlorobenzene. The ee values remained quite low even in chlorobenzene at 10 °C, with the highest ee value obtained (25%) in dichloromethane at -78 °C. As noted previously, we synthesized the bipodal Cu(I) catalyst **16** by replacing one of the phenyl legs with a smaller and sterically less hindered Me group. It was designed while keeping in mind that the tripodal framework might be sterically too bulky to show catalytic activity with sterically demanding substrates. Not surprisingly, the bipodal catalyst showed inferior ee values by comparison to the tripodal analog, at essentially comparable yields in different solvents. One possible explanation of the lower ee values in the case of **16** is the lack of rigidity of this catalyst.

Table 4. Asymmetric Aziridination of Styrene by PhINTs Catalytic Data Mediated by **16** at 30 °C, 10 °C and 0 °C in Various Solvents[a]

Solvent	Temp (°C)	Yield(%)	% ee
CH_3CN	30	90	0
CH_3CN	0	25	10
CH_2Cl_2	0	20	8
CH_2Cl_2	-78	5	25
C_6H_6	10	55	20
C_6H_5Cl	30	80	12
C_6H_5Cl	10	50	8
Pentane	30	65	5
Pentane	10	50	15

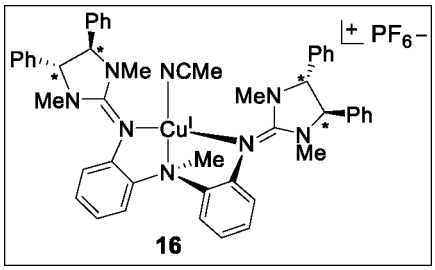

16

[a]Conditions: Styrene, 2.0 mmol; PhINTs, 0.25 mmol; cat **16**, 0.0125 mmol (5 mol %); MS (5 Å), 20 mg; solvent , 200 mg; 12 h.

Catalytic Studies with a Soluble Nitrene Source**.** We also pursued catalytic studies using a soluble source of nitrene, since PhINTs has a polymeric structure and is insoluble in common solvents. The soluble NTs o- propoxyphenyliminoiodane **27** (prepared according to the literature protocol, Scheme 25) can be delivered slowly to the reaction in a suitable solvent over a period of time through a syringe pump. This might be helpful in controlling the rate of the reactions, and hence, affecting reactivity and selectivity. Compound **27** should be stored in the refrigerator and protected from the light to increase its shell life. It exhibits good solubility in dichloromethane, chloroform, and to lesser extent, in acetonitrile. The solubility in dichloromethane is 0.250 g/mL, however this soluble source of NTs proved to be unstable in chlorinated solvents.

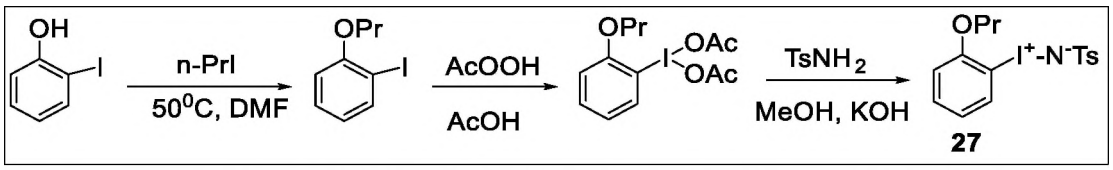

Scheme 25. Synthesis of a Soluble NTs Source (**27**)

Initially, we screened the solvents acetonitrile, dichloromethane and 1,1,3,3-hexafluoro isopropanol (HFIP), in which the nitrene source **27** is soluble enough at 30 °C and was added over a period of 1.0 h with the assistance of a syringe pump.

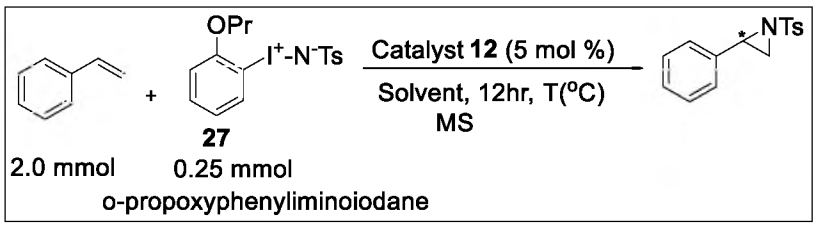

Scheme 26. Asymmetric Aziridination of Styrene with a Soluble NTs **27** Mediated by **12**

In the case of the Cu(I) tripodal catalyst **12** with soluble NTs **27** as a nitrene source (Scheme 26), we observed that at 30 °C in acetonitrile, the yield dropped to 65 % as compared to 99 % when PhINTs was used as a nitrene source (Table 5). Dichloromethane also gave comparable yield (55%), but in HFIP, the yield obtained (40%) was even lower. Similar results were obtained with the deuterated Cu (I) analog **13** and the bipodal Cu(I) **16** catalyst. As expected, ee (%) values are close to zero at this temperature. The lower yields are also consistent with the instability of **27** in various solvents.

We then explored the styrene aziridination reaction in the same solvents at 10 °C and 0 °C (Table 6). The yields dropped significantly for all three chiral catalysts in all solvents.

Table 5. Asymmetric Aziridination Catalytic Data with Soluble NTs **27**[a] at 30 ^{0}C

Solvent	Yield (%) Catalyst **12**	ee (%) Catalyst **12**	Yield (%) Catalyst **14**	ee (%) Catalyst **14**	Yield (%) Catalyst **16**	ee (%) Catalyst **16**
CH_3CN	65	0	60	0	55	0
CH_2Cl_2	60	5	50	0	52	0
HFIP	40	0	30	0	35	0
CH_2Cl_2+C_6H_5Cl[b]	55	5	45	0	50	0

[a]Conditions: Styrene, 2.0 mmol; Soluble NTs **27**, 0.25 mmol; catalyst, 0.0125 mmol (5 mol %); MS (5 Å), 20 mg; solvent , 0.900 mL; 12 h. [b]CH_2Cl_2 (200 mg) and C_6H_5Cl (700 mg)

Modest ee values (53%) were obtained for **12** at 0 ^{o}C, marking an improvement versus PhINTs. As noted with PhINTs, we did not observe any significant ee values with the chiral catalysts **13** and **16**. In the case of the soluble form of NTs (**27**) as a nitrene source, the best balance between yield and ee values is obtained with catalyst **12** in dichloromethane at 0 ^{o}C. The modest yields observed, raised questions about the stability of the soluble nitrene source **27** over a period of time when delivered slowly through a syringe pump. We thus obtained a series of ^{1}H NMR spectra of **27** in several deuterated solvents, namely $CDCl_3$, CD_3CN and d-HFIP at regular time intervals. We observed that in the case of $CDCl_3$ and CD_3CN, **27** decomposed slowly, as we noticed smaller peaks developing besides those attributed to **27**. In contrast, when we used d-HFIP as the solvent, the soluble NTs was stable even after 16 hours. However, the solubility of **27** in HFIP is inferior to that observed in dichloromethane or acetonitrile, and also HFIP did not prove to be a good solvent for aziridination reactions.

Table 6. Asymmetric Aziridination with Soluble NTs **27** at 10 °C and 0 °C.

Solvent	Yield (%) Catalyst **12**		ee (%) Catalyst **12**		Yield (%) Catalyst **14**		ee (%) Catalyst **14**		Yield (%) Catalyst **16**		ee (%) Catalyst **16**	
	10 °C	**0 °C**	**10 °C**	**0 °C**	**10 °C**	**0 °C**	**10 °C**	**0 °C**	**10 °C**	**0 °C**	**10 °C**	**0 °C**
CH_3CN	12	45	20	20	30	35	25	20	25	30	20	20
CH_2Cl_2	40	**35**	45	**53**	25	30	35	35	25	30	20	20
CH_2Cl_2+C_6H_5Cl	30	35	40	43	20	25	25	20	25	25	10	10
HFIP	30	25	10	15	25	20	10	10	25	20	0	0

[a]Conditions: Styrene, 2.0 mmol; Soluble NTs **27**, 0.25 mmol; catalyst, 0.0125 mmol (5 mol %); MS (5 Å), 20 mg; solvent , 0.900 mL; 12 h. [b]CH_2Cl_2 (200 mg), C_6H_5Cl (700 mg)

Asymmetric Cyclopropanation Reactions**.** We also attempted a preliminary screening of a series of asymmetric cyclopropanation reactions of styrene (Scheme 27) with methyl 2-diazo-2-phenylacetate (prepared according to a literature protocol), as a carbene source. The diazocarbene was dissolved in the solvent of choice (MeCN, benzene, chlorobenzene, pentane, CH_2Cl_2, fluorobenzene, trifluoroethanol) and added

slowly via syringe pump to the flask containing 5 equiv. of styrene and 5 mol % of the catalyst **12**. The reaction mixture was stirred vigorously for 12 hours at a specific temperature.

After completion of the reaction, the products were isolated by column chromatography (silica gel) and quantified by ^{1}H NMR in $CDCl_3$ versus an internal standard (4′-methoxyacetophenone). The % ee values were calculated with the assistance of chiral HPLC on a commercial (R, R)-Whelk-O1 column.

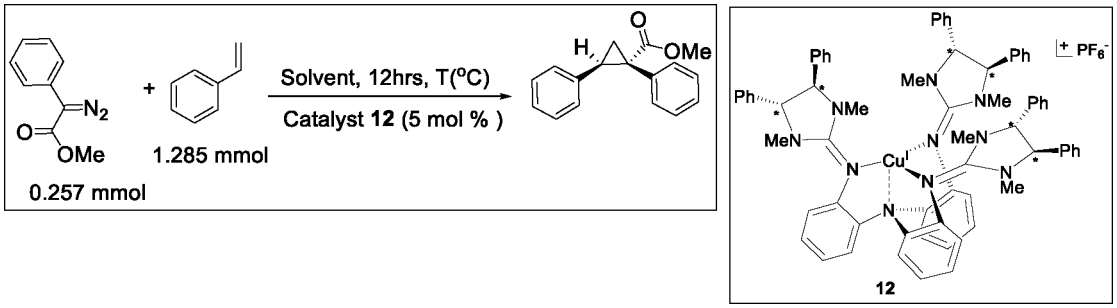

Scheme 27. Asymmetric Cyclopropanation Reaction of Styrene Mediated by Catalyst **12**

The yield was only 15% in dichloromethane with 1 mol% catalyst **12** loading, however, at 5 mol %, the yield increased significantly to 70% (Table 7). All other solvents provided lower yields. As expected, on decreasing the temperature from 30 °C to -78 °C, the yields dropped to 40% in dichloromethane. Trifluoroethanol (CF_3CH_2OH) also gave modest yield (55%) at 0 °C.

In all case examined, the ee values remain low even at very low temperatures. It is very likely that this catalyst is quite bulky for handling the sterically demanding carbene source and does not permit close contact with the chiral auxiliary.

Table 7. Asymmetric Cyclopropanation Catalytic Data of Styrene Mediated by **12**[a]

Solvent	Temp (°C)	Yield (%)	ee (%)
CH_2Cl_2	30[b]	15	5
CH_2Cl_2	30	70	8
CH_2Cl_2	0	50	10
CH_2Cl_2	-78	40	12
CH_3CN	0	15	0
CF_3CH_2OH	0	55	10
C_6H_5Cl	10	45	15
C_6H_6	10	30	8
Pentane	30	35	10

[a]Conditions: Styrene, 1.285 mmol; methyl 2-diazo-2-phenylacetate, 0.257 mmol; catalyst **12**, 0.0125 mmol (5 mol %); solvent , 2.0 mL; 12 h. [b]catalyst **12**, 0.0025 mmol (1 mol %).

2.6. MISCELLANEOUS SYNTHESIS OF LIGANDS, INTERMEDIATES AND METAL COMPLEXES FOR FUTURE DEVELOPMENT

We also designed a cyclic chiral ligand featuring N–^{i}Pr guanidinyl-arms. Having N–^{i}Pr arm might be more advantageous, as it is less prone to oxidative demethylation as compared to N-Me arm. Moreover, ^{i}Pr group might help in restricting the movement of the guanidinyl-arms perpendicular to the ligand and thus might be more useful in achieving higher selectivity. On the other hand, the possibility of making the ligand too bulky for any significant catalytic activity still exists.

For the synthesis of this chiral ligand scaffold possessing N–^{i}Pr guanidinyl-arms, we start from commercially available chiral 1R, 2R-(+)-1, 2- diphenylethylenediamine and add 1 equiv. of acetone in methanol. The reaction is stirred for 1 h at rt and then 3 equiv. of $NaBH_4$ was added and the mixture was stirred for another 3h at rt to give monoalkylated amine (1R,2R)-N1-isopropyl-1,2-diphenylethane-1,2-diamine **17**.

The compound was isolated through extraction procedure with dichloromethane and the product was obtained as a yellowish viscous liquid (92%) (Scheme 28).

The above procedure was repeated for dialkylation to provide (1R,2R)-N,N′-Diisopropyl 1,2-diphenylethylenediamine **18** (Scheme 28) as a white solid (83%). By means of ^{1}H-NMR, we observed that both the methyls of the isopropyl group appeared as doublets and, therefore, are localized in different chemical environments as shown by discrete chemical shift values. Indeed, ^{1}H-NMR of **18** shows that Me of the N-^{i}Pr arm resolves to give two different doublet peaks at 1.13-1.12 and 1.09-1.07 ppm in $CDCl_3$.

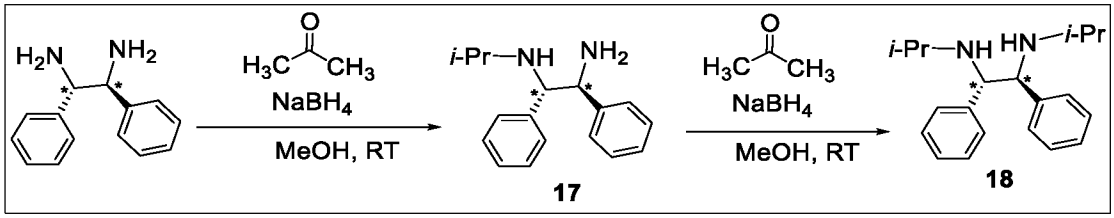

Scheme 28. Synthesis of (1R,2R)-N,N′-Diisopropyl 1,2-diphenylethylenediamine **18**

This **18**.2HCl salt and 1 equiv. of triethyl orthoformate were heated at 100 °C for 16 h to afford (4R,5R)-1,3-diisopropyl-4,5-diphenyl-4,5-dihydro-1H-imidazol-3-ium chloride **19** (67.5%) as a colorless solid (Scheme 29).

The Synthesis of the Chloro Imidazolium Salt **20** can be achieved by two methods. Method A. MeMgCl (3M Et_2O, 1.2 equiv.) was added to (4R,5R)-1,3-diisopropyl-4,5-diphenyl-4,5-dihydro-1H-imidazol-3-ium **19** in THF, followed by 1.4 equiv. of hexachloroethane and stirred for 24 h at room temperature to afford (4R,5R)-2-chloro-1,3-diisopropyl-4,5-diphenyl-4,5-dihydro-1H-imidazol-3-ium chloride **20** (Scheme 30) as a light yellowish solid (60%).

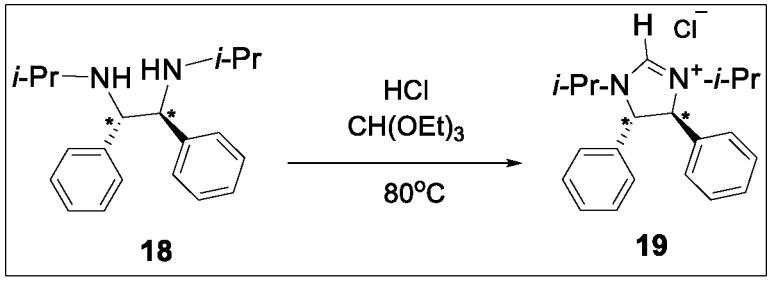

Scheme 29. Synthesis of Compound **19**

Method B. Initially, we tried to synthesize the N–^{i}Pr arm appended chloro imidazolium salt **20** by adopting a methodology (Scheme 31) similar as to the synthesis of N–Me arm appended chloro imidazolium salt **3** albeit in low yields (~10%). Therefore, we adopted the alternative methodology noted above (Method A, Scheme 26) for its synthesis, which increased its yield to 60%. In the methodology B, compound **18** was dissolved in acetonitrile and then 1.08 equiv. of di-tert-butyl dicarbonate (BOC_2O) and 1.08 equiv. of 4-dimethylaminopyridine (DMAP) were added and stirred for 24 h at room temperature. The compound (4R, 5R)-1,3-diisopropyl-4,5-diphenylimidazolidin-2-one (**21)** was obtained as a pure white solid (85%). The isopropylated urea **21** is then converted **20** by using 5 equiv. of oxalyl chloride upon refluxing for 20 h.

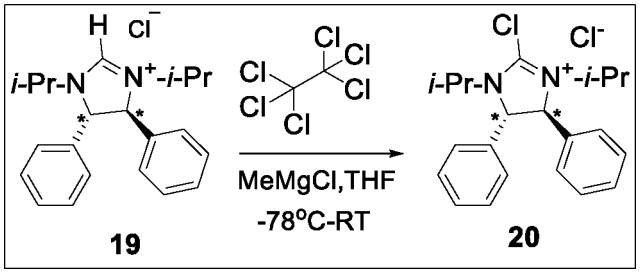

Scheme 30. Synthesis of Chloro Imidazolium Salt **20** (Method A)

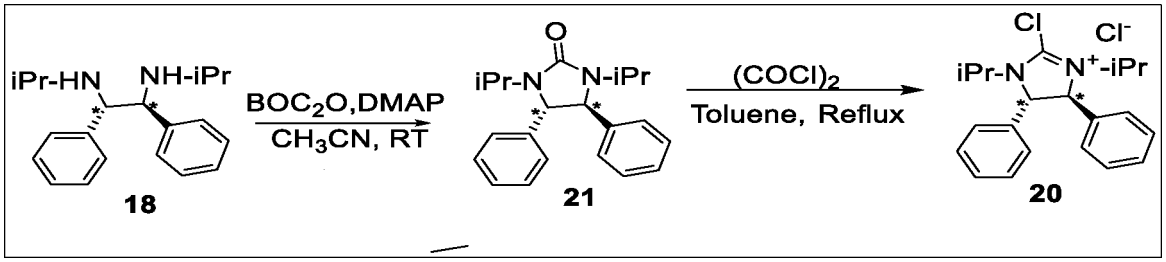

Scheme 31. Synthesis of Compound **20** (Method B)

Synthesis of a Bipodal Biphenyl amido-aniline Scaffold (N_2N-$C_6H_4NH_2$) with Chiral Cyclic Guanidinyl Arms**.** We have also synthesized the chiral ligand with two different substituted N-arm i.e., a combination of N−Me arm and N− ^{i}Pr arm (**25**, Scheme 32). In this way, we are breaking the symmetry of the ligand in the initial stage, which in turn might make the catalyst more useful in achieving higher selectivities in catalytic reactions. For the synthesis of this chiral catalyst, we convert mono substituted N-^{i}Pr armed chiral amine **17** to the corresponding urea **22** using 1.09 equiv. of di-tert-butyl dicarbonate (BOC_2O) and 0 9 equiv. of 4-dimethyaminopyridine (DMAP). The compound (4R,5R)-1-isopropyl-4,5-diphenylimidazolidin-2-one (**22**) was obtained as a pure white solid (80%).

We then alkylate the N-H arm of the urea **22** first by deprotonating it with 2 equiv. of sodium hydride and then alkylating it with 2.5 equiv. of methyl iodide to give the desired chiral ligand with two different N-substituted arms, (4R,5R)-1-isopropyl-3-methyl-4,5-diphenylimidazolidin-2-one (**23),** as a white solid (77%). The chiral ligand **23** was further converted into the (4R,5R)-2-chloro-3-isopropyl-1-methyl-4,5-diphenyl-4,5-dihydro-1H-imidazol-3-ium chloride **24** using 5 equiv. of oxalyl chloride in refluxing toluene for 20 hours.

The chloro imidazolium salt **24** is then coupled with our parent 2, 2′, 2″-triaminotriphenylamine in the presence of 3 equiv. of triethylamine to afford ligand **25** in the form of a white solid (70%), which was recrystallized further from acetonitrile to give X-ray quality crystals. Figure. 9 shows the ORTEP diagram of the compound **25**.

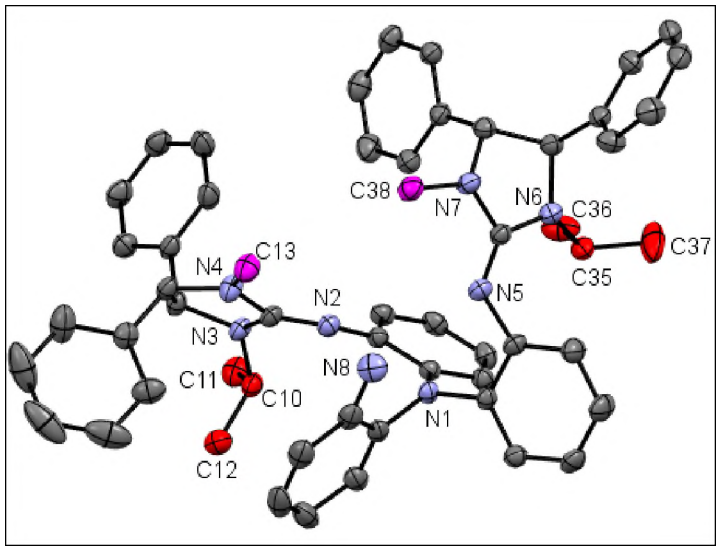

Figure 9. ORTEP Diagram of Compound **25**

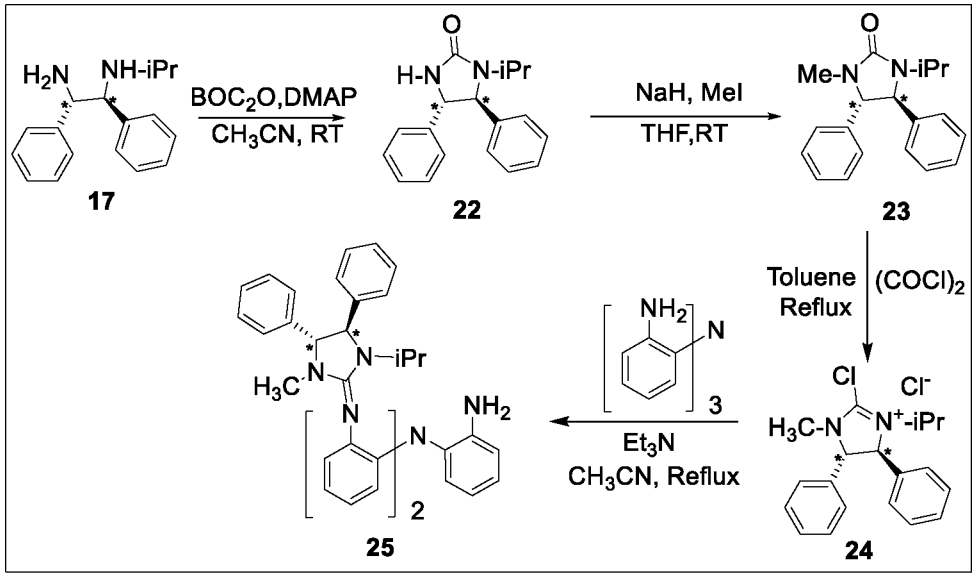

Scheme 32. Synthesis of Compound **25**

Apparently, due to the steric bulk of the ligand, only two legs of the triphenylamine core are substituted, instead of the expected three legs. The unsubstituted NH_2 arm of the ligand **25** can be further exploited in many useful ways in the future.

Synthesis of Tripodal Triphenyl amido-amine Ligand with tert-Butyl Substitution **(2-NH(^{t}Bu)-C_6H_4)$_3$N).** In 2018, our group reported a library of trisamido-amine ligands (L^1H_3−$L^{15}H_3$) used for C─N bond construction methodology. All ligands possess the 2,2′,2″- triaminotriphenylamine (trphen) scaffold with a variety of pendent arms (aryl, acyl, alkyl). Primary and secondary substituents as in the case of Me and ^{i}Pr can be easily installed, but once there is no hydrogen atom attached to the carbon, it becomes significantly more difficult to synthesize the corresponding ligands, because of steric bulk and lack of general methodologies.

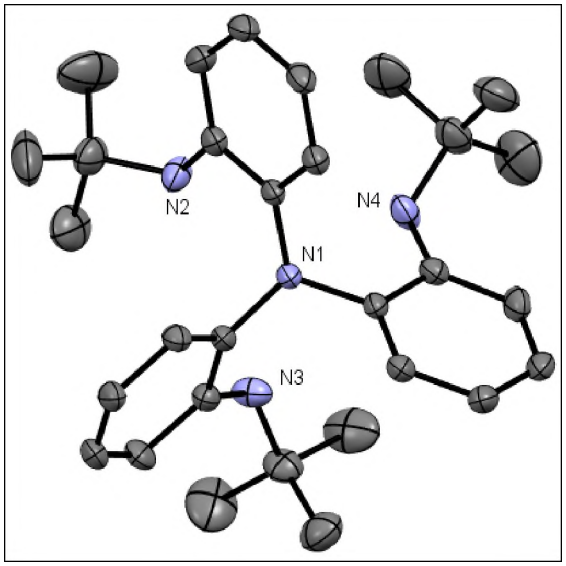

Figure 10. ORTEP Diagram of tert butylated Tripodal Ligand **26**

This is illustrated for the synthesis of the tripodal tert-butyl armed ligand (**26**) which we achieved after significant effort. Initially, when we tried the reaction under a

multitude of conditions (Scheme 33) and with the assistant of various t-Bu precursors, the yields obtained were very low (≤ 5%). Finally, we succeeded (Scheme 34) upon using neat t-Bu 2,2,2-trichloroacetimidate at room temperature in a fast reaction (15min).

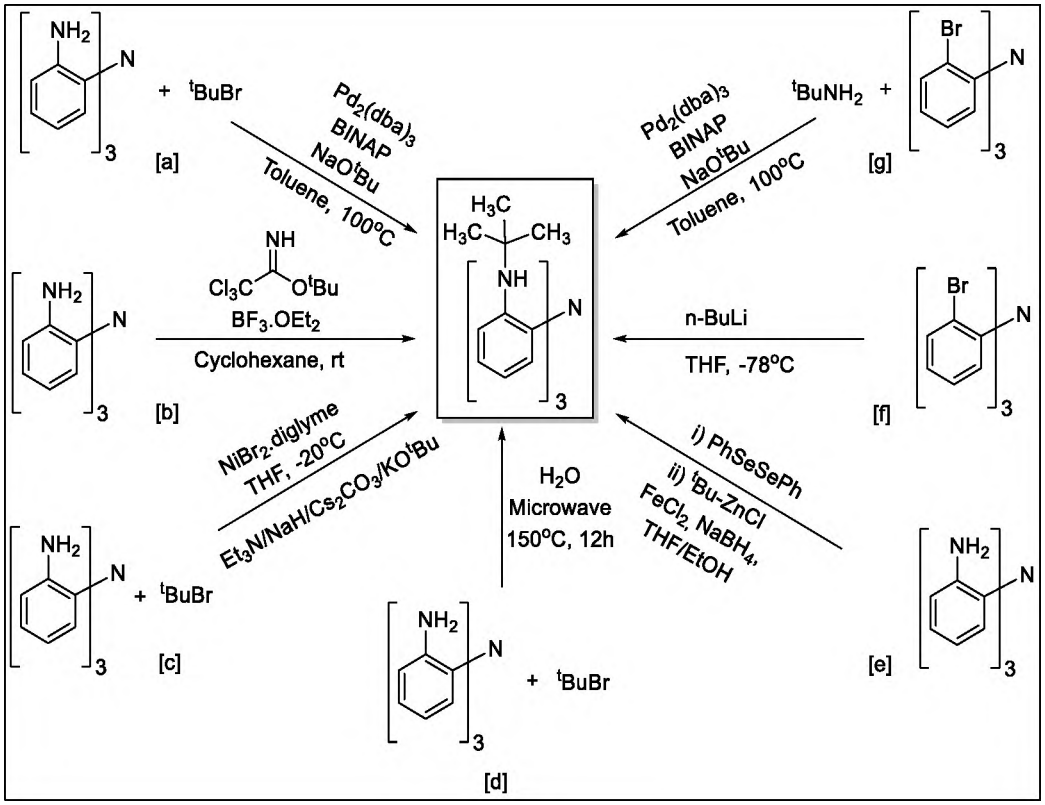

Scheme 33. Synthetic Routes Attempted for the Synthesis of the tert butylated Tripodal Ligand (**26**)

Our parent ligand $(2\text{-}NH_2\text{-}C_6H_4)_3N$ and $Cu(OTf)_2$ were mixed together and to these solids 7.5 equiv. of tert-butyl 2,2,2-trichloroacetimidate[15] was added and the mixture was stirred for 15 minutes to afford 2-(1^1-azaneyl)-N-(tert-butyl)aniline (**26**) (85%) as a white solid. The ligand was further recrystallized from hexane to afford crystals for X-ray diffraction analysis (Figure. 10). The ^{1}H-NMR spectrum shows the Me of the tert-butyl group at 1.19 ppm in $CDCl_3$.

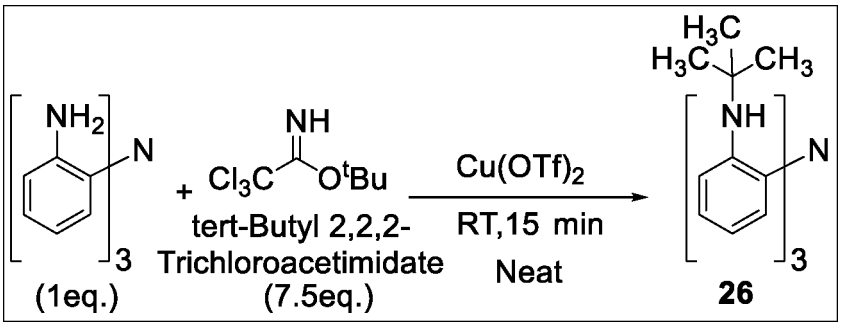

Scheme 34. Successful Synthetic Route for the Synthesis of tert butylated Tripodal Ligand (**26**)

2. CONCLUSION AND FUTURE DIRECTIONS

The following are the major findings and future endeavors for this work:

1. The Cu(I) chiral tripodal scaffold, featuring N─Me arms (**12**, 5 mol %) provides moderate yields and ee values in the aziridination of styrene and other para-substituted styrenes in chlorobenzene at 10 °C. The deuterated analog **13** (N─CD_3 arm) and the bipodal [N_2NMe] catalyst **16** showed inferior ee values by comparison to the tripodal analog **12**, at essentially comparable yield in different solvents. The substrate scope for asymmetric aziridination is quite limited in the literature and unfunctionalized alkenes (such as styrenes) have proven to be especially challenging feedstock. Future experiments will concentrate on further catalyst development featuring more elaborate secondary interactions. We will also be conducting amination reactions (ethyl benzene, adamantane) with our chiral Cu catalysts; nitrene insertion into C─H bonds is more challenging than C=C aziridinations.

2. Since there is still controversy whether C=C aziridinations proceed in a concerted or a stepwise manner, through a putative metal– nitrenoid intermediate, this mechanistic differentiation requires further attention for selectivity purposes, by

providing careful evaluation of the time elapsed between the first and second C−N bond construction. Besides focusing on the reactivity and the selectivity aspect, future efforts will also explore the metal-centered events associated with the electron chemistry of the Cu chiral cyclic guanidinyl catalyst, which might be different from analogous steps in the two- electron chemistry of Rh catalysts.

3. To further extend the library of chiral guanidinyl reagents, we have synthesized a key precursor, (4R,5R)-2-chloro-1,3-diisopropyl-4,5-diphenyl-4,5-dihydro-1H-imidazol-3-ium chloride **20** (featuring N-^{i}Pr arm**)**. The next goal will be to couple it with the parent ligand 2, 2′, 2″-triaminotriphenylamine, and further metallate the corresponding chiral ligand with Cu(I) sources, in order to be used in catalytic studies for comparative purposes. We have also synthesized the bipodal biphenyl amido amine scaffold **25** based on the usual chiral cyclic guanidinyl moeity featuring a combination of N−Me arm and N− ^{i}Pr arms . The unsubstituted NH_2 can be exploited in many different ways to generate unsymmetrical ligands that can be further metalated with Cu(I) sources and used for catalytic studies.

4. We also designed the corresponding Ru(II) reagent, $[Ru^{II}(DMDPI_3\text{-trphen})](PF_6)_2$ (Scheme 35, **28**) for comparative catalytic and mechanistic studies.

The synthesis of the chiral reagent **28** requires extensive heating of the ligand $DMDPI_3$-trphen (**4)** and 1 equiv. of $[Ru(CH_3CN)_6](PF_6)_2$ in THF at 55 °C. The filtrate was evaporated to give **28** as a white solid, identified by ^{1}H-NMR. X-ray structure of this compound is pending.

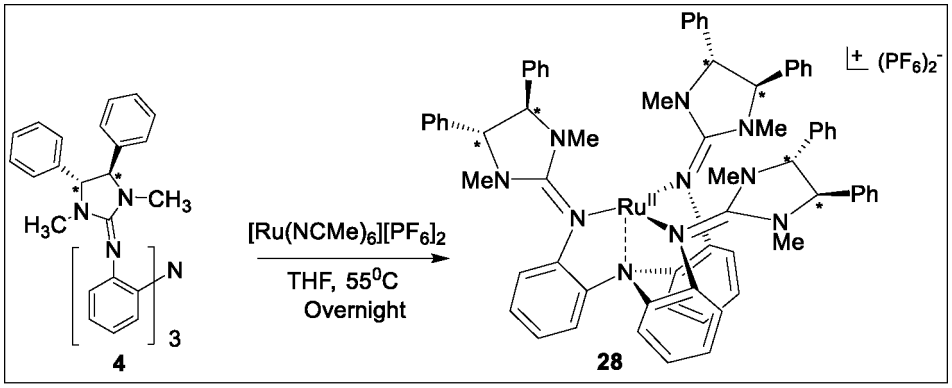

Scheme 35. Synthesis of Chiral $[Ru^{II}(DMDPI_3\text{-trphen})](PF_6)_2$ (**28**)

5. Moreover, we have also designed a similar catalyst, but with chiral moieties appended from the N atoms. In this way, the chirality may be more easily transferred to the metal cavity due to the proximity of these chiral groups to the metal center (Scheme 36). The synthetic methodology relies on the commercially available chiral S-(α)-methylbenzylamine (**29**) which reacts with glyoxal in toluene to form imine (**30**, Scheme 36). Stereoselective addition of phenylmagnesium bromide to the chiral bis-imine results in the formation of chiral diamine **31.** It was then converted into the imidazolinium salt **32** by using triethylorthoformate ($CH(OEt)_3$) as an electrophile. The imazadolinium salt is further converted to chloro salt **33** using methylmagnesium chloride as a base and hexachloroethane as an electrophile. So far, we have synthesized the chiral diamine **31** (according to the literature protocol)[16].

6. In this work , we have placed more emphasis on aziridination reactions, but we are also interested in cyclopropanation reactions. We have already conducted a few of the cyclopropanation reactions with the chiral Cu catalyst **12** and methyl 2-diazo-2-phenylacetate as a carbene source, but with limited success.

Our next step will be to work with different acceptor-donor carbene sources which might be of more synthetic value if they are more electrophilic and less bulky (Scheme 37).

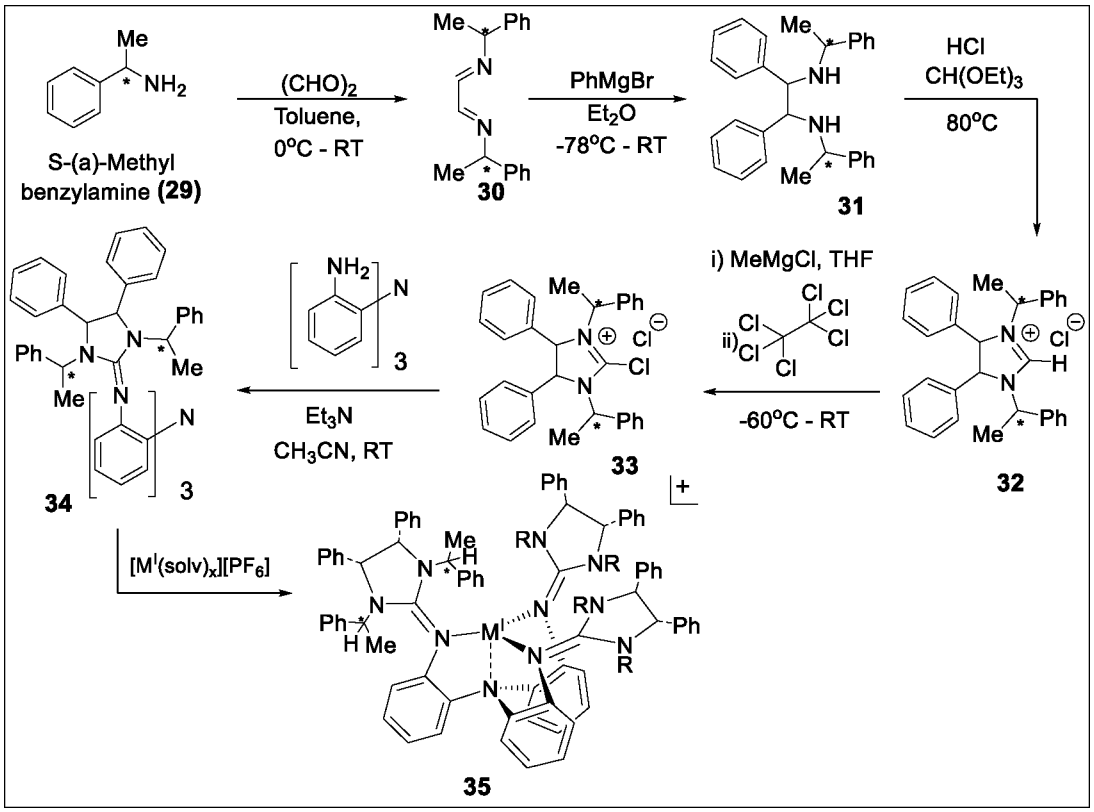

Scheme 36. Synthetic Methodology for the Catalyst with Chirality Attached to the Nitrogen.

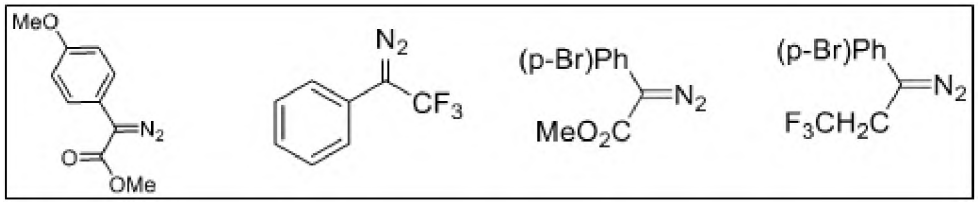

Scheme 37. Different Carbene Sources to be Considered in this Study

7. We have finally synthesized a tripodal triphenyl amido-amine ligand with tert-butyl substitution (**26**). Initially, we tried to deprotonate the ligand by using potassium

hydride (KH) as a base, but we observed through NMR that most of the ligand **26** remained unreacted. The next target will be to deprotonate by using stronger bases such as n-butyllithium, and metalate with first-row transition metals (Mn, Fe and Co) for use in catalytic nitrene transfer chemistry.

ACKNOWLEDGEMENTS

This work was generously supported by the National Institute of General Medical Sciences of the National Institutes of Health under Award Number R15GM117508 (to P.S.), and in part by the National Science Foundation through grant CHE-0412959 (to P.S.).

REFERENCES

(1) Li, Z.; Conser, K. R.; Jacobsen, E. N. Asymmetric alkene aziridination with readily available chiral diimine-based catalysts. *J. Am. Chem. Soc.* **1993**, *115*, 5326−5327.

(2) Evans, D. A.; Faul, M. M.; Bilodeau, M. T.; Anderson, B. A.; Barnes, D. M. Bis(oxazoline)-copper complexes as chiral catalysts for the enantioselective aziridination of olefins. *J. Am. Chem.Soc.* **1993**, *115*, 5328−5329.

(3) Evans, D. A.; Nelson, S.G. Chiral Magnesium Bis(sulfonamide) Complexes as Catalysts for the Merged Enolization and Enantioselective Amination of *N*-Acyloxazolidinones. A Catalytic Approach to the Synthesis of Arylglycines. *J. Am. Chem. Soc.* **1997**, *119*, 6452−6453.

(4) Lebel, H.; Cedric, S.; Leogane, O.; Trudel, C.; Parmentier., M. Stereoselective Rhodium-Catalyzed Amination of Alkenes. *Org. Lett.* **2011**, *13*, 5460-5463.

(5) Fiori, K. W.; Du Bois, J. Catalytic Intermolecular Amination of C−H Bonds: Method Development and Mechanistic Insights. *J. Am. Chem. Soc.* **2007**, *129*, 562-568.

(6) Nishioka, Y.; Uchida, T.; Katsuki, T.; Enantio- and Regioselective Intermolecular Benzylic and Allylic C─H Bond Amination. *Angew. Chem., Int. Ed.* **2013**, *52*, 1739-1742.

(7) Tao, J.; Jin, L.; Zhang, P. X. Synthesis of chiral *N*-phosphoryl aziridines through enantioselective aziridination of alkenes with phosphoryl azide via Co(II)-based metalloradical catalysis. *Beilsten J. Org. Chem.* **2014**, *10*, 1282-89.

(8) Prier, C. K; Zhang, R. K.; Buller, R. K.; Chen, S.B; Arnold, F.H.. Enantioselective, intermolecular benzylic C-H amination catalysed by an engineered iron-haem enzyme. *Nat. Chem.* **2017**, *9*, 629-634.

(9) Farwell, C. C.; Zhang, R. K.; McIntosh, J. A.; Hyster, T. K.; Arnold, F. H Enantioselective Enzyme-Catalyzed Aziridination Enabled by Active-Site Evolution of a Cytochrome P450. *ACS Cent. Sci.* 2015, *1*, 89−93.Evans, D. A.; Woerpel, A. K.; Hinman,M.M.; Faul, M.M. Bis(oxazolines) as chiral ligands in metal-catalyzed asymmetric reactions. Catalytic, asymmetric cyclopropanation of olefins. *J. Am. Chem. Soc.* **1991**, *113*,726-728.

(10) Evans, D. A.; Woerpel, A. K.; Hinman,M.M.; Faul, M.M. Bis(oxazolines) as chiral ligands in metal-catalyzed asymmetric reactions. catalytic, asymmetric cyclopropanation of olefins. *J. Am. Chem. Soc.* **1991**, *113*,726-728.

(11) Chen, Y.; Fields, K. B.; Zhang P. X. Bromoporphyrins as Versatile Synthons for Modular Construction of Chiral Porphyrins: Cobalt-Catalyzed Highly Enantioselective and Diastereoselective Cyclopropanation. *J. Am. Chem. Soc.* **2004**, *126*, 14718-14719.

(12) Adly, F.G.; Gardiner, M.G.; Ghanem, A. Design and Synthesis of Novel Chiral Dirhodium(II) Carboxylate Complexes for Asymmetric Cyclopropanation Reactions. *Chem Eur. J.* **2016**, *22*, 3447-3461.

(13) Qin, C.; Davies, H. M.L. Role of Sterically Demanding Chiral Dirhodium Catalysts in Site-Selective C–H Functionalization of Activated Primary C–H Bonds. *J. Am. Chem. Soc.* **2014**, 136, 27, 9792-9796.

(14) Bagchi, V.; Paraskevopoulou, P.; Das, P.; Chi, L.; Wang, Q.; Choudhury, A.; Mathieson, J. S.; Cronin, L.; Pardue, D. B.; Cundari, T. R.; Mitrikas, G.; Sanakis, Y.; Stavropoulos, P. A Versatile Tripodal Cu(I) Reagent for C–N Bond Construction via Nitrene-Transfer Chemistry: Catalytic Perspectives and Mechanistic Insights on C–H Aminations/Amidinations and Olefin Aziridinations. *J. Am. Chem. Soc.* **2014**, *136*, 11362−11381.

(15) Cran, J.W; Vidhani D.V; Krafft, M.E. Copper-catalyzed N-tert-butylation of aromatic amines under mild conditions using tert-butyl 2,2,2-trichloroacetimidate. *Synlett.* **2014**, 1550-1554.

(16) Mastranzo, Virginia M. Use of diamines containing the α-phenylethyl group as chiral ligands in the asymmetric hydrosilylation of prochiral ketones. *Tetrahedron* **2002**, *60*, 1781-1789

SECTION

2. SUMMARY AND CONCLUSIONS

The first part of this study explores the synthesis and characterization of a family of fifteen Mn(II) anionic complexes supported by a N_3N^{3-} triphenylamido-amine framework and various carbonaceous arms (aryl, acyl, and alkyl). The anionic character of the complexes attenuates the reactivity for aziridination of aromatic olefins, but enhances selectivity versus aliphatic olefins, especially with Mn(II) complexes. Electrochemical data support a wide range of Mn^{II}/Mn^{III} redox potentials. Among all 15 Mn(II) complexes, L^8Mn(II), bearing the CF_3CO residue, was found out to be the most anodically shifted, stabilizing the Mn(II) oxidation state. On the other hand., L^{13}Mn(II), which bears electron-releasing substituents was found out to be most oxidizable, and also among a subset of very few Mn(II) complexes that show semi-reversible waves. L^8Mn(II) proved to be the highest yielding catalyst (75%) in the aziridination of styrene by PhINTs as a nitrogen source. The yields correlate largely with the redox potential of all fifteen Mn(II) compounds used in this study, in as much as the higher the redox potential of the catalyst, the higher the yield of the aziridination reaction tends to be. Hence, the reactivity of the library of Mn(II) catalysts in nitrene transfer to olefins is governed by the electrophilicity of the putative metal-nitrene active species.

Once L^8Mn(II) was identified as the highest yielding catalyst, the catalytic aziridination reaction with different types of substrates was explored in a comparative study that involved the L^8Mn, L^8Fe and L^8Co analogs. In the case of para-substituted styrenes, all three catalysts afforded good to high yields of aziridines in comparable

ranges. In sharp contrast, styrenes with α or β substitution show a drastic drop in the yield and loss of stereochemistry, most likely because of steric encumbrance. Most importantly, out of all three catalysts, L^8Co proved to be superior in terms of yield and retention of stereochemistry with respect to cis/trans isomerizations. The comparative reaction profile study also highlights differences in the rate of aziridine formation by the three metals (L^8Mn, L^8Fe and L^8Co), indicating that the rate of aziridine formation by Co(II)-catalyzed reactions is much faster than that of the kinetically more comparable Fe and Mn systems. In the case of aliphatic olefins, the yield is drastically reduced, as compared to that for the aromatic olefins. However, aliphatic olefins exhibit better stereocontrol than aromatic congeners upon aziridination, presumably due to faster ring closure.

Competitive aziridination of styrene versus aliphatic olefins by PhINTs demonstrated that all three catalysts are favoring aziridination of aromatic olefins over aliphatic olefins. Importantly, this trend is significantly more enhanced for Mn catalyzed reactions, and consistently in the order Mn > Co > Fe. Overall, these results are consistent with an inverse reactivity/selectivity correlation, with the exception of Fe(II)-mediated reactions, which are ill behaved. Attenuated aziridination reactivity of the anionic L^8Mn reagent enables differentiation of styrene and 1-hexene by a practicable margin (62:1) versus a modest edge (5:1) previously reported by Evans and co-workers with Cu reagents. Mechanistic (Hammett plots, secondary KIE, cis/trans isomerization) and computational studies (DFT) showed that the formation of aziridine follows a stepwise mechanism with the generation of a carboradical intermediate. The first step is a slow, rate determining step, characterized by $N_{TS} - C_\beta$ bond formation and generation of a radical $C\alpha$ site. The second step consist of the aziridine ring closing (N_{TS}-C_α bond

formation) and occurs as a much faster event, determining the stereochemistry of the product. The computationally calculated results agreed with the experimental evidence and suggested L^8Co to be more reactive and selective than L^8Mn and L^8Fe analogues in the aziridination of styrene. Isopentene was modeled as an alternative substrate to study the competition between styrene and acyclic aliphatic olefins. As expected, the activation energy barrier of the initial N_{TS} – C bond forming step for the Mn(II) mediated aziridination of isopentene (32.8Kcal/mol), is significantly higher than that for styrene (25.1 kcal/mol). The calculated HOMO energy of styrene was 0.7eV higher than that of isopentene, which makes styrene a better nucleophile for attack by the electrophilic nitrene catalyst, yielding a lower activation energy barrier. Conversely the activation energy for the second N_{TS} – C bond formation (aziridine ring closure) is lower for isopentene (3.4 kcal/mol) than that for styrene (4.7 kcal/mol). Interestingly, radical clock experiments reveal that the aliphatic radical exhibits longer lifetime in the Co rather than the Mn-mediated reaction, in sharp contrast to the stereocontrol studies in styrene aziridinations. More extensive experimentation with aliphatic olefins will further shed light on these intriguing variations.

The second part of the study focuses on the high-spin Co(II) complexes (S=3/2) supported by all ligands (L^1H_3-$L^{15}H_3$) used in the first study, as well as two new ligands, $L^{16}H_3$ and $L^{17}H_3$. Amongst all seventeen Co(II) compounds, the catalytically important $[K(L^4)Co^{II}]_n$ exhibits the highest symmetry (strictly C_3 symmetry). This compound is characterized by an exclusive four-coordinate [N_3N] ligand field, and an open metalated cavity fortified by the three –CO^tBu arms. The electrochemical properties of a panel of representative Co^{II} compounds were studied by cyclic voltammetry. The results are

consistent with the electronic character of the ligands and prior electrochemical data obtained for the analogous Mn^{II} complexes, although the potentials of the Co^{II} compounds have been shifted anodically, as expected, by a factor of 0.4-0.7 V, and are also associated with significant ligand oxidation.

Surprisingly, L^4Co (70%) was found out to be the most productive catalyst out of all the seventeen cobalt complexes, followed very closely by L^8Co (69%), in spite of the fact that L^8Co is anodically shifted by 500 mV versus L^4Co, and is potentially less congested. As opposed to the corresponding L^xMn^{II} reagents (x = 1-15) that reveal a dominant relationship between increasing styrene aziridination yields with anodically shifting Mn^{II}/Mn^{III} redox potentials (i.e., with increased electrophilicity), the Co^{II} catalysts provide yields that indicate a more complex pattern of electronic and steric contributions. Moreover, L^4Co is significantly faster in achieving the maximum yield than L^8Co. At the 1.0 h mark, the rate of aziridine formation is completed by 88% for L^4Co, whereas it is 65% in case of L^8Co.

The aziridination yields for the para-substituted styrenes in case of L^4Co, except for the parent styrene, are only slightly inferior to those previously reported for L^8Co. In the case of bulkier substrates (α- and β-substituted styrenes), L^8Co was on average more productive than L^4Co, possibly due to the more voluminous reaction cavity of L^8Co. Mechanistic (Hammett plots, secondary KIE, cis/trans isomerization) showed that the formation of aziridine mediated by L^4Co also follows a stepwise mechanism with the generation of a carboradical intermediate. The cis- and trans-β-*d*-styrene aziridinations, mediated by L^4Co and L^8Co, showed modest inverse KIE values, highlighting the preponderance of N_{TS}-C_β formation (sp^2 to sp^3) in the rate determining step. The ratio of

cis/trans aziridine (94:6) resulting from the L^4Co-mediated aziridination of cis-*β-d*-styrene is more pronounced than that provided by L^8Co (cis/trans aziridine: 89/11), signifying the interference of even smaller energy barriers in aziridine-ring closure (formation of the second N_{TS}-Cα bond) in the case of L^4Co. All these kinetic and mechanistic results cannot be solely explained by the general electrophilicity criterion noted for the Mn(II) library of reagents.

The structure and electronic description of the presumptive [L^4Co]NTs intermediate were explored by DFT calculations, highlighting how a small ligand modification can result in a major electronic rearrangement. All three spin states (quartet, sextet, doublet) of [L^4Co]NTs generated large activation barriers for the initial step (~50 kcal/mol; N_{TS}-Cβ bond formation). London dispersion forces are attractive forces present between the highly polarizable bulky and rigid alkyl substituents such as tert -Bu group and are currently emerging as stabilizing factors in highly congested organic and inorganic compounds. The corresponding barriers were reduced by approximately 20 kcal/mol on applying London dispersion-corrected DFT. However, these barriers are still significant by comparison to the reaction of [L^8Co]NTs (sextet) and styrene (23.4 kcal/mol, N_{TS}-Cβ bond formation). Spin-density calculations also revealed that the non-coordinating arm of [L^4Co]NTs is one-electron oxidized, resulting in the formation of *N*-aryl amidyl radical. The corresponding arm of [L^8Co]NTs is redox innocent because the electron withdrawing CF_3 residue protects it from a similar one-electron oxidation. The single-electron distribution of the *N*-aryl amidyl radical in [L^4Co]NTs is spread throughout the non-coordinating arm, with almost half of the spin density being localized on the N atom (Figure. 2.1). This enables more favorable reactivity channels in case of

[L^4Co]NTs as compared to [L^8Co]NTs. *N*-aryl amidyl radicals are known to add to alkenes, at least intramolecularly and might provide stabilizing effect in case of [L^4Co]NTs. Further experimentation and attendant DFT calculations will be required to understand the anomalous behavior of high spin Co(II) complexes (higher reactivity for styrene aziridination despite of lower electrophilicity) and further explore whether reagents with other rigid alkyl substituents (such as the adamantyl group) can be superior mediators of nitrene-transfer chemistry by stabilizing the metal nitrene moiety.

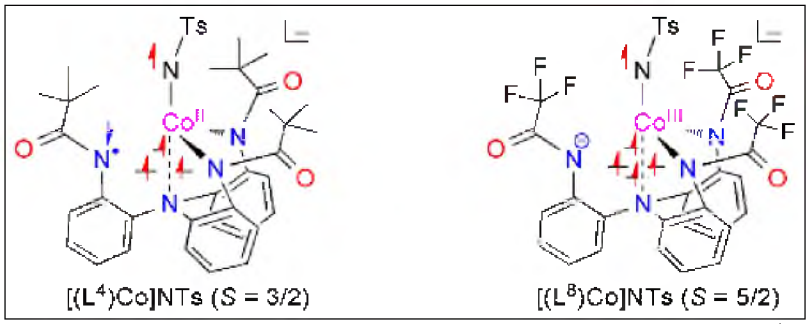

Figure 2.1. Schematic distribution of spins in the ground state of [L^4Co]NTs and [L^8Co]NTs

The third part of this dissertation consists of a preliminary effort to study the intermolecular aziridination of alkenes catalyzed by metal reagents (Cu, Ag) supported by bulky ligands with a chiral framework**.** We synthesized a tripodal triphenyl amido-amine scaffold [N_3N] with chiral cyclic guanidinyl framework and also a bipodal bisphenyl amido-methyl amine scaffold [N_2N-Me] with the same chiral cyclic guanidinyl moeity, both possessing superior rigidity and permitting the incorporation of chiral centers in the backbone of the cyclic framework. Enantioselective intermolecular C─N bond construction has been reported in the literature mostly relying on Pt-group transition metals such as Rh, Ru and Ir. The major problem with these metals is that they are quite

expensive and toxic. We opted for using mostly earth abundant first-row transition metals such as Cu.

We first explored asymmetric aziridination reactions with styrene (a notoriously challenging substrate) and PhINTs as a nitrene source, in the presence of 5 mol% of Cu(I) cyclic chiral guanidinyl catalyst with N-Me pendent arms. The best balance between yield and ee values was found in chlorobenzene at 10 ^{o}C (yield, 70%; ee, 60%). The Jacobsen group used copper reagents bearing C_2-symmetric chiral salen-framework, while Evans' group used Cu(I) bis(oxazoline) compounds for asymmetric aziridination of styrenes at -78 ^{o}C and 0 ^{o}C, respectively. The % ee value with our Cu(I) cyclic chiral guanidinyl catalyst with N-Me arm catalyst is moderate (60 ee%), at roughly the same level as that achieved in the iconic work of Jacobsen and Evans, although the temperature required (10 ^{o}C) is higher. The % ee values remain modest with p-substituted styrenes with the parent styrene providing the best yield and ee values. We also designed Cu(I) cyclic chiral guanidinyl catalyst with N—CD_3 arm to impede any oxidative demethylation as compared to the N—Me arm. Although this catalyst shows good reactivity, ee values were surprising very low to non-existent. The corresponding bipodal Cu(I) cyclic chiral guanidinyl catalyst also showed inferior ee values by comparison to the tripodal analog, at essentially comparable yields in different solvents. One possible explanation of the lower ee values in the case of the bipodal analog catalyst is the lack of rigidity. We also expanded the library of chiral cyclic guanidine frameworks by employing two N— ^{i}Pr arms and also a combination of N−Me/N− ^{i}Pr arms . For the future studies, the goal will be to metallate them with Cu(I) and use them in catalytic studies for asymmetric alkene aziridination and C—H amination reactions.

APPENDIX A.

COMPARATIVE NITRENE-TRANSFER CHEMISTRY TO OLEFINIC SUBSTRATES MEDIATED BY A LIBRARY OF ANIONIC Mn(II) TRIPHENYLAMIDO-AMINE REAGENTS AND M(II) CONGENERS (M = Fe, Co, Ni) FAVORING AROMATIC OVER ALIPHATIC ALKENES

1. EXPERIMENTAL SECTION

1.1. GENERAL CONSIDERATIONS

All operations were performed under anaerobic conditions under a pure dinitrogen or argon atmosphere using Schlenk techniques on an inert gas/vacuum manifold or in a dry-box (O_2, H_2O < 1 ppm). Anhydrous diethyl ether, methylene chloride, acetonitrile, tetrahydrofuran, hexane, pentane, benzene, toluene, dimethylformamide, dimethylacetamide, and dimethylsulfoxide were purchased from Sigma-Aldrich. Ethanol and methanol were distilled over the corresponding magnesium alkoxide, and acetone was distilled over Drierite. Solvents were degassed by three freeze-pump-thaw cycles. Unless otherwise noted, all other reagents were purchased at the highest purity available. Potassium hydride was provided as dispersion in mineral oil and was thoroughly washed prior to use with copious amounts of tetrahydrofuran followed by hexane. Ligands L^1H_3, L^2H_3–L^6H_3, L^7H_3, L^8H_3,[2] L^9H_3,[2] $L^{10}H_3$, $L^{13}H_3$,[4] and compounds [K(MeCN)(L^8)Fe^{II}–NCMe] (**8c**),[2] [$K(THF)_x$][(L^1)Mn^{II}–THF] (**1**) and (Ph_4P)[(L^1)Mn^{II}–THF]•3THF (**Xb**)[5] have been prepared according to literature methods.

^1H and ^{13}C NMR spectra were recorded on Varian XL-400, Varian INOVA/ UNITY 400 MHz Unity Plus and a Varian 300 Unity Plus NMR spectrometers. IR spectra were obtained on a Perkin-Elmer 883 IR spectrometer and FT-IR spectra on Nicolet Nexus 470 and 670, Magna 750 FT-IR ESP and Shimadzu IR-Affinity-1 spectrometers. UV-vis spectra were obtained on a Hewlett-Packard 8452A diode array, Varian Cary 50 and Varian Cary 300 spectrophotometers. EI and FAB mass spectra were obtained on a Finnigan MAT-90 mass spectrometer. ESI and APCI mass spectra were obtained on a Thermo-Finnigan TSQ7000 triple-quadrupole mass spectrometer, equipped

with the API2 source and Performance Pack (ThermoFinnigan, San Jose, CA). HRMS data were collected on a Thermo Fisher Scientific LTQ-Orbitrap XL hybrid mass spectrometer, using the Orbitrap analyzer for acquisition of high-resolution accurate mass data. Samples were infused using the integrated syringe pump at 3 μL/min and ionization was *via* the electrospray source with source settings at their defaults. In general, settings for the ion optics were determined automatically during the regular tuning and calibration of the instrument. For high-resolution data, the Orbitrap analyzer is set to a resolution of 100000. Microanalyses were done by Galbraith Laboratories, Knoxville, TN, Quantitative Technologies Inc., Whitehouse, NJ, and on an in-house Perkin-Elmer 2400 CHN analyzer.

1.2. OTHER PHYSICAL MEASUREMENTS

(a) X-ray crystallography**.** Intensity data sets for all the compounds were collected on a Bruker Smart Apex diffractometer using graphite monochromated Mo Kα radiation (λ = 0.71073 Å) from a fine focus sealed tube X-ray source. Suitable crystals were selected and mounted on a glass fiber using super glue. The data were collected at low temperatures (140–150 K) and room temperature for metal complexes and purely organic compounds, respectively, employing a scan of 0.3° in ω with an exposure time of 20 s/frame using SMART software. The cell refinement and data reduction were carried out with SAINT while the program SADABS was used for the absorption correction.[7] The structures were solved by direct methods using SHELXS-97 and difference Fourier syntheses. Full-matrix least-squares refinement against $|F^2|$ was carried out using the SHELXTL-PLUS[8] suite of programs. All non-hydrogen atoms were refined anisotropically. Hydrogen atoms were placed geometrically and held in the riding mode

during the final refinement. Pertinent crystallographic data are collected in Tables S1-S3, and selective interatomic distances and angles are reported in Tables S4-S8. ORTEPS are shown in Figures 3-6 and S1-S4.

Table S1. Summary of Crystallographic Data for Metal Compounds $[K(THF)_6][(L^2)Mn^{II}–THF]$ (**2**), $[K(THF)_2(L^3)Mn^{II}–THF]$ (**3**), $[K_2(DMA)_3(L^4)_2Mn^{II}{}_2]$ (**4**), $[K(THF)_4(L^5)Mn^{II}–THF]$ (**5**), $[K(NCMe)][(L^6)Mn^{II}–NCMe]•MeCN$ (**6**) and $\{[K(DMA)(L^7)Mn^{II}]_2\}_2•3Et_2O$ (**7**)

	L^2Mn^{II}	**L^3Mn^{II}**	**L^4Mn^{II}**	**L^5Mn^{II}**	**L^6Mn^{II}**	**L^7Mn^{II}**
formula	$C_{88}H_{131}KMnN_4O_7$	$C_{54}H_{45}F_{18}KMnN_4O_3$	$C_{78}H_{105}Mn_2K_2N_{11}O_9$	$C_{56}H_{61}Cl_6KMnN_4O_5$	$C_{45}H_{36}KMnN_7O_3$	$C_{148}H_{198}K_4Mn_4N_{20}O_{19}$
M_r	1451.01	1233.98	1528.81	1176.83	816.85	2937.42
crystal system	Triclinic	Triclinic	Triclinic	Monoclinic	Monoclinic	Triclinic
space group	$P\bar{1}$	$P\bar{1}$	$P\bar{1}$	$P2_1/n$	$P2_1/n$	$P\bar{1}$
a (Å)	13.4244(15)	12.729(4)	11.759(2)	11.3910(7)	11.7651(7)	12.421(3)
b (Å)	15.4608(17)	14.584(4)	13.541(3)	20.1796(14)	21.2221(12)	13.222(3)
c (Å)	21.041(2)	16.701(5)	26.426(5)	24.4880(18)	16.4682(9)	24.754(5)
α (deg)	92.203(2)	112.045(5)	86.003(3)	90.00	90.00	89.650(4)
β (deg)	93.4740(10)	92.891(6)	80.023(3)	93.742(3)	95.4680(10)	77.831(4)
γ (deg)	102.8050(10)	99.020(5)	73.719(2)	90.00	90.00	72.506(3)
V (Å^3)	4244.7(8)	2817.7(14)	3977.1(14)	5617.0(7)	4093.1(4)	3783.3(13)
Z	2	2	2	4	4	1
D_{calcd} (g cm^{-3})	1.135	1.454	1.277	1.392	1.326	1.289
T (K)	130(2)	223(2)	130(2)	100(2)	137(2)	293(2)
λ (Å)	0.71073	0.71073	0.71073	0.71073	0.71073	0.71073
μ (mm^{-1})	0.258	0.413	0.483	0.645	0.473	0.505
$R_1{}^a$ (I>2σ(I))	0.0823	0.0689	0.0884	0.0403	0.0436	0.0714
$wR_2{}^b$ (I>2σ(I))	0.2295	0.1774	0.2382	0.0861	0.1096	0.1764

$||F_c||/\Sigma|F_o|$. ^{b} $wR_2 = [\Sigma w(F_o^2 - F_c^2)^2/\Sigma w(F_o^2)^2]^{1/2}$

.

Table S2. Summary of Crystallographic Data for Metal Compounds $[K(DMA)(L^{8})Mn^{II}–DMA]_n$ (**8a**), $[K(NCMe)(L^{8})Mn^{II}–NCMe]$ (**8b**), $[K(L^{9})Mn^{II}]_n$ (**9**), $[K_2(THF)_3(L^{10})_2Mn^{II}_2]$•2THF (**10**), $[K(THF)_3(L^{11})Mn^{II}–THF]$•0.75 Pentane (**11**), $[K(L^{12})Mn^{II}–THF]$•THF (**12**), $[K(THF)_3][(L^{13})Mn^{II}–THF]$ (**13**) and $[K(L^{15})Mn^{II}]$•0.5DMA•0.5hexane (**15**)

	$L^{8}Mn^{II}$–DMA	**$L^{8}Mn^{II}$–MeCN**	**$L^{9}Mn^{II}$**	**$L^{10}Mn^{II}$**	**$L^{11}Mn^{II}$**	**$L^{12}Mn^{II}$**	**$L^{13}Mn^{II}$**	**$L^{15}Mn^{II}$**
formula	$C_{32}H_{30}F_9KMnN_6O_5$	$C_{28}H_{18}F_9KMnN_6O_3$	$C_{27}H_{33}KMnN_4$	$C_{86}H_{118}K_2Mn_2N_8O_{17}$	$C_{61}H_{77}KMnN_4O_4$	$C_{50}H_{55}KMnN_4O_2$	$C_{58}H_{71}KMnN_4O_4$	$C_{53}H_{47.5}F_9KMnN_{4.5}O_{6.5}$
M_r	842.65	751.52	507.61	1723.96	1024.30	838.02	982.23	1116.49
crystal system	Monoclinic	Monoclinic	Monoclinic	Monoclinic	Triclinic	Monoclinic	Monoclinic	Monoclinic
space group	Cc	$P2_1/c$	$P2_1/c$	C2/c	$P\bar{1}$	$P2_1/n$	$P2_1/n$	$P2_1/n$
a (Å)	18.3717(12)	10.661(7)	9.4583(12)	18.8633(15)	11.719(10)	11.527(2)	12.4818(15)	12.3883(15)
b (Å)	10.8662(7)	18.766(12)	13.3572(17)	21.7465(17)	12.417(10)	13.729(3)	21.792(3)	18.995(2)
c (Å)	19.0286(12)	15.752(10)	20.218(3)	22.5199(18)	21.770(19)	27.724(5)	20.039(2)	21.656(3)
α (deg)	90.00	90.00	90.00	90.00	91.221(12)	90.00	90.00	90.00
β (deg)	94.3070(10)	100.699(10)	98.800(2)	102.7590(10)	100.827(11)	92.471(4)	105.708(2)	101.457(2)
γ (deg)	90.00	90.00	90.00	90.00	100.424(12)	90.00	90.00	90.00
V (Å^3)	3788.0(4)	3097(3)	2524.2(6)	9009.8(12)	3055(4)	4383.3(15)	5247.3(11)	4994.5(11)
Z	4	4	4	4	2	4	4	4
D_{calcd} (g cm^3)	1.478	1.612	1.336	1.271	1.114	1.270	1.264	1.485
T (K)	130(2)	200(2)	137(2)	136(2)	130(2)	130(2)	130(2)	137(2)
λ (Å)	0.71073	0.71073	0.71073	0.71073	0.71073	0.71073	0.71073	0.71073
μ (mm^{-1})	0.549	0.656	0.710	0.440	0.329	0.440	0.380	0.438
$R_1{}^a$ (I>2σ(I))	0.0516	0.0668	0.0951	0.0546	0.0771	0.0549	0.0398	0.0917

Table S2. Summary of Crystallographic Data for Metal Compounds [K(DMA)(L^8)Mn^{II}–DMA]$_n$ (**8a**), [K(NCMe)(L^8)Mn^{II}–NCMe] (**8b**), [K(L^9)Mn^{II}]$_n$ (**9**), [K_2(THF)$_3$(L^{10})$_2Mn^{II}_2$]•2THF (**10**), [K(THF)$_3$(L^{11})Mn^{II}–THF]•0.75 Pentane (**11**), [K(L^{12})Mn^{II}–THF]•THF (**12**), [K(THF)$_3$][(L^{13})Mn^{II}–THF] (**13**) and [K(L^{15})Mn^{II}]•0.5DMA•0.5hexane (**15**) (cont.)

wR_2[b] (I>2σ(I))	0.1418	0.1768	0.1642	0.1354	0.1823	0.1321	0.1028	0.0917

[a] $R_1 = \Sigma||F_o| - |F_c||/\Sigma|F_o|$. [b] $wR_2 = [\Sigma w(F_o^2 - F_c^2)^2/\Sigma w(F_o^2)^2]^{1/2}$.

Table S3. Summary of Crystallographic Data for Metal Compounds [K(MeCN)(L^8)Co^{II}–NCMe] (**8d**), [K(DMA)$_3$(L^8)Ni^{II}]$_2$ (**8e**), [K(DMA)(L^{14})Fe^{II}]•DMA (**14b**) and [K(DMA)(L^{14})Co^{II}]•DMA (**14c**), and Ligands $L^{11}H_3$ and $L^{15}H_3$

	L^8Co^{II}–MeCN	**L^8Ni^{II}**	**$L^{14}Fe^{II}$**	**$L^{14}Co^{II}$**	**$L^{11}H_3$**	**$L^{15}H_3$**
formula	$C_{28}H_{18}CoF_9KN_6O_3$	$C_{36}H_{39}F_9KN_7NiO_6$	$C_{41}H_{51}FeKN_6O_{11}$	$C_{41}H_{51}CoKN_6O_{11}$	$C_{45}H_{48}N_4$	$C_{48}H_{39}F_9N_4O_6$
M_r	755.51	934.55	898.83	901.91	644.87	938.83
crystal system	Monoclinic	Monoclinic	Orthorhombic	Orthorhombic	Triclinic	Monoclinic
space group	$P2_1/c$	$P2_1/n$	$P2_12_12_1$	$P2_12_12_1$	$P\bar{1}$	$P2_1/c$
a (Å)	10.696(3)	9.133(8)	11.1683(17)	11.0919(7)	9.1381(9)	19.360(3)
b (Å)	18.855(6)	29.15(3)	18.406(3)	18.3376(11)	12.0237(12)	10.0615(16)
c (Å)	15.813(5)	16.125(14)	21.830(3)	21.9261(13)	17.8361(19)	29.486(4)
α (deg)	90.00	90.00	90.00	90.00	96.278(2)	90
β (deg)	101.378(5)	95.392(12)	90.00	90.00	90.360(2)	128.675(7)
γ (deg)	90.00	90.00	90.00	90.00	111.214(2)	90

Table S3. Summary of Crystallographic Data for Metal Compounds [K(MeCN)(L^8)Co^{II}–NCMe] (**8d**), [K(DMA)$_3$(L^8)Ni^{II}]$_2$ (**8e**), [K(DMA)(L^{14})Fe^{II}]•DMA (**14b**) and [K(DMA)(L^{14})Co^{II}]•DMA (**14c**), and Ligands $L^{11}H_3$ and $L^{15}H_3$ (cont.)

V (Å^3)	3126.1(17)	4274(7)	4487.4(12)	4459.7(5)	1813.7(3)	4484.0(12)
Z	4	4	4	4	2	4
D_{calcd} (g cm^{-3})	1.605	1.453	1.330	1.343	1.181	1.391
T (K)	243(2)	220(2)	293(2)	137(2)	130(2)	295(2)
λ (Å)	0.71073	0.71073	0.71073	0.71073	0.71073	0.71073
μ (mm^{-1})	0.777	0.642	0.492	0.542	0.069	0.117
R_1[a] (I>2σ(I))	0.0606	0.0564	0.0344	0.0520	0.1174	0.0628
wR_2[b] (I>2σ(I))	0.1398	0.1475	0.0904	0.1125	0.2273	0.1537

[a] $R_1 = \Sigma||F_o| - |F_c||/\Sigma|F_o|$. [b] $wR_2 = [\Sigma w(F_o^2 - F_c^2)^2/\Sigma w(F_o^2)^2]^{1/2}$.

Table S4. Selected Interatomic Distances (Å) for Metal Compounds $(Ph_4P)[(L^1)Mn^{II}–THF]$•3THF (**Xb**),[5] $[K(THF)_6][(L^2)Mn^{II}–THF]$ (**2**), $[K(THF)_2(L^3)Mn^{II}–THF]$ (**3**), $[K_2(DMA)_3(L^4)_2Mn^{II}_2]$ (**4**), $[K(THF)_4(L^5)Mn^{II}–THF]$ (**5**), $[K(NCMe)][(L^6)Mn^{II}–NCMe]$•MeCN (**6**), $\{[K(DMA)(L^7)Mn^{II}]_2\}_2$•3$Et_2O$ (**7**), $[K(DMA)(L^8)Mn^{II}–DMA]_n$ (**8a**), $[K(NCMe)(L^8)Mn^{II}–NCMe]$ (**8b**), $[K(L^9)Mn^{II}]_n$ (**9**), $[K_2(THF)_3(L^{10})_2Mn^{II}_2]$•2THF (**10**), $[K(THF)_3(L^{11})Mn^{II}–THF]$•0.75 Pentane (**11**), $[K(L^{12})Mn^{II}–THF]$•THF (**12**), $[K(THF)_3][(L^{13})Mn^{II}–THF]$ (**13**) and $[K(L^{15})Mn^{II}]$•0.5DMA•0.5hexane (**15**)

	L^1Mn^{II} [5]	**L^2Mn^{II}**	**L^3Mn^{II}**	**L^4Mn^{II}**	**L^5Mn^{II}**	**L^6Mn^{II}**	**L^7Mn^{II}**	**L^8Mn^{II} –DMA**	**L^8Mn^{II} –MeCN**
Mn(1)–N(1)	2.316(3)	2.2959(19)	2.350(3)		2.3385(16)	2.386(2)	2.543(2)	2.475(3)	2.440(4)
Mn(1)–N(2)	2.113(3)	2.105(2)	2.102(4)		2.1284(17)	2.141(2)	2.152(2)	2.224(4)	2.161(3)
Mn(1)–N(3)	2.084(3)	2.113(2)	2.126(3)	2.148(5)	2.0839(17)	2.1541(19)	2.140(3)	2.171(3)	2.165(3)
Mn(1)–N(4)	2.088(3)	2.105(2)	2.120(3)	2.163(5)	2.0972(17)	2.155(2)	2.189(3)	2.158(3)	2.174(3)
Mn(1)–N(5)						2.171(2)			2.176(4)
Mn(1)–O(1)	2.228(3)	2.2175(18)	2.198(3)	2.083(4)	2.2266(14)				
Mn(1)–O(2)				2.395(5)				2.042(3)	
Mn(1)–O(3)									
Mn(1)–O(4)						2.044(3)			
Mn(1)–O(5)			2.094(4)						
Mn(1)–O(6)					2.039(2)				
Mn(1)–K(1)			3.4554(18)						
Mn(1)–K(2)			3.8582(18)						
Mn(2)–N(5)					2.133(3)				
Mn(2)–N(6)					2.140(3)				
Mn(2)–N(7)			2.175(5)		2.184(2)				
Mn(2)–N(8)			2.152(5)		2.639(3)				

Table S4. Selected Interatomic Distances (Å) for Metal Compounds $(Ph_4P)[(L^1)Mn^{II}–THF]•3THF$ (**Xb**),[5] $[K(THF)_6][(L^2)Mn^{II}–THF]$ (**2**), $[K(THF)_2(L^3)Mn^{II}–THF]$ (**3**), $[K_2(DMA)_3(L^4)_2Mn^{II}_2]$ (**4**), $[K(THF)_4(L^5)Mn^{II}–THF]$ (**5**), $[K(NCMe)][(L^6)Mn^{II}–NCMe]•MeCN$ (**6**), $\{[K(DMA)(L^7)Mn^{II}]_2\}_2•3Et_2O$ (**7**), $[K(DMA)(L^8)Mn^{II}–DMA]_n$ (**8a**), $[K(NCMe)(L^8)Mn^{II}–NCMe]$ (**8b**), $[K(L^9)Mn^{II}]_n$ (**9**), $[K_2(THF)_3(L^{10})_2Mn^{II}_2]•2THF$ (**10**), $[K(THF)_3(L^{11})Mn^{II}–THF]•0.75$ Pentane (**11**), $[K(L^{12})Mn^{II}–THF]•THF$ (**12**), $[K(THF)_3][(L^{13})Mn^{II}–THF]$ (**13**) and $[K(L^{15})Mn^{II}]•0.5DMA•0.5$hexane (**15**) (cont.)

Mn(2)–O(3)	2.088(4)	2.045(2)	
Mn(2)–O(4)	2.070(5)		
Mn(2)–O(6)	2.342(5)		
Mn(2)–K(1)	3.4192(18)		
Mn(2)–K(2)	3.8944(19)		

	L^9Mn^{II}	**$L^{10}Mn^{II}$**	**$L^{11}Mn^{II}$**	**$L^{12}Mn^{II}$**	**$L^{13}Mn^{II}$**	**$L^{15}Mn^{II}$**
Mn(1)–N(1)	2.212(4)	2.540(2)	2.359(3)	2.345(2)	2.3356(14)	2.429(4)
Mn(1)–N(2)	2.036(5)	2.101(2)	2.139(3)	2.098(2)	2.1102(14)	2.179(4)
Mn(1)–N(3)	2.085(6)	2.158(2)	2.144(3)	2.122(2)	2.1367(14)	2.158(4)
Mn(1)–N(4)	2.094(5)	2.137(2)	2.125(3)	2.114(2)	2.1024(14)	2.178(4)
Mn(1)–N(5)						
Mn(1)–O(1)				2.273(3)	2.2481(13)	
Mn(1)–O(2)						
Mn(1)–O(3)		2.0902(19)	2.272(3)			
Mn(1)–O(4)						2.446(4)
Mn(1)–O(5)						
Mn(1)–O(6)						2.366(4)

Table S4. Selected Interatomic Distances (Å) for Metal Compounds $(Ph_4P)[(L^1)Mn^{II}–THF]•3THF$ (**Xb**),[5] $[K(THF)_6][(L^2)Mn^{II}–THF]$ (**2**), $[K(THF)_2(L^3)Mn^{II}–THF]$ (**3**), $[K_2(DMA)_3(L^4)_2Mn^{II}_2]$ (**4**), $[K(THF)_4(L^5)Mn^{II}–THF]$ (**5**), $[K(NCMe)][(L^6)Mn^{II}–NCMe]•MeCN$ (**6**), $\{[K(DMA)(L^7)Mn^{II}]_2\}_2•3Et_2O$ (**7**), $[K(DMA)(L^8)Mn^{II}–DMA]_n$ (**8a**), $[K(NCMe)(L^8)Mn^{II}–NCMe]$ (**8b**), $[K(L^9)Mn^{II}]_n$ (**9**), $[K_2(THF)_3(L^{10})_2Mn^{II}_2]•2THF$ (**10**), $[K(THF)_3(L^{11})Mn^{II}–THF]•0.75$ Pentane (**11**), $[K(L^{12})Mn^{II}–THF]•THF$ (**12**), $[K(THF)_3][(L^{13})Mn^{II}–THF]$ (**13**) and $[K(L^{15})Mn^{II}]•0.5DMA•0.5hexane$ (**15**) (cont.)

Mn(1)–K(2)	3.7971(8)
Mn(2)–N(5)	
Mn(2)–N(6)	
Mn(2)–N(7)	
Mn(2)–N(8)	
Mn(2)–O(3)	
Mn(2)–O(4)	
Mn(2)–O(6)	
Mn(2)–K(1)	
Mn(2)–K(2)	

Table S5. Selected Interatomic Distances (Å) for Metal Compounds [K(MeCN)(L^8)Co^{II}–NCMe] (**8d**), [K(DMA)$_3$(L^8)Ni^{II}]$_2$ (**8e**), [K(DMA)(L^{14})Fe^{II}]•DMA (**14b**) and [K(DMA)(L^{14})Co^{II}]•DMA (**14c**)

	L^8Co^{II}–MeCN	**L^8Ni^{II}**	**$L^{14}Fe^{II}$**	**$L^{14}Co^{II}$**
Co(1)–N(1)	2.345(4)			2.222(2)
Co(1)–N(2)	2.060(3)			2.017(2)
Co(1)–N(3)	2.076(3)			2.019(2)
Co(1)–N(4)	2.069(3)			2.030(2)
Co(1)–N(5)	2.055(5)			
Co(1)–O(1)				2.163(2)
Ni(1)–N(1)		2.038(3)		
Ni(1)–N(2)		1.987(3)		
Ni(1)–N(3)		1.972(2)		
Ni(1)–N(4)		1.982(3)		
Fe(1)–N(1)			2.2602(17)	
Fe(1)–N(2)			2.0621(17)	
Fe(1)–N(3)			2.0592(17)	
Fe(1)–N(4)			2.0624(18)	
Fe(1)–O(3)			2.1526(15)	

Table S6. Selected Interatomic Distances (Å) for Ligands $L^{11}H_3$ and $L^{15}H_3$

	$L^{11}H_3$		$L^{15}H_3$
N(1)–C(16)	1.424(4)	N(1)–C(33)	1.434(4)
N(1)–C(1)	1.427(4)	N(1)–C(1)	1.437(4)
N(1)–C(31)	1.446(4)	N(1)–C(7)	1.438(4)
N(2)–C(2)	1.384(4)	N(2)–C(2)	1.404(4)
N(2)–C(7)	1.418(4)	N(2)–C(7)	1.344(5)
N(3)–C(17)	1.406(4)	N(3)–C(18)	1.414(4)
N(3)–C(22)	1.425(4)	N(3)–C(23)	1.355(4)
N(4)–C(32)	1.401(4)	N(4)–C(34)	1.408(4)
N(4)–C(37)	1.425(4)	N(4)–C(39)	1.325(5)

Table S7. Selected Angles (°) for Metal Compounds $(Ph_4P)[(L^1)Mn^{II}–THF]•3THF$ (**Xb**),[5] $[K(THF)_6][(L^2)Mn^{II}–THF]$ (**2**), $[K(THF)_2(L^3)Mn^{II}–THF]$ (**3**), $[K_2(DMA)_3(L^4)_2Mn^{II}_2]$ (**4**), $[K(THF)_4(L^5)Mn^{II}–THF]$ (**5**), $[K(NCMe)][(L^6)Mn^{II}–NCMe]•MeCN$ (**6**), $\{[K(DMA)(L^7)Mn^{II}]_2\}_2•3Et_2O$ (**7**), $[K(DMA)(L^8)Mn^{II}–DMA]_n$ (**8a**), $[K(NCMe)(L^8)Mn^{II}–NCMe]$ (**8b**), $[K(L^9)Mn^{II}]_n$ (**9**), $[K_2(THF)_3(L^{10})_2Mn^{II}_2]•2THF$ (**10**), $[K(THF)_3(L^{11})Mn^{II}–THF]•0.75$ Pentane (**11**), $[K(L^{12})Mn^{II}–THF]•THF$ (**12**), $[K(THF)_3][(L^{13})Mn^{II}–THF]$ (**13**) and $[K(L^{15})Mn^{II}]•0.5DMA•0.5hexane$ (**15**)

	L^1Mn^{II} [5]	**L^2Mn^{II}**	**L^3Mn^{II}**	**L^4Mn^{II}**	**L^5Mn^{II}**	**L^6Mn^{II}**	**L^7Mn^{II}**	**L^8Mn^{II} –DMA**	**L^8Mn^{II} –MeCN**
N(2)–Mn(1)–N(4)	114.68(12)	116.19(8)	106.81(14)		123.70(7)	112.15(7)	113.57(10)	112.36(14)	113.60(12)
N(2)–Mn(1)–N(3)	115.19(11)	114.53(8)	105.05(14)		101.40(6)	110.74(8)	108.36(10)	109.75(13)	109.13(12)
N(4)–Mn(1)–N(3)	114.92(12)	114.07(8)	128.36(13)	100.99(19)	116.40(7)	112.75(7)	105.15(10)	105.35(13)	107.29(11)
N(2)–Mn(1)–N(1)	76.39(10)	76.35(7)	76.64(12)		73.46(6)	73.08(7)	70.22(9)	69.48(13)	71.32(11)
N(4)–Mn(1)–N(1)	77.03(11)	77.18(7)	74.19(12)		75.77(6)	72.89(7)	70.51(8)	70.81(11)	71.42(11)
N(3)–Mn(1)–N(1)	76.91(10)	76.81(8)	75.01(11)		77.60(6)	73.22(7)	69.61(9)	70.47(11)	70.50(11)
N(1)–Mn(1)–N(5)						174.92(7)			178.44(12)
N(2)–Mn(1)–N(5)						110.69(8)			107.14(13)
N(3)–Mn(1)–N(5)						101.99(8)			110.43(13)
N(4)–Mn(1)–N(5)						108.02(8)			109.27(13)
N(1)–Mn(1)–O(1)	173.52(10)	173.97(7)	158.16(12)		154.60(5)				
N(2)–Mn(1)–O(1)	100.23(11)	99.17(7)	125.20(12)		91.46(6)				
N(3)–Mn(1)–O(1)	109.57(11)	101.78(8)	96.55(13)	106.49(18)	126.29(6)				
N(4)–Mn(1)–O(1)	99.73(11)	108.61(7)	97.02(13)	108.66(18)	97.20(6)				
N(3)–Mn(1)–O(2)				57.19(18)					
N(4)–Mn(1)–O(2)				90.45(17)					
N(1)–Mn(1)–O(3)									
N(2)–Mn(1)–O(3)									
N(3)–Mn(1)–O(3)									
N(4)–Mn(1)–O(3)									
N(1)–Mn(1)–O(4)								177.11(13)	

Table S7. Selected Angles (°) for Metal Compounds $(Ph_4P)[(L^1)Mn^{II}–THF]$•3THF (**Xb**),[5] $[K(THF)_6][(L^2)Mn^{II}–THF]$ (**2**), $[K(THF)_2(L^3)Mn^{II}–THF]$ (**3**), $[K_2(DMA)_3(L^4)_2Mn^{II}_2]$ (**4**), $[K(THF)_4(L^5)Mn^{II}–THF]$ (**5**), $[K(NCMe)][(L^6)Mn^{II}–NCMe]$•MeCN (**6**), $\{[K(DMA)(L^7)Mn^{II}]_2\}_2$•$3Et_2O$ (**7**), $[K(DMA)(L^8)Mn^{II}–DMA]_n$ (**8a**), $[K(NCMe)(L^8)Mn^{II}–NCMe]$ (**8b**), $[K(L^9)Mn^{II}]_n$ (**9**), $[K_2(THF)_3(L^{10})_2Mn^{II}_2]$•2THF (**10**), $[K(THF)_3(L^{11})Mn^{II}–THF]$•0.75 Pentane (**11**), $[K(L^{12})Mn^{II}–THF]$•THF (**12**), $[K(THF)_3][(L^{13})Mn^{II}–THF]$ (**13**) and $[K(L^{15})Mn^{II}]$•0.5DMA•0.5hexane (**15**) (cont.)

N(3)–Mn(1)–O(5)	128.13(19)	
N(4)–Mn(1)–O(5)	119.82(18)	
N(1)–Mn(1)–O(6)		178.27(8)
N(2)–Mn(1)–O(6)		109.26(9)
N(3)–Mn(1)–O(6)		112.08(9)
N(4)–Mn(1)–O(6)		108.44(9)
O(1)–Mn(1)–O(2)	157.73(16)	
O(1)–Mn(1)–O(5)	90.25(17)	
O(2)–Mn(1)–O(5)	89.91(17)	
O(6)–Mn(1)–O(4)		
K(1)–Mn(1)–N(1)		
K(1)–Mn(1)–N(2)		
K(1)–Mn(1)–N(3)	152.90(14)	
K(1)–Mn(1)–N(4)	100.69(14)	
K(1)–Mn(1)–O(1)	50.65(12)	
K(1)–Mn(1)–O(2)	138.46(11)	
K(1)–Mn(1)–O(3)		
K(1)–Mn(1)–O(5)	49.85(13)	
K(2)–Mn(1)–N(1)		
K(2)–Mn(1)–N(2)		
K(2)–Mn(1)–N(3)	92.54(14)	

Table S7. Selected Angles (°) for Metal Compounds $(Ph_4P)[(L^1)Mn^{II}–THF]$•3THF (**Xb**),[5] $[K(THF)_6][(L^2)Mn^{II}–THF]$ (**2**), $[K(THF)_2(L^3)Mn^{II}–THF]$ (**3**), $[K_2(DMA)_3(L^4)_2Mn^{II}_2]$ (**4**), $[K(THF)_4(L^5)Mn^{II}–THF]$ (**5**), $[K(NCMe)][(L^6)Mn^{II}–NCMe]$•MeCN (**6**), $\{[K(DMA)(L^7)Mn^{II}]_2\}_2$•3$Et_2O$ (**7**), $[K(DMA)(L^8)Mn^{II}–DMA]_n$ (**8a**), $[K(NCMe)(L^8)Mn^{II}–NCMe]$ (**8b**), $[K(L^9)Mn^{II}]_n$ (**9**), $[K_2(THF)_3(L^{10})_2Mn^{II}_2]$•2THF (**10**), $[K(THF)_3(L^{11})Mn^{II}–THF]$•0.75 Pentane (**11**), $[K(L^{12})Mn^{II}–THF]$•THF (**12**), $[K(THF)_3][(L^{13})Mn^{II}–THF]$ (**13**) and $[K(L^{15})Mn^{II}]$•0.5DMA•0.5hexane (**15**) (cont.)

K(2)–Mn(1)–O(1)	160.12(12)	
K(2)–Mn(1)–O(2)	41.31(11)	
K(2)–Mn(1)–O(3)		
K(2)–Mn(1)–O(5)	82.18(13)	
K(1)–Mn(1)–K(2)	112.23(4)	
N(2)–Mn(2)–N(4)		
N(2)–Mn(2)–N(3)		
N(4)–Mn(2)–N(3)		
N(2)–Mn(1)–N(1)		
N(4)–Mn(2)–N(1)		
N(5)–Mn(2)–N(6)		105.54(10)
N(5)–Mn(2)–N(7)		112.87(10)
N(5)–Mn(2)–N(8)		68.73(9)
N(6)–Mn(2)–N(7)		103.69(10)
N(6)–Mn(2)–N(8)		68.32(9)
N(7)–Mn(2)–N(8)	103.5(2)	68.60(8)
N(5)–Mn(2)–O(3)		106.66(9)
N(6)–Mn(2)–O(3)		113.26(9)
N(8)–Mn(2)–O(3)		175.36(8)
N(3)–Mn(2)–O(8)	132.61(19)	
N(4)–Mn(2)–O(8)	104.4(2)	

Table S7. Selected Angles (°) for Metal Compounds $(Ph_4P)[(L^1)Mn^{II}–THF]•3THF$ (**Xb**),[5] $[K(THF)_6][(L^2)Mn^{II}–THF]$ (**2**), $[K(THF)_2(L^3)Mn^{II}–THF]$ (**3**), $[K_2(DMA)_3(L^4)_2Mn^{II}_2]$ (**4**), $[K(THF)_4(L^5)Mn^{II}–THF]$ (**5**), $[K(NCMe)][(L^6)Mn^{II}–NCMe]•MeCN$ (**6**), $\{[K(DMA)(L^7)Mn^{II}]_2\}_2•3Et_2O$ (**7**), $[K(DMA)(L^8)Mn^{II}–DMA]_n$ (**8a**), $[K(NCMe)(L^8)Mn^{II}–NCMe]$ (**8b**), $[K(L^9)Mn^{II}]_n$ (**9**), $[K_2(THF)_3(L^{10})_2Mn^{II}_2]•2THF$ (**10**), $[K(THF)_3(L^{11})Mn^{II}–THF]•0.75$ Pentane (**11**), $[K(L^{12})Mn^{II}–THF]•THF$ (**12**), $[K(THF)_3][(L^{13})Mn^{II}–THF]$ (**13**) and $[K(L^{15})Mn^{II}]•0.5DMA•0.5$hexane (**15**) (cont.)

N(7)–Mn(2)–O(6)	92.69(19)
N(8)–Mn(2)–O(6)	58.11(18)
O(3)–Mn(2)–O(4)	90.31(18)
O(3)–Mn(2)–O(6)	91.43(16)
O(4)–Mn(2)–O(6)	155.95(17)
K(1)–Mn(2)–N(7)	84.94(15)
K(1)–Mn(2)–N(8)	152.90(16)
K(1)–Mn(2)–O(3)	61.43(13)
K(1)–Mn(2)–O(4)	48.80(13)
K(1)–Mn(2)–O(6)	148.29(11)
K(2)–Mn(2)–N(7)	66.66(15)
K(2)–Mn(2)–N(8)	94.69(16)
K(2)–Mn(2)–O(3)	76.11(13)
K(2)–Mn(2)–O(4)	160.91(13)
K(2)–Mn(2)–O(6)	40.23(11)
K(1)–Mn(2)–K(2)	112.19(4)

Table S7. Selected Angles (°) for Metal Compounds $(Ph_4P)[(L^1)Mn^{II}–THF]•3THF$ (**Xb**),[5] $[K(THF)_6][(L^2)Mn^{II}–THF]$ (**2**), $[K(THF)_2(L^3)Mn^{II}–THF]$ (**3**), $[K_2(DMA)_3(L^4)_2Mn^{II}_2]$ (**4**), $[K(THF)_4(L^5)Mn^{II}–THF]$ (**5**), $[K(NCMe)][(L^6)Mn^{II}–NCMe]•MeCN$ (**6**), $\{[K(DMA)(L^7)Mn^{II}]_2\}_2•3Et_2O$ (**7**), $[K(DMA)(L^8)Mn^{II}–DMA]_n$ (**8a**), $[K(NCMe)(L^8)Mn^{II}–NCMe]$ (**8b**), $[K(L^9)Mn^{II}]_n$ (**9**), $[K_2(THF)_3(L^{10})_2Mn^{II}_2]•2THF$ (**10**), $[K(THF)_3(L^{11})Mn^{II}–THF]•0.75$ Pentane (**11**), $[K(L^{12})Mn^{II}–THF]•THF$ (**12**), $[K(THF)_3][(L^{13})Mn^{II}–THF]$ (**13**) and $[K(L^{15})Mn^{II}]•0.5DMA•0.5$hexane (**15**) (Cont.).

	L^9Mn^{II}	**$L^{10}Mn^{II}$**	**$L^{11}Mn^{II}$**	**$L^{12}Mn^{II}$**	**$L^{13}Mn^{II}$**	**$L^{15}Mn^{II}$**
N(2)–Mn(1)–N(4)	111.0(2)	119.45(9)	112.60(12)	111.20(9)	119.65(6)	111.05(16)
N(2)–Mn(1)–N(3)	121.47(19)	107.22(9)	112.59(12)	122.55(9)	112.44(6)	110.34(16)
N(4)–Mn(1)–N(3)	118.19(19)	101.39(9)	119.40(11)	106.72(9)	111.30(6)	110.45(16)
N(2)–Mn(1)–N(1)	81.07(18)	69.76(8)	77.07(10)	75.81(9)	75.81(5)	71.84(15)
N(4)–Mn(1)–N(1)	78.68(16)	71.39(8)	77.28(11)	75.90(9)	76.54(5)	71.16(15)
N(3)–Mn(1)–N(1)	79.6(2)	70.71(8)	75.80(10)	73.50(8)	76.22(5)	72.10(15)
N(1)–Mn(1)–N(5)						
N(2)–Mn(1)–N(5)						
N(3)–Mn(1)–N(5)						
N(4)–Mn(1)–N(5)						
N(1)–Mn(1)–O(1)				154.90(8)	178.81(5)	
N(2)–Mn(1)–O(1)				97.93(9)	103.02(5)	
N(3)–Mn(1)–O(1)				90.58(8)	104.13(5)	
N(4)–Mn(1)–O(1)				128.19(9)	104.33(5)	
N(3)–Mn(1)–O(2)						
N(4)–Mn(1)–O(2)						
N(1)–Mn(1)–O(3)		177.56(8)	105.12(10)			
N(2)–Mn(1)–O(3)		108.60(8)	99.93(11)			
N(3)–Mn(1)–O(3)		111.66(8)	104.81(11)			
N(4)–Mn(1)–O(3)		108.35(8)	176.71(10)			

Table S7. Selected Angles (°) for Metal Compounds $(Ph_4P)[(L^1)Mn^{II}$–THF]•3THF (**Xb**),[5] $[K(THF)_6][(L^2)Mn^{II}$–THF] (**2**), $[K(THF)_2(L^3)Mn^{II}$–THF] (**3**), $[K_2(DMA)_3(L^4)_2Mn^{II}_2]$ (**4**), $[K(THF)_4(L^5)Mn^{II}$–THF] (**5**), $[K(NCMe)][(L^6)Mn^{II}$–NCMe]•MeCN (**6**), $\{[K(DMA)(L^7)Mn^{II}]_2\}_2$•$3Et_2O$ (**7**), $[K(DMA)(L^8)Mn^{II}$–DMA]$_n$ (**8a**), $[K(NCMe)(L^8)Mn^{II}$–NCMe] (**8b**), $[K(L^9)Mn^{II}]_n$ (**9**), $[K_2(THF)_3(L^{10})_2Mn^{II}_2]$•2THF (**10**), $[K(THF)_3(L^{11})Mn^{II}$–THF]•0.75 Pentane (**11**), $[K(L^{12})Mn^{II}$–THF]•THF (**12**), $[K(THF)_3][(L^{13})Mn^{II}$–THF] (**13**) and $[K(L^{15})Mn^{II}]$•0.5DMA•0.5hexane (**15**) (Cont.).

N(3)–Mn(1)–O(4)			68.31(14)
N(4)–Mn(1)–O(4)			98.12(14)
N(3)–Mn(1)–O(5)			
N(4)–Mn(1)–O(5)			
N(1)–Mn(1)–O(6)			130.75(13)
N(2)–Mn(1)–O(6)			96.38(14)
N(3)–Mn(1)–O(6)			150.35(14)
N(4)–Mn(1)–O(6)			69.31(14)
O(1)–Mn(1)–O(2)			
O(1)–Mn(1)–O(5)			
O(2)–Mn(1)–O(5)			
O(6)–Mn(1)–O(4)			82.24(12)
K(1)–Mn(1)–N(1)	69.01(15)	124.03(5)	
K(1)–Mn(1)–N(2)	148.68(12)	156.22(7)	
K(1)–Mn(1)–N(3)	45.44(12)	96.14(6)	
K(1)–Mn(1)–N(4)	72.75(15)	57.97(6)	
K(1)–Mn(1)–O(1)			
K(1)–Mn(1)–O(2)			
K(1)–Mn(1)–O(3)		56.83(5)	

Table S7. Selected Angles (°) for Metal Compounds $(Ph_4P)[(L^1)Mn^{II}$–THF]•3THF (**Xb**),[5] $[K(THF)_6][(L^2)Mn^{II}$–THF] (**2**), $[K(THF)_2(L^3)Mn^{II}$–THF] (**3**), $[K_2(DMA)_3(L^4)_2Mn^{II}_2]$ (**4**), $[K(THF)_4(L^5)Mn^{II}$–THF] (**5**), $[K(NCMe)][(L^6)Mn^{II}$–NCMe]•MeCN (**6**), $\{[K(DMA)(L^7)Mn^{II}]_2\}_2$•3$Et_2O$ (**7**), $[K(DMA)(L^8)Mn^{II}$–DMA]$_n$ (**8a**), $[K(NCMe)(L^8)Mn^{II}$–NCMe] (**8b**), $[K(L^9)Mn^{II}]_n$ (**9**), $[K_2(THF)_3(L^{10})_2Mn^{II}_2]$•2THF (**10**), $[K(THF)_3(L^{11})Mn^{II}$–THF]•0.75 Pentane (**11**), $[K(L^{12})Mn^{II}$–THF]•THF (**12**), $[K(THF)_3][(L^{13})Mn^{II}$–THF] (**13**) and $[K(L^{15})Mn^{II}]$•0.5DMA•0.5hexane (**15**) (Cont.).

K(2)–Mn(1)–N(2)	80.27(6)
K(2)–Mn(1)–N(3)	49.99(6)
K(2)–Mn(1)–N(4)	150.80(7)
K(2)–Mn(1)–O(1)	
K(2)–Mn(1)–O(2)	
K(2)–Mn(1)–O(3)	82.10(5)
K(2)–Mn(1)–O(5)	
K(1)–Mn(1)–K(2)	112.935(16)
N(2)–Mn(2)–N(4)	
N(2)–Mn(2)–N(3)	
N(4)–Mn(2)–N(3)	
N(2)–Mn(1)–N(1)	
N(4)–Mn(2)–N(1)	
N(5)–Mn(2)–N(6)	
N(5)–Mn(2)–N(7)	
N(5)–Mn(2)–N(8)	
N(6)–Mn(2)–N(7)	
N(6)–Mn(2)–N(8)	
N(7)–Mn(2)–N(8)	

Table S7. Selected Angles (°) for Metal Compounds $(Ph_4P)[(L^1)Mn^{II}$–THF]•3THF (**Xb**),[5] $[K(THF)_6][(L^2)Mn^{II}$–THF] (**2**), $[K(THF)_2(L^3)Mn^{II}$–THF] (**3**), $[K_2(DMA)_3(L^4)_2Mn^{II}_2]$ (**4**), $[K(THF)_4(L^5)Mn^{II}$–THF] (**5**), $[K(NCMe)][(L^6)Mn^{II}$–NCMe]•MeCN (**6**), $\{[K(DMA)(L^7)Mn^{II}]_2\}_2$•3$Et_2O$ (**7**), $[K(DMA)(L^8)Mn^{II}$–DMA]$_n$ (**8a**), $[K(NCMe)(L^8)Mn^{II}$–NCMe] (**8b**), $[K(L^9)Mn^{II}]_n$ (**9**), $[K_2(THF)_3(L^{10})_2Mn^{II}_2]$•2THF (**10**), $[K(THF)_3(L^{11})Mn^{II}$–THF]•0.75 Pentane (**11**), $[K(L^{12})Mn^{II}$–THF]•THF (**12**), $[K(THF)_3][(L^{13})Mn^{II}$–THF] (**13**) and $[K(L^{15})Mn^{II}]$•0.5DMA•0.5hexane (**15**) (Cont.).

N(8)–Mn(2)–O(3)	
N(3)–Mn(2)–O(8)	
N(4)–Mn(2)–O(8)	
N(7)–Mn(2)–O(3)	
N(7)–Mn(2)–O(4)	
N(7)–Mn(2)–O(6)	
N(8)–Mn(2)–O(6)	
O(3)–Mn(2)–O(4)	
O(3)–Mn(2)–O(6)	
O(4)–Mn(2)–O(6)	
K(1)–Mn(2)–N(7)	
K(1)–Mn(2)–N(8)	
K(1)–Mn(2)–O(3)	
K(1)–Mn(2)–O(4)	
K(1)–Mn(2)–O(6)	
K(2)–Mn(2)–N(7)	
K(2)–Mn(2)–N(8)	
K(2)–Mn(2)–O(3)	
K(2)–Mn(2)–O(4)	

Table S8. Selected Angles (°) for Metal Compounds [K(MeCN)(L^8)Co^{II}–NCMe] (**8d**), [K(DMA)$_3$(L^8)Ni^{II}]$_2$ (**8e**), [K(DMA)(L^{14})Fe^{II}]•DMA (**14b**) and [K(DMA)(L^{14})Co^{II}]•DMA (**14c**), and Ligands $L^{11}H_3$ and $L^{15}H_3$

	L^8Co^{II}–MeCN	**$L^{14}Co^{II}$**
N(2)–Co(1)–N(4)	111.52(14)	121.19(10)
N(2)–Co(1)–N(3)	115.40(14)	110.05(10)
N(4)–Co(1)–N(3)	110.05(13)	115.83(10)
N(2)–Co(1)–N(1)	73.53(13)	76.25(10)
N(2)–Co(1)–N(5)	105.44(15)	
N(4)–Co(1)–N(5)	107.45(15)	
N(3)–Co(1)–N(5)	106.45(15)	
N(5)–Co(1)–N(1)	178.96(13)	
N(4)–Co(1)–N(1)	73.18(13)	78.60(10)
N(3)–Co(1)–N(1)	73.98(13)	78.83(9)
N(1)–Co(1)–O(1)		167.36(9)
N(2)–Co(1)–O(1)		91.44(9)
N(3)–Co(1)–O(1)		108.64(9)
N(4)–Co(1)–O(1)		106.06(9)

Table S8. Selected Angles (°) for Metal Compounds [K(MeCN)(L^8)Co^{II}–NCMe] (**8d**), [K(DMA)$_3$(L^8)Ni^{II}]$_2$ (**8e**), [K(DMA)(L^{14})Fe^{II}]•DMA (**14b**) and [K(DMA)(L^{14})Co^{II}]•DMA (**14c**), and Ligands $L^{11}H_3$ and $L^{15}H_3$ (cont.)

	L^8Ni^{II}
N(2)–Ni(1)–N(4)	114.63(10)
N(2)–Ni(1)–N(3)	109.91(11)
N(4)–Ni(1)–N(3)	131.79(9)
N(2)–Ni(1)–N(1)	82.90(8)
N(3)–Ni(1)–N(1)	84.77(8)
N(4)–Ni(1)–N(1)	83.31(9)

	$L^{14}Fe^{II}$
N(2)–Fe(1)–N(1)	75.02(7)
N(2)–Fe(1)–N(4)	106.51(7)
N(2)–Fe(1)–N(3)	122.90(7)
N(4)–Fe(1)–N(1)	77.58(6)
N(4)–Fe(1)–N(3)	115.34(7)
N(3)–Fe(1)–N(1)	77.94(7)
N(1)–Fe(1)–O(3)	164.96(6)
N(2)–Fe(1)–O(3)	90.06(6)
N(3)–Fe(1)–O(3)	109.59(7)
N(3)–Fe(1)–O(3)	109.20(6)

	$L^{11}H_3$
C(16)–N(1)–C(1)	119.1(3)
C(31)–N(1)–C(16)	117.9(2)
C(1)–N(1)–C(31)	118.6(2)
C(7)–N(2)–C(2)	123.5(3)
C(22)–N(3)–C(17)	123.2(3)
C(37)–N(4)–C(32)	122.0(3)

	$L^{15}H_3$
C(33)–N(1)–C(1)	115.4(3)
C(33)–N(1)–C(17)	116.3(3)
C(1)–N(1)–C(17)	115.4(3)
C(7)–N(2)–C(2)	128.2(3)
C(23)–N(3)–C(18)	127.6(3)
C(39)–N(4)–C(34)	129.3(3)

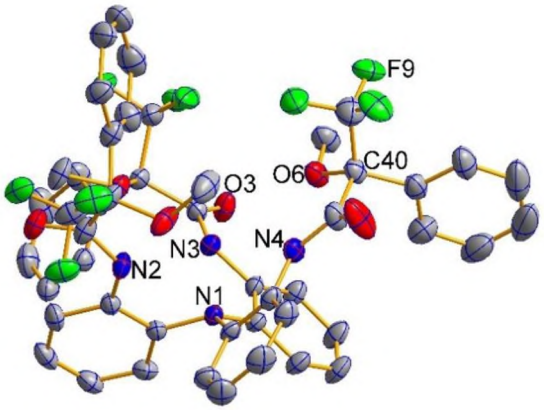

Figure S1. ORTEP Diagram of Ligand $L^{15}H_3$ (drawn with 40% thermal ellipsoids). Selective interatomic distances [Å] and angles [°]:

N(1)–C(1) = 1.437(4), N(1)–C(7) = 1.438(4), N(1)–C(33) = 1.434(4), C(1)–N(1)–C(17) = 115.4(3), C(33)–N(1)–C(17) = 116.3(3), C(1)–N(1)–C(33) = 115.4(3).

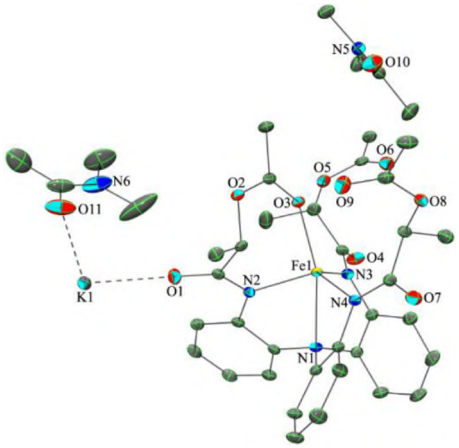

Figure S2. ORTEP Diagram of Compound [K(DMA)(L^{14})Fe^{II}]•DMA (**14b**; drawn with 40% thermal ellipsoids). Selective interatomic distances [Å] and angles [°]:

Fe(1)–N(1) = 2.2602(17), Fe(1)–N(2) = 2.0621(17), Fe(1)–N(3) = 2.0592(17), Fe(1)–N(4) = 2.0624(18), Fe(1)–O(3) = 2.1526(15), N(1)–Fe(1)–N(2) = 75.02(7), N(1)–Fe(1)–N(3) = 77.94(7), N(1)–Fe(1)–N(4) = 75.02(7), N(2)–Fe(1)–N(3) = 122.90(7), N(2)–Fe(1)–N(4) = 106.51(7), N(3)–Fe(1)–N(4) = 115.34(7).

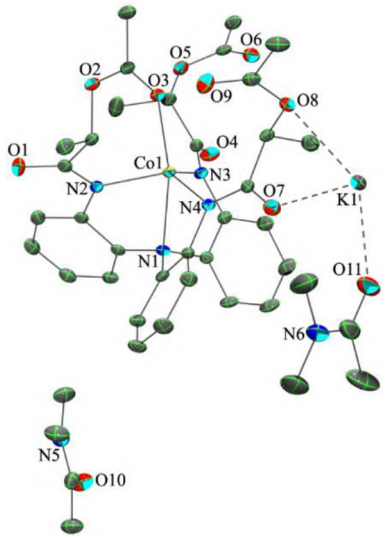

Figure S4. ORTEP Diagram of Compound [K(DMA)(L^{14})Co^{II}]•DMA (**14c**; drawn with 40% thermal ellipsoids). Selective interatomic distances [Å] and angles [°].

Co(1)–N(1) = 2.222(2), Co(1)–N(2) = 2.017(2), Co(1)–N(3) = 2.019(2), Co(1)–N(4) = 2.030(2), Co(1)–O(1) = 2.163(2), N(1)–Co(1)–N(2) = 76.25(10), N(1)–Co(1)–N(3) = 78.83(9), N(1)–Co(1)–N(4) = 78.60(10), N(2)–Co(1)–N(3) = 110.05(10), N(2)–Co(1)–N(4) = 121.19(10), N(3)–Co(1)–N(4) = 115.83(10).

(b) Electrochemistry. Cyclic voltammetry was carried out with an Eco Chemie Autolab PGSTAT100 electrochemical workstation fitted in a Dry Box and controlled with a General Purpose Electrochemical Software (GPES) or with a Bipotentiostat AFCBP1 from Pine Instrument Company fitted in a Dry Box and controlled with the PineChem 2.7.9 software. Experiments were performed using a gold disk working electrode (1.6 mm diameter) and a Ag/Ag^{+} (0.01 M $AgNO_3$ and 0.1 or 0.5 M ($^{n}Bu_4N$)PF_6, in acetonitrile or dimethylformamide) non-aqueous reference electrode (Bioanalytical Systems, Inc.) with a prolonged bridge (0.1 or 0.5 M ($^{n}Bu_4N$)PF_6 in acetonitrile or dimethylformamide). A thin Pt foil or gauge (8 cm^2, Sigma-Aldrich) was

employed as counter electrode. The working electrode was polished using successively 6, 3, 1 μm diamond paste on a DP-Nap polishing cloth (Struers, Westlake, OH), washed with water, acetone and air-dried. The Pt foil and gauge electrodes were cleaned in a H_2O_2/H_2SO_4(conc) solution (1/4 v/v) and oven-dried.

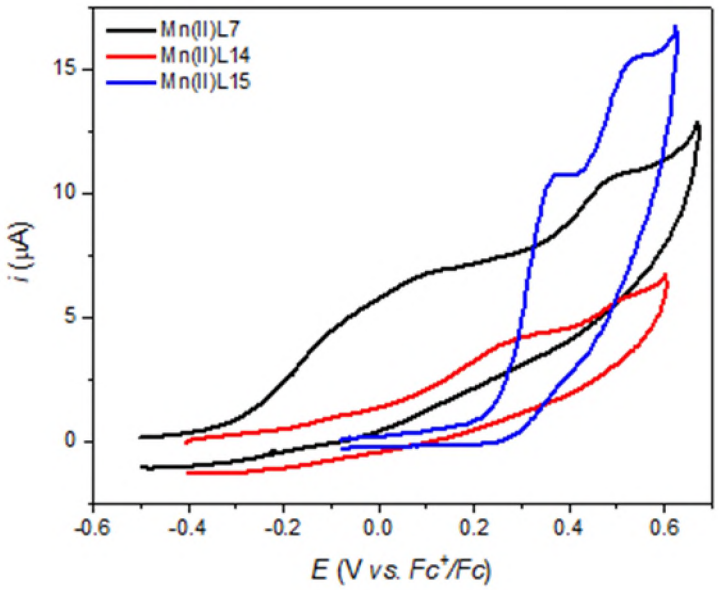

Figure S5**.** Cyclic voltammograms of Mn^{II} compounds bearing acyl-ligands:

CV of compounds shown in Fig 5. $\{[K(DMA)(L^7)Mn^{II}]_2\}_2$•$3Et_2O$ (**7**), $[K(DMA)(L^{14})Mn^{II}]$•DMA (**14a**) and $[K(L^{15})Mn^{II}]$•0.5DMA•0.5hexane (**15**) in DMF/$(^nBu_4N)PF_6$, as indicated, with a Au disk electrode (1.6 mm in diameter); scan rate 0.1 V/s.

The concentrations of the samples were between 1 and 3 mM and that of $(^nBu_4N)PF_6$ (supporting electrolyte) was 0.1 or 0.5 M. The potential sweep rate varied between 10–1000 mV/s. All potentials are reported versus the ferrocenium/ferrocene

(Fc^+/Fc) couple. Electrochemical data are collected in Table 1, and cyclic voltammograms are shown in Figures 7, 8, and S5.

1.3. LIGAND SYNTHESIS

[(2,4,6-Trimethylphenyl)-NH-(2-C_6H_4)]$_3$N **($L^{11}H_3$).** $Pd_2(dba)_3$ (0.0912 g, 0.1 mmol) and BINAP (0.1866 g, 0.3 mmol) were added in a 100 mL Schlenk flask along with toluene (10.0 mL), and the mixture was stirred for 15 minutes. To the cherry-red solution was added (2-NH_2-C_6H_4)$_3$N (0.580 g, 2.0 mmol), sodium *tert*-butoxide (1.96 g, 20.0 mmol), and 2-bromomesitylene (3.6 g, 18.0 mmol) and the reaction mixture was refluxed for 72 hours. The solution was then filtered to remove solids, and the solvent was evaporated (rotary evaporator) to afford a dark brown solid that was purified by column (silica) chromatography with petroleum ether /ethyl acetate (50:1 v/v). The product can be further recrystallized from THF and petroleum ether to afford colorless crystals of the compound (0.65 g, 50%). Crystals suitable for x-ray crystallography can be grown by slow diffusion of pentane into concentrated THF solutions of the product. ^{1}H NMR ($CDCl_3$, 7.26 ppm): δ 7.18 (d, 3H, aryl), 6.92 (t, 3H, aryl), 6.76 (d, 6H, aryl), 6.70 (t, 3H, aryl), 6.14 (d, 3H, aryl), 5.54 (s, 3H, N*H*), 2.22 (s, 9H), 1.79 (s, 9H), 1.45 (s, 9H). ^{13}C NMR ($CDCl_3$, 77.16 ppm): δ 141.3, 135.9, 135.6, 135.2, 135.0, 132.0, 129.2, 129.0, 126.0, 118.0, 112.4, 21.0, 17.8, 17.2. IR (KBr, cm^{-1}): 3362, 3333, 2907, 2844, 1495, 1479, 1450, 1310, 1266, 1232, 1153, 1105, 1033, 852, 751, 741, 737, 716, 617, 595, 555, 418. MS-FAB (*m/z*): calcd. 644.90; found 644.89. Elemental analysis: Calcd. for $C_{45}H_{48}N_4$: C, 83.81; H, 7.50; N, 8.69. Found C, 83.74; H, 7.48; N, 8.75.

[(3,5-Dimethylphenyl)-NH-(2-C_6H_4)]$_3$N **($L^{12}H_3$).** $Pd_2(dba)_3$ (0.0456 g, 0.05 mmol) and BINAP (0.0933 g, 0.15 mmol) were added in a 100 mL Schlenk flask,

followed by toluene (10.0 mL), and the mixture was stirred for 15 minutes. To the cherry-red solution was added (2-NH_2-C_6H_4)$_3$N (0.580 g, 2.0 mmol), sodium tert-butoxide (1.44 g, 15.0 mmol), and 3,5-dimethylbromobenzene (1.110 g, 6.0 mmol) and the reaction mixture was refluxed for 24 hours. The solution was separated from solids by filtration, and the solvent was evaporated (rotary evaporator) to afford a dark brown solid that was purified by column (silica) chromatography with petroleum ether/ethyl acetate (50:1 v/v). Solvent evaporation affords colorless $L^{12}H_3$ (0.73 g, 61%). ^{1}H NMR ($CDCl_3$, 7.26 ppm): δ 7.34 (d, 3H, J = 7.6 Hz, aryl), 7.11-7.06 (m, 6H, aryl), 6.87 (t, 3H, J = 7.6 Hz, aryl), 6.49 (s, 3H, aryl), 6.34 (s, 6H, aryl), 5.63 (s, 3H, N*H*), 2.11 (s, 18H, Me). ^{13}C NMR ($CDCl_3$, 77.16 ppm): δ 142.9, 139.2, 139.0, 136.2, 126.7, 126.3, 123.5, 121.6, 118.7, 116.8, 21.8. IR (KBr, cm^{-1}): 3354, 3024, 2915, 2361, 2336, 1607, 1584, 1520, 1481, 1333, 1269, 1167, 1039, 827, 747, 667. MS-FAB (*m*/*z*): calcd. 602.82; found 602.83. Elemental analysis: Calcd. for $C_{42}H_{42}N_4$: C, 83.68; H, 7.02; N, 9.29. Found C, 83.72; H, 7.05; N, 9.34.

[(*S*)-(-)-$CH_3COOCH(CH_3)$-CONH-(2-C_6H_4)]$_3$N **($L^{14}H_3$).** To a stirred solution of (2-NH_2-C_6H_4)$_3$N (1.16 g, 4.0 mmol) and triethylamine (1.70 mL, 12.0 mmol) in dichloromethane (50 mL) was slowly added (*S*)-(-)-acetoxypropionyl chloride (1.50 mL, 12.0 mmol) at 0 °C by means of a syringe, and the mixture was allowed to warm up to room temperature and then stirred overnight. The solvent was removed under reduced pressure and the crude residue was purified by column chromatography with petroleum ether/ethyl acetate (5:1) to give the product as a yellow solid (2.15 g, 85 %). ^{1}H NMR ($CDCl_3$, 7.26 ppm): δ 8.38 (s, 3H, NH), 7.65 (m, 3H, aryl), 7.16-7.07 (m, 6H, aryl), 6.82 (m, 3H, aryl), 5.00 (q, 1.65/3H, J = 6.7 Hz, C*H*), 4.87 (q, 1.35/3H, J = 6.8 Hz, C*H*), 2.07

(s, 4.95/9H, OCH_3), 1.99 (s, 4.05/9H, OCH_3), 1.11 (d, 9H, J = 6.8 Hz, CH_3). ^{13}C NMR ($CDCl_3$, 77.16 ppm): δ 169.2, 168.8, 138.5, 129.9, 127.2, 126.6, 125.2, 124.4, 70.4, 70.3, 21.2, 17.7, 17.3. IR (KBr, cm^{-1}): 3256, 2988, 2361, 2336, 1748, 1695, 1596, 1539, 1447, 1371, 1229, 1091, 1043, 916, 756, 667. MS-FAB (*m*/*z*): calcd. 632.67; found 632.66. Elemental analysis: Calcd. for $C_{33}H_{36}N_4O_9$: C, 62.65; H, 5.74; N, 8.86. Found C, 62.54; H, 5.69; N, 8.74.

[PhC(CF_3)(OCH_3)-CONH-(2-C_6H_4)]$_3$N **($L^{15}H_3$).** To a stirred solution of (2-NH_2-C_6H_4)$_3$N (0.29 g, 1.0 mmol) and triethylamine (0.42 mL, 3.0 mmol) in dichloromethane (30 mL) was slowly added α-methoxy-α-trifluoromethylphenylacetyl chloride (0.57 mL, 3.0 mmol) at 0 °C by means of a syringe, and the mixture was allowed to warm up to room temperature and then stirred overnight. The solvent was removed under reduced pressure and the crude residue was purified by column chromatography with petroleum ether/ethyl acetate (5:1) to give the product as a grayish solid (0.61 g, 69 %). The compound can be crystalized from layering hexane over a concentrated solution of the compound in chloroform. ^{1}H NMR ($CDCl_3$, 7.26 ppm): δ 9.17 (s, 1H, NH), 9.16 (s, 1H, NH), 9.06 (s, 1H, NH), 8.64 (d, 2H, J = 7.9 Hz, aryl), 8.58 (d, 1H, J = 8.2 Hz, aryl), 7.54 (m, 2H, Ph), 7.43 (m, 4H, Ph), 7.33-7.23 (m, 6H, Ph), 7.20-7.13 (m, 3H, Ph), 6.96-6.89 (m, 3H, aryl), 6.86 (m, 6H, aryl), 7.16-7.07 (m, 6H, aryl), 6.82 (m, 3H, aryl), 3.12 (s, 3H, OCH_3), 3.09 (s, 3H, OCH_3), 2.69 (s, 3H, OCH_3). ^{13}C NMR ($CDCl_3$, 77.16 ppm): δ 164.55, 164.40, 164.34, 135.47, 135.30, 134.68, 131.77, 131.61, 131.57, 131.44, 131.32, 131.20, 129.75, 129.57, 129.54, 129.03, 128.93, 128.88, 128.83, 128.79, 127.68, 127.61, 127.56, 127.20, 126.93, 126.86, 126.65, 126.12, 126.02, 125.59, 125.53, 125.47, 125.13, 124.85, 124.75, 122.04, 121.90, 121.62, 84.27 (q, $^2J_{C\text{-}F}$ = 26.0 Hz, *C*-CF_3), 84.22 (q, $^2J_{C\text{-}F}$

= 25.7 Hz, *C*-CF_3), 84.18 (q, $^2J_{C\text{-}F}$ = 25.7 Hz, *C*-CF_3), 55.06, 54.87, 54.55. ^{19}F ($CFCl_3$, 0.00 ppm): δ -68.49, -68.60, -68.65. IR (KBr, cm^{-1}): 3853, 3431, 2924, 2852, 2631, 2337, 1844, 1750, 1653, 1554, 1457, 1419, 1261, 1156, 1100, 802, 668, 459, 415. MS-FAB (*m/z*): calcd. 881.85; found 881.86. Elemental analysis: Calcd. for $C_{48}H_{39}N_4O_6F_6$: C, 65.38; H, 4.46; N, 6.35. Found C, 65.44; H, 4.49; N, 6.40.33)–N(1)–C(17) = 116.3 (3), C(1)–N(1)–C(33) = 115.4(3).

1.4. SYNTHESIS OF Mn^{II} COMPLEXES

[K(THF)$_6$][(L^2)Mn^{II}-THF] **(2).** The ligand L^2H_3 (0.428 g, 0.5 mmol) was dissolved in degassed THF (15.0 mL), and KH (0.060 g, 1.5 mmol) was added to this solution. The mixture was allowed to stir overnight, followed by addition of anhydrous $MnCl_2$ (0.063 g, 0.5 mmol). This mixture was stirred for an additional 24 hours to afford a green-brown solution. The solution was refrigerated (–30 °C) overnight and the insoluble salts were filtered off on an anaerobic frit. The filtrate was reduced to 2.0 mL by evaporation, and was allowed to stand at –30 °C to afford light brown crystalline material, suitable for X-ray diffraction analysis (0.372 g, 51%). IR (KBr, cm^{-1}): 3389, 3047, 2953, 2895, 2858, 1580, 1474, 1440, 1426, 1388, 1358, 1327, 1308, 1244, 1200, 1153, 1124, 1107, 1043, 994, 972, 901, 847, 742, 707, 622. UV–vis (THF, nm): λ_{max} (ε (M^{-1} cm^{-1})) 298 (36000). Elem. Anal. calcd. for $C_{88}H_{131}N_4O_7MnK$: C, 72.83; H, 9.10; N, 3.86. Found C, 72.77; H, 9.06; N, 3.81.

[K(THF)$_2$(L^3)Mn^{II}-THF] **(3).** The ligand L^3H_3 (0.463 g, 0.5 mmol) was dissolved in degassed THF (15.0 mL), and KH (0.060 g, 1.5 mmol) was added to this solution. The mixture was allowed to stir overnight, followed by addition of anhydrous $MnCl_2$ (0.063

g, 0.5 mmol). This mixture was stirred for an additional 24 hours to afford a yellow solution. The solution was refrigerated (–30 °C) overnight and the insoluble salts were filtered off on an anaerobic frit. The filtrate was evaporated to dryness, and the residue was extracted with hexane (3 × 10 mL) and filtered. The filtrate was reduced to 10 mL and was allowed to stand at –30 °C to afford pale yellow crystalline material, suitable for X-ray diffraction analysis (0.399 g, 65%). IR (KBr, cm^{-1}): 3055, 2965, 2915, 2850, 1617, 1581, 1479, 1379, 1274, 1175, 1126, 1045, 995, 960, 754, 699, 681. UV–vis (THF

$[K_2(DMA)_3(L^4)_2Mn^{II}_2]$ **(4).** The ligand L^4H_3 (0.271 g, 0.5 mmol) was dissolved in degassed DMA (5.0 mL), and KH (0.060 g, 1.5 mmol) was added to this solution. The mixture was allowed to stir overnight, followed by addition of anhydrous $MnCl_2$ (0.063 g, 0.5 mmol). This mixture was stirred for an additional 24 hours to afford a light yellow-brown solution. The solution was refrigerated (–30 °C) overnight and the insoluble salts were filtered off on an anaerobic frit. Diethyl ether (30.0 mL) was carefully layered over the DMA solution, and the system is allowed to slowly mix at room temperature to afford pale yellow crystalline material, suitable for X-ray diffraction analysis (0.261 g, 68%). IR (KBr, cm^{-1}): 3045, 2944, 2913, 2859, 1636, 1556, 1520, 1513, 1473, 1442, 1412, 1396, 1349, 1318, 1270, 1213, 1172, 1104, 1095, 1034, 1014, 959, 942, 931, 897, 753, 652, 623, 591, 503. UV–vis (DMA, nm): λ_{max} (ε (M^{-1} cm^{-1})) 319 (45600). Elem. Anal. calcd. for $C_{78}H_{105}N_{11}O_9Mn_2K_2$: C, 61.26; H, 6.93; N, 10.08. Found C, 61.34; H, 6.96; N, 10.13.

$[K(THF)_4(L^5)Mn^{II}–THF]$ **(5).** The ligand L^5H_3 (0.363 g, 0.5 mmol) was dissolved in degassed THF (15.0 mL), and KH (0.060 g, 1.5 mmol) was added to this solution. The mixture was allowed to stir overnight, followed by addition of anhydrous $MnCl_2$ (0.063 g, 0.5 mmol). This mixture was stirred for an additional 24 hours to afford a green-brown

solution. The solution was refrigerated (–30 °C) overnight and the insoluble salts were filtered off on an anaerobic frit. The filtrate was reduced to 3.0 mL by evaporation, and pentane was carefully layered over the THF solution. The mixture was allowed to stand at room temperature to afford light green crystalline material, suitable for X-ray diffraction analysis (0.352 g, 60%). IR (KBr, cm^{-1}): 3386, 3090, 3049, 2964, 2867, 1567, 1526, 1469, 1438, 1320, 1224, 1154, 1100, 1047, 977, 955, 862, 833, 794, 750, 619, 587, 572, 544, 489. UV–vis (THF, nm): λ_{max} (ε (M^{-1} cm^{-1})) 314 (28000), 394 (sh). Elem. Anal. calcd. for $C_{56}H_{61}N_4Cl_6O_5MnK$: C, 57.13; H, 5.23; N, 4.76. Found C, 57.27; H, 5.18; N, 4.82.

[K(NCMe)][(L^6)Mn^{II}–NCMe]•MeCN **(6).** The ligand L^6H_3 (0.301 g, 0.5 mmol) was dissolved in degassed THF (15.0 mL), and KH (0.060 g, 1.5 mmol) was added to this solution. The mixture was allowed to stir overnight, followed by addition of anhydrous $MnCl_2$ (0.063 g, 0.5 mmol). This mixture was stirred for an additional 24 hours to afford a pale yellow solution. The solution was refrigerated (–30 °C) overnight and the insoluble salts were filtered off on an anaerobic frit. The filtrate was evaporated to dryness, and the residue was dissolved in acetonitrile (10.0 mL). This solution was reduced to approximately 5.0 mL by evaporation, and was refrigerated (–30 °C) to afford pale yellow crystalline material, suitable for X-ray diffraction analysis (0.278 g, 68%). IR (KBr, cm^{-1}): 3046, 2964, 2865, 1579, 1518, 1478, 1438, 1407, 1255, 1169, 1155, 1132, 1090, 1043, 1024, 927, 897, 795, 751, 698, 629. UV–vis (MeCN, nm): λ_{max} (ε (M^{-1} cm^{-1})) 256 (30000), 290 (sh). Elem. Anal. calcd. for $C_{45}H_{36}N_7O_3MnK$: C, 66.15; H, 4.44; N, 12.01. Found C, 66.31; H, 4.46; N, 11.89.

$\{[K(DMA)(L^7)Mn^{II}]_2\}_2 \cdot 3Et_2O$ **(7).** The ligand L^7H_3 (0.250 g, 0.5 mmol) was dissolved in degassed DMA (5.0 mL), and KH (0.060 g, 1.5 mmol) was added to this solution. The mixture was allowed to stir overnight, followed by addition of anhydrous $MnCl_2$ (0.063 g, 0.5 mmol). This mixture was stirred for an additional 24 hours to afford a light yellow-brown solution. The solution was refrigerated (–30 °C) overnight and the insoluble salts were filtered off on an anaerobic frit. Diethyl ether (30.0 mL) was carefully layered over the DMA solution, and the system is allowed to slowly mix at –30 °C to afford pale yellow crystalline material, suitable for X-ray diffraction analysis (0.270 g, 80%). IR (KBr, cm^{-1}): 3853, 3801, 3744, 3628, 2966, 2867, 1652, 1623, 1540, 1513, 1486, 1446, 1396, 1311, 1279, 1250, 1091, 1037, 942, 889, 747, 621, 592, 473. UV–vis (DMA, nm): λ_{max} (ε (M^{-1} cm^{-1}) 290 (12600). Elem. Anal. calcd. for $C_{34}H_{42}N_5O_4MnK$ (7 – ether): C, 60.16; H, 6.24; N, 10.32. Found C, 60.24; H, 6.29; N, 10.33.

$[K(DMA)][(L^8)Mn^{II}–DMA]$**(8a).** The ligand L^8H_3 (0.289 g, 0.5 mmol) was dissolved in degassed DMA (5.0 mL), and KH (0.060 g, 1.5 mmol) was added to this solution. The mixture was allowed to stir overnight, followed by addition of anhydrous $MnCl_2$ (0.063 g, 0.5 mmol). This mixture was stirred for an additional 24 hours to afford a light yellow solution. The solution was refrigerated (–30 °C) overnight and the insoluble salts were filtered off on an anaerobic frit. Diethyl ether (30.0 mL) was carefully layered over the DMA solution, and the system is allowed to slowly mix at room temperature to afford pale yellow crystalline material, suitable for X-ray diffraction analysis (0.262 g, 62%). IR (KBr, cm^{-1}): 3432, 2964, 2361, 1634, 1588, 1483, 1262, 1248, 1164, 1130, 1035, 929, 800, 775, 562. UV–vis (DMA, nm): λ_{max} (ε (M^{-1} cm^{-1}))

300 (38000). Elem. Anal. calcd. for $C_{32}H_{30}N_6F_9O_5MnK$: C, 45.54; H, 3.59; N, 9.96. Found C, 45.54; H, 3.52; N, 9.89.

[K(MeCN)(L^8)Mn^{II}–NCMe] **(8b).** The ligand L^8H_3 (0.289 g, 0.5 mmol) was dissolved in degassed THF (15.0 mL), and KH (0.060 g, 1.5 mmol) was added to this solution. The mixture was allowed to stir overnight, followed by addition of anhydrous $MnCl_2$ (0.063 g, 0.5 mmol). This mixture was stirred for an additional 12 hours to afford an almost colorless solution. The solution was refrigerated (–30 °C) overnight and the insoluble salts were filtered off on an anaerobic frit. The filtrate was evaporated to dryness, the residue was dissolved in acetonitrile (3.0 mL) and the mixture was allowed to stand at –30 °C to afford light pink crystalline material, suitable for X-ray diffraction analysis (0.174 g, 46%). IR (KBr, cm^{-1}): 3256, 3047, 3019, 2929, 2548, 1620, 1510, 1478, 1446, 1407, 1251, 1163, 1127, 1037, 1014, 941, 928, 921, 773, 764, 756, 745, 725, 624, 598, 561, 548, 476. UV–vis (MeCN, nm): λ_{max} (ε (M^{-1} cm^{-1})) 246 (20000), 288 (13000). Elem. Anal. calcd. for $C_{28}H_{18}N_6F_9O_3MnK$: C, 44.75; H, 2.41; N, 11.18. Found C, 44.61; H, 2.43; N, 11.25.

An identical procedure is followed for the synthesis of off-white [K(MeCN)(L^8)Fe^{II}–NCMe] (**8c**, previously reported)[2] and violet [K(MeCN)(L^8)Co^{II}–NCMe] (**8d**), by employing anhydrous $FeCl_2$ and $CoCl_2$, respectively. The corresponding nickel complex $[K(DMA)_3(L^8)Ni(II)]_2$ (**8e**) has been isolated as orange-red crystals from DMA/diethyl ether solutions, by following the procedure detailed for **8a**.

[K(MeCN)(L^8)Co^{II}–NCMe] **(8d).** Yield: 0.238 g, 63%. IR (KBr, cm^{-1}): 3433, 2918, 1631, 1482, 1451, 1251, 1133, 1034, 948. UV–vis (MeCN, nm): λ_{max} (ε (M^{-1} cm^{-}

^{1})) 284 (14700). Elem. Anal. calcd. for $C_{28}H_{18}N_6F_9O_3CoK$: C, 44.51; H, 2.40; N, 11.12. Found C, 44.57; H, 2.42; N, 11.19.

$[K(DMA)_3(L^8)Ni^{II}]_2$ **(8e).** Yield: 0.292 g, 62%. IR (KBr, cm^{-1}): 3444, 2929, 1711, 1547, 1485, 1454, 1255, 1160, 1018, 941, 802, 757, 722. UV–vis (DMA, nm): λ_{max} (ε (M^{-1} cm^{-1})) 290 (22100). Elem. Anal. calcd. for $C_{72}H_{78}N_{14}F_{18}O_{12}Ni_2K_2$: C, 46.27; H, 4.21; N, 10.49. Found C, 46.31; H, 4.19; N, 10.53.

$[K(L^9)Mn^{II}]_n$ **(9).** The ligand L^9H_3 (0.208 g, 0.5 mmol) was dissolved in degassed THF (15.0 mL), and KH (0.060 g, 1.5 mmol) was added to this solution. The mixture was allowed to stir overnight, followed by addition of anhydrous $MnCl_2$ (0.063 g, 0.5 mmol). This mixture was stirred for an additional 12 hours to afford a yellow-brown solution. The solution was refrigerated (–30 °C) overnight and the insoluble salts were filtered off on an anaerobic frit. The filtrate was reduced to 5.0 mL by evaporation, and pentane was layered over the THF solution. The mixture was allowed to stand at –30 °C to afford light yellow crystalline material. Crystals suitable for X-ray diffraction analysis can be obtained by diffusion of pentane into a concentrated THF solution of the compound (0.155 g, 61%). IR (KBr, cm^{-1}): 3387, 3058, 3035, 2955, 2858, 1581, 1504, 1465, 1440, 1379, 1361, 1316, 1259, 1171, 1043, 980, 892, 816, 741, 625. UV–vis (THF, nm): λ_{max} (ε (M^{-1} cm^{-1})) 310 (43000). Elem. Anal. calcd. for $C_{27}H_{33}N_4MnK$: C, 63.87; H, 6.56; N, 11.04. Found C, 63.74; H, 6.59; N, 10.98.

$[K_2(THF)_3(L^{10})_2Mn^{II}_2]$•2THF **(10).** The ligand $L^{10}H_3$ (0.295 g, 0.5 mmol) was dissolved in degassed THF (15.0 mL), and KH (0.060 g, 1.5 mmol) was added to this solution. The mixture was allowed to stir overnight, followed by addition of anhydrous $MnCl_2$ (0.063 g, 0.5 mmol). This mixture was stirred for an additional 24 hours to afford

a yellow-brown solution. The solution was refrigerated (–30 °C) overnight and the insoluble salts were filtered off on an anaerobic frit. The filtrate was reduced to 5 mL, and pentane (10 mL) was layered over the THF solution. The mixture was allowed to stand at –30 °C to afford light yellow crystalline material, suitable for X-ray diffraction analysis (0.250 g, 58%). IR (KBr, cm^{-1}): 3050, 2965, 2918, 2874, 1612, 1578, 1535, 1480, 1445, 1384, 1361, 1279, 1251, 1166, 1111, 1041, 1019, 829, 795, 772, 747, 655, 620. UV–vis (THF, nm): λ_{max} (ε (M^{-1} cm^{-1})) 290 (17000). Elem. Anal. calcd. for $C_{86}H_{118}N_8O_{17}Mn_2K_2$: C, 59.92; H, 6.90; N, 6.50. Found C, 59.82; H, 6.86; N, 6.58.

[$K(THF)_3(L^{11})Mn^{II}$–THF]•0.75 Pentane **(11).** The ligand $L^{11}H_3$ (0.322 g, 0.5 mmol) was dissolved in degassed THF (15.0 mL), and KH (0.060 g, 1.5 mmol) was added to this solution. The mixture was allowed to stir overnight, followed by addition of anhydrous $MnCl_2$ (0.063 g, 0.5 mmol). This mixture was stirred for an additional 24 hours to afford a dark brown solution. The solution was refrigerated (–30 °C) overnight and the insoluble salts were filtered off on an anaerobic frit. The filtrate was reduced to approximately 3 mL by evaporation and layered with pentane (10 mL) to afford pale yellow crystalline material upon standing at –30 °C. Crystals suitable for X-ray diffraction analysis can be obtained by slow diffusion of pentane into concentrated THF solutions of the compound at room temperature (0.343 g, 67%). IR (KBr, cm^{-1}): 3371, 2965, 2906, 2850, 1579, 1475, 1437, 1318, 1262, 1210, 1149, 1036, 857, 736, 698, 616, 580, 557. UV–vis (THF, nm): λ_{max} (ε (M^{-1} cm^{-1})) 310 (6100). Elem. Anal. calcd. for $C_{61}H_{77}N_4O_4MnK$ (**11** – pentane): C, 71.53; H, 7.58; N, 5.47. Found C, 71.68; H, 7.53; N, 5.39.

[K(L^{12})Mn^{II}–THF]•THF **(12).** The ligand $L^{12}H_3$ (0.301 g, 0.5 mmol) was dissolved in degassed THF (15.0 mL), and KH (0.060 g, 1.5 mmol) was added to this solution. The mixture was allowed to stir overnight, followed by addition of anhydrous $MnCl_2$ (0.063 g, 0.5 mmol). This mixture was stirred for an additional 24 hours to afford a brown solution. The solution was refrigerated (–30 °C) overnight and the insoluble salts were filtered off on an anaerobic frit. The filtrate was reduced to approximately 3 mL by evaporation and layered with pentane (10 mL) to afford pale yellow crystalline material upon standing at –30 °C. Crystals suitable for X-ray diffraction analysis can be obtained by slow diffusion of pentane into concentrated THF solutions of the compound at room temperature (0.243 g, 58%). IR (KBr, cm^{-1}): 3372, 3000, 2907, 2853, 1583, 1474, 1328, 1255, 1156, 1105, 1039, 837, 807, 745, 686, 676, 621, 569. UV–vis (THF, nm): λ_{max} (ε (M^{-1} cm^{-1})) 282 (13600). Elem. Anal. calcd. for $C_{58}H_{71}N_4O_4MnK$: C, 71.66; H, 6.61; N, 6.69. Found C, 71.77; H, 6.69; N, 6.62.

[K$(THF)_3$(L^{13})Mn^{II}–THF] **(13).** The ligand $L^{13}H_3$ (0.301 g, 0.5 mmol) was dissolved in degassed THF (15.0 mL), and KH (0.060 g, 1.5 mmol) was added to this solution. The mixture was allowed to stir overnight, followed by addition of anhydrous $MnCl_2$ (0.063 g, 0.5 mmol). This mixture was stirred for an additional 24 hours to afford a brown solution. The solution was refrigerated (–30 °C) overnight and the insoluble salts were filtered off on an anaerobic frit. The filtrate was reduced to approximately 3 mL by evaporation and layered with pentane (10 mL) to afford yellow crystalline material upon standing at –30 °C. Crystals suitable for X-ray diffraction analysis can be obtained by slow diffusion of pentane into concentrated THF solutions of the compound at room temperature (0.280 g, 57%). IR (KBr, cm^{-1}): 3369, 3247, 3039, 2966, 2936, 2906, 2863,

1576, 1473, 1438, 1414, 1317, 1259, 1204, 1149, 1091, 1043, 910, 848, 764, 734, 621. UV–vis (THF, nm): λ_{max} (ε (M^{-1} cm^{-1})) 316 (14000), 364 (11000). Elem. Anal. calcd. for $C_{58}H_{71}N_4O_4MnK$: C, 70.91; H, 7.29; N, 5.71. Found C, 70.98; H, 7.33; N, 5.64.

[K(DMA)(L^{14})Mn^{II}]•DMA **(14a).** The ligand $L^{14}H_3$ (0.316 g, 0.5 mmol) was dissolved in degassed DMA (5.0 mL), and KH (0.060 g, 1.5 mmol) was added to this solution. The mixture was allowed to stir overnight, followed by addition of anhydrous $MnCl_2$ (0.063 g, 0.5 mmol). This mixture was stirred for an additional 24 hours to afford a light yellow-brown solution. The solution was refrigerated (–30 °C) overnight and the insoluble salts were filtered off on an anaerobic frit. Diethyl ether (20.0 mL) was carefully layered over the DMA solution, and pentane (10.0 mL) was layered over ether, and the system was allowed to slowly mix at room temperature to afford off-white amorphous material, not suitable for X-ray diffraction analysis (0.290 g, 65%). IR (KBr, cm^{-1}): 3384, 2360, 2335, 1748, 1684, 1652, 1558, 1540, 1447, 1235, 1090, 1041, 927, 763, 667. UV–vis (DMA, nm): λ_{max} (ε (M^{-1} cm^{-1}) 295 (36000). Elem. Anal. calcd. for $C_{41}H_{51}N_6O_{11}MnK$: C, 54.84; H, 5.72; N, 9.36. Found C, 54.99; H, 5.66; N, 9.42.The corresponding [K(DMA)(L^{14})M^{II}]•DMA complexes (M = Fe (**14b**), Co(**14c**)) were prepared according to the same methodology, and afforded yellow-brown (Fe) and violet (Co) crystalline materials, both suitable for X-ray analysis.

[K(DMA)(L^{14})Fe^{II}]•DMA **(14b).** (0.270 g, 60%). IR (KBr, cm^{-1}): 3446, 2361, 2336, 1733, 1717, 1615, 1576, 1559, 1480, 1448, 1259, 1081, 1037, 41, 763, 667. UV–vis (DMA, nm): λ_{max} (ε (M^{-1} cm^{-1}) 290 (23500). Elem. Anal. calcd. for $C_{41}H_{51}N_6O_{11}FeK$: C, 54.79; H, 5.72; N, 9.35. Found C, 54.86; H, 5.68; N, 9.39.

[K(DMA)(L^{14})Co^{II}]•DMA **(14c).** (0.285 g, 65%). IR (KBr, cm^{-1}): 3435, 2963, 2919, 1740, 1637, 1480, 1448, 1399, 1262, 1083, 1034, 801, 762, 640. UV–vis (DMA, nm): λ_{max} (ε (M^{-1} cm^{-1}) 285 (15500). Elem. Anal. calcd. for $C_{41}H_{51}N_6O_{11}CoK$: C, 54.60; H, 5.70; N, 9.32. Found C, 54.64; H, 5.71; N, 9.36.

[K(L^{15})Mn^{II}]•0.5DMA•0.5Hexane **(15).** The ligand $L^{15}H_3$ (0.235 g, 0.5 mmol) was dissolved in degassed DMA (5.0 mL), and KH (0.060 g, 1.5 mmol) was added to this solution. The mixture was allowed to stir overnight, followed by addition of anhydrous $MnCl_2$ (0.063 g, 0.5 mmol). This mixture was stirred for an additional 24 hours to afford a yellow-brown solution. The solution was refrigerated (–30 °C) overnight and the insoluble salts were filtered off on an anaerobic frit. Diethyl ether (20.0 mL) was carefully layered over the DMA solution, and hexane (10.0 mL) was layered over ether, and the system was allowed to slowly mix at room temperature to afford yellowish crystalline material suitable for X-ray diffraction analysis (0.270 g, 62%). IR (KBr, cm^{-1}): 3368, 3058, 2954, 1612, 1572, 1499, 1483, 1370, 1154, 1068, 918, 753, 641. UV–vis (DMA, nm): λ_{max} (ε (M^{-1} cm^{-1}) 305 (27500). Elem. Anal. calcd. for $C_{53}H_{47.5}N_{4.5}F_9O_{6.5}MnK$: C, 57.02; H, 4.29; N, 5.65. Found C, 56.89; H, 4.23; N, 5.73.

1.5. CATALYTIC AND MECHANISTIC STUDIES

General Catalytic Olefin Aziridination Procedure**.** In a typical experiment, a 20 mL screw-cap vial containing a small magnetic bar was charged in sequence with the catalyst (0.0125 mmol), N-(*p*-tolylsulfonyl)imido]phenyliodinane (93.3 mg, 0.25 mmol), molecular sieves (5Å) (20 mg), olefin (2.0 mmol) and solvent (0.200 mL) (chlorobenzene, unless otherwise stated). The reaction mixture was stirred vigorously for

24 hours (unless otherwise stated). After completion of the reaction, the products were isolated by column chromatography (silica gel) and quantified by ^{1}H NMR (in $CDCl_3$ or CD_3CN) versus an internal standard (4′-methoxyacetophenone).

Table S9. Yields of Aziridination/Amination of Olefins by [L^8M^{II}–NCMe][K(NCMe)] (M = Mn, Fe, Co)

Entry No.	Substrate	Products		Yield (%) CH_2Cl_2/PhCl L^8Mn	Yield (%) PhCl L^8Fe	Yield (%) PhCl L^8Co
1.		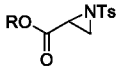	R = Me	polymer	polymer	polymer
2.			R = tBu	polymer	polymer	polymer
3.	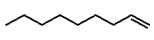	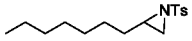		15	10	32
4.		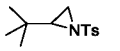		7	12	6
5.		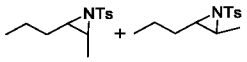		4, 2	3, 2	18, 19
6.		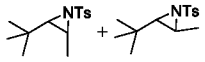		trace	trace	trace

All aziridination and allylic/benzylic amination products (Tables 3 and S9) are known compounds, and have been identified with the assistance of ^{1}H and ^{13}C NMR spectra, as well as HRMS data, by comparison to spectroscopic features reported for authentic samples in the literature.

Reaction Profile for the Aziridination of Styrene Mediated by [K(NCMe)(L^8)M^{II}–NCMe] (M = Mn, Fe, Co). The general procedure for olefin aziridination was followed, albeit in 0.50 mL of d^5-chlorobenzene at 30 °C, in the presence of a known amount of an internal standard for integration purposes (1,2-di-*p*-tolylethane). A 5.0 μL aliquot was sampled at regular time intervals, diluted in $CDCl_3$, and used for ^{1}H NMR analysis.

Integration data from three independent trials per catalyst were employed to obtain kinetic profiles.

Competitive Aziridinations of Styrene versus Non-Conjugated Olefins (Allylbenzene, 4-Phenyl-1-Butene, 1-Hexene) Mediated by [K(NCMe)(L^8)M^{II}–NCMe] (M = Mn, Fe, Co) and Other Catalysts**.** The general aziridination procedure was followed, with the exception that 1.0 mmol of each competing olefin (styrene and non-conjugated styrene) was used. Reactions catalyzed by [Cu(NCMe)$_4$](PF$_6$) (5 mol%) and [Rh$_2$(OAc)$_4$] (2.0 mol%) were conducted in MeCN and CH_2Cl_2, respectively.

Hammett Plots**.** The general aziridination of olefins was conducted mediated by [K(MeCN)(L^8)Mn^{II}–NCMe] (M = Mn, Fe, Co), with the exception that the olefin mixture was composed of 1.0 mmol of styrene and 1.0 mmol of a *p*-X-styrene (X = MeO, Me, ^{t}Bu, F, Cl, CF_3, NO_2). At the end of the reaction the mixture was flash chromatographed on silica gel (hexane, then petroleum ether/ethyl acetate 10:1) in order to recover the aziridination products and evaluate their ratio by quantitative ^{1}H-NMR analysis (in CD_3CN). For *p*-MeO-styrene, direct extraction by petroleum ether/ethyl acetate (10:1) is preferred, because the corresponding aziridine is unstable on silica. Hammett plots as a function of polar (σ_{mb}) and spin-delocalization ($\sigma_{JJ}^{\bullet}$) parameters are shown in Figure 9 for all three catalysts. Hammett plots as a function of the resonance-responsive σ+ parameter for Mn^{II}- and Co^{II}-mediated reactions are shown in Figure S6 (Fe^{II}-related data show poor correlation).

Table S10. Competitive Aziridination Reactions of *para*-substituted Styrenes *vs.* Styrene by PhI=NTs in the presence of [K(MeCN)(L^8)Mn^{II}–NCMe]

X	$\sigma_{JJ'}$	σ_{mb}	av. ratio	$A\times\sigma_{JJ'} + B\times\sigma_{mb} + C$ [b]	log(av. ratio)
F	-0.02	-0.24	1.572	0.14428	0.19645
CF_3	-0.01	0.49	0.759	-0.12731	-0.11976
H	0	0	1	0.06351	0
Me	0.15	-0.29	1.716	0.24988	0.23452
Cl	0.22	0.11	1.498	0.13396	0.17551
MeO	0.23	-0.77	3.165	0.47259	0.50037
^{t}Bu	0.26	-0.22	1.659	0.27942	0.21985
NO_2	0.36	0.86	0.852	-0.07895	-0.06956

[a] Reaction conditions: **8b**, 0.0125 mmol; *para*-substituted styrene, 1.0 mmol; Styrene, 1.0 mmol; PhI=NTs, 0.25 mmol; Chlorobenzene, 0.200 mL; Molecular Sieves (5Å), 20 mg; t = 24 hours. [b] A = 0.51; B = -0.38; C = 0.06; R^2 = 0.95.

Table S11. Competitive Aziridination Reactions of *para*-substituted Styrenes *vs.* Styrene by PhI=NTs in the presence of [K(MeCN)(L^8)Fe^{II}–NCMe] (**8c**) [a]

X	$\sigma_{JJ'}$	σ_{mb}	av. ratio	$A\times\sigma_{JJ'} + B\times\sigma_{mb} + C$ [b]	log(av. ratio)
F	-0.02	-0.24	1.547	0.14327	0.18949
CF_3	-0.01	0.49	0.904	-0.05515	-0.04383
H	0	0	1	0.08197	0
Me	0.15	-0.29	1.610	0.19706	0.20683
Cl	0.22	0.11	1.525	0.10353	0.18327
MeO	0.23	-0.77	2.306	0.34791	0.36286
^{t}Bu	0.26	-0.22	1.348	0.20371	0.12969
NO_2	0.36	0.86	0.840	-0.06977	-0.07577

[a] Reaction conditions: **8c**, 0.0125 mmol; *para*-substituted styrene, 1.0 mmol; Styrene, 1.0 mmol; PhI=NTs, 0.25 mmol; Chlorobenzene, 0.200 mL; Molecular Sieves (5Å), 20 mg; t = 24 hours. [b] A = 0.24; B = -0.28; C = 0.08; R^2 = 0.84

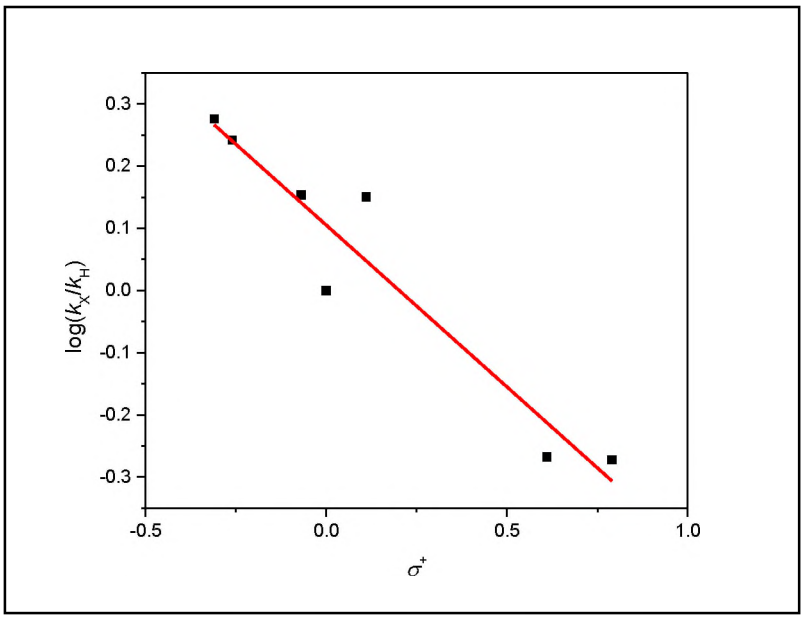

Figure S6. Linear free energy correlation of $\log(k_X/k_H)$ vs. σ^+ for aziridination of para-substituted styrenes by $[L^8M^{II}–solv]^-$ (M = Mn (top) or Co (bottom)). Fe provides a poor correlation.

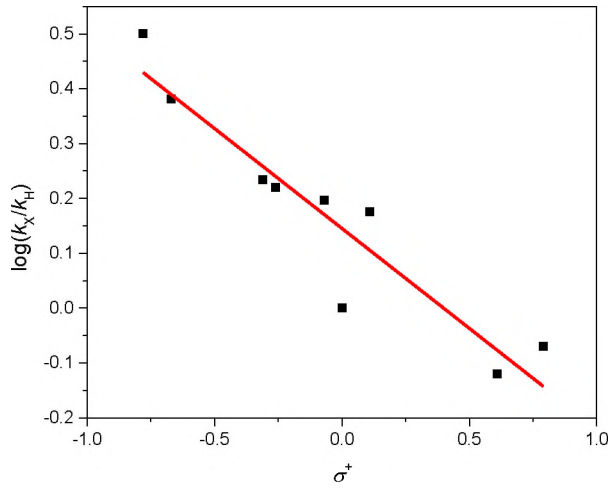

Figure S6. Linear free energy correlation of $\log(k_X/k_H)$ vs. σ^+ for aziridination of para-substituted styrenes by $[L^8M^{II}–solv]^-$ (M = Mn (top) or Co (bottom)). Fe provides a poor correlation.(cont.)

Competitive Aziridinations of Deuterated Styrenes vs. Styrene (KIE). In order to determine values of secondary deuterium kinetic isotope effects (k_H/k_D), a panel of deuterated styrenes (α-d^1-styrene, *cis*- and *trans*-β-d^1-styrene, β-d^2 styrene) was used

together with styrene (0.5 mmol each), and was subjected to aziridination (three trials) by PhI=NTs (0.125 mmol) in the presence of [K(MeCN)(L^8)M^{II}–NCMe] (6.25 μmol; M = Mn, Fe, Co) and molecular sieves (5Å, 10 mg) in chlorobenzene (0.100 mL), according to the general olefin aziridination procedure noted above. Prior to mixing with any other reagents, an aliquot (5.0 μl) of the original mixture of styrenes was retained for ^{1}H-NMR analysis ($CDCl_3$, 120 s relaxation delay). After completion of the reaction (24 h), the mixture was flash chromatographed on silica gel, first with hexane to remove the styrenes, and then with petroleum ether/ethyl acetate (10: 1 v/v) to recover the aziridination products. The ratio of $d^0/d^{1,2}$ aziridines is evaluated by ^{1}H NMR (CD_3CN, 120 s relaxation delay) and compared to the ratio of the starting $d^0/d^{1,2}$ styrenes in order to extract secondary KIE values.

Stereochemical Scrambling in Aziridinations of Deuterated Styrenes**.** The aziridination of *cis*- and *trans*-*β*-d^1-styrene (synthesized by following a literature report),[10] mediated by [K(MeCN)(L^8)M^{II}–NCMe] (M = Mn, Fe, Co), was conducted according to the general procedure for olefin aziridinations. The isolated aziridines were dissolved in $CHCl_3$ (700 μL)/$CDCl_3$(20 μL) and loaded in a precision NMR tube. Extensive ^{2}H NMR data were collected (90 s relaxation delay) for three independent reaction trials, in order to quantify the relative deuterium content at the *cis* and *trans* *β*-carbon sites of the aziridination products.

Radical Probe**.** The general olefin aziridination protocol noted above was applied to the radical clock *trans*-2-phenyl-1-vinylcyclopropane (synthesized according to a literature report) in the presence of catalysts [K(MeCN)(L^8)M^{II}–NCMe] (M = Mn, Fe, Co), both in the presence and absence of added $TsNH_2$ (1.0 equiv. vs the radical probe).

Copper catalysts $[Cu(NCMe)_4](PF_6)$ and $[Cu(TMG_3\text{-trphen})](PF_6)$[9] have also been employed for comparative purposes under the same conditions, with the exception of conducting the catalytic reaction in acetonitrile in lieu of chlorobenzene. Upon reaction completion, the mixture was extracted with hexane/ethyl acetate (3: 1 v/v) and the residue resulting after solvent evaporation was analyzed by ^{1}H NMR to evaluate the ratio of ring-closed (aziridines (**17**)) and ring-open products (olefinic diamine **19**, and conjugate diene **20**; see Scheme 2). The products were identified by their spectroscopic features (^{1}H NMR, ^{13}C NMR, ESI-MS) and literature precedence (**20**). The diastereomeric aziridines (previously reported,[11] but not fully characterized) and the olefinic diamine **19** were further purified by column chromatography.

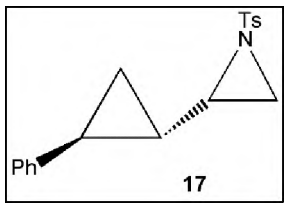

Figure S7. Closed aziridine product

Data for 17 (diast. a+b)**.** ^{1}H NMR (400 MHz, CD_3CN, 1.94 ppm): δ 7.83-7.77 (m, 2H, aryl(Ts)), 7.48-7.42 (m, 2H, Ph), 7.24-7.17 (m, 2H, aryl(Ts)), 7.15-7.09 (m, 1H, Ph), 6.89 (m, 2H, Ph), 2.87-2.81 (m, 0.50H, C*H*(azir, a)), 2.73-2.67 (m, 0.5H, C*H*(azir, b)), 2.61 (m, 1H, CH_2(azir)), 2.47 (s, 1.5H, Me(Ts, a)), 2.46 (s, 1.5H, Me(Ts, b)), 2.25 (dd, 0.5H, J = 4.5 , 0.4 Hz, CH_2(azir, b)), 2.22 (dd, 0.5H, J = 4.5 , 0.3 Hz, CH_2(azir, a)), 1.65 (m, 0.5H, PhC*H*(cy, b)), 1.45 (m, 0.5H, PhC*H*(cy, a)), 1.21 (m, 0.5H, C*H*(cy, a)), 1.10 (m, 0.5H, C*H*(cy, b)), 0.94-0.74 (m, 2H, CH_2(cy)). ^{13}C NMR (CD_3CN, 118.26 ppm): δ

145.8, 145.7, 142.5, 142.3, 135.5, 135.4, 130.5, 130.4, 128.9, 128.8, 128.5, 128.4, 126.23, 126.21, 126.18, 126.09, 42.3, 41.1, 33.2, 33.1, 22.6, 22.1, 21.4, 21.2, 20.6, 13.2, 11.8.

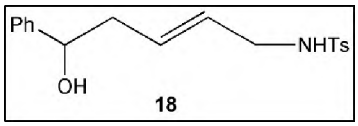

Figure S8. Open aminated product

Data for 18**.** ^{1}H NMR (400 MHz, CD_3CN, 1.94 ppm): δ 7.68 (d, 2H, J = 8.3 Hz, aryl(Ts)), 7.37 (dd, 2H, J = 8.6, 0.6 Hz, aryl(Ts)), 7.35-7.26 (m, 4H, Ph), 7.25-7.21 (m, 1H, Ph), 5.57-5.48 (m, 2H, C*H*=CH, N*H*Ts), 5.38-5.30 (m, 1H, CH=C*H*), 4.35 (td, 1H, J = 6.5, 4.1 Hz, C*H*OH), 3.39 ('t', 2H, J = 6.1 Hz, CH_2NHTs), 3.17 (d, 1H, J = 4.1 Hz, O*H*) 2.41 (s, 3H, Me(Ts)), 2.29 ('t', 2H, J = 6.7 Hz, CH_2). ^{13}C NMR ($CDCl_3$, 77.16 ppm): δ 145.9, 144.3, 138.4, 130.8, 130.5, 129.0, 128.6, 127.9, 127.8, 126.7, 73.6, 45.7, 42.9, 21.4.

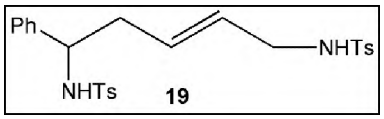

Figure S9. Open di-aminated product

Data for 19**.** ^{1}H NMR (400 MHz, $CDCl_3$, 7.26 ppm): δ 7.72 (d, 2H, J = 8.2 Hz, aryl(Ts)), 7.55 (d, 2H, J = 8.2 Hz, aryl(Ts)), 7.34-7.30 (m, 2H, Ph), 7.18-7.13 (m, 5H, aryl(Ts, 4H), Ph (1H)), 7.03-7.00 (m, 2H, Ph), 5.43-5.29 (m, 2H, C*H*=C*H*), 5.00 (d, 1H, J = 7.4 Hz, CHN*H*Ts), 4.51 (t, 1H, J = 5.9 Hz, CH_2N*H*Ts), 4.35 (dt, 1H, J = 7.2, 6.7 Hz, C*H*NHTs), 3.43 (dd, 2H, J = 5.8, 5.4 Hz, CH_2NHTs), 2.43 (s, 3H, Me(Ts)), 2.38 (m, 2H, CH_2NHTs), 2.36 (s, 3H, Me(Ts)). ^{13}C NMR ($CDCl_3$, 77.16 ppm): δ 143.8, 143.5, 140.3,

137.7, 136.9, 130.0, 129.7, 129.6, 129.1, 128.7, 127.7, 127.4, 127.3, 126.6, 57.4, 45.2, 40.3, 21.8, 21.7. HRMS (ESI) *m/z*: $[M + H]^+$ calcd for $C_{25}H_{29}N_2O_4S_2$ 485.15633; found 485.15674.

1.6. COMPUTATIONAL METHODS

Density functional theory employing the B3LYP functional along with the 6-31+G(d) basis set is used in the Gaussian09 software package for all reported calculations. Previous calculations on similar Cu guanidino complexes has indicated the accuracy of the calculation with this level of theory.[9] All calculations were done assuming 1 atm and 298.15 K and all possible spin states were evaluated. Two transition states were calculated for each metal (Co, Fe, Mn), for initial and subsequent C–N bond formation of aziridine. For the products, separate aziridine and catalyst are favored free energy-wise, aziridine-catalyst complexes were thus not discussed in the present calculations.

REFERENCES

(1) Çelenligil-Çetin, R.; Paraskevopoulou, P.; Dinda, R.; Staples, R. J.; Sinn, E.; Rath, N. P.; Stavropoulos, P. Synthesis, Characterization, and Reactivity of Iron Trisamidoamine Complexes that Undergo both Metal- and Ligand-Centered Oxidative Transformation. *Inorg. Chem.* **2008**, *47*, 1165–1172.

(2) Paraskevopoulou, P.; Ai, L.; Wang, Q.; Pinnapareddy, D.; Acharrya, R.; Dinda, R.; Çelenligil-Çetin, R.; Floros, G.; Sanakis, Y.; Choudhury, A.; Rath, N. P.; Stavropoulos, P. Synthesis and Characterization of a Series of Structurally and Electronically Diverse Fe(II) Complexes Featuring a Family of Triphenylamido-amine Ligands. *Inorg. Chem.* **2010**, *49*, 108-122.

(3) Jones, M. B.; MacBeth, C. E. Tripodal Phenylamine-Based Ligands and Their Co^{II} Complexes. *Inorg. Chem.* **2007**, *46*, 8117–8119.

(4) Bagchi, V.; Raptopoulos, G.; Das, P.; Christodoulou, S.; Wang, Q.; Ai, L.; Choudhury, A.; Pitsikalis, M.; Paraskevopoulou, P.; Stavropoulos, P. Synthesis and characterization of a family of Co(II) triphenylamido-amine complexes and catalytic activity in controlled radical polymerization of olefins. *Polyhedron* **2013**, *52*, 78–90.

(5) Çelenligil-Çetin, R.; Paraskevopoulou, P.; Lalioti, N.; Sanakis, Y.; Staples, R. J.; Rath, N. P.; Stavropoulos, P. Metalloradical Complexes of Manganese and Chromium Featuring an Oxidatively Rearranged Ligand. *Inorg. Chem.* **2008**, *47*, 10998-11009.

(6) Bruker, SMART **2002**, Bruker AXS Inc., Madison, Wisconsin, USA.

(7) Bruker, SAINT and SADABS **2008**, Bruker AXS Inc., Madison, Wisconsin, USA.

(8) Sheldrick, G. M. A short history of *SHELX*. *Acta Cryst.* **2008**, *A64*, 112-122.

(9) Bagchi, V.; Paraskevopoulou, P.; Das, P.; Chi, L.; Wang, Q.; Choudhury, A.; Mathieson, J. S.; Cronin, L.; Pardue, D. B.; Cundari, T. R.; Mitrikas, G.; Sanakis, Y.; Stavropoulos, P. A Versatile Tripodal Cu(I) Reagent for C−N Bond Construction via Nitrene-Transfer Chemistry: Catalytic Perspectives and Mechanistic Insights on C−H Aminations/Amidinations and Olefin Aziridinations. *J. Am. Chem. Soc.* **2014**, *136*, 11362–11381.

(10) Peng, T.-S.; Gladysz, J. A. Mechanism of Equilibration of Diastereomeric Chiral Rhenium Alkene Complexes of the Formula $[(\eta^5\text{-}C_5H_5)Re(NO)(PPh_3)(H_2C{=}CHR)]^+BF_4^-$. The Metal Traverses between Alkene Enantiofaces without Dissociation! *J. Am. Chem. Soc.* **1992**, *114*, 4174-4181.

(11) Baik, J. S.; Lee, N. H. Mechanistic Studies on the O_2-mediated Oxidation of Olefins in the Presence of (Schiff-base)Mn(III) Catalyst and $NaBH_4$. *Bull. Korean Chem. Soc.* **2006**, *27*, 765-768.

(12) Xing, D.; Yang, D. Gold(I)-Catalyzed Highly Regio- and Stereoselective Decarboxylative Amination of Allylic *N*-Tosylcarbamates via Base-Induced Aza-Claisen Rearrangement in Water. *Org. Lett.* **2010**, *12*, 1068-1071.

(13) Stephens, P. J.; Devlin, F. J.; Chabalowski, C. F.; Frisch, M. J. Ab Initio Calculation of Vibrational Absorption and Circular Dichroism Spectra Using Density Functional Force Fields. *The Journal of Physical Chemistry* **1994**, 98, 11623-11627.

(14) Frisch, M. J.; Trucks, G. W.; Schlegel, H. B.; Scuseria, G. E.; Cheeseman, J. R.; Scalmani, G.; Barone, V.; Mennucci, B.; Petersson, G. A.; Nakatsuji, H.; Caricato, M.; Li, X.; Hratchian, H. P.; Izmaylov, A. F.; Bloino, J.; Zheng, G.; Sonnenberg, J. L.; Hada, M.; Ehara, M.; Toyota, K.; Fukuda, R.; Hasegawa, J.; Ishida, M.; Nakajima, T.; Honda, Y.; Kitao, O.; Nakai, H.; Vreven, T.; Montgomery, J. A. J.; Peralta, J. E.; Ogliaro, F.; Bearpark, M.; Heyd, J. J.; Brothers, E.; Kudin, K. N.; Staroverov, V. N.; Kobayashi, R.; Normand, J.; Raghavachari, K.; Rendell, A.; Burant, J. C.; Iyengar, S. S.; Tomasi, J.; Cossi, M.; Rega, N.; Millam, J. M.; Klene, M.; Knox, J. E.; Cross, J. B.; Bakken, V.; Adamo, C.; Jaramillo, J.; Gomperts, R.; Stratmann, R. E.; Yazyev, O.; Austin, A. J.; Cammi, R.; Pomelli, C.; Ochterski, J. W.; Martin, R. L.; Morukuma, K.; Zakrzewski, V. G.; Voth, G. A.; Salvador, P.; Dannenberg, J. J.; Dapprich, S.; Daniels, A. D.; Farkas, O.; Foresman, J. B.; Ortiz, J. V.; Ciolowski, J.; Fox, D. J. Gaussian 09, B.01; Gaussian, Inc.: Wallingford, CT, 2009.

APPENDIX B.

IS THE ELECTROPHILICITY OF THE METAL NITRENE THE SOLE PREDICTOR OF METAL-MEDIATED NITRENE TRANSFER TO OLEFINS? SECONDARY CONTRIBUTING FACTORS AS REVEALED BY A LIBRARY OF HIGH-SPIN Co(II) REAGENTS

1. EXPERIMENTAL SECTION

1.1. GENERAL CONSIDERATIONS

All operations were performed under anaerobic conditions under a pure dinitrogen or argon atmosphere using Schlenk techniques on an inert gas/vacuum manifold or in a dry-box (O_2, H_2O < 1 ppm). Anhydrous diethyl ether, methylene chloride, acetonitrile, tetrahydrofuran, hexane, pentane, benzene, toluene, dimethylformamide, dimethylacetamide, and dimethylsulfoxide were purchased from Sigma-Aldrich (Millipore). Ethanol and methanol were distilled over the corresponding magnesium alkoxide, and acetone was distilled over drierite. Solvents were degassed by three freeze-pump-thaw cycles, unless otherwise stated. All other reagents were purchased at the highest purity available. Potassium hydride was provided as dispersion in mineral oil and was thoroughly washed prior to use with copious amounts of tetrahydrofuran followed by hexane. Ligands L^1H_3,[1] L^2H_3–L^6H_3,[2] L^7H_3,[3] L^8H_3,[2] L^9H_3,[2] $L^{10}H_3$,[4] $L^{11}H_3$,[5] $L^{12}H_3$,[5] $L^{13}H_3$,[4] $L^{14}H_3$,[5] $L^{15}H_3$,[5] and compounds $[K(L^3)Co^{II}–NCMe]_n$ (**3**),[4] $[K(THF)_6][(L^5)Co^{II}]$•1.5THF (**5**),[4] $[K(THF)_2(L^8)Co^{II}]_n$ (**8a**),[4] $[K(NCMe)(L^8)Co^{II}–NCMe]_n$ (**8b**),[5] $[K_2(L^9)_2Co^{II}_2]_n$ (**9**),[4] $\{[K_2(DMA)_3(L^{10})_2Co^{II}_2]$•$0.5Et_2O\}_n$ (**10**),[4] and $[K(NCMe)_3(L^{13})Co^{II}–NCMe]$ (**13**),[4] have been prepared according to literature methods.

^1H and ^{13}C NMR spectra were recorded on Varian XL-400, Varian INOVA/ UNITY 400 MHz Unity Plus and a Varian 300 Unity Plus NMR spectrometers. IR spectra were obtained on a Perkin-Elmer 883 IR spectrometer and FT-IR spectra on Nicolet Nexus 470 and 670, Magna 750 FT-IR ESP and Shimadzu IR-Affinity-1 spectrometers. UV-vis spectra were obtained on a Hewlett-Packard 8452A diode array, Varian Cary 50 and Varian Cary 300 spectrophotometers. EI and FAB mass spectra were

obtained on a Finnigan MAT-90 mass spectrometer. ESI and APCI mass spectra were obtained on a Thermo-Finnigan TSQ7000 triple-quadrupole mass spectrometer, equipped with the API2 source and Performance Pack (ThermoFinnigan, San Jose, CA). HRMS data were collected on a Thermo Fisher Scientific LTQ-Orbitrap XL hybrid mass spectrometer, using the Orbitrap analyzer for acquisition of high-resolution accurate mass data.Samples were infused using the integrated syringe pump at 3 μL/min and ionization was *via* the electrospray source with source settings at their defaults. In general, settings for the ion optics were determined automatically during the regular tuning and calibration of the instrument. For high-resolution data, the Orbitrap analyzer is set to a resolution of 100000. Microanalyses were done by Galbraith Laboratories, Knoxville, TN, Quantitative Technologies Inc., Whitehouse, NJ, and on an in-house Perkin-Elmer 2400 CHN analyzer.

1.2. LIGAND SYNTHESIS

$[CH_3\text{-}NH\text{-}(2\text{-}C_6H_4)]_3N$ **($L^{16}H_3$).** A suspension of $(2\text{-}NH_2\text{-}C_6H_4)_3N$ (0.58 g, 2.0 mmol) and KH (0.24 g, 6.0 mmol) in THF (20 mL) was stirred at room temperature for 12 hours. Methyl iodide (0.85 g, 6.0 mmol) was then added slowly, and the resulting reaction mixture was stirred for an additional 6 hours. The solid formed was removed by filtration and the solvent evacuated to dryness to afford a white solid that was further purified by column chromatography (silica gel). The fragment eluted with petroleum ether/ethyl acetate (40:1 v/v) was collected and the product was isolated after removal of the solvent mixture (0.38 g, 57%). ^1H NMR ($CDCl_3$, 7.26 ppm): δ 7.08 (td, 3H, J = 7.7, 1.5 Hz, aryl), 6.88 (dd, 3H, J = 7.7, 1.5 Hz, aryl), 6.62 (m, 6H, aryl), 3.93 (q, 3H, J = 4.7

Hz, N*H*), 2.74 (d, 9H, J = 5.1 Hz, Me). ^{13}C NMR ($CDCl_3$, 77.16 ppm): δ 144.0, 132.4, 125.9, 125.2, 116.9, 110.8, 30.8. IR (KBr, cm^{-1}): 3416, 3044, 2899, 2815, 2112, 1914, 1596, 1582, 1506, 1423, 1264, 1224, 1167, 1063, 1038, 739, 623, 473. MS-FAB (*m*/*z*): calcd. 332.45; found 332.43. Elemental analysis: Calcd. for $C_{21}H_{24}N_4$: C, 75.87; H, 7.28; N, 16.85. Found C, 75.84; H, 7.30; N, 16.86.

[(*S*)-(+)-2,2-Dimethylcyclopropane-CONH-(2-C_6H_4)]$_3$N•0.10$CHCl_3$ **($L^{17}H_3$).** To a stirred solution of (2-NH_2-C_6H_4)$_3$N (0.58 g, 2.0 mmol) and triethylamine (0.61 g, 6.0 mmol) in dichoromethane (25.0 mL), (*S*)-(+)-2,2-dimethylcyclopropane-1-carbonyl chloride (0.80 g, 6.0 mmol; prepared from the corresponding carboxylic acid and thionyl chloride) was slowly added by means of a syringe at 0 °C. The mixture was allowed to warm up to room temperature, and was further stirred overnight. The solvent was removed under reduced pressure and the crude residue was purified by column chromatography (petroleum ether/ethyl acetate) to afford the product as a white solid (0.78 g, 67%). Crystals for X-ray diffraction analysis were obtained from chloroform. ^{1}H NMR ($CDCl_3$, 7.26 ppm): 8.38 (s, 3H, N*H*), 7.81 (d, 3H, J = 7.8 Hz, aryl), 7.11 (t, 3H, J = 7.4 Hz, aryl), 6.99 (t, 3H, J = 7.3 Hz, aryl), 6.79 (d, 3H, J = 7.8 Hz, aryl), 1.24 (t, 3H, J = 5.8/6.9 Hz, cy-C*H*), 1.04 (t, 3H, J = 3.9/4.6 Hz, cy-CH_2), 0.93 (s, 3H, Me), 0.77 (s, 3H, Me), 0.66 (dd, 3H, J = 7.4, 4.2 Hz, cy-CH_2). ^{13}C NMR ($CDCl_3$, 77.16 ppm): δ 170.0, 138.2, 132.4, 125.6, 125.3, 124.8, 124.4, 29.3, 26.8, 22.5, 20.3, 18.4. IR (KBr, cm^{-1}): 3373, 3264, 3234, 2946, 2869, 1685, 1672, 1642, 1594, 1522, 1446, 1398, 1374, 1292, 1264, 1187, 1174, 1187, 1118, 1037, 978, 859, 757, 737, 623, 488. Elemental analysis: Calcd. for $C_{36}H_{42}N_4O_3$ (**$L^{17}H_3$** – 0.10 $CHCl_3$): C, 74.71; H, 7.32; N, 9.68. Found C, 74.68; H, 7.34; N, 9.71.

1.3. SYNTHESIS OF COBALT(II) COMPLEXES

[K(2.2.2-cryptand)][(L^1)Co^{II}]•3THF **(1).** To a THF (15.0 mL) solution of the ligand L^1H_3 (0.343 g, 0.5 mmol) KH (0.060 g, 1.5 mmol) was added, and the mixture was stirred overnight. Anhydrous $CoCl_2$ (0.065 g, 0.5 mmol) was added to this solution, and the mixture was allowed to stir for an additional 24 hours to afford a deep green solution. The solution was refrigerated (–30 °C) overnight, and the insoluble salts were filtered off on a fine porosity anaerobic frit. The filtrate was then added to 2.2.2-cryptand (0.188 g, 0.5 mmol), and the solution was stirred for 1.0 hour. The solution was then reduced to 5.0 mL under vacuum, and pentane (30.0 mL) was carefully layered over the THF solution and was allowed to mix slowly at –30 °C to afford crystalline green material suitable for x-ray diffraction analysis (0.310 g, 45%). IR (KBr, cm^{-1}): 3527, 32187, 2943, 2863, 1645, 1658, 1583, 1565, 1541, 1489, 1435, 1375, 1329, 1278, 1246, 1210, 1158, 1109, 1028, 1005, 948, 823, 725, 705, 665, 623, 591, 572, 475, 428, 408. UV–vis (THF): λ_{max} (ε (M^{-1} cm^{-1})) 305 (21000). Elem. Anal. calcd. for $C_{78}H_{111}N_6O_9CoK$: C, 68.14; H, 8.14; N, 6.11. Found C, 68.38; H, 8.17; N, 6.07.

[K(2.2.2-cryptand)][(L^2)Co^{II}]•1.5 Pentane **(2).** To a THF (15.0 mL) solution of the ligand L^2H_3 (0.428 g, 0.5 mmol), KH (0.060 g, 1.5 mmol) was added, and the mixture was stirred overnight. Anhydrous $CoCl_2$ (0.065 g, 0.5 mmol) was added to this solution, and the mixture was allowed to stir for an additional 24 hours to afford a deep green-brown solution. The solution was refrigerated (–30 °C) overnight, and the insoluble salts were filtered off on a fine porosity anaerobic frit. The filtrate was then added to 2.2.2-cryptand (0.188 g, 0.5 mmol), and the solution was stirred for 1.0 hour. The solution was then reduced to 3.0 mL under vacuum, and pentane (30.0 mL) was carefully layered over

the THF solution and was allowed to mix slowly at –30 °C to afford crystalline green material suitable for x-ray diffraction analysis (0.340 g, 47%). IR (KBr, cm^{-1}): 3868, 3092, 2938, 2759, 1646, 1628, 1576, 1545, 1532, 1512, 1487, 1435, 1326, 1317, 1298, 1263, 1242, 1198, 1146, 1098, 1032, 988, 889, 823, 798, 767,675, 645, 640, 598, 583, 557, 504, 487.466, 445. UV–vis (THF): λ_{max} (ε (M^{-1} cm^{-1})) 383 (27000). Elem. Anal. calcd. for $C_{78}H_{111}N_6O_6CoK$ (**2** – 1.5 Pentane): C, 70.61; H, 8.43; N, 6.33. Found C, 70.50; H, 8.47; N, 6.27.

[K(THF)$_3$(L^2_{re})Co^{II}–THF] (2b) and [($L^2_{re,ox}$)Co^{II}–THF]•0.5 Pentane **(2c).** Anhydrous THF (15.0 mL, Sigma-Aldrich product, not further degassed) was added to the ligand L^2H_3 (0.428 g, 0.5 mmol) and KH (0.060 g, 1.5 mmol), and the mixture was stirred overnight. Anhydrous $CoCl_2$ beads (0.065 g, 0.5 mmol) were added to this solution, and the mixture was allowed to stir for an additional 24 hours to afford a deep brown-green solution. The solution was refrigerated (–30 °C) overnight, and the insoluble salts were filtered off on a fine porosity anaerobic frit. The filtrate was then reduced to a small volume (2.0 mL) under vacuum, and refrigerated (–35 °C) for several days to afford yellow-brown crystals of **2b**, suitable for x-ray diffraction analysis. The crystalline material was filtered off, and the green-brown filtrate was again refrigerated (–35 °C) to afford an additional small crop of **2b** (combined yield: 0.205 g, 33%). After filtration of **2b**, pentane (30.0 mL) was carefully layered over the green THF filtrate, and was allowed to mix slowly at –35 °C to afford crystalline green **2c**, suitable for x-ray diffraction analysis (0.160 g, 31%). **2b**, IR (KBr, cm^{-1}): 3952, 3922, 3863, 3529, 3085, 2752, 1696, 1621, 1530, 1513, 1480, 1423, 1335, 1311, 1252, 1241, 1182, 1152, 1073, 1036, 975, 880, 725, 715, 675, 583, 550, 503, 483, 460, 440. UV–vis (THF): λ_{max} (ε (M^{-1} cm^{-1})) 375

(21000). Elem. Anal. calcd. for $C_{76}H_{107}N_4O_4CoK$: C, 73.69; H, 8.71; N, 4.52. Found C, 73.29; H, 8.68; N, 4.61. **2c**, IR (KBr, cm^{-1}): 3945, 3867, 3842, 3673, 3290, 2865, 2678, 1685, 1611, 1578, 1525, 1493, 1446, 1320, 1245, 1190, 1162, 1136, 1085, 1045, 978, 925, 857, 745, 721, 667, 580, 527,490, 465, 428. UV–vis (THF): λ_{max} (ε (M^{-1} cm^{-1})) 305 (25000). Elem. Anal. calcd. for $C_{64}H_{83}N_4OCo$ (**2c** – 0.5 Pentane): C, 78.17; H, 8.51; N, 5.70. Found C, 78.01; H, 8.46; N, 5.79.

[$K(L^4)Co^{II}$]•Diethyl ether **(4).** The ligand L^4H_3 (0.271 g, 0.5 mmol) was dissolved in degassed DMA (5.0 mL), and KH (0.060 g, 1.5 mmol) was added to this solution. The mixture was allowed to stir overnight, followed by addition of anhydrous $CoCl_2$ (0.065 g, 0.5 mmol). This mixture was stirred for an additional 24 hours to afford a light green-brown solution. The solution was refrigerated (–30 °C) overnight and the insoluble salts were filtered off on an anaerobic frit. Diethyl ether (30.0 mL) was carefully layered over the DMA solution, and the system was allowed to slowly mix at room temperature to afford light green crystalline material. Crystals suitable for x-ray diffraction analysis were obtained by slow diffusion of diethyl ether into a DMA solution of the title compound (0.173 g, 54%). FT-IR (KBr, cm^{-1}): 3448, 3057, 2948, 2863, 1654, 1638, 1596, 1577, 1560, 1536, 1477, 1449, 1389, 1357, 1337, 1276, 1251, 1217, 1174, 1107, 1035, 1023, 965, 853, 800, 771, 762, 741, 668, 628, 593, 580, 553, 507, 476, 460. UV–vis (THF): λ_{max} (ε (M^{-1} cm^{-1})) 368 (23000). Elem. Anal. calcd. for $C_{33}H_{39}N_4O_3CoK$ (**4** – Diethyl ether): C, 62.13; H, 6.17; N, 8.79. Found C, 62.33; H, 6.21; N, 8.83.

[$K(NCMe)(L^6)Co^{II}$–NCMe]•2MeCN **(6).** The ligand L^6H_3 (0.301 g, 0.5 mmol) was dissolved in degassed THF (15.0 mL), and KH (0.060 g, 1.5 mmol) was added to this solution. The mixture was allowed to stir overnight, followed by addition of anhydrous

$CoCl_2$ (0.065 g, 0.5 mmol). This mixture was stirred for an additional 24 hours to afford a violet solution. The solution was refrigerated (–30 °C) overnight and the insoluble salts were filtered off on an anaerobic frit. The filtrate was evaporated to dryness, and the residue was dissolved in acetonitrile (10.0 mL). This solution was reduced to approximately 5.0 mL by evaporation, and was refrigerated (–30 °C) to afford violet crystalline material, suitable for x-ray diffraction analysis (0.232 g, 54%). IR (KBr, cm^{-1}): 3411, 3056, 1596, 1583. 1539, 1473, 1446, 1362, 1271, 1241, 1155, 1134, 1038, 933, 750, 718, 697, 590, 518. UV–vis (MeCN): λ_{max} (ε (M^{-1} cm^{-1})) 276 (29000). Elem. Anal. calcd. for $C_{47}H_{39}N_8O_3CoK$: C, 65.50; H, 4.56; N, 13.00. Found C, 65.33; H, 4.52; N, 13.09.

$[K_2(DMA)_4][K(L^7)_2Co^{II}_2]_2$•2DMA **(7).** The ligand L^7H_3 (0.250 g, 0.5 mmol) was dissolved in degassed DMA (5.0 mL), and KH (0.060 g, 1.5 mmol) was added to this solution. The mixture was allowed to stir overnight, followed by addition of anhydrous $CoCl_2$ (0.065 g, 0.5 mmol). This mixture was stirred for an additional 24 hours to afford a green-brown solution. The solution was refrigerated (–30 °C) overnight and the insoluble salts were filtered off on an anaerobic frit. Diethyl ether (30.0 mL) was carefully layered over the DMA solution, and the system was allowed to slowly mix at room temperature to afford green-brown crystalline material suitable for x-ray diffraction analysis (0.205 g, 56%). IR (KBr, cm^{-1}): 3058, 2959, 2866, 1635, 1594, 1543, 1480, 1468, 1408, 1252, 1218, 1159, 1087, 1035, 965, 944, 745, 636, 590, 470. UV–vis (DMA): λ_{max} (ε (M^{-1} cm^{-1})) 285 (35000). Elem. Anal. calcd. for $C_{36}H_{46.5}N_{5.5}O_{4.5}CoK$: C, 59.53; H, 6.45; N, 10.61. Found C, 59.48; H, 6.47; N, 10.58.

$[K(DMA)_3(L^8)Co^{II}]_2$ **(8c).** The ligand L^8H_3 (0.289 g, 0.5 mmol) was dissolved in degassed DMA (5.0 mL), and KH (0.060 g, 1.5 mmol) was added to this solution. The mixture was allowed to stir overnight, followed by addition of anhydrous $CoCl_2$ (0.065 g, 0.5 mmol). This mixture was stirred for an additional 24 hours to afford a grey-blue solution. The solution was refrigerated (–30 °C) overnight and the insoluble salts were filtered off on an anaerobic frit. Diethyl ether (30.0 mL) was carefully layered over the DMA solution, and the system was allowed to slowly mix at –35 °C to afford light grey-blue crystalline material suitable for x-ray diffraction analysis (0.240 g, 51%). IR (KBr, cm^{-1}): 3878, 3788, 3735, 3646, 3570, 3498, 3423 3376, 2981, 2978, 2855, 2797, 2738, 2656, 2587, 1695, 1678, 1576, 1543, 1487, 1459, 1384, 1367, 1259, 1145, 1095, 1023, 996, 921, 879, 764, 711, 686, 623, 589, 470, 438, 412. UV–vis (DMA): λ_{max} (ε (M^{-1} cm^{-1})) 357 (27000). Elem. Anal. calcd. for $C_{36}H_{39}N_7F_9O_6CoK$: C, 46.26; H, 4.205; N, 10.49. Found C, 46.72; H, 4.31; N, 10.41.

$[K(THF)(L^{11}H)Co^{II}–OH]_2$ **(11).** The ligand $L^{11}H_3$ (0.322 g, 0.5 mmol) was dissolved in degassed THF (15.0 mL), and KH (0.060 g, 1.5 mmol) was added to this solution. The mixture was allowed to stir overnight, followed by addition of anhydrous $CoCl_2$ (0.065 g, 0.5 mmol). The mixture was stirred for an additional 24 hours to afford a green-blue solution that progressively decomposes, eventually yielding a blue solid and a light green filtrate. The filtrate was reduced to approximately 3 mL by evaporation and layered with pentane (20 mL) to afford very few green crystals of the title compound. This compound was identified by single X-ray diffraction analysis, but its amount was otherwise insufficient for other analytical/diagnostic data collection.

$[K(THF)_3(L^{12})Co^{II}]\bullet THF$ **(12).** To a THF (15.0 mL) solution of the ligand $L^{12}H_3$ (0.301 g, 0.5 mmol) KH (0.060 g, 1.5 mmol) was added, and the mixture was stirred overnight. Anhydrous $CoCl_2$ (0.065 g, 0.5 mmol) was added to this solution, and the mixture was allowed to stir for an additional 24 hours to afford a green-brown solution. The solution was refrigerated (–30 °C) overnight, and the insoluble salts were filtered off on a fine porosity anaerobic frit. The filtrate was then reduced to 3.0 mL, and pentane (30.0 mL) was carefully layered over the THF solution and allowed to mix slowly at –30 °C to afford crystalline green-brown material suitable for x-ray diffraction analysis (0.235 g, 48%). IR (KBr, cm^{-1}): 3322, 3011, 2914 2853, 2726, 1575, 1469, 1333, 1298, 1246, 1196, 1152, 1028, 952, 827, 734, 687, 588. UV–vis (THF): λ_{max} (ε (M^{-1} cm^{-1})) 266 (12500). Elem. Anal. calcd. for $C_{58}H_{71}N_4O_4CoK$: C, 70.63; H, 7.26; N, 5.68. Found C, 70.58; H, 7.27; N, 5.70.

$[K(DMA)(L^{14})Co^{II}]\bullet DMA$ **(14).** The chiral ligand $L^{14}H_3$ (0.316 g, 0.5 mmol) was dissolved in degassed DMA (5.0 mL), and KH (0.060 g, 1.5 mmol) was added to this solution. The mixture was allowed to stir overnight, followed by addition of anhydrous $CoCl_2$ (0.065 g, 0.5 mmol). This mixture was stirred for an additional 24 hours to afford a violet solution. The solution was refrigerated (–20 °C) overnight, and the insoluble salts were filtered off on an anaerobic frit. Diethyl ether (20 mL) was carefully layered over the DMA filtrate, and pentane (10 mL) was layered over the diethyl ether. The setup was allowed to stand at room temperature to afford blue-violet crystalline material, suitable for x-ray diffraction analysis (0.262 g, 58%). IR (KBr, cm^{-1}): 2981, 1719, 1599, 1533, 1477, 1445, 1393, 1369, 1230, 1081, 1035, 929, 866, 754, 619, 547, 484. UV–vis

(DMA): λ_{max} (ε (M^{-1} cm^{-1})) 285 (28000). Elem. Anal. calcd. for $C_{41}H_{51}N_6O_{11}CoK$: C, 54.58; H, 5.70; N, 9.32. Found C, 54.51; H, 5.66; N, 9.21.

[$K(THF)_3(L^{15})Co^{II}$]•THF **(15).** The ligand $L^{15}H_3$ (0.469 g, 0.5 mmol) was dissolved in degassed DMA (5.0 mL), and KH (0.060 g, 1.5 mmol) was added to this solution. The mixture was allowed to stir overnight, followed by addition of anhydrous $CoCl_2$ (0.065 g, 0.5 mmol). This mixture was stirred for an additional 24 hours to afford a violet solution. The solution was refrigerated (–20 °C) overnight, and the insoluble salts were filtered off on an anaerobic frit. Diethyl ether (20 mL) was carefully layered over the DMA filtrate, and pentane (10 mL) was layered over the diethyl ether. The setup was allowed to stand at room temperature to afford a pink solid, not suitable for x-ray diffraction analysis. X-ray quality pink crystals were obtained from concentrated tetrahudrofuran solutions stored at –35 °C (0.350 g, 56%). IR (KBr, cm^{-1}): 3350, 3125, 2965, 1695, 1576, 1487, 1455, 1360, 1156, 1043, 905, 786, 655, 418. UV–vis (THF): λ_{max} (ε (M^{-1} cm^{-1})) 300 (26000). Elem. Anal. calcd. for $C_{64}H_{68}N_4F_9O_{10}CoK$: C, 54.50; H, 4.57; N, 4.24. Found C, 54.58; H, 4.60 ; N, 4.27.

[$K(L^{16})Co^{II}$–THF]•0.5Pentane **(16).** The ligand $L^{16}H_3$ (0.166 g, 0.5 mmol) was dissolved in THF (15.0 mL), and KH (0.060 g, 1.5 mmol) was added to this solution. The mixture was allowed to stir overnight, followed by addition of anhydrous $CoCl_2$ (0.065 g, 0.5 mmol). Stirring was resumed for an additional 24 hours to afford a dark red-brown solution that was subsequently filtered and reduced under vacuum to 3.0 mL. Pentane (30.0 mL) was carefully layered over the concentrated THF solution and allowed to mix slowly at –30 °C to provide red-brown crystalline material suitable for x-ray diffraction analysis (0.205 g, 82%). IR (KBr, cm^{-1}): 3634, 3415, 3045, 2853, 2814, 2776, 1593,

1500, 1454, 1278, 1225, 1158, 1033, 866, 725, 595. UV–vis (THF): λ_{max} (ε (M^{-1} cm^{-1})) 280 (13500). Elem. Anal. calcd. for $C_{25}H_{29}N_4O_1CoK$ (**16** – 0.5Pentane): C, 60.11; H, 5.85; N, 11.22. Found C, 60.17; H, 5.86; N, 11.16.

$[K(THF)_2(L^{16}{}_{re})Co^{II}]_2$ **(16b).** The procedure described for the preparation of **16** was followed, with the exception that the THF employed (anhydrous, Sigma-Aldrich) was not further degassed. The compound was isolated from THF/pentane as brown crystals (0.205 g, 72%). IR (KBr, cm^{-1}): 3998, 3767, 3675, 3589, 3478, 3305, 2976, 2943, 2890, 2786, 2687, 2587, 1687, 1649, 1578, 1590, 1478, 1455, 1390, 1372, 1245, 1133, 1101, 1068, 1059, 976, 949, 887, 765, 723, 688, 629, 521, 478, 445, 408. UV–vis (THF): λ_{max} (ε (M^{-1} cm^{-1})) 295 (23000). Elem. Anal. calcd. for $C_{29}H_{37}N_4O_2CoK$: C, 60.93; H, 6.52; N, 9.80. Found C, 60.48; H, 6.46; N, 9.89.

$[K(THF)K(L^{17})_2Co^{II}{}_2]_2$•3Pentane **(17).** The chiral ligand $L^{17}H_3$ (0.289 g, 0.5 mmol) was dissolved in THF (15.0 mL) and KH (0.060 g, 1.5 mmol) was added to the solution. The mixture was allowed to stir overnight, followed by addition of anhydrous $CoCl_2$ (0.065 g, 0.5 mmol) and continuous stirring for an additional 24 hours to afford a violet solution. The solution was then refrigerated overnight (–30 °C) and the insoluble salts were filtered off on a fine porosity anaerobic frit. The filtrate was reduced to 3.0 mL under vacuum and pentane was carefully layered over the concentrated THF solution to provide x-ray diffraction quality violet crystals upon standing at –30 °C (0.277 g, 78%). IR (KBr, cm^{-1}): 3060, 2993, 2939, 2865, 1597, 1536, 1478, 1420, 1372, 1340, 1296, 1195, 1119, 1035, 972, 747, 621. UV–vis (THF): λ_{max} (ε (M^{-1} cm^{-1})) 303 (27000). Elem. Anal. calcd. for $C_{38}H_{43}N_4O_{3.5}CoK$ (**17** – 3Pentane): C, 64.30; H, 6.11; N, 7.89. Found C, 64.37; H, 6.13; N, 7.85.

1.4. X-RAY CRYSTALLOGRAPHY

Intensity data sets for all the compounds were collected on either a Bruker Smart Apex or a Bruker Apex II diffractometer using graphite monochromated Mo (λ = 0.71073 Å) or Cu (λ = 1.54178 Å) Kα radiation from a fine focus sealed tube X-ray source. Suitable crystals were selected and mounted on a glass fiber using super glue. The datasets were collected at low temperatures (140–150 K) and room temperature for metal complexes and purely organic compounds, respectively, employing a scan of 0.3° in ω with an exposure time of 20 s/frame using Apex III or SMART software.[6,7] The cell refinement and data reduction were carried out with SAINT, while the program SADABS was used for the absorption correction.[8] The structures were solved by direct methods using SHELXS-97 and difference Fourier syntheses.[9] Full-matrix least-squares refinement against $|F^2|$ was carried out using the SHELXTL-PLUS[8] suite of programs. All non-hydrogen atoms were refined anisotropically. Hydrogen atoms were placed geometrically and held in the riding mode during the final refinement. Crystal structures of (L^1)Co (**1**), (L^4)Co (**4**), ($L^2_{re,ox}$)Co (**2c**), (L^{15})Co (**15**), (L^{16})Co (**16**), and (L^{17})Co (**17**) contained volatile solvent molecules in the void space. The diffuse scattering from the disordered or partly evaporated solvents residing in the voids were treated as a diffuse contribution to the overall scattering without specific atom positions by SQUEEZE/PLATON.[10] All structures were finally refined with SHELX-2014 using SHELXle.[11] Pertinent crystallographic data are collected in Table S1. ORTEP diagrams and selective metrical parameters for compounds **4**, **6**, **7**, **8c**, **14**, **15** and **17** are shown in Figure 3, for **16** in Figure 4, for **1**, **2**, **11** and **12** in Figure 5, for ligands $L^{16}H_3$ and $L^{17}H_3$ in Figure S1, **2b** and **2c** in Figure S2, and for **16b** in Figure S3.

Table S1. Summary of Crystallographic Data for Compounds **1**, **2**, **4** and **6**

	L^1Co^{II} (1)	**L^2Co^{II} (2)**	**L^4Co^{II} (4)**	**L^6Co^{II} (6)**
formula	$C_{78}H_{111}N_6O_9CoK$	$C_{85.5}H_{129}N_6O_6CoK$	$C_{37}H_{49}N_4O_4CoK$	$C_{47}H_{39}N_8O_3CoK$
M_r	1374.75	1434.97	711.83	861.89
crystal system	Monoclinic	Triclinic	Trigonal	Monoclinic
space group	$P2_1/n$	$P\bar{1}$	$P\bar{3}$	$P2_1/n$
a (Å)	12.794(19)	13.456(3)	10.469(2)	10.271(3)
b (Å)	24.93(4)	13.795(3)	10.469(2)	23.557(6)
c (Å)	23.62(4)	25.747(6)	19.966(4)	18.471(5)
α (deg)	90	79.209(7)	90	90
β (deg)	94.697(15)	78.532(6)	90	102.559(3)
γ (deg)	90	62.283(6)	120	90
V (Å^3)	7508(20)	4121.7(16)	1895.1(9)	4362.5(19)
Z	4	2	2	4
D_{calcd} (g cm^{-3})	1.216	1.156	1.247	1.312
T (K)	200(2)	100(2)	130(2)	220(2)
λ (Å)	0.71073	0.71073	0.71073	0.71073
μ (mm^{-1})	0.343	0.312	0.604	0.539
R_1[a] (I>2sigma(I))	0.1484	0.1100	0.0908	0.0793
wR_2[b] (I>2sigma(I))	0.3389	0.2065	0.2397	0.1575

[a] $R_1 = \Sigma||F_o| - |F_c||/\Sigma|F_o|$. [b] $wR_2 = [\Sigma w(F_o^2 - F_c^2)^2/\Sigma w(F_o^2)^2]^{1/2}$.

Table S1. Summary of Crystallographic Data for Compounds **7**, **8c**, **11**, and **12** (cont.).

	L^7Co^{II} (7)	L^8Co^{II} (8c)	$L^{11}Co^{II}$ (11)	$L^{12}Co^{II}$ (12)
formula	$C_{144}H_{186}N_{22}O_{18}Co_4K_4$	$C_{72}H_{78}N_{14}F_{18}O_{12}Co_2K_2$	$C_{49}H_{55}N_4O_2CoK$	$C_{58}H_{71}N_4O_4CoK$
M_r	2905.26	1869.54	830.00	986.21
crystal system	Triclinic	Monoclinic	Monoclinic	Monoclinic
space group	$P\bar{1}$	$P2_1/n$	$P2_1/c$	$P2_1/c$
a (Å)	20.156(7)	9.0733(2)	13.187(8)	21.72(4)
b (Å)	20.622(7)	29.2751(7)	20.522(11)	13.60(3)
c (Å)	21.581(8)	15.9177(4)	16.050(10)	18.90(4)
α (deg)	64.584(6)	90	90	90
β (deg)	81.644(7)	93.542(2)	97.064(19)	108.20(3)
γ (deg)	67.502(6)	90	90	90
V (Å^3)	7483(5)	4220.01(17)	4311(4)	5303(18)
Z	2	2	2	4
D_{calcd} (g cm^{-3})	1.289	1.471	1.279	1.235
T (K)	140(2)	150(2)	140(2)	140(2)
λ (Å)	0.71073	1.54178	0.71073	0.71073
μ (mm^{-1})	0.615	4.889	0.538	0.451
R_1[a] (I>2sigma(I))	0.0803	0.0336	0.0561	0.1176
wR_2[b] (I>2sigma(I))	0.2080	0.0835	0.0935	0.1945

[a] $R_1 = \Sigma||F_o| - |F_c||/\Sigma|F_o|$. [b] $wR_2 = [\Sigma w(F_o^2 - F_c^2)^2/\Sigma w(F_o^2)^2]^{1/2}$.

Table S1. Summary of Crystallographic Data for Compounds **2c**, **16b** and Ligands $L^{16}H_3$ and $L^{17}H_3$ (cont.).

formula	$C_{66.5}H_{89}N_4OCo$	$C_{58}H_{74}N_8O_4Co_2K_2$	$C_{21}H_{24}N_4$	$C_{36.10}H_{42.10}N_4Cl_{10.30}O_3$
M_r	1019.34	1143.31	332.44	590.67
crystal system	Triclinic	Monoclinic	Orthorhombic	Orthorhombic
space group	$P\bar{1}$	$C2/c$	$P2_12_12_1$	$P2_12_12_1$
a (Å)	14.0187(7)	38.308(3)	12.2246(6)	12.0185(17)
b (Å)	14.1991(7)	22.5718(17)	16.7598(9)	15.962(2)
c (Å)	17.7928(9)	31.324(2)	36.1289(19)	17.715(2)
α (deg)	71.2280(10)	90	90	90
β (deg)	81.0670(10)	124.6010(10)	90	90
γ (deg)	61.5330(10)	90	90	90
V (Å^3)	2947.9(3)	22294(3)	7402.2(7)	3398.5(8)
Z	2	16	16	4
D_{calcd} (g cm^{-3})	1.148	1.362	1.193	1.154
T (K)	137(2)	136(2)	293(2)	150(2)
λ (Å)	0.71073	0.71073	0.71073	0.71073
μ (mm^{-1})	0.335	0.798	0.072	0.097
R_1[a] (I>2sigma(I))	0.0673	0.0488	0.0688	0.0745
wR_2[b] (I>2sigma(I))	0.1876	0.1199	0.1291	0.1875

[a] $R_1 = \Sigma||F_o| - |F_c||/\Sigma|F_o|$. [b] $wR_2 = [\Sigma w(F_o^2 - F_c^2)^2/\Sigma w(F_o^2)^2]^{1/2}$.

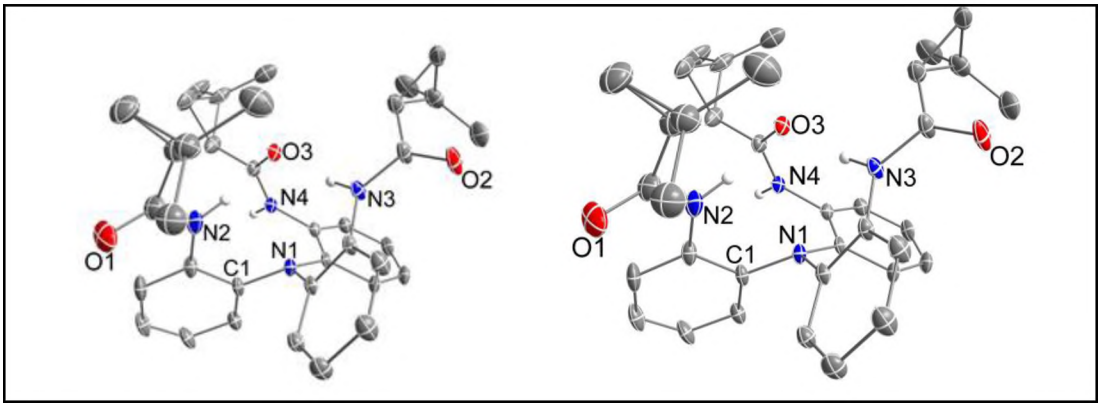

Figure S1. ORTEP diagrams of ligands $L^{16}H_3$ (left) and $L^{17}H_3$ (right), drawn with 40% thermal ellipsoids. Selective interatomic distances (Å) and angles (°).

$L^{16}H_3$, N(1)–C(1) = 1.438(4), N(1)–C(15) = 1.439(4), N(1)–C(8) = 1.445(4), N(2)–C(2) = 1.369(5), N(2)–C(7) = 1.446(5), N(3)–C(9) = 1.383(5), N(3)–C(14) = 1.444(5), N(4)–C(16) = 1.370(5), N(4)–C(20) = 1.443(5), C(1)–N(1)–C(15) = 116.0(3), C(1)–N(1)–C(8) = 116.0(3), C(8)–N(1)–C(15) = 115.7(2), C(2)–N(2)–C(7) = 123.2(4), C(9)–N(3)–C(14) = 122.1(3), C(16)–N(4)–C(20) = 123.0(3); $L^{17}H_3$, N(1)–C(1) = 1.419(6), N(1)–C(13) = 1.423(6), N(1)–C(25) = 1.421(6), N(2)–C(2) = 1.389(8), N(2)–C(7) = 1.349(7), N(3)–C(14) = 1.391(7), N(3)–C(19) = 1.347(7), N(4)–C(26) = 1.411(6), N(4)–C(31) = 1.335(7), O(1)–C(7) = 1.183(8), O(2)–C(19) = 1.233(6), O(3)–C(31) = 1.242(6), C(1)–N(1)–C(13) = 116.5(4), C(1)–N(1)–C(25) = 117.7(4), C(13)–N(1)–C(25) = 117.6(2), C(2)–N(2)–C(7) = 127.6(5), C(14)–N(3)–C(19) = 127.3(4), C(26)–N(4)–C(31) = 124.8(4), O(1)–C(7)–N(2) = 123.7(7), O(2)–C(19)–N(3) = 123.2(5), O(3)–C(31)–N(4) = 122.8(5).

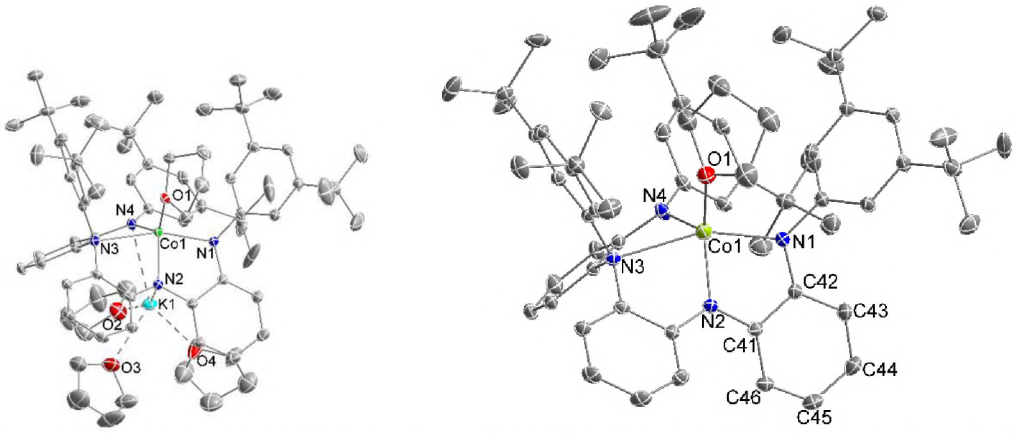

Figure S2. ORTEP diagrams of $[K(THF)_3(L^2_{re})Co^{II}–THF]$ (**2b**) (left) and $[(L^2_{re,ox})Co^{II}–THF]$•0.5Pentane (**2c**) (right), drawn with 40% thermal ellipsoids. Hydrogen atoms are omitted for clarity. Selective interatomic distances (Å) and angles (°).

2b, Co(1)–N(1) = 2.0094(17), Co(1)–N(2) = 1.9739(17), Co(1)–N(3) = 2.4036(17), Co(1)–N(4) = 1.9709(17), Co(1)–O(1) = 2.0904(15), Co(1)–[N(2), N(3), N(4)] = 0.57(2) (distance of Co from mean plane), N(2)–Co(1)–N(4) = 113.66(7), N(2)–Co(1)–N(3) = 76.84(6), N(3)–Co(1)–N(4) = 78.69(6), N(2)–Co(1)–N(1) = 83.18(7), N(4)–Co(1)–N(1) = 114.39(7), N(3)–Co(1)–N(1) = 159.44(6), N(3)–Co(1)–O(1) = 87.19(6), N(2)–Co(1)–O(1) = 107.16(6), N(4)–Co(1)–O(1) = 131.95(6), N(1)–Co(1)–O(1) = 94.18(6); **2c**, Co(1)–N(1) = 2.032(2), Co(1)–N(2) = 1.9520(19), Co(1)–N(3) = 2.471(2), Co(1)–N(4) = 1.942(2), Co(1)–O(1) = 2.062(2), N(1)–C(42) = 1.359(3), N(2)–C(41) = 1.364(3), C(41)–C(42) = 1.444(3), C(42)–C(43) = 1.425(3), C(43)–C(44) = 1.374(4), C(44)–C(45) = 1.399(4), C(45)–C(46) = 1.374(3), C(46)–C(41) = 1.420(3), N(2)–Co(1)–N(4) = 120.06(9), N(4)–Co(1)–N(1) = 114.88(9), N(2)–Co(1)–N(1) = 82.36(8), N(2)–Co(1)–O(1) = 118.91(8), N(4)–Co(1)–O(1) = 114.34(9), N(1)–Co(1)–O(1) = 98.82(8), N(3)–Co(1)–N(1) = 157.61(8), N(3)–Co(1)–N(2) = 75.27(8), N(3)–Co(1)–N(4) = 76.67(8), N(3)–Co(1)–O(1) = 92.86(8).

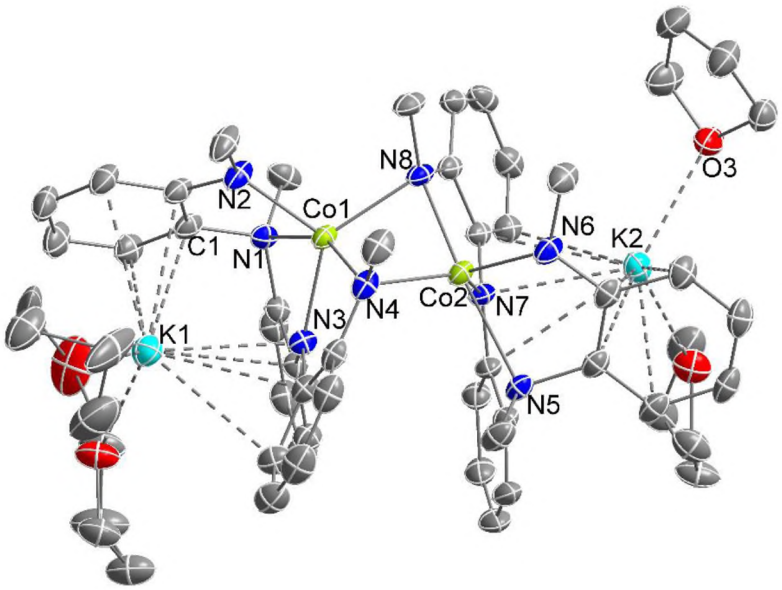

Figure S3. ORTEP diagram of $[K(THF)_2(L^{16}_{re})Co^{II}]_2$ (**16b**), drawn with 40% thermal ellipsoids. Hydrogen atoms are omitted for clarity. Selective interatomic distances (Å) and angles (°).

Co(1)–N(1) = 2.3527(17), Co(1)–N(2) = 1.9661(18), Co(1)–N(3) = 1.9840(17), Co(1)–N(4) = 2.1326(17), Co(1)–N(8) = 2.0859(18), Co(2)–N(5) = 2.3310(17), Co(2)–N(6) = 1.9680(18), Co(2)–N(7) = 1.9855(17), Co(2)–N(8) = 2.1274(17), Co(2)–N(4) = 2.0900(18), N(2)–Co(1)–N(4) = 109.55(7), N(2)–Co(1)–N(3) = 115.02(2), N(3)–Co(1)–N(4) = 79.98(7), N(2)–Co(1)–N(1) = 78.83(7), N(4)–Co(1)–N(1) = 155.56(6), N(3)–Co(1)–N(1) = 75.74(6), N(3)–Co(1)–N(8) = 132.14(7), N(2)–Co(1)–N(8) = 112.24(7), N(4)–Co(1)–N(8) = 91.39(7), N(1)–Co(1)–N(8) = 106.92(6), N(6)–Co(2)–N(7) = 114.53(8), N(6)–Co(2)–N(8) = 109.36(7), N(7)–Co(2)–N(8) = 80.07(7), N(6)–Co(2)–N(5) = 78.94(7), N(7)–Co(2)–N(5) = 76.11(6), N(8)–Co(2)–N(5) = 156.06(6), N(6)–Co(2)–N(4) = 113.06(7), N(7)–Co(2)–N(4) = 131.79(7), N(8)–Co(2)–N(4) = 91.43(7), N(5)–Co(2)–N(4) = 106.18(7).

1.5. OTHER PHYSICAL MEASUREMENTS

(a) Electrochemistry**.** Cyclic voltammetry was carried out with a Bipotentiostat AFCBP1 from Pine Instrument Company fitted in a Dry Box and controlled with the Aftermath 1.2.5876 software, or with an Eco Chemie Autolab PGSTAT100 electrochemical workstation fitted in a Dry Box and controlled with a General Purpose Electrochemical Software (GPES). Experiments were performed using a gold disk working electrode (1.6 mm diameter) and a Ag/Ag^+ (0.01 M $AgNO_3$ and 0.1 or 0.5 M (^{n}Bu$_4$N)PF_6 in acetonitrile, dimethylformamide or dimethylacetamide) non-aqueous reference electrode (Bioanalytical Systems, Inc.) with a prolonged bridge (0.5 M (^{n}Bu$_4$N)PF_6 in acetonitrile, dimethylformamide or dimethylacetamide). A thin Pt gauge (8 cm^2, Sigma-Aldrich) was employed as counter electrode. The working electrode was polished using successively 6, 3, 1 μm diamond paste on a DP-Nap polishing cloth (Struers, Westlake, OH), washed with water, acetone and air-dried. The Pt gauge electrodes were cleaned in a H_2O_2/H_2SO_4(conc) solution (1/4 v/v) and oven-dried. The concentration of the samples was 3 mM and that of (^{n}Bu$_4$N)PF_6 (supporting electrolyte) was 0.5 M. The potential sweep rate varied between 40–500 mV/s. All potentials are reported versus the ferrocenium/ferrocene (Fc^+/Fc) couple. Cyclic voltammograms of compounds **3**-**7**, **8a**, **9**, **10**, **13**, **17** are shown in Figure 6, and corresponding electrochemical data in Table S2.

Table S2. Electrochemical Data for Selected Co^{II} Compounds (first oxidation waves)

Compound	**Solvent**	$E_{1/2}$ **(or** $E_{p,a}$**)** **(V vs.** Fc^+/Fc**)**	ΔE **(mV)**
$[K(L^3)Co^{II}–NCMe]$ (**3**)[4]	MeCN	-0.090	72
$[K(L^4)Co^{II}]•Et_2O$ (**4**)	DMF	0.221	
$[K(THF)_6][(L^5)Co^{II}]•1.5THF$ (**5**)[4]	DMF	-0.258	102
$[K(MeCN)(L^6)Co^{II}–NCMe]•2MeCN$ (**6**)	DMF	0.259	
$[K_2(DMA)_4][K(L^7)_2Co^{II}_2]_2•2DMA$ (**7**)	DMF	0.172	
$[K(THF)_2(L^8)Co^{II}]$ (**8a**)[4]	DMF	0.719	
$[K_2(L^9)_2Co^{II}_2]$ (**9**)[4]	DMF	-0.654, -0.500	88, 75
$[K_2(DMA)_3(L^{10})_2Co^{II}_2]•0.5Et_2O$ (**10**)[4]	DMA	0.559	
$[K(NCMe)_3(L^{13})Co^{II}–NCMe]$ (**13**)[4]	MeCN	-0.665	78
$[K(THF)K(L^{17})_2Co^{II}_2]_2•3Pentane$ (**17**)	DMF	0.032, 0.388	

(b) EPR spectroscopy**.** X-band EPR measurements were performed with a Bruker ER 200D instrument equipped with an ESR-9 Oxford cryostat and an Anritsu microwave frequency counter, and on a Bruker EMX-Plus (X-Band, 9.2 GHz) (Dept. of Chemistry, Washington University, St. Louis). Simulations of the EPR spectra were carried out with the program SPINCOUNT kindly provided to us by Prof. M. P. Hendrich (Dept. of Chemistry, Carnegie Mellon University, Pittsburgh, PA, U.S.A.). EPR spectra of Co(II) compounds **3**-**7**, **8a**, **9**, **10**, **13**-**15** and **17** were recorded in frozen DMF solutions. EPR spectra obtained at 10 K are shown in Figure 7, and the corresponding EPR parameters are collected in Table S3.

Table S3. EPR Parameters for the Co(II) Complexes Examined

Complex	Site	E/D	$\sigma_{E/D}$[a, b]	$g_{0\perp}$[c]	$g_{0\parallel}$[c]	$A_\perp$[d] (MHz)	$A_\parallel$[e] (MHz)	R(%)[f, g]
3	1	0.048	0.015	2.19	2.03	60	290	53
	2	0.130	0.050	2.19	2.05	50	290	47
4	1	0.048	0.015	2.26	2.00	65	280	50
	2	0.129	0.025	2.35	2.00	80	320	50
5	1	0.105	0.040	2.22	2.05	75	240	100
6	1	0.070	0.025	2.185	2.10	55	200	16
	2	0.125	0.060	2.25	2.17	90	200	84
7	1	0.035	0.010	2.225	2.03	60	250	59
	2	0.120	0.055	2.250	2.00	85	270	41
8a	1	0.052	0.020	2.280	2.00	75	250	14
	2	0.190	0.070	2.260	2.00	90	290	86
9	1	0.037	0.016	2.22	2.01	40	258	100
10	1	0.030	0.010	2.25	2.03	40	226	14
	2	0.128	0.065	2.18	2.00	70	250	86
13	1	0.018	0.011	2.188	2.02	30	290	100
14	1	0.119	0.015	2.22	2.08	65	225	100
15[h]	1	0.333	0.080			n.d	n.d	100
17	1	0.041	0.020	2.22	2.03	50	250	20
	2	0.115	0.070	2.24	2.09	70	240	80

[a]Distribution parameter on *E/D* introduced in the simulations. [b]A residual linewidth σ_B of 20-30 G was used. [c]Estimated error: ±0.02. [d]Estimated error: ±20%. [e]Estimated error: ±5%. [f]Relative abundance of the species assuming equal values for $|D|$; [g]Estimated error: ±10%. [h]The spectrum was simulated with g_{0y} =2.30, $g_{0x} = g_{0z}$ =1.99.

1.6. CATALYTIC AND MECHANISTIC STUDIES

(a) General Catalytic Olefin Aziridination Procedure**.** In a typical experiment, a 20 mL screw-cap vial containing a small magnetic bar was charged in sequence with the catalyst (0.0125 mmol with respect to Co), N-(*p*-tolylsulfonyl)imido]-phenyliodinane (93.3 mg, 0.25 mmol), molecular sieves (5Å) (20 mg), olefin (2.0 mmol) and solvent (0.200 g) (chlorobenzene, unless otherwise stated). The reaction mixture was stirred vigorously at 30 °C for 24 hours (unless otherwise stated). After completion of the reaction, the products were isolated by column chromatography (silica gel) and quantified

by ^{1}H NMR (in $CDCl_3$ or CD_3CN) versus an internal standard (4′-methoxyacetophenone).

Table S4. Yields of Aziridination/Amination of Olefins by [K(L^4)Co^{II}]•Et_2O (**4**)[a]

Entry No.	Substrate	Products		Yield (%)[b] PhCl L^4Co	Yield (%)[c] PhCl L^8Co
1.		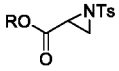	R = Me	polymer	polymer
2.			R = tBu	polymer	polymer
3.	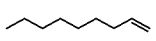	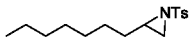		9	32
4.		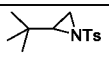		12	6
5.		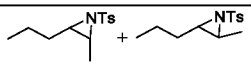		8, 17	18, 19
6.		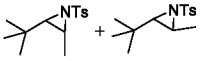		7/8	trace

[a]Conditions: **4**, 0.0125 mmol (5 mol %); PhINTs, 0.25 mmol; olefin, 2.0 mmol; MS 5 Å, 20 mg; PhCl, 0.200 g; room temperature; 24 h. [b]This work. [c]Ref. 5.

All aziridination and/or allylic/benzylic amination products (Tables 1, 2 and S4) are known compounds, and have been identified with the assistance of ^{1}H and ^{13}C NMR spectra, as well as HRMS data, by comparison to spectroscopic features reported for authentic samples in the literature.[12]

For the competitive aziridination of styrene versus 1-hexene, mediated by [K(L^4)Co^{II}]•Diethyl ether (**4**), the general aziridination procedure noted above was followed, with the exception that 1.0 mmol of each olefin was used.

(b) Evaluation of the Reaction Profile**.** The general styrene aziridination procedure was followed in the presence of catalysts [K(L^4)Co^{II}]$_n$ (**4**), [K_2(DMA)$_4$][K(L^7)$_2Co^{II}_2$]$_2$•2DMA (**7**) and [K(DMA)$_3$(L^8)Co^{II}]$_2$ (**8c**) (5 mol% with respect to Co) in chlorobenzene (0.500 g) at 30 °C. The same type and size of screw-cap vials (20 mL) and magnetic stir bars were used. The catalysts were similarly pulverized

prior to use, and the stirring speed was kept constant by the same stir plate. At predetermined time intervals, the reaction was quenched via addition of silica gel, and the mixture was subsequently chromatographed as noted above. Aziridination yields were evaluated for each datapoint by means of at least two independent experiments, following the methodology noted under the general protocol.

(c) Hammett Plots. The general aziridination of olefins was conducted mediated by [K(L^4)Co^{II}]•Diethyl ether (**4**), with the exception that the olefin mixture was composed of 1.0 mmol of styrene and 1.0 mmol of a *p*-X-styrene (X = Me, ^{t}Bu, F, Cl, CF_3, NO_2). At the end of the reaction the mixture was flash chromatographed on silica gel (hexane, then petroleum ether/ethyl acetate 10:1) in order to recover the aziridination products and evaluate their ratio by quantitative ^{1}H-NMR analysis in CD_3CN (Table S5). A linear free- energy correlation of $\log(k_X/k_H)$ as a function of polar (σ_{mb}) and spin-delocalization ($\sigma_{JJ}^{\bullet}$) parameters is shown in Figure 8.

Table S5. Competitive Aziridination Reactions of *para*-substituted Styrenes *vs.* Styrene by PhI=NTs in the presence of L^4Co (**4**) [a]

X	$\sigma_{JJ^{\bullet}}$	σ_{mb}	k_X/k_H	$A\times\sigma_{JJ}^{*} + B\times\sigma_{mb} + C$ [b]	$\log(k_X/k_H)$
F	-0.02	-0.24	1.560	0.15802	0.19312
CF_3	-0.01	0.49	0.537	-0.25706	-0.27003
H	0	0	1	0.03019	0
Me	0.15	-0.29	1.884	0.27464	0.27508
Cl	0.22	0.11	1.328	0.08054	0.12320
^{t}Bu	0.26	-0.22	1.794	0.29118	0.25382
NO_2	0.36	0.86	0.529	-0.27887	-0.27654

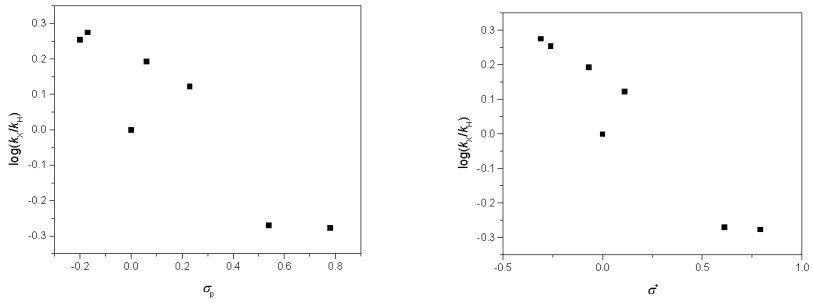

Figure S4. Free energy correlation of $\log(k_X/k_H)$ vs σ_p (left) and σ^+ (right) for the aziridination of para-substituted styrenes (X = Me, ^{t}Bu, F, Cl, CF_3, NO_2) mediated by [K(L^4)Co^{II}]•Diethyl ether (**4**).

Competitive Aziridinations of Deuterated Styrenes vs. Styrene (KIE)**.** In order to determine values of secondary deuterium kinetic isotope effects (k_H/k_D), a panel of deuterated styrenes (α-d^1-styrene, *cis*- and *trans*-β-d^1-styrene)[12] was used together with styrene (1.0 mmol each), and was subjected to aziridination (three trials) by PhI=NTs (0.25 mmol) in the presence of [K(L^4)Co^{II}]•Diethyl ether (**4**) or [K(DMA)$_3$(L^8)Co^{II}]$_2$ (**8c**) (5 mol%) and molecular sieves (5Å, 25 mg) in chlorobenzene (0.500 g), according to the general olefin aziridination procedure noted above. Prior to mixing with any other reagents, an aliquot (5.0 μl) of the original mixture of styrenes was retained for ^{1}H-NMR analysis ($CDCl_3$, 120 s relaxation delay). The reaction was quenched after two hours, and the mixture was flash chromatographed on silica gel, first with hexane to remove the styrenes, and then with petroleum ether/ethyl acetate (10: 1 v/v) to recover the aziridination products. The ratio of d^0/d^1 aziridines is evaluated by ^{1}H NMR (CD_3CN, 120 s relaxation delay) and compared to the ratio of the starting d^0/d^1 styrenes in order to extract secondary KIE values (Table 3).

(e) Stereochemical Scrambling in Aziridinations of Deuterated Styrenes. The aziridination of *cis*- and *trans*-β-d^1-styrene (synthesized by following a literature

report),[13] mediated by [K(L^4)Co^{II}]•Diethyl ether (**4**) or [K(DMA)$_3$(L^8)Co^{II}]$_2$ (**8c**), was conducted according to the general procedure for olefin aziridinations. The isolated aziridines were dissolved in $CHCl_3$ (700 μL)/$CDCl_3$(20 μL) and loaded in a precision NMR tube. Extensive ^2H NMR data were collected (90 s relaxation delay) for three independent reaction trials, in order to quantify the relative deuterium content at the *cis* and *trans* β-carbon sites of the aziridination products (Table 4).

1.7. COMPUTATIONAL STUDIES

Density functional theory employing the B3LYP[14] functional along with the 6-31+G(d) basis set is used in the Gaussian09[15] software package for all reported calculations. Previous calculations on similar Mn(II), Fe(II) and Co(II) complexes have indicated the accuracy of the calculation with this level of theory.[5] All calculations were done assuming 1 atm and 298.15 K and all possible spin states were evaluated. Optimized geometries for the three spin states of [L^4Co]NTs (doublet, quarter, sextet) are shown in Table S6, and have also been deposited as .xyz files. DFT structures for [L^4Co]NTs in three spin states, optimized at the B3LYP/6-31+G(d) level of theory, are shown in Figure 9. Spin densities on the calculated lowest-energy spin state of the putative cobalt nitrenoid intermediates for quartet [L^4Co]NTs and sextet [L^8Co]NTs are shown in Figure 10.

Table S6. Optimized Geometries for Three Spin States of [L^{4}Co]NTs. First Column is Atomic Number. Columns 2 - 4 are Cartesian Coordinates (in Å).

Doublet [L^{4}Co]NTs

27	0.658143000	-1.046889000	0.126397000
7	2.060378000	1.555907000	-0.295306000
7	1.486678000	-0.926806000	-1.621855000
7	-0.536102000	2.823858000	-0.367141000
7	1.921656000	-0.531054000	1.623195000
7	-1.231125000	-1.069420000	0.144744000
6	1.210895000	2.763181000	-3.725168000
1	1.152852000	3.707546000	-4.260454000
6	0.894547000	1.555822000	-4.362255000
1	0.577941000	1.550052000	-5.402796000
6	0.992379000	0.355632000	-3.667736000
1	0.762196000	-0.578907000	-4.164907000
6	1.391734000	0.311523000	-2.317466000

Table S7. Optimized Geometries for Three Spin States of [L^{4}Co]NTs. First Column is Atomic Number. Columns 2 - 4 are Cartesian Coordinates (in Å) (cont.)

6	1.660045000	1.541845000	-1.674035000
6	1.593553000	2.747336000	-2.390047000
1	1.823527000	3.676448000	-1.877308000
6	1.664819000	2.537768000	0.610533000
6	0.375216000	3.222553000	0.518587000
6	0.107492000	4.269993000	1.472012000
1	-0.828386000	4.806056000	1.365624000

Table S8. Optimized Geometries for Three Spin States of [L^{4}Co]NTs. First Column is Atomic Number. Columns 2 - 4 are Cartesian Coordinates (in Å)

6	0.975711000	4.572453000	2.491585000
1	0.729213000	5.351006000	3.209587000
6	2.190342000	3.855581000	2.604963000
1	2.882209000	4.074699000	3.414032000
6	2.520895000	2.875386000	1.685912000
1	3.459770000	2.348914000	1.797713000
6	3.234331000	0.772546000	0.016342000
6	3.165811000	-0.220670000	1.014591000
6	4.345193000	-0.931397000	1.306113000
1	4.313299000	-1.686037000	2.084533000
6	5.531252000	-0.681332000	0.619025000
1	6.423805000	-1.252889000	0.864425000
6	5.573210000	0.288185000	-0.390173000
1	6.490864000	0.475569000	-0.941843000
6	4.420078000	1.011983000	-0.686711000

Table S9. Optimized Geometries for Three Spin States of [L^{4}Co]NTs. First Column is Atomic Number. Columns 2 - 4 are Cartesian Coordinates (in Å) (cont.)

1	4.423486000	1.765594000	-1.469126000
6	0.607292000	-0.906156000	3.741228000
6	-2.919139000	2.835129000	-1.007241000
6	2.176218000	-3.372963000	-1.674007000
8	-2.024453000	-2.720224000	-1.604937000
8	-1.909591000	-3.422041000	0.844470000
6	-3.866298000	-1.852994000	0.066818000
6	-4.659053000	-1.548606000	-1.038434000

Table S10. Optimized Geometries for Three Spin States of [L^4Co]NTs. First Column is Atomic Number. Columns 2 - 4 are Cartesian Coordinates (in Å) .

6	-5.984406000	-1.146529000	-0.843496000
1	-4.241627000	-1.636131000	-2.036248000
6	-5.710263000	-1.356096000	1.539782000
1	-3.768384000	-2.018063000	2.213714000
6	-6.529425000	-1.039337000	0.442514000
1	-6.602086000	-0.913131000	-1.708583000
1	-6.114211000	-1.286771000	2.548356000
6	-7.959928000	-0.596382000	0.653933000
1	-8.005419000	0.359871000	1.191862000
1	-8.482603000	-0.466031000	-0.299876000
1	-8.522266000	-1.328163000	1.248232000
16	-2.151389000	-2.367528000	-0.171112000
6	-1.597307000	3.595513000	-0.781657000

Table S11. Optimized Geometries for Three Spin States of [L^4Co]NTs. First Column is Atomic Number. Columns 2 - 4 are Cartesian Coordinates (in Å) (cont.)

8	-1.480541000	4.796192000	-1.056195000
6	1.911029000	-0.503742000	2.995723000
8	2.896197000	-0.152479000	3.666774000
6	2.183641000	-1.933212000	-2.262860000
8	2.797010000	-1.762265000	-3.323433000
6	-3.305516000	2.099883000	0.294557000
1	-3.434345000	2.807012000	1.125473000
1	-4.254682000	1.567141000	0.155915000
1	-2.546928000	1.363782000	0.574302000
6	-4.023871000	3.830848000	-1.397130000

Table S12. Optimized Geometries for Three Spin States of [L^4Co]NTs. First Column is Atomic Number. Columns 2 - 4 are Cartesian Coordinates (in Å)

1	-4.182844000	4.581446000	-0.614075000
1	-3.771221000	4.366594000	-2.317893000
6	-2.717176000	1.808268000	-2.145041000
1	-2.404307000	2.304185000	-3.071926000
1	-1.959413000	1.067160000	-1.880579000
1	-3.661882000	1.283443000	-2.338921000
6	1.216115000	-4.202173000	-2.562455000
1	1.533245000	-4.158070000	-3.609914000
1	1.224672000	-5.252675000	-2.240826000
1	0.186736000	-3.834403000	-2.489418000
6	1.732575000	-3.490307000	-0.209798000

Table S13. Optimized Geometries for Three Spin States of [L^4Co]NTs. First Column is Atomic Number. Columns 2 - 4 are Cartesian Coordinates (in Å) (cont.)

1	2.383764000	-2.930019000	0.468218000
1	0.678567000	-3.206044000	-0.058206000
1	1.766869000	-4.540341000	0.109253000
6	3.607054000	-3.940525000	-1.793846000
1	3.621619000	-4.988378000	-1.464830000
1	3.956662000	-3.887547000	-2.827992000
1	4.309592000	-3.375400000	-1.169058000
6	0.230939000	-2.366665000	3.415467000
1	1.057827000	-3.045592000	3.662156000
1	-0.640642000	-2.671203000	4.010480000
1	-0.035074000	-2.519399000	2.367758000
6	0.856820000	-0.798310000	5.258789000

Table S14. Optimized Geometries for Three Spin States of [L^4Co]NTs. First Column is Atomic Number. Columns 2 - 4 are Cartesian Coordinates (in Å).

1	1.667642000	-1.460357000	5.579619000
1	1.134930000	0.220418000	5.546149000
6	-0.546237000	0.052323000	3.372381000
1	-0.274124000	1.091474000	3.594945000
1	-0.823513000	-0.008222000	2.317692000
1	-1.438326000	-0.196661000	3.964255000

Quartet [L^4Co]NTS

27	0.801160000	-0.723918000	0.309227000
7	1.487775000	1.153672000	-1.072744000
7	2.726341000	-0.449745000	0.830843000
7	0.446853000	-1.376668000	-1.541945000
7	-0.837399000	2.774513000	-0.388283000
7	-0.715532000	-0.551707000	1.247795000
6	4.572730000	0.087607000	-2.948195000
1	5.017538000	0.219728000	-3.931078000
6	5.201601000	-0.703355000	-1.979286000
1	6.146643000	-1.192680000	-2.204781000
6	4.624154000	-0.877119000	-0.723940000
1	5.116854000	-1.482984000	0.026909000
6	3.397501000	-0.265455000	-0.398799000
6	2.777170000	0.523010000	-1.387760000
6	3.356283000	0.698159000	-2.646986000
1	2.842884000	1.298855000	-3.390947000

Table S15. Optimized Geometries for Three Spin States of [L^4Co]NTs. First Column is Atomic Number. Columns 2 - 4 are Cartesian Coordinates (in Å).

6	0.534792000	0.983292000	-2.160952000
6	0.045686000	-0.321110000	-2.399600000
6	-0.861614000	-0.481412000	-3.468315000
1	-1.261195000	-1.466416000	-3.667365000
6	-1.231288000	0.592886000	-4.272948000
1	-1.937109000	0.431429000	-5.084909000

Table S16. Optimized Geometries for Three Spin States of [L^4Co]NTs. First Column is Atomic Number. Columns 2 - 4 are Cartesian Coordinates (in Å).

6	-0.693772000	1.865886000	-4.051037000
1	-0.966093000	2.706399000	-4.683990000
6	0.192719000	2.051798000	-2.994192000
1	0.603786000	3.036921000	-2.796917000
6	1.557822000	2.366548000	-0.332888000
6	0.381238000	3.170021000	-0.020171000
6	0.576988000	4.381234000	0.734577000
1	-0.301236000	4.983497000	0.936097000
6	1.809725000	4.763919000	1.206063000
1	1.916727000	5.671547000	1.794512000
6	2.931172000	3.959661000	0.919095000
1	3.915923000	4.238127000	1.284851000
6	2.800737000	2.800344000	0.163508000
1	3.688950000	2.216672000	-0.036277000
6	-3.262576000	3.132415000	-0.020675000
6	0.947759000	-3.840517000	-1.177971000

Table S17. Optimized Geometries for Three Spin States of [L^4Co]NTs. First Column is Atomic Number. Columns 2 - 4 are Cartesian Coordinates (in Å).

8	-2.143200000	-0.005332000	3.281162000
6	-3.319753000	-1.385278000	1.370884000
6	-3.261592000	-1.906999000	0.075857000
6	-4.551564000	-1.180046000	1.992177000

Table S18. Optimized Geometries for Three Spin States of [L^4Co]NTs. First Column is Atomic Number. Columns 2 - 4 are Cartesian Coordinates (in Å) (cont.)

6	-4.443476000	-2.226195000	-0.591599000
1	-2.300715000	-2.036548000	-0.412629000
6	-5.729245000	-1.506041000	1.312141000
1	-4.583208000	-0.761463000	2.993321000
6	-5.696019000	-2.033857000	0.014316000
1	-4.390988000	-2.623575000	-1.603674000
1	-6.688745000	-1.342646000	1.799779000
6	-6.969616000	-2.374240000	-0.727287000
1	-7.109886000	-1.721934000	-1.599674000
1	-6.953820000	-3.407554000	-1.096962000
1	-7.848999000	-2.261540000	-0.083387000
16	-1.797303000	-1.056984000	2.297753000
6	0.622707000	-2.624942000	-2.094629000
8	0.536047000	-2.862005000	-3.308701000
6	-1.906252000	3.637025000	-0.539554000
8	-1.787800000	4.702762000	-1.153107000
6	3.478340000	-0.283522000	1.974955000
8	4.670078000	0.061898000	1.940641000
6	-0.195132000	-4.864955000	-1.374710000

Table S19. Optimized Geometries for Three Spin States of [L^4Co]NTs. First Column is Atomic Number. Columns 2 - 4 are Cartesian Coordinates (in Å).

1	0.025426000	-5.784577000	-0.816510000
1	-1.149821000	-4.472051000	-1.002275000
6	2.271263000	-4.454872000	-1.689446000
1	2.503578000	-5.368655000	-1.125880000
1	2.194501000	-4.703383000	-2.751872000
1	3.106394000	-3.755158000	-1.561341000
6	1.085418000	-3.538162000	0.317693000
1	1.933160000	-2.874588000	0.524665000
1	0.168892000	-3.126931000	0.756912000
1	1.287767000	-4.465871000	0.869907000
6	2.107661000	-1.866689000	3.447585000
1	2.812944000	-2.677189000	3.220566000
1	1.731478000	-2.023494000	4.466581000
1	1.247473000	-1.958596000	2.784006000
6	1.780734000	0.643693000	3.608969000
1	2.271402000	1.623580000	3.551577000
1	0.954166000	0.626917000	2.895725000
1	1.347902000	0.537610000	4.612187000
6	3.886120000	-0.422711000	4.447747000
1	3.418629000	-0.554224000	5.432598000
1	4.639170000	-1.207655000	4.314398000
1	4.409272000	0.537936000	4.432486000
6	-3.162463000	2.936735000	1.509016000
1	-2.929018000	3.884266000	2.013521000

Table S20. Optimized Geometries for Three Spin States of [L^{4}Co]NTs. First Column is Atomic Number. Columns 2 - 4 are Cartesian Coordinates (in Å)

1	-4.122493000	2.578179000	1.900687000
1	-2.402497000	2.200966000	1.784793000
6	-4.352679000	4.167121000	-0.344450000
1	-5.319650000	3.809389000	0.032535000
1	-4.138784000	5.136399000	0.119782000
1	-4.439394000	4.331622000	-1.423697000
6	-3.595419000	1.788310000	-0.704422000
1	-3.668477000	1.908972000	-1.792270000
1	-2.829344000	1.038911000	-0.497398000
1	-4.557160000	1.411602000	-0.333983000

Sextet [L^{4}Co]NTs

Table S21. Optimized Geometries for Three Spin States of [L^{4}Co]NTs. First Column is Atomic Number. Columns 2 - 4 are Cartesian Coordinates (in Å).

27	0.555034000	-0.882148000	-0.313099000
7	2.074087000	0.960258000	0.790510000
7	1.877314000	-0.347048000	-1.679871000
7	-0.292756000	2.572647000	0.576730000
7	1.273924000	-1.637432000	1.437541000
7	-1.197928000	-0.669263000	-0.660326000
6	2.952484000	3.769706000	-1.522466000
1	3.239777000	4.816994000	-1.465817000
6	2.849206000	3.120137000	-2.758247000
1	3.041473000	3.664357000	-3.680152000

Table S22. Optimized Geometries for Three Spin States of [L^4Co]NTs. First Column is Atomic Number. Columns 2 - 4 are Cartesian Coordinates (in Å).

6	2.500048000	1.773871000	-2.822315000
1	2.430642000	1.281447000	-3.782771000
6	2.238825000	1.024003000	-1.657023000
6	2.308030000	1.708168000	-0.421856000
6	2.677516000	3.056118000	-0.359009000
1	2.743300000	3.538262000	0.612875000
6	1.453177000	1.554955000	1.907694000
6	0.240485000	2.360660000	1.777552000
6	-0.325738000	2.910482000	2.983693000
1	-1.224117000	3.508762000	2.884466000
6	0.210716000	2.661647000	4.225539000
1	-0.251985000	3.080375000	5.115834000
6	1.357051000	1.846880000	4.333703000
1	1.787762000	1.633024000	5.308352000
6	1.956985000	1.314277000	3.197775000
1	2.835124000	0.690930000	3.310858000
6	3.082520000	-0.052965000	1.056263000
6	2.657679000	-1.346393000	1.425948000
6	3.653999000	-2.310948000	1.677443000
1	3.346381000	-3.307886000	1.970344000
6	5.006055000	-2.001053000	1.554091000
1	5.750640000	-2.770573000	1.746681000
6	5.408833000	-0.715027000	1.172748000
1	6.462903000	-0.473279000	1.062486000

Table S23. Optimized Geometries for Three Spin States of [L^4Co]NTs. First Column is Atomic Number. Columns 2 - 4 are Cartesian Coordinates (in Å).

6	4.440492000	0.255208000	0.922539000
1	4.727950000	1.254454000	0.609417000
6	-0.698499000	-2.706885000	2.600250000
6	-1.640863000	4.290475000	-0.600417000
6	2.061476000	-2.630708000	-2.779806000
8	-2.348730000	0.896654000	-2.309558000
8	-2.044987000	-1.563190000	-2.862251000
6	-3.865713000	-0.873149000	-1.080500000
6	-4.397019000	0.011065000	-0.134187000
6	-4.554263000	-2.031096000	-1.437653000
6	-5.628711000	-0.280596000	0.449419000
1	-3.854233000	0.909065000	0.147701000
6	-5.790747000	-2.306587000	-0.842777000
1	-4.125020000	-2.700582000	-2.176203000
6	-6.345420000	-1.440850000	0.108068000
1	-6.038995000	0.407241000	1.186976000
1	-6.328602000	-3.210000000	-1.125152000
6	-7.678593000	-1.739495000	0.757579000
1	-8.130369000	-2.647927000	0.343510000
1	-7.571816000	-1.884197000	1.841018000
1	-8.389131000	-0.915252000	0.611777000
16	-2.268557000	-0.505153000	-1.843330000
6	-1.556375000	3.105070000	0.383908000
8	-2.556030000	2.631585000	0.926994000

Table S24. Optimized Geometries for Three Spin States of [L^4Co]NTs. First Column is Atomic Number. Columns 2 - 4 are Cartesian Coordinates (in Å).

6	0.801363000	-2.298803000	2.547042000
8	1.519807000	-2.558341000	3.527096000
6	2.521217000	-1.156136000	-2.594114000
8	3.455993000	-0.772993000	-3.310199000
6	-3.116669000	4.647973000	-0.840613000
1	-3.629866000	4.903313000	0.093174000
1	-3.178323000	5.509836000	-1.518221000
1	-3.650802000	3.809599000	-1.298408000
6	-0.909238000	5.491157000	0.047264000
1	-0.956515000	6.357392000	-0.625477000
1	-1.372184000	5.780946000	1.000206000
1	0.146678000	5.263767000	0.229996000
6	-0.963765000	3.933758000	-1.941017000
1	0.097616000	3.715370000	-1.806213000
1	-1.434845000	3.058734000	-2.396680000
1	-1.057444000	4.785626000	-2.629340000
6	1.398682000	-2.709643000	-4.176932000
1	2.087659000	-2.351648000	-4.948803000
1	1.129119000	-3.750350000	-4.403440000
1	0.481170000	-2.111197000	-4.213187000
6	1.070700000	-3.155971000	-1.734653000
1	1.486914000	-3.133863000	-0.720286000
1	0.108720000	-2.627748000	-1.777618000
1	0.827796000	-4.206765000	-1.943487000

Table S25. Optimized Geometries for Three Spin States of [L^4Co]NTs. First Column is Atomic Number. Columns 2 - 4 are Cartesian Coordinates (in Å)..

6	3.325157000	-3.518819000	-2.756739000
1	3.053521000	-4.561173000	-2.971796000
1	4.048890000	-3.178945000	-3.502281000
1	3.810452000	-3.489344000	-1.772949000
6	-1.108400000	-3.532832000	1.362902000
1	-0.456519000	-4.407785000	1.239668000
1	-2.137745000	-3.895640000	1.486648000
1	-1.083139000	-2.946310000	0.443587000
6	-0.921474000	-3.577081000	3.853759000
1	-1.980690000	-3.861908000	3.914047000
1	-0.317902000	-4.491181000	3.820718000
1	-0.649485000	-3.039574000	4.766795000
6	-1.577312000	-1.440921000	2.722668000
1	-1.288402000	-0.854257000	3.603714000
1	-1.509202000	-0.802919000	1.840073000
1	-2.630469000	-1.730484000	2.840407000

REFERENCES

(1) Çelenligil-Çetin, R.; Paraskevopoulou, P.; Dinda, R.; Staples, R. J.; Sinn, E.; Rath, N. P.; Stavropoulos, P. Synthesis, Characterization, and Reactivity of Iron Trisamidoamine Complexes that Undergo both Metal- and Ligand-Centered Oxidative Transformation. *Inorg. Chem.* **2008**, *47*, 1165-1172.

(2) Paraskevopoulou, P.; Ai, L.; Wang, Q.; Pinnapareddy, D.; Acharrya, R.; Dinda, R.; Çelenligil-Çetin, R.; Floros, G.; Sanakis, Y.; Choudhury, A.; Rath, N. P.; Stavropoulos, P. Synthesis and Characterization of a Series of Structurally and Electronically Diverse Fe(II) Complexes Featuring a Family of Triphenylamido-amine Ligands. *Inorg. Chem.* **2010**, *49*, 108-122.

(3) Jones, M. B.; MacBeth, C. E. Tripodal Phenylamine-Based Ligands and Their Co^{II} Complexes. *Inorg. Chem.* **2007**, *46*, 8117-8119.

(4) Bagchi, V.; Raptopoulos, G.; Das, P.; Christodoulou, S.; Wang, Q.; Ai, L.; Choudhury, A.; Pitsikalis, M.; Paraskevopoulou, P.; Stavropoulos, P. Synthesis and characterization of a family of Co(II) triphenylamido-amine complexes and catalytic activity in controlled radical polymerization of olefins. *Polyhedron* **2013**, *52*, 78-90.

(5) Bagchi, V.; Kalra, A.; Das, P.; Paraskevopoulou, P.; Gorla, S.; Ai, L.; Wang, Q.; Mohapatra, S.; Choudhury, A.; Sun, Z.; Cundari, T. R.; Stavropoulos, P. Comparative Nitrene-Transfer Chemistry to Olefinic Substrates Mediated by a Library of Anionic Mn(II) Triphenylamido-Amine Reagents and M(II) Congeners (M = Fe, Co, Ni) Favoring Aromatic over Aliphatic Alkenes. *ACS Catal.* **2018**, *8*, 9183-9206.

(6) Bruker's APEX3, SAINT and SHELXTL. **2017**, Bruker AXS Inc., Madison, Wisconsin, USA.

(7) Bruker's SMART **2002**, Bruker AXS Inc., Madison, Wisconsin, USA.

(8) Bruker's SAINT, SADABS, SHELXTL-PLUS, **2008**, Bruker AXS Inc., Madison, Wisconsin, USA.

(9) Sheldrick, G. M. A short history of SHELX, *Acta Cryst.* **2008**, *A64*, 112.

(10) Spek, A. L. PLATON SQUEEZE: a tool for the calculation of the disordered solvent contribution to the calculated structure factors, Acta Cryst, 2015, C71, 9-18.

(11) Sheldrick, G.M.; Hubshle, C. B.; Dittrich, B. Shelxle: A Qt graphical user interface for SHELXL, *J. Appl. Cryst.* **2011**, *44*, 1281-1284.

(12) Bagchi, V.; Paraskevopoulou, P.; Das, P.; Chi, L.; Wang, Q.; Choudhury, A.; Mathieson, J. S.; Cronin, L.; Pardue, D. B.; Cundari, T. R.; Mitrikas, G.; Sanakis, Y.; Stavropoulos, P. A Versatile Tripodal Cu(I) Reagent for C−N Bond Construction via Nitrene-Transfer Chemistry: Catalytic Perspectives and Mechanistic Insights on C−H Aminations/Amidinations and Olefin Aziridinations. *J. Am. Chem. Soc.* **2014**, *136*, 11362–11381.

(13) Peng, T.-S.; Gladysz, J. A. Mechanism of Equilibration of Diastereomeric Chiral Rhenium Alkene Complexes of the Formula [(η^5-C_5H_5)Re(NO)(PPh_3)(H_2C=CHR)]$^+BF_4^-$. The Metal Traverses between Alkene Enantiofaces without Dissociation! *J. Am. Chem. Soc.* **1992**, *114*, 4174-4181.

(14) Stephens, P. J.; Devlin, F. J.; Chabalowski, C. F.; Frisch, M. J. Ab Initio Calculation of Vibrational Absorption and Circular Dichroism Spectra Using Density Functional Force Fields. *J. Phys. Chem.* **1994**, 98, 11623-11627.

(15) Frisch, M. J.; Trucks, G. W.; Schlegel, H. B.; Scuseria, G. E.; Cheeseman, J. R.; Scalmani, G.; Barone, V.; Mennucci, B.; Petersson, G. A.; Nakatsuji, H.; Caricato, M.; Li, X.; Hratchian, H. P.; Izmaylov, A. F.; Bloino, J.; Zheng, G.; Sonnenberg, J. L.; Hada, M.; Ehara, M.; Toyota, K.; Fukuda, R.; Hasegawa, J.; Ishida, M.; Nakajima, T.; Honda, Y.; Kitao, O.; Nakai, H.; Vreven, T.; Montgomery, J. A. J.; Peralta, J. E.; Ogliaro, F.; Bearpark, M.; Heyd, J. J.; Brothers, E.; Kudin, K. N.; Staroverov, V. N.; Kobayashi, R.; Normand, J.; Raghavachari, K.; Rendell, A.; Burant, J. C.; Iyengar, S. S.; Tomasi, J.; Cossi, M.; Rega, N.; Millam, J. M.; Klene, M.; Knox, J. E.; Cross, J. B.; Bakken, V.; Adamo, C.; Jaramillo, J.; Gomperts, R.; Stratmann, R. E.; Yazyev, O.; Austin, A. J.; Cammi, R.; Pomelli, C.; Ochterski, J. W.; Martin, R. L.; Morukuma, K.; Zakrzewski, V. G.; Voth, G. A.; Salvador, P.; Dannenberg, J. J.; Dapprich, S.; Daniels, A. D.; Farkas, O.; Foresman, J. B.; Ortiz, J. V.; Ciolowski, J.; Fox, D. J. Gaussian 09, B.01; Gaussian, Inc.: Wallingford, CT, 2009.

APPENDIX C.

STUDIES DIRECTED TOWARDS THE INTERMOLECULAR AZIRIDINATION OF ALKENES CATALYZED BY METAL REAGENTS (Cu, Ag) SUPPORTED BY BULKY LIGANDS WITH A CHIRAL FRAMEWORK

1. EXPERIMENTAL SECTION

1.1. GENERAL CONSIDERATIONS

All operations were performed under anaerobic conditions under a pure dinitrogen atmosphere using Schlenk techniques on an inert gas/vacuum manifold or in a dry-box (O_2, H_2O < 1 ppm). Anhydrous diethyl ether, methylene chloride, acetonitrile, tetrahydrofuran, hexane, pentane, benzene, toluene, dimethylformamide and dimethylacetamide were purchased from Sigma-Aldrich (Millipore). Solvents were degassed by three freeze-pump-thaw cycles. Unless otherwise noted, all other reagents were purchased at the highest purity available. ^{1}H and ^{13}C NMR spectra were recorded on Varian XL-400, Varian INOVA/ UNITY 400 MHz Unity Plus (Missouri S&T),. IR spectra were obtained on a Perkin-Elmer 883 IR spectrometer and FT-IR spectra on Nicolet Nexus 470 and 670, Magna 750 FT-IR ESP and Shimadzu IR-Affinity-1 spectrometers. UV-vis spectra were obtained on a Hewlett-Packard 8452A diode array, Varian Cary 50 and Varian Cary 300 spectrophotometers. EI and FAB mass spectra were obtained on a Finnigan MAT-90 mass spectrometer. Elemental analysis were conducted at Galbraith laboratories.

1.2. X-RAY CRYSTALLOGRAPHY

Intensity data sets for all the compounds were collected on a Bruker Smart Apex diffractometer using graphite monochromated Mo Kα radiation (λ = 0.71073 Å) from a fine focus sealed tube X-ray source. Suitable crystals were selected and mounted on a glass fiber using super glue. The data were collected at low temperatures (140–150 K) and room temperature for metal complexes and purely organic compounds, respectively,

employing a scan of 0.3° in ω with an exposure time of 20 s/frame using SMART software.1 The cell refinement and data reduction were carried out with SAINT2 while the program SADABS was used for the absorption correction. The structures were solved by direct methods using SHELXS-973 and difference Fourier syntheses. Full-matrix least-squares refinement against |F2 | was carried out using the SHELXTL-PLUS3 suite of programs. All non-hydrogen atoms were refined anisotropically. Hydrogen atoms were placed geometrically and held in the riding mode during the final refinement.

1.3. SYNTHESIS OF TRIPODAL LIGANDS

Synthesis of (4R, 5R)-1,3-dimethyl-4,5-diphenylimidazolidin-2-imine-trphen ($DMDPI_3$- trphen) **(4).**

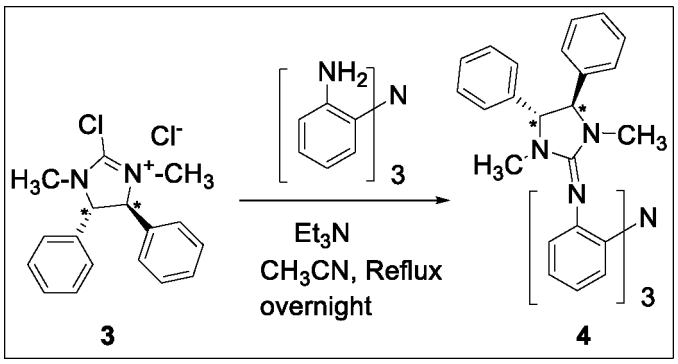

Scheme S1. Synthesis of $DMDPI_3$- trphen

(4R,5R)-2-chloro-1,3-dimethyl-4,5-diphenyl-4,5-dihydro-1H-imidazol-3-ium chloride (**3**) was prepared according to the literature protocol[1].

Compound **3** (0.995 g, 3.0 mmol) was dissolved in anhydrous acetonitrile (30.0 mL) in a Schlenk flask inside an inert atmosphere glove box. In another Schlenk flask, $(2\text{-}NH_2\text{-}C_6H_4)_3N$ (0.3g, 1.0 mmol) and triethylamine (0.432 mL, 3.0 mmol) were dissolved in a minimum amount of acetonitrile (15.0 mL). Both flasks were brought

outside the glove box with a sealed septum and were connected to a gas- vacuum Schlenk line under nitrogen. The flask containing $(2\text{-}NH_2\text{-}C_6H_4)_3N$ was cooled to 0 ^oC and then **3** was added to it slowly over a period of time via canula. The mixture was then refluxed overnight to produce a clear solution. The acetonitrile was evaporated under vacuum. The resulting solid was dissolved in dichloromethane (60.0 mL) and then washed first with a solution of 5% HCl (30.0 mL) and then with 50 % NaOH (50.0 mL). The solvent was removed under reduced pressure and the crude residue was purified by silica column chromatography with hexane/ethyl acetate (50:50 v/v) followed by $MeOH/CH_2Cl_2$ (1−5%) to give the product **4** in the form of a whitish solid which was further recrystallized from acetonitrile and diethyl ether carefully layered over the MeCN solution. (0.725 g, 70 %).^{1}H-NMR ($CDCl_3$, 7.26 ppm): δ 7.30- 7.28 (m, 6H, aryl), 7.10-7.07 (m, 4H, aryl), 6.96-6.94 (dd, 2H, aryl), 6.77-6.75 (td, 2H, aryl), 3.81 (br s, 2H, CH of the cyclic ring), 2.26 (br s, 6H, Me). ^{13}C NMR ($CDCl_3$, 77.16 ppm): δ 171.0, 128.8, 128.4, 128.7, 127.4, 127.2, 60.3, 21.0. IR (KBr, cm^{-1}): ν 3085, 3002, 2963, 2876, 2747, 1610, 1589, 1435, 1355, 1279, 1128, 1019, 836, 725.

Synthesis of 1,3-dimethyl-d_3--4,5-diphenylimidazolidin-2-imine-trphen (d-$DMDPI_3$-trphen) **(7).** The ligand was synthesized exactly in the same manner as the procedure described above for the synthesis of the ligand **4** , with the exception that the source of alkylating agent is deuterated iodomethane (CD_3I), as detailed below.

The synthesis of (4R,5R)-1,3-bis(methyl-d_3)-4,5-diphenylimidazolidin-2-one **(5)**. (4R,5R)-4,5-Diphenylimidazolidin-2-one (**1**) was synthesized [1]according to the literature protocol. The white solid obtained of **1** (3.0 g, 12.6 mmol) was dissolved in THF (60.0 mL) and sodium hydride was added (0.907g, 37.8mmol) to this solution.

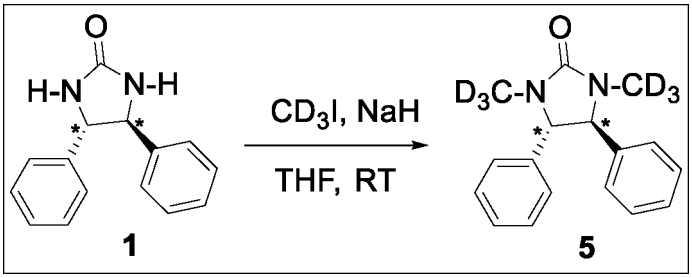

Scheme S2. Synthesis of deuterated urea.

The reaction was allowed to stir at room temperature for 30 min. CD_3I (2.9 mL, 46.6 mmol) was slowly added to the reaction mixture at 0 °C and allowed to stir at room temperature overnight. The resulting mixture was passed through a short column packed with celite.The solvent was then evaporated under reduced pressure and purified by silica column chromatography with hexane/ethyl acetate (70:30, v/v) to give (4R,5R)-1,3-bis(methyl-d_3)-4,5-diphenylimidazolidin-2-one (**5**) as a white solid (2.75 g, 80%). ^{1}H-NMR ($CDCl_3$, 7.26 ppm): δ 7.36- 7.33 (m, 6H, aryl), 7.15- 7.12 (m, 4H, aryl), 4.08 (s, 2H, CH of the cyclic ring).

Synthesis of (4R,5R)-2-chloro-1,3-bis(methyl-d_3)-4,5-diphenyl-4,5-dihydro-1H-imidazol-3-ium chloride **(6)** The urea (1.0 g, 3.6 mmol) (**5**) was dissolved in a minimum amount of toluene (15.0 mL) in a Schlenk flask. The flask was cooled to 0 ^{o}C, and then oxalyl chloride (1.5 mL, 18 mmol) was added. The reaction mixture was then refluxed for 24 h to afford a white solid. The solid was filtered and washed with diethyl ether under inert atmosphere to afford (4R,5R)-2-chloro-1,3-bis(methyl-d_3)-4,5-diphenyl-4,5-dihydro-1H-imidazol-3-ium chloride **(6)** as pure white solid (1.0 g, 83%). ^{1}H-NMR ($CDCl_3$, 7.26 ppm): δ 7.43- 7.41 (m, 6H, aryl), 7.27- 7.25 (m, 4H, aryl), 5.14 (s, 2H, CH of the cyclic ring).

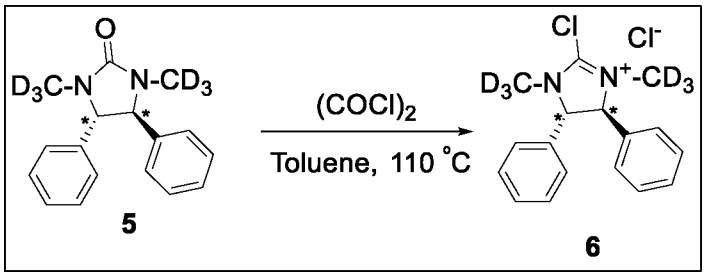

Scheme S3. Synthesis of deuterated chloro salt.

Synthesis of 1,3-dimethyl-d_3--4,5-diphenylimidazolidin-2-imine- trphen (d-DMDPI$_3$-trphen**) (7).**

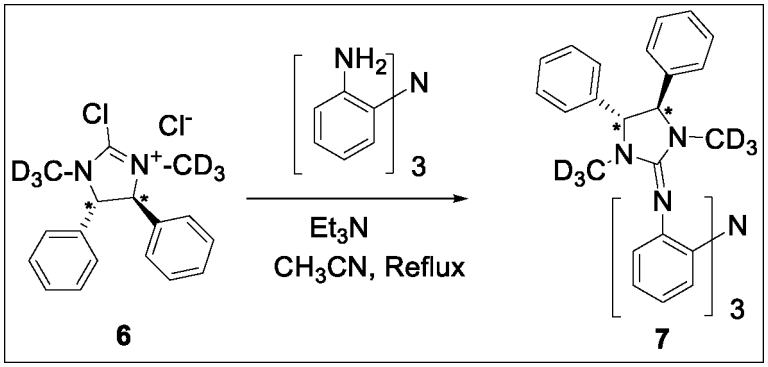

Scheme S4. Synthesis of (d-DMDPI$_3$-trphen).

Compound **6** (0.985 g, 3.0 mmol) was dissolved in anhydrous acetonitrile (30.0 mL) in a Schlenk flask inside an inert atmosphere glove box. In another Schlenk flask, (2-NH_2-C_6H_4)$_3$N (0.3g, 1.0 mmol) and triethylamine (0.432 mL, 3.0 mmol) were dissolved in a minimum amount of acetonitrile (15.0 mL). Both flasks were brought outside the glove box with a sealed septum and were connected to a gas-vacuum Schlenk line under nitrogen. The flask containing (2-NH_2-C_6H_4)$_3$N was cooled to 0 ^{o}C, and then the MeCN solution of **6** was added to it slowly over a period of time via canula. The mixture was then refluxed overnight to produce a clear solution. The acetonitrile was evaporated under vacuum. The resulting solid was dissolved in dichloromethane (60.0

mL) and washed first with a solution of 5% HCl (30.0 mL) and then with 50 % NaOH (50.0 mL). The solvent was removed under reduced pressure and the crude residue was purified by silica column chromatography with hexane/ethyl acetate (50:50 v/v) followed by MeOH/CH_2Cl_2 (1−5%) to give the product d-DMDPI$_3$-trphen **(7)** in the form of a white solid (0.685 g, 65%).^{1}H-NMR ($CDCl_3$, 7.26 ppm): δ 7.32- 7.30 (m, 6H, aryl), 7.12- 7.08 (m, 4H, aryl), 6.97-6.95 (dd, 2H, aryl), 6.80-6.78 (td, 2H, aryl), 3.85 (br s, 2H, CH of the cyclic ring).

1.4. SYNTHESIS OF BIPODAL LIGANDS

Synthesis of N-methyl-2-nitro-*N*-(2-nitrophenyl)benzenamine **(9)**.

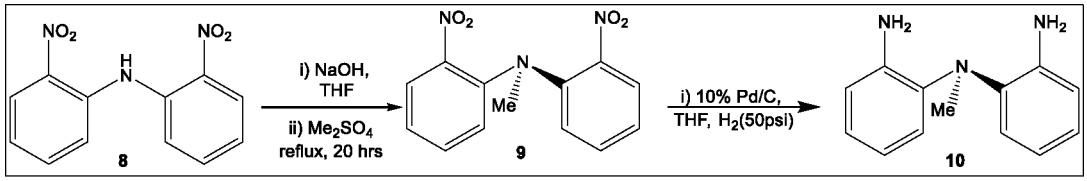

Scheme S5. Synthesis of bipodal diamine.

Bis(2-nitrophenyl)amine **(8)** (prepared according to the literature protocol[2] ; 5.44 g, 21.0 mmol) was dissolved in THF (50 mL) to give a dark brown solution. The solution changed to purple after addition of sodium hydroxide (2.10 g, 0.05 mmol). Me_2SO_4 (8.0 mL, 84.3 mmol) was added to the purple solution slowly and the mixture was refluxed for 20 minutes. The mixture was poured into water (100 mL) and extracted with ethyl acetate (20 mL x 3). The combined organic layers were dried over sodium sulfate overnight. The solvent was removed under vacuum and the crude residue was purified by recrystallization from EtOH to give the product N-Methyl-2-nitro-*N*-(2-nitrophenyl)benzenamine **(9)** as yellow needle crystal (5.9 g, 97%).

^{1}H-NMR ($CDCl_3$, 7.26 ppm,): δ 7.20 (d, J = 7.2 Hz, 2H, aryl), 7.31 (d, J = 8.4 Hz, 2H, aryl), 7.60 (d, J = 7.2 Hz, 2H, aryl), 7.72 (d, J = 8.4 Hz, 2H, aryl), 3.74 (s, 3H, Me).

Synthesis of N-methyl-2,2-diamino-diphenylamine **(10)**. A one- liter pressure flask was charged with N-methyl-2-nitro-N-(2-nitrophenyl)benzenamine **(9)** (5.46 g, 0.01 mol) and Pd/C (1.4 g, 10% Pd) in THF (50.0 mL). High purity nitrogen was first bubbled through this mixture for 0.5 h, and then the flask was pressurized with 50 psig hydrogen gas, and the mixture was allowed to stir at room temperature for 2 h. The flask was disconnected from hydrogen carefully, and the mixture was filtered quickly. The resulting solid was washed with THF (200 mL) and the solvent was removed under vacuum to afford **10** as a white solid (3.83 g, 90 %).^{1}H-NMR ($CDCl_3$, 7.26 ppm): δ 6.69-6.74 (m, 4H, aryl), 6.91-6.98 (m, 4H, aryl), 3.79 (br s, 4H, NH), 3.05 (s 3H, Me).

Synthesis of 1,3-bis(methyl)-4,5-diphenylimidazolidin-2-imine-biphen ($DMDPI_3$-biphen**) (11).** Compound **3** (0.995 g, 3.0 mmol) was dissolved in anhydrous acetonitrile (30.0 mL) in a Schlenk flask inside an inert atmosphere glove box. In another Schlenk flask, $(2\text{-}NH_2\text{-}C_6H_4)_2NMe$ **(10)** (0.3 g, 1.4 mmol) and triethylamine (0.432 mL, 3.0 mmol) were dissolved in a minimum amount of acetonitrile (15.0 mL). Both flasks were brought outside the glove box with a sealed septum and were connected to a gas-vacuum Schlenk line under nitrogen. The flask containing $(2\text{-}NH_2\text{-}C_6H_4)_3N$ was cooled to 0 ^oC, and then the MeCN solution of **3** was added to it slowly over a period of time via canula. The mixture was refluxed overnight to produce a clear solution. The acetonitrile was evaporated under vacuum. The resulting solid was dissolved in dichloromethane (60.0 mL), and washed first with a solution of 5% HCl (30.0 mL) and then with 50 % NaOH (50.0 mL). The solvent was removed under reduced pressure and the crude residue was

purified by silica column chromatography with hexane/ethyl acetate (50:50 v/v) followed by MeOH/CH_2Cl_2 (1−5%) to give the title product **11** in the form of a white solid (0.745 g, 75%). ^{1}H-NMR ($CDCl_3$, 7.26 ppm): δ 7.32- 7.31 (m, 14H, aryl), 7.15- 7.12 (m, 8H, aryl), 6.90-6.86 (m, 6H, aryl) 3.91 (s, 4H, CH of the cyclic ring), 3.58 (s, 3H, Me), 2.31 (s, 12H, Me)

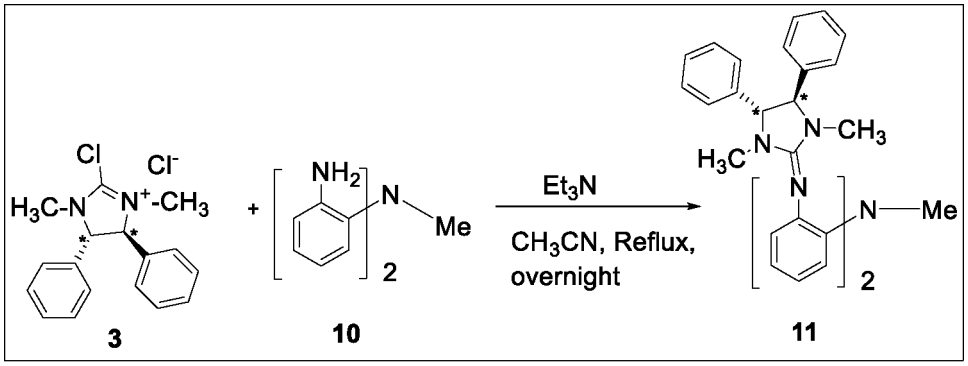

Scheme S6. Synthesis of bipodal ligand.

1.5. SYNTHESIS OF METAL COMPLEXES

Synthesis of [Cu^I(DMDPI$_3$-trphen)][PF_6] **(12).** The ligand DMDPI$_3$-trphen **(4)** (0.30 g, 0.290 mmol) was dissolved in degassed THF (15.0 mL), and [$Cu(CH_3CN)_4$][PF_6] (0.108 g, 0.290 mmol) was added to this solution. The mixture was stirred overnight to give an off-white precipitate.

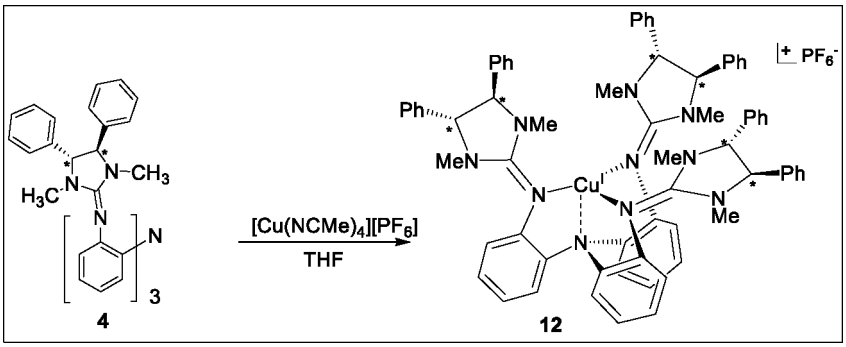

Scheme S7. Synthesis of [Cu^I(DMDPI$_3$-trphen)][PF_6].

The solid was then filtered off on an anaerobic vacuum frit. The filtrate was evaporated and the solid obtained was further dissolved in minimum amount of acetonitrile (2.0 mL) and carefully layered with diethyl ether. The solution was allowed to stand at – 30 °C to afford off white crystalline material of **12** (0.288 g, 80%), suitable for X-ray diffraction analysis. ^{1}H-NMR (CD_3CN, 1.94 ppm): δ 7.35- 7.32 (m, 6H, aryl), 7.25- 7.27 (m, 4H, aryl), 7.18- 7.15 (td, 1H, aryl), 7.11- 7.09 (dd, 2H, aryl), 6.86- 6.83 (td, 1H, aryl), 4.30-4.32 (d, 1H, J= 7.18, CH of the cyclic ring), 3.82-3.83 (d, 1H, J= 7.56, CH of the cyclic ring), 2.82 (s, 3H, Me), 2.05 (s, 3H, Me). ^{13}C NMR ($CDCl_3$, 77.16 ppm): δ 161.44, 147.2 139.9, 139.6, 139.4. 127.84. 127.49. 127.29, 126.31, 125.86, 123.77, 122.19, 73.55, 77.51, 35.09, 33.46. FT-IR (KBr, cm^{-1}): ν 3534, 2928, 2870, 1561, 1523, 1478, 1434, 1418, 1405, 1284, 1278, 1158, 1027, 867, 848, 810, 759, 738, 547. UV−vis (MeCN, nm): λ_{max} (ε (M^{-1} cm^{-1})) 295 (31000).

Synthesis of [Cu^{I}(d-DMDPI$_3$-trphen][PF_6] **(13)**.

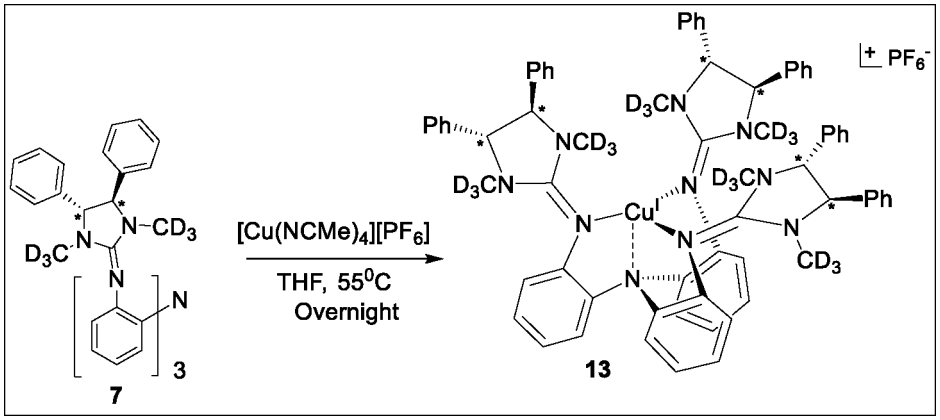

Scheme S8. Synthesis of [Cu^{I}(d-DMDPI$_3$-trphen][PF_6].

The ligand **7** (0.30 g, 0.285 mmol) was dissolved in degassed THF (15.0 mL), and [$Cu(CH_3CN)_4$][PF_6] (0.106 g, 0.285 mmol) was added to this solution. The mixture was

heated and stirred overnight at 50 ^{o}C in a sealed Schlenk flask with a glass stopper, and then filtered on an anaerobic vacuum frit. The filtrate was evaporated, and the solid obtained was further dissolved in a minimum amount of acetonitrile (2.0 mL) and carefully layered with diethyl ether. The solution was allowed to stand at – 30 °C to afford off white crystalline material of **13** (0.277 g, 78%). ^{1}H-NMR (CD_3CN, 1.94 ppm): δ 7.48- 7.40 (m, 6H, aryl), 7.33- 7.27 (m, 4H, aryl), 7.20- 7.16 (td, 1H, aryl), 7.13- 7.11 (dd, 2H, aryl), 6.95- 6.92 (t, 1H, aryl), 4.33-4.32 (td, 1H, J= 7.27, CH of the cyclic ring), 3.95-3.93 (d, 1H, J= 7.74, CH of the cyclic ring).

Synthesis of $[Cu^{I}(DMDPI_3\text{-trphen})][(B(C_6F_5)_4]$ **(14).**

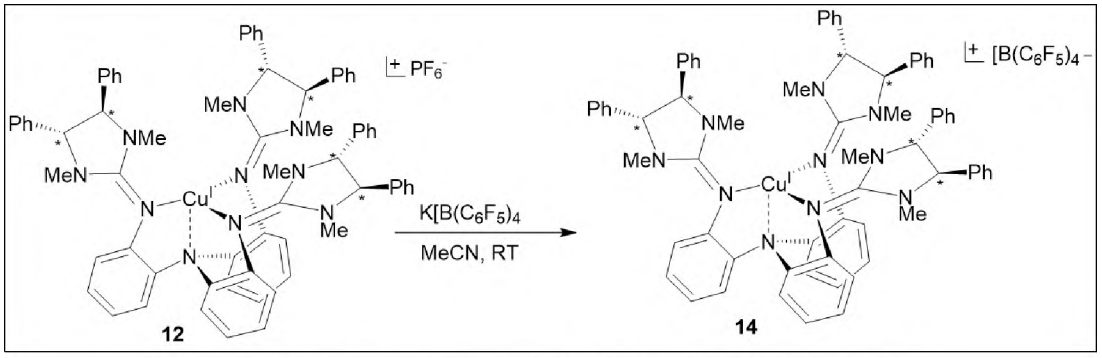

Scheme S9. Synthesis of $[Cu^{I}(DMDPI_3\text{-trphen})][(B(C_6F_5)_4]$.

The metal complex $[Cu^{I}(DMDPI_3\text{-trphen})][PF_6]$ **(12)** (0.30 g, 0.241 mmol) was dissolved in acetonitrile and potassium tetrakis pentafluorophenylborate $K[(B(C_6F_5)_4]$ (0.225g, 0.313mmol) was added to this solution. The mixture was stirred overnight to give a white precipitate, which was filtered off on an anaerobic vacuum frit. The filtrate was evaporated, and **14** was obtained as a white solid (0.180 g, 75%). ^{1}H-NMR (CD_3CN, 1.94 ppm): δ 7.47- 7.40 (m, 6H, aryl), 7.31- 7.29 (m, 4H, aryl), 7.20- 7.16 (td, 1H, aryl), 7.14- 7.12 (dd, 2H, aryl), 6.96- 6.94 (td, 1H, aryl), 4.34-4.32 (d, 1H, J= 7.29, CH of the

cyclic ring), 3.96-3.94 (d, 1H, J= 7.34, CH of the cyclic ring), 2.99 (s, 3H, Me), 1.80 (s, 3H, Me).

Synthesis of [Ag^{I}(DMDPI$_3$-trphen)][PF_6] **(15).** The ligand DMDPI$_3$-trphen **(4)** (0.30 g , 0.290 mmol) was dissolved in degassed acetonitrile (15.0 mL) and $AgPF_6$ (0.073 g, 0.290 mmol) was added to this solution. The mixture was stirred overnight to give an off-white precipitate, which was filtered off on an anaerobic vacuum frit. The filtrate was reduced to approximately 2.0 mL and carefully layered with diethyl ether. The solution was allowed to stand at – 30 °C to afford white crystalline material of **15** (0.291 g, 78%) suitable for X-ray diffraction analysis. ^{1}H-NMR (CD_3CN, 1.94 ppm): 7.38- 7.41 (m, 6H, aryl), 7.28- 7.31 (m, 4H, aryl), 7.22- 7.20 (td, 1H, aryl), 7.16- 7.13 (dd, 2H, aryl), 6.93- 6.96 (td, 1H, aryl), 4.35-4.37 (d, 1H, J= 7.20, CH of the cyclic ring), 3.85-3.87 (d, 1H, J= 7.60, CH of the cyclic ring), 2.90 (s, 3H, Me), 2.09 (s, 3H, Me).

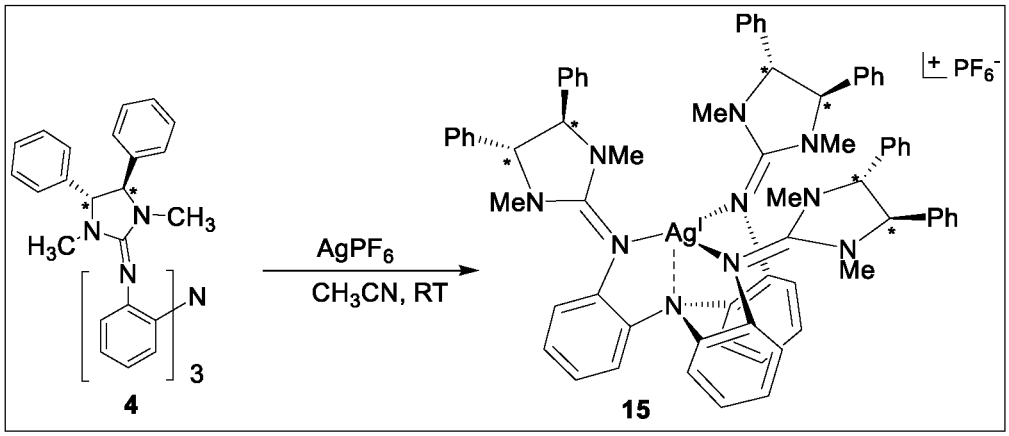

Scheme S10. Synthesis of [Ag^{I}(DMDPI$_3$-trphen)][PF_6].

Synthesis of [Cu^{I}(DMDPI$_3$-biphen)][PF_6]. Et_2O **(16)**. The ligand DMDPI$_3$-biphen) **(11)** (0.30 g , 0.423 mmol) was dissolved in degassed THF (15.0 mL), and [$Cu(CH_3CN)_4$][PF_6] (0.157 g, 0.423 mmol) was added to this solution.

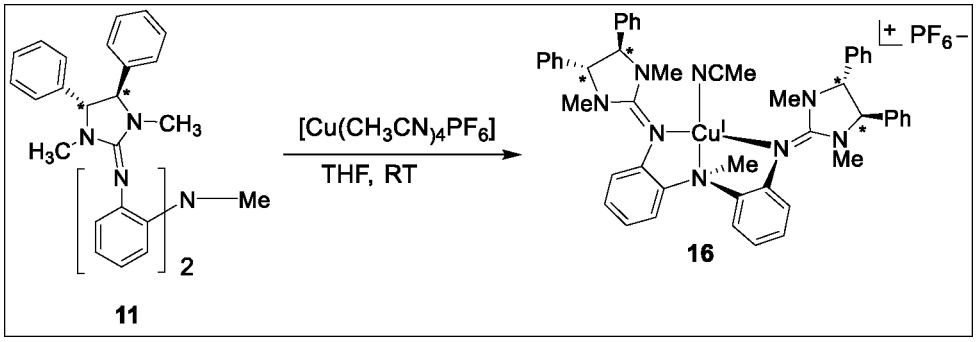

Scheme S11. Synthesis of $[Cu^{I}(DMDPI_3\text{-biphen})][PF_6]$. Et_2O.

The mixture was stirred overnight to give a orange-yellow precipitate which was filtered on an anaerobic vacuum frit. The filtrate was evaporated and the solid obtained was further dissolved in a minimum amount of acetonitrile (2.0 mL) and carefully layered with diethyl ether. The solution was allowed to stand at – 30 °C to afford light white crystalline material of **16** (0.318 g, 82%), suitable for X-ray diffraction analysis. .

Synthesis of $[Ru^{II}(DMDPI_3\text{-trphen})][PF_6]_2$ **(28)**.

The ligand $DMDPI_3$-trphen (**4)** (0.30 g , 0.290 mmol) was dissolved in degassed THF (15.0 mL), and $[Ru(CH_3CN)_6](PF_6)_2$ (0.184 g, 0.290 mmol) was added to this solution. The mixture was heated at 50 ° C in a sealed Schlenk flask with a glass stopper and stirred overnight. The solution filtered on an anaerobic vacuum frit, the filtrate was evaporated, and the white solid **28** was obtained. X-ray diffraction analysis is pending for this compound. ^{1}H-NMR (CD_3CN, 1.94 ppm): δ 7.43- 7.40 (m, 6H, aryl), 7.28- 7.26 (m, 4H, aryl), 7.20- 7.18 (td, 1H, aryl), 7.10- 7.05 (dd, 2H, aryl), 6.90- 6.88 (td, 1H, aryl), 4.73-4.70 (d, 1H, J= 10.01, CH of the cyclic ring), 4.53-4.51 (d, 1H, J= 10.03, CH of the cyclic ring), 2.88 (s, 3H, Me), 2.10 (s, 3H, Me).

The schematic synthesis of $[Ru^{II}(DMDPI_3\text{-trphen})][PF_6]_2$ has been depicted below.

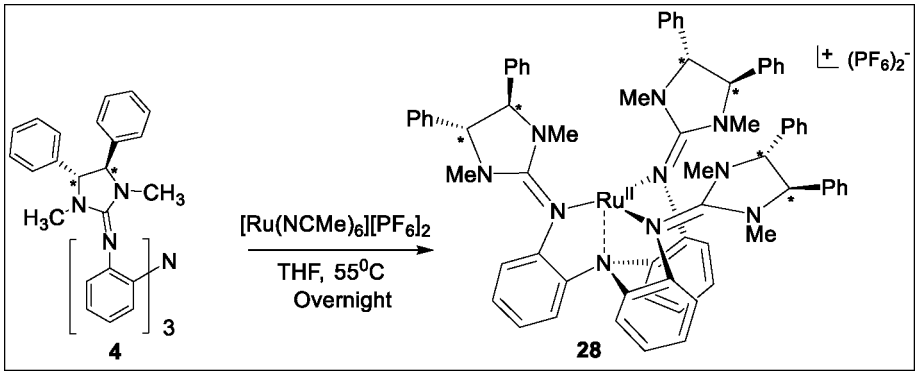

Scheme S12. Synthesis of $[Ru^{II}(DMDPI_3\text{-trphen})][PF_6]_2$.

1.6. MISCELLANEOUS SYNTHESIS OF LIGANDS AND INTERMEDIATES FOR FUTURE DEVELOPMENT

Synthesis of (1R,2R)-N,N′-Diisopropyl 1,2-diphenylethylenediamine (**18**).

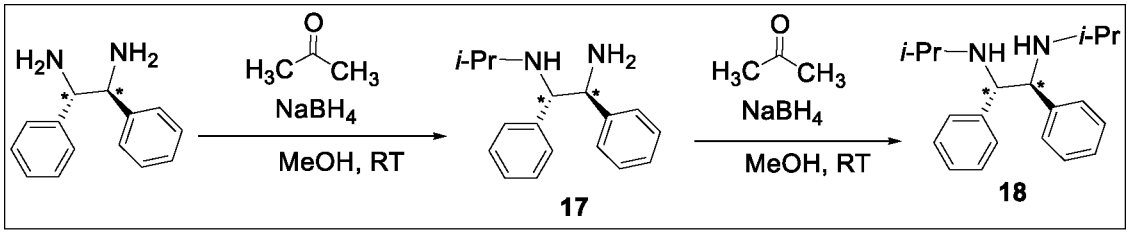

Scheme S13. Synthesis of NH-isoprpyl diamine.

To a stirred solution of chiral 1R, 2R-(+)-1, 2- diphenylethylenediamine (1 g, 4.7 mmol) in CH_3OH (60.0 mL) was added acetone (0.348 mL, 4.7 mmol). The resulting solution was stirred for 1 h at room temperature. $NaBH_4$ (0.535 g, 14.1 mmol) was added to the flask at 0 °C. After allowing the mixture to warm to ambient temperature and stirring for 3 h, a saturated $NaHCO_3$ solution (50.0 mL) was added to the flask and the mixture was extracted with CH_2Cl_2 (3 x 100 mL). The combined organic layers were dried over $MgSO_4$, filtered, and concentrated under reduced pressure to give the monoalkylated amine (1R,2R)-N1-isopropyl-1,2-diphenylethane-1,2-diamine **(17)** as a yellowish viscous liquid (1.10 g , 92%) which was pure, and was used for the next step

without any further purification. ^{1}H-NMR ($CDCl_3$, 7.26 ppm): δ 7.29- 7.17 (m, 10H, aryl), 4.06-4.04 (d, 1H, J= 7.35 Hz, CH of the cyclic ring), 3.90-3.88 (d, 1H, J= 7.23 Hz, CH of the cyclic ring), 2.68-2.58 (sept, 1H, CH), 1.85 (s, 3H, NH), 1.05-1.02 (dd, 6H, J=6.73 Hz, CH_3).

The above procedure was repeated for dialkylation purposes to provide (1R,2R)-N,N′-diisopropyl 1,2-diphenylethylenediamine (**18)** as a white solid**.** Compound **17** (1.0 g, 0.0039 mmol), acetone (0.3 mL, 0.0039 mmol) and sodium hydride (0.446 g, 0.0117 mmol) were used for this reaction. The solid obtained was pure and was used for the next step without any further purification (1.05 g, 83%). ^{1}H-NMR ($CDCl_3$, 7.26 ppm): δ 7.27- 7.15 (m, 10H, aryl), 3.86 (s, 2H, CH of the cyclic ring), 2.74-2.64 (sept, 2H, CH), 1.99 (s, 2H, NH), 1.13-1.12 (d, 3H, J=6.15 Hz, CH_3), 1.09-1.07 (d, 3H, J=6.36 Hz, CH_3).

Synthesis of (4R,5R)-1,3-diisopropyl-4,5-diphenyl-4,5-dihydro-1H-imidazol-3-ium chloride **(19)**.

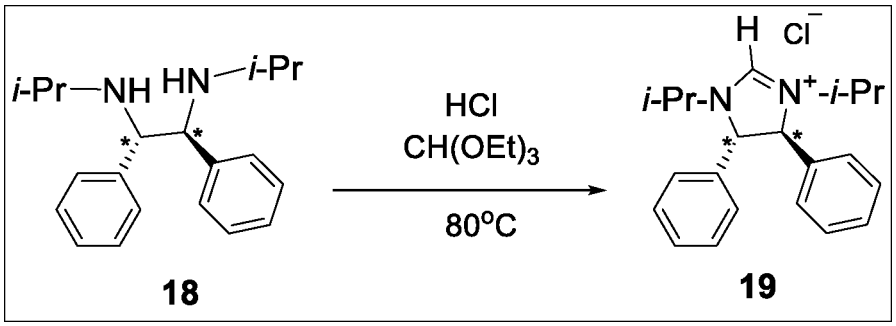

Scheme S14. Synthesis of N-isoprpyl imidazolium salt.

(1R,2R)-N,N′-Diisopropyl 1,2-diphenylethylenediamine **18** was dissolved in minimum amount of dichloromethane (20.0mL) and then drops of 37% dilute HCl were added to the solution until a white solid precipitated out. The solid was filtered, washed with diethyl ether and dried thoroughly under reduced pressure. This **18.**2HCl salt (0.8 g,

2.16 mmol), and triethyl orthoformate (3.6 mL, 2.16 mmol) were added to a 100 mL Schlenk flask and 2-3 drops of formic acid were added to this solution. The reaction mixture was then heated at 100 °C for 16 h. The solution was allowed to reach ambient temperature and was concentrated under reduced pressure. The crude residue was purified by flash column chromatography (1−5% MeOH/CH_2Cl_2) on silica gel (50-60 mL). The orange solid obtained was dissolved in minimum amount of CH_2Cl_2 (5.0 mL), and Et_2O (35.0 mL) was added to precipitate the title compound. The precipitate was filtered, washed with a 1:10 mixture of CH_2Cl_2 and Et_2O, and dried under reduced pressure to afford the title compound **19** (0.5 g, 67.5%) as a colorless solid. ^{1}H-NMR ($CDCl_3$, 7.26 ppm): δ 10.26 (s, 1H, CH), 7.27- 7.24 (m, 4H, aryl), 7.05- 7.03 (m, 4H, aryl), 4.65 (s, 2H, CH of the cyclic ring), 3.78-3.68 (sept, 2H, CH), 1.36-1.34 (d, 3H, J= 6.83 Hz, CH_3), 1.01-1.00 (d, 3H, J= 6.74 Hz, CH_3).

Synthesis of (4R,5R)-2-chloro-1,3-diisopropyl-4,5-diphenyl-4,5-dihydro-1H-imidazol-3-ium chloride **(20)**.

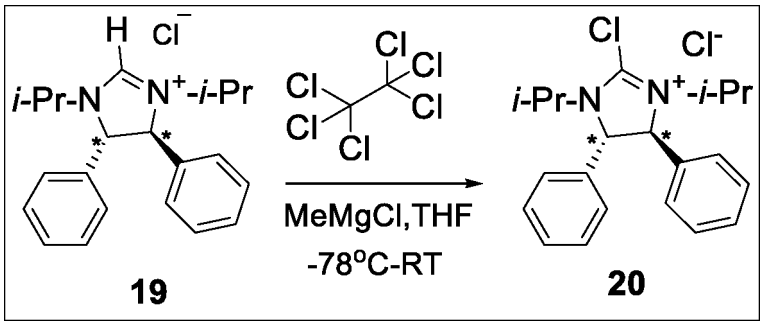

Scheme S15. Synthesis of N-isoprpyl imidazolium chloro salt.

Method A**.** MeMgCl (3M Et_2O, 0.583 mL, 1.75 mmol) was added dropwise to a cooled (0 °C) suspension of (4R,5R)-1,3-diisopropyl-4,5-diphenyl-4,5-dihydro-1H-imidazol-3-ium chloride **(19)** (0.5 g, 1.45 mmol) in THF (15 mL), followed by stirring for

another 30 min to afford a clear solution. The mixture was then cooled to –78 °C and a solution of hexachloroethane (0.480 g, 2.03 mmol) in THF (10 mL) was added dropwise. The reaction mixture was brought to room temperature and stirred for a further 24 h. The solvent was dried under vacuum and the solid obtained was washed with THF and then with Et_2O on an anerobic frit to yield the title compound **20** as a light yellowish solid (0.328 g, 60%). ^{1}H-NMR ($CDCl_3$, 7.26 ppm): δ 7.48- 7.44 (m, 10H, aryl), 5.03 (s, 2H, CH of the cyclic ring), 4.66-4.55 (sept, 2H, CH), 1.40-1.39 (d, 3H, J= 6.73 Hz, CH_3), 1.07-1.06 (d, 3H, J= 6.87 Hz, CH_3).

Method B**.** Compound **20** can also be synthesized via another route albeit in low yields (~ 10%). In this methodology, compound **(18)** (0.54 g, 1.82 mmol) was dissolved in acetonitrile (80.0 mL) and then di-tert-butyl dicarbonate (0.433 g, 1.98 mmol) and 4-dimethylaminopyridine (0.241g, 1.98 mmol) were added to the MeCN solution of **18**. The reaction was allowed to stir at room temperature for 24 h under nitrogen. The solvent was then evaporated under reduced pressure and purified by silica column chromatography using hexane/ethyl acetate (90:10, v/v).

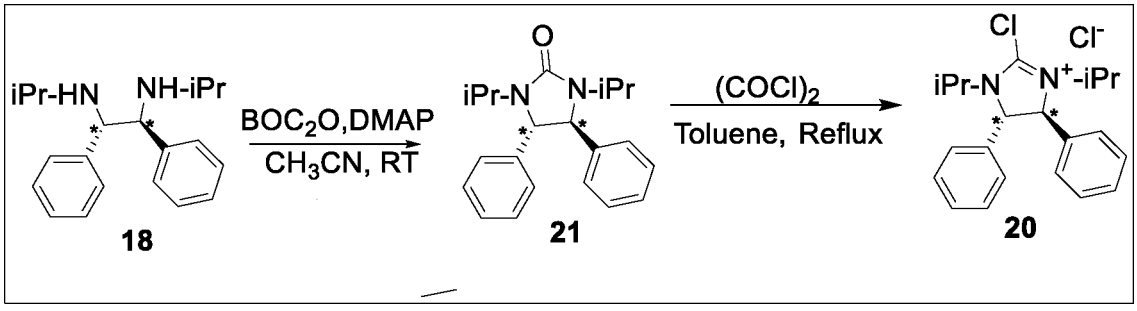

Scheme S16. Synthesis of N-isoprpyl imidazolium chloro salt (Method B).

The product (4R,5R)-1,3-diisopropyl-4,5-diphenylimidazolidin-2-one **(21)** was obtained as pure white solid (0.498 g, 85%). ^{1}H-NMR ($CDCl_3$, 7.26 ppm): δ 7.27- 7.11

(m, 10H, aryl), 4.13 (s, 2H, CH of the cyclic ring), 3.98-3.88 (sept, 2H, CH), 1.14-1.13 (d, 3H, J= 6.81 Hz, CH_3), 0.82-0.81 (d, 3H, J= 6.85 Hz, CH_3).

The urea **(21)** (0.5 g, 1.55 mmol) was dissolved in a minimum amount of toluene (15.0 mL) in a Schlenk flask. The flask was cooled to 0 °C and then oxalyl chloride (0.664 mL, 7.75 mmol) was added to the toluene solution. The reaction mixture was then refluxed for 20 h to afford a white solid. The solid was further filtered and washed with diethyl ether under inert atmosphere to give **20** as a pure white solid (47 mg, 8%)

Synthesis of (4R,5R)-1-isopropyl-4,5-diphenylimidazolidin-2-one (22) To a solution of (1R,2R)-N1-isopropyl-1,2-diphenylethane-1,2-diamine **(17)** (0.5 g, 1.96 mmol) in acetonitrile (70.0 mL), was added di-tert-butyl dicarbonate (0.467 g, 2.14 mmol) and 4-dimethylaminopyridine (0.261 g, 2.14 mmol). The reaction mixture was stirred at room temperature for 24 h. The solvent was then evaporated under reduced pressure. The solid obtained was further purified by silica column chromatography using hexane/ethyl acetate (80:20, v/v) to give (4R,5R)-1-isopropyl-4,5-diphenylimidazolidin-2-one (**22)** as a pure white solid (0.437 g, 80%). ^{1}H-NMR ($CDCl_3$, 7.26 ppm): δ 7.33-7.29 (m, 6H, aryl), 7.20- 7.17 (m, 4H, aryl), 4.90 (br s, 1H, NH),4.47-4.46 (d, 1H, J= 6.57 Hz, CH of the cyclic ring), 4.35-4.33 (d, 1H, J= 6.75 Hz, CH of the cyclic ring), 3.97-3.87 (sept, 1H, CH), 1.85 (s, 3H, NH), 1.19-1.17 (d, 3H, J= 6.80 Hz, Me), 0.90-0.88 (d, 3H, J= 6.91 Hz, Me).

Synthesis of (4R,5R)-1-isopropyl-3-methyl-4,5-diphenylimidazolidin-2-one **(23)**. Compound **22** (0.22 g, 0.784 mmol) was dissolved in anhydrous THF (60.0 mL), and sodium hydride was added (0.037 g, 1.568 mmol) to the THF solution. The reaction was allowed to stir at room temperature for 30 min.

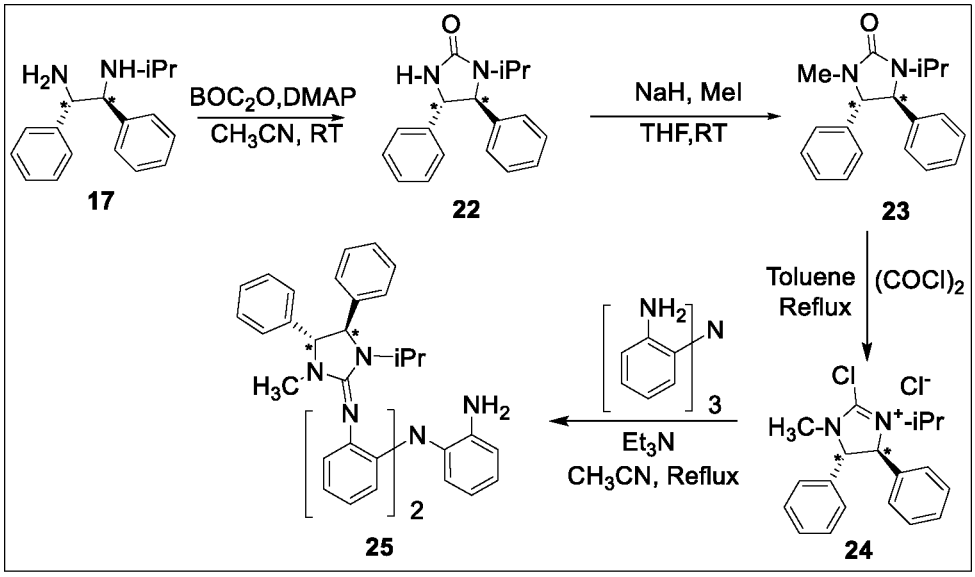

Scheme S17. Synthesis of (IMDP$_2$-biphen)

Methyl iodide (0.122 mL, 1.96 mmol) was then slowly added to the reaction mixture at 0 °C, and allowed to stir at room temperature overnight. After that, the mixture was passed through a short column packed with celite. The solvent was evaporated under reduced pressure, and the product was purified by silica column chromatography with hexane/ethyl acetate (90:10, v/v) to give (4R,5R)-1-isopropyl-3-methyl-4,5-diphenylimidazolidin-2-one **(23)** as a white solid (0.177 g, 77%). ^{1}H-NMR ($CDCl_3$, 7.26 ppm): δ 7.16- 7.13 (m, 6H, aryl), 7.03- 7.01 (m, 4H, aryl), 4.15-4.13 (d, 1H, J= 7.88 Hz, CH of the cyclic ring), 4.05-4.04 (d, 1H, J= 7.14 Hz, CH of the cyclic ring), 2.62 (s, 3H, Me), 3.84-3.73 (sept, 1H, CH), 1.17-1.15 (d, 3H, J= 6.77 Hz, Me), 0.88-0.86 (d, 3H, J= 6.90 Hz, Me).

Synthesis of (4R,5R)-2-chloro-3-isopropyl-1-methyl-4,5-diphenyl-4,5-dihydro-1H-imidazol-3-ium chloride **(24).** The white solid **23** (0.5 g, 1.7 mmol) was dissolved in a minimum amount of toluene (15.0 mL) in a Schlenk flask. The flask was cooled to 0 °C and then oxalyl chloride (0.728 mL, 8.5 mmol) was added to it. The reaction mixture was

then refluxed for 24 h to afford a white solid. The solid precipitated was filtered and washed first with toluene and then with diethyl ether under inert atmosphere to give (4R,5R)-2-chloro-3-isopropyl-1-methyl-4,5-diphenyl-4,5-dihydro-1H-imidazol-3-ium chloride (**24)** as a pure white solid (0.475 g, 80). ^{1}H-NMR ($CDCl_3$, 7.26 ppm): δ 7.68-7.65 (m, 4H, aryl), 7.13- 7.10 (m, 6H, aryl), 5.32-5.29 (d, 1H, J= 11.57 Hz, CH of the cyclic ring), 4.89-4.79 (d, 1H, J= 11.67 Hz, CH of the cyclic ring), 4.19-4.09 (sept, 1H, CH), 3.12 (s, 3H, Me), 1.20-1.18 (d, 3H, J= 7.02 Hz, Me), 0.95-0.94 (d, 3H, J= 6.76 Hz, Me).

Synthesis of 2-((2-(4R,5R)-1-isopropyl-3-methyl-4,5-diphenylimidazolidin-2-ylidene)amino)-phenyl)-l2-azaneyl)aniline ($IMDP_2$-biphen) **(25).** Compound **24** (1.04 g, 3.0 mmol) was dissolved in anhydrous acetonitrile (30.0 mL) in a Schlenk flask inside an inert atmosphere glove box. In another Schlenk flask, $(2\text{-}NH_2\text{-}C_6H_4)_3N$ (0.3g, 1.0 mmol) and triethylamine (0.432 mL, 3.0 mmol) were dissolved in a minimum amount of acetonitrile (15.0 mL). Both flasks were brought outside the glove box with a sealed septum and were connected to a gas-vacuum Schlenk line under nitrogen. The flask containing $(2\text{-}NH_2\text{-}C_6H_4)_3N$ was cooled to 0 ^{o}C and then the MeCN solution of **24** was added to it slowly over a period of time via canula. The mixture was then refluxed overnight to produce a clear solution. The acetonitrile was evaporated under vacuum . The resulting solid was dissolved in dichloromethane (60.0 mL) and then washed first with a solution of 5% HCl (30.0 mL) and then with 50 % NaOH (50.0 mL). The solvent was removed under reduced pressure and the crude residue was purified by silica column chromatography with hexane/ethyl acetate (50:50 v/v) followed by $MeOH/CH_2Cl_2$ ((1−5%) to give the title product **25** in the form of a white solid (0.590g, 70%). The

compound was recrystallized from acetonitrile to give X-ray quality crystals. ^{1}H-NMR (CD_3CN, 1.94 ppm): δ 7.40- 6.61 (m, 33H, aryl), 5.09 (br s, 2H, CH of the cyclic ring), 4.22 (br s, 2H, CH of the cyclic ring), 3.77 (br s, 2H, CH), 2.26 (br s, 6H, Me), 1.02- 0.65 (br s, 12H, Me).

Synthesis of 2-(l^1-azaneyl)-N-(tert-butyl)aniline (26, 2-NH(^{t}Bu)-$C_6H_4)_3$N).

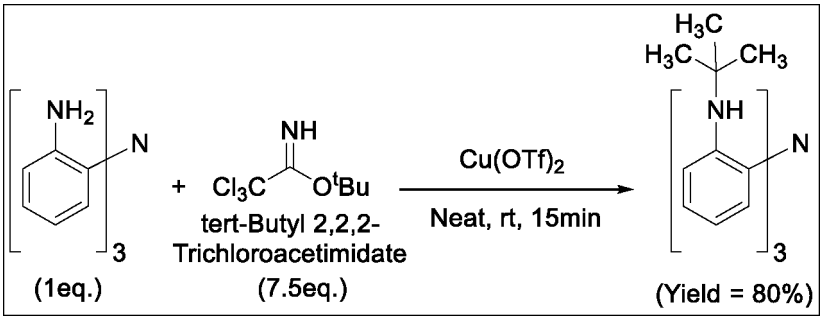

Scheme S18. Synthesis of tripodal tert-butyl ligand.

A 20.0 mL vial was charged with $(2\text{-}NH_2\text{-}C_6H_4)_3N$ (0.2 g, 0.689 mmol) and $Cu(OTf)_2$ (0.0372 g, 0.103 mmol). To these solids, tert-butyl-2,2,2-trichloroacetimidate (1.13 g, 5.17 mmol) was added slowly and the mixture was stirred for 15 minutes to provide a brown solid in an exothermic reaction. The solid was dissolved in ethyl acetate and washed with a saturated sodium bicarbonate solution. The organic layer was collected and evaporated under reduced pressure. The crude residue was purified by silica column chromatography with hexane/ethyl acetate (97:3 v/v) to give the title compound **26** as a pure white solid (0.267 g, 85%). The compound was recrystallized from hexane to afford crystals for X-ray diffraction analysis. ^{1}H-NMR ($CDCl_3$, 7.26 ppm): δ 6.99-6.95 (td, 1H, aryl), 6.86-6.83 (td, 2H, aryl), 6.53-6.49 (td, 1H, aryl), 3.92 (s, 1H, NH), 1.19 (s, 9H, ^{t}Bu). ^{13}C-NMR ($CDCl_3$, 77.16 ppm): δ 142.1, 133.5, 125.2, 116.2, 113.9, 29.9

1.7. CATALYTIC STUDIES

General Catalytic Olefin Aziridination Procedure at Room Temperature**.** In a typical experiment, a 20 mL screw-cap vial containing a small magnetic bar was charged in sequence with the catalyst (0.0125 mmol), N-(p-tolylsulfonyl)imido]phenyliodinane (PhINTs) (93.3 mg, 0.25 mmol) or *o*-propoxyphenyliminoiodane (**27**) (prepared according to the literature protocol[3], 107.8 g, 0.25 mmol), molecular sieves (5Å) (20 mg), olefin (2.0 mmol) and solvent (0.200 mL). The reaction mixture was stirred vigorously for 12 hours (unless otherwise stated). After completion of the reaction, the products were isolated by column chromatography (silica gel) and quantified by ^{1}H NMR (in $CDCl_3$ or CD_3CN) versus an internal standard (4′- methoxyacetophenone). All aziridinated products are known compounds and have been identified with the assistance of ^{1}H and ^{13}C NMR spectra by comparison to spectroscopic features reported for authentic samples in the literature.

General Catalytic Olefin Aziridination Procedure with PhINTs at Lower Temperatures.

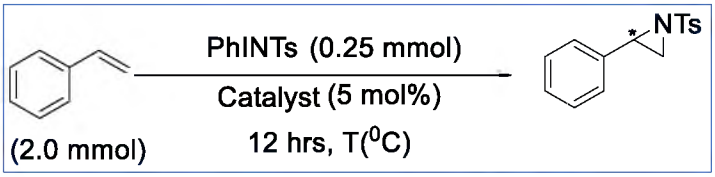

Scheme S19. Catalytic Olefin Aziridination with PhINTs

In a typical experiment, a 10.0 mL round bottom flask containing a small magnetic bar was charged in sequence with the catalyst (0.0125 mmol), N-(p-tolylsulfonyl)imido]phenyliodinane (93.3 mg, 0.25 mmol) and molecular sieves (5Å, 20 mg). In another 20.0 mL screw-capped vial, olefin (2.0 mmol) and solvent (0.200 mL)

was added. The small round bottom flask was cooled to the desired temperature using a chiller or a suitable solvent bath system. For maintaining the temperature below 0 °C, solvent bath systems were used. The olefin and solvent mixture were also cooled to the same desired temperature in a separate flask and then added to the flask containing the catalyst. The mixture was stirred vigorously for 12 hours (unless otherwise stated) at the specific temperature. After completion of the reaction, the products were isolated by column chromatography (silica gel) and quantified by ^{1}H NMR (in $CDCl_3$ or CD_3CN) versus an internal standard (4′- methoxyacetophenone).

General Catalytic Olefin Aziridination Procedure with o-Propoxyphenyliminoiodane at Lower Temperatures**.**

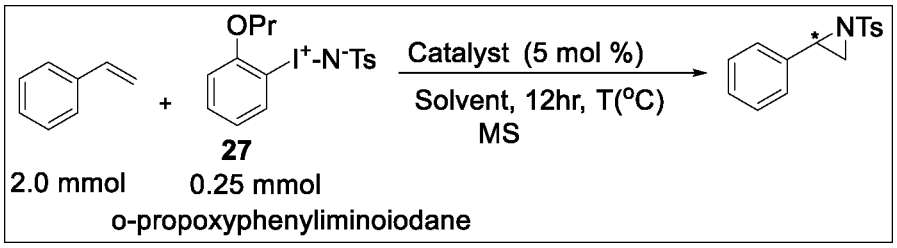

Scheme S20. Catalytic Olefin Aziridination with soluble NTs

In a typical experiment, a 10.0 mL round bottom flask containing a small magnetic bar was charged with the catalyst (0.0125 mmol) and molecular sieves (5Å) (20 mg). In another 20.0 mL screw-capped vial, *o*-propoxyphenyliminoiodane (107.8 g, 0.25 mmol) was dissolved completely in a chosen solvent (0.800 mL). In another 20.0 mL screw-capped vial, olefin (2.0 mmol) was added. The round bottom flask containing the catalyst was cooled to the desired temperature using a chiller or a suitable solvent bath system. The olefin was first added to the flask at the desired temperature, and then the o-propoxyphenyliminoiodane **27** was added via a syringe pump slowly over a period

of 1 hour. The reaction mixture was then stirred for 12 hours (unless otherwise stated) at the specific temperature. After completion of the reaction, the products were isolated by column chromatography (silica gel) and quantified by ^{1}H NMR (in $CDCl_3$ or CD_3CN) versus an internal standard (4′- methoxyacetophenone).

General Catalytic Olefin Cyclopropanation Procedure at Room Temperature. In a typical experiment, a 20 mL screw-cap vial containing a small magnetic bar was charged in sequence with the catalyst **12** (15.98 mg, 0.01285 mmol), methyl 2-diazo-2-phenylacetate (45.2 mg, 0.257 mmol, prepared according to the literature protocol[4]), molecular sieves (5Å, 20 mg), styrene (0.135 g, 1.3 mmol) and solvent (1.0 mL). The reaction mixture was stirred vigorously for 12 hours (unless otherwise stated). After completion of the reaction, the products were isolated by column chromatography (silica gel) and quantified by ^{1}H NMR (in $CDCl_3$ or CD_3CN) versus an internal standard (4′-methoxyacetophenone). All cyclopropanated product are known compounds and have been identified with the assistance of ^{1}H and ^{13}C NMR spectra by comparison to spectroscopic features reported for authentic samples in the literature.

General Catalytic Olefin Cyclopropanation Procedure at Low Temperatures.

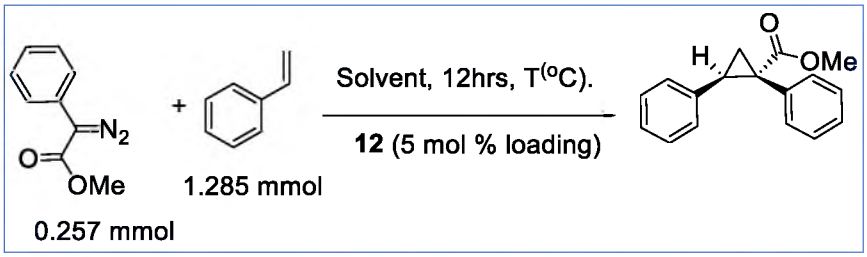

Scheme S21. Catalytic Olefinic cyclopropanation

In a typical experiment, a 10.0 mL small round bottom flask containing a small magnetic bar was charged with the catalyst **12** (15.98 mg, 0.01285 mmol) and molecular

sieves (5Å) (20 mg). In another 20.0 mL screw-capped vial, methyl 2-diazo-2-phenylacetate (45.2 mg, 0.257 mmol (107.8 g, 0.25 mmol) was dissolved completely in the solvent of choice (1.5- 2.0 mL; solvent used: MeCN, benzene, chlorobenzene, pentane, CH_2Cl_2, fluorobenzene, trifluoroethanol). In another 20.0 mL screw-capped vial, styrene (0.133 g, 1.285 mmol) was added. The catalyst-containing round bottom flask was cooled to the desired temperature using a chiller or a suitable solvent bath system. The olefin was first added to the flask at the desired temperature, followed by methyl 2-diazo-2-phenylacetate added via a syringe slowly over a period of 1 hour. The reaction mixture was then stirred for 12 hours (unless otherwise stated) at the specific temperature. After completion of the reaction, the products were isolated by column chromatography (silica gel) and quantified by ^1H NMR (in $CDCl_3$ or CD_3CN) versus an internal standard (4′- methoxyacetophenone).

HPLC Analysis of Chiral Aziridines. All aziridines were purified by column chromatography and then were analyzed by HPLC (HITACHI) on a commercial (R, R)-Whelk-O1 column. The conditions used for running the HPLC were: Flow rate, 0.7 ml/min; Mobile phase, Hexane/Isopropanol (70/30, Isocratic Elution); Wavelength, 254 nm; Retention time (R_t), 30 min. The samples were dissolved in the same solvent system as the mobile phase. The efficiency of the chirality transfer is measured as enantiomeric excess [% ee = (R-S)/(R+S) x 100].

HPLC Analysis of Chiral Cyclopropanated Product. The conditions used for running the HPLC were: Flow rate, 0.7 ml/min; Mobile phase, Hexane/Isopropanol (99/2, Isocratic Elution); Wavelength, 254 nm; Retention time (R_t), 30 min.

Typical HPLC Graphs and ee Evaluation for Representative Aziridination of Styrenes.

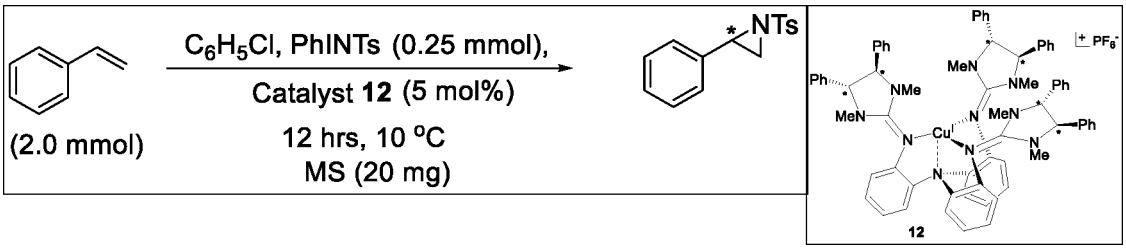

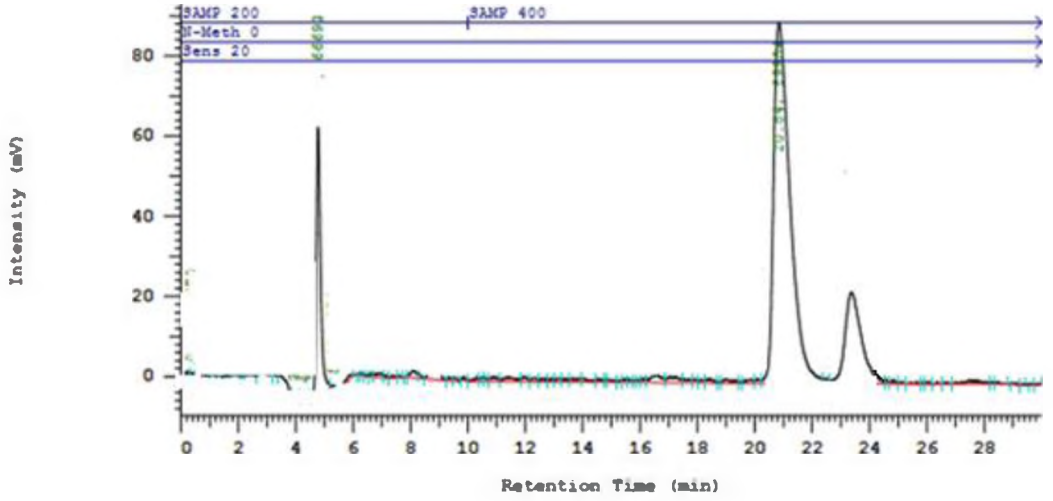

Retention time (R_t)	Peak Area	Height
20.84	3570013	89984
23.37	920943	22686

[% ee= (89984-22686)/(89984+22686) x 100] = 60%

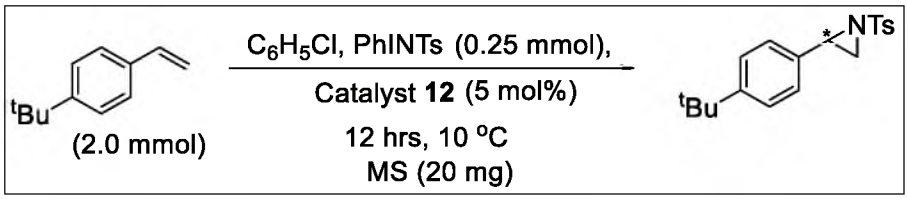

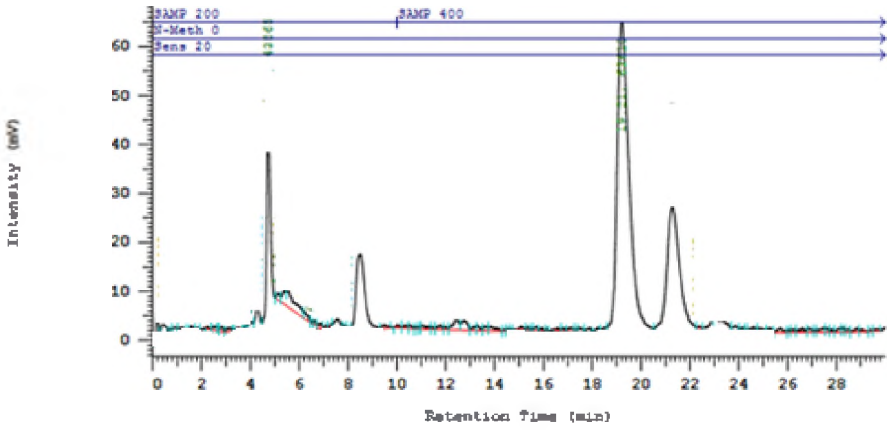

Retention time (Rt)	Peak Area	Height
19.21	2181915	67610
21.29	920631	25690

[%ee=(67610-25690)/(67610+25690) x 100] = 45%

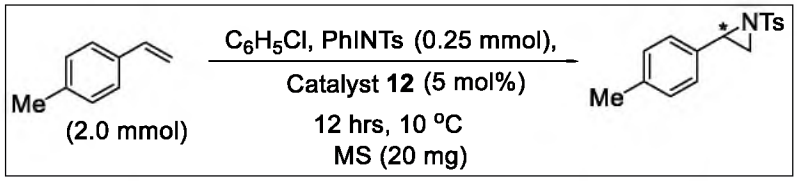

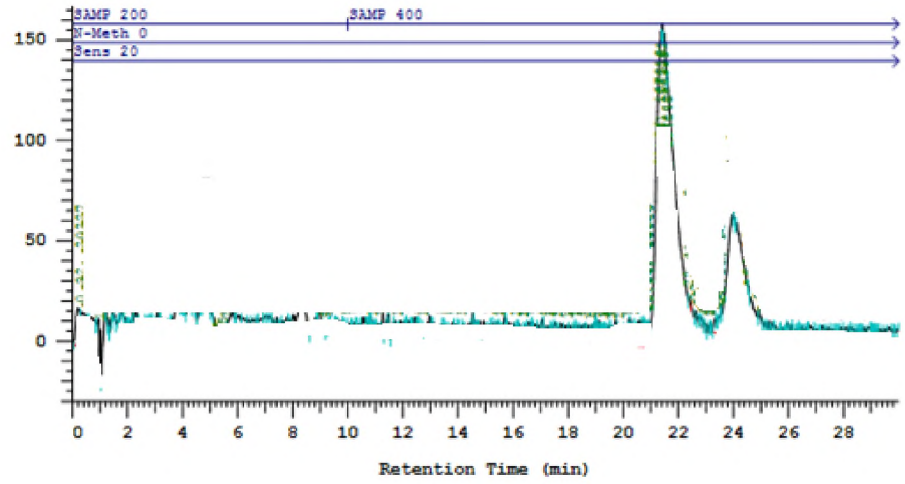

Retention time (Rt)	Peak Area	Height
21.41	629149	161162
24.08	198624	54895

[%ee= (161162-54895)/(161162-54895) x 100] = 50%

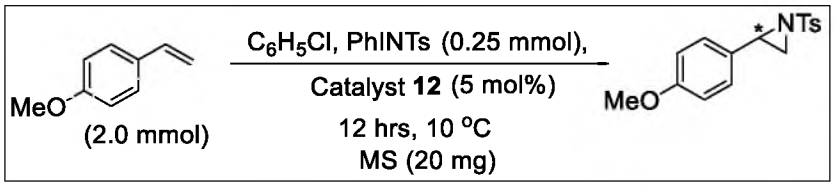

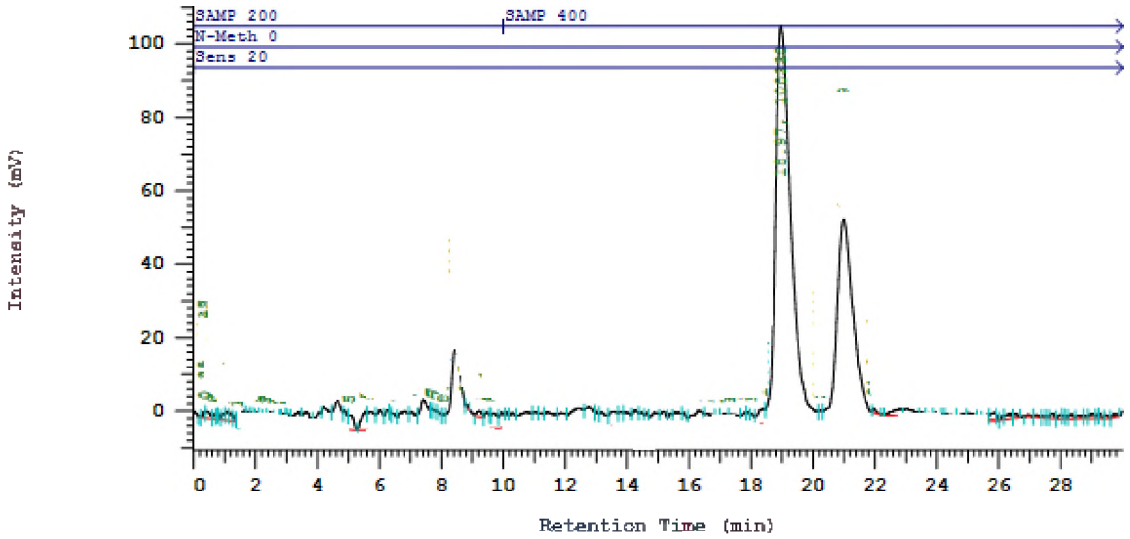

Retention time (Rt)	Peak Area	Height
19.17	2783108	84158
21.21	1351800	35521

[%ee= (84158-35521)/(84158+35521) x 100] = 40%

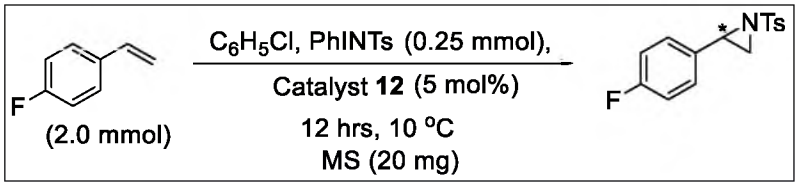

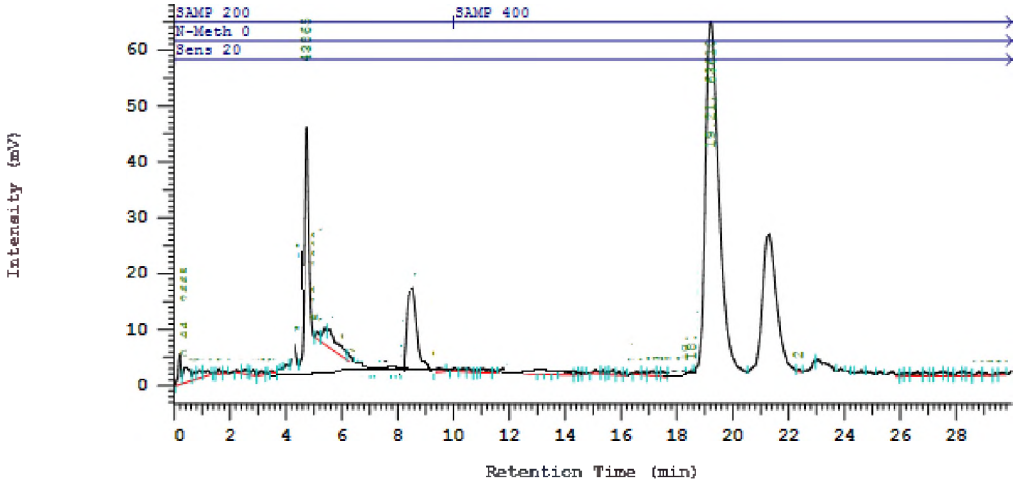

Retention time (Rt)	Peak Area	Height
19.21	4082118	76610
21.83	1271800	25690

[% ee= (76610-25690)/(76610-25690) x 100] = 50%

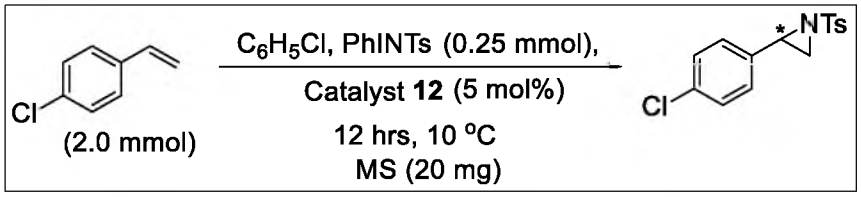

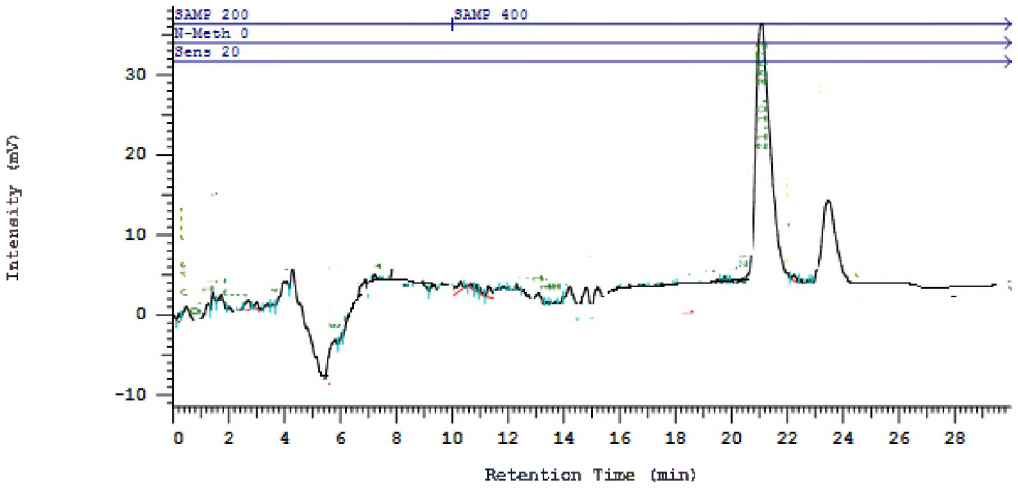

Retention time (Rt)	Peak Area	Height
21.10	2230719	40872
23.43	758609	13678

[% ee= (40872-13678)/(40872-13678) x 100] = 50%

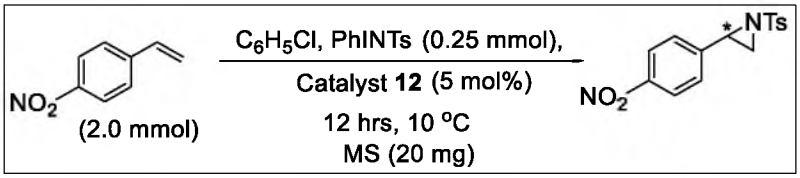

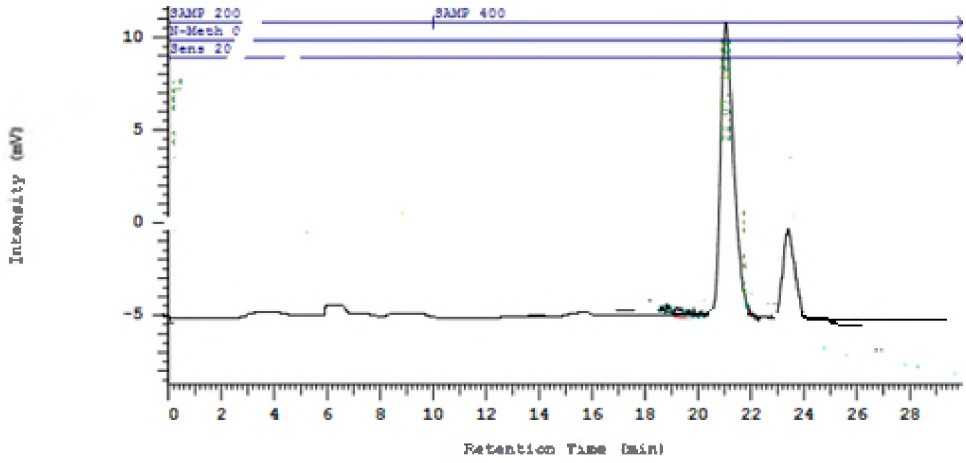

Retention time (Rt)	Peak Area	Height
21.07	682808	18366
23.42	23449	5796

[% ee= (18366-5796)/(18366+5796) x 100] = 51%

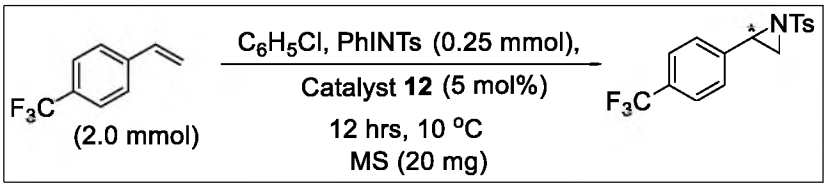

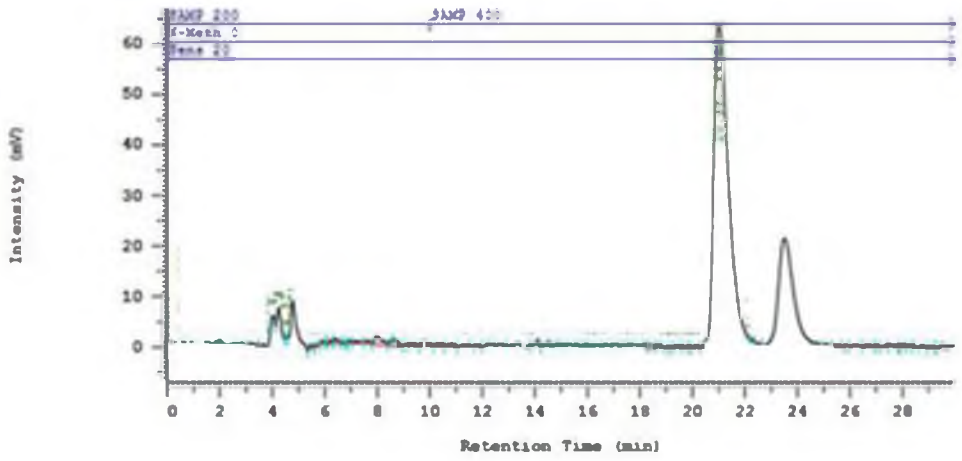

Retention time (R_t, min)	Peak Area	Height
20.99	3470013	64243
23.51	920943	21537

[% ee= (64243- 21537)/(64243+21537) x 100] = 50%

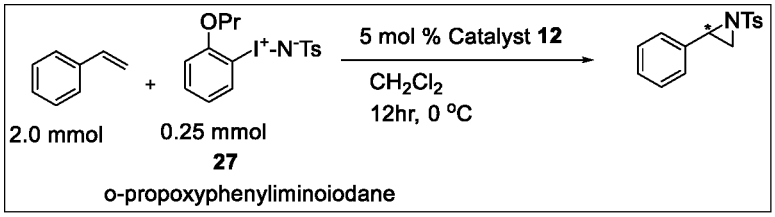

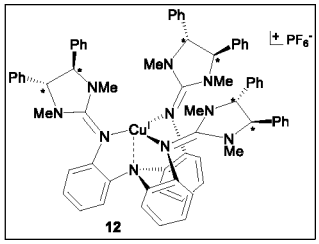

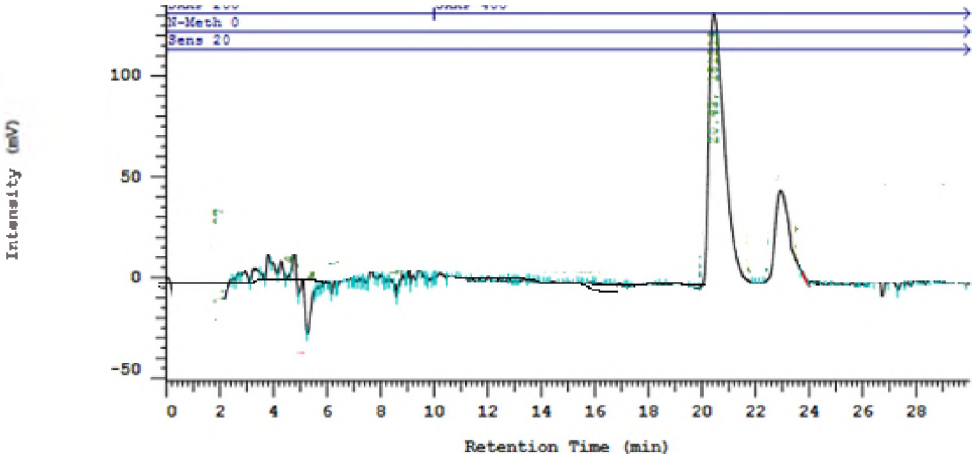

Retention time (Rt)	Peak Area	Height
20.51	4239801	140974
23.92	1286479	44837

[% ee= (140974-44837)/(140974+44837) x 100] = 53%

Typical HPLC Graphs and ee Evaluation for Representative Cyclopropanation of Styrene.

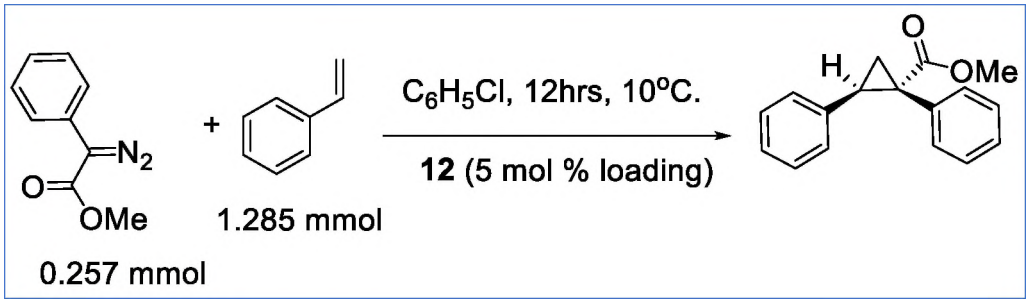

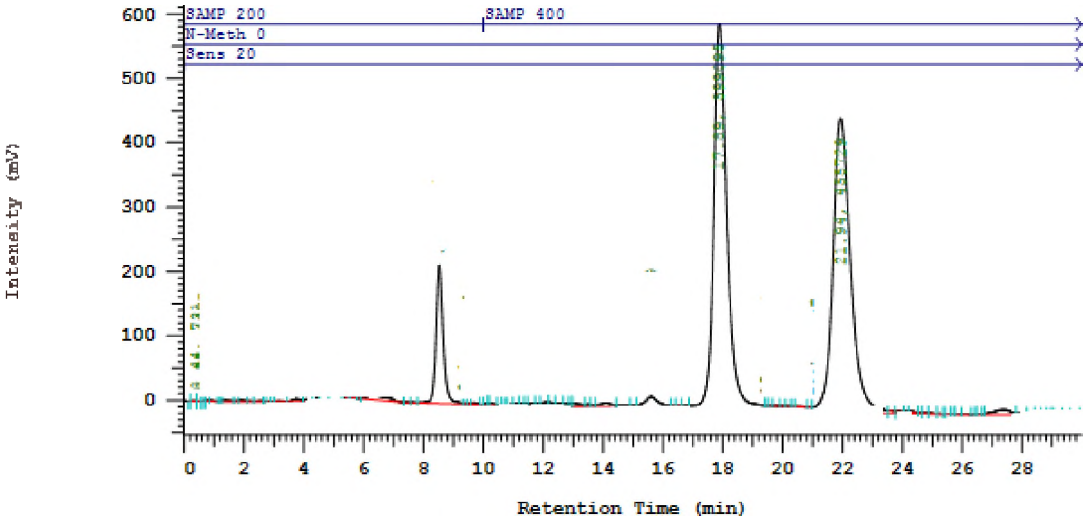

Retention time (Rt)	Peak Area	Height
17.89	12276804	599095
21.94	8919115	435729

[% ee= (599095- 435729)/(599095+435729) x 100] = 15%

REFERENCES

(1) Wu, L.; Li, G.; He, M.; Wang, Y.; Zhao, G.; Tang, Z. First example of an organocatalytic asymmetric Mannich reaction between aldimines of glycinates and sulphonyl imines. *Can. J. Chem.* **2016**, *94*, 769-772.

(2) Ren, P; Vechorkin, O; Allmen, K.V.; Kim; Scopelleti., R; Hu, X. A Structure-Activity Study of Ni-Catalyzed Alkyl-Alkyl Kumada Coupling. Improved Catalysts for Coupling of Secondary Alkyl Halides. *J. Am. Chem. Soc*. **2011**, *133*, 7084-7095.

(3) Hsueh, N.; Clarkson, G.J.; Shipman, M. Functionalization of Alkenes through Telescoped Continuous Flow Aziridination Processes. *Org. Lett*. **2016**, *18*, 4908-4911.

(4) Chen, P. A.; Setthakarn, K; May, J.A. A Binaphthyl-Based Scaffold for a Chiral Dirhodium(II) Biscarboxylate Ligand with α-Quaternary Carbon Centers. *ACS Catal*. **2017**, *7*, 6155-6161.

BIBLIOGRAPHY

1. Olah, G. A.; Molnar, A. *Hydrocarbon Chemistry*; John Wiley & Sons: New York, NY, **1995**. Taube, H. Observations on Atom-Transfer Reactions *Mechanistic Aspects of Inorganic Reactions*, Rorabacher, D. B., Endicott, J. F., Eds.; *ACS Symposium Series* Chapter 7. **1982**, *198*, 151-179.

2. Taube, H. Observations on Atom-Transfer Reactions *Mechanistic Aspects of Inorganic Reactions*, Rorabacher, D. B., Endicott, J. F., Eds.; *ACS Symposium Series* Chapter 7. **1982**, *198*, 151-179.

3. Holm, R. H.; Kennepohl, P.; Solomon, E. I. Structural and Functional Aspects of Metal Sites in Biology. *Chem. Rev.* **1996**, *96*, 2239-2314.

4. Mayer, J. M. Understanding Hydrogen Atom Transfer: From Bond Strengths to Marcus Theory. *Acc. Chem. Res.* **2011**, *44*, 36-46.

5. (a) Atienza, C. C. H.; Bowman, A. C.; Lobkovsky, E.; Chirik, P. J. Photolysis and Thermolysis of Bis(imino)pyridine Cobalt Azides: C−H Activation from Putative Cobalt Nitrido Complexes *J. Am. Chem. Soc.* **2010**, *132*, 16343-16345. (b) Berry, J. F.; Bill, E.; Bothe, E.; DeBeer George, S.; Mienert, B.; Neese, F.; Wieghardt,K. An Octahedral Coordination Complex of Iron(VI) *Science* **2006**, *312*, 1937-1941. (c) DuBois, J.; Tomooka, C. S.; Hong, J.; Carreira, E. M. Nitridomanganese(V) Complexes: Design, Preparation, and Use as Nitrogen Atom-Transfer Reagents *Acc. Chem. Res.* **1997**, *30*, 364-372.

6. (a) Holm, R. H. Metal-centered oxygen atom transfer reactions *Chem. Rev.* **1987**, *87*, 1401-1449. (b) Murray, L. J.; Lippard, S. J. Substrate Trafficking and Dioxygen Activation in Bacterial Multicomponent Monooxygenases. *Acc. Chem. Res.* **2007**, *40*, 466-474. (c) Cooper, H. L. R.; Mishra, G.;Huang, X.; Pendler-Cudlip, M.; Austin, R. N.; Shanklin, J.; Groves, J. T. Parallel and Competitive Pathways for Substrate Desaturation, Hydroxylation, and Radical Rearrangement by the Non-heme Diiron Hydroxylase AlkB.. *J. Am. Chem. Soc.* **2012**, *134*, 20365-20375. (d) Chen, M. S.; White, M. C. Combined Effects on Selectivity in Fe-Catalyzed Methylene Oxidation. *Science* **2010**, *327*, 566-571.

7. (a) Donahue, J. P. Thermodynamic Scales for Sulfur Atom Transfer and Oxo-for-Sulfido Exchange Reactions. *Chem. Rev.* **2006**, *106*, 4747-4783. (b)Yang, L.; Tehranchi, J.; Tolman, W. B. Reactions of $Ph_3Sb{=}S$ with Copper(I) Complexes Supported by N-Donor Ligands: Formation of Stable Adducts and S-Transfer Reactivity. *Inorg. Chem.* **2011**, *50*, 2606-2612. (c) Wang, J.-J.; Kryatova, O.P.; Rybak-Akimova, E. V.; Holm, R. H. Comparative Kinetics and Mechanism of Oxygen and Sulfur Atom Transfer Reactions Mediated by Bis(dithiolene) Complexes of Molybdenum and Tungsten. *Inorg. Chem.* **2004**, *43*, 8092-8101.

8. (a) Matyjaszewski, K. Atom Transfer Radical Polymerization (ATRP): Current Status and Future Perspectives. *Macromolecules* **2012**, *45*, 4015-4039. (b) Pintauer, T.; Matyjaszewski, K. Atom transfer radical addition and polymerization reactions catalyzed by ppm amounts of copper complexes. *Chem. Soc. Rev.* **2008**, *37*, 1087-1097. (c) Ouchi, M.; Terashima, T.; Sawamoto, M. Transition Metal-Catalyzed Living Radical Polymerization: Toward Perfection in Catalysis and Precision Polymer Synthesis. *Chem. Rev.* **2009**, *109*, 4963-5050.

9. (a) Hartwig, J. F. Borylation and Silylation of C–H Bonds: A Platform for Diverse C–H Bond Functionalizations. *Acc. Chem. Res.* **2012**, *45*, 864-873. (b) Mkhalid, I. A. I.; Barnard, J. H.; Marder, T. B.; Murphy, J. M.; Hartwig, J. F. C−H Activation for the Construction of C−B Bonds. *Chem. Rev.* **2010**, *110*, 890-931. (c) Obligacion, J. V.; Semproni, S. P.; Chirik, P. J. Cobalt-Catalyzed C–H Borylation. *J. Am. Chem. Soc.* **2014**, *136*, 4133-4136.

10. (a) Doyle, M. P.; Forbes, D. C. Recent Advances in Asymmetric Catalytic Metal Carbene Transformations. *Chem. Rev.* **1998**, *98*, 911-935. (b) Davies, H.M. L.; Beckwith, R. E. J. Catalytic Enantioselective C−H Activation by Means of Metal−Carbenoid-Induced C−H Insertion. *Chem. Rev.* **2003**, *103*, 2861-2903. (c) Davies, H. M. L.; Manning, J. R. Catalytic C–H functionalization by metal carbenoid and nitrenoid insertion. *Nature* **2008**, *451*, 417-424.

11. Roth, J. P.; Lovell, S.; Mayer, J. M. Intrinsic Barriers for Electron and Hydrogen Atom Transfer Reactions of Biomimetic Iron Complexes. *J. Am. Chem. Soc.* **2000**, *122*, 5486-5498.

12. (a) Waidmann, C. R.; Zhou, X.; Tsai, E. A.; Kaminsky, W.; Hrovat, D. A.; Borden, W. T.;Mayer, J. M. Slow Hydrogen Atom Transfer Reactions of Oxo- and Hydroxo-Vanadium Compounds: The Importance of Intrinsic Barriers. *J. Am. Chem. Soc.* **2009**, *131*, 4729- 4743. (b) Waidmann, C. R.; Zhou, X.; Tsai, E. A.; Kaminsky, W.; Hrovat, D. A.; Borden, W. T.;Mayer, J. M. Slow Hydrogen Atom Transfer Reactions of Oxo- and Hydroxo-Vanadium Compounds: The Importance of Intrinsic Barriers. *J. Am. Chem. Soc.* **2009**, *131*, 4729-4743.

13. (a) Zalatan, D.N.; Du Bois, J. Metal-Catalyzed Oxidations of C–H to C–N Bonds. *Top. Curr. Chem.* **2010**, *292*, 347-378. (b) Roizen, J. L.;Harvey, M. E.; Du Bois, J. Metal-Catalyzed Nitrogen-Atom Transfer Methods for the Oxidation of Aliphatic C–H Bonds. *Acc. Chem. Res.* **2012**, *45*, 911-922. (c) Gephart, R. T., III; Warren, T. H. Copper-Catalyzed sp^3 C–H Amination. *Organometallics* **2012**, *31*, 7728-7752. (d) Collet, F.;Lescot, C.; Dauban, P. Catalytic C–H amination: the stereoselectivity issue. *Chem. Soc.Rev.* **2011**, *40*, 1926-1936.

14. (a) Evano, G.; Blanchard, N.; Toumi, M. Copper-Mediated Coupling Reactions and Their Applications in Natural Products and Designed Biomolecules Synthesis. *Chem. Rev***2008**, *108*, 3054-3131. (b) Monnier, F.; Taillefer, M. Catalytic C–C, C–N, and C–O Ullmann-Type Coupling Reactions: Copper Makes a Difference. *Angew. Chem. Int. Ed.* **2008**, *47*, 3096-3099. (c) Hartwig, J. F.;Kawatsura, M.; Hauck, S. I.; Shaughnessy, K. H.; Alcazar-Roman, L. M. Room-Temperature Palladium-Catalyzed Amination of Aryl Bromides and Chlorides and Extended Scope of Aromatic C–N Bond Formation with a Commercial Ligand. *J. Org. Chem.* **1999**, *64*, 5575-5580. (d) Wolfe, J. P.; Buchwald, S. L. Scope and Limitations of the Pd/BINAP-Catalyzed Amination of Aryl Bromides. *J. Org. Chem.* **2000**, *65*, 1144-1157. (e) Lam, P. Y. S.; Clark, C. G.;Saubern, S.; Adams, J.; Winters, M. P.; Chan, D. M. T.; Combs, A. New aryl/heteroaryl C–N bond cross-coupling reactions via arylboronic acid/cupric acetate arylation. *Tetrahedron Lett.* **1998**, *39*, 2941-2944. (f) Rao, K.S.; Wu, T.-S. Chan-Lam coupling reactions: synthesis of heterocycles. *Tetrahedron* **2012**, *68*, 7735-7754. (15) (a) *Aziridines and Epoxides in Organic Synthesis*; Yudin, A. K., Ed.; Wiley-VCH: Weinheim, 2006. (b) Padwa, A. "Aziridines and Azirines: Monocyclic" in *Comprehensive Heterocyclic Chemistry III*, Katritzky, A. R.; Ramsden, C. A.; Scriven, E. F. V.; Taylor, R. J. K., Eds.; Elsevier Science: Amsterdam, 2008, Vol. 1, pp 1-104 (c) Sweeney, J. B. Aziridines: epoxides' ugly cousins? *Chem. Soc. Rev.* **2002**, *31*, 247-258. (d) Lapinsky, D. J. Three-Membered Ring Systems. *Prog. Heterocycl. Chem.* **2015**, *27*, 61-85.

15. (a) Tomasz, M.; Mitomycin C. Small, fast and deadly (but very selective). *Chem. Biol.* **1995**, *2*, 575-579. (b) Coleman, R. S.; Li, J.; Navarro, A. Total Synthesis of Azinomycin A. *Angew. Chem. Int. Ed.* **2001**, *40*, 1736-1739. (c) Zhao, Q.; He, Q.; Ding, W.; Tang, M.; Kang, Q.; Yu, Y.; Deng, W.; Zhang, Q.; Fang, J.; Tang, G.; Liu, W. Characterization of the Azinomycin B Biosynthetic Gene Cluster Revealing a Different Iterative Type I Polyketide Synthase for Naphthoate Biosynthesis. *Chem. Biol.* **2008**, *15*, 693-705. (d) Ogasawara, Y.; Liu, H.-W. Biosynthetic Studies of Aziridine Formation in Azicemicins. *J. Am. Chem. Soc.* **2009**, *131*, 18066-18068. (e) Nakao, Y.; Fujita, M.; Warabi, K.; Matsunaga, S.; Fusetani, N. Miraziridine A, a Novel Cysteine Protease Inhibitor from the Marine Sponge *Theonella* aff. *Mirabilis*. *J. Am. Chem. Soc.* **2000**, *122*, 10462-10463. (f) Liu, Y.; Li, M.; Mu, H.; Song, S.; Zhang, Y.; Chen, K.; He, X.; Wang, H.; Dai, Y.; Lu, F.; Yan, Z.; Zhang, H. Identification and characterization of the ficellomycin biosynthesis gene cluster from *Streptomyces ficellus*. *Appl. Microbiol. Biotechnol.* **2017**, *101*, 7589-7602. (g) Foulke-Abel, J.; Agbo, H.; Zhang, H.; Mori, S.; Watanabe, C. M. H. Mode of action and biosynthesis of the azabicycle-containing natural products azinomycin and ficellomycin. *Nat. Prod. Rep.* **2011**, *28*, 693-704.

16. (a) Ismail, F. M. D.; Levitsky, D. O.; Dembitsky, V. M. Aziridine alkaloids as potential therapeutic agents. *Eur. J. Med. Chem.* **2009**, *44*, 3373-3387. (b) Ballereau, S.; Andrieu-Abadie, N.; Saffon, N.; Génisson, Y. Synthesis and biological evaluation of aziridine-containing analogs of phytosphingosine. *Tetrahedron* **2011**, *67*, 2570-2578. (c) Dorr, R. T.; Wisner, L.; Samulitis, B. K.; Landowski, T. H.; Remers, W. A. Anti-tumor activity and mechanism of action for a cyanoaziridine-derivative, AMP423. *Cancer Chemother. Pharmacol.* **2012**, *69*, 1039-1049. (d) Pillai, B.; Cherney, M. M.; Diaper, C. M.; Sutherland, A.; Blanchard, J. S.; Vederas, J. C.; James, M. N. G. Structural insights into stereochemical inversion by diaminopimelate epimerase: An antibacterial drug target. *Proc. Natl. Acad. Sci. U.S.A.* **2006**, *103*, 8668-8673.

17. (a) Rotstein, B. H.; Zaretsky, S.; Rai, V.; Yudin, A. K. Small Heterocycles in Multicomponent Reactions. *Chem. Rev.* **2014**, *114*, 8323-8359. (b) Huang, C.-Y. Doyle, A. G. The Chemistry of Transition Metals with Three-Membered Ring Heterocycles. *Chem. Rev.* **2014**, *114*, 8153-8198. (c) Stankovic, S.; D'hooghe, M.; Catak, S.; Eum, H.; Waroquier, M.; Van Speybroeck, V.; De Kimpe, N.; Ha, H.-J. Regioselectivity in the ring opening of non-activated aziridines. *Chem. Soc. Rev.* **2012**, *41*, 643-665. (d) Lu, P. Recent developments in regioselective ring opening of aziridines. *Tetrahedron* **2010**, *66*, 2549-2560. (e) Schneider, C. Catalytic, Enantioselective Ring Opening of Aziridines. *Angew. Chem. Int. Ed.* **2009**, *48*, 2082-2084.

18. (a) Moon, H. K.; Kang, S.; Yoon, H. J. Aziridine-functionalized polydimethylsiloxanes for tailorable polymeric scaffolds: aziridine as a clickable moiety for structural modification of materials. *Polym. Chem.* **2017**, *8*, 2287-2291. (b) Chen, R.; Chen, J. S.; Zhang, C.; Kessler, M. R. Rapid room-temperature polymerization of bio-based multiaziridine-containing compounds. *RSC Adv.* **2015**, *5*, 1557-1563.

19. (a) Degennaro, L.; Trinchera, P.; Luisi, R. Recent Advances in the Stereoselective Synthesis of Aziridines. Chem. Rev. 2014, 114, 7881-7929. (b) Pellissier, H. Recent Developments in Asymmetric Aziridination. Adv. Synth. Catal. 2014, 356, 1899-1935. (c) Pellissier, H. Recent developments in asymmetric aziridination. Tetrahedron 2010, 66, 1509-1555. (d) Singh, G. S.; D'hooghe, M.; De Kimpe, N. Synthesis and Reactivity of C-Heteroatom-Substituted Aziridines. Chem. Rev. 2007, 107, 2080-2135. (e) Watson, I. D. G.; Yu, L.; Yudin, A. K. Advances in Nitrogen Transfer Reactions Involving Aziridines. Acc. Chem. Res. 2006, 39, 194-206. (f) Osborn, H. M. I.; Sweeney, J. The asymmetric synthesis of aziridines. Tetrahedron: Asymmetry 1997, 8, 1693-1715. (g) Tanner, D. Chiral Aziridines–Their Synthesis and Use in Stereoselective Transformations. Angew. Chem. Int. Ed. 1994, 33, 599-619.

20. (a) Fiori, K. W.; Du Bois, J. "Catalytic Intermolecular Amination of C−H Bonds: Method Development and Mechanistic Insights" *J. Am. Chem. Soc.* **2007**, *129*, 562-568. (b) Zalatan, D. N.; Du Bois, J. Understanding the Differential Performance of $Rh_2(esp)_2$ as a Catalyst for C−H Amination. *J. Am. Chem. Soc.* **2009**, *131*, 7558-7559. (c) Fiori, K. W.; Espino, C. G.; Brodsky, B. H.; Du Bois, J. A mechanistic analysis of the Rh-catalyzed intramolecular C–H amination reaction. *Tetrahedron* **2009**, *65*, 3042-3051. (d) Liang, C.;Collet, F.; Robert-Peillard, F.; Muller, P.; Dodd, R. H.; Dauban, P. Toward a Synthetically Useful Stereoselective C−H Amination of Hydrocarbons. *J. Am. Chem. Soc.* **2008**, *130*,343-350. (e) Liang, C.; Robert-Peillard, F.; Fruit, C.; Muller, P.;Dodd, R. H.; Dauban, P. Efficient Diastereoselective Intermolecular Rhodium-CatalyzedC-H Amination. *Angew. Chem. Int. Ed.* **2006**, *45*, 4641-4644. (f) Jat, J. L.; Paudyal, M. P.; Gao, H.; Xu, Q.-L.; Yousufuddin, M.;Devarajan, D.; Ess, D. H.; Kurti, L.; Falck, J. R. Direct Stereospecific Synthesis of Unprotected N-H and N-Me Aziridines from Olefins. *Science* **2014**, *343*, 61-65

21. (a) Harvey, M. E.; Musaev, D.; Du Bois, J. A Diruthenium Catalyst for SelectiveIntramolecular Allylic C–H Amination: Reaction Development and Mechanistic InsightGained through Experiment and Theory. *J. Am. Chem. Soc.* **2011**, *133*, 17207-17216. (b) Leung, S. K.-Y.; Tsui, W.-M.; Huang, J.-S.; Che, C.-M.; Liang, J.-L.; Zhu, N. Imido Transfer from Bis(imido)ruthenium(VI) Porphyrins to Hydrocarbons:Effect of Imido Substituents, C−H Bond Dissociation Energies, and RuVI/V Reduction Potentials. *J. Am. Chem. Soc.* **2005**, *127*, 16629-16640. (c) Liang, J.-L.; Huang, J.-S.; Yu, X.-Q.; Zhu, N.; Che, C.-M. Metalloporphyrin-Mediated Asymmetric Nitrogen-Atom Transfer to Hydrocarbons: Aziridination of Alkenes and Amidation of Saturated C−H Bonds Catalyzed by Chiral Ruthenium and Manganese Porphyrins" *Chem. Eur. J.* **2002**, *8*, 1563-1572. (d) Au, S.-M.; Huang, J.-S.; Yu, W.-Y.; Fung, W.-H.; Che, C.-M. Aziridination of Alkenes and Amidation of Alkanes by Bis(tosylimido)ruthenium(VI) Porphyrins. A Mechanistic Study. *J. Am. Chem. Soc.* **1999**,*121*, 9120-9132. (e) Xiao, W.; Wei, J.; Zhou, C.-Y.; Che, C.-M. [RuIV(F20-TPP)Cl_2] efficiently catalysed inter- and intra-molecular nitrene insertion into sp^3 C–H bonds of hydrocarbons using phosphoryl azides as nitrene sources. *Chem. Commun.***2013**, *49*, 4619-4621. (f) Zdilla, M. J.; Dexheimer, J. L.; Abu-Omar, M. M. Hydrogen Atom Transfer Reactions of Imido Manganese(V) Corrole: One Reaction with Two Mechanistic Pathways. *J. Am. Chem. Soc.* **2007**, *129*, 11505-11511. (g) Nishioka, Y.; Uchida, T.; Katsuki, T. Enantio- and Regioselective Intermolecular Benzylic and Allylic C-H Bond Amination. *Angew. Chem. Int. Ed.* **2013**, *52*, 1739-1742. (h) Kohmura, Y.; Katsuki, T. Mn(salen)-catalyzed enantioselective C-H amination. *Tetrahedron Lett.* **2001**, *42*, 3339-3342.

22. (a) King, E. R.; Hennessy, E. T.; Betley, T. A. Catalytic C−H Bond Amination from High-Spin Iron Imido Complexes. *J. Am. Chem. Soc.* **2011**, *133*, 4917-4923. (b) Paradine, S. M.; White, M. C. Iron-Catalyzed Intramolecular Allylic C–H Amination. *J. Am. Chem. Soc.* **2012**, *134*, 2036-2039

23. (a) Lu, H.; Jiang, H.; Wojtas, L.; Zhang, X. P. Selective Intramolecular C-H Amination through the Metalloradical Activation of Azides: Synthesis of 1,3-Diamines under Neutral and Nonoxidative Conditions. *Angew. Chem. Int. Ed.* **2010**, *49*, 10192-10196. (b) Lu, H.; Tao, J.; Jones, J. E.; Wojtas, L.; Zhang, X. P. Cobalt(II)-Catalyzed Intramolecular C−H Amination with Phosphoryl Azides: Formation of 6- and 7-Membered Cyclophosphoramidates. *Org. Lett.* **2010**, *12*, 1248-1251. (c) Lu, H.; Subbarayan, V.; Tao, J.; Zhang, X. P. Cobalt(II)-Catalyzed Intermolecular Benzylic C−H Amination with 2,2,2-Trichloroethoxycarbonyl Azide ($TrocN_3$). *Organometallics* **2010**, *29*, 389-393.

24. (a) Wiese, S.; McAfee, J. L.; Pahls, D. R.; McMullin, C. L.; Cundari, T. R.; Warren, T. H. C–H Functionalization Reactivity of a Nickel–Imide. *J. Am. Chem. Soc.* **2012**, *134*, 10114-10121. (b) Kogut, E.; Wiencko, H. L.; Zhang, L.; Cordeau, D. E.;Warren, T. H. A Terminal Ni(III)−Imide with Diverse Reactivity Pathways. *J. Am. Chem. Soc.* **2005**, *127*, 11248-11249. (c) Laskowski, C. A.; Miller, A. J.M.; Hillhouse, G. L.; Cundari, T. R. A Two-Coordinate Nickel Imido Complex That Effects C−H Amination. *J. Am. Chem. Soc.* **2011**, *133*, 771-773. (d) Iluc,V. M.; Miller, A. J. M.; Anderson, J. S.; Monreal, M. J.; Mehn, M. P.; Hillhouse, G. L. Synthesis and Characterization of Three-Coordinate Ni(III)-Imide Complexes. *J. Am. Chem. Soc.* **2011**, *133*, 13055-13063. (e) Harrold, N. D.;Waterman, R.; Hillhouse, G. L.; Cundari, T. R. Group-Transfer Reactions of Nickel−Carbene and −Nitrene Complexes with Organoazides and Nitrous Oxide that Form New C=N, C=O, and N=N Bonds. *J. Am. Chem. Soc.* **2009**, *131*, 12872-12873.

25. Paradine, S. M.; Griffin, J. R.; Zhao, J.; Petronico, A. L.; Miller, S. M.; White, M. C. A manganese catalyst for highly reactive yet chemoselective intramolecular C(sp^3)–H amination. *Nat. Chem.* **2015**, *7*, 987-994.

26. Alderson, J. M.; Phelps, A. M.; Scamp, R. J.; Dolan, N. S.; Schomaker, J. M. LigandControlled, Tunable Silver-Catalyzed C–H Amination. *J. Am. Chem. Soc.* **2014**, *136*,16720-16723

27. Paradine, S. M.; Griffin, J. R.; Zhao, J.; Petronico, A. L.; Miller, S. M.; White, M. C. A manganese catalyst for highly reactive yet chemoselective intramolecular C(sp^3)–H amination. *Nat. Chem.* **2015**, *7*, 987-994.

28. Hennessy, E. T.; Betley, T. A. Complex N-Heterocycle Synthesis via Iron-Catalyzed, Direct C–H Bond Activation. *Science.* **2013**, *340*, 591-595.

29. Takamatsu, K.; Hirano, K.; Satoh, T.; Miura, M. Synthesis of Indolines by Copper Mediated Intramolecular Aromatic C–H Amination. *J. Org. Chem.* **2015**, *80*, 3242-3249.

30. Yang, M.; Su, B.; Wang, Y.; Chen, K.; Jiang, X.; Zhang, Y.-F.; Zhang, X.-S.; Chen, G.; Cheng, Y.; Cao, Z.; Guo, Q.-Y.; Wang, L.; Shi, Z.-J. Silver-catalysed direct amination of unactivated C–H bonds of functionalized molecules. *Nat. Commun.* **2014**, *5*, 4707.

31. Corbin, D. R.; Schwarz, S.; Sonnichsen, G. C. Methylamines synthesis: A review. *Catal. Today* **1997**, *37*, 71-102

32. Yuzawa, H.; Kumagai, J.; Yoshida, H. Reaction Mechanism of Benzene and Substituted Benzenes by Aqueous Ammonia over Platinum-Loaded Titanium Oxide Photocatalyst. *J.Phys. Chem.* **2013**, *117*, 11047-11058.

33. Hagemeyer, A.; Borade, R.; Desrosiers, P.; Guan, S.; Lowe, D. M.; Poojary, D. M.; Turner, H.; Weinberg, H.; Zhou, X.; Armbrust, R.; Fengler, G.; Notheis, U. Application of combinatorial catalysis for the direct amination of benzene to aniline. *Appl. Catal. A:General* **2002**, *227*, 43-61.

34. Dequirez, G.; Pons, V.; Dauban, P. Nitrene Chemistry in Organic Synthesis: Still in Its Infancy?. *Angew. Chem. Int. Ed.* **2012**, *51*, 7384-7395.

35. Starkov, P.; Jamison, T. F.; Marek, I. Electrophilic Amination: The Case of Nitrenoids. *Chem. Eur. J.* **2015**, *21*, 5278-5300.

36. Driver, T. G. Recent advances in transition metal-catalyzed *N*-atom transfer reactions of Azides. *Org. Biomol. Chem.* **2010**, *8*, 3831-3846.

37. Kuznetsova, N. I.; Kuznetsova, L. I.; Detusheva, L. G.; Likholobov, V. A.; Pez, G. P.;Cheng, H. Amination of benzene and toluene with hydroxylamine in the presence of transition metal redox catalysts. *J. Mol. Catal. A: Chem.* **2000**, *161*, 1-9.

38. Citterio, A.; Gentile, A.; Minisci, F.; Navarrini, V.; Serravalle, M.; Ventura, S. Polar Effects in Free Radical Reactions. Homolytic Aromatic Amination by the Amino Radical Cation,$\bullet^{+}NH_3$: Reactivity and Selectivity. *J. Org. Chem.* **1984**, *49*, 4479-4482

39. Tomat, R.; Rigo, A. Electrochemical Production of $NH_2^{\bullet}$ Radicals by the System $Cu^{2+}/VO_2^{+}/NH_2OH$ and their Reactions with Benzene and Toluene. *J. Electroanal. Chem.***1977**, *75*, 629-635.

40. Tomat, R.; Rigo, A. Reactivities of Aromatic Compounds Towards the Amino Radical. *J. Electroanal. Chem.* **1975**, *63*, 329-337.

41. Driver, T. G. Recent advances in transition metal-catalyzed *N*-atom transfer reactions of Azides. *Org. Biomol. Chem.* **2010**, *8*, 3831-3846.

42. (a) Lu, H.; Jiang, H.; Wojtas, L.; Zhang, X. P. Selective Intramolecular C-H Amination through the Metalloradical Activation of Azides: Synthesis of 1,3-Diamines under Neutral and Nonoxidative Conditions. *Angew. Chem. Int. Ed.* **2010**, *49*, 10192-10196.

43. Lu, H.; Tao, J.; Jones, J. E.; Wojtas, L.; Zhang, X. P. Cobalt(II)-Catalyzed Intramolecular C−H Amination with Phosphoryl Azides: Formation of 6- and 7-Membered Cyclophosphoramidates. *Org. Lett.* **2010**, *12*, 1248-1251.

44. (c) Lu, H.; Subbarayan, V.; Tao, J.; Zhang, X. P. Cobalt(II)-Catalyzed Intermolecular Benzylic C−H Amination with 2,2,2-Trichloroethoxycarbonyl Azide ($TrocN_3$).*Organometallics* **2010**, *29*, 389-393.

45. Starkov, P.; Jamison, T. F.; Marek, I. Electrophilic Amination: The Case of Nitrenoids.*Chem. Eur. J.* **2015**, *21*, 5278-5300.

46. Starkov, P.; Jamison, T. F.; Marek, I. Electrophilic Amination: The Case of Nitrenoids.*Chem. Eur. J.* **2015**, *21*, 5278-5300. 46. Rappaport, Z.; Liebman, J. F. The Chemistry of Hydroxylamines, Oximes and Hydroxamic Acids; *Wiley: Hoboken, NJ*, **2008**; Vol. *2*.

47. Moreau, Y.; Chen, H.; Derat, E.; Hirao, H.; Bolm, C.; Shaik, S. NR Transfer Reactivity of Azo-Compound I of P450. How Does the Nitrogen Substituent Tune the Reactivity of the Species toward C–H and C=C Activation?. *J. Phys. Chem. B* **2007**, *111*, 10288-10299

48. Li, L.; Zhang, J. Lewis Acid-catalyzed [3+2]Cyclo-addition of Alkynes with N-Tosyl-aziridines via Carbon–Carbon Bond Cleavage: Synthesis of Highly Substituted 3-Pyrrolines. *Org. Lett.* **2011**, *13*, 5940-5943. (b) Dauban, P.; Dodd, R. H. PhI=NSes: A New Iminoiodinane Reagent for the Copper-Catalyzed Aziridination of Olefins. *J. Org. Chem.* **1999**, *64*, 5304-5307.

49. Warner, D. L.; Hibberd, A. M.; Kalman, M.; Klapars, A.; Vedejs, E. *N*-Silyl Protecting Groups for Labile Aziridines: Application toward the Synthesis of *N*-H Aziridinomitosenes. *J. Org. Chem.* **2007**, *72*, 8519-8522.

50. Kornecki, K. P.; Briones, J. F.; Boyarskikh, V.; Fullilove, F.; Autschbach, J.; Schrote, K. E.; Lancaster, K. M.; Davies, H. M. L.; Berry, J. F. Direct Spectroscopic Characterization of a Transitory Dirhodium Donor-Acceptor Carbene Complex. *Science* **2013**, *342*, 351-354

51. Collins, L. R.; van Gastel, M.; Neese, F.; Fürstner, A. Enhanced Electrophilicity of Heterobimetallic Bi–Rh Paddlewheel Carbene Complexes: A Combined Experimental, Spectroscopic, and Computational Study. *J. Am. Chem. Soc.* **2018**, *140*, 13042-13055

52. Corona, T.; Ribas, L.; Rovira, M.; Farquhar, E. R.; Ribas, X.; Ray, K.; Company, A.Characterization and Reactivity Studies of a Terminal Copper–Nitrene Species. *Angew.Chem. Int. Ed.* **2016** (Early View).

53. Kundu, S.; Miceli, E.; Farquhar, E.; Pfaff, F. F.; Kuhlmann, U.; Hildebrandt, P.; Braun, B.;Greco, C.; Ray, K. Lewis Acid Trapping of an Elusive Copper–Tosylnitrene Intermediate Using Scandium Triflate. *J. Am. Chem. Soc.* 2012, *134*, 14710-14713.

54. Carsch, Kurtis M.; DiMucci, Ida M.; Iovan, Diana A.; Li, Alex; Zheng, Shao-Liang; Titus, Charles J.; Lee, Sang Jun; Irwin, Kent D.; Nordlund, Dennis; Lancaster, Kyle M; Betley, Theodore A. Synthesis of a copper-supported triplet nitrene complex pertinent to copper-catalyzed amination. *Science*. **2019**, *365*, 1138-1143.

55. (a) Mansuy, D.; Mahy, J.-P.; Dureault, A.; Bedi, G.; Battioni, P. Iron- and manganese-porphyrin catalysed aziridination of alkenes by tosyl- and acyl-iminoiodobenzene. *J. Chem. Soc., Chem. Commun.* **1984**, 1161-1163. (b) Mahy, J.-P.; Battioni, P.; Mansuy, D. Formation of an Iron(III) Porphyrin Complex with a Nitrene Moiety Inserted into a Fe–N Bond during Alkene Aziridination by [(Tosylimido)iodo]benzene Catalyzed by Iron(III) Porphyrins. *J. Am. Chem. Soc.* **1986**, *108*, 1079-1080.

56. (a) Li, Z.; Quan, R. W.; Jacobsen, E. N. Mechanism of the (Diimine)copper-Catalyzed Asymmetric Aziridination of Alkenes. Nitrene Transfer via Ligand-Accelerated Catalysis. *J. Am. Chem. Soc.* **1995**, *117*, 5889-5890. (b) Li, Z.; Conser, K. R.; Jacobsen, E. N. Asymmetric Alkene Aziridination with Readily Available Chiral Diimine-Based Catalysts. *J. Am. Chem. Soc.* **1993**, *115*, 5326-5327.

57. Evans, D. A.; Faul, M. M.; Bilodeau, M. T.; Anderson, B. A.; Barnes, D. M. Bis(oxazoline)-copper complexes as chiral catalysts for the enantioselective aziridination of olefins. *J. Am. Chem. Soc.* **1993**, *115*, 5328-5329.

58. Lebel, H.; Parmentier, M. Copper-catalyzed enantioselective aziridination of styrenes. *Pure App. Chem.* **2010**, *82*, 1827-1833.

59. Subbarayan, V.; Jin, L.-M.; Cui, X.; Zhang, X. P. Room temperature activation of aryloxysulfonyl azides by [Co(II)(TPP)] for selective radical aziridination of alkenes via metalloradical catalysis. *Tetrahedron Lett.* **2015**, *56*, 3431-3434.

60. Jones, J. E.; Ruppel, J. V.; Gao, G.-Y.; Moore, T. M.; Zhang, X. P. Cobalt-Catalyzed Asymmetric Olefin Aziridination with Diphenylphosphoryl Azide. *J. Org. Chem.* **2008**, *73*, 7260-7265.

61. (a) Hazelard, D.; Nocquet, P.-A.; Compain, P. Catalytic C–H amination at its limits: challenges and solutions. *Org. Chem. Front.* **2017**, *4*, 2500-2521. (b) Collet, F.; Lescot, C.; Dauban, P. Catalytic C–H amination: the stereoselectivity issue. *Chem. Soc. Rev.* **2011**, *40*, 1926-1936. (c) Zalatan, D.N.; Du Bois, J. Metal-Catalyzed Oxidations of C–H to C–N Bonds. *Top. Curr. Chem.* **2010**, *292*, 347-378. (d) Díaz-Requejo, M. M.; Pérez, P. J. Coinage Metal Catalyzed C−H Bond Functionalization of Hydrocarbons. *Chem Rev.* **2008**, *108*, 3379-3394.

62. Palucki, M.; Finney, N. S.; Pospisil, P. J.; Güler, M. L.; Ishida, T.; Jacobsen, E. N. The Mechanistic Basis for Electronic Effects on Enantioselectivity in the (salen)Mn(III)-Catalyzed Epoxidation Reaction. *J. Am. Chem. Soc.* **1998**, *120*, 948-954.

63. (a) Paradine, S. M.; Griffin, J. R.; Zhao, J.; Petronico, A. L.; Miller, S. M.; White, M. C. A manganese catalyst for highly reactive yet chemoselective intramolecular C(sp^3)–H amination. *Nat. Chem.* **2015**, *7*, 987-994. (b) Clark, J. R.; Feng, K.; Sookezian, A.; White, M. C. Manganese-catalysed benzylic C(sp^3)–H amination for late-stage functionalization. *Nat. Chem.* **2018**, *10*, 583-591.

64. Bagchi, V.; Paraskevopoulou, P.; Das, P.; Chi, L.; Wang, Q.; Choudhury, A.; Mathieson, J. S.; Cronin, L.; Pardue, D. B.; Cundari, T. R.; Mitrikas, G.; Sanakis, Y.; Stavropoulos, P. A Versatile Tripodal Cu(I) Reagent for C–N Bond Construction via Nitrene-Transfer Chemistry: Catalytic Perspectives and Mechanistic Insights on C–H Aminations/Amidinations and Olefin Aziridinations. *J. Am. Chem. Soc.* **2014**, *136*, 11362-11381.

65. Hennessy, E. T.; Liu, R. Y.; Iovan, D. A.; Duncan, R. A.; Betley, T. A. Iron-mediated intermolecular N-group transfer chemistry with olefinic substrates. *Chem. Sci.* **2014**, *5*, 1526-1532.

66. Chan, K.-H.; Guan, X.; Lo, V. K.-Y.; Che, C.-M. Elevated Catalytic Activity of Ruthenium(II)–Porphyrin-Catalyzed Carbene/Nitrene Transfer and Insertion Reactions with N-Heterocyclic Carbene Ligands. *Angew. Chem. Int. Ed.* **2014**, *53*, 2982-2987.

67. Ma, Z.; Zhou, Z.; Kürti, L. Direct and Stereospecific Synthesis of N-H and N-Alkyl Aziridines from Unactivated Olefins Using Hydroxylamine-O-Sulfonic Acids. *Angew. Chem. Int. Ed.* **2017**, *56*, 9886-9890.

68. Evans, D. A.; Faul, M. M.; Bilodeau, M. T. Development of the Copper-Catalyzed Olefin Aziridination Reaction. *J. Am. Chem. Soc.* **1994**, *116*, 2742-2753.

69. Klotz, K. L.; Slominski, L. M.; Hull, A. V.; Gottsacker, V. M.; Mas-Ballesté, R.; Que, L., Jr.; Halfen, J. A. Non-heme iron(II) complexes are efficient olefin aziridination catalysts. *Chem. Commun.* **2007**, 2063-2065.

70. Xu, Q.; Appella, D. H. Aziridination of Aliphatic Alkenes Catalyzed by *N*-Heterocyclic Carbene Copper Complexes. *Org. Lett.* **2008**, *10*, 1497-1500.

71. Lebel, H.; Huard, K.; Lectard, S. *N*-Tosyloxycarbamates as a Source of Metal Nitrenes: Rhodium-Catalyzed C−H Insertion and Aziridination Reactions. *J. Am. Chem. Soc.* **2005**, *127*, 14198-14199.

72. Dolan, N. S.; Scamp, R. J.; Yang, T.; Berry, J. F.; Schomaker, J. M. Catalyst-Controlled and Tunable, Chemoselective Silver-catalyzed Intermolecular Nitrene Transfer: Experimental and Computational Studies. *J. Am. Chem. Soc.* **2016**, *138*, 14658-14667.

73. a) Schrock, R. R. Transition Metal Complexes That Contain a Triamidoamine Ligand. *Acc. Chem. Res.* **1997**, 30, 1, 9–16. (b) Greco, G. E.; Schrock, R. R. Synthesis ofTriamidoamine Ligands of the Type (ArylNHCH2CH2)3N and Molybdenum and TungstenComplexes That Contain an $[(ArylNCH_2CH_2)_3N]^{3-}$ Ligand. *Inorg. Chem.* **2001**, 40, 16, 3850–3860. (c) Greco, G. E.; Schrock, R. R. Synthesis, Structure, and Electrochemical Studies of Molybdenum and Tungsten Dinitrogen, Diazenido, and Hydrazido Complexes That Contain Aryl-Substituted Triamidoamine Ligands. *Inorg. Chem.* **2001**, 40, 16, 3861–3878

VITA

Anshika Kalra received her Bachelor of Science in Chemistry from Panjab University, India in May 2011. She completed her Master of Science in Chemistry with specialization in Inorganic Chemistry from Panjab University in May 2013. She started her Ph.D program in the Department of Chemistry at Missouri University of Science and Technology, Rolla, MO in 2015 under the guidance of Dr. Pericles Stavropoulos. Her specialization was synthetic organometallic chemistry and homogeneous catalysis. Her research involved the development of tripodal and bipodal frameworks first-row transition metal reagents for selective C–N bond construction methodologies. In July 2021, she received her Ph.D in Chemistry from Missouri University of Science and Technology.